

APRIL 1, 1993

ANCHAM

# *Analytical* CHEMISTRY



*Analytical Chemistry in the  
Aftermath of the Gulf War*

**359 A**

# SCALE UP RELIABILITY

## Simple, Economical and Direct

Produced to the Same Exacting Specifications,  
E. Merck Silica Based Chromatography Products Provide  
the Highest Performance with Identical Selectivity and  
Guaranteed Reproducibility Regardless of the  
Method and Size of Your Sample

...Makes the Transfer from  
Analytical to Prep and  
Production Scale Easy,  
Reliable, and Reproducible

Use HPTLC to Economically Scan  
Chemistries to Determine the Best  
Selectivity

E. Merck HPTLC plates are available in a wide range of bonded phases which provide a fast, easy, and direct method for product screening. HPTLC can be particularly useful for "In-Process" control during prep LC with Lobar® Prepacked Columns.

Lobar Prepacked Glass LC Columns Offer  
Convenience, Economy, and Performance  
for Preparative Chromatography in the Lab

Lobar Glass Columns are packed with E. Merck LiChrorep® materials which are guaranteed to provide identical selectivity. They are a convenient and cost-effective alternative to HPLC for isolating prep quantities of product. Available in three sizes to accommodate a variety of loading capacities.

LiChrorep Packing Materials Guarantee  
Selectivity and Reproducibility for Scale Up

E. Merck has produced LiChrorep packing materials with the same guaranteed selectivity for over 20 years. Available in four different particle size ranges, scale up reproducibility is guaranteed.

**ORDER DIRECT**

For more information call 800/922-1084 or write:

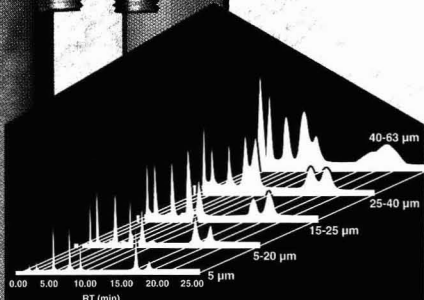


## EM SEPARATIONS

A Division of EM Industries, Inc.

480 Democrat Road • Gibbstown, New Jersey 08027  
(609) 224-0742 • (800) 922-1084 • FAX: (609) 423-4389

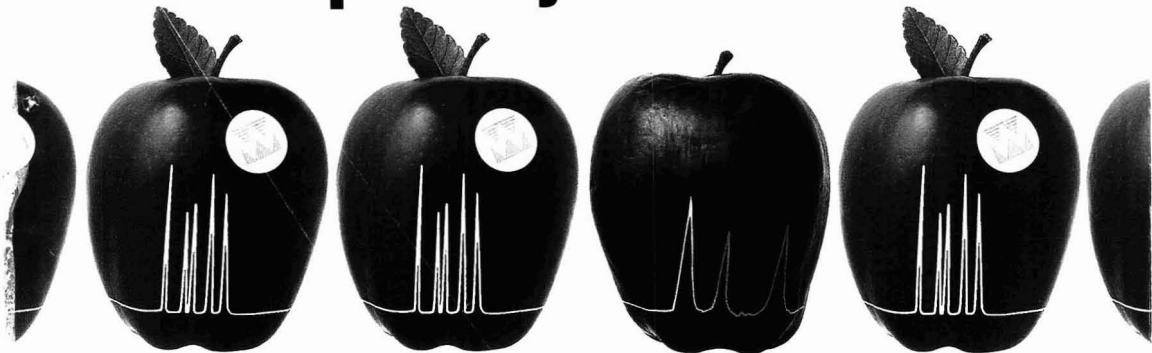
CIRCLE 24 ON READER SERVICE CARD



Guaranteed  
reproducibility over 5  
different particle sizes



# Why let one bad apple spoil all your work?



## Get reproducible results with Whatman.

**Call 1-800-242-7530  
for a free sample and more information.**

Reproducibility problems are more than just frustrating: They cast doubt on the validity of your analysis. Why not get the reproducible results you need from Whatman?

Whatman has the most complete line of sample prep products in the industry—over 500 in all—and every one is unconditionally guaranteed to work within your exacting tolerances. In fact, reproducible results are the #1 reason so many professionals have made the switch to Whatman.

Our technical staff is ready to help you improve your method's reproducibility—whether your problems are procedural or involve the shortcomings of another manufacturer's product.

So the next time you're less than satisfied with the results you're getting, call Whatman. We'll spoil you, not your work.

CIRCLE 96 ON READER SERVICE CARD

### Whatman®

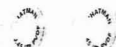
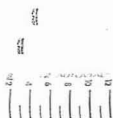
Whatman Laboratory Division

Whatman Inc., 9 Bridewell Place, Clifton, New Jersey 07014

Telephone: 201-773-5800 Telex: 133426 Fax: 201-472-6949

Whatman (word and device) and Whatman (word only) are trademarks of Whatman Paper Ltd. 746-11-203

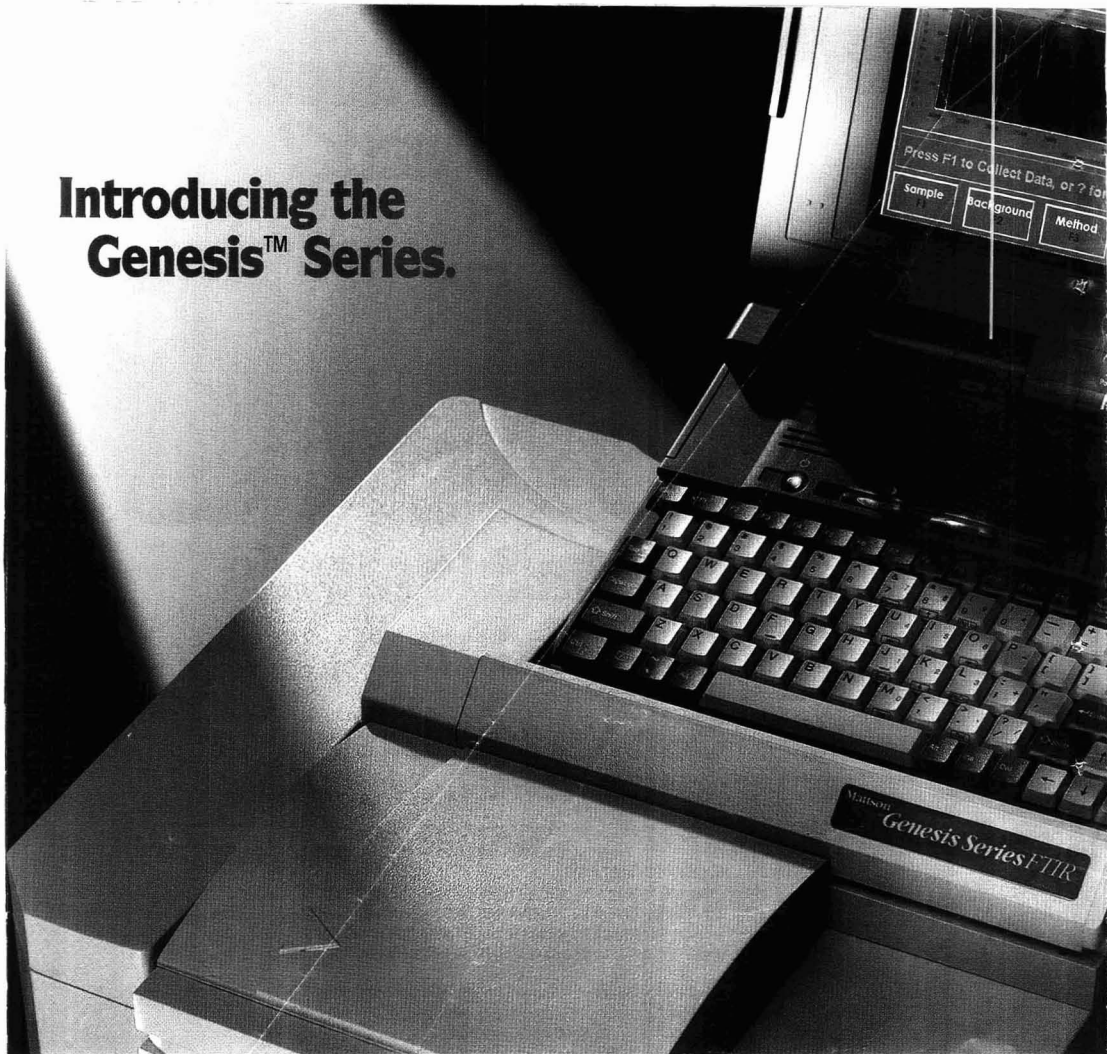
**The reproducible results you need. Guaranteed.**



SPE OCS-1



# Introducing the Genesis™ Series.



## A new age in FTIR spectroscopy begins.

**It's simplicity.** For the first time ever, spectroscopists and non-spectroscopists alike can start gathering spectra *instantly*. Without special training. Without memorizing cryptic commands. As the acknowledged leader in easy-to-use software, we're proud to announce that Genesis *is* simplicity.

**Without sacrifice.** New microelectronic technology gives you the performance you demand, and the large sample compartment you need, in a revolutionary new design: Genesis is the smallest spectrometer ever made. Yet, it's Designed For Ruggedness and Reliability (DFR<sup>2</sup>).™

**It's ahead of its time.** We designed Genesis like we design all of our instruments — with an eye to the future. It's ready to evolve with changes in technology. It's ready to grow with *you*.

**Welcome to the new age of FTIR.**

Call (608) 831-5515 and ask about Genesis today. Or fax us at 608-831-2093.



**Mattson**  
Revolutionary. Evolutionary.

**UNICAM**  
ANALYTICAL SYSTEMS

1001 Fourier Drive Madison, WI 53717

Cahn, Orion, Mattson and Unicam are  
operating divisions of Analytical Technology, Inc.

© 1992, Mattson Instruments, Inc.

CIRCLE 60 ON READER SERVICE CARD



Registered in U.S. Patent and Trademark Office;  
©Copyright 1993 by the American Chemical Society

EDITOR: **ROYCE W. MURRAY**, University of North Carolina

ASSOCIATE EDITORS: **Catherine C. Fenselau**, University of Maryland Baltimore County, **William S. Hancock**, Genentech, **James W. Jorgenson**, University of North Carolina, **Robert A. Osteryoung**, North Carolina State University, **Edward S. Yeung**, Iowa State University/Ames Laboratory

Editorial Headquarters, research section  
Department of Chemistry  
Venable and Kenan Laboratories  
University of North Carolina  
Chapel Hill, NC 27599-3290  
Phone: 919-962-2541  
Fax: 919-962-2542  
E-mail: Murray @ uncx1.oit.unc.edu

Editorial Headquarters, A-page section  
1155 Sixteenth St., N.W.  
Washington, DC 20036  
Phone: 202-872-4570  
Fax: 202-872-4574  
E-mail: rmh96 @ acs.org

Managing Editor: Mary Warner

Senior Editor: Louise Voress

Associate Editor: Grace K. Lee

Assistant Editor: Felicia Wach

Editorial Assistant: Deborah Noble

Contributing Editor: Marcia Vogel

Head, Graphics and Production: Leroy L. Corcoran

Art Director: Alan Kahan

Designers: Peggy Corrigan, Robert Sargent

Production Editor: Elizabeth Wood

Electronic Composition: Wanda R. Gordon

Circulation: David Schulbaum

#### LabGuide

Managing Editor of Directories and Databases:  
Kathleen Strum

Associate Editor: Joanne Mullican

Assistant Editor: Susan Barclay

Journals Dept., Columbus, Ohio

Editorial Office Manager: Mary E. Scanlan

Journals Editing Managers: Kathleen E. Duffy,  
Anne C. O'Melia, Joseph E. Yurvati

Associate Editor: Lorraine Gibb

Assistant Editor: Brenda S. Wooten

Advisory Board: Michelle V. Buchanan, Bruce Chase, M. Bonner Denton, Joseph G. Gordon, David M. Haaland, Joel M. Harris, Timothy D. Harris, Franz Hillenkamp, Kiyokatsu Jinno, Dennis C. Johnson, Richard A. Keller, Philip D. LaFleur, Gary E. Maciel, Geraldine Richmond, Ralph Riggan, Michael Thompson  
Ex Officio: Joseph L. Glajch

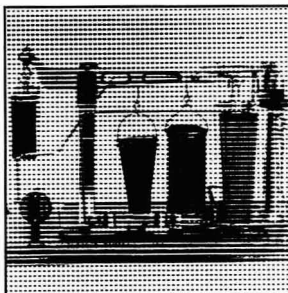
Instrumentation Advisory Panel: Anna Brajter-Toth, Raymond E. Clement, Therese M. Cottcn, Norman J. Dovichi, Jack D. Henion, Mary Ellen P. McNally, John W. Olesik, Dallas L. Raosenstein, J. Michael Ramsey

#### Publications Division

Director: Robert H. Marks

Head, Special Publications: Anthony Durniak

Head, Journals: Charles R. Bertsch



## REPORT 344 A

**A look back at scientific instrumentation.** Historic instruments are an endangered species. John T. Stock of the University of Connecticut focuses on the development of various types of instrumentation, emphasizing the value of historical instruments as an important part of the scientist's heritage



## ANALYTICAL APPROACH 359 A

**On the cover.** Analytical chemistry in the aftermath of the Gulf War. The 1991 Gulf War ended with Iraq's acceptance of the cease-fire terms embodied in U. N. Security Council Resolution 687. D. L. Donohue and Rolf Zeisler of the International Atomic Energy Agency describe the role of the IAEA laboratories in inspecting Iraqi nuclear installations

Cover photo by Imtek Imaging/Masterfile

## UPCOMING RESEARCH

337 A

## EDITORIAL

341 A

**The handsome 600-pound gorilla.** Mass spectrometry is assuming a more central role as a vigorous player in measurement science frontiers

## NEWS

343 A

**1994 Waters symposium proposals.** • **EAS award nominations.** • **Genetic bit analysis for horses and humans.** • **1994 Bomem-Michelson award**

## FOCUS

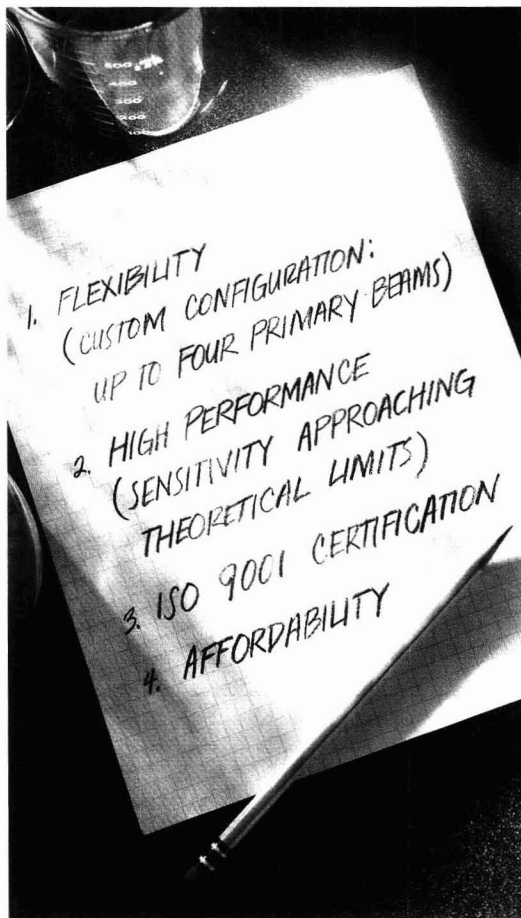
353 A

**Molecular dosimetry.** Cancer researchers are using molecular dosimetry to measure the reactivity of carcinogens with target DNA molecules and to determine whether there are threshold levels of exposure

## NEW PRODUCTS AND MANUFACTURERS' LITERATURE

356 A

# Every Research-Grade FT-IR Should Have These Four Features. Only One Does.



Before you buy an FT-IR, compare it to the Perkin-Elmer System 2000 FT-IR Spectrometer.

The System 2000 is the only FT-IR with an optical bench that can be equipped with up to four identical *primary* beams. That means uncompromised



*The System 2000:  
performance plus versatility.*

optical performance and unsurpassed applications versatility.

It's the only FT-IR with Dynascan™—an interferometer immune to tilt and shear problems. That means performance approaching theoretical limits. And Perkin-Elmer is the only manufacturer whose FT-IR spectrometers are all certified as designed and manufactured under the strict quality requirements of ISO 9001. That means assurance of reliability and performance.

The System 2000 is without question the price/performance leader. That means you can't buy a higher performance FT-IR for anywhere near the price.

Superior features. Superior performance. Superior value. That means the System 2000 is the only research-grade FT-IR you need.

For more information, contact your local Perkin-Elmer office. For product literature in the U.S., call 1-800-762-4000.

**PERKIN ELMER**

The Perkin-Elmer Corporation, 761 Main Avenue, Norwalk, CT 06850-0012, U.S.A.  
Perkin-Elmer Ltd., Post Office Lane, Beaconsfield, Bucks HP9 1QA, U.K.  
Bodenseewerk Perkin-Elmer GmbH, Postfach 10 11 64, 7770 Ueberlingen, Germany  
Dynascan is a trademark of The Perkin-Elmer Corporation.

Circle 72 for information only. Circle 73 for Sales Call.



ANALYTICAL CHEMISTRY (ISSN 0003-2700) is published semimonthly by the American Chemical Society, 1155 Sixteenth St., N.W., Washington, DC 20036. Second-class postage paid at Washington, DC, and additional mailing offices. Postmaster: Send address changes to ANALYTICAL CHEMISTRY, Member & Subscriber Services, P.O. Box 3337, Columbus, OH 43210.

Canadian GST Reg. No. R127571347.

**Copyright Permission:** An individual may make a single reprographic copy of an article in this publication for personal use. Reprographic copying beyond that permitted by Section 107 or 108 of the U.S. Copyright Law is allowed, provided that the appropriate per-copy fee is paid through the Copyright Clearance Center, Inc., 27 Congress St., Salem, MA 01970. For reprint permission, write Copyright Administrator, Publications Division, ACS, 1155 Sixteenth St., N.W., Washington, DC 20036.

**Registered names and trademarks, etc.,** used in this publication, even without specific indication thereof, are not to be considered unprotected by law.

#### Subscription and Business Information

**1993 subscription rates** include air delivery outside the U.S., Canada, and Mexico. Canadian subscriptions are subject to 7% GST.

	Members	Nonmembers (personal)	Nonmembers (institutional)
U.S.	\$ 36	\$ 78	\$ 415
Canada and Mexico	72	114	451
Europe	117	230	496
Other countries	141	254	520

**Nonmember rates in Japan:** Rates above do not apply to nonmember subscribers in Japan, who must enter subscription orders with Maruzen Company Ltd., 3-10, Nihonbashi 2-chrome, Chuo-ku, Tokyo 103, Japan. Tel: (03) 272-7211.

**For multi-year and other rates,** call toll free 800-227-5558 in the U.S. and Canada; in the Washington, DC, metropolitan area and outside the U.S., call 202-872-4363; fax 202-872-4615.

**Single issues,** current year, \$16.00 except review issue, \$50.00, and LabGuide, \$50.00; **back issues and volumes and microform editions** available by single volume or back issue collection. For information or to order, call the number listed for subscription orders by phone; or write the Microform & Back Issues Office at the Washington address.

**Subscription orders by phone** may be charged to VISA, MasterCard, or American Express. Call toll free 800-333-9511 in the continental U.S.; in the Washington, DC, metropolitan area and outside the continental U.S., call 202-872-8065. Mail orders for new and renewal subscriptions should be sent with payment to American Chemical Society, Department L-0011, Columbus, OH 43268-0011.

**Changes of address** must include both old and new addresses with ZIP code and a recent mailing label. Send all address changes to the ACS Columbus address. Please allow 6 weeks for change to become effective. **Claims for missing numbers** will not be allowed if loss was due to failure of notice of change of address to be received in the time specified: if claim is dated (a) North America—more than 90 days beyond issue date, (b) all other foreign—more than 180 days beyond issue date. Hard copy claims are handled at the ACS Columbus address.

**ACS membership information:** Lorraine Bowlin (202-872-4567)

## Articles

- Fluorescence Detection and Size Measurement of Single DNA Molecules** **849**  
*Alonso Castro, Frederic R. Fairfield, and E. Brooks Shera\**
- Fiber Optic pH Sensor Based on Phase Fluorescence Lifetimes** **853**  
*Richard B. Thompson\* and Joseph R. Lakowicz*
- Flow Injection Donnan Dialysis Preconcentration of Trace Metal Cations for Inductively Coupled Plasma Atomic Emission Spectrometry** **857**  
*Narasimhan Kasthurikrishnan and John A. Koropchak\**
- Luminescence Rule of Polycyclic Aromatic Hydrocarbons in Micelle-Stabilized Room-Temperature Phosphorescence** **863**  
*Jin Weijun and Liu Changsong\**
- Detection of Liquid Injection Using an Atmospheric Pressure Ionization Radiofrequency Plasma Source** **866**  
*Jianguo Zhao and David M. Lubman\**
- Collisional Fragmentation of Glycoproteins by Electrospray Ionization LC/MS and LC/MS/MS: Methods for Selective Detection of Glycopeptides in Protein Digests** **877**  
*Michael J. Huddleston, Mark F. Bean\*, and Steven A. Carr\**
- Chiral Separation of Basic Drugs Using Cyclodextrin-Modified Capillary Zone Electrophoresis** **885**  
*Michel W. F. Nielsen*
- Kinetic Detection Method for the Quantification of Isoenzymes on Electrophoretic Media** **894**  
*Robin S. Hampton and Sarah C. Rutan\**
- Capillary Electrophoresis/Electrospray Ionization Mass Spectrometry: Improvement of Protein Detection Limits Using On-Column Transient Isotachophoretic Sample Preconcentration** **900**  
*Toni J. Thompson, Frantisek Foret, Paul Vouros, and Barry L. Karger\**
- Graphitized Carbon Black Extraction Cartridges for Monitoring Polar Pesticides in Water** **907**  
*Antonio Di Corcia\*, Roberto Samperi, Antonio Marcomini, and Susanna Stelluto*
- Determination by Heteronuclear NMR Spectroscopy of the Complete Structure of the Cell Wall Polysaccharide of *Streptococcus sanguis* Strain K103** **913**  
*G. Prabhakar Reddy, Chi-Chou Chang, and C. Allen Bush\**
- Effect of Model Organic Compounds on Potentiometric Stripping Analysis Using a Cellulose Acetate Membrane-Covered Electrode** **922**  
*Joseph H. Aldstadt and Howard D. Dewald\**
- Voltammetric Study on a Condensed Monolayer of a Long Alkyl Cyclodextrin Derivative as a Channel Mimetic Sensing Membrane** **927**  
*Kazunori Odashima, Minoru Kotato, Masao Sugawara, and Yoshio Umezawa\**

\*Corresponding author

continued on p. 335 A

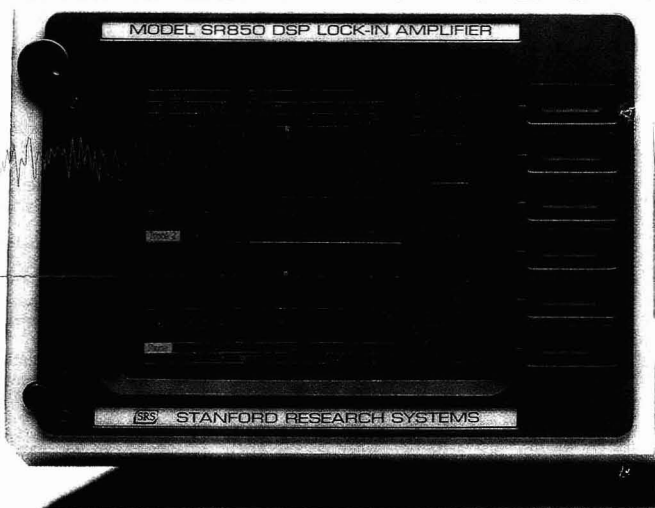
# Seeing is Believing

## ANALOG LOCK-IN



## DIGITAL LOCK-IN

Both amplifiers are locked to a 350 Hz reference with 10  $\mu\text{V}$  sensitivity, 60 dB dynamic reserve, and a 300 ms, 12 dB time constant. The interfering signal is 10 mV at 600 Hz. Both outputs are recorded by the SR850's 16 bit A/D inputs.



Don't be limited by your analog lock-in amplifier. Look at the difference when measuring a signal embedded in noise under identical instrument settings. The analog lock-in is noisy and has a sizeable error, while the SR850 DSP Lock-In Amplifier is quiet and accurate!

The SR850 uses digital signal processing to replace the traditional analog demodulator, low pass filters, and DC amplifiers. The result is no gain error, output drift or stability tradeoff for using high dynamic reserve. The SR850 also has features that no other lock-in can match; polar graphs of R and Theta, direct printing or plotting from the instrument, detection of any harmonic up to 102 kHz, a sweeping synthesized reference source, and much more.

We're so sure that the SR850 DSP Lock-In Amplifier will make your measurements better, we want you to see for yourself. Just call our application engineers at (408) 744-9040, tell them how you're using your analog lock-in, and we'll send you an SR850 for two weeks so you can see the difference.

Performance, Presentation, Ease of use. Seeing is Believing.



- 100 dB dynamic reserve without prefilters
- 0.001° phase resolution
- 0.001 Hz - 102 kHz operation
- \$7500

The introductory price of \$4750 has been extended until June 15th.



## STANFORD RESEARCH SYSTEMS

1290 D. Reamwood Avenue, Sunnyvale, CA 94089  
TEL (408)744-9040 • FAX (408)744-9049

CIRCLE 82 ON READER SERVICE CARD



**Editorial Information**

**Instructions for authors** of AC RESEARCH are published in the January 1 issue, p. 91. Guidelines for the INSTRUMENTATION, REPORT, ANALYTICAL APPROACH, and A/C INTERFACE features are published in the January 1 issue, p. 90. Please consult these instructions and guidelines prior to submitting a manuscript for consideration for publication.

**Manuscripts for publication** in AC RESEARCH (4 copies of text and illustrative material) should be submitted to the Editor at the University of North Carolina address. Please include a signed copyright status form; a copy of this document appears on p. 95 of the January 1 issue. Manuscripts for publication in the A-page section should be submitted to the Washington editorial staff.

**For individual reprints** of AC RESEARCH or A-page articles, please contact the authors directly. Bulk reprints of individual articles are available from ACS. For information, write or call the Distribution office at the ACS Washington address (202-872-4539; fax 202-872-4615).

**ACS Division of Analytical Chemistry**  
Chair, Joseph L. Glajch (508-671-8413)  
Secretary, Sarah Rutan (804-367-1298)

**ACS Information**

Library Services	202-872-4515
Education Division	202-872-4388
Meetings Dept.	202-872-4397
Member Services	202-872-4414
Employment Services	202-872-6120
Public Outreach	202-872-4091

**Supplementary material** is noted in the table of contents with a ■. It is available as photocopy (\$10.00 for up to 3 pages and \$1.50 per page for additional pages, plus \$2.00 for foreign postage) or as 24X microfiche (\$10.00, plus \$1.00 for foreign postage). Canadian residents should add 7% GST. See supplementary material notice at end of journal article for number of pages. Orders must state whether for photocopy or for microfiche and give complete title of article, names of authors, journal, issue date, and page numbers. Prepayment is required and prices are subject to change. Order from Microforms & Back Issues Office at the ACS Washington address.

The paper used in this publication meets the minimum requirements of American National Standard for Information Sciences—Permanence of Paper for Printed Library Materials, ANSI Z39.48-1984.

**Journals Department**  
American Chemical Society  
2540 Orlentangy River Road  
P.O. Box 3330  
Columbus, OH 43210  
614-447-3600, Ext. 3171  
TELEX 6842086; Fax 614-447-3745

**Member & Subscriber Services**  
American Chemical Society  
P.O. Box 3337  
Columbus, OH 43210  
614-447-3776  
800-333-9511

Advertising Office: Centcom, Ltd., 1599 Post Road East, P.O. Box 231, Westport, CT 06881

The American Chemical Society and its editors assume no responsibility for the statements and opinions advanced by contributors. Views expressed in the editorials are those of the editors and do not necessarily represent the official position of the American Chemical Society.

**Scanning Tunneling Microscopy of Carbon Surfaces: Relationships between Electrode Kinetics, Capacitance, and Morphology for Glassy Carbon Electrodes**

*Mark T. McDermott, Christie Allred McDermott, and Richard L. McCreery\**

**937****Technical Notes****Fluorocarbon-Based Immobilization of a Fluoroionophore for Preparation of Fiber Optic Sensors**

*Timothy L. Blair, Tadeusz Cynkowski, and Leonidas G. Bachas\**

**945****Detection of Carbohydrates by Capillary Electrophoresis with Pulsed Amperometric Detection**

*Thomas J. O'Shea, Susan M. Lunte\*, and William R. LaCourse*

**948****Ion Chromatography of Sulfur Dioxide, Sulfate Ion, and Dithionate Ion in Aqueous Mineral Leachates**

*Lloyd M. Petrie\*, M. Emmelyn Jakel, Richard L. Brandvig, and Joseph G. Kroening*

**952****Multiplexed Fluorescence Detector for Capillary Electrophoresis Using Axial Optical Fiber Illumination**

*John A. Taylor and Edward S. Yeung\**

**956****Differential Visualization of Transparent Testa Mutants in *Arabidopsis thaliana***


*John J. Sheahan and Garry A. Rechnitz\**

**961****Author Index****964**

# FT-IR down-time?

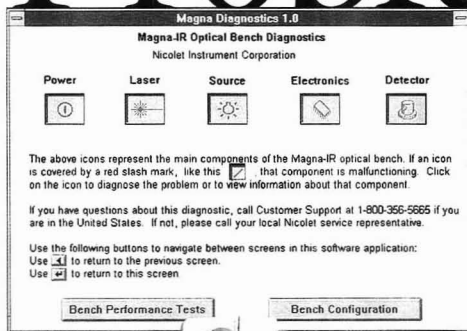


# No Problem!

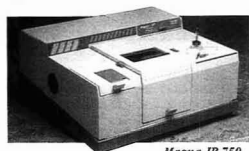
 Nicolet's new Magna-IR™ and Impact™ spectrometers with OMNIC™ software will change the way you think about FT-IR technology.

You can easily replace the source, laser, detectors, and power supply—without getting in over your head. The only tool kit you'll ever need is a screwdriver.

Nicolet offers the first FT-IR systems with user-changeable components. Each is pinned-in-place, eliminating complicated alignment adjustments and a service call. This saves you time and money.



Plus, you are ensured of reliable FT-IR performance through Nicolet's advanced diagnostics program. With a click of the mouse, you are instantly updated on the system's operating status.



Magna-IR 750

*No guessing.  
No waiting.  
No problem!*

Contact Nicolet at 800-356-8088 for an eye opening demonstration or circle the reader service number to receive more information.

**Nicolet**

INSTRUMENTS OF DISCOVERY  
The intelligent FT-IR choice!

5225 Verona Road / Madison, WI 53711-4495 / TEL: 608/271-3333 / FAX: 273-5046

CIRCLE 64 ON READER SERVICE CARD



# UPCOMING RESEARCH

## Second Dissociation Constant of 3-(*N*-Morpholino)-2-hydroxypropanesulfonic Acid and pH of Its Buffer Solutions

Certified pH values and selected thermodynamic properties for the second in a series of pH buffer standards specifically designed for physiological measurements are determined at temperatures from 0 to 50 °C.

**Y. C. Wu, P. A. Berezansky, Daming Feng, and W. F. Koch\***, Inorganic Analytical Research Division, National Institute of Standards and Technology, Gaithersburg, MD 20899

## Time-of-Flight Secondary Ion Mass Spectrometry of Poly(alkyl methacrylates)

A high-resolution TOF-SIMS study of acrylic polymers in the mass range 800–3500 is reported. Polymers show repeating patterns of clusters of individual lines; the patterns are related to the mechanism of chain fracture and cluster structure to hydrogen transfer reactions.

**Paul A. Zimmerman and David M. Hercules\***, Department of Chemistry, University of Pittsburgh, Pittsburgh, PA 15260 and **Alfred Benninghoven**, Physikalisches Institut der Universität Münster, Wilhelm-Klemm Strasse 10, Münster, Germany

## Reduction of Secondary Ion Mass Spectrometry Matrix Effect for High Dose Chromium and Cobalt Implanted Silicon

The energy spectrum of  $^{52}\text{Cr}^+$  proves that energy filtering can be used to significantly reduce the SIMS matrix effect caused by high Cr or Co concentration in the Si substrate.

**Chunsheng Tian\* and Gerhard Stinger**, Institut für Analytische Chemie, Technische Universität Wien, Getreidemarkt 9/151, A-1060 Wien, Austria and **Henning Bubert**, Institut für Spektrochemie und angewandte Spektroskopie, Bunsen-Kirchhoff-Strasse 11, D-4600 Dortmund 1, Germany

## Micro Flow Rate Particle Beam Interface for Capillary Liquid Chromatography/Mass Spectrometry

A commercially available particle beam interface is modified to accommodate the micro flow rate from a packed capillary column. The modified device exhibits improved sensitivity, better response to high-water-content mobile phases, and no noticeable instrument contamination as a result of mobile-phase introduction.

**Achille Cappiello\* and Fabrizio Bruner**, Istituto di Scienze Chimiche, Università di Urbino, P. Rinascimento 6, 61029 Urbino, Italy

These articles are scheduled to appear in AC RESEARCH in the near future.

\*Corresponding author

## Quantitative Microdialysis under Transient Conditions

A method for quantitative microdialysis under transient conditions allows simultaneous determination of extracellular analyte concentration and probe recovery. In vivo recovery is shown to be subject to change following drug administration.

**R. J. Olson and J. B. Justice, Jr.\***, Department of Chemistry, Emory University, Atlanta, GA 30322

## Multidimensional Gas Chromatography with Parallel Cryogenic Traps

Successful implementation of MDGC with two parallel cryogenic traps using chromatographic conditions compatible with GC/IR/MS requirements is described. It is suggested that MDGC systems employing more than two parallel cryogenic traps and multiple analytical GC columns could be useful.

**N. Rangunathan, Kevin A. Krock, and Charles L. Wilkins\***, Department of Chemistry, University of California, Riverside, Riverside, CA 92521

## Kalman Filter-Optimized Simulation for Step Voltammetry

An extended Kalman filter is used to optimize a generalized step voltammetry simulation. Double-layer-corrected estimates of charge-transfer parameters are obtained from experimental voltammograms in a single pass by fitting the filter-optimized simulation model.

**Robert S. Bear, Jr., and Steven D. Brown\***, Department of Chemistry and Biochemistry, University of Delaware, Newark, DE 19716

## Homogeneous Electrochemical Immunoassay Using a Perfluorosulfonated Ionomer-Modified Electrode as Detector for a Cationic-Labeled Hapten

A Nafion film-modified electrode is used to detect a cobaltocenium-labeled amphetamine in the low-nmol range. The electrochemical technique is combined with homogeneous competitive immunoassay of amphetamine.

**Benoit Limoges and Chantal Degrand\***, Université Blaise Pascal de Clermont-Ferrand, Thermodynamique et Electrochimie en Solution, URA 434, Laboratoire d'Electrochimie Organique, 24 Avenue des Landais, 63177 Aubière, France, **Pierre Brossier**, Université de Bourgogne, Faculté de Pharmacie, Unité d'Immunoanalyse, 7 Boulevard Jeanne D'Arc, 21033 Dijon, France, and **Ronald L. Blankespoor**, Department of Chemistry, Calvin College, 3201 Burton S. E., Grand Rapids, MI 49546

## Miniaturized Diameter Flexible Amperometric Lactate Probe

Amperometric lactate electrodes are built by sequentially adsorbing a high molecular weight redox polycation and lactate oxidase on the tip of an epoxy-embedded bundle of carbon fibers.

**Dan Li Wang and Adam Heller\***, Department of Chemical Engineering, University of Texas at Austin, Austin, TX 78712

S A R T O R I U S   K N O W S

# Quality



After a century-long history of innovation, Sartorius is among the first companies to be certified under ISO 9001 standards.

**We passed the test...**



**and we're sharing the results.**

Last year Sartorius AG was awarded ISO 9001 certification. And after experiencing firsthand the intense ISO auditing processes, we know how difficult it is to reach their high standards.

*And we know how to make it easier for you . . . by supplying complete documentation on all Sartorius instruments, including ready-to-use maintenance and servicing forms; and by designing many new product features—specially-engineered for QA ease and enhancement.*

Quality Assurance certification is an important business move in today's global market. But with Sartorius as your partner, ISO 9000 can be an easy move . . . to success.

**sartorius**

140 Wilbur Place  
Bohemia, Long Island, NY 11716  
Phone: 800-635-2906  
FAX: 516-563-5065

CIRCLE 80 ON READER SERVICE CARD

**Langmuir-Derived Equations for the Prediction of Solid Adsorbent Breakthrough Volumes of Volatile Organic Compounds in Atmospheric Emission Effluents**

Equations are developed for the prediction of Tenax GC breakthrough volumes in high-concentration mixtures of VOCs and for important competitive adsorption effects.

**Pau Comes, Norbert Gonzalez-Flesca, and Tamara Ménard**, INERIS, Groupe Air, Parc Technologique Alata, BP 2, 60550-Verneuil-en-Halatte, France and **Joan O. Grimalt\***, Department of Environmental Chemistry (CID-CSIC), Jordi Girona, 18 08034-Barcelona, Catalonia, Spain

**Analysis of a Recombinant Protein Preparation on Physical Homogeneity and State of Aggregation**

An analytical method based on time-resolved fluorescence is proposed to determine the homogeneity of protein preparations and to detect high molecular weight protein contaminants or aggregates in solution.

**J. C. Brochon\*, P. Tauc, F. Mérola, and B. M. Schoot**, LURE, CNRS-CEA-MEN, Centre Universitaire Paris-Sud, Bât. 209D, F91405 Orsay, France, and **ROUSSEL-UCLAF**, Centre de Recherche, F93230 Romainville, France

**Determination of Equilibrium Constants by Chemometric Analysis of Spectroscopic Data**

The analysis described is general and determines both the equilibrium constant and the spectral responses of the components. The proposed method, which is more accurate than traditional single-point approaches to analyzing spectroscopic titration data, may replace these methods because of its relative simplicity.

**Mikael Kubista\*, Robert Sjöback, and Bo Albinsson**, Department of Physical Chemistry, Chalmers University of Technology, S-412 96 Gothenburg, Sweden

**Solventless Collection of Analytes by Rapid Depressurization after Static Supercritical Fluid Extraction**

Following static SFE, analytes can be efficiently collected by rapidly depressurizing the CO<sub>2</sub> effluent through a small i.d. stainless steel tube into a capped vial.

**David J. Miller\* and Steven B. Hawthorne**, Energy and Environmental Research Center, University of North Dakota, Box 8213, University Station, Grand Forks, ND 58202 and **Mary Ellen P. McNally**, E. I. du Pont de Nemours and Company, Du Pont Agricultural Products Experiment Station, Wilmington, DE 19880-0402

**Continuous-Flow Fast Atom Bombardment Liquid Chromatography/Mass Spectrometry of Carotenoids**

Microbore HPLC is combined on line with continuous-flow FABMS for molecular weight and retention time identification of carotenoids. The sensitivity of this LC/MS method is comparable to UV-vis absorbance photodiode array detection.

**Richard B. van Breeman\*, Harold H. Schmitz, and Steven J. Schwartz**, Department of Chemistry, Box 8204, and Department of Food Science, Box 7624, North Carolina State University, Raleigh, NC 27695-8204

**Potentiometric Discrimination of Organic Amines by a Liquid Membrane Electrode Based on a Lipophilic Hexaester of Calix[6]arene**

A liquid membrane electrode based on a long aryl hexaester of calix[6]arene that has an inclusion cavity for organic guests can discriminate organic amines according to their steric shapes.

**Kazunori Odashima, Kenichi Yagi, Koji Tohda, and Yoshi Umezawa\***, Department of Chemistry, Faculty of Science, Hokkaido, Kita 10-Jo Nishi 8-Chome, Sapporo, Hokkaido 060, Japan

**Tandem Time-of-Flight Mass Spectrometer**

A compact TOF/TOF instrument incorporates two dual-stage reflectron analyzers and a collision cell for obtaining structural information by collision-induced dissociation.

**Timothy J. Cornish and Robert J. Cotter\***, Middle Atlantic Mass Spectrometry Laboratory, Department of Pharmacology and Molecular Sciences, The Johns Hopkins University School of Medicine, Baltimore, MD 21205

**Partial Least Squares Techniques in the Energy Dispersive X-ray Fluorescence Determination of Sulfur-Graphite Mixtures**

Partial least squares fitting is applied to evaluation of spectra in the ED-XRF determination of sulfur in graphite. The PLS method can predict sulfur concentrations with an accuracy better than 5% in the concentration range of 2-60% sulfur.

**Jurgen Swerts and Piet Van Espen\***, University of Antwerp, Department of Chemistry, Micro and Trace Analysis Centre, Universiteitsplein 1, 2610 Wilrijk, Belgium, and **Paul Geladi**, University of Umeå, Department of Organic Chemistry, S901 87 Umeå, Sweden

**Chemical Modification by Ascorbic Acid and Oxalic Acid in Graphite Furnace Atomic Absorption Spectrometry**

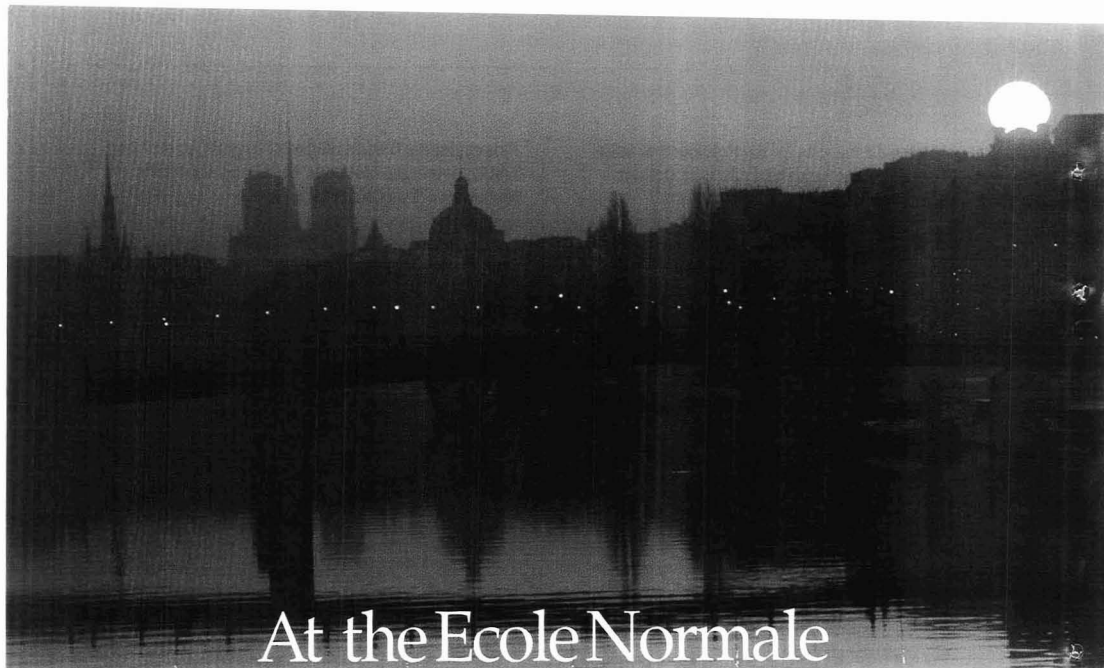
Pyrolysis of ascorbic acid and oxalic acid in a heated graphite tube atomizer produces elevated levels of H<sub>2(g)</sub> and CO<sub>(g)</sub>. The extent of the shift in appearance temperature of Pb shows correlation with variations in the levels of H<sub>2(g)</sub> and CO<sub>(g)</sub> produced by pyrolysis.

**John P. Byrne**, University of Technology Sydney, P.O. Box 123, Broadway NSW 2007, Australia, and **Chuni L. Chakrabarti\*, Glen F. R. Gilchrist, Marc M. Lamoureux, and Peter Bertels**, Centre for Analytical and Environmental Chemistry, Department of Chemistry, Carleton University, Ottawa, Ontario K1S 5B6 Canada

**Affinity Electrophoresis in Multisectional Polyacrylamide Slab Gels Is a Useful and Convenient Technique for Measuring Binding Constants of Aryl Sulfonamides to Bovine Carbonic Anhydrase B<sup>1</sup>**

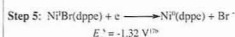
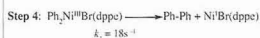
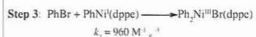
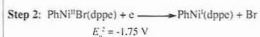
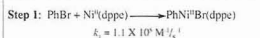
Convenient preparations of heterogeneous multisectional polyacrylamide slab gels are described. The gels contain immobilized affinity ligands and are used to measure binding constants of ligand to protein.

**Yen-Ho Chu, James K. Chen, and George M. Whitesides\***, Department of Chemistry, Harvard University, Cambridge, MA 02138



At the Ecole Normale Supérieure in Paris, scientists are synthesizing polyaryls for optoelectronics using nickel (II) or palladium (II) as catalysts—and *electrochemistry* as the analytical tool. More and more, in laboratories around the world, scientists are studying mechanisms and rates of redox reactions using the electrochemical analyzers BAS has pioneered. So should you.

**BAS. Around the world, around the lab.**



**Bioanalytical  
Systems, Inc.**

2701 Kent Avenue  
West Lafayette, IN 47906  
PH (317) 463-4527  
FAX (317) 497-1102

BAS Japan • 36-4, 1-Chome • Oshiage, Sumida-Ku • Tokyo 131, Japan • PH (81) 3 3624 0367 • FAX (81) 3 3624 0940  
 BAS Europe • Dellingsstraat, 34-1, B-2800 Mechelen Belgium • PH (32) 15 43 22 31 • FAX (32) 15 43 23 85

CIRCLE 10 ON READER SERVICE CARD



## The Handsome 600-Pound Gorilla

Who is the handsome 600-pound gorilla beating up on analytical problems these days? I suspect I'd get several volunteers for such a statement, but I'm picking mass spectrometry as this month's gorilla for another edition of my discussions of analytical chemistry frontiers.

Molecular MS has for decades been an important analytical tool for molecular formula, mass, and structure identification. Researchers have successfully deciphered the fragmentation chemistry of the electron impact ionization source, and GC has been wed with digital data storage systems and moderate-cost time-of-flight and quadrupole mass analyzers. Ultrahigh resolution and tandem instruments also played a substantial role in mass spectral research and applications.

There is a certain parallel between the introduction of  $^{13}\text{C}$  and multidimensional techniques into proton NMR spectroscopy and recent developments in MS. Important discoveries have taken place, and the pace of change has quickened. Although classical mass spectral approaches remain a solid foundation of analytical applications, there is a vastly broadened horizon of challenges and opportunities. Mass spectrometric experiments are under development to probe the three-dimensional structures or folding of biopolymers.

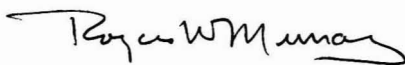
The drivers of change are several. Matrix-assisted laser desorption, fast atom bombardment, and electrospray ion sources have opened more routine ways to volatilization and ionization, including multiple ionization, of large mass structures. Tandem or multiple mass analysis can be done with high resolution and mass accuracy on four-sector combinations or at moderate cost with quadrupole devices. Probably most important are the sophisticated new techniques of inducing gas-phase dissociation chemistry with controllable energy deposition and reactive target

gases as well as the opportunity to use time as a variable in ion-molecule reactions with cyclotron resonance and quadrupole ion storage devices. The elucidation of large mass structures requires more delicate and chemically versatile ways to pry such structures apart.

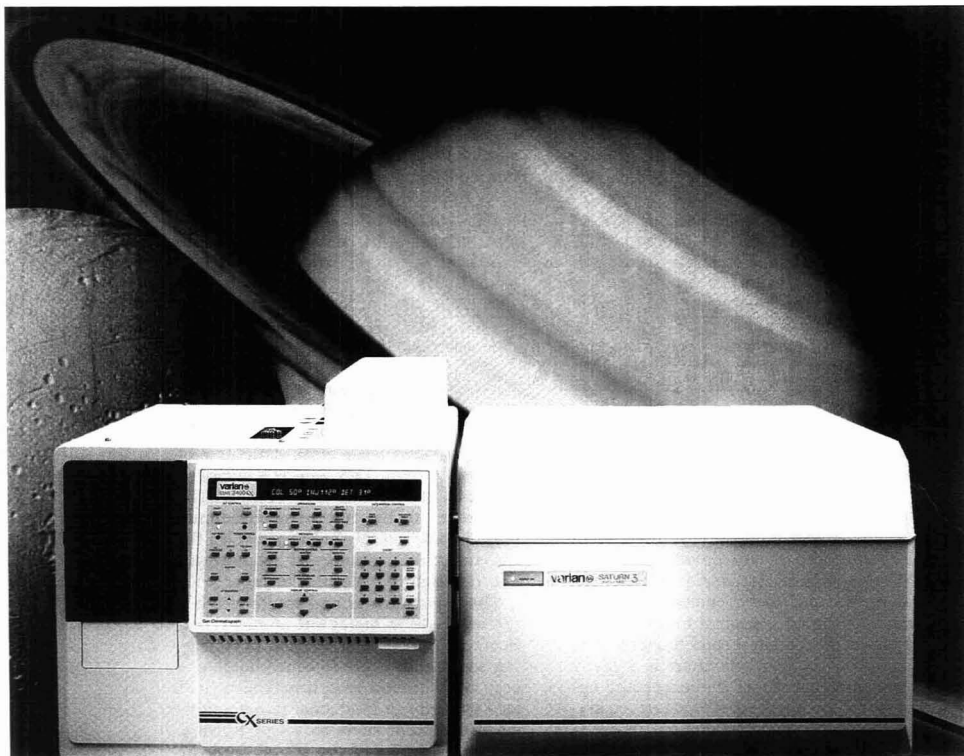
The applications that can be envisioned through these new advances are most obvious and exciting in the biomolecular area. Coupled with new separations capabilities and principles emerging in capillary electrophoresis, CZE/MS may assume a future importance rivaling that of GC/MS. Drinking the full content of this new cup will require research aimed at understanding the newly accessible dissociation chemistry of very diverse large mass structures of biological origin. This will be a substantial task, and choices of its focus will be important to the field; the dividends may include greatly enhanced roles for the analytical community in analysis and research in molecular biology.

The opportunities and challenges are not confined to biological applications. Surface-induced dissociation is emerging as another route to controllable energy deposition in ions; it may also yield new wrinkles in functional group analysis of molecular surfaces. I look forward to incorporation of the recent innovations into simplified low-cost instruments useful for routine monitoring/sensing applications in the human and natural environment.

It is good to see MS assuming a more central role as a vigorous player in measurement science frontiers. It should commensurately assume a larger place in our undergraduate- and graduate-level curricula as well as in continuing education. The opportunities for young scholars in this field seem quite bright.



# Superior GC/MS sensitivity for any sample.



## Saturn 3's new Wave~Board sets standards no benchtop quad can match.

ISO 9001  
REGISTERED

You won't want to purchase a new benchtop GC/MS before you find out about new Saturn 3 Wave~Board technology. It provides the sensitivity and selectivity you need for even the most complex application.

For the awesome details, call  
1-800-941-1826 in the USA and  
1-800-387-2216 in Canada.

- New Wave~Board Scan Function
- Unsurpassed EI→CI time programming
- Advanced quantitation
- Superior automated reporting
- Stay tuned for future Wave~Board modes

GC • GC/MS • HPLC • AAS • ICP-AES • ICP-MS • UV-Vis-NIR • NMR • Sample Preparation • Vacuum Products

varian 

CIRCLE 93 ON READER SERVICE CARD

## 1994 Waters Symposium Proposals

Proposals are solicited for the 1994 James L. Waters Annual Symposium, which will recognize the collaborative work of groups involved in the invention, development, and implementation of analytical instrumentation of established exceptional importance. Previous symposia have covered GC, atomic absorption spectrometry, and IR spectrometry; this year's symposium will be on NMR spectroscopy.

Proposals should include recommendations for the analytical instrumentation to be recognized as well as names of inventors, entrepreneurs producing and marketing commercial instruments, and additional researchers at the forefront of the technology. Proposals should also recommend speakers who can authoritatively address the invention, production, and use of the instrumentation. Proposals should be submitted by April 30 to Chair, Waters Symposium Committee, Society for Analytical Chemists of Pittsburgh, Conference Office, Suite 332, 300 Penn Center Blvd., Pittsburgh, PA 15235-5503. Proposals for the 1995 symposium are also being accepted.

## EAS Awards Nominations

The Eastern Analytical Symposium (EAS) requests nominations for the 1994 awards in the fields of analytical chemistry, near-IR spectroscopy, separation sciences, and magnetic resonance. Each award recognizes an individual who has helped to shape these respective fields. Each award winner will be presented with a plaque at the 1994 annual meeting, which will be held Nov. 14-18 in Somerset, NJ. In addition, the winner of the Award for Achievements in the Fields of Analytical Chemistry will receive a \$1000 honorarium; other award winners will receive \$500 each.

Nominations, consisting of a biographical sketch and a letter specifying the nominee's accomplishments, should be sent to Chair, EAS Awards Committee, P.O. Box 633, Montchanin, DE 19710-0633. Nominations are held active for three years. Deadline is Sept. 30.

## Genetic Bit Analysis for Horses and Humans

When purchasing a race horse, the potential owner has a keen interest in the animal's bloodlines—who an animal's parents are determines not only the price of the horse, but whether the animal "has it in 'im" to be worth the investment of time and money.

Breeding records, blood tests, and markings are part of the system currently used for determining a horse's parentage. These methods can be expensive and complicated, and they are not always conclusive. Scientists at Molecular Tool, a biotechnology company in Baltimore, MD, have developed a technique called genetic bit analysis (GBA) for the horse racing industry as a way to im-

prove upon the current system. GBA is based on enzyme-linked immunosorbent assay (ELISA).

Horse chromosomes, like human chromosomes, occur in pairs. A nucleotide at a particular site on one chromosome of a pair has a corresponding nucleotide on the other chromosome. The corresponding nucleotides may be identical or different, because each one is inherited from a different parent. If a foal's nucleotides at the two corresponding sites on a particular chromosome match one or both nucleotides at the same corresponding sites of the (supposed) parents, that horse is likely to be one of the foal's parents.

The test developed by Molecular Tool checks 20 different sites. The greater the number of nucleotide matches, the more likely that animal is indeed the foal's parent. The test verifies to a probability of 97% the identity of the foal's parents.

The financial backing of the horse racing industry was critical to GBA development. Once the technique proved effective for horses, it was only natural that it should be extended to humans. Working with The Johns Hopkins Medical Institutes, Molecular Tool is using GBA for human chromosomes. Researchers are designing tests that can identify individuals who have genetic diseases, with a goal of doing 50,000 tests per year. Because GBA promises to be quick, accurate, easily automated, and inexpensive, the company hopes that this biotechnological advance will be able to contribute to lowering medical costs.

## 1994 Bomem-Michelson Award

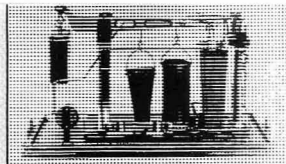
Nominations are sought for the Bomem-Michelson Award, which is given annually at the Pittsburgh Conference to a scientist who has advanced the techniques of vibrational, molecular, Raman, or electronic spectroscopy. Contributions may be theoretical or experimental. The award consists of a medal and an honorarium.

Nominees must be at least 37 years of age and actively working in the fields mentioned above. Nominating and seconding letters, a curriculum vitae, and descriptions of specific research efforts should be sent to David Cameron, BP Research, 4440 Warrensville Center Rd., Cleveland, OH 44128. Deadline is May 1.

## For Your Information

NIST is making available its first set of certified soil standard reference materials. Three different soil samples are certified for baseline, moderate, and high levels of trace elements monitored by the EPA. Laboratories will be able to assess the actual percentages of toxic chemicals recovered by their own methods. Commercial reference material producers will also be able to evaluate the quality of their products. The reference materials (SRMs 2709, 2710, and 2711) cost \$193 each. To purchase, contact NIST, Standard Reference Materials Program, Rm. 205, Bldg. 202, Gaithersburg, MD 20899-0001 (301-975-6776; fax 301-948-4403).

# A Backward Look at Scientific Instrumentation



## John T. Stock

Department of Chemistry  
University of Connecticut  
Storrs, CT 06269-3060

I well remember the time when we were told that the balance, buret, and other volumetric glassware were the prospective chemist's best friends. In my London high school, we were taught to push measuring equipment to the limit. I recall two "zero-cost" experiments. We had to estimate, to the nearest 0.1 mL, the volumes of water contained in a series of 100-mL measuring cylinders. Then came the "weighing by swings" of separate small objects A and B, when we noted the sum of these two weights. Finally, we weighed A and B together and learned that, however good the balance, satisfactory agreement of the two totals required a self-consistent set of weights! In this REPORT I focus the development of various types of instrumentation, emphasizing the value of historical instruments as an important part of the scientist's heritage.

## Balances

My first encounter with balances occurred when, as a small boy, I was taken to the Science Museum in London. I quickly passed by exhibits without buttons or handles to make things move. However, I recall being stopped by the collection of historic balances. I was impressed by the Ramsden "cone beam" instrument shown in Figure 1. Later, I read that this balance had come into being at the behest of the tax collector—the British government needed accurate figures for the specific gravities of alcohol-water mixtures so that the proper duty on "spirituous liquors" could be levied. Some four decades later, as Honorary Research Fellow, I reported on the museum's entire collection of balances (1).

Eventually, these studies were extended (2, 3). When searching for historic instruments, or even for facts about them, one often reaches an apparent dead end. This occurred while I was searching for the balances used to re-establish the Imperial pound after the British standards of weights and measures had been destroyed in a fire in 1834. I found the location of the smallest balance and also learned of the fate of the mid-sized one (2). However, I could not trace the major instrument (4). William Hallows Miller (1801–80), who described the lengthy work of re-establishment, gave the following account of this balance.

These comparisons were made with a balance of extreme delicacy procured from Mr. Barrow. In its construction it nearly resembles the balances of the late Mr. T. C. Robinson. The beam is made sufficiently strong to carry a kilogramme in each pan. The middle knife edge is about 1.93 inch long, and rests, when the balance is in action, throughout its whole length on a single plane surface of quartz. The surfaces of quartz which rest upon the extreme knife edges, and from which the pans are suspended, are also plane. The distance between the extreme knife edges is about 15.06, and the length of each about 1.05. . . .

Despite numerous inquiries and searches since 1965, this balance has not been found. This is doubly serious; not only is there a loss of a superb example of instrument making, but also the balance was the means by which a national standard was re-established.

Despite the failure to achieve the main objective, the inquiries did enlighten me in other directions. I had not known that Henry Barrow (1790–1870), who made the missing balance, was hired at the request of then Captain George Everest (1790–1866) as instrument maker for the Great Trigonometrical Survey of India (5).

Like many others, I had regarded the so-called chainomatic balance as an American invention of 1916. In this type of balance, the adjustable drag of a fine chain is used to eliminate the need for weights smaller than 0.1 g. In fact, the principle had been described a quarter century earlier, and a "chain balance" was available in France before 1899 (6).

Although requiring great care in design, construction, and adjustment, the two-pan balance is essentially a simple device and shows that an instrument does not have to be complicated to be valuable. An extreme example is the surgeon's one-piece scalpel. Another is the blowpipe, which has a most interesting history (7). Between 1751 and 1863, no fewer than 11 elements were discovered with the aid of this highly portable device. The buret, appearing as a one-piece pour-type vessel nearly two centuries ago, acquired the vertical form with stopcock in 1846 (8).

Given that their literary output was often limited to bills, trade cards, and the like, the early instrument makers tend to be forgotten. Their memorials lie in the discoveries made by the scientists who used the instruments. Such users often became expert glass workers; great mechanical ability was claimed less frequently. Charles Vernon Boys (1855–1944) possessed such ability in the highest degree. His professional career began at London's Royal School of Mines, where he worked on an unusual technique for measuring electrolytic conductivity and then on the production of extremely fine quartz torsion fibers (9).

In 1798, Henry Cavendish (1731–1810) determined the gravitational constant. He torsionally measured the attraction between massive lead balls and smaller ones hanging from the ends of a 6-foot-long beam. When Boys described his redetermi-



nation of this constant in 1895, he used tiny gold balls suspended from a beam only 0.9 in. long. Another striking application of Boys' mechanical ability was the "radio-mechanical balance," reportedly able to detect heat equivalent to that given off by a candle a mile away. Both of the Boys instruments as well as his fiber-making equipment are in the London Science Museum.

When the coal-gas industry began in the early 1800s, its output was used for open-flame lighting. Accordingly, the quality of the gas was assessed by its illuminating power. Toward the end of the century, the use of gas spread to lighting by gas mantles (10) and heating. Eventually, a declared calorific value of the gas became a legal requirement. Boys became a gas referee in 1897 and developed the flow calorimeter, which became the official British test instrument. He then designed and built the extremely complicated recording gas calorimeter shown in Figure 2. However, Boys did not despise the simple; in Figure 3, he is shown with another interest—soap bubbles!

#### Optical instrumentation

The development of optical devices gave the instrument makers a new problem. Often they depended on a subcontractor to provide lenses and other components. The first need for the maker of optical devices was defect-free glasses of differing refractive indices. Composite lenses could then be made from these materials, so that the spherical and chromatic aberrations associated with one-piece lenses could be minimized. This led to a considerable improvement in telescope lenses during the 18th century (11). Obviously, this improvement passed to the design of optical instruments in general.

Figure 4 shows French optician Charles Chevalier (1804–59) and

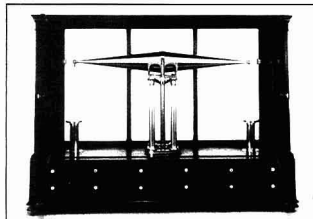


**Figure 1.** Ramsden balance, 1789. The pans and suspensions are missing. (Reproduced with permission of the Trustees of the Science Museum, London.)

British physicist Charles Wheatstone (1804–75). Chevalier made lenses for Jules Duboscq (1817–86), inventor of a colorimeter widely used until well into the present century (12). Duboscq was a pioneer in stereoscopic and other photography, and his existing daguerreotypes are highly regarded.

#### Electrical instrumentation

Progress in all fields of science often depends upon the availability of suitable electrical instrumentation, as described in a previous report (13). The development of methods for the measurement of electric current is

## REPORT

described in a Science Museum monograph (14). The laying of transatlantic cables, begun in 1858, fostered the development of high-sensitivity galvanometers. Knowing that telegraphic signals from across the Atlantic were very weak, William Thomson (1824–1907), later Lord Kelvin, realized that he needed a "frictionless pen" to record on the traveling paper tape. In his "siphon recorder," patented in 1867, ink was fed to a fine glass tube mounted on the deflection coil, so that the tip of the tube was just clear of the tape. An applied potential between the tip and a plate beneath the tape caused the continuous ejection of ink in tiny

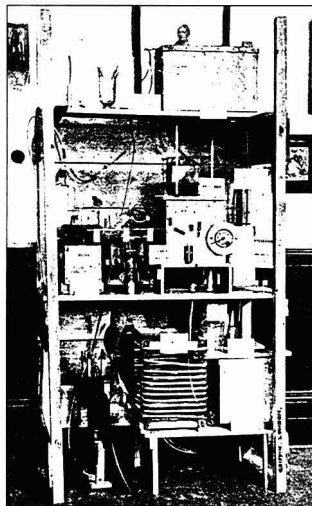


**Figure 2.** Recording gas calorimeter, 1922.

drops (15). Thus, "ink-jet" printing is by no means new.

The siphon recorder was, of course, merely a detector. The problem of the quantitative recording of very small voltages or currents was taken up by Hugh Longbourne Callendar (1863–1930). Figure 5 shows his recorder, patented in 1897, designed for platinum-resistance thermometry. A sensitive galvanometer exerts its control by energizing one or another of a pair of relays, according to the direction of the galvanometer deflection. The pen is then driven by clockwork across the chart, until a contact on a slidewire has returned the deflection to zero.

Other examples of power-assisted small-signal recording are the "thread recorder," in which the freely moving pointer of the galvanometer is periodically depressed on an inked thread above the chart roll, and the Leeds and Northrup "Micromax" and earlier potentiometric recorders. In forms such as the steam-engine indicator, "X–Y" response developed quite early in the engineering industry. The laboratory electrical X–Y recorder owes its origin to home workshop activities in the period 1936 to 1938 (16).

#### Mechanics and hydraulics

Automation or mechanization in the fields of mechanics and hydraulics appeared more than 1000 years ago. More recent examples are the 1728 pattern-weaving loom, which was controlled by punched cards, and the Boulton–Watt steam-engine governor of 1788. About 1880, examples of



**Figure 3.** Charles Vernon Boys. (Reproduced with permission of the Trustees of the Science Museum, London.)

mechanization in the laboratory began to appear (17). These were simple devices to control heating by gas for a fixed time, or for evaporation to a predetermined stage. Somewhat more complicated were arrangements for mechanizing the tedious washing of a gravimetric precipitate and for the repetitive raising and lowering of mercury levels, which were needed in high-vacuum pumping systems.

Figure 6 shows an arrangement of the same period for the repeated agitation of the gas-liquid interface in a selected absorption vessel of an Orsat gas analyzer. Water from A runs continuously into cylinder B. In this cylinder, a long test tube is placed over the central tube, the lower end of which is at E. Air pressure, caused by the rising water, is transmitted from G through H, J, M, and N to the bottle on the right, so that the liquid level in the absorption vessel is depressed. When the water level in the cylinder reaches D, the rapid siphoning through the central tube relieves the pressure, thus restoring the level in the absorption vessel. The cycle then repeats.

Widespread furnace operation made flue-gas carbon dioxide monitors important industrial analytical instruments. (An account of the history of these devices has appeared [18]). The first patents were granted in Germany in 1893. For several years after this, manual flue-gas monitoring was still commonly practiced. By 1916, however, the use of

recording monitors had become so widespread that the U.S. Bureau of Mines issued an extensive bulletin on the performance of competing devices. At that time, some of the devices involved quite complicated glassware, as indicated in Figure 7.

Some other examples of early industrial mechanization are the processing of photographic, dyeing, or cooking operations; the dosing of water to remove turbidity; and a fractional distillation installation of 1907, which relied on the assumption that boiling point and density increase together (19). By the 1920s, the theory and practice of distillation had greatly developed; sophisticated column controls were then in use.

**Electrochemistry**

In 1873, Willoughby Smith (1828-91) observed that the electrical resistance of a bar of selenium decreased when the bar was exposed to light. This discovery led to the light-sensitive selenium cells used in various early devices. A picture telegraphy apparatus was described in 1881. A more practical example was the comparison photometer shown in Figure 8, which was reproduced from the 1907 patent (20). Selenium in the cell is rapidly oscillated between positions a and b. The distances of the light sources i and j are then adjusted so that the signal of the detector, a meter or telephone receiver, remains unchanged.

A more striking application used the selenium cell in a complicated

mechanization of water softening by the lime-soda process (21). This apparatus sampled the treated water, added reagents such as phenolphthalein, photoscopically assessed the state of the sample, adjusted the dosing with the softening agents if necessary and, finally, emptied the sampling vessel.

A paper published in 1923, when alkali-metal photoelectric cells had become available, commented that only a few industrial applications of light-sensitive cells had been proposed (22). Typical applications were for counting, control of liquid level and, more ambitious, optical Marsh-testing for arsenic, a catalyst poison in burner gases involved in the production of sulfuric acid.

In 1776, Cavendish made the first quantitative comparisons of electrolytic conductivity. His only "indicator" was the highly subjective experience of electric shock! Much later came developments such as high-precision absolute measurements, conductometric titrimetry, and conductometric monitoring (23). Monitoring that uses the marked change in conductivity caused by the presence of very low concentrations of electrolytes is crucial for the assessment of the quality of distilled or demineralized water. On the other hand, modern industrial electrodeless instrumentation can handle materials such as hot sodium hydroxide solution, oleum, and raw sewage.

The Nernst equation, formulated in 1889, is a cornerstone of electrochemistry. One of Walther Nernst's



Figure 4. Charles Chevalier (left) and Charles Wheatstone, ca. 1843.

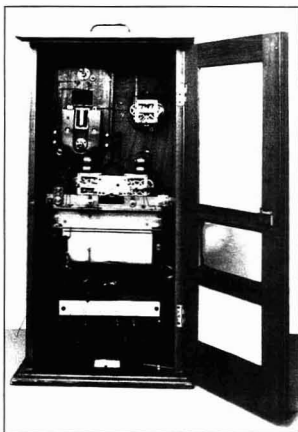


Figure 5. Callendar recorder, 1897.

(Reproduced with permission of the Trustees of the Science Museum, London.)

P R E S E N T I N G

# The Absolute Detector... at your fingertips!

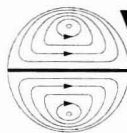
Brought to you by the people who *invented* laser light scattering, the miniDAWN® is an inexpensive, easy-to-use multi-angle light scattering detector that can be coupled to almost any HPLC line for absolute macromolecular characterization. It determines molecular weights and sizes for a broad range of polymers without making assumptions about your samples. It can also reveal a wealth of information that goes unseen by UV, RI and other detection technologies.

*Solves aggregation and calibration problems.* You can use the miniDAWN to see what your samples are doing *in solution* as well as to distinguish among protein and microgel aggregation states without column calibration.

*From the #1 Light Scattering Company.*

With installations in more than 25 countries, Wyatt Technology is the pioneer and world's leading manufacturer of laser light scattering instrumentation for absolute macromolecular characterization. Call us today to get your free 10-page brochure on the miniDAWN. You'll see immediately that the miniDAWN is *absolutely* smarter and faster than any other detector on the market.

- MWs FROM 1000 TO MORE THAN 1 MILLION G/MOLE!
- NO COLUMN CALIBRATION.
- NO PUMP SPEED DEPENDENCE.
- EASY TO USE!



**Wyatt  
Technology**  
CORPORATION

802 East Cota Street  
Santa Barbara, California 93103  
Telephone: (805) 963-5904  
Fax: (805) 965-4898

© 1992 by Wyatt Technology Corporation.

CIRCLE 118 ON READER SERVICE CARD

ANALYTICAL CHEMISTRY, VOL. 65, NO. 7, APRIL 1, 1993 • 347 A

colleagues at Leipzig was Robert Behrend (1856–1926), who eventually published about 100 papers (24). With one remarkable exception, essentially all of these concerned organic chemistry. The exception was his 1893 account, in which he described the application of Nernst's work to the measurement of the solubilities of sparingly soluble mercurous salts. Behrend realized that his technique could be used to follow the course of precipitation reactions; he described the first potentiometric titrations, those of halides with silver nitrate solution.

Recent collaborative reports have discussed the choice of the hydrogen electrode as the base for the electromotive series, and the development

of the pH meter and the glass pH electrode (25). By 1909, Haber and Klemensiewicz had developed the glass electrode and had used it in potentiometric acid–base titrimetry. Because of the high electrical resistance of the glass membrane, observations had to be made with a quadrant electrometer. The transformation of the glass electrode from a specialized item into a routine pH-measuring device had to await developments in electronics. In the interim, pH measurements were made colorimetrically or, by use of electrode systems of low electrical resistance, potentiometrically.

Although the hydrogen electrode meets this electrical requirement, it needs a supply of hydrogen and is susceptible to deactivation by "poisoning." Nevertheless, this electrode was used in industry (26). In response to the deactivation problem, a robust electrode system with easily replaceable platinum elements was patented in 1923. The system, which incorporated a calomel reference electrode, was used in a scheme that permitted the recording of the pH of a flowing stream and governed the making of additions to keep the pH constant.

Although limited to samples in which the pH was less than about 8, the simplicity of the platinum–quinhydrone electrode made it a widely used alternative to the hydrogen electrode in the period before the general advent of the glass electrode (27). Successful attempts were made

to record the pH of flowing streams by continuous dosing with a solution of quinhydrone.

When pH measurements accurate to within 0.1–0.2 units are acceptable, the antimony–antimony oxide electrode, another low-resistance device, can be used with the added advantages of robustness and simplicity. Figure 9 shows a typical antimony–calomel unit of the early 1930s. The indicator electrode is simply elemental antimony, which acquires its oxide coating during use. By the late 1930s, industrial users of the antimony electrode numbered in the hundreds.

At a symposium held in Atlanta in the spring of 1991 to mark the bicentenary of the birth of Michael Faraday (1791–1868), one of the papers outlined the pathway leading from the report of the electrolysis of water in 1800 to the enunciation of the laws of electrolysis in 1834 (28). To determine the total amount of electricity used in an experiment, Faraday devised several forms of the voltameter, based on the gasometric measurement of the products of the electrolysis of water. These procedures were studied by other workers, who made increasingly accurate measurements of the electrochemical equivalent of water (29).

Believing that metal deposition from aqueous solution was a secondary process, Faraday sought quantitative data from the much more difficult electrolysis of fused salts. The crystalline nature of the deposited silver gave problems when he tried fused silver chloride. A few months after Faraday's 1834 publication,

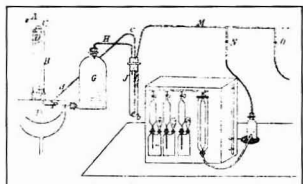


**Figure 6.** Partially mechanized gas analyzer, 1880.

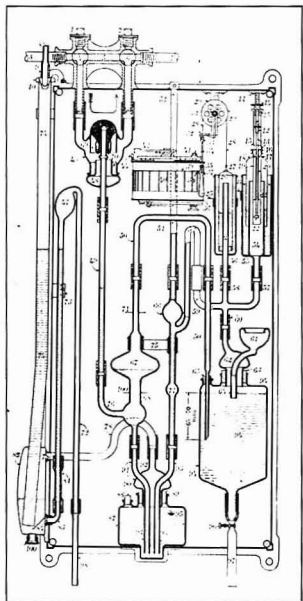


**Figure 7.** Interior of Sarco carbon dioxide monitor, 1907.

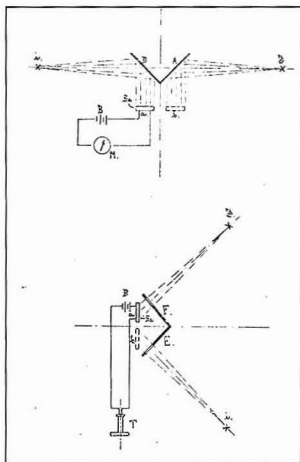


**Figure 8.** Selenium cell comparison photometer, 1907.

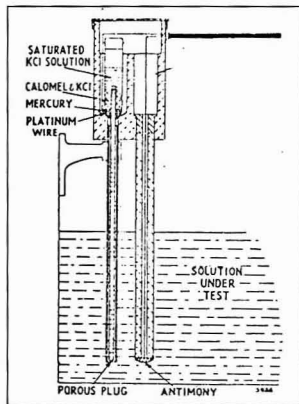


**Figure 9.** Industrial antimony–calomel pH electrode system, ca. 1930.

Carlo Matteucci (1811–68) described the (aqueous) silver-deposition voltameter. As an added irony, the Faraday constant, now known to within a few parts per million, is based on the silver voltameter. Nobel Laureate Theodore William Richards (1868–1928) was one of the many who successively improved the precision of the silver voltameter (30). In 1902 he suggested that the anachronistic term, voltameter, should be replaced by the descriptive term, coulometer. During the period 1908–47, the ampere was internationally defined in terms of the rate of deposition of silver from aqueous silver nitrate solution. Various other chemical and electromechanical coulometers came into use, followed by electronic coulometers.

Two major areas of electrolysis do not require the attainment of 100% current efficiency, however desirable. The first is electropreparation, described in the vast literature of laboratory organic syntheses (31–33). Some of these syntheses have reached industrial scale. The massive production of aluminum, sodium hydroxide, and chlorine are examples of inorganic applications (34). Intense hardness, which may hinder or prevent the use of conventional tools, does not affect electromachining, which involves selective anodic destruction of the metal to be shaped or drilled (35).

The other area is electrogravimetry, at one time a major technique for the determination of certain metals. On the basis of his short paper of 1864, Oliver Wolcott Gibbs (1822–1908) is usually named as the originator of this technique. However, the German railway chemist, C. Luckow, claimed to have been using the method since 1860. It is likely that this claim was well founded; certainly Luckow, and not Gibbs, went on to develop the technique (36). By changing conditions such as pH, it is sometimes possible to analyze mixtures by successive deposition.

A notable advance in both the preparative and the analytical aspects of electrolysis came from the realization that selectivity depends largely on control of the potential of the working electrode. Henry Julius Sand (1873–1944), known mainly for the chronopotentiometric equation that bears his name, was a leading exponent of internal-electrolysis, controlled-potential, and microchemical electrogravimetry (37).

The use of controlled cathode potential by Fritz Haber (1868–1934) made possible the elucidation of the

reaction stages in the electroreduction of nitrobenzene (38). He, like Sand and others, had to control the potential manually; the potentiostat did not appear until 1942.

The introduction of the electric light bulb brought forth the problem of assessing a customer's usage of the dc electricity then being supplied. Thomas Alva Edison (1847–1931) did this by passing a known fraction of the current through amalgamated zinc electrodes immersed in zinc sulfate solution. Periodically, the anode was reweighed to assess the cost (39). In 1882, Edison used this principle in a meter incorporating a balance beam, the periodic tilting of which operated a mechanical counter.

In response to the increasing use of commercial electricity, various other electrolytic meters appeared. Typical is a prepayment meter. Copper electrodes in copper sulfate solution are used; the anode hangs from the right-hand end of the balance beam, which operates a mercury switch that is normally in the open position. Coins inserted in the meter are guided into the larger bucket, causing the beam to tilt, the switch to close, and the electrolysis to begin. Eventually, the decrease in anode weight allows the beam to return to its original position; the supply is interrupted until a further payment is made. Although attempts were made to retain electrolytic meters when power supplies changed from dc to ac, they were eventually supplanted by electromechanical instruments.

The determination of quantities of electricity by measuring the products of electrolysis began with Faraday. A typical reverse approach, coulometric titration, involving the quantitative generation of a titrant by a known

quantity of electricity, was not described until 1938 (40). The intervention of World War II probably delayed developments, but eventually coulometric titration at constant current became a widely used technique. A great advantage is simplicity. Neither potentiostat nor coulometer is needed; the measured variable is merely that of time.

The massive literature on coulometric titration (41, 42) contains many examples of automation or mechanization (43, 44). Apparently, the first example (not a constant-current device) was that shown diagrammatically in Figure 10. This titrator was originally designed during World War II for the continuous bromometric determination of mustard gas in air (45). Developed later as an industrial instrument, the titrator found other uses, such as monitoring mercaptan odorants in town gas supplies. The contaminated air is pumped into the central compartment, causing the sulfuric acid-potassium bromide electrolyte solution to circulate. Negative feedback controls the rate of generation of bromine so that a very slight excess is maintained in the cell.

The determination of acids in chloride medium was one of the earliest coulometric titrations (40). A platinum cathode and a silver anode were used, and an added pH indicator solution provided visual end-point detection. This type of technique is obviously inapplicable in the presence of any substance more easily reduced

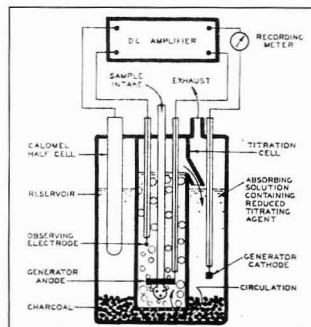


Figure 10. Continuous coulometric recorder, 1948.

(Reproduced from Reference 45.)

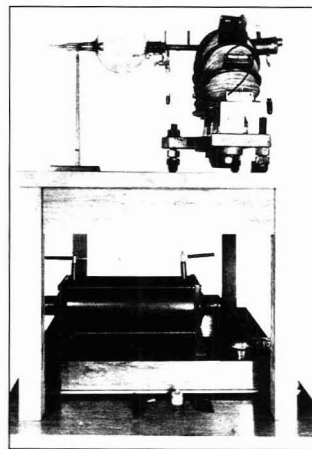


Figure 11. Aston mass spectrograph, 1919.

(Reproduced with permission of the Trustees of the Science Museum, London.)



than hydrogen ions or water. This difficulty was overcome by external titrant generation. In 1951, this approach was used in a mechanized constant-current acid-base titrator.

**The value of historic instruments**

Compared with most modern equipment, the devices that have been described are generally simple. However, instrumentation experts, like other progressives, stand on the shoulders of their predecessors. Some years ago, I pointed out that historic instruments are an endangered species (46). It is easy to cannibalize or to jettison an obsolescent instrument. This may not matter unless the instrument in question is unique or is the last of its kind. Although plentiful in their day, early examples of carbon dioxide monitors or process controllers (47) are now rarely encountered. Aston's first mass spectrograph (Figure 11) is obviously unique. We are still making unique instruments—the prototypes on which production models are based!

A damaged or even incomplete historic instrument can sometimes be restored. Apart from the experts in

museum workshops, there are specialists whose restorative skill is matched by the respect they have for instruments on which they work (48). The great museums of the world are much more than mere exhibitors. They guard the scientific heritage of our successors, they educate, and they are centers of research. On my regular visits to the London Science Museum, I am always amazed by the numbers of school parties of all ages that arrive daily. Perhaps, as I did, these visitors begin with a little "handle-turning." But they soon pass on to a realization of what we owe to science and technology!

This work was partially carried out under the Research Fellowship Program of the Science Museum, London.

**References**

- (1) Stock, J. T. *Development of the Chemical Balance*; Science Museum: London, 1969; p. 13.
- (2) Stock, J. T. *J. Chem. Educ.* **1968**, *45*, 254-57.
- (3) Stock, J. T. *Anal. Chem.* **1973**, *45*, 974A-980A.
- (4) Stock, J. T. In *The History and Preservation of Chemical Instrumentation*; Stock, J. T.; Orna, M. V., Eds.; Reidel: Boston, 1986; p. 244.

- (5) Stock, J. T. *Bull. Sci. Instrum. Soc.* **1986** (9), 11-12.
- (6) Stock, J. T. *Bull. Hist. Chem.* **1990**(8), 12-15.
- (7) Jensen, W. B. In *The History and Preservation of Chemical Instrumentation*; Stock, J. T.; Orna, M. V., Eds.; Reidel: Boston, 1986; pp. 123-49, 244.
- (8) Szabadvary, F. *History of Analytical Chemistry*; Pergamon: New York, 1966; p. 236.
- (9) Stock, J. T. *Bull. Sci. Instrum. Soc.* **1989** (23), 2-6.
- (10) Stock, J. T. *J. Chem. Educ.* **1991**, *68*, 801-03.
- (11) Jaecks, D. H. In *The History and Preservation of Chemical Instrumentation*; Stock, J. T.; Orna, M. V., Eds.; Reidel: Boston, 1986; pp. 51-65, 244.
- (12) Stock, J. T. Submitted.
- (13) Stock, J. T. *Anal. Chem.* **1980**, *52*, 1518A-1523A.
- (14) Stock, J. T.; Vaughan, D. *The Development of Instruments to Measure Electric Current*; Science Museum: London, 1983.
- (15) Green, D.; Lloyd, J. T. *Kelvin's Instruments and the Kelvin Museum*; The University: Glasgow, 1970; p. 34.
- (16) Moseley, F. L. Presented at the 178th National Meeting of the American Chemical Society, Washington, DC, Sept. 1979; paper 11.
- (17) Stock, J. T. *Educ. Chem.* **1983**, *20*, 7-10.
- (18) Stock, J. T. *Trends Anal. Chem.* **1983**, *2*(1), 14-17.
- (19) Stock, J. T. *Amer. Lab.* **1984**, *16*(6), 14-21.
- (20) Bumb, H. German Patent 191,075, 1907.

# INDUSTRIAL & ENGINEERING CHEMISTRY RESEARCH



Editor: Donald R. Paul  
University of Texas, Austin  
Published by the American Chemical Society

## Quality information that gives you the leading edge

Covering the broad, interdisciplinary field of chemical engineering and industrial chemistry, *Industrial & Engineering Chemistry Research* delivers peer-reviewed, monthly reports with a focus on the fundamental and theoretical aspects of chemical engineering, process design and development, and product R&D.

A typical issue contains original studies in the areas of kinetics and catalysis, materials and interfaces, process engineering and design, separations, and other topics, with an emphasis on new areas of science and technology.

## Don't miss a single issue, Subscribe Today!

**Call Toll Free (U.S. only):** 1-800-333-9511  
**Outside the U.S.:** 614-447-3776  
**FAX:** 614-447-3671

**Or Write:**  
American Chemical Society  
Member and Subscriber Services  
P.O. Box 3337  
Columbus, OH 43210

Volume 32 (1993)	Canada	All Other		
Printed	U.S. & Mexico	Europe*	Countries*	
<b>ACS Members</b>				
One Year	\$ 64	\$ 84	\$108	\$120
Two Years	\$115	\$155	\$203	\$227
<b>Nonmembers</b>	<b>\$567</b>	<b>\$587</b>	<b>\$611</b>	<b>\$623</b>

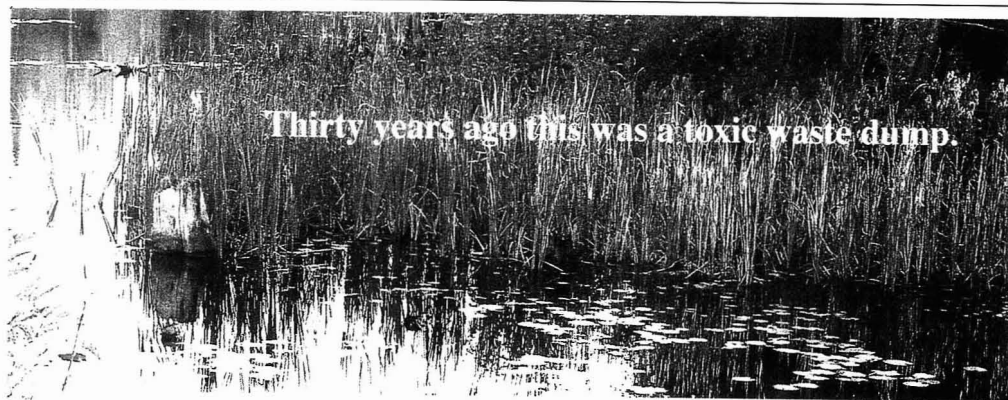
\* Air Service Included.

Member subscription rates are for personal use only. Subscriptions are based on a calendar year. Foreign payment must be made in U.S. currency by international money order, UNESCO coupons, or U.S. bank draft, or order through your subscription agency. For nonmember rates in Japan, contact Maruzen Co., Ltd. This publication is available on microfilm, microfiche, and the full text is available online on STN International.

- (21) Stock, J. T. *Trends Anal. Chem.* **1983**, 2(11), 261-62.
- (22) Logan, L. *Ind. Eng. Chem.* **1923**, 15, 40-43.
- (23) Stock, J. T. *Anal. Chem.* **1984**, 56, 561 A-565 A.
- (24) Stock, J. T. *J. Chem. Educ.* **1992**, 69, 197-99.
- (25) Jaselskis, B.; Moore, C. E.; Von Smolinski, A. In *Electrochemistry, Past and Present*; Stock, J. T.; Orna, M. V., Eds.; ACS Symposium Series No. 390; American Chemical Society: Washington, DC, 1989; Chapters 9, 18, and 19.
- (26) Stock, J. T. *Bull. Hist. Chem.* **1991** (10), 31-34.
- (27) Stock, J. T. *J. Chem. Educ.* **1989**, 66, 910-12.
- (28) Stock, J. T. *Bull. Hist. Chem.* **1991** (11), 86-92.
- (29) Stock, J. T. *J. Chem. Educ.*, in press.
- (30) Stock, J. T. *J. Chem. Educ.* **1992**, 69, 949-52.
- (31) Fichter, F. *Organische Elektrochemie*; Steinkopff: Dresden, 1942.
- (32) Allen, M. J. *Organic Electrode Processes*; Chapman & Hall: London, 1958.
- (33) Baizer, M. M. In *Electrochemistry, Past and Present*; Stock, J. T.; Orna, M. V., Eds.; ACS Symposium Series No. 390; American Chemical Society: Washington, DC, 1989; Chapter 13.
- (34) Leddy, J. J. In *Electrochemistry, Past and Present*; Stock, J. T.; Orna, M. V., Eds.; ACS Symposium Series No. 390; American Chemical Society: Washington, DC, 1989; Chapter 33.
- (35) McGeough, J. A.; Barker, M. B. In *Electrochemistry, Past and Present*; Stock, J. T.; Orna, M. V., Eds.; ACS Symposium Series No. 390; American Chemical Society: Washington, DC, 1989; Chapter 39.
- (36) Stock, J. T. *Bull. Hist. Chem.* **1990**(7), 17-19.
- (37) Stock, J. T. In *Electrochemistry, Past and Present*; Stock, J. T.; Orna, M. V., Eds.; ACS Symposium Series No. 390; American Chemical Society: Washington, DC, 1989; Chapter 32.
- (38) Stock, J. T. *J. Chem. Educ.* **1988**, 65, 337-38.
- (39) Stock, J. T. *J. Chem. Educ.* **1989**, 66, 417-19.
- (40) Ewing, G. W. In *Electrochemistry, Past and Present*; Stock, J. T.; Orna, M. V., Eds.; ACS Symposium Series No. 390; American Chemical Society: Washington, DC, 1989; Chapter 27.
- (41) Lingane, J. J. *Electroanalytical Chemistry*, 2nd ed.; Interscience: New York, 1958; Chapters 20, 21.
- (42) Stock, J. T. *Anal. Chem.* **1984**, 56, 1 R-7 R.
- (43) Stock, J. T. *Trends Anal. Chem.* **1981**, 7(3), 59-62.
- (44) Stock, J. T. *Trends Anal. Chem.* **1982**, 7(5), 117-20.
- (45) Shaffer, P. A.; Briglio, A.; Brockman, J. A. *Anal. Chem.* **1948**, 20, 1008-14.
- (46) Stock, J. T. *Chem. Eng. News* **1979**, 57(31), 30.
- (47) Stock, J. T. *Trans. Newcomen Soc.* **1987-88**, 59, 15-29.
- (48) Read, W. J. In *The History and Preservation of Chemical Instrumentation*; Stock, J. T.; Orna, M. V., Eds.; Reidel: Boston, 1986; pp. 157-62.



John T. Stock is emeritus professor of chemistry at the University of Connecticut. Born in England, he received the Ph.D. and D.Sc. from the University of London. After extensive industrial and academic experience he joined the faculty of the University of Connecticut in 1956. As an analytical chemist, he has been a long-term contributor to ANALYTICAL CHEMISTRY, both in the A pages and in the biennial reviews. His interest in the design, construction, and history of scientific instruments, aroused in his youth, has developed throughout his life. He organized the ACS symposia on the history of chemical instrumentation in 1979 and 1985, and on the history of electrochemistry in 1988. He received the University of Connecticut Alumni Award for excellence in teaching in 1977 and the Dexter Award for outstanding contributions to the history of chemistry in 1992.



Thirty years ago this was a toxic waste dump.

That's when PolyScience first introduced organic standards.

In 1963 — a year after Rachel Carson published *Silent Spring* — PolyScience began offering volatile organic standards. Since that time, while the implementation of environmental policies changed the very nature of this wetland, PolyScience has become the standard for standards.

Every organic and inorganic substance with our name on it is triple-checked for purity. Whether it's an EPA 502.2 mixture, chlorinated insecticides or naphthenes — our standards are your best scientific reference. And they'll remain a constant in standards excellence for another thirty years.



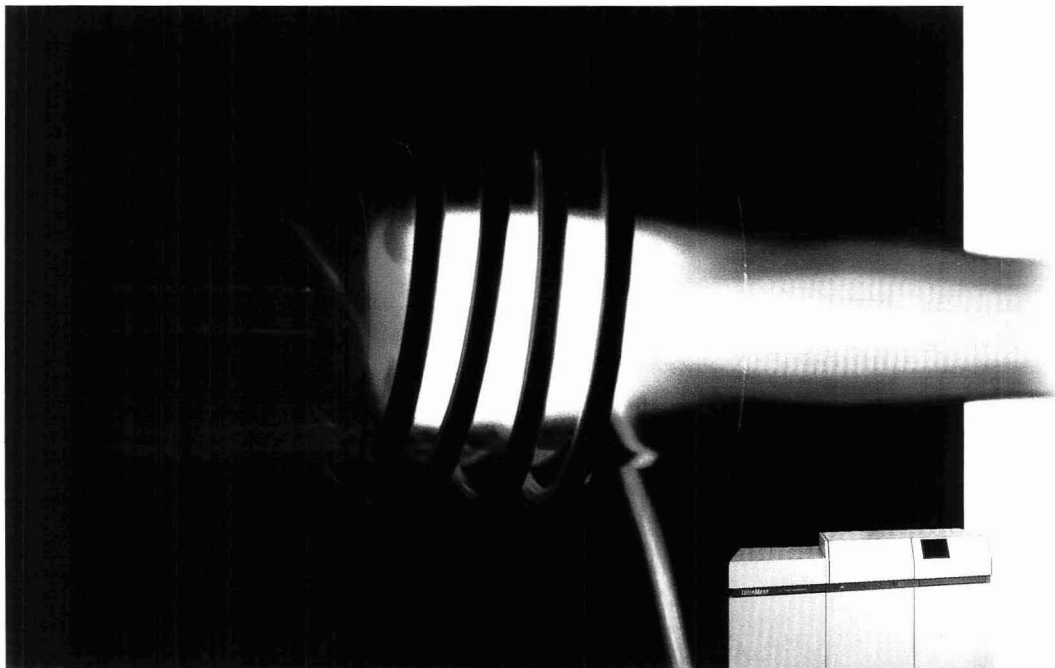
**PolyScience**

7800 Merrimac Avenue • Niles, Illinois 60714  
800/229-7589 • In Illinois: 708/965-0611

Constantly PolyScience. Because Life Varies.

CIRCLE 70 ON READER SERVICE CARD

# The first fully automated ICP-MS.



You asked for a totally automated ICP-MS. And Varian delivered. Our new UltraMass ICP-MS is fast, easy to use, and provides unprecedented flexibility in multitasking software.

UltraMass controls and stores all parameters in a method, allowing a variety of sample matrices to run without stopping. It will also display a full mass spectrum, the zoom of a specific mass, and statistical results simultaneously on one screen.

Scout, a unique safety device, ensures that large peaks can be measured without damage to the detector. And

powerful service diagnostics software can help to reduce downtime, making this the ideal instrument for every laboratory.

You will also get the high standard of quality assured by an ISO 9001 registered business, along with outstanding post-sales support. For further details, call Varian at 1-800-944-1826 in the US and 1-800-387-2216 in Canada.



# Molecular Dosimetry

*Cancer researchers are using molecular dosimetry to measure the reactivity of carcinogens with target DNA molecules and to determine whether there are threshold levels of exposure.*

**“W**arning: The Surgeon General Has Determined That Smoking May Be Dangerous To Your Health.” But how dangerous? And how much tobacco smoke is enough to cause the variety of cancers, heart disease, and birth defects that well-established epidemiological and animal exposure studies have shown it causes?

For the more than 3000 identified compounds in tobacco smoke, as well as for a myriad of environmental and food-related contaminants and toxins, policy makers and public health officials have the unenviable job of trying to figure out, on the basis of these types of studies, the biological risk to humans exposed to these compounds.

Many compounds, including known toxins and carcinogens, produce a wide range of reactions in individuals, and lesions or tumors may not appear until years after an exposure.

## **FOCUS**

Some carcinogens interact with each other, some initiate tumors, some promote tumors, and some must be metabolized to produce an actively genotoxic form. These complications make it difficult to quantitate the carcinogenicity of a compound by using gross measures of external or internal exposure. “Total body burden,” or the concentration of toxin taken up by the body, is used as a measure of internal exposure. But because of physiological and metabolic differences among individuals and among species, the amount of toxin present does not necessarily reflect how much damage it will cause.

Molecular dosimetry is one way cancer researchers are beginning to quantify the potency of carcinogens and to determine whether there are threshold levels of exposure to them. This technique measures the chemical reactivity of a potential or known carcinogen, mutagen, or other genotoxin with a host “target molecule”—

generally DNA. Most models of carcinogenicity assume that the genotoxin acts by mutating or damaging DNA, but in molecular dosimetry some proteins are also examined as easily obtainable indicators with similar reactivity. Many genotoxic agents are electrophilic species that form covalent adducts with bases along the DNA strand and with certain amino acid residues in proteins.

Steven Tannenbaum, of the Department of Chemistry and the Division of Toxicology at the Massachusetts Institute of Technology, says, “Molecular dosimetry at MIT really started about 30 years ago with Gerald Wogan’s first studies of aflatoxin adduction to DNA.” Researchers took what had been discovered in animal experiments—the observation that the carcinogen formed adducts with DNA and proteins—and tried to use quantification of the adducts as a measure of the effective dose, or the amount of genotoxin that actually reaches and affects the DNA. “The key to doing molecular dosimetry [effectively] is the use of new analytical techniques that can measure adduct concentrations at the femtomole levels that might be found in people,” says Tannenbaum.

One advantage of measuring the reactivity of genotoxic agents with DNA is that although physiology and metabolism vary widely among species and among individuals, the mechanisms of DNA regulation, transcription, and translation are fairly consistent among vertebrates. Because the chemistry of purified DNA is even more uniform, it may be more accurate to extrapolate rates of DNA-adduct formation among species than it is to extrapolate rates of tumor formation. Another advantage of molecular dosimetry is that it can be performed on human urine or blood samples *in vitro* rather than requiring harmful *in vivo* exposure to potential carcinogens.

### **Tracking down the adducts**

Tannenbaum’s group uses GC/MS with negative ion chemical ioniza-

tion (NICI) or electron ionization (EI) detection to measure the adduct-forming capabilities of aromatic amines and PAHs—particularly reactive metabolites of benzo[*a*]pyrene (BaP)—with hemoglobin (Hb) or DNA. In many studies of humans, Hb is obtainable in greater quantity than DNA and its adducts have been used as surrogates or biomarkers for DNA adduct formation at critical sites, although actual rates of adduct formation for Hb and DNA may differ. Hb is found enclosed in red blood cells (RBCs), and its accessibility as a target is similar to that of DNA, which is enclosed within the nucleus.

To measure the rate of adduct formation in Hb for known PAHs, Tannenbaum isolates RBCs from human blood, incubates them with known doses of purified active forms of the carcinogens, washes and lyses them, removes the membranes by centrifugation, and precipitates the Hb (which now presumably contains adducts with PAH residues) from the cytosol by adding HCl and acetone. The isolated Hb is washed with 1-butanol to remove free PAHs and sulfur-bonded adducts to glutathione (GSH), a coprecipitating peptide that plays an important role in scavenging toxins from the body and is also studied in molecular dosimetry.

The Hb is digested to completion with a nonselective protease, and individual amino acids are extracted with ethyl acetate and separated by either C<sub>18</sub> HPLC or GC/MS. The PAHs used are diastereomers of BaP epoxides (the actively genotoxic forms of BaP). When Hb from 1 mL of whole blood is mixed with 350 nmol of epoxide, the resulting amino

acid-BaP adducts, isolated in the form of diols and tetrols, can be detected in the single-femtomole range.

Part of the attraction of molecular dosimetry is that it permits chemists to predict how active a potential carcinogen might be in vivo, although extrapolation of structure-function characteristics cannot be substituted for testing any particular carcinogen experimentally. According to Tannenbaum, simple chemical properties such as electrophilicity are better for predicting carcinogenic activity of small alkylating agents than of larger compounds. With bulky carcinogenic agents, steric factors and chirality come into play, and it becomes harder to predict genotoxicity from the compounds' chemical structures. In addition, the method of hydrolyzing the adducts—acid- or base-catalyzed, or neutral—can affect whether the adducts are recovered as *syn* or *anti* forms.

Optimal GC/MS detection methods vary by the type of carcinogen being tested and by the target molecule, says Tannenbaum. Most of his group's MS methods were developed for small derivatized adducts with MW < 1000. Because Hb adduct esters with BaP analogues are somewhat labile, the adducts are derivatized before GC/MS is performed. Analysis of the adducts by GC/MS is semi-automated for aromatic amines but not, as yet, for PAHs, because the derivatization method for NICI-MS detection of PAH adducts is trickier. For most PAH-Hb adducts, NICI-MS results in much less fragmentation than does EI-MS. "With NICI, the advantage over EI is in the signal-to-noise ratio, not in

the sensitivity," says Tannenbaum.

HPLC with fluorescence line-narrowing spectroscopy (FLNS) is another adduct detection method being used by Tannenbaum's group. Tannenbaum says, "We picked up the technique from Gerald Small's group [at Iowa State University]. FLNS is comparable in sensitivity to GC/MS, but no one has done a side-by-side comparison yet." (See also Jankowiak, R.; Small, G. J. *Anal. Chem.* **1989**, *61*, 1023 A–1031 A.) Tannenbaum says he is planning a comparative study of the two methods in the next year and adds that although FLNS is still primarily qualitative, his group has figured out a way to make it quantitative for Hb adducts.

**"Real-life" molecular dosimetry**

Molecular dosimetry can also be used to monitor real-life adduct formation in people who have been exposed to environmental carcinogens. Tannenbaum's group has assayed blood samples from smokers for BaP-like adducts by isolating Hb from RBCs, hydrolyzing it with protease, passing the digest solution twice over an immunoaffinity column with a monoclonal antibody ligand raised against PAH adducts, and concentrating the eluted adducts. Originally the adducts were analyzed by synchronous fluorescence spectroscopy at  $\Delta\lambda = 34$  nm, and the amount of pyrene-like fluorescent species was calculated by using a *trans-anti*-[<sup>14</sup>C]BaP-tetrol standard curve. Tannenbaum says his group has since abandoned that method for the more accurate GC/MS and FLNS techniques. Typical in vivo environmental concentrations are 0.2–10 pmol/g of Hb.

Although Hb adducts provide a convenient and abundant source of information on genotoxicity, DNA adducts are most closely tied to the initiation of carcinogenesis and mutagenesis, and they indicate longer exposure to genotoxins. They can be determined in target tissues such as liver, kidney, bone marrow, and germ-line cells, but fairly invasive procedures must be used to collect the samples. However, products of DNA repair and excision are often excreted intact in urine and can be determined by several methods.

Gerald Wogan, director of the Division of Toxicology at MIT, has carried out small-scale population studies in China and in Gambia, West Africa, to determine the relationship between dietary intake of aflatoxin and formation of adducts to DNA or

**Table I. Biomarkers for carcinogenicity assessment by molecular dosimetry**

Biomarker	Matrix	Half-life	Exposure	Significance
GSH adduct metabolites	Urine	Hours	Acute	Detoxification or metabolic activation
Serum albumin adducts	Peripheral blood	~ 25 days	Short-term	General internal exposure, likely genotoxic
Hemoglobin adducts	Peripheral blood	~ 120 days	Semichronic	Effective dose, likely genotoxic
DNA adducts	Target tissues	> 120 days	Chronic	Effective dose, genotoxic
DNA adduct repair products	Urine		Chronic	Effective dose, possible detoxification with repair



to serum albumin, a biomarker for short-term exposure. Aflatoxin, a mycotoxin produced by *Aspergillus flavus*, can contaminate cereals, peanuts, and other foods. It has been linked to increased incidences of liver cancer in China and Africa. Wogan's group used monoclonal antibody immunoaffinity chromatography, followed by HPLC with UV or fluorescence detection, to detect DNA-aflatoxin adducts and aflatoxin breakdown products in urine samples.

Other DNA adduct detection methods include  $^{32}\text{P}$  postlabeling, a less instrumentally complex method that is nonselective and has a detection limit of less than one adduct per  $10^9$  or  $10^{10}$  nucleotide bases in samples of 1–10 g DNA. The DNA is digested with endonucleases to nucleotide-3'-monophosphates and enzymatically radiolabeled with [ $\gamma$ - $^{32}\text{P}$ ]-ATP at the 5'-position. The labeled adducts are resolved by four-directional TLC for a fingerprint of adduct nucleotides and quantified by autoradiography.

#### Molecular dosimetry as an epidemiological tool

Molecular dosimetry is not the ultimate measuring tool for carcinogenic risk, says Tannenbaum, but rather part of an overall scheme of toxic exposure assessment performed at several levels, each providing a different type of information. The chemical interaction of a purified known agent with a purified target molecule in an isolated system determines the effective dose once the agent has access to the target molecule. Uptake and adduction in intact cells indicate some of the localized physiological and metabolic factors that influence the target molecule's exposure to an agent. Whole-body controlled-exposure studies in animals are needed to determine the toxicokinetics of exposure to an agent, and large population studies—many of them morbidity and mortality evaluations—indicate the outcomes of exposure.

Because each level of exposure evaluation gives a different piece of information, the *in vitro* methods of molecular dosimetry are not likely to replace animal exposure studies altogether, says Tannenbaum. "Molecular dosimetry may simplify animal studies—it may even shorten them by helping direct their focus on the most likely agents and mechanisms—but ultimately, it's not likely to replace them," he remarks.

Still, prospects are good that molecular dosimetry will become part of standard regulatory genotoxicity risk

assessment schemes to provide more precise information on the action of agents on human target molecules. In 1991 the International Agency for Research on Cancer assigned a group to meet in Lyon, France, to evaluate carcinogenic risks. The group concluded, "As the range of data on mechanisms of action of carcinogens increases, so the set of possible . . . substantive types of evidence available . . . will increase. At the same time, inclusion in human studies of measures related to mechanisms

(e.g., molecular dosimetry . . .) will increase the scope and sensitivity of epidemiological research" (*Cancer Res.* 1992, 52, 2357–61).

Although molecular dosimetry will not replace animal testing or epidemiological outcome studies outright, it may change some of the current risk classifications by providing a refined connection between exposure and genotoxicity and by giving epidemiologists a new molecular tool for assessing carcinogenic risk.

Deborah Noble

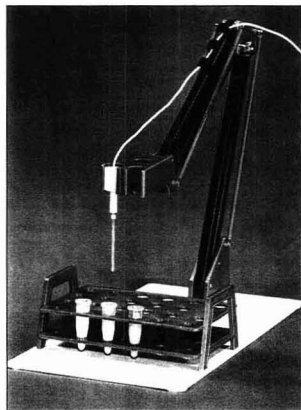
**CHEAP  
CHEAP  
CHEAP**

Finally there's something to chirp about. Introducing the HPC-222 Mass Flow Controller from Teledyne Hastings-Raydist. It's the most economical and accurate mass flow controller you can buy for low flow applications. With a piezoelectric valve actuator to simplify valve construction, the HPC-222 reduces power requirements and increases efficiency. And it's compact and light weight enough for all your gas flow measuring and controlling needs, like gas chromatography and pollution monitoring. For more information on the HPC-222, call us today. We'll give you something to chirp about too.

**TELEDYNE  
HASTINGS-RAYDIST**

P.O. Box 1436 • Hampton VA 23661  
1-800-950-2468

# NEW PRODUCTS



**PHG-1 glass combination pH microprobe** has a tip diameter of 1.2 mm to allow pH measurement in sample volumes down to 1  $\mu$ L for biotechnology applications. It can be immersed in harsh buffers as well as solutions of pH 0–14. Physitemp **401**

## Instrumentation

**CE system.** HP 3D capillary electrophoresis system is fully automated with random access for up to 48 samples. The system includes on-capillary detection using a diode array detector, extended light path capillaries for increased sensitivity, and a self-aligning mechanism for capillary changeover time of under 2 min. Forced-air cooling controls capillary temperatures from 10 °C below ambient to 60 °C. Hewlett Packard **402**

**Immunoassay.** Real-time process monitor for immunoassays is used to monitor purification, fermentation, and other biopharmaceutical production processes. The monitor tracks concentration and purity of products or contaminants by passing part of the process stream through an immunoassay-based sensor cartridge or a perfusion chromatography column at high flow rate. Assays are performed in cycles of 15–20 s or

1 min, depending on the application. PerSeptive Biosystems **403**

**Particle size analysis.** Micro Volume Module for LS series laser diffraction particle size analyzers accommodates small samples of 1–50 mg in a 12-mL diluent volume. The wetted surfaces are corrosion- and solvent-resistant, and the module handles viscosity up to 100 centipoise, with variable-speed stirring and run times of 10 s. Coulter **404**

**TOFMS.** LaserTec BenchTop matrix-assisted laser desorption time-of-flight mass spectrometer for biopolymer molecular weight determinations has automated control of laser intensity and sample position tracking for unattended operation. Equipped with a 0.7-m linear flight tube and a nitrogen laser, the spectrometer provides a video sample monitor for viewing individual samples and a joystick for fast manual operation. The carousel holds 24 samples. Vestec **405**

**NMR.** Unityplus 750-Hz NMR spectrometer, designed for commercial biochemical structure determinations, is available with as many as six interchangeable rf channels that can be configured for indirect detection, triple and quadruple resonance experiments, and other applications. Varian **406**

**Spectrophotometry.** Model 920 UV–vis spectrophotometer features true double-beam, full double monochromator optics and is externally controlled via an IBM-compatible computer. The instrument has continuously variable spectral slit width, with stray light < 0.0003 % T at 220 nm and photometric noise < 0.00005 AU rms, and can scan up to 7000 nm/min. Automated accessories include a routine sipper, batch sampler, gel scanner, reflectance attachments, and ambient cell holders with up to 14 cell positions. GBC **407**

**HPLC.** LC-295 UV–vis detector has programmable wavelength selection for up to 20 wavelength changes per run, allowing users to choose the op-

timal wavelength for each sample component. The detector uses dual-beam optics and has a range of 195–600 nm. It includes autozero correction for each wavelength change and self-checks the deuterium lamp and the energy throughput for both beams. Perkin Elmer **408**

**Mercury analysis.** High-speed cold-vapor mercury analyzer features on-line sample digestion and follows EPA Method 245.2. The system can run 40 samples per hour and has a detection limit of 40 ppb. A DOS-controlled 76-position autosampler and data acquisition software are included. Columbia Analytical Instruments **409**

**XRD.** Materials Research Diffractometer with modular construction maps regions of reciprocal space in epitaxial and thin-film structure studies, and can identify strain, stress, and wafer curvature in single-crystal and polycrystalline materials. The diffractometer incorporates a computer-controlled Bartels four-crystal monochromator and can be equipped with a diffracted beam analyzing crystal for measurements by triple-axis technique. It also uses a conventional divergence slit and parallel plate collimator for analysis of polycrystalline and textured materials. Optical configurations can be switched in seconds, and samples are handled on a wafer stage, 75-mm  $x$ - $y$  translation stage, or an open Eulerian cradle. Philips Analytical **410**

## Software

**Data acquisition.** ChromTalk chromatography interface software collects data in the background from up to 12 instruments simultaneously. The software monitors incoming data and converts it, performs calculations, checks for quality control samples, and transfers to a LIMS automatically. Labtronics **411**

For more information, please circle the appropriate numbers on one of our Reader Service Cards.



**Titrimetric Metrohm dynamic titrator** performs acid-base, redox, precipitation, complexometric, Karl Fischer, and other titration methods, as well as amperometric or voltammetric titrations with an integrated polarizer. The titrator can be interfaced with a printer, balance, sample changer, or PC. Brinkmann 412

**Spectrometry.** SpecInfo Online database on STN International contains 114,000 NMR, IR, and MS spectra of organic compounds. Users can search by entering a chemical structure online, entering a complete NMR spectrum as a list of peak positions, or editing an NMR spectrum selected from the database. The database software can also predict NMR spectra from entered structures for later comparison with experimental results. Chemical Concepts 413

**Chromatography.** Konikrom chromatography data system performs data acquisition and storage; peak integration, timing, and identification; detector response calibration; quantitation; chromatogram reprocessing; and visual analysis. Up to two instruments with four detectors each or vice versa can be supported. The system works within Windows for multitasking data acquisition, methods development, calibration, and calculation and chromatogram-editing functions. Konik 414

## Manufacturers' Literature

**Chromatography.** *Waters Column* newsletter features Nova-Pak C<sub>18</sub> columns and applications for the extraction of mycolic acid from tubercular cultures, isolation of antisense oligonucleotides, and high-perfor-

mance GPC of epoxy resins. Chromatograms and protocol notes, along with ordering information for columns, are included. 32 pp. Millipore/Waters Chromatography 415

**Process chemistry.** *Guidelines for Auditing Process Safety Management Systems* describes alternatives for developing audit programs in chemical process safety management. Pre- and postaudit activities, protocols, data gathering, methods, sources, and organizational changes are discussed. 136 pp. American Institute of Chemical Engineers 416

**Clinical chemistry.** Brochure describes Reply clinical chemistry analyzer and has sections on reagents, ISE benefits, data processing, and instrument support as well as information on the automated features. 8 pp. Olympus 417

**SFE.** Training videotapes describe applications for SFE methods using CO<sub>2</sub> for determination of fat content in foods; EPA Method 3560 determination of environmental pollutants; and general sample preparation, including polymer analyses. 15 min. Isco 418

**XRF.** Brochure discusses on-line elemental analysis by XRF and includes descriptions and photographs of liquid analyzers, coating gauges, granular sample analyzers, and other instruments from the Model 600 series. 12 pp. Asoma 419

## Catalogs

**Laboratory supplies.** Catalog contains a separations feature section with complete listings for filtration and chromatography products. Also included are bioreactors, a UV cross-linker, anemometers, fiber-optic illuminators, and a 24-page section of immunochemicals. Whatman 420

**Gases.** European version of specialty gases catalog contains products for environmental compliance monitoring, supercritical fluid techniques, and toxic organic measurements as well as specialty gases and gas-handling equipment. Information on concentration ranges, shipping, cylinder sizes and contents, and maximum allowable concentrations is provided. Also included are metric conversions, DIN valve outlets and connections, and other format changes for European customers. Scott Specialty Gases 421

## Automatically Convert Hard Copy Graphs to (x,y) Data

with **UN-SCAN-IT™**



IBM & Mac Versions!

**UN-SCAN-IT™**  
Turns Any Scanner Into an Automated (x,y) Digitizing System for Under \$350.

4.5328, 1.1776  
4.3427, 1.1822  
4.5428, 1.1822  
4.7429, 1.1822  
5.1431, 1.1544  
5.3432, 1.7743

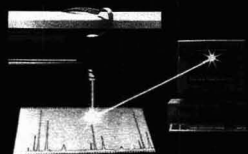
**AUTOMATICALLY DIGITIZE:**

- strip chart output
- (x,y) recorder output
- instrumental output
- published graphs
- old graphs & drawings
- any hard copy graph...

The (x,y) data can be saved in ASCII or HPGL format and imported into almost any commercial graphics or spreadsheet program. The UN-SCAN-IT software can also be used to re-scale graphs, integrate peak areas, smooth data, perform regression analysis, take derivatives, etc.

If you have a plotter...

**UN-PLOT-IT™**

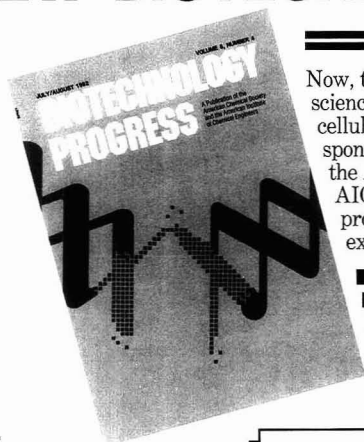


**UN-PLOT-IT™** Turns Your Plotter Into an Automated Digitizing System.

Call: 1-800-227-5558  
FAX: (202) 872-6067

Order from:  
**ACS Software**

# VITAL *NEW* COVERAGE OF *NEW* BIOTECHNOLOGY CONCEPTS



## Basic science ... and the applications

Now, there's a journal that links you with information on the basic science and the applications of breakthroughs in molecular and cellular biology. It's *Biotechnology Progress*, a new journal co-sponsored by the American Institute of Chemical Engineers and the American Chemical Society. Originally started in 1985 by AIChE, *Biotechnology Progress* is now a bimonthly journal that provides research articles, notes, state-of-the-art reviews, and expert commentaries on concepts and trends in these areas:

- Bioseparations
- Bioconversion
- Bioreactor technology
- Applied molecular biology
- Bioanalysis
- Formulation
- Product delivery
- Biocatalytic processes
- Applied biochemistry
- Bioinstrumentation
- Biomedical engineering

### Editor

Jerome S. Schultz  
Center for Biotechnology  
& Bioengineering  
University of Pittsburgh  
1132 Benedum Engineering Hall  
(412) 648-7956

### Associate Editor, Reviews

M.C. Flickinger  
University of Minnesota

## A sampling of articles

*Alpha-Amylase Fermentation with Bacillus Amyloliquefaciens in an Aqueous Two-Phase System*, K.-M. Park and N.S. Wang

*Formation of Bioerodible Polymeric Microspheres and Microparticles by Rapid Expansion of Supercritical Solutions*, J.W. Tom and P.G. Debenedetti

*Metabolic Activity Control of the L-Lysine Fermentation by Restrained Growth Fed-Batch Strategies*, R.D. Kiss and G. Stephanopoulos

*Intracellular Ice Formation During Freezing of Hepatocytes Cultured in a Double Gel*, A. Hubel, M. Toner, E.G. Cravalho, M.L. Yarmush, and R.G. Tompkins

*Cell Death in the Thin Films of Bursting Bubbles*, R.S. Cherry and C.T. Hulle

*Antibody-Targeted Photolysis: In Vitro Immunological, Photophysical, and Cytotoxic Properties of Monoclonal Antibody-Dextran-Sn(IV) Chlorin c6 Immunoconjugates*, S. L. Rakestraw, W.E. Ford, R.G. Tompkins, M.A.J. Rodgers, W.P. Thorpe, and M.L. Yarmush

## Call For Papers

Biotechnology Progress provides exposure among both chemical researchers and engineers, plus publication of accepted manuscripts usually within 4 to 6 months after submission, and research notes within just 2 to 3 months *without page charges*. Articles are abstracted in Chemical Abstracts.

### Please select your method of payment:

Payment enclosed (Payable to the American Chemical Society)

Bill me

Charge my:  Visa/MasterCard or  
 American Express

Account No. \_\_\_\_\_

Expiration date: \_\_\_\_\_

Signature: \_\_\_\_\_

Print name: \_\_\_\_\_

Foreign payment must be made in U.S. dollars by international money order, UNESCO coupons, or U.S. bank draft. Orders accepted through your subscription agency. For nonmember rates in Japan, contact: Maruzen Co., Ltd., 3-10 Nihonbashi 2-chome, Chuo-ku, Tokyo, 103, Japan.

**Yes**, I want to receive bimonthly issues of *Biotechnology Progress*. My 1993 subscription is covered by the ACS pro-rata refund guarantee.

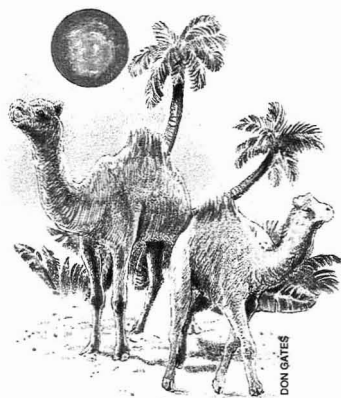
### Please check one:

	U.S.	Canada & Mexico	Europe (Air Service included)	All Other Countries (Air Service included)
ACS/AIChE Members	1 year <input type="checkbox"/> \$ 30	<input type="checkbox"/> \$ 38	<input type="checkbox"/> \$ 47	<input type="checkbox"/> \$ 53
Nonmembers	1 year <input type="checkbox"/> \$ 325	<input type="checkbox"/> \$ 333	<input type="checkbox"/> \$ 342	<input type="checkbox"/> \$ 348
Name	_____			
Address	_____			
City	_____	State	_____	Zip
	_____		_____	_____

### Mail this coupon to:

Biotechnology Progress, Member & Subscriber Services, American Chemical Society, Dept. L-0011, Columbus, OH 43268-0011  
Or Call: 1-800-333-9511 (U.S. only) or (614) 447-3776 FAX: (614) 447-3671

# **ANALYTICAL APPROACH**



## **Analytical Chemistry in the Aftermath of the Gulf War**

---

### **D. L. Donohue and Rolf Zeisler**

International Atomic Energy Agency  
Wagramerstrasse 5  
P.O. Box 100  
A-1400 Seibersdorf  
Austria

---

The 1991 Gulf War came to an end with the acceptance by Iraq of the cease-fire terms embodied in United Nations Security Council Resolution 687. This resolution specifically called upon the International Atomic Energy Agency (IAEA), assisted by the U.N. Special Commission, to carry out inspections of all Iraqi nuclear installations and to develop a plan to destroy, remove, or render harmless all items related to the development of nuclear weapons or nuclear-weapons-usable material.

Within two weeks of that resolution, an IAEA Action Team was formed. Its first inspection, which took place within six weeks, consisted of sorting through the rubble of the buildings in Tuwaitha, the main research center of the Iraq

Atomic Energy Commission. The team took custody of all nuclear materials and visited the Tarmiya site. As time went on, other inspections by the IAEA in collaboration with the U.N. Special Commission enabled investigators to obtain a clearer picture of what had been a multibillion-dollar clandestine program to produce a nuclear weapon.

The IAEA Action Team succeeded in implementing, on very short notice, a comprehensive program of inspection activities by calling upon an impressive range of technical and administrative resources within the IAEA and its member states. The IAEA laboratories in Seibersdorf, Austria, played an important role in this effort by performing hundreds of analytical measurements on samples brought back by inspectors. These analytical results were used to plan subsequent inspections and to verify the declarations made by the Iraqi authorities about their activities prior to the war. In this ANALYTICAL APPROACH we will describe some of the contributions made by the IAEA

laboratories to ensure the success of the Action Team's mission, and we will attempt to convey some of the challenges we faced during this project.

### **Background**

Two specific laboratories in the IAEA's Department of Research and Isotopes were responsible for supporting the Action Team. The Chemical Analysis and Isotopic Analysis Units of the Safeguards Analytical Laboratory (SAL) and the Chemistry Unit of the Physics, Chemistry, and Instrumentation (PCI) Laboratory performed the majority of the measurements. Additional analytical support was provided by government laboratories in the member states, the Austrian Research Center in Seibersdorf, the Atom Institute of the Austrian Universities in Vienna, and a commercial analytical laboratory.

In the initial phases of the project, inspectors and analytical chemists were confronted with the need to define what, if any, undeclared nuclear

activities had taken place; where and, if possible, when they took place; and by what means they were accomplished. To answer these questions, it was important to consider all aspects of the suspect process when the sample collection and analysis system was designed.

Considering the degree of destruction of the Iraqi facilities and the Iraqis' efforts to conceal certain aspects of their program, it was necessary to collect a large number of environmental or construction material samples to search for unusual traces of nuclear materials. To facilitate this sampling, inspectors were supplied with materials such as filter papers for smear samples and plastic or glass bottles for bulk samples. At the laboratory, the samples were coded and split into three parts: one sample for assay in the IAEA laboratories, one for possible analysis in a laboratory outside the IAEA, and one for archival purposes.

The initial goal of the analytical chemists was to quickly answer the following questions:

- Is there radioactive material in the sample? What radionuclides are present?
- Are uranium or other actinide elements present in the sample?
- Are isotopically disturbed uranium or compounds of uranium that are indicative of a particular enrichment process present?
- What are the quantities of radionuclides, fission products, or actinide elements in the samples?

It was imperative that the inspectors and chemists closely coordinate their efforts in determining the best method of sample treatment, priorities for analysis, and where to send the subsamples for outside measurements. The inspectors requested a variety of measurements to aid in the investigation of both declared and undeclared nuclear activities in Iraq. The range of sample types shown in Table I includes environmental samples from nuclear facilities, construction materials used in U enrichment or Pu production, and nuclear-grade process materials.

**Analytical capabilities**

**SAL.** The analysis of nuclear materials for U and Pu content as well as isotopic composition was and still is the main work performed by the SAL in support of IAEA safeguards under the nonproliferation treaty and other agreements. In this article, however, we will focus on the types of samples (including some listed in Table I)

that were unique to the inspections in Iraq or those that required the application or development of new analytical methods and protocols.

The techniques selected for analysis by the SAL (1) require high precision and accuracy, high selectivity for U or Pu and, in some cases, high sensitivity (because of the problems associated with shipping large samples). Table II lists the analytical techniques applied at the SAL for analysis of the samples obtained by the Action Team. Certain techniques

such as high-resolution gamma ray spectrometry and X-ray fluorescence (XRF) spectrometry can be used to measure a large number of isotopes or elements. For this reason, these methods were used extensively in screening the non-nuclear material samples, whereas the more traditional Safeguards Analytical techniques were used for the nuclear material samples.

**PCI Laboratory.** The PCI Laboratory performs a broad range of measurements in support of IAEA

**Table I. Analytical measurements requested for samples obtained by the IAEA Action Team**

Sample category	Sample type	Information requested
Non-nuclear materials		Presence and amount of U and Pu
Environmental	Smears Vegetation Soil Debris Rocks, ores Water	Presence of other radionuclides Presence and amount of F, Cl, U, and Pu isotopes Presence of high explosives
Construction materials	Graphite Steel Beryllium Unknown metals	Purity, type, or identity
Nuclear materials	U metal U compounds Pu compounds Po U, Pu waste and scrap	Amount of U and Pu Amount of U and Pu isotopes Amount of Po Compounds of U and Pu Trace elements in U compounds

**Table II. Analytical techniques used at the SAL**

Analytical technique	Component measured
High-resolution gamma ray spectrometry	Pu isotopic abundances Amount of <sup>241</sup> Am, <sup>237</sup> Np Presence of radionuclides
Alpha particle spectrometry	<sup>238</sup> Pu abundance Presence of <sup>210</sup> Po
X-ray fluorescence spectrometry	Major, minor, trace elemental analysis
K-edge densitometry	Amount of U, Pu, Th, Np in solutions
McDonald/Savage potentiometric titration	Amount of Pu in pure nuclear materials
NBL modified Davies/Gray potentiometric titration	Amount of U in pure nuclear materials
Optical emission spectrometry	Trace elements in U compounds
Thermal ionization MS	U, Pu isotopic abundances
Isotope dilution MS	Amount of U, Pu in small samples





## DEVELOPING A CHEMICAL HYGIENE PLAN

Joy A. Young  
Warren K. Kingsley  
George H. Wahl, Jr.

PUBLISHED BY  
THE AMERICAN CHEMICAL SOCIETY

## Developing a Chemical Hygiene Plan

This essential "how-to" book tells you what you need to know to comply with the federal regulation known as the "OSHA Laboratory Standard" which requires chemical hygiene plans. Developed by the ACS Committee on Chemical Safety, the guide presents hygiene plans that can be modified according to the particulars of individual laboratories. Among the topics covered in this valuable book you'll find

- application of the OSHA Laboratory Standard
- history of the OSHA Laboratory Standard
- standard operating procedures
- control measures and equipment
- records and recordkeeping

In addition, several appendices are provided, including employee information and training techniques, exposure assessment procedures, the elements of an emergency procedure plan, the OSHA Laboratory Standard, a list of contacts for states that have OSHA-approved state plans, and a list of acronyms.

This reference is critical to all lab supervisors who must have in place by January 31, 1991, a chemical hygiene plan that outlines specific work practices and procedures ensuring employee protection from health hazards associated with hazardous chemicals.

by Jay A. Young, Warren K. Kingsley, and George H. Wahl

Developed by the Committee on Chemical Safety of the American Chemical Society

72 pages (1990) Paperbound  
ISBN 0-8412-1876-5 LC 90-4672-1  
\$18.95

O • R • D • E • R • F • R • O • M

American Chemical Society  
Distribution Office, Dept. 67  
1155 Sixteenth St., N.W.  
Washington, DC 20036

or CALL TOLL FREE

# 800-227-5558

(in Washington, D.C. 872-4363) and use your credit card!

Announcing the Acclaimed ACS Short Course!

# Modern FT-NMR Spectrometry: Principles and Practice

Sunday-Friday, May 16-21, 1993

Virginia Tech

Blacksburg, Virginia

.....  
*Gain Hands-On Experience with This  
Powerful Analytical Tool!*

### In Just 5 1/2 Days, You'll

- ◆ Learn the basics and specifics of operating and maintaining Fourier Transform NMR spectrometers
- ◆ Gain an operational knowledge of FT-NMR spectrometers and state-of-the-art techniques
- ◆ Use basic 2-D experiments (COSY, HETCOR, etc.) to solve structural problems
- ◆ Prepare NMR samples for  $^{13}\text{C}$  and  $^1\text{H}$  data collection at the instrument consoles
- ◆ Optimize and maintain FT-NMR spectrometers on a daily basis
- ◆ Perform T $^1$ , NOE, and quantitative NMR
- ◆ AND MUCH, MUCH MORE!

### About the Laboratory

Participants will use a variety of FT-NMR spectrometers during the course. The laboratory is equipped with the following instruments: Varian Unity-400 MHz, Bruker WP-270 MHz, Bruker WP-200 MHz, Bruker MSL-300 MHz, Joel FX-200 MHz, and Bruker NR-80 MHz

### Course Director

Harry C. Dorn, Professor of Chemistry, Virginia Tech

.....  
For more information, phone the ACS Continuing Education Department at (800) 227-5558 (TOLL FREE) or (202) 872-4508. FAX (202) 872-6336. Or mail the coupon below.

**YES!**

Please send me information on *Modern FT-NMR Spectrometry: Principles and Practice*, an ACS Short Course to be held May 16-21, 1993 at Virginia Tech in Blacksburg, VA.

Name \_\_\_\_\_

Title \_\_\_\_\_

Organization \_\_\_\_\_

Address \_\_\_\_\_

City, State, Zip \_\_\_\_\_

Mail to: American Chemical Society, Dept. of Continuing Education, Meeting Code VPI93, 1155 Sixteenth Street, N.W. Washington, DC 20036.

programs. The activities of the PCI Laboratory range from the measurement of radionuclides in the environment (e.g., the international Chernobyl project) to the provision of quality control standards under the Analytical Quality Control Services program. Techniques for the screening and analysis of inspection samples from Iraq, which are divided between destructive and nondestructive analysis methods, are shown in Table III.

To determine F and Cl, neutron activation analysis (NAA) with automated equipment can be used for the rapid evaluation of a large number of samples (2). Gamma ray spectrometry was used extensively to screen samples for radioactivity and to detect the presence of uranium above the background level of  $\sim 1 \mu\text{g/g}$  of sample. Also measured by gamma ray spectrometry were fission product elements that remained in the samples after reprocessing of the spent reactor fuel. The advantage of this method is that results are provided quickly, without elaborate sample preparation. Another advantage is the broad range for detecting radionuclides without requiring prior knowledge of sample composition.

XRF analysis, whether with excitation by an X-ray tube or by a radioisotopic source such as  $^{109}\text{Cd}$ , is also a rapid screening technique with a detection limit for uranium of  $\sim 1 \mu\text{g}/\text{cm}^2$ . Most other elements of interest (except for the lightest ones) were also measured by this method, and it was ideal for determining the composition of metals, powders, or solutions. Quantitative information can be obtained if appropriate standards are available.

Among the destructive analytical techniques used, laser fluorometry offers the highest sensitivity and accuracy for uranium determination (3). This method relies on the optical fluorescence of uranium compounds following illumination by UV laser light. The sample preparation for such measurements involves ashing the specimen in air at  $500^\circ\text{C}$  to remove all organic components, followed by dissolution in hot nitric acid. In some cases, it is necessary to use a solvent extraction procedure to chemically separate the U from interfering elements. The final measurement by laser fluorometry is performed in a phosphate medium to achieve a high luminescence yield.

Information about the concentration of uranium and many other elements in dissolved samples was ob-

tained with inductively coupled plasma optical emission spectrometry (ICP-OES). This method was especially useful for measuring the trace elements in water samples from the pool of the Soviet IRT-5000 reactor and from the spent-fuel storage ponds. The presence in such samples of elements from the fuel cladding or core would be indicative of corrosion or damage to the fuel and would have had serious consequences. The ICP-OES results, in conjunction with the pH and conductivity measurements, gave a consistent picture of the integrity of the fuel rods in these locations.

Finally, certain measurements of Pu in Iraqi samples were performed with alpha particle spectrometry. The sensitivity and selectivity of this method for Pu is quite high; it has a detection limit of  $< 1 \text{ ng}$  (4). Quantitation of the amount of Pu present was accomplished by the addition of a  $^{239}\text{Pu}$  tracer of known quantity. Interference by U in this measurement is minimal because it has lower specific activity and emits lower alpha particle energies.

#### Sample-handling protocol

The analytical schemes applied to the non-nuclear material samples were specially developed to allow the inspectors to make rapid and selective measurements without demanding optimum performance in terms of precision. Another important objective was to obtain as much information as possible from a sample before it was destroyed by further chemical processing.

Usually, a preliminary measurement was performed to screen samples for the presence of important components such as uranium, plutonium, or other radionuclides. Initial screening for uranium was performed by workers at the Austrian

Research Center in Seibersdorf. They used alpha particle counting in an ionization chamber for the highest sensitivity. In both the SAL and the PCI laboratory, additional screening was carried out with high-resolution gamma ray spectrometry and energy-dispersive XRF spectrometry. Gamma ray spectrometry has a high sensitivity (nanogram to microgram levels) for radionuclides with relatively short half-lives, as in the case for many fission products and certain isotopes of Pu. The XRF method was used to screen for the presence of uranium, with a detection limit of  $\sim 1 \mu\text{g}/\text{cm}^2$ . Because uranium is a naturally occurring element that is present in soil at a concentration of  $\sim 1 \mu\text{g/g}$ , there were certain analytical problems associated with the "blank" levels, primarily in the environmental samples.

Following initial screening measurements, samples that showed elevated levels of U or Pu were measured by other nondestructive methods, such as NAA (for F and Cl content), before being submitted for chemical dissolution and further destructive analysis. Care was taken in the chemical treatment of the samples to minimize the danger of contamination. The primary methods used for the determination of U content—laser fluorometry and isotope dilution MS along with other complementary methods—were especially valuable in the analysis of uranium ores from Al Qaim, as discussed below.

The chemical treatment of samples containing U or Pu depended on the matrix. Filter paper smears were digested in nitric acid; soils, ores, and rocks were dissolved in nitric/hydrofluoric acid; and graphite or metal pieces with suspected surface contamination were leached with nitric or hydrochloric acid. Certain an-

**Table III. Analytical techniques used at the PCI Laboratory**

Analytical technique	Component measured
<b>Nondestructive analysis</b>	
Neutron activation analysis	F, Cl, U
Gamma ray spectrometry	U and radionuclides (fission products)
X-ray fluorescence spectrometry	U and elemental composition
Conductivity and pH	Ionic concentration of solutions
<b>Destructive analysis</b>	
Laser fluorometry	U
Inductively coupled plasma optical emission spectrometry	U and trace elements
Alpha particle spectrometry	U and Pu

alytical techniques such as isotope dilution MS required that the samples undergo further chemical processing steps. Thus the analysis of one sample could involve a significant amount of effort and measurements with several analytical techniques.

More than 500 environmental or smear samples and nearly 600 nuclear material samples from the 15 Action Team inspections in 1991 and 1992 were analyzed at Seibersdorf.

#### External analytical support

In addition to the measurements performed at Seibersdorf, selected samples were distributed to laboratories outside of the IAEA that could offer special analytical services or a rapid response for screening measurements. The Austrian Research Center in Seibersdorf supplied alpha particle measurements for the screening of non-nuclear material samples for the presence of U and, in collaboration with the Atom Institute of the Austrian Universities in Vienna, carried out NAA. Samples of steel were sent to a commercial metallurgical laboratory to determine their type and, therefore, their usefulness for building gas centrifuge components (used for uranium enrichment). Government laboratories in several member states accepted samples on which they performed highly sensitive and precise measurements.

#### Results of analytical measurements: selected examples

Several cases will be described in which analytical measurements were performed on non-nuclear material samples supplied by the Action Team. These cases exemplify the range of measurement techniques applied and demonstrate how the results of such analyses can be combined with the inspectors' observations for a more complete understanding of the nuclear activities under investigation.

#### Evidence of electromagnetic separation of uranium isotopes.

The revelation that Iraq had been using the electromagnetic isotope separation (EMIS) process for enriching  $^{235}\text{U}$  came as a surprise to many people in the scientific community. It was not until the third inspection that the Iraqi authorities admitted to the existence of this program and described their activities in detail. This declaration by the Iraqis contained information about the

large facilities at Tarmiya and Ash Sharquat, the number of isotope separators (calutrons) that were operating at Tuwaitha and Tarmiya, and the amount of  $^{235}\text{U}$  that was successfully separated. The Action Team was shown parts of the isotope separators that had been dismantled, destroyed, and buried in an attempt to conceal this program. A few parts from the ion sources and collectors of the calutrons were brought back for analysis. In addition, samples were taken from the declared product batches, covering a range of  $^{235}\text{U}$  enrichment from depleted (< 0.1 wt%) to ~ 6 wt%.

Figures 1 and 2 show photos of an ion source and collector pieces from a 1200-mm calutron declared to have been in operation at Tarmiya. These graphite pieces were scraped with a razor blade to remove ~ 1 g of powder from the surface that was then

leached in nitric acid to dissolve the uranium. This was followed by isotopic measurements using a thermal ionization mass spectrometer (Finnigan MAT-261). Results are shown in Table IV. The ion sources that were sampled for analysis contained only natural uranium. The data from the sampled collector pieces showed enrichments not exceeding 6%.

The Iraqi authorities declared five batches of uranium nitrate product solution from the EMIS process work at Tarmiya. These were said to contain several hundred grams of enriched uranium with a  $^{235}\text{U}$  content of between 3 and 6 wt%, as well as other recovered material with depleted or near-natural  $^{235}\text{U}$  abundance. The product solutions had been removed from five tanks at Tarmiya and buried in plastic bottles. Each bottle was sampled by the IAEA inspectors; the samples

Table IV. Results of isotopic measurements for calutron pieces

Sample I.D.	$^{235}\text{U}$ abundance (wt %)	Remarks
Ion source 1	0.71	Natural U
Ion source 2	0.71	Natural U
Collector 1-1	0.76	Slightly enriched
Collector 1-2	5.82	Enriched
Collector 1-3	4.76	Enriched
Collector 1-4	0.39	Slightly depleted
Collector 1-5	6.84	Enriched
Collector 2-1	0.06	Highly depleted
Collector 2-2	5.94	Enriched
Collector 2-3	4.22	Enriched
Collector 2-4	0.79	Slightly enriched

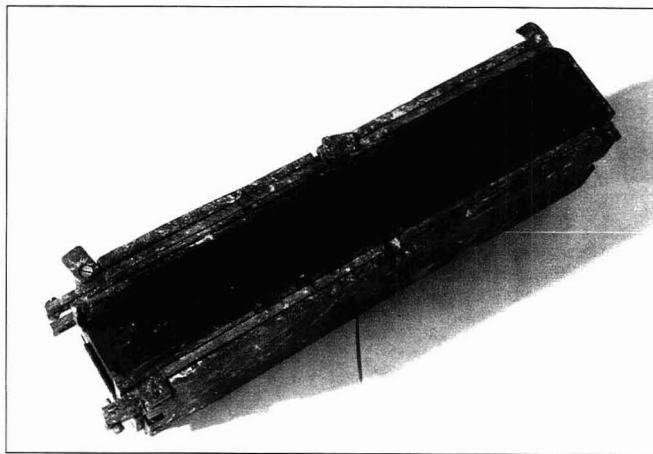


Figure 1. Ion source from electromagnetic isotope separator.

were analyzed at the SAL with thermal ionization MS to determine the isotopic composition and with isotope dilution MS to determine the uranium content (Table V).

The measured isotope information closely matches the declared information. Investigators combined the concentration data with the measured volumes of solution in the bottles to determine the total amount of material present.

**Evidence of plutonium production.** In 1991 Iraq declared that it had established a program for reprocessing spent fuel to recover Pu. This was carried out by dissolving one "exempted" spent-fuel assembly from the 10% enriched fuel for the Soviet IRT-5000 reactor, yielding

~ 2.26 g of Pu. It was subsequently discovered that the Iraqis also irradiated natural U fuel pins in the IRT-5000 reactor. This resulted in production of an additional 2.7 g of Pu.

IAEA inspectors sampled all of these plutonium-bearing materials and sent them to Seibersdorf for immediate analysis. By using the most rapid analytical method, high-resolution gamma ray spectrometry, a measurement of the Pu isotopic abundances (except for  $^{242}\text{Pu}$ ) and the  $^{241}\text{Am}$  content was obtained. From these data, it was possible to infer the most recent date of chemical processing of the samples, which gave an approximate timetable for the undeclared activities. Table VI

contains the isotopic data obtained in this manner. The  $^{239}\text{Pu}$  abundances and the estimated separation dates were used to confirm the irradiation and reprocessing activities that were eventually declared.

**Uranium recovery from phosphate ores.** A large fraction of uranium materials from the EMIS process came from domestic uranium mines at Al Jesira and Al Qaim. The amount of uranium obtained can be estimated from the weight of ore processed and the concentration of uranium in the ores. This information would represent the upper limit on the amount of indigenously produced uranium starting materials that were available for the EMIS process or other processes in Iraq. Relatively small differences (10–20%) in the uranium concentration in these ores could lead to differences of many tons in the total production.

Ore samples were brought back to Seibersdorf by the inspection teams; the U content was determined by gamma ray spectrometry and, after dissolution, by laser fluorometry, ICP-OES, and isotope dilution MS. The results for each ore sample obtained from the different techniques agreed within the uncertainty limits. Inspectors used these data to check the accuracy of the declared throughput of the uranium plant.

**Identification of construction materials.** Investigators collected a group of samples to determine the nature of certain industrial processes used in Iraq and their possible connection to clandestine nuclear activity. For example, it was suspected that several pieces of steel were being used to make gas centrifuge equipment for uranium enrichment. Special types of steel (maraging steel) are needed for making the rotors of gas centrifuges that must withstand very high stress (5). The types can be identified by their elemental compositions (18% Ni, 12% Co, and 4–5% Mo) and by their metallurgical properties. The samples received were small irregular pieces, each weighing ~ 5 g. They were analyzed by wavelength-dispersive XRF spectrometry, using a commercially available instrument. Three types of ordinary stainless steel were found, none of which was the special type used for centrifuge rotors.

XRF spectrometry was also used to investigate a heavy gray metal cylinder ~ 15 cm long and 2.5 cm in diameter that might have been part of development work relevant to nuclear weapons. Investigators determined

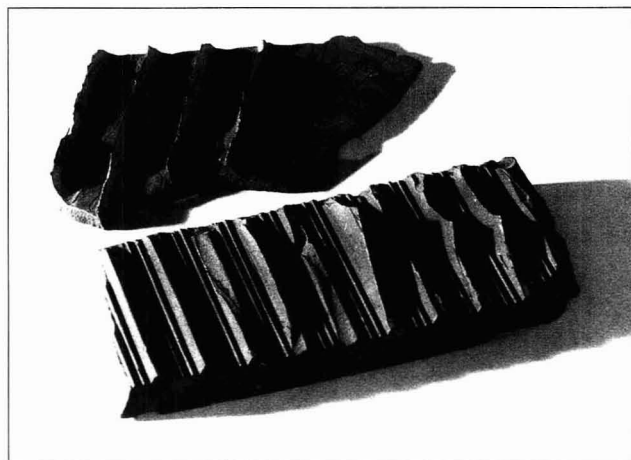


Figure 2. Graphite collector pieces from electromagnetic isotope separator.

Table V. Results of measuring uranium nitrate solutions

Sample	Declared $^{235}\text{U}$ (wt %)	Measured $^{235}\text{U}$ (wt %)	Measured U concentration (mg/g)
Tank 1-1	<0.1	0.088	0.781
Tank 1-2	<0.1	0.094	0.787
Tank 2-1	0.1–0.5	0.176	0.583
Tank 2-2	0.1–0.5	0.176	0.581
Tank 3-1	0.5–1.0	0.614	0.294
Tank 3-2	0.5–1.0	0.614	0.295
Tank 4-1	1–5	3.23	0.702
Tank 4-2	1–5	3.26	0.130
Tank 5-1	5–10	5.80	1.221
Tank 5-2	5–10	5.81	0.647
Tank 5-3	5–10	5.81	0.992
Tank 5-4	5–10	5.80	0.517
Tank 5-5	5–10	5.81	0.800

that the sample was 50% W, 20–25% Co, 1–2% Cu, and 1–2% Nb. There were obviously other components (primarily light elements) that could not be measured. These data, combined with the measured density of the sample (13.5 g/cm<sup>3</sup>), were consistent with the conclusion that this was a bar of sintered tungsten carbide with cobalt as the binder. Such materials are commonly used for making machine tools.

**Detection of <sup>210</sup>Po.** Documents returned by the sixth inspection team revealed that the Iraqis had been working on radioisotope neu-

tron generators for triggering a chain reaction in a nuclear explosive device. These neutron generators can be made with beryllium and the alpha particle-emitting isotope <sup>210</sup>Po. Therefore, the presence of <sup>210</sup>Po in samples would support evidence of the existence of this program and would possibly indicate where the work had been carried out.

One smear sample from a glove box that had been removed from Tuwaitha and buried in the desert showed unusually high alpha particle activity, according to contamination readings in the field. Smear

samples were taken and returned to Seibersdorf, where an alpha particle energy spectrum was taken, as shown in Figure 3. The dashed spectrum resulted from a control standard containing <sup>238</sup>Pu, <sup>239</sup>Pu, and <sup>240</sup>Pu, which was used to establish the calibration of the energy axis. The solid-line spectrum is that of the smear sample, which clearly shows a peak at 5.3 MeV, in agreement with the expected energy for alpha particles from <sup>210</sup>Po. Results from a government laboratory in a member state confirmed this interpretation.

**Measurement of water samples from fuel storage pits.** In addition to the investigation of nuclear activities, the Action Team was given the task of removing all highly enriched nuclear fuel—both fresh and irradiated—from Iraq. The fuel is present in several locations; it is in the reactor pool and the spent-fuel storage pool of the Soviet IRT-5000 reactor as well as in 14 pits in a storage location outside of Tuwaitha. Before arranging the transport of this fuel, it is of critical importance to know whether the fuel has corroded to the point of releasing fission products into the surrounding water. Samples of ~100 mL were taken from each location and brought back to Seibersdorf for analysis. The samples were screened for radioactivity with gamma ray spectrometry, followed by pH and conductivity measurements as well as trace element analysis by ICP-OES to look for evidence of corrosion of the cladding (aluminum and magnesium).

In all cases, radiation measurements were at or near background levels, and only small amounts of <sup>137</sup>Cs appeared in the suspended solid material. The pH and Mg and Al concentrations did not suggest any significant corrosion of the fuel cladding. These types of measurements will be continued to monitor the integrity of the spent fuel until it can be removed from Iraq.

## Conclusions

These examples demonstrate the range of analytical techniques used at Seibersdorf to evaluate samples brought back by the Action Team. The information derived from the analyses proved to be of critical importance in verifying the Iraqi declarations and planning follow-up activities. The value of the analytical results can also be measured by what was *not* found, namely convincing evidence of yet undeclared nuclear programs. In this respect, we

Table VI. Results of Pu isotopic analysis

Reprocessed fuel batch	<sup>239</sup> Pu abundance (wt %)	Pu content (g)	Estimated separation date
Exempted—1	87.38	0.565	2/89
Exempted—2	87.38	0.902	1/89
Exempted—3	87.38	0.100	2/89
Exempted—4	87.36	0.097	10/88
Natural—1	94.54	0.047	7/90
Natural—2	94.57	0.036	7/90
Natural—3	95.89	0.050	*
Natural—4	98.32	1.087	8/90
Natural—5	99.10	0.498	3/90
Natural—6	97.95	0.842	12/90

\*Note: <sup>241</sup>Am could not be measured because of the presence of fission products.

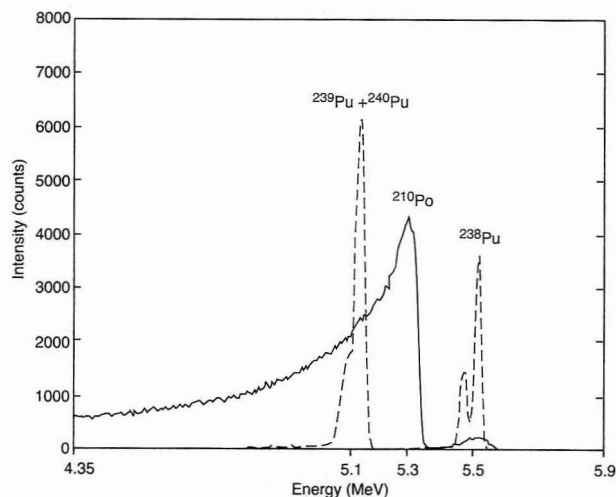


Figure 3. Alpha particle spectrum of smear sample (solid line) and Pu control standard (dashed line).

rely on the sensitivity and selectivity of the analytical methods for uranium, plutonium, and other important components of the samples.

This project taught us some valuable lessons. We learned that there must be prior consultation with analysts in planning the sampling effort. Here, the emphasis is on the choice of sampling and analysis methods that will give accurate data, free from interferences and blank effects.

Investigators must validate sampling methods, keeping in mind the requirements and potential problems associated with the techniques that will be applied. Also, analytical methods that give rapid, reliable results must be chosen. In critical instances, verification by independent methods should be employed.

Finally, inference methods that take into account the sources of random and systematic error inherent in the data should be applied to the results. In many cases, this analytical uncertainty can make the difference between a correct conclusion and a faulty one.

The IAEA was fortunate to have the proper analytical capabilities in place

so that it could rapidly mobilize in support of this unprecedented inspection effort. In the future, it will be necessary to build on the experience gained thus far and to strengthen the analytical expertise available to the IAEA to respond to changing needs.

The authors thank the staff of the Safeguards Analytical Laboratory; the Physics, Chemistry, and Instrumentation Laboratory; the director of the IAEA laboratories; and the staff of the IAEA Action Team for their indispensable contribution to this work.

**References**

- (1) *Handbook of Nuclear Safeguards Measurement Methods*; Rodgers, D. R., Ed.; U.S. Nuclear Regulatory Commission: Washington, DC, 1983; NUREG/CR-2078.
- (2) Salahis, A.; Grass, F.; Beuch, F.; Kaser, T.; Seidel, E.; Ott, S. *J. Trace Microprobe Tech.* **1988**, *6*, 229.
- (3) Ghods-Esphahani, A.; Veselsky, J. C.; Zepeda, E.; Peiris, M.A.R.K. *Radiochim. Acta* **1990**, *50*, 155.
- (4) LaRosa, J. J.; Coopar, E. L.; Ghods-Esphahani, A.; Jansta, V.; Makarewicz, M.; Shawky, S.; Vajda, N. *J. Environ. Radioact.* **1992**, *17*, 183.
- (5) Floreen, S. In *Metals Handbook Ninth Edition*; American Society for Metals: Metals Park, OH, 1978; Vol. 1, pp. 445-52.



*D. L. Donohue (left) is on his third assignment to the IAEA as head of the Isotopic Analysis Unit in the Safeguards Analytical Laboratory. He received B.S. and M.S. degrees in chemistry from the University of Virginia. In 1974 he joined the Analytical Chemistry Division of Oak Ridge National Laboratory. While at ORNL, he studied at the University of Tennessee, Knoxville, and graduated in 1979 with a Ph.D. in chemistry.*

*Rolf Zeisler is head of the Chemistry Unit in the Physics, Chemistry, and Instrumentation Laboratory of the IAEA laboratories in Seibersdorf, Austria. Previously he worked with the Nuclear Methods Group of the National Institute of Standards and Technology. He received his diploma in chemistry and his Ph.D. from the Technical University in Munich.*

**For Those Involved in the Vital Field  
of Surface and Colloid Chemistry**

# Langmuir

**The ACS Journal of Surfaces and Colloids**

Each month, *Langmuir* subscribers receive broad coverage that brings together research from all aspects of the field: ultra-high vacuum surface chemistry and spectroscopy, heterogeneous catalysis, and all aspects of interface chemistry involving fluids, and disperse systems.

- Langmuir publishes peer-reviewed research in:**
- \* "Wet" Surface Chemistry \* "UHV" Surface Chemistry
  - \* Disperse Systems \* Electrochemistry
  - \* Surface Structure; tunneling electron microscopy

**EDITOR**  
William A. Steele, The Pennsylvania State University

**ASSOCIATE EDITORS**  
A. Bradshaw, Max Planck Institute, Germany  
R.L. Rowell, University of Massachusetts  
J.T. Yates, Jr., University of Pittsburgh

1993 Rates	ACS Members* Nonmembers		
	1 year	2 years	1 year
U.S.	\$ 68	\$122	\$715
Canada & Mexico	\$ 89	\$164	\$736
Europe**	\$116	\$218	\$763
All Other Countries**	\$129	\$244	\$776

\* Member rate is for personal use only.  
\*\* Air service included. ISSN 0743-7465

**For more information or to subscribe, write:**  
American Chemical Society  
Member and Subscriber Services  
P.O. Box 3337  
Columbus, OH 43210

**In a hurry?**  
Call Toll Free (800)333-9511 (within the U.S.) or  
(614) 447-3776 (outside the U.S.) or Fax your order  
to (614)447-3671.



## INDEX TO ADVERTISERS IN THIS ISSUE

CIRCLE INQUIRY NO.	ADVERTISERS	PAGE NO.
10	<b>Bioanalytical Systems, Inc.</b> Kissinger Advertising Associates	340A
24	<b>EM Separations</b> Scientific Marketing Services, Inc.	IFC
50	<b>Leco Corporation</b> Lecom	OBC
60	<b>*Mattson Instruments, Inc.</b> Fourier Court Advertising	330A
64	<b>*Nicolet Analytical Instruments</b> Nicolet Advertising	336A
72, 73	<b>*Perkin-Elmer Corporation</b> Keiler Advertising	332A
70	<b>*PolyScience</b>	351A
80	<b>Sartorius Corporation</b> Dunlap, Schulze Associates	338A
82	<b>Stanford Research Systems</b>	334A
106	<b>Teledyne Hastings-Raydist</b> TRL Productions	355A
92, 93	<b>*Varian</b> Lanig Associates	342A, 352A
96	<b>Whatman</b>	329A
118	<b>*Wyatt Technology Corporation</b>	347A

Advertising Management for the American Chemical Society Publications

### CENTCOM, LTD.

*President*  
**James A. Byrne**  
*Executive Vice President*  
**Benjamin W. Jones**

**Joseph P. Stenza, Production Director**

1599 Post Road East  
P.O. Box 231  
Westport, Connecticut 06881-0231  
(Area Code 203) 256-8211  
Fax No. 203-256-8175

### DIRECTOR, ADVERTISING SALES, LABORATORY PRODUCTS

**Bruce E. Poorman**

### ADVERTISING PRODUCTION MANAGER

**Jane F. Gatenby**

### SALES REPRESENTATIVES

Philadelphia, PA . . . CENTCOM, LTD. GSB Building, Suite 405, 1 Belmont Ave., Bala Cynwyd, PA. 19004. Telephone: 215-667-9666, FAX: 215-667-9353

New York/New Jersey . . . Dean A. Baldwin, John F. Raftery, CENTCOM, LTD., Schoolhouse Plaza, 720 King Georges Post Road, Fords, NJ 08863, Telephone: 908-738-8200, FAX: 908-738-6128

Westport, CT/Boston, MA. . . Dean A. Baldwin, Michael J. Pak, CENTCOM, LTD., 1599 Post Road East, P.O. Box 231, Westport, CT 06881-0231. Telephone: 203-256-8211, FAX: 203-256-8175

Cleveland, OH. . . Bruce E. Poorman, Dean A. Baldwin, CENTCOM, LTD., 325 Front St., Suite 2, Berea, OH 44017. Telephone: 216-234-1333, FAX: 216-234-3425

Chicago, IL. . . Michael J. Pak, CENTCOM, LTD., 540 Frontage Rd., Northfield, IL. 60093. Telephone: 708-441-6383, FAX: 708-441-6382

Houston, TX/Atlanta, GA. . . Edward M. Black, CENTCOM, LTD., P.O. Box 820966, Houston, TX 77082-0966. Telephone: 713-493-1560, FAX: 713-493-6673

San Francisco, CA. . . Paul M. Butts, CENTCOM, LTD., Suite 808, 2672 Bayshore Parkway, Mountain View, CA 94043. Telephone: 415-969-4604, FAX: 415-969-2104

United Kingdom, Scandinavia and Europe (Except: Germany, Switzerland, Austria) . . . Malcolm Thiele, Technomedia Ltd., Wood Cottage, Shurlock Row, Reading RG10 0QE, Berkshire, England. Telephone: 0734-343302, FAX: 0734-343848

Germany, Switzerland, Austria . . . InterMedia Partners, GmbH, Deutscher Ring 40, 5600 Wuppertal 11, Germany. Telephone: (0202) 711091, FAX: (0202) 712431

Tokyo, Japan . . . Sumio Oka, International Media Representatives Ltd., 1-11-5-502, Tamazutsumi, Setagaya-ku, Tokyo 158 Japan. Telephone: 502-0656, Telex #22633, FAX: 5706-7349

Asia (Except Japan) . . . Bruce E. Poorman, CENTCOM, LTD., 325 Front St., Suite 2, Berea, OH 44017. Telephone: 216-234-1333, FAX: 216-234-3425

South America . . . Bruce E. Poorman, CENTCOM, LTD., 325 Front St., Suite 2, Berea, OH 44017. Telephone: 216-234-1333, FAX: 216-234-3425

\*See ad in ACS LabGuide.

**The American Chemical Society Presents  
A Four-Day, Hands-On Short Course  
Covering the Techniques and  
Instrumentation of . . .**

# Supercritical Fluid Fractionation/ Extraction/ Chromatography

Newly  
Revised . . .  
Completely  
Updated!

Monday - Thursday, May 10-13, 1993

Virginia Tech

Blacksburg, Virginia

## Seven Key Ways You'll Benefit From Attending This Course:

1. Learn to interpret SFF, SFC and SFE data
2. Discover why SFE offers distinct advantages over conventional extraction
3. Learn state-of-the-art techniques for performing SFF/SFE/SFC
4. Know which SFC and SFE strategies to use when your analyte will not dissolve in  $\text{CO}_2$
5. Gain hands-on experience working with chromatographs, column detectors, and extraction devices
6. Understand the limitations of SFF/SFE/SFC
7. Obtain guidelines for column selection

**Instructor:** Larry T. Taylor, Professor of Chemistry,  
Virginia Tech

To register or to obtain more information about this unique short course, call the Continuing Education Short Course Department at (800) 227-5558 (TOLL FREE) or (202) 872-4508. FAX (202) 872-6336. Or mail the coupon to: American Chemical Society, Dept. of Continuing Education, Meeting Code VPI93, 1155 Sixteenth Street, N.W., Washington, DC 20036.

Please send me a free brochure describing the ACS Short Course, *Supercritical Fluid Fractionation/Extraction/Chromatography*, to be held May 10-13, 1993 at Virginia Tech in Blacksburg, VA.

Name \_\_\_\_\_

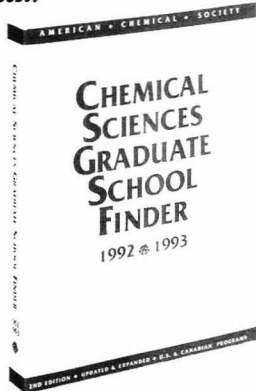
Title \_\_\_\_\_

Organization \_\_\_\_\_

Address \_\_\_\_\_

City, State, Zip \_\_\_\_\_

**Graduate School . . . where to go,  
what to study, how much does it  
cost?**



## Chemical Sciences Graduate School Finder 1992-1993

If these are the questions you're asking others, or just yourself, here is the book for you. This concise and easy-to-use guide provides undergraduate chemistry students with information necessary for selecting a graduate program to suit their needs and goals.

Includes listings from major educational institutions in the United States and Canada offering courses leading to a Master's or Ph.D degree in chemistry and allied fields. Provides information on the size and make-up of student population, admission and degree requirements, costs and financial aid, faculty members and their research specialties, and the institution's research facilities and equipment.

Also included is a section on how to apply to graduate school, a checklist of things to do, and perforated pages with preprinted postcards for requesting materials from graduate schools.

### Contents

- How To Use This Guide
- Planning for Graduate Work in Chemistry
- Alphabetical List of Schools
- Graduate School Listings
- Fields of Study Index
- Geographic Index

620 pages (1992) Paperbound

ISBN 0-8412-2522-2

\$44.95

ACS Student Affiliates \$17.00

O R D E R F O R M

American Chemical Society  
Distribution Office, Dept. 50  
1155 Sixteenth St., N.W.  
Washington, DC 20036

or CALL TOLL FREE

**800-227-5558**

(in Washington, D.C. 872-4363) and use your credit card!

# AC RESEARCH

## Fluorescence Detection and Size Measurement of Single DNA Molecules

Alonso Castro, Frederic R. Fairfield, and E. Brooks Shera\*

*Biophysics and Theoretical Biology Groups, Los Alamos National Laboratory, Los Alamos, New Mexico 87545*

We have developed a technique for the detection and size discrimination of single DNA molecules in a hydrodynamically focused flowing solution. Double-stranded  $\lambda$  DNA molecules at  $3 \times 10^{-15}$  M were stained with the fluorescent dye TOTO-1 and were individually detected. The technique makes use of a frequency-doubled mode-locked Nd:YAG laser to repetitively excite the molecules as they traverse the tightly focused laser beam. The flowing sample solution was hydrodynamically focused down to a 20- $\mu$ m-diameter stream by a rapidly flowing water sheath. The sheath flow technique is well suited for laser-induced fluorescence detection of small-volume, low-concentration samples. The emitted fluorescence photon burst originating from a single DNA molecule was detected with a microchannel plate photomultiplier based single-photon counter, which used time-gated electronics for Raman and Rayleigh scattering rejection. In addition, a mixture of  $\lambda$  DNA and smaller single-cut fragments has been simultaneously detected and identified by size. The advantages over other techniques for the detection and size determination of DNA fragments are discussed.

### INTRODUCTION

The detection and identification of minute amounts of nucleic acids is required in many fields, such as molecular biology, biotechnology, medical diagnostics, and forensic analysis. Radioactive labeling is the most widely used technique for the detection of trace amounts of DNA,<sup>1,2</sup> primarily because of its sensitivity, which extends down to the picogram range. However, the difficulties associated with the lifetime, handling, and disposal of radioactive reagents have created an interest in alternative detection strategies. Recently, for example, Rye et al.<sup>3</sup> have developed a method for the detection of DNA in agarose gels based on fluorescence emission. This method has a sensitivity of 4 pg per band, which approaches that of radiolabeling methods. Nevertheless, many applications require the detection of even smaller

samples of DNA. Currently, the polymerase chain reaction technique (PCR)<sup>4,5</sup> is widely used to amplify specific DNA sequences, making detection more feasible. Although PCR is a highly effective amplification mechanism, the use of many PCR cycles may introduce ambiguities arising from contamination and by mechanisms not yet fully understood.<sup>6-7</sup> It is for these reasons that it is important to develop more accurate, sensitive, and faster techniques for the detection of small amounts of DNA.

In this paper, we describe the use of our recently developed technique of single molecule detection<sup>8,9</sup> to efficiently detect single DNA molecules in a hydrodynamically focused flowing solution. The technique involves repetitive laser excitation of individual molecules, detection of the emitted fluorescence light with a microchannel plate photomultiplier based single-photon counter, time-gated electronics, and signal processing. The signature of the passage of individual molecules is a burst of photons that occurs as the molecule traverses the laser beam.

Since the fluorescence quantum yield of DNA is very small, we use a modified version of the staining technique used by Hirschfield<sup>10</sup> in his early observations of individual protein molecules. In the present experiments we stained the native DNA with the fluorescent dye TOTO-1<sup>11</sup> (a dimer of thiazole orange). TOTO-1, which intercalates between the DNA bases, has a binding affinity constant nearly 1000 times larger than that of the most widely used DNA intercalator, ethidium bromide.<sup>12</sup> Also, when bound to DNA, the TOTO-1-DNA complex fluorescence quantum yield increases by a factor of 1100 compared to that of free TOTO-1.<sup>3</sup> This makes it an excellent candidate for ultrasensitive detection of DNA molecules.

In the present experiments, we demonstrate the detection of full length duplex  $\lambda$  phage DNA molecules (48 502 base pairs). In addition, a mixture of  $\lambda$  DNA and smaller single-

\* Author to whom correspondence should be addressed at Mail Stop D434.

(1) Sambrook, J.; Fritsch, E. F.; Maniatis, T. *Molecular Cloning*, 2nd ed.; Cold Spring Harbor Laboratory Press: New York, 1989; pp 6.21, E.21.

(2) Maxam, A. M.; Gilbert, W. *Methods Enzymol.* 1980, 65, 499-559.

(3) Rye, H. S.; Yue, S.; Wenner, D. E.; Quesada, M. A.; Haugland, R. P.; Mathies, R. A.; Glazer, A. N. *Nucleic Acids Res.* 1992, 20, 2803-2812.

(4) Scharf, S. J.; Horn, G. T.; Erlich, H. A. *Science* 1986, 233, 1076-1078.

(5) Bej, A. K.; Mahbubani, M. H.; Atlas, R. M. *Crit. Rev. Biochem. Biophys.* 1991, 26, 301-334.

(6) Dunning, A. M.; Talmud, P.; Humphries, S. E. *Nucleic Acids Res.* 1988, 16, 10393.

(7) Kwoh, S.; Higuchi, R. *Nature* 1989, 339, 237.

(8) Shera, E. B.; Seitzinger, N. K.; Davies, L. M.; Keller, R. A.; Soper, S. A. *Chem. Phys. Lett.* 1990, 174, 553-557.

(9) Soper, S. A.; Davies, L. M.; Shera, E. B. *J. Opt. Soc. Am. B.* 1992, 9, 1761-1769.

(10) Hirschfield, T. *Appl. Opt.* 1976, 15, 2965-2966.

(11) Molecular Probes, Inc., Eugene, OR.

(12) Huang, Z., Molecular Probes, Inc., personal communication.

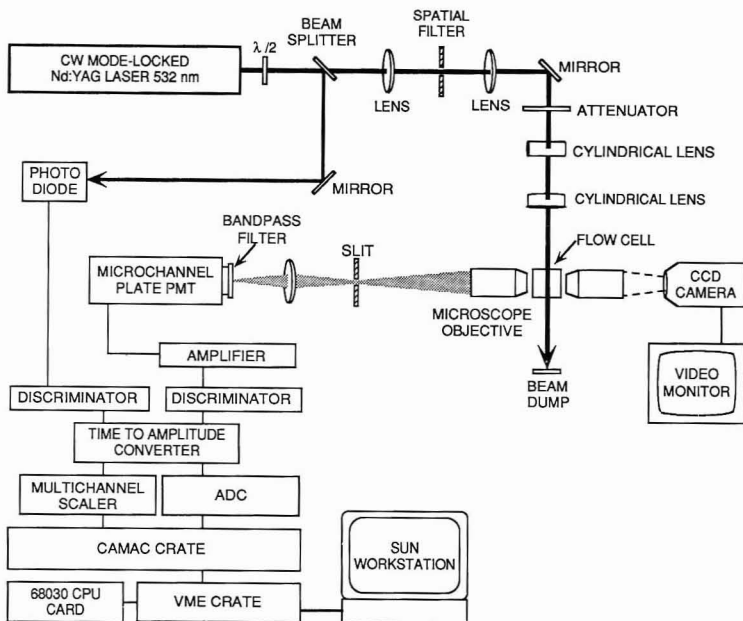


Figure 1. Schematic drawing of the experimental set-up.

cut fragments have been simultaneously detected and identified by size.

### EXPERIMENTAL SECTION

A schematic drawing of the apparatus we have used for the detection of single molecules is shown in Figure 1. A Spectra-Physics 3800 frequency-doubled mode-locked Nd:YAG laser producing 70-ps pulses at 532-nm wavelength and 82-MHz repetition rate was used as the excitation source. The laser output was directed through a variable neutral density filter which attenuated the laser intensity to 50–70 mW. The laser beam was focused into the sample cell by a pair of crossed cylindrical lenses to yield a  $500 \times 10\text{-}\mu\text{m}$  spot (horizontal and vertical  $1/e^2$  values, respectively). This arrangement provided uniform excitation along the entire cross section of the hydrodynamically focused sample stream (see below). The sheath flow cell was constructed from a glass square-bore capillary with inside dimensions of  $800 \times 800 \mu\text{m}$  (Figure 2). The sample was gravity fed through a  $100\text{-}\mu\text{m}$ -diameter stainless steel hypodermic needle into the square cell. A sheath of water was pumped by a Harvard Apparatus Model 22 syringe pump through a  $0.1\text{-}\mu\text{m}$  Millipore filter and into the square cell at about  $0.8 \text{ mL/h}$ . This rapidly flowing water sheath hydrodynamically focused the sample stream to a final diameter of  $20 \mu\text{m}$ . The combined use of a large horizontal beam dimension and a small stream diameter should permit homogeneous illumination of the sample, such that all molecules experience identical laser excitation intensities. This modification of the tightly focused Gaussian laser beam profile used in previous experiments<sup>8</sup> was required if meaningful fluorescence intensity measurements are to be made. The detection volume created by the intersection of the laser beam and the focused sample stream was  $3 \text{ pL}$ . The sheath flow technique<sup>13</sup> is well suited for laser-induced fluorescence of low-concentration samples because of the small probing volume produced, which provides low background fluorescence and uniform excitation of the sample. Fluorescent light was collected by a  $40\times 0.65 \text{ N.A.}$  microscope objective, spatially filtered by a

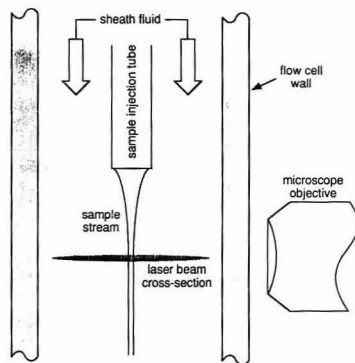
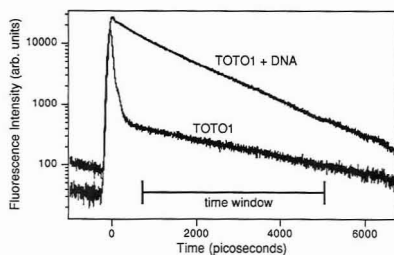


Figure 2. Cross section of the sheath flow cell (not to scale). The sheath liquid flows through a glass square-bore cell ( $0.8\text{-mm}$  i.d.) and hydrodynamically focuses the sample stream from the  $100\text{-}\mu\text{m}$ -i.d. injection tube down to  $20 \mu\text{m}$ . The laser beam travels perpendicular to the drawing plane.

$1.2 \times 0.4\text{-mm}$  rectangular slit, spectrally filtered by a  $555/30 \text{ nm}$  eight-cavity Omega Optics interference filter, and detected by a Hamamatsu R1562U microchannel-plate photomultiplier tube cooled to  $0^\circ\text{C}$ . The MCP-PMT signal was amplified by a Hewlett-Packard 8447F amplifier, shaped by a Tennelec TC454 discriminator and sent to the gate and stop inputs of a Tennelec TC863 time to amplitude converter (TAC). A fraction of the laser beam was split off by a beam splitter and sent to a fast photodiode to provide the start pulses for the TAC. A time-gate window was set such that both prompt Raman and Rayleigh scattering were rejected, and only delayed fluorescence photons were detected.<sup>8</sup> Events occurring during the time window were counted by a CAMAC Joergel S3 multichannel scaler. The CAMAC bus was interfaced via a CES Model CBD-8210 VME interface to a Sun workstation. The data stream from the scaler was stored on disk



**Figure 3.** Time-delay histograms for a  $2 \times 10^{-12}$  M solution of DNA-TOTO-1 complex in TE buffer (upper curve) and for a similar solution without DNA, i.e., TOTO-1 in TE buffer (lower curve). The position of the time-gate window used to reject Raman and Rayleigh scattering is shown.

for off-line analysis and was also analyzed in real-time using a VME-bus color monitor driven by the Sun computer. This display provides a chart-recorder-style graph of the photon bursts that occur as individual DNA molecules pass through the laser beam, thus facilitating rapid experimental optimization.

Determination of the sample stream flow velocity was accomplished in a separate measurement by observation of 1- $\mu$ m fluorescent microspheres as they flowed through the detection volume. A microscope objective imaged the detection volume into a CCD video camera whose output was recorded and analyzed frame-by-frame. The linear flow velocity was determined in this way to be 700  $\mu$ m/s, which corresponds to a transit time through the laser beam of about 20 ms. A similar procedure was employed to determine the sample stream diameter, which was considered to be the same for microspheres and DNA, since the effects of diffusion are negligible in both cases under our experimental conditions.

$\lambda$  DNA (full-length and *Xba* I digest) and TOTO-1 were purchased from New England Biolabs (Massachusetts) and Molecular Probes (Eugene, OR), respectively. Sample solutions were prepared by diluting the  $\lambda$  DNA in TE buffer (10 mM Tris, 1 mM EDTA, pH 8.0) to the desired concentration. TOTO-1 was added to yield a final base pair to dye ratio of 5:1. Water was deionized and doubly distilled prior to use, and all solutions were prepared immediately before each experiment.

## RESULTS

**(a) Time-Gate Optimization and Estimation of the  $\lambda$  DNA-TOTO-1 Complex Fluorescence Lifetime.** In order to determine the position of the time-gate window for best rejection of Raman and Rayleigh scattering, a time-delay histogram of the TAC output was accumulated for a  $2 \times 10^{-12}$  M  $\lambda$  DNA solution in TE buffer to which TOTO-1 was added at a base pair to dye ratio of 5:1. The results of this measurement are depicted in Figure 3, where the position of the selected time-gate window is shown. The fluorescence lifetime was determined to be approximately 1.7 ns. Also shown in Figure 3 is the time-delay histogram for a TOTO-1 solution in TE buffer at the same concentration, but without  $\lambda$  DNA (the prompt peak due to Raman and Rayleigh scattering is clearly evident). A comparison of the two curves indicates the large enhancement in TOTO-1 fluorescence upon intercalation into DNA.

**(b) Detection of Single Full-Length  $\lambda$  DNA Molecules.** To demonstrate the detection of individual DNA molecules, we used a flowing sample consisting of  $3 \times 10^{-15}$  M  $\lambda$  DNA molecules (48 kbp) stained with TOTO-1 at a base pair to dye ratio of 5:1 in TE buffer. At this concentration, the probability of a DNA molecule occupying the detection volume is 0.004. The probability of two molecules occupying the detection volume at the same time is then  $1.6 \times 10^{-5}$ . Thus, the detection of two or more DNA molecules at the same time is unlikely. The results of the experiment are shown in Figure 4. Each

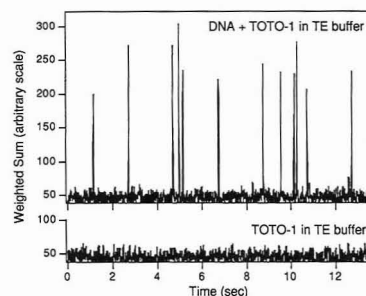


**Figure 4.** Weighted sum plots for a  $3 \times 10^{-15}$  M solution of DNA-TOTO-1 complex in TE buffer (top) and for a similar solution without DNA, i.e., TOTO-1 in TE buffer (bottom).

observed peak is the integrated photon burst emitted by an individual DNA molecule as it traverses the laser beam. An average of 400 photons per  $\lambda$  DNA molecule were obtained. The total number of detected molecules,  $N$ , for the 819.2-s data stream was 346. This quantity is in agreement with the estimated value of 326, as calculated by the equation

$$N = c\sigma vT$$

where  $c$  is the concentration,  $\sigma$  is the sample stream cross-sectional area,  $v$  is the stream flow velocity, and  $T$  is the duration of the experiment. The comparison of the observed and computed number of DNA molecules indicates that the detection efficiency is 100% within our estimated experimental error.

For better visualization of the photon bursts, the data stream was subjected to a weighted sum algorithm given by

$$S(t) = \sum_{\tau=0}^{k-1} w(\tau) d(t + \tau)$$

where  $k$  covers a time interval of the order of the molecular passage time,  $d(t + \tau)$  is the data point at time  $t + \tau$ , and  $w(\tau)$  are weights that resemble the photon burst shape (a double-sided symmetrical ramp was used in the present case). The experiments were also performed under identical conditions with a similar sample solution except that DNA was not added, i.e., TOTO-1 in TE buffer at the same concentration. The resulting data stream is shown at the bottom of Figure 4. No photon bursts were detected in this case.

**(c) Simultaneous Detection of  $\lambda$  DNA and  $\lambda$  *Xba* I Digest.** In a second series of experiments, a mixture of  $\lambda$  DNA (48 kbp) and  $\lambda$  DNA *Xba* I digest was used. The *Xba* I digest of  $\lambda$  DNA yields two fragments of about 24 kbp each. The concentration of the mixture components was adjusted to obtain a 1:1 ratio of large (48 kbp) to small (24 kbp) fragments at  $3 \times 10^{-15}$  M each. Since the amount of intercalated dye is proportional to the DNA size,<sup>3</sup> one would expect to observe fluorescent molecules of two different brightnesses corresponding to the two DNA fragment sizes. This is indeed the case, as shown by the histogram plot of the number of peaks vs peak amplitude in Figure 5. The distribution centered at about 150 intensity units corresponds to 24 kb DNA pieces, and the one centered at 300 corresponds to 48 kb DNA pieces, yielding the expected 2:1 intensity ratio. Thus, we have been able to quantify the detection of DNA molecules of different sizes with a resolution of 12–15%, as determined by the widths of the histograms in Figure 5. Once again, the number of detected molecules was in agreement with the calculated value: 651 vs 640, respectively.

We believe that the size resolution in the present measurements is limited primarily by two factors: (1) statistical

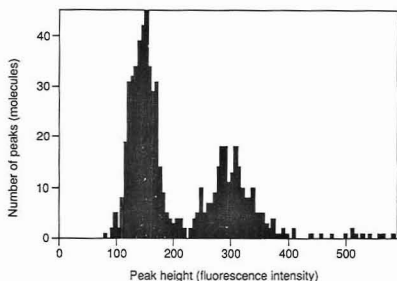


**Figure 5.** Histogram of the number of molecules vs fluorescence intensity for a mixture of  $\lambda$  DNA (48 kbp) and  $\lambda$  DNA *Xba* digest (24 kbp) at  $3 \times 10^{-15}$  M each.

fluctuations in the number of photons detected from individual molecules (shot noise) and (2) lack of uniformity of laser illumination across the sample stream caused by imperfections in the glass capillary and by diffraction effects.

### DISCUSSION

The present results suggest techniques that may be useful in developing biotechnological, clinical, and forensic methods that do not require extensive DNA amplification using PCR or other methods. As mentioned, the sensitivity limit for fluorescence detection of DNA in agarose gels is of the order of  $4 \times 10^{-12}$  g/band.<sup>5</sup> A similar sensitivity can be achieved with radioactive labeling methods. In the present case, the detection and size identification of a single 24 kbp DNA

fragment translates into a sensitivity limit of  $3 \times 10^{-17}$  g. However, the size resolution of gel electrophoresis can be only a few percent or less, depending on the fragment sizes being separated, and may be as small as 0.2% for sequencing gels, whereas our technique has a current size resolution of 12–15%. Nevertheless, in many cases, only a few DNA lengths may be present in a sample, and high resolution is not required. We are currently working to improve the resolution of our technique to differentiate among DNA fragments which differ in size by a few percent.

For comparison, another technique which uses fluorescence emission for the detection of DNA is flow cytometry. Determination of the DNA content of a single *Escherichia coli* bacteria has been reported using this technique.<sup>14</sup> However, the DNA content of the *E. coli* genome is about  $4 \times 10^6$  base pairs, more than 100 times greater than that of the single fragments detected in the present experiments.

The sensitive detection of other individual biological molecules has important applications. Our current single fluorophore detection limit allows us to study solutions of concentrations in the sub-femtomolar range. Potential applications include the detection and measurement of low levels of pollutants or toxins, and the study of hormones directly at their biologically active levels of  $10^{-12}$  M and below. Currently, these concentrations are only detectable through indirect biological means.

### ACKNOWLEDGMENT

The authors would like to thank Lloyd Davis, Carol Harger, and Steven Soper for helpful discussions and Mark Peters for technical assistance.

RECEIVED for review November 10, 1992. Accepted January 2, 1993.

(14) Steen, H. B. In *Flow cytometry and sorting*, 2nd ed.; Melamed, R. M., Lindmo, T., Mendelsohn, M., Eds.; Wiley-Liss: New York, 1990; Chapter 29.



# Fiber Optic pH Sensor Based on Phase Fluorescence Lifetimes

Richard B. Thompson\* and Joseph R. Lakowicz

Center for Fluorescence Spectroscopy and Department of Biological Chemistry, School of Medicine, University of Maryland, 108 North Greene Street, Baltimore, Maryland 21201

**A fiber optic pH sensor based on single fiber phase fluorescence lifetime measurements of commercially available fluorescence indicators is described. The apparatus is a straightforward modification of an existing phase fluorometer and exhibits accuracy and precision of approximately 0.02 pH unit. The approach is applicable to other analytes and indicators, as well as evanescent wave sensing schemes.**

## INTRODUCTION

Fiber optic chemical sensors represent an emerging technology likely to have important applications in clinical diagnosis, pollution monitoring, oceanography, chemical process monitoring, and other fields.<sup>1-4</sup> Fiber optic sensors offer the capability of continuous determination of chemical analytes in remote, inaccessible, hazardous, or in vivo environments. Many different analytes have been determined or quantitated using fiber optic sensors, including ions, small molecules, and macromolecules. While some chemical sensors based on absorbance and other phenomena have been described,<sup>5,6</sup> most fiber optic sensors are based on photoluminescence effects, especially fluorescence.<sup>7</sup> The sine qua non of fluorescence-based sensors is transducing the presence or concentration of the analyte as a change in fluorescence observable through a length of optical fiber. While performing fluorometry through optical fibers is not trivial,<sup>8,9</sup> much of the effort in the field is directed at achieving desirable levels of sensitivity, selectivity, dynamic range, and accuracy through development of the transducing mechanism.

Among the fluorescence-based sensors, most have relied upon monitoring a change in fluorescence intensity at a single wavelength which is correlated with the presence and amount of the analyte. While the virtues of fluorescence in analytical chemistry are well-known, the drawbacks of intensity measurements are also well-known, including the susceptibility to photobleaching and quenching, variation in probe concentration, inner filter effects, scattering, source level variations, susceptibility to temperature variations, and the presence of interfering fluorescent materials and Raman scatter. Some of these problems are straightforward to address, but others cannot be alleviated for many applications. Recognizing this, many workers have employed fluorescent

techniques wherein the presence of the analyte causes a wavelength shift in the excitation or emission, permitting the amount of analyte to be correlated with the ratio of fluorescence intensities at two wavelengths. These ratiometric techniques are relatively insensitive to photobleaching or the fluorophore amount, source intensity fluctuations, quenching, and influences such as temperature; they are also easier to calibrate. Among the analytes determined in this way are pH,<sup>10</sup> Ca<sup>2+</sup>,<sup>11</sup> Mg<sup>2+</sup>, and inhalation anesthetics.<sup>12</sup> Unfortunately, this approach is not immune to inner filter effects or fluorescent interferents, and it is evidently difficult to design fluorescent indicators that have the requisite selectivity for and sensitivity to a particular analyte and also exhibit a suitable shift in fluorescence excitation or emission. It is particularly difficult to envision such indicators for analytes other than atoms or small molecules.

Recently, Lakowicz,<sup>13</sup> Wolfbeis,<sup>14</sup> and others<sup>7</sup> have shown that the presence or level of an analyte can be correlated with a change in fluorescence lifetime of a suitable indicator and that this approach has some important advantages over analytical methods based on fluorescence intensity changes. Among these advantages are insensitivity to excitation source fluctuations, scattering or absorption of excitation or emission, variation in fluorophore levels due to washout or photobleaching, facile calibration, and reduced susceptibility to fluorescent interferents and influences such as temperature. Lakowicz and Szmajcinski<sup>15</sup> also demonstrated an important advantage of the lifetime approach, namely a broad dynamic range. Of course, an ordinary pH indicator operating under the law of mass action will exhibit 10-90% of its total response (absorbance or fluorescence intensity) over a range of 100-fold in concentration, and the total dynamic range cannot be more than about 3 orders of magnitude or so because greater absorbance or fluorescence measurement precision is difficult to achieve in practice. By judicious selection of excitation and emission wavelengths to favor particular forms of the indicator, Lakowicz and Szmajcinski showed that a single indicator (not exhibiting multiple equilibria), such as carboxy-SNARF-6, could measure pH over a range from pH 5.5 to 10. This property is of particular interest when an indicator cannot be synthesized with precisely the desired equilibrium constant. Moreover, it seems likely that the design of indicators exhibiting lifetime changes in the presence of the analyte may be easier than for those exhibiting wavelength shifts. Finally, instrumentation for the measurement of fluorescence lifetimes has become simpler and cheaper, due to advances in laser, electronics, and computer technology.<sup>13,16-19</sup> For all these reasons, fluorescence lifetime-based chemical analysis is likely to grow.

\* To whom correspondence should be addressed.

(1) Wolfbeis, O. S. Ed. *Biosensors* CRC Press: Boca Raton, FL, 1991; 3 Vols.

(2) Wise, D., Wingard, L., Eds. *Biosensors with Fiber Optics*; Humana Press: Clifton, NJ, 1991.

(3) Seitz, W. R. *Anal. Chem.* 1984, 56, 16A-34A.

(4) Wolfbeis, O. S., Ed. *Proc. SPIE—Int. Soc. Opt. Eng.* 1991, 1510, 42 pp.

(5) Villarruel, C. A.; Dominguez, D. D.; Dandridge, A. *Proc. SPIE—Int. Soc. Opt. Eng.* 1987, 798, 225-9.

(6) Butler, M. A. *Appl. Phys. Lett.* 1984, 45, 1007-9.

(7) Thompson, R. B. In *Topics in Fluorescence Spectroscopy Vol. II: Biochemical Applications*; Lakowicz, J. R., Ed.; Plenum Press: New York, 1991; pp 345-65.

(8) Thompson, R. B.; Levine, M.; Kondracki, L. *Appl. Spectrosc.* 1990, 44, 117-22.

(9) Bright, F. V.; Monnig, C. A.; Hietje, G. M. *Anal. Chem.* 1986, 58, 3139-44.

(10) Zhujun, Z.; Seitz, W. R. *Anal. Chim. Acta* 1984, 160, 47-54.

(11) Tsieng, R. Y. *Methods Enzymol.* 1989, 172, 230-41.

(12) Yager, P. Y.; Thompson, R. B.; Merlo, S. U.S. Pat. No. 5,094,819, 1992.

(13) Lakowicz, J. R. *Laser Focus World* 1992, 28 (5), 60-80.

(14) Lippitsch, M. E.; Pusterhofer, J.; Leiner, M. J. P.; Wolfbeis, O. S. *Anal. Chim. Acta* 1988, 205, 1-6.

(15) Lakowicz, J. R.; Szmajcinski, H. Submitted for publication to *Anal. Chem.*

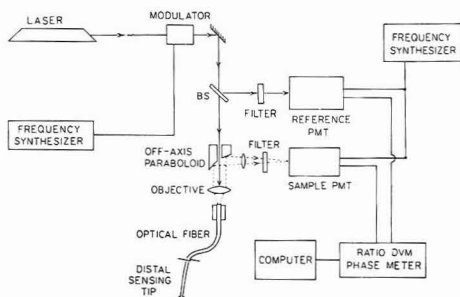


**Figure 1.** Apparatus for measuring phase fluorescence lifetimes through a single optical fiber. The cuvette holder in a commercial phase fluorometer is replaced by the off-axis paraboloid, objective, and fiber holder as described in the text.

From the point of view of optical fiber sensors, lifetime-based sensing offers additional advantages. First, due to microbending, mode transformation, and passage through slip rings, the apparent fluorescence intensities measured through multimode optical fibers can fluctuate, even if other factors such as source intensity are held constant. These problems are reduced or absent for single mode fibers, but such fibers are difficult to use for routine fluorescence sensing. For remote sensing applications such as in oceanography, ease of calibration of the lifetime approach is a decisive advantage; we note that wavelength ratiometric approaches require distance-dependent calibration in most fibers due to the steep wavelength dependence of fiber transmission with length. Hietje and Bright<sup>9</sup> and later Bright<sup>24</sup> described fiber optic phase fluorometers which differ somewhat from the apparatus described in Figure 1. In particular, they used much more powerful laser sources in a two-fiber configuration, and measured fluorescence lifetimes of several compounds. The two-fiber configuration, where excitation and emission are conducted through different fibers, has some drawbacks<sup>7</sup> including unsuitability for evanescent wave excitation, the difficulty of constructing the sensing tip, occasional problems with getting good registration between the portion of sample illuminated and the fluorescence collected, and the additional complexity and cost of the second fiber. While they did not use their devices for sensing per se, the data in Bright<sup>24</sup> are comparable to ours. Apart from the drawbacks of the two-fiber approach, the apparatus of Bright should be satisfactory for lifetime-based sensing.

For these reasons we chose to adapt our existing fiber optic sensor design<sup>8,20</sup> to the measurement of fluorescence lifetimes using the frequency domain technique and apply this apparatus to the measurement of pH as an example. We note that this approach is not only feasible with pH but other chemical analytes as well.

#### EXPERIMENTAL SECTION

**Apparatus.** The fiber optic phase fluorometer is a modification of our existing design,<sup>8,20</sup> adapted for use with a commercial

(16) Imasaka, T.; Ishibashi, N. *Anal. Chem.* 1990, 62 (3), 363A-71A.  
(17) Thompson, R. B.; Frisoli, J. S.; Lakowicz, J. R. *Anal. Chem.* 1992, 64, 2075-2078.

(18) Feddersen, B.; Piston, D.; Gratton, E. *Rev. Sci. Instrum.* 1989, 60, 2929-36.

(19) Lakowicz, J. R., Ed. *Topics in Fluorescence Spectroscopy*; Plenum Press: New York, 1991; 3 Vols.

(20) Golden, J. P.; Shriver-Lake, L. C.; Anderson, G. P.; Thompson, R. B.; Ligler, F. S. *Opt. Eng.* 1992, 31, 1458-1462.

(21) Thompson, R. B.; Gratton, E. *Anal. Chem.* 1988, 60, 670-4.

(22) Berlow, R., Ed. *Merck Manual of Diagnosis and Therapy*, 13th ed.; Merck, Sharp, and Dohme: Rahway, NJ, 1977; Chapter 24.

(23) Wait, D. R. *Deep Sea Res.*, in press.

(24) Bright, F. V. *Proc. SPIE-Int. Soc. Opt. Eng.* 1988, 909, 23-8.

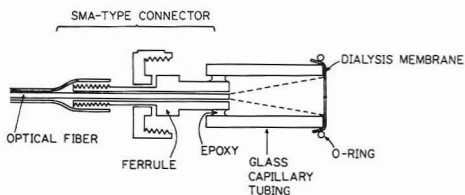


**Figure 2.** Distal sensing tip schematic. Glass capillary tubing is epoxied to an SMA connector attached to the distal end of the fiber. The dialysis membrane is secured by the O-ring, forming a small chamber that contains the c-SNAFL-2 dextran conjugate.

phase fluorometer (ISS K2, Champaign, IL); the apparatus is depicted schematically in Figure 1. The turret is removed from the sample chamber and replaced with a 6- × 6-in. breadboard, on which are mounted an off-axis parabolic mirror (Janos A8037-105), with a 0.062-in. hole along its mechanical axis, and a precision fiber positioner (Newport-Klinger FP-1015), with its microscope objective replaced with a 25-mm *f*/1 synthetic fused-silica lens (Newport-Klinger SBX-019); both positioner and mirror are conveniently mounted on small three-axis translators. The optical fiber (General Fiber Optics Catalog No. 16-200S 200- $\mu$ m core plastic clad silica, 2-5 m long) is held in the positioner with a fiber holder, a glass capillary tube, or an SMA 905 connector (Amphenol). In addition, the emission polarizer holder was removed and replaced with a 75-mm focal length fused-silica lens (Newport-Klinger SBX 025) to focus the fluorescence emission on the PMT photocathode. Excitation was provided by a Liconix 4214NB helium cadmium laser (442 nm, 10 mW cw) or an Ion Laser Technology 5000 Series air-cooled argon ion laser (50 mW all lines). For alignment purposes it was convenient to launch a HeNe laser beam back down the fiber into the fluorescence collection optics. Excitation intensity was enhanced by insertion and adjustment of a  $1/4$  wave plate (Karl Lambrecht, Chicago, IL) in the laser beam prior to its passage through the beam-splitting polarizer.

For some experiments the fluorescent indicators were dissolved in solution at low micromolar concentrations and the distal end of the fiber was dipped therein. For sensing applications the indicator was immobilized at the distal end by covalent attachment to 70 000 molecular weight dextran and confined in a chamber adapted from an SMA 905 connector (Figure 2) or a Zeppzauer tube. Dialysis tubing stretched over the end permits passage of ions while retaining the indicator.

**Reagents.** Resorufin (sodium salt), carboxy-SNAFL-2, and SNAFL-2 dextran were products of Molecular Probes, and Rose Bengal was from Aldrich; all were used without further purification. Water was distilled and passed through a Milli-Q water purification system; buffer salts were analytical reagent grade and were used without further purification.

#### RESULTS AND DISCUSSION

We decided to compare the precision and relative accuracy of the fiber optic phase fluorometer depicted in Figure 1 to those routinely achieved with non fiber optic instrumentation in order to determine if the approach was feasible and to form some estimate of the accuracy and precision by which analytes such as pH might be determined by this method. We took the results in ref 15 as being perfectly accurate with regard to what phase angle, demodulation ratio, or complete frequency response of a given indicator corresponds to a particular pH. Our goal is to assess any *additional* error introduced by the use of an optical fiber in the measurements. Our assessment of accuracy is therefore based on the closeness of our results to those in ref 15 and on the  $\chi^2$  for fits to complete frequency responses. The  $\chi^2$  is an indicator of accuracy because in this case, where we have a good understanding of the form of the data (the model) and an independent measure of the precision of the data from the standard deviations of the measurements at each frequency,

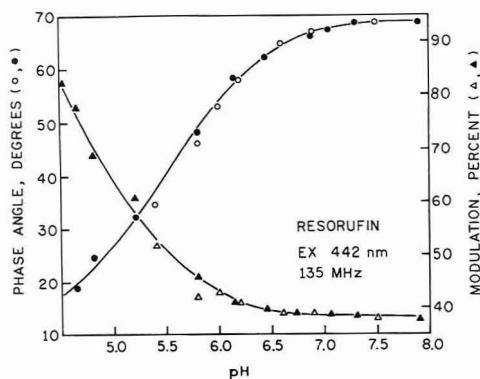


**Figure 3.** pH-dependent phase shifts (circles) and demodulation factors (triangles) measured for resorufin in a cuvette (filled symbols) and through an optical fiber (open symbols). The cuvette data are from ref 15.

the  $\chi_R^2$  cannot be low for an inaccurate result. Thus we measured the phase shift and demodulation of resorufin in 0.1 M citrate-phosphate buffer solutions at various pH's using resorufin at pH 7.5 as a standard and compared them with the results of Lakowicz and Szmazcinski,<sup>15</sup> as depicted in Figure 3. The conditions of excitation (442 nm), modulation frequency (135 MHz), and emission filtration (Corning 3-76) match those of Lakowicz and Szmazcinski, except that an additional 2-mm path length fused-silica liquid filter containing 1% potassium dichromate in water was inserted in the detection optical train between the 3-76 filter and the off-axis paraboloid to prevent photoluminescence being excited in the 3-76 by stray laser light;<sup>8</sup> we do not anticipate that this affected the results much, as the liquid filter does not absorb appreciably at the wavelengths of resorufin emission. For the samples at lower pH the detector gain and/or the amount of the resorufin indicator in the sample were increased to obtain adequate intensity; a virtue of this method is that these factors do not affect the results much,<sup>13</sup> as can also be seen in Figure 3.

It is evident from Figure 3 that the apparent phase angles and demodulation factors are very similar to those measured previously by Lakowicz and Szmazcinski,<sup>15</sup> and thus it is quite feasible to measure pH through an optical fiber by this method. The low fluorescence intensity and quantum yield of resorufin at low pH prevented acquisition of data in this case at pH's below 5.4. We note that the modulated laser power launched in the fiber was less than 0.5 mW and that more powerful excitation should increase the fluorescence intensity and permit measurements at lower pH using resorufin. Note that using much higher laser power or high peak powers with a small fiber core can result in damage to the core or nonlinear effects. Apparently, the data obtained through the optical fiber are not much less accurate than those observed in a cuvette, and their precision as indicated by the standard deviations of the individual measurements is less good, but comparable. The average standard deviations of the phase and modulation data in Figure 3 measured through an optical fiber (three repetitions each of sample and reference) are 0.351° and 0.007, respectively, which are about 2-fold larger than the values typically seen in this laboratory, when samples are measured in cuvettes, and used in calculating  $\chi_R^2$ . Much of this difference can be attributed to the low fluorescence intensity due to modest excitation power and to the inefficiency of optical fibers for collecting emission.

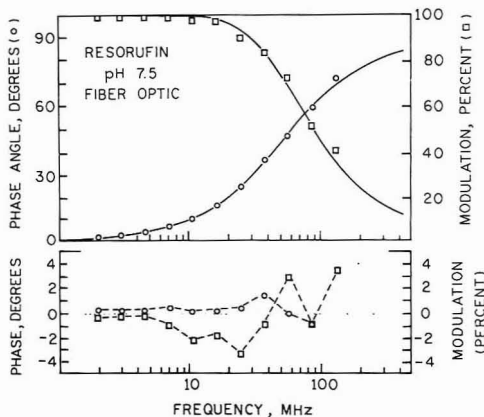


**Figure 4.** Frequency-dependent phase shifts (circles) and demodulation ratios (squares) measured through 2 m of optical fiber for resorufin in 0.1 M potassium phosphate buffer pH 7.5 versus Rose Bengal as a standard.

As an independent measure of the accuracy of the method, and its utility at frequencies other than 135 MHz, we measured the frequency-dependent phase shifts and demodulation ratios of resorufin in 0.1 M sodium, potassium phosphate pH 7.5 buffer using Rose Bengal as a reference<sup>21</sup> and used these data to determine its fluorescence lifetime in the usual manner. The best fit value for the results shown in Figure 4 was a single component of  $3.36 \pm 0.11$  ns, in good agreement with the results of Lakowicz and Szmazcinski<sup>15</sup> (2.96 ns), which were obtained in 80 mM Tris-HCl buffer at pH 7.3. The accuracy of the individual phase and modulation measurements can be deduced from the resulting value of  $\chi_R^2$  when the average standard deviations of the phase and modulation measurements (0.351° and 0.7%, respectively) are employed in the calculation. The resulting  $\chi_R^2$  is 9.9, indicating that the measurements are reasonably accurate.

Our results indicate that rather accurate and precise pH measurements can be made with this apparatus. In the case of resorufin, in the pH range roughly from 5 to 6, where the phase angle varies approximately linearly with pH, a change of 1.0 pH units corresponds to a phase of 27° (Figure 3) or 0.037 pH unit/deg. Thus if we ordinarily obtain accuracy and precision in our phase measurements of 0.35°, we can expect pH measurements accurate to 0.015 pH unit. For some applications, such as blood pH monitoring<sup>22</sup> or microbial cell growth monitoring, this accuracy is adequate, but for other applications, such as monitoring oceanic CO<sub>2</sub>, it is not.<sup>23</sup> Resorufin represents a favorable case in that it exhibits a very large lifetime (and thus phase) difference between the protonated and unprotonated forms, whereas other probes are not so good; of course, the phase difference cannot be greater than 90°. However, the precision of these measurements might be very much improved in a phase fluorometer optimized for operation at a single frequency, rather than the more flexible, broad-band commercial phase fluorometer used in these experiments. Note also that given the ability to vary the wavelengths of excitation and emission for a particular probe, the optimum response can be achieved.<sup>15</sup>

Comparable results were obtained for the pH indicator carboxy-SNAFL-2 in solution using an argon ion laser for excitation, using a different excitation wavelength (514 nm) than those of Lakowicz and Szmazcinski (543 and 563 nm). In particular, Figure 5 depicts phase angles and demodulations measured through the optical fiber using the apparatus depicted in Figure 1 and in a cuvette. The slight systematic

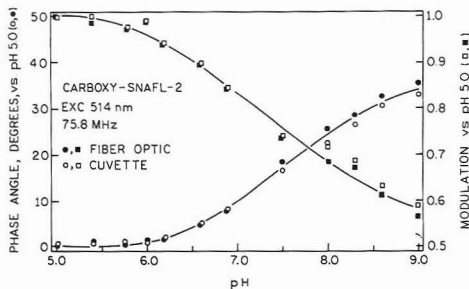


**Figure 5.** pH-dependent phase shifts (circles) and demodulation ratios (squares) measured for carboxy-SNAFL-2 in a cuvette (open symbols) and for carboxy-SNAFL-2 conjugated to dextran through an optical fiber (filled symbols).

error apparent at high pH suggests that some slight aging of the samples may have occurred over a 1-month period, but otherwise they appear to be quite robust. In many cases it is impractical to add a fluorescent indicator such as resorufin or carboxy-SNAFL-2 to a sample whose pH is to be determined. In these cases it is preferable to immobilize an indicator at the distal end of the fiber. In this instance we chose to encapsulate carboxy-SNAFL-2 as a conjugate to 70 000 molecular weight dextran in the distal cuvette chamber depicted in Figure 2. Dialysis tubing secured over the end served to prevent leakage of the SNAFL-dextran, while permitting the passage of protons. In addition to being convenient, the isolation of the indicator from some fluorescent interferers which may be present in solution is also an advantage.<sup>2</sup> The rapidity of response of pH probes is of importance in many applications, and therefore the kinetics of the phase shift of carboxy-SNAFL-2 immobilized in the distal cuvette-type probe in Figure 2 were measured as the pH was abruptly varied. The results of such an experiment are depicted in Figure 6. Under these conditions of rapid mixing, the estimated time for mixing is 10–15 s, which is somewhat more than the instrumental time constant of the ISS phase fluorometer. The drift in phase angle was about 1 deg in a period of 2 h. In the experiment depicted in Figure 6, a time constant of over 2 h is observed. This is overtly slow for nearly all applications, and clearly the slow response can be attributed to slow diffusion through the dialysis tubing and mixing within the distal cuvette chamber. Since some miniature electrochemical pH probes exhibit time constants of less than 30 s, it is evident that the fiber optic sensor time constant could also be improved by miniaturization of the sensing tip and substitution of a different membrane or by covalently attaching the fluorescent indicator to the distal end of the fiber.

In these experiments, the results are unaffected by demodulation of the excitation due to modal or material dispersion due to the short length (2–5 m) of fiber employed.<sup>7</sup>

(25) Berndt, K. W.; Gryczynski, I.; Lakowicz, J. R. *Rev. Sci. Instrum.* 1990, 61, 1816–20.

(26) Patonay, G.; Antoine, M. D. *Anal. Chem.* 1991, 63, 321A–7A.

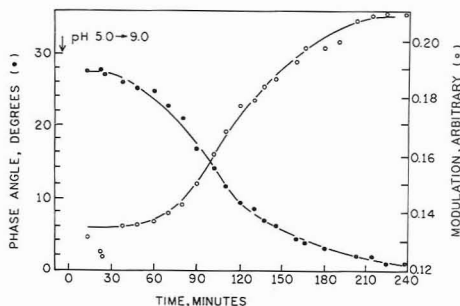


**Figure 6.** Time response of fiber optic sensor. The sensing tip depicted in Figure 2 is switched from a pH 5.0 buffer solution to a pH 9.0 buffer solution at time  $T = 0$ , and the phase angle (filled circles) and modulation (open circles) was monitored at intervals.

The plastic clad silica fiber employed here has a bandwidth of approximately 15–20 MHz km and an estimated material dispersion of several hundred picoseconds per kilometer per nanometer. For more remote experiments, it might be necessary to employ gradient index multimode fibers with bandwidths due to modal dispersion of 400 MHz km, which is a higher frequency response than the detector used in these experiments, the Hamamatsu R928 PMT. For multikilometer sensing, it might be necessary to employ single mode fibers with single frequency near-IR lasers, but fluorescent indicators useful with such excitation sources are not yet available.

## CONCLUSIONS

It is difficult to predict the ultimate performance achievable with the fiber optic lifetime-based sensor, but there seems to be no overt barrier to performance comparable to typical pH electrodes. Obviously, the fiber approach is unsuited to routine applications which require low cost, but for other applications it is likely to be useful or even indispensable. Among the important issues remaining are improved accuracy and precision, together with faster response time. A really useful development would be the synthesis of fluorescent lifetime indicators excitable by diode lasers. Phase fluorometry using diode lasers as a source is straightforward,<sup>17,25</sup> and this approach has many advantages from the standpoint of cost, durability, detection limits, low interference, and simplicity.<sup>16,26</sup> In addition, light of red and near-IR wavelengths is much less attenuated in optical fibers than shorter wavelengths, which is important for remote sensing applications.

## ACKNOWLEDGMENT

The authors wish to especially thank Dr. Henry Szmazinski for sharing his data prior to publication and the Office of Naval Research for support.

RECEIVED for review July 16, 1992. Accepted December 3, 1992.

# Flow Injection Donnan Dialysis Preconcentration of Trace Metal Cations for Inductively Coupled Plasma Atomic Emission Spectrometry

Narasimhan Kasthurikrishnan and John A. Koropchak\*

Department of Chemistry and Biochemistry, Southern Illinois University, Carbondale, Illinois 62901-4409

The on-line combination of flow injection Donnan dialysis (FIDD) with inductively coupled plasma atomic emission spectrometry (ICP-AES) is shown to provide enrichment factors of over 200 for cations with an 8-min dialysis time, allowing nanogram per liter level detection limits. These results are obtained for receiver solutions consisting either of  $\text{Sr}^{2+}$  or  $\text{Mg}^{2+}$ , providing complementary free spectral ranges and the applicability of FIDD-ICP-AES to trace metal cation analysis for both transition and rare earth elements. The enrichment factors obtained are linear over a wide range of concentrations and limits of detection (LODs) approximately 100 times lower than for direct aspiration are obtained using modest experimental conditions. Additional improvements in enrichment factors are obtained with increases in dialysis time and/or final sample solution temperature. A signal enhancement factor of 650 with an LOD of 11 ng/L for monovalent silver cation is demonstrated using a 30-min dialysis, a 42 °C final solution temperature, and longer lengths of cation-exchange tubing.

Donnan dialysis is a process which can preconcentrate a given ionic species, either cation or anion, into a concentrated electrolyte solution by establishing an ionic strength gradient across an ion-exchange membrane.<sup>1</sup> The electrolyte solution of higher ionic strength, known as the receiver solution, is maintained at a lower volume than the sample solution containing the ion of interest.<sup>2</sup> For cation Donnan dialysis, cation-exchange membranes are used. These membranes are highly permselective to cations; that is, in principle anions cannot diffuse through the membrane. Under the influence of the ionic strength gradient, cations from the receiver diffuse into the sample solution. Since anions are impermeable to the membrane, cations from the sample solution must diffuse through the membrane into the receiver in order to maintain electroneutrality. The latter process is the phenomenon termed Donnan dialysis. As the volume difference between the receiver and sample solution is large and the sample ions are efficiently transported to the receiver, preconcentration within the receiver results. Of the two types of cation-exchange membranes that are commonly used, tubular cation-exchange membranes have shown to provide higher enrichment than flat cation exchange membranes due to their decreased receiver volume to surface area ratio.<sup>3</sup> On-line studies of tubular cation-exchange membranes of various thickness have determined better preconcentration factors per unit time for the thin-wall membranes.<sup>4</sup> This is due to the increased transport rate across the membrane, as Donnan dialysis is constrained by the processes that occur in the bulk of the membrane.

With Donnan dialysis, one can reject counterion interferences,<sup>5</sup> normalize matrices,<sup>3,5</sup> and achieve sample matrix independent enrichment over a wide range of conditions.<sup>6</sup> The compatibility of Donnan dialysis with voltammetry,<sup>3</sup> high-pressure ion-exchange chromatography,<sup>7</sup> pulse polarography,<sup>3</sup> and flame atomic absorption spectrometry (FAAS) has been described.<sup>4</sup> With FAAS on-line tubular experiments, a compromise between optimum Donnan dialysis flow rate (static) and the high flow rate (3-6 mL/min) of FAAS had to be achieved. ICP-AES measurements provide considerably lower LODs and require much lower flow rates as compared to FAAS. Replacing FAAS with ICP-AES should result in better limits of detection (LODs) with a Donnan dialysis process. The approach to combine Donnan dialysis in a continuous-flow mode with ICP-AES has been demonstrated using conventional- and low-flow nebulizer systems.<sup>8</sup> Previously, FAAS or ICP-AES experiments performed with continuous aspiration of the receiver solution containing 3-10% dissolved solids resulted in nebulizer, burner, or torch blockage.<sup>5</sup> On-line preconcentration studies with the use of a tubular ion-exchange membrane and flow injection technique (flow injection Donnan dialysis or FIDD) have provided high enrichment factors and about 100 times lower LODs than for direct aspiration with FAAS within approximately 5 min.<sup>4</sup> With flow injection techniques, the sample that is preconcentrated in the receiver solution is fed to the nebulizer or torch for only short periods of time, alleviating blockage problems. Thus, the extension of FIDD to ICP emission techniques appears promising.

In this work we are demonstrating the applicability of flow injection Donnan dialysis (FIDD) with ICP-AES as the detector for a wide variety of cations. Since the selection of receiver solution plays an important role in FIDD, the ideal receiver solution for ICP-AES is discussed. Particular attention is paid to the various interferences involved in a typical ICP-AES experiment, such as spectral and matrix interferences that affect the signal enhancement. The difference between signal enhancement factor (SEF) and enrichment factor (EF) is elucidated, and the importance of variables such as dialysis time and temperature on signal enhancement is characterized. Discussion of results describing the concentration independence of SEF and dispersion effects on signal enhancements are included.

## EXPERIMENTAL SECTION

Donnan dialysis studies were performed using 0.33-mm-i.d × 0.51-mm-o.d thin wall Nafion 811 cation-exchange tubing (Perma Pure Products, Toms River, NJ). These dimensions are for the dry tubing. In order to maximize contact with the sample solution,

(1) Wallace, R. M. *Ind. Eng. Chem. Process Design Dev.* 1967, 6, 423.  
(2) Cox, J. A.; Gray, T.; Yoon, K. S.; Twardowski, Z. *Analyst (London)* 1984, 109, 1603.  
(3) Cox, J. A.; Twardowski, Z. *Anal. Chem.* 1980, 52, 1503.  
(4) Koropchak, J. A.; Allen, L. *Anal. Chem.* 1989, 61, 1410.

(5) Koropchak, J. A.; Dabek-Zlotorzynska, E. *Appl. Spectrosc.* 1987, 41, 1231.

(6) Cox, J. A.; Twardowski, Z. *Anal. Chem. Acta* 1980, 119, 39.

(7) DiNunzio, J. E.; Jubara, M. *Anal. Chem.* 1983, 55, 1013.

(8) Koropchak, J. A.; Dabek-Zlotorzynska, E. *Anal. Chem.* 1988, 60, 328.



the tubing was loosely coiled around a three-prong holder. The dialysis experimental set up used was very similar to the one described previously.<sup>4</sup> The cation-exchange membranes were stored in deionized distilled water (DDW) at all times, except when dialyzing. Unless stated otherwise, all dialysis experiments were carried out for 8 min at room temperature (23 °C). No extensive pretreatment of the membrane was necessary before the start of a dialysis experiment other than flushing the membrane with carrier to achieve base line signal followed by injection of 5-mL receiver solution. Once the base-line signal was obtained, the injection loop (i.e. the tubular ion-exchange membrane) was washed externally with DDW, filled with receiver solution, removed from DDW, and inserted into the sample solution. Stirring of the sample solution and timing of the dialysis began. Stirring here was achieved magnetically using a hot plate stirrer. At the end of the predetermined time of dialysis, the sample was injected, the signal measured, the flow to the ICP disconnected, and the membrane flushed with higher flow rates of the carrier after replacing the membrane in DDW to ensure a quick return of the signal to the base line. Though the optimum operating sample volume is 500 mL, or more, for Donnan dialysis,<sup>4</sup> the sample volume was fixed at 350 mL for these studies for convenient sample handling purposes. The length of the cation-exchange membrane tubing used in these studies was 0.95 m for most studies, and the nitric acid carrier solution concentration was 1 M. To demonstrate higher enrichment factors for some studies, a 500-mL sample solution volume and a 2-m length tubing was used. The flow rate of the carrier stream for the flow injected dialysates was 1.5 mL/min for all the elements except for Pb and Tl where the flow rate was 1.3 mL/min. All solutions were prepared from analytical reagent-grade (or better) salts or acids dissolved in DDW or dilute nitric acid. All glassware was scrupulously cleaned by soaking in nitric acid followed by storage with DDW until usage. Limits of detection reported here are based on 3 × standard deviation of the blank.

The spectrometric measurement system consisted of a Perkin-Elmer (Norwalk, CT) 5500 ICP modified with a dynamic background correction facility. The spectrometer was purged with nitrogen gas for studies with short wavelengths (below 200 nm). The monochromator for this system is a Czerny-Turner design with a 408-mm focal length and a grating having 2880 lines/mm and blazed at 210 nm. A Wavetek (San Diego, CA) Sweep/Trigger VCG Model 1114 provided the modulation of frequency and amplitude for a quartz refraction plate located prior to the exit slit of the spectrometer. A Keithley (Cleveland, OH) Model 485 picoammeter provided the signal amplification, and a Stanford Research Systems (Palo Alto, CA) SR 510 lock-in-amplifier provided the final background corrected signals. The output from the lock-in-amplifier was connected to a Fisher Recordall Series 5000 linear chart recorder for almost all the studies, except for cases where the output from the picoammeter was input to a Multitech 700 PC via a Metrabyte (Taunton, MA) DAS-8 interface. The computer used for signal readout in this case was equipped with Asystant Plus Software (MacMillan, New York). The computer data acquisition was used primarily for the collection and storage of wide wavelength range spectral scans.

A cross-flow nebulizer was used for all studies. Direct aspiration linear calibration curves for various elements were obtained by feeding the sample solution into the cross flow ICP nebulizer with a Gilson (Middleton, WI) Minipuls 2 peristaltic pump. In most cases, plasma operating conditions were 14 L/min coolant, 1 L/min auxiliary, and 1.1 KW of power. Measurements were made in the normal analytical zone (NAZ) at 15-mm observation height above the load coil, except in the case of Tl<sup>+</sup> where the height was 18 mm. Dispersion values are reported as the ratio of the true analyte concentration to the observed concentration of the analyte at the detector. The observed concentration at the detector was determined by injecting the same analyte concentration through the membrane. Matrix effects are expressed as the percent reduction in signal intensity of the analyte to the true signal intensity of the analyte in the absence of a matrix.

## RESULTS AND DISCUSSION

Throughout this report we will be describing Donnan dialysis in terms of signal-enhancement factors (SEFs) as

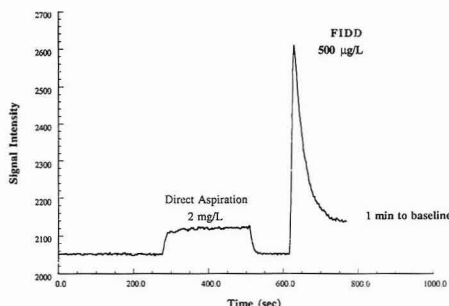


Figure 1. Typical raw data for Donnan dialysis (500 µg/L) and direct aspiration (2 mg/L) of Pb<sup>2+</sup> with a 3-min dialysis and room temperature sample solution using a Mg<sup>2+</sup> receiver.

opposed to enrichment factor (EFs). The EF is the ratio of the concentration of the ionic species of interest after dialysis in the receiver to that of its initial concentration in the sample and thus describes the exact level of preconcentration. The SEF is the ratio of the peak signal for on-line Donnan dialysis to the steady-state signal resulting from direct aspiration at the optimized flow rate of that particular instrument (an ICP-AES in this case). In an ideal case, the SEF observed should be the same as the EF. With an ICP-AES and FIDD combination, matrix effects, dispersion, and spectral interferences may cause the SEF to differ from the EF. Matrix effects occur when the analyte of interest is present in a highly concentrated matrix. More often than not, the analyte signal intensity is reduced due to the matrix, and thus the SEF obtained is lower than the EF. But, it is possible that the analyte signal intensity may be enhanced for certain elements under different conditions of operation. In such cases, the SEF obtained would be higher than the EF. Dispersion effects are associated with flow injection techniques and generally reduce the analyte signal intensity, resulting in a lower SEF. Spectral interferences are of various types, and like matrix effects can either reduce or enhance analyte signal intensity, resulting in lower or higher SEFs. Thus the deviation of SEF from EF may be positive or negative due to the above mentioned factors.

Figure 1 shows typical raw data for the Donnan dialysis process signal where a 0.5 mg/L Pb<sup>2+</sup> sample solution was dialyzed for 3 min. At the end of the 3 min of preconcentration, the sample was injected and the signal measured. Figure 1 shows the peak sharpness and shape of the Donnan dialysis signal. Data acquisition was terminated with 1 min remaining for the signal to reach base line. Since direct aspiration of a 2 mg/L Pb<sup>2+</sup> solution provided a signal height (background subtracted) of about 70 units on the Y axis, direct aspiration of a 500 µg/L solution would give a signal height of 17.5 units, assuming a linear calibration curve. The standard deviations obtained for blank solutions by both direct aspiration and Donnan dialysis were observed to be the same. Thus, if one were to calculate an SEF for Pb<sup>2+</sup> in this case, it would be the ratio of the respective signal heights by Donnan dialysis and direct aspiration. In this case, the calculated SEF would be 570/17.5 or 32.

An important step in performing a FIDD-ICP technique is to select the receiver which would yield the best SEF and be compatible with the ICP. Unlike studies of FIDD-FAAS, for measurements using an ICP various types of spectral interferences, which might limit the selection of receiver electrolyte, need to be considered. The problem created by line overlap interference may lead to positive errors in SEF determinations and degraded signal-to-noise ratios, especially



Table I. Receiver Effect\*

receiver	SEF		
	Cu	Pb	Tl
0.2 M magnesium sulfate, 0.5 mM aluminum nitrate, 0.1 M nitric acid		85	84
0.5 M strontium nitrate, 1.2 mM aluminum nitrate, 0.1 M nitric acid	75	80	72
0.25 M strontium nitrate, 0.25 M cesium nitrate, 1.2 mM aluminum nitrate, 0.1 M nitric acid	65	80	71
0.25 M strontium nitrate, 0.25 M rubidium nitrate, 1.2 mM aluminum nitrate, 0.1 M nitric acid	65	81	76

\* The wavelengths for the elements are the same as given in Table II. SEF signal enhancement factor. Flow rates: 1.3 mL/min for Pb and Tl, 1.5 mL/min for Cu. The room temperature was 20 °C.

if the receiver is the contributing source. This spectral problem caused by concomitant line overlap may be eliminated simply by choosing an alternate wavelength where there is no overlap from the interferent. But the detection limits for the alternate analyte line wavelength may be worse and some compromise may be required. The important criteria involved in selecting a receiver electrolyte are the valencies of the receiver cations and their affinities for exchange sites on the membrane. Previous studies have shown that a 0.2 M  $Mg^{2+}$ -0.5 mM  $Al^{3+}$  combination at pH 1 yields similar EFs for monovalent as well as divalent sample cations.<sup>2</sup> The  $Al^{3+}$  cation present in the receiver solution has strong affinity for negative exchange sulfonate sites on the membrane, thereby allowing lower selectivity analyte ions to diffuse efficiently.<sup>9</sup> This is because volume diffusion (movement of analyte ions across solvent filled channels of the membrane) instead of chemical kinetics will limit the rate of transport in such a case.<sup>10</sup> For the selection of counterions to the receiver cations, sulfate anions are preferred as they are less Donnan permeable than chlorides and nitrate.<sup>11</sup> Our studies with various receivers resulted in similar SEFs as shown in Table I. Studies were performed with three different elements using four different receiver combinations. All the elements behaved similarly, except for slightly higher SEFs with the magnesium receiver. The results obtained in Table I allow the flexibility of choosing an alternate receiver electrolyte for the preconcentration step in the case of a line overlap spectral problem. Thus, in case of a spectral line overlap interference from the receiver electrolyte, one can switch to an alternate receiver electrolyte without sacrificing SEFs. This is important, as SEFs are a direct reflection of the preconcentrating efficiency of the Donnan dialysis process. Secondly, no compromise in LODs is required, as there is no need to choose an alternate wavelength of the analyte.

Figures 2 and 3 depict the spectral scans obtained during the continuous input of primarily magnesium and strontium receiver, respectively. Clearly, the strontium receiver is preferable for wavelengths ranging from 248 to 330 nm, whereas the magnesium receiver is more suitable for the wavelength range of 218–275 nm. Other than the prominent clean spectral regions of the receivers, a closer look at the two spectra reveals their complementary nature. The high amount of dissolved solids in the receiver is shown by the intense

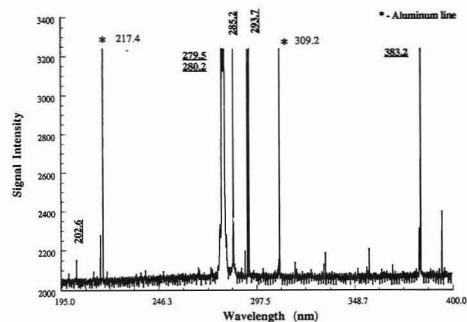


Figure 2. Spectrum obtained during continuous aspiration of the  $Mg^{2+}$  receiver (0.2 M magnesium sulfate, 0.5 mM aluminum sulfate, and 0.1 M nitric acid). Asterisk-marked numbers show prominent aluminum lines, and the underlined numbers in bold print stand for magnesium lines.

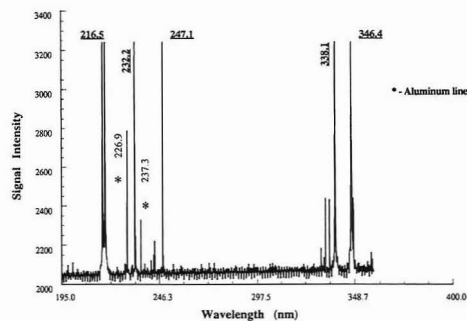


Figure 3. Strontium receiver spectrum obtained with continuous aspiration of the  $Sr^{2+}$  receiver (0.5 M strontium nitrate, 1.2 mM aluminum nitrate, and 0.1 M nitric acid). Asterisk-marked numbers show prominent aluminum lines, and the underlined numbers in bold print stand for strontium lines.

peaks for both magnesium and strontium. Thus, a possibility of wing overlap spectral interference exists, and for the same reason it would be unwise to choose the magnesium receiver for an element of wavelength 278 nm or strontium receiver for an element of wavelength 215 nm. An example of such a case would be divalent cadmium at 214.45 nm where one is restricted to the use of the magnesium receiver. Since aluminum is present in very low concentrations within the receiver, there are only a few intense aluminum lines in the spectra. Though the wavelength scans shown here provide the necessary information about the choice of receiver, a confirmatory study of the selected receiver should be done at the wavelength desired by actual injection through the membrane at the highest sensitivity level possible. This eliminates interference from any weak lines that are not visible in the spectra obtained. For example,  $Cu^{2+}$  at 324.7-nm wavelength suffered from spectral line overlap interference from the magnesium receiver, whereas there was no interference in the case of strontium receiver. Once the extent of interference, if any, is known, the analyst has the choice of either avoiding the interfering spectral region or operating at such high concentration levels of the analyte so as to render the contribution from the interferent insignificant. In our studies with a wide range of elements, we used the magnesium receiver for all elements except  $Cu^{2+}$ , where a strontium-based receiver was used due to line overlap spectral interference from magnesium.

(9) DiNunzio, J. E.; Wilson, R. L.; Gatchell, F. P. *Talanta* 1983, 30, 57.

(10) Cox, J. A.; Twardowski, Z. *Anal. Lett.* 1980, 13 (A 14), 1283.

(11) Cox, J. A.; Gajek, R.; Litwinski, G. R.; Carnahan, J. W.; Trochimczuk, W. *Anal. Chem.* 1982, 54, 1153.

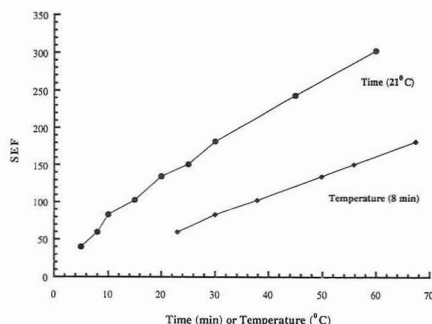


**Figure 4.** Signal enhancement factors as a function of dialysis time for sample solutions fixed at 21 °C (●) and as a function of sample solution temperature with an 8-min dialysis time (◆). The magnesium receiver was used for all experiments.

Of the parameters that affect the Donnan dialysis pre-concentration process, the dialysis time, and temperature of the sample solution are particularly important. We investigated the effect of these variables using a fixed membrane tubing length, stirring rate, and sample volume. The effects of sample solution temperature and dialysis time for divalent cadmium with a magnesium receiver are shown in Figure 4. For the solution temperature studies, the dialysis time was fixed at 8 min, and for the dialysis time study, the sample solution was maintained at room temperature (23 °C). For higher temperature studies, a temperature gradient of the sample solution from room temperature to the final desired temperature was achieved within the fixed 8-min dialysis by varying the rate of increase. SEFs were found to increase from 60 to 180 as the final temperature of the sample solution was varied from room temperature to 65 °C. The increase in SEF with increased temperatures results from the increased transfer rate across the membrane. An earlier study reported an increase of 4% in the transfer rate across the membrane per degree for  $\text{Li}^+$  using a KCl receiver and a temperature-controlled bath.<sup>12</sup> Our studies were performed by providing a temperature gradient rather than constant maintenance of temperature. In addition to  $\text{Cd}^{2+}$ , our studies performed with other elements ( $\text{Zn}^{2+}$ ,  $\text{Pb}^{2+}$ ) confirmed the trend of increased SEFs with increased temperatures. Figure 4 also shows SEFs increasing from 40 to over 300 as the dialysis time increased from 5 to 60 min. Using the combination of high sample temperatures and longer dialysis times, exceedingly high SEFs can be obtained. Increases in temperature and time provide increases in SEF that are additive of the two effects. For example an 8-min dialysis of  $\text{Cd}^{2+}$  with the sample solution at 21 °C provided an SEF of 64 (reference SEF), and increasing the dialysis time to 15 min at 21 °C gave an SEF of 100 (an increase of 36 in SEF). An increase in temperature from 21 to 36 °C with 8-min dialysis provided a SEF of 98 with an increase of 2.67/°C in SEF (35 increase in SEF). When an experiment was performed with a dialysis time to 15 min and a sample solution temperature of 34 °C, an SEF of 134 was obtained (an increase of 70 in SEF). The net increase in SEF (70) is thus found to be approximately the sum of the cumulative increases in SEF (36 + 35) that would be obtained if the experiments for increasing dialysis time and temperature are performed separately. This additive effect helps one to predict the SEF that would be obtained when both time and temperature are varied. Of the other variables, previous workers have reported that increasing the rate of stirring

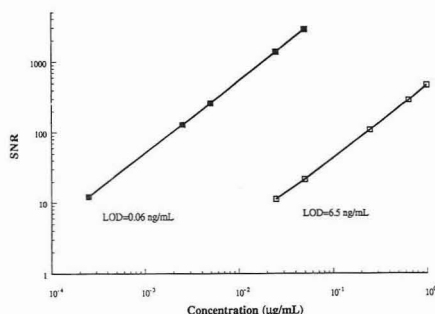


**Figure 5.** A log-log plot of signal to noise ratio against concentration for  $\text{Ag}^+$  with FIDD-ICP-AES (■) and with direct aspiration (□). The magnesium receiver, an 8-min dialysis, and room temperature solutions were employed for FIDD-ICP-AES.

**Table II.** Comparison of Detection Limits<sup>a</sup>

element	wavelength (nm)	limit of detection (µg/L)		SEF
		direct aspiration	Donnan dialysis	
Ag(I)	328.06	6.5	0.06	120
Cd(II)	214.43	6.42	0.10	64
Cr(III)	205.55	19.00	0.5	38
Cu(II)	324.75	4.45	0.04	113
Fe(II)	238.20	8.2	0.13	70
Ni(II)	221.60	22.9	0.3	70
Pb(II)	220.35	62	0.8	85
Tl(I)	190.86	162	1.82	108
Zn(II)	213.80	4.5	0.06	96
La(III)	333.75	13	0.28	45
Nd(III)	401.23	42	0.84	50

<sup>a</sup> The SEFs obtained here are with 8-min dialysis at room temperature (21–23 °C) using strontium receiver for copper and magnesium receiver for all other elements. SEF, signal enhancement factor. Plasma operating conditions are mentioned in the Experimental Section. The valencies of the cations are given in parentheses.

from 4 to 7 Hz has doubled the transport rate, resulting in increased SEFs.<sup>12</sup>

Typical log-log plots of SNR versus concentration obtained using either Donnan dialysis or direct aspiration for  $\text{Ag}^+$  are shown in Figure 5 with their respective detection limits. The plot shows the high linearity of response obtained after Donnan dialysis of a wide range of analyte concentrations, confirming the concentration independence of SEF. The significant difference in the LODs for direct aspiration (6.5 µg/L) and Donnan dialysis (0.06 µg/L) for silver is a representation of the preconcentrating efficiency of Donnan dialysis process for that element. These results were obtained for a moderately short dialysis time (8 min) and low sample solution temperature (23 °C).

The applicability of Donnan dialysis to a wide variety of cations is evident from Table II, which lists the various elements studied, the wavelength chosen, both Donnan dialysis and direct aspiration LODs, and their respective signal enhancement factors. For the determination of this data, a relatively short dialysis time, low sample temperature (23 °C), and 350-mL sample volume were chosen as compromise conditions of convenience. By using higher sample temperatures or longer dialysis times, lower LODs and higher SEFs can be obtained. It is clear that one can detect concentrations as low as 40 ng/L with Donnan dialysis for  $\text{Cu}^{2+}$  and nanogram per liter levels of the other elements for these compromise conditions. Hence, the combination of FIDD and ICP-AES provides nanogram per liter detection limits with very short

(12) Cox, J. A.; DiNunzio, J. E. *Anal. Chem.* 1977, 49, 1272.

dialysis times at room temperature. Of the transition elements,  $\text{Cr}^{3+}$  is known to form kinetically inert complexes, and the replacement of water molecules that are coordinated to  $\text{Cr}^{3+}$  by other ligands is a slow process at room temperature. The  $\text{Cr}^{3+}$  complexes persist in solution even under thermodynamically unstable conditions, making chromium substitution inert. One hypothesis is that the slow kinetics of ligand exchange is the cause for the lower SEF of trivalent chromium ion. In addition to the trivalent chromium from transition elements, the table also includes SEF data for a few trivalent ions from the lanthanide series. In these cases, the SEFs are also lower than those for mono- and divalent transition elements, but are slightly higher than for  $\text{Cr}^{3+}$ . Although the slow kinetics of ligand exchange may limit the SEF in case of  $\text{Cr}^{3+}$ , the additional SEF data for trivalent lanthanides indicates a possibility of SEFs being lower with trivalent cation Donnan dialysis in general. In such a case, the difference in SEFs for the mono- and divalent transition elements compared with trivalent cations could be explained. The difference in SEFs between  $\text{Cr}^{3+}$  and lanthanide trivalent cations could be due to the added effect of slow kinetics of ligand exchange with  $\text{Cr}^{3+}$ . Preconcentration of trivalent rare earth elements by Donnan dialysis has been described, and lower enrichment factors were reported, compared to divalent cations.<sup>9</sup> Cox and DiNunzio observed that trivalently charged cations would be more susceptible to interference effects from multicharged cations in the sample compared to divalent cation.<sup>12</sup> We performed preliminary studies with a divalent ( $\text{Pb}^{2+}$ ) and a trivalent ( $\text{Cr}^{3+}$ ) sample cation by adding increasing concentrations of a trivalent cation ( $\text{Nd}^{3+}$ ) to serve the purpose of an interferent. The results obtained by us indicate no difference in behavior among the di- and trivalent cations in the presence of an interferent. An interference was observed in both cases only when the typical ionic strength limit of Donnan dialysis (0.01  $\mu$ ) was reached. Further investigation into the behavior of trivalent cations is presently underway.

Based on our definition of SEF, the EF should be higher with FIDD-ICP-AES as measurements with ICP-AES suffer from matrix effects considering that the concentration of  $\text{Mg}^{2+}$  in the receiver is 24 g/L. Moreover, with any flow injection technique, band broadening (dispersion) is a common occurrence. Dispersion can occur both by convection and diffusion. With narrow tubing sizes, diffusion perpendicular to the flow direction (radial diffusion) might occur. In such a case, the signals obtained would be Gaussian-shaped due to the combined effect of convection and radial diffusion. The signal shapes that we obtain indicate that convection was the main dispersion phenomenon with FIDD under the operating conditions described. Dispersion is governed by the tubing length, flow rate, and sample volume. Increased dialyzed sample volumes will decrease dispersion, whereas larger transport tube lengths will result in an increase. Previously with on-line continuous analysis, SEFs were reported to be higher with longer lengths of tubing.<sup>5,8</sup> With FIDD-FAAS, however, EFs were reported to show an optimum between 0.5 and 1 m for the thick-wall membranes and then reduce further with increasing lengths.<sup>4</sup> This is because sample to receiver volume ratio decreases with increasing lengths of the tubing. The above trend was not continued below 0.5 m due to substantial dispersion effects that occurred with reduced receiver sample volumes. Thus in FIDD, a compromise between membrane length and receiver sample volume is desired. As our studies involved thinner membranes, the optimum tubing length should shift from that of thicker membranes to longer membrane lengths. This is explained by the fact that it would take longer lengths of thinner membranes compared to thicker for a fixed receiver

Table III. Comparison of SEF and EF<sup>a</sup>

element	SEF	dispersion	matrix effects (%)	EF
Cd(II)	64	2.0	24	159
Cr(III)	38	2.0	20	93
Cu(II)	113	2.0	9	230
Ni(II)	70	2.0	18	167
Tl(II)	108	1.8	18	234
Zn(II)	96	2.0	8	209

<sup>a</sup> The wavelengths and plasma operating conditions for the elements were the same as given in Table II. The comparison between SEF and EF is made for an 8-min dialysis time.

sample volume which is crucial due to its dispersion effects. Our studies found the optimum length to be around 2 m for the type of membrane that we used. Another factor of significance with FIDD that affects the SEF is the extra-injector flow volume. The effect of low and high volumes on SEFs have been studied.<sup>4</sup> By minimizing this volume, dispersion effects are lower and higher SEFs can be attained.

Table III lists the matrix effects and dispersion levels determined for various elements, showing that the actual EFs are higher than the SEFs that we are reporting throughout. Most ICP-AES instruments operated under recommended conditions in the presence of a high dissolved solids matrix cause a depression in signal. Matrix effect studies previously done show that neither the nebulizer nor the changes in test solution uptake rate are responsible for this depression.<sup>13</sup> Most studies that we performed were under conditions typically optimum for multielement analysis, although measurements were made in a single element mode. Signal depressions of about 18–25% for  $\text{Ni}^{2+}$ ,  $\text{Cd}^{2+}$ ,  $\text{Cr}^{3+}$ ,  $\text{Fe}^{2+}$ ,  $\text{Pb}^{2+}$ , and  $\text{Tl}^{+}$  were observed with the magnesium receiver compared to measurements using a dilute  $\text{HNO}_3$  sample matrix. For  $\text{Cu}^{2+}$ , there was less than 10% depression with the strontium receiver.  $\text{Zn}^{2+}$  at the chosen wavelength showed an 8% depression with the magnesium receiver. The studies shown here tend to agree with those reported by Thompson.<sup>13</sup> It is important to emphasize, however, that the matrix of the receiver solution is not significantly altered by the dialysis process such that the matrix of the analyte after dialysis is essentially constant from sample to sample, independent of the original sample composition. Thus, these results only illustrate the difference between SEFs and EFs for FIDD-ICP-AES, and not a matrix interference.

We investigated the combined effect of various optimum parameters on the SEF for  $\text{Ag}^{+}$ . Figure 6 shows the signal resulting from the Donnan dialysis of 60 ng/L silver with a 30-min dialysis time, a 0.7 °C/min temperature gradient (initial and final values being 21 and 42 °C, respectively), 500-mL sample volume, and 2-m tubing length. A signal to noise ratio (SNR) of 16.2 was obtained for this concentration, corresponding to an SEF of 650. This improvement in SEF by a factor of 5.4 over an 8-min dialysis at room temperature is due to the additive nature of the various effects of higher temperature, longer tubing length, larger sample volume, and longer dialysis time. The figure shows that the signal obtained for the dialysis is entirely due to the analyte, as the blank dialysis performed under identical conditions with the magnesium receiver did not result in a change in the background level. The detection limit for FIDD-ICP-AES was lowered from 60 ng/L to 11 ng/L by using the higher temperature, longer dialysis time, larger sample volume, and longer tubing length. The combined effect of the various parameters is a way to attain low LODs for ultratrace analyses.

(13) Thompson, M.; Ramsey, M. H. *Analyst* 1985, 110, 1413.

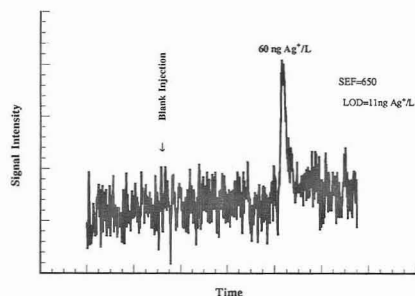


**Figure 6.** A plot of signal intensity vs time for silver with magnesium receiver is obtained with a 30-min dialysis, temperature gradient of 0.7 deg/min (initial, 21 °C; final, 42 °C), and 2 m of tubing. The analyte concentration was 60 ng/L. The arrow indicates the instant when the dialysate of a blank solution (DDW) was injected after performing a dialysis under conditions similar to that for the analyte.

### CONCLUSION

An attractive feature of FIDD for preconcentration is that hardware requirements are minimally different than those for direct aspiration analysis. Only the tubing and a stirrer are required beyond the typical instrumental setup for ICP-AES, making it a simple, low-cost addition to the experiment. SEFs of approximately 100 can be obtained for an 8-min dialysis of a room temperature solution. One can achieve increased SEFs and much lower LODs by increasing the temperature of the sample and by increasing the dialysis time. If in addition to the above we increase the sample

volume, optimize the tubing length for a particular type of membrane, and minimize dead volumes, LODs down to picograms per liter can be realized. Thus, if one deems it necessary to achieve a certain fixed SEF, a variety of factors can be adjusted to achieve that level. Another feature of the technique is that all cations from the sample are simultaneously preconcentrated with cation Donnan dialysis. Thus, the technique is amenable to simultaneous multielement analysis with ICP-AES, using a direct reading spectrometer. As is true of cation preconcentration with a cation-exchange membrane, anion preconcentration can be performed with an anion-exchange membrane. However, the SEFs obtained in the latter case would be significantly lower as good-quality tubular anion-exchange membranes are still unavailable. Neutral, or counterionic metal forms are not extracted during the Donnan dialysis process, and hence, the process can be used for metal speciation studies.<sup>14</sup> If Donnan dialysis is combined with ICP-MS, in addition to the possibility of extremely low LODs, some counterion isobaric interferences might be reduced. The main limitations to the Donnan dialysis technique are its ability to function only in a specified range of ionic strengths and the requirement for relatively large sample volumes for highest enrichment.

### ACKNOWLEDGMENT

We are grateful to Perma Pure Corp. for providing us with the cation-exchange membranes. We also thank the Office of Research Development and Administration, SIU-C, for financial support of this project.

(14) Cox, J. A.; Slonawska, K.; Gatchell, D. K. *Anal. Chem.* 1984, 56, 850.

RECEIVED for review October 26, 1992. Accepted January 2, 1993.

# Luminescence Rule of Polycyclic Aromatic Hydrocarbons in Micelle-Stabilized Room-Temperature Phosphorescence

Jin Weijun and Liu Changsong\*

Department of Chemistry, Shanxi University, Taiyuan 030006, People's Republic of China

**This paper studies the effect of the triplet energy on micelle-stabilized room-temperature phosphorescence (MS-RTP) of polycyclic aromatic hydrocarbons (PAHs). The results of the experiments show that it is difficult or impossible to induce MS-RTP of PAHs when the triplet energy is less than about 14 000 cm<sup>-1</sup>, which may be a critical value for inducing MS-RTP of PAHs. In addition, this paper also discusses the effects of ring size and linearity on MS-RTP of PAHs.**

Room-temperature phosphorimetry (RTP) has been developed rapidly since 1974. Winefordner and co-workers<sup>1,2</sup> established the general use of RTP as an analytical technique because of its simplicity, high sensitivity, and good selectivity.<sup>3,4</sup> Establishment of the MS-RTP method, especially chemical deoxygenation MS-RTP, is one of the major technical advances in the use of RTP.<sup>5-8</sup> RTP has been applied to the determination of trace amounts of many organic compounds of biochemical and environmental interest.<sup>9</sup> MS-RTP is useful for analysis of PAHs in the environment,<sup>5,10,11</sup> as is solid-substrate RTP.<sup>9</sup>

Vo-Dinh<sup>9</sup> conducted a study of the effect of ring size and molecular linearity on the phosphorescence wavelength of PAHs. In this paper, the effects of the triplet energy and the ring size and linearity of PAHs on the intensity ratio,  $I_P/I_F$ , as well as on RTP and fluorescence intensities, etc. in the micelle system have been studied. The results of these experiments indicate that for MS-RTP the effect of the ring size and linearity on RTP and RTP wavelengths is in accordance with the literature.<sup>9</sup> On the other hand, our experiments also show that  $I_P/I_F$  decreases rapidly with the decrease of the triplet energy of PAHs. That is, fluorescence intensities increase, while phosphorescence intensities decrease, relatively, with a decrease in the triplet energy. Thus, it will most likely be difficult or impossible to induce MS-RTP of PAHs when the triplet energy is less than about 14 000 cm<sup>-1</sup>.

## EXPERIMENTAL SECTION

**Instruments.** All records of luminescence spectra and measurement of luminescence intensities were carried out with

(1) Paynter, R. A.; Wellons, S. L.; Winefordner, J. D. *Anal. Chem.* 1974, 46, (6), 736.

(2) Wellons, S. L.; Paynter, R. A.; Winefordner, J. D. *Spectrochim. Acta* 1974, 30A, 2133.

(3) Parker, R. T.; Freedlander, R.; Dunlap, R. B. *Anal. Chim. Acta* 1980, 120, 1-17.

(4) Lue Yen-Bower, E.; Ward, J. L.; Walden, G.; Winefordner, J. D. *Talanta* 1980, 27, 380-382.

(5) Cline Love, L. J.; Skrilec, M.; Habarta, J. G. *Anal. Chem.* 1980, 52 (4), 754.

(6) Skrilec, M.; Cline Love, L. J. *Anal. Chem.* 1980, 52 (11), 1559-1564.

(7) Diaz Garcia, M. E.; Sanz-Medel, A. *Anal. Chem.* 1986, 58, 1436-1440.

(8) Wei, Yansheng; Liu, Changsong; Zheng, Sushe *Fenxi Huaxue* 1990, 18 (3), 228.

(9) Vo-Dinh, T. *Room Temperature Phosphorimetry for Chemical Analysis*; Wiley: New York, 1984.

(10) Cline Love, L. J.; Skrilec, M. *Am. Lab.* 1981, 13 (3), 103-107.

(11) Jin, Weijun; Liu, Changsong *Proceeding of International 4th Beijing Conference and Exhibition on Instrumental Analysis, C161*; Science Press: Beijing & New York, 1991.

a MPF-4 fluorescence spectrophotometer (HITACHI), equipped with a thermostatic cell holder. The spectrometer used a 150-W xenon arc lamp as the excitation light source and a R<sub>4486F</sub> photomultiplier (Hamamatsu Co.) as the detector.

**Reagents.** Anthracene and naphthalene, chemical grades, were supplied by Shanghai Reagent Corp. and recrystallized from warm ethyl alcohol. Phenanthrene, chrysene, and benz[a]anthracene (purum) were purchased from Fluka. Fluoranthene, 1,5-dimethylnaphthalene, fluorene, benzo[a]pyrene, perylene, and pyrene are HPLC grade from Fluka which were obtained from The Institute of Coal Chemical Research, Academia Sinica, Shanxi, P. R. China. Stock solutions of PAHs were prepared by dissolving PAHs in an aqueous 0.5 mol/L sodium dodecyl sulfate (SDS) solution, respectively.

SDS, purchased from Shen Yang reagent factory, was twice recrystallized from warm ethyl alcohol (95%, AR). Thallous nitrate, sodium sulfite, etc., Analyzed Reagent Grade, were purchased from Shanghai Reagent Co. Sub-boiling doubly distilled water was used to prepare all solutions.

The luminescence intensities shown in Table I and Figure 1 are "uncorrected spectra". The 12-nm slit was used for excitation, and the 9-nm slit was used for emission.

## RESULTS AND DISCUSSION

**Relationship between the Triplet Energy and  $I_P/I_F$ .** In the previous paper,<sup>11</sup> we mentioned that in the presence of thallous nitrate, the fluorescence of phenanthrene and 1,5-dimethylnaphthalene is almost quenched, but the fluorescence of fluoranthene, pyrene, and benz[a]anthracene is still very intense. In addition, the literature<sup>7</sup> reported that perylene does not display MS-RTP. In our experiment, perylene and anthracene do not display MS-RTP either. Generally, anthracene, which is a very weak phosphor, can only display weak RTP in a very rigid environment, for example, in  $\beta$ -CD-paper substrate.<sup>12</sup> We try to explain why these phenomena appear from the triplet-singlet energy differences  $\Delta E(T-S)$ . The triplet energies of PAHs studied and the  $I_P/I_F$  ratios corresponding to  $[Ti^{+}] = 0.025$  and  $0.035$  mol/L are listed in Table I, and their interrelation is given in Figure 1.

From Figure 1, we can see that  $I_P/I_F$  decreases rapidly with a decrease in the triplet energy and tends toward zero when the triplet energy is less than 14 000 cm<sup>-1</sup>. There is an exception for fluorene. Although its  $I_P$  and  $I_F$  are very strong under the experimental conditions, the  $I_P/I_F$  is small. Theoretically, the nonradiative rate constant corresponding to the intersystem crossing (ISC) process  $T_1 \rightarrow S_0$  strongly depends on the magnitude of the energy gap  $\Delta E(T_1-S_0)$ , that is, the rate constant increases exponentially with decreasing  $\Delta E(T_1-S_0)$ .<sup>9,13,14</sup> The intersystem crossing rate is so great that radiative transition cannot occur when the triplet energy is less than about 14 000 cm<sup>-1</sup>. The phosphorescence wavelengths of anthracene reported in the literature<sup>12</sup> are 674 and 690 nm. The former responds to maximum phosphorescence intensity. The triplet energy converted by 674 nm is 14 928

(12) Vo-Dinh, T.; Alak, A. M. *Appl. Spectros.* 1987, 14 (6), 963.

(13) Rohatgi-mukherjee, K. K. *Fundamentals of Photochemistry*; John Wiley & Sons: New York, 1978.

(14) Siebrand, W. J. *Chem. Phys.* 1967, 47 (7), 2411-2422.

Table I. Triplet Energy of Some PAHs and the  $I_P/I_F$  Ratio<sup>a</sup>

compd	no. of benzene rings	linearity <sup>b</sup>	triplet energy, cm <sup>-1</sup>	$I_P/I_F$ ratio		
				[Tl <sup>+</sup> ] = 0.025 mol/L	[Tl <sup>+</sup> ] = 0.035 mol/L	wavelength, nm <sup>d</sup>
				$E_X$	$E_{FM}$	$E_{PM}$
fluorene			21 888	0.32	0.52	276 312 457
phenanthrene	3	B	21 014	4.5	6.5	294 365 476
naphthalene	2	L	20 980	2.7	4.1	284 328 477
1,5-dimethylnaphthalene	2	L	20 385	2.2	3.0	297 338 491
chrysene	4	B	19 510	1.6	2.3	324 364 513
fluoranthene			18 287	0.77	0.95	361 442 547
pyrene	4	B	16 748	0.88	1.2	335 390 597
benzo[ <i>a</i> ]anthracene	4	B	16 573	0.40	0.58	360 389 603
benzo[ <i>a</i> ]pyrene	5	B	14 510	0.0048	0.0075	381 408 689
anthracene	3	L	15 035 <sup>c</sup>			
perylene	5		12 600 <sup>c</sup>			
naphthacene	4	L	10 140 <sup>c</sup>			

<sup>a</sup> Temperature: 25–26 °C. [SDS]: 0.05 or 0.03 mol/L. [Na<sub>2</sub>SO<sub>3</sub>]: 0.06 mol/L. pH ~ 7. [PAHs]: 5 × 10<sup>-6</sup> mol/L. <sup>b</sup> L = linearity, B = bent. <sup>c</sup> From ref 14. <sup>d</sup>  $E_{FM}$  = fluorescence wavelength,  $E_{PM}$  = phosphorescence wavelength.

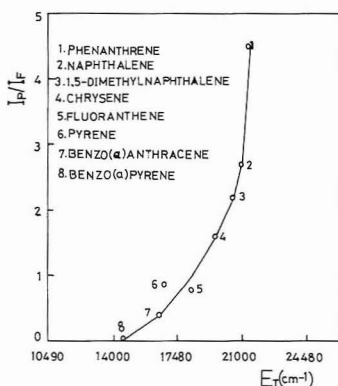


Figure 1. Interrelation between the triplet energy ( $E_T$ ) and the  $I_P/I_F$  ratio.

cm<sup>-1</sup>. The triplet energy of anthracene reported in the literature<sup>15</sup> is 43 kcal/mol, i.e., 15 035 cm<sup>-1</sup>. Therefore anthracene is a weak phosphor. The triplet energies of perylene and naphthacene reported in the literature<sup>15</sup> are 36 and 29 kcal/mol, i.e., 12 600 and 10 140 cm<sup>-1</sup>, respectively. Thus it is very difficult or impossible to induce their MS-RTP.

Actually, the phosphorescence or triplet yields of PAHs and their susceptibility to increase by heavy-atom (HA) perturbation are the result of a complex interplay of radiative and radiationless transition rates. The three main radiationless processes that compete with the luminescence or radiation process are  $S_1 \rightarrow S_0$ ,  $S_1 \rightarrow T_1$ , and  $T_1 \rightarrow S_0$ . The nonradiative rate constants of these processes are closely related to the individual energy separation between the electronic states corresponding to the process.<sup>9,13,14,16</sup> The rate constants of internal conversion ( $S_1 \rightarrow S_0$ ) and intersystem crossing ( $S_1 \rightarrow T_1$ ,  $T_1 \rightarrow S_0$ ) are very important factors in determining the RTP yield. However,  $T_n$  states may intervene between  $S_1$  and  $T_1$ , but none may intervene between  $T_1$  and  $S_0$ . Thus the phosphorescence and intersystem crossing are directly interrelated by a common electronic transition,  $T_1 \rightarrow S_0$ . If the effects of the three processes above on phosphorescence were considered simultaneously, it would

Table II. Triplet Energies and Tl<sup>+</sup>/Na<sup>+</sup> Ratios Corresponding to Maximum RTP Intensities<sup>a</sup>

PAHs	triplet energy, cm <sup>-1</sup>	Tl <sup>+</sup> /Na <sup>+</sup> mole ratio, %
phenanthrene	21 740	31.3
fluoranthene	18 510	38.5
benzo[ <i>a</i> ]anthracene	16 520	46.7

<sup>a</sup> [Na<sup>+</sup>] = [SDS] + 2[Na<sub>2</sub>SO<sub>3</sub>]; Tl<sup>+</sup>/Na<sup>+</sup> = [Tl<sup>+</sup>]/([Na<sup>+</sup>] + [Tl<sup>+</sup>]).

be more difficult to interpret them clearly. But it is not appropriate to attribute completely the factors that affect the phosphorescence yield to  $T_1 \rightarrow S_0$  processes. The other aspects still require further study.

**Relationship between Triplet Energy and the Tl<sup>+</sup>/Na<sup>+</sup> mole ratio.** Generally, PAHs show intense fluorescence, and no phosphorescence can be detected in the SDS system. Only external HA perturbation, via thallos ions, is added to the SDS system; fluorescence is quenched and phosphorescence is enhanced. Thallos ions, as SDS counterions, partly replace Na<sup>+</sup> on the micelle surface and further form thallos dodecyl sulfate (TIDS). However, TIDS is easily precipitated at lower temperature and the Tl<sup>+</sup>/Na<sup>+</sup> mole ratio is less than 30% in the system.<sup>5</sup> Nugara et al.<sup>17</sup> reported that the Tl<sup>+</sup>/Na<sup>+</sup> mole ratio can reach 50% without precipitation with a mixed micelle system. Maximum phosphorescence intensities of naphthalene are obtained when the Tl<sup>+</sup>/Na<sup>+</sup> ratio is 30%. In our experiments, the Tl<sup>+</sup>/Na<sup>+</sup> ratio can be close to 50% because of adopting a higher temperature, 25–26 °C. For a given PAH,  $I_P/I_F$  increased with an increase in Tl<sup>+</sup> concentration or reached a maximum value and then decreased with a further increase in Tl<sup>+</sup> concentration. Generally, phosphorescence intensities show a steady increase when the Tl<sup>+</sup> concentration ranges from 0 to 0.025 or 0.035 mol/L, but phosphorescence and fluorescence intensities decrease simultaneously when the Tl<sup>+</sup> concentration is more than 0.025 or 0.035 mol/L. The experiments show that the Tl<sup>+</sup>/Na<sup>+</sup> ratio is not the same in the SDS system for various PAHs when phosphorescence intensities reach maximum. It may also be concerned with the triplet energy of the PAHs. The triplet energies and Tl<sup>+</sup>/Na<sup>+</sup> ratios of PAHs corresponding to maximum RTP intensities are shown in Table II. Because it is difficult to induce RTP at lower triplet energies, a higher Tl<sup>+</sup> ion concentration and an intense magnetic field would be required. However, the Tl<sup>+</sup> ion concentration cannot be increased indefinitely because of the solubility of TIDS, the quenching of Tl<sup>+</sup> ion at high concentration, and other action.<sup>17</sup>

(15) Bartrop, J. A.; Coyle, J. D. *Principles of Photochemistry*, 2nd ed.; 1978.

(16) Dreeskamp, H.; Pabst, J. *Chem. Phys. Lett.* 1979, 61 (2), 262–265.

(17) Nugara, N. E.; King, A. D., Jr. *Anal. Chem.* 1989, 61 (13), 1431–1435.



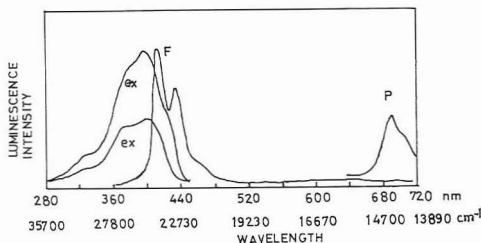


Figure 2. Excitation and emission spectra of benzo[a]pyrene. Conditions: [SDS], 0.05 mol/L; [thallous nitrate], 0.035 mol/L; [benzo[a]pyrene],  $2 \times 10^{-5}$  mol/L. Key: F = fluorescence ( $I = 3300$ ); P = phosphorescence ( $I = 25$ ).

**Effect of Ring Size and Linearity on the RTP.** Our results on the effect of ring size and linearity on the RTP wavelength are in accordance with the literature,<sup>9</sup> as shown in Table I. On the other hand, PAHs which possess linearity and large ring sizes fluoresce easily but, relatively, bent PAHs phosphoresce easily. For example, anthracene is an intense fluorescence compound but naphthalene and phenanthrene are intense phosphors.

**Analytical Considerations.** Phosphorescence spectra are usually located in the red regions. This is an aspect of RTP selectivity. As shown in Figure 2, for benzo[a]pyrene, the excitation and emission wavelengths are 381 and 689 nm, respectively; little emission occurs at 689 nm. Therefore, although benzo[a]pyrene has a very low  $I_P/I_F$  ratio, analytical selectivity of MS-RTP using the feature of its longer excitation and emission wavelengths is higher than for fluorometry. Therefore, MS-RTP not only may reduce a complex sepa-

ration procedure but also may "pick out"<sup>18</sup> benzo[a]pyrene from a complex environmental sample.

## CONCLUSION

The relationship between the triplet energy and the  $I_P/I_F$  and  $Tl^+/Na^+$  ratios has been demonstrated. The effect of the ring size and linearity of PAHs on MS-RTP is shown. Analytically, sensitivity and selectivity should be considered simultaneously to decide whether MS-RTP or fluorometry should be chosen for PAHs analysis. Several primary beneficial predictions can be made on the basis of our results which may shorten the experimental procedure; for example, for analysts, they can judge by the  $E_T$  value if a certain PAH is of intense MS-RTP. This is helpful for selecting the proper analytical methods (fluorometry or phosphorimetry) for this compound. The effect of  $E_T$  on the  $Tl^+/Na^+$  ratio and phosphorescence yields is only one of various factors. Other factors still need further study. We believe that the conclusion of this experiment is also significant for use with other RTP methods for PAH analysis, for example, solid-substrate RTP.

## ACKNOWLEDGMENT

This work was supported by the National Natural Science Foundation of China and Shanxi Provincial Natural Science Foundation.

RECEIVED for review May 11, 1992. Accepted September 18, 1992.

**Registry No.** Fluorene, 86-73-7; phenanthrene, 85-01-8; naphthalene, 91-20-3; 1,5-dimethylnaphthalene, 571-61-9; chrysene, 218-01-9; fluoranthene, 206-44-0; pyrene, 129-00-0; benzo[a]anthracene, 56-55-3; benzo[a]pyrene, 50-32-8; anthracene, 120-12-7; perylene, 198-55-0; naphthacene, 92-24-0; thallous nitrate, 10102-45-1; sodium sulfite, 7757-83-7.

(18) Vo-Dinh, T.; Hooyman, J. R. *Anal. Chem.* 1979, 51 (12), 1915-1921.

# Detection of Liquid Injection Using an Atmospheric Pressure Ionization Radiofrequency Plasma Source

Jianguo Zhao and David M. Lubman\*

Department of Chemistry, The University of Michigan, Ann Arbor, Michigan 48109

**An atmospheric pressure rf plasma source which operates in a variety of different buffer gases has been developed as an ionization method for organic samples introduced by liquid injection into atmospheric pressure ionization mass spectrometry (API/MS). The rf source can operate in He at <1 W of load power at 165 kHz. It can also be sustained in Ar, N<sub>2</sub>, air, and CO<sub>2</sub> at a load power of <15 W. In most cases studied, the protonated molecule, MH<sup>+</sup>, is observed with little or no fragmentation even under the relatively high current conditions of the discharge. However, using increasingly higher acceleration voltages between the skimmers in the differentially pumped region between atmospheric pressure and high vacuum, one can induce fragmentation via collision-induced dissociation. This can be assisted in these experiments via the use of a heavy buffer gas. The detection limits achieved for rf/API plasma detection are typically in the low femtomole region for small organic molecules including neurotransmitters, PTH-amino acids, steroids, drugs, pesticides, and explosives. The detection can be performed with quantitation over at least 4 orders of magnitude.**

## INTRODUCTION

There has been great interest over the last decade in the development of new methods for interfacing liquid chromatography to mass spectrometric detection. In particular, atmospheric pressure ionization has served as a highly sensitive means of performing ionization for liquid injection into mass spectrometry.<sup>1-12</sup> Moreover, API methods provide a convenient means for separation of the liquid carrier and analyte, thus avoiding the introduction of large amounts of liquid effluent directly into the mass spectrometer pumping station. The operation of atmospheric pressure ionization sources is based upon the generation of kiloelectron volt electrons that ionize the components in the air, which initiate charge or proton transfer through a series of ion/molecule reactions.<sup>2</sup> Since this is essentially chemical ionization at atmospheric pressure, the method is very efficient for molecules which have a high proton or electron affinity. In addition, the protonated molecule is generally observed for easy identification in the positive mode while M<sup>-</sup> or (M-H)<sup>-</sup> is observed in the negative mode.

The methods used as API sources traditionally have included the Ni  $\beta$  or corona discharge, both of which have been successfully used as ionization sources for liquid chromatography mass spectrometric detection.<sup>2-4,8,10</sup> Ni  $\beta$  sources have been widely used in commercial API and electron capture devices because of their long-term reliability; however, Ni  $\beta$  sources produce a relatively small electron density and, as a result, generally require a large volume in which to efficiently ionize the sample. Corona discharge sources produce a higher electron density than Ni  $\beta$  sources, but still have the disadvantage of a small discharge current (<1  $\mu$ A) located close to the orifice (1-4 mm) so that a limited sampling time may result in incomplete ionization. Also, the ion-molecule reactions and the resulting products may vary depending on the background and the distance between the needle and the orifice and may be easily saturated at high sample concentration levels.

In an attempt to enhance detection of liquid injection via API/MS, several new ionization sources have been recently developed. In our own laboratory an atmospheric pressure dc plasma source in helium has been used as a means of ionization for organic samples introduced by liquid injection into API/MS.<sup>13-15</sup> This plasma source operates in the abnormal glow discharge regime<sup>13</sup> and can operate typically up to 1 mA of current at atmospheric pressure, i.e., 3 orders of magnitude greater than the corona source. Even at the high currents used in this plasma source, soft ionization is routinely obtained with little or no fragmentation, even with relatively labile molecules. This relatively soft ionization is obtained under these conditions since the ionization mechanism ultimately still appears to be proton transfer via ion-molecule reactions. In addition, detection limits for small organic molecules reaching down into the low femtomole level are routinely obtained with linear quantitation over at least 3-4 orders of magnitude. The main limitation of this dc plasma, though, is that it can operate only in helium and not in other buffer gases.

In other work, microwave sources have also been used to ionize organic molecules at both atmospheric pressure and at reduced pressure.<sup>12,16</sup> Microwave-induced plasma sources have been used quite extensively as atomic ionization sources for some time.<sup>17-21</sup> However, in recent work Satzger developed a low-power atmospheric pressure microwave-induced helium plasma source in which the He plasma could be maintained at a low (10-30 W) power level.<sup>12</sup> This source could ionize

- (1) Thomson, B. A.; Iribarne, J. V. *J. Chem. Phys.* 1979, 71, 4451-63.
- (2) Carroll, D. L.; Dzidic, I.; Horning, E. C.; Stillwell, R. N. *Appl. Spectrosc. Rev.* 1981, 17, 337-406.
- (3) Thomson, B. A.; Iribarne, J. V. *Anal. Chem.* 1982, 54, 2219-24.
- (4) Sakairi, M.; Kambara, H. *Mass Spectrosc.* 1983, 31, 87-95.
- (5) Spangler, G. E.; Cohen, M. J. In *Plasma Chromatography*; Carr, T. W., Ed.; Plenum Press: New York, 1984; p 1.
- (6) Covey, T. R.; Lee, E. D.; Bruins, A. P.; Henion, J. D. *Anal. Chem.* 1985, 58, 1451A-61A.
- (7) Yamashita, M.; Fenn, J. B. *J. Phys. Chem.* 1984, 88, 4451-9.
- (8) Bruins, A. P.; Covey, T. R.; Henion, J. D. *Anal. Chem.* 1987, 59, 2642-6.
- (9) Sakairi, M.; Kambara, H. *Anal. Chem.* 1988, 60, 774-80.
- (10) Sakairi, M.; Kambara, H. *Anal. Chem.* 1989, 61, 1159-64.
- (11) Ketkar, S. N.; Dulak, J. G.; Fite, W. L.; Buchner, J. D.; Dheandhanoo, S. *Anal. Chem.* 1989, 61, 260-4.
- (12) Shen, W. L.; Satzger, R. D. *Anal. Chem.* 1991, 63, 1960-4.

- (13) Sofer, I.; Zhu, J.; Lee, H. S.; Antos, W.; Lubman, D. M. *Appl. Spectrosc.* 1990, 44, 1391-5.
- (14) Zhao, J.; Zhu, J.; Lubman, D. M. *Anal. Chem.* 1992, 64, 1426-33.
- (15) Ma, C.; Michael, S. M.; Chien, M.; Zhu, J.; Lubman, D. M. *Rev. Sci. Instrum.* 1992, 63, 139-48.
- (16) Poussel, E.; Mermet, J. M.; Deruaz, D.; Beaugrand, C. *Anal. Chem.* 1988, 60, 923-7.
- (17) Wilson, D. A.; Vickers, G. H.; Hietje, G. M. *Anal. Chem.* 1987, 59, 1664-70.
- (18) Heppner, R. A. *Anal. Chem.* 1983, 55, 2170-4.
- (19) Quimby, B. D.; Sullivan, J. J. *Anal. Chem.* 1990, 62, 1027-34.
- (20) Carnahan, J. W.; Gelhausen, J. M. *Anal. Chem.* 1989, 61, 674-7.
- (21) Calzada, M. D.; Quintero, M. C.; Camero, A.; Gallego, M. *Anal. Chem.* 1992, 64, 1374.

organic molecules with production of the molecular ion, although usually accompanied by rather extensive fragmentation. In addition, the plasma could operate stably only using He as the plasma gas. In other work, Mermert and co-workers<sup>16</sup> developed a microwave-induced plasma at low pressure (<0.1 Torr) as a soft ionization source for mass spectrometry. By adjustment of the power and the pressure, molecular ions were obtained for a number of organic compounds, although generally accompanied by rather extensive fragmentation. Several rare gas buffers could be used in this low pressure MIP, and relatively low power (<50 W) was employed.

In the present work we introduce the atmospheric pressure rf plasma as a novel ionization source for organic molecules for API/MS. The rf discharges have been used for low pressure plasma ionization for atomic analysis<sup>22,23</sup> for some time. Also, atmospheric pressure helium rf discharges have been used as excitation sources for atomic emission spectrometry in a graphite furnace.<sup>24,25</sup> However, in this work we present a high current rf plasma at atmospheric pressure that can softly ionize organic molecules. This rf plasma can be coupled to liquid injection methods for ionization and detection at significantly high flow rates. Using the rf plasma source, very soft ionization can be obtained for a range of organic molecules of biological interest. Generally only the  $MH^+$  ion is obtained, with little or no fragmentation unless decomposition occurs in the nebulization process. This rf plasma source can operate at very low power levels, i.e., ~1 W, in helium buffer. In addition, the rf plasma can operate in a host of buffer gases at 1 atm, including He,  $N_2$ , air, Ar, and  $CO_2$ , unlike the dc plasma. In addition, we demonstrate the effectiveness of the high current available in the plasma source for detection of trace quantities of sample in the femtomole range, with quantitation over several orders of magnitude. Moreover, fragmentation for structural analysis can be performed using collision-induced dissociation (CID) in the low pressure region between the two differentially pumped skimmers, which varies as a function of the buffer gas and voltage used. Indeed, it is demonstrated that the use of heavy buffer gases in the rf plasma source can be used to induce significant CID in the differentially pumped region as compared to a He buffer.

## EXPERIMENTAL SECTION

The atmospheric pressure rf plasma source used in this work is shown in Figure 1. The system consists of a heated pneumatic nebulizer, a vaporization chamber, a plasma ionization chamber, and a differentially pumped dual orifice interface. This setup is very similar to that used in previous work for the dc plasma source<sup>14</sup> with several modifications and, thus, will be described in limited detail here. The basic device consists of a liquid chromatography pump which delivers the sample, dissolved in a solvent, through the heated pneumatic nebulizer assembly to the vaporization chamber, where the sample is vaporized and the solvent is removed. The sample then passes through a duct into a second chamber, where it is ionized by the rf plasma source in 1 atm of buffer gas. The resulting ions pass through a pair of differentially pumped skimmers, which sample the on-axis component of the ion beam. The ions are then mass analyzed and detected by a SpectraEL atmospheric pressure ionization quadrupole mass spectrometer.

The LC pump delivery, nebulization, vaporization, and ionization setup are very similar to that used with the dc plasma.<sup>14</sup> In the case of the rf plasma source, liquid flow rates from 10

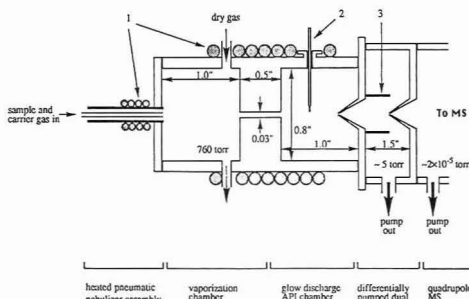


**Figure 1.** Atmospheric pressure ionization setup for rf plasma: (1) heating coils; (2) tungsten electrode insulated with ceramic tube; (3) ion beam condenser.

$\mu L/min$  up to 1 mL/min were used, although in most of the experiments described in this work the flow rate was in the 35  $\mu L/min$  flow range. The solvent was generally 50:50 methanol:water, but other solvent combinations were sometimes used to dissolve the peptides. The operation of the actual ionization source was very similar to the dc source, except that an rf power supply was used instead. In the case of helium as the buffer gas, the plasma was ignited and maintained at <1-W load power. The forward power generated by the supply was 2–5 W. This low power could produce breakdown in He over the temperature range between 25 and 350 °C at a typical frequency of 165 kHz which was used in these experiments.

The rf power supply used was an ENI Model HPG-2, which has special shielded cables and connectors so that rf is not radiated into the laboratory environment. This rf power supply has a built-in impedance matching unit. The impedance matching is achieved by changing the rf at a certain rf power level until the load power indication is maximized, followed by rotating the impedance matching switch until the load power to forward power ratio is maximum. The frequency for the best impedance matching in most cases is 165 kHz. This power supply is capable of generating rf over the frequency range of 125–375 kHz at a maximum forward power of 200 W. However, this capability is almost 2 orders of magnitude more power than was required in most of these experiments described herein. Indeed a simple and relatively inexpensive rf generator could be used as an ionization source in these experiments. A higher frequency, i.e., 13.6 MHz, rf source was also used in these experiments; however, the 125–250 kHz rf range was found to produce the most stable plasma. The peak-to-peak voltage in the experiments using the ENI Model HPG-2 unit could be measured directly from an output on the back of the unit onto an oscilloscope. In addition, a procedure of measuring the rf power dissipated in the plasma provides a way of determining the discharge current. The average discharge current generated in the plasma can be found as  $I = P/V$  where  $P$  = the power dissipated in the plasma and  $V$  = RMS voltage. The result is that in He, for example, at a power dissipated in the plasma of 1 W, a peak-to-peak voltage of 2000 V results and a discharge current of 1.40 mA is obtained. Of course, in an rf plasma the sum of the currents is 0 since there is no net charge flow from one electrode to another. But there is a charge flow at all times with different magnitudes and directions. The discharge current calculated herein is a dc equivalent current.

The plasma could be operated stably in every one of several different buffer gases used, although higher power was often required to maintain the plasma and the power needed varied as a function of the buffer gas. In the case of  $N_2$  at least 15 W (forward) power was required, whereas in  $CO_2$  14 W was used, and usually some small amount of He was needed to produce breakdown. Of course, higher powers could always be used to increase the current and, thus, the number of ions produced in these experiments. The flow of gas in the nebulizer and the flow of dry gas must be optimized for each gas in order to optimize the signal produced by the rf plasma source.

(22) Duckworth, D. C.; Marcus, R. K. *Anal. Chem.* 1989, 61, 1879–86.

(23) Duckworth, D. C.; Marcus, R. K. *Appl. Spectrosc.* 1990, 44, 649–55.

(24) Sturgeon, R. E.; Willie, S. N.; Luong, V.; Berman, S. S.; Dunn, J. G. *J. Anal. At. Spectrom.* 1989, 4, 669–72.

(25) Liang, D. C.; Blades, M. W. *Spectrochim. Acta* 1989, 44B, 1059–63.

Table I. Radiofrequency Plasma Ionization Spectra in Helium

molecule	MW	mp (°C)	T (°C)	major peaks					
Peptides									
Tyr-Gly-Gly-Phe-Leu	555	290	556 (MH <sup>+</sup> ) (17)	406 (13)	329 (23)	297 (73)	216 (100)	200 (40)	129 (20)
Phe-Phe-Phe-Phe-Phe	753	290	754 (MH <sup>+</sup> ) (3)	502 (8)	419 (29)	295 (100)			
Phe-Phe-Phe-Phe	606	290	607 (MH <sup>+</sup> ) (11)	419 (24)	295 (100)	164 (23)			
Phe-Gly-Phe-Gly	426	270	427 (MH <sup>+</sup> ) (11)	330 (60)	232 (20)	219 (37)	202 (100)		
Phe-Gly-Gly-Phe	426	290	427 (MH <sup>+</sup> ) (41)	291 (100)	235 (19)	220 (35)	70 (30)	63 (89)	
Gly-Gly-Phe-Leu	392	270	393 (MH <sup>+</sup> ) (100)	334 (21)	298 (21)	277 (56)	262 (63)	245 (24)	203 (11)
Phe-Phe-Phe	459	290	460 (MH <sup>+</sup> ) (100)	419 (33)	295 (81)	164 (47)	116 (52)		
Phe-Gly-Gly	279	230	280 (MH <sup>+</sup> ) (100)	205 (28)	120 (7)	74 (67)			
Gly-Gly-Leu	245	230	246 (MH <sup>+</sup> ) (100)						
Gly-Gly-Phe	279	260	280 (MH <sup>+</sup> ) (31)	164 (100)	119 (77)				
Gly-Leu-Tyr	351	290	352 (MH <sup>+</sup> ) (20)	370 (MH + H <sub>2</sub> O) <sup>+</sup> (16)	220 (100)	203 (29)	219 (8)	204 (5)	
Gly-Phe-Phe	369	290	370 (MH <sup>+</sup> ) (6)	351 (9)	291 (100)	219 (8)	204 (5)		
Leu-Trp	319	260	320 (MH <sup>+</sup> ) (59)	302 (MH - H <sub>2</sub> O) <sup>+</sup> (100)	981 (18)	903 (32)	750 (16)	179 (18)	
Gramicidin S	1141	315	1142 (MH <sup>+</sup> ) (100)						
PTH-Amino Acids									
PTH-serine	222	195	223 (MH <sup>+</sup> ) (100)						
PTH-glutamate	264	205	265 (MH <sup>+</sup> ) (100)						
PTH-proline	232	195	233 (MH <sup>+</sup> ) (100)						
PTH-aspartate	249	205	250 (MH <sup>+</sup> ) (100)						
Drugs									
cocaine hydrochloride	339	187	205	304 (MH - HCl) <sup>+</sup> (100)					
caffeine	194	235	230	195 (MH <sup>+</sup> ) (100)					
dibucaine hydrochloride	379	90	205	345 (MH - HCl) <sup>+</sup> (100)					
thebaine	311	192	205	312 (MH <sup>+</sup> ) (100)					
eserine	275	107	150	276 (MH <sup>+</sup> ) (100)					
atropin	289	116	120	290 (MH <sup>+</sup> ) (100)					
papaverine	339	225	205	340 (MH <sup>+</sup> ) (100)					
oxycodone	315	220	230	316 (MH <sup>+</sup> ) (100)					
lidocaine	234	69	150	235 (MH <sup>+</sup> ) (100)					
prazepam	324	146	175	325 (MH <sup>+</sup> ) (100)					
amitriptyline hydrochloride	313	200	175	278 (MH - HCl) <sup>+</sup> (100)					
codeine	299	155	200	300 (MH <sup>+</sup> ) (100)					
methadone hydrochloride	345	230	210	310 (MH - HCl) <sup>+</sup> (100)					
Steroids									
estrone	270	260	265	271 (MH <sup>+</sup> ) (100)					
cholesterol	386	149	230	369 (MH - H <sub>2</sub> O) <sup>+</sup> (100)					
estradiol	272	179	230	273 (MH <sup>+</sup> ) (100)	255 (MH - H <sub>2</sub> O) <sup>+</sup> (12)	305 (MH + MeOH) <sup>+</sup> (12)			
Antibiotics									
penicillin G	334	217	120	335 (MH <sup>+</sup> ) (47)	157 (100)				
ampicillin	349	199	205	350 (MH <sup>+</sup> ) (100)	157 (60)				
valinomycin	1110	190	300	1111 (MH <sup>+</sup> ) (100)	670 (19)				
tetracycline	444	175	175	445 (MH <sup>+</sup> ) (160)	427 (MH - H <sub>2</sub> O) <sup>+</sup> (53)	397 (15)	255 (11)	143 (10)	129 (15)
Vitamins									
thiamine hydrochloride	337	260	120	144 (100)					
nicotinic acid	123	239	230	124 (MH <sup>+</sup> ) (100)					
nicotinamide	122	130	230	123 (MH <sup>+</sup> ) (100)					
pyridoxine	169	160	230	170 (MH <sup>+</sup> ) (100)					
ascorbic acid	176	192	215	177 (MH <sup>+</sup> ) (100)					
Explosives									
TNT	227	80	150	227 (M <sup>+</sup> ) (100)	257 (M + NO) <sup>-</sup> (15)	244 (M + OH) <sup>-</sup> (11)	210 (M - OH) <sup>-</sup> (11)	197 (M - NO) <sup>-</sup> (36)	
RDX	222	203	230	222 (M <sup>+</sup> ) (7)	268 (M + NO <sub>2</sub> ) <sup>-</sup> (100)	325 (40)	101 (44)		
HMX	296	278	315	296 (M <sup>+</sup> ) (5)	326 (M + NO) <sup>-</sup> (100)	336 (82)	364 (21)	395 (18)	
Pesticides									
azinfos-ethyl	345	53	205	346 (MH <sup>+</sup> ) (100)	158 (29)	133 (22)			
diazinon	304	90 <sup>a</sup>	175	305 (MH <sup>+</sup> ) (100)					
methidathion	302	40	120	303 (MH <sup>+</sup> ) (100)					
phosmet	319	72	230	320 (MH <sup>+</sup> ) (100)	193 (10)	161 (57)			
fenamiphos	303	49	175	304 (MH <sup>+</sup> ) (100)					
chlormephos	234	85 <sup>a</sup>	175	235 (MH <sup>+</sup> ) (100)					
fenitrothion	277	118 <sup>a</sup>	120	278 (MH <sup>+</sup> ) (100)	156 (93)				
malathion	330	157 <sup>a</sup>	150	331 (MH <sup>+</sup> ) (100)	205 (6)				

Table I. (Continued)

molecule	MW	mp (°C)	T (°C)	major peaks				
				Pesticides				
ronnel	321	42	175	322 (MH <sup>+</sup> ) (100)	156 (22)	140 (47)	125 (47)	109 (53)
dimethoate	229	52	175	230 (MH <sup>+</sup> ) (100)				
				Catecholamines				
tyramine	137	164	175	138 (MH <sup>+</sup> ) (100)				
melatonin	232	116	150	233 (MH <sup>+</sup> ) (100)				
DOPA	197	272	275	198 (MH <sup>+</sup> ) (100)				
serotonin	212	168	205	177 (MH - HCl) <sup>+</sup> (100)				
norepinephrine	169	148	160	170 (MH <sup>+</sup> ) (100)	152 (MH - H <sub>2</sub> O) <sup>+</sup> (11)			
homovanillic acid	182	143	160	183 (MH <sup>+</sup> ) (100)	138 (MH - COOH) <sup>+</sup> (3)			
normetanephrine	219	207	215	184 (MH - HCl) <sup>+</sup> (100)	166 (MH - HCl - H <sub>2</sub> O) <sup>+</sup> (7)			
phenylephrine	203	140	150	168 (MH - HCl) <sup>+</sup> (100)	150 (MH - HCl - H <sub>2</sub> O) <sup>+</sup> (2)			
vanilmandelic acid	198	134	150	181 (MH - H <sub>2</sub> O) <sup>+</sup> (100)	153 (MH - H <sub>2</sub> O - CO) <sup>+</sup> (10)			

° Boiling point.

The mass spectrometer is an atmospheric pressure ionization quadrupole mass spectrometer. This device can scan up to 1200 amu with a resolution of up to 1000, although generally only nominal unit resolution was used to enhance the sensitivity. The detector was a high-gain channeltron electron multiplier (Detector Technology DT203) which was set up in the pulse-counting mode. The typical scan rate used was 50 amu/s over a range of 260–520 amu. The signal was accumulated in the pulse-counting mode and subsequently stored in a computer. When the sensitivity was evaluated, the mass spectrometer was set to monitor a single ion at a preselected mass (usually the MH<sup>+</sup>) and a counter (RIDL Model 49-28) was used to obtain the ion and background counts. The mass range was calibrated with aniline (MH<sup>+</sup>, 94) and also iodine, which produces peaks at *m/z* 127 (I<sup>+</sup>) and 254 (I<sub>2</sub><sup>+</sup>). The quadrupole was resonated periodically to keep the rf in phase for optimum performance.

The peptides, small biologicals, and drugs were obtained from Sigma Chemical Co. and used without further purification. The organophosphorus pesticide samples were obtained from the Environmental Protection Agency Repository, Research Triangle Park, NC, with the exception of malathion, which was obtained from Chem Service (West Chester, PA). The explosives were obtained courtesy of L. Van de Kieft of Ballistic Research Laboratories (Aberdeen Proving Ground, MD). For safety, the samples were prepared in solution under a chemical hood, and in all cases, polyethylene gloves and face masks were used since many of these compounds are readily absorbed through the skin. The effluent of the atmospheric pressure ionization chamber was flowed into an air exhaust unit. In the case of the explosives, one needs to prevent static electricity discharges that may ignite them. Thus, it is essential that a wooden spatula is used in handling the compound and to discharge static electricity buildup prior to sample preparation.

## RESULTS AND DISCUSSION

**Soft Ionization.** One of the key issues in the use of API sources is the ability to obtain soft ionization. The mass spectral results obtained upon liquid injection of various organic compounds into the API/rf plasma source is shown in Table I. The results in this table were obtained for the rf plasma in 1 atm of helium at ~1 W of rf load power. However, as to be shown later, these compounds could all be detected in rf plasmas in other buffer gases including Ar, N<sub>2</sub>, air, and CO<sub>2</sub>, and the mass spectral patterns observed were very similar under comparable conditions to those used to obtain the results in Table I. In almost every compound studied, the molecular ion, MH<sup>+</sup>, was obtained. Indeed, as shown in Table I, in many cases the molecular ion was observed with no or little accompanying fragmentation. Even in the case of

Table II. Sensitivities of Selected Compounds Detected by rf Plasma Ionization in Helium<sup>a</sup>

molecule	MW	mp	SIM	T (°C)	detection limit
Gly-Gly-Leu	245		246 (MH <sup>+</sup> )	235	1 ng
PTH-Ser	222		223 (MH <sup>+</sup> )	235	4 pg
cocaine	339	187	304 (MH - HCl) <sup>+</sup>	200	4 pg
estrone	270	260	271 (MH <sup>+</sup> )	260	170 pg
valinomycin	1110	190	1111 (MH <sup>+</sup> )	235	45 pg
nicotinamide	122	130	123 (MH <sup>+</sup> )	200	20 pg
TNT	227	80	227 (M <sup>+</sup> )	175	4.8 pg
dimethoate	229	52	230 (MH <sup>+</sup> )	150	3.5 pg
tyramine	137	164	138 (MH <sup>+</sup> )	200	1.5 pg

<sup>a</sup> The solvents are CH<sub>3</sub>COOH/CH<sub>3</sub>CN (9:1) for valinomycin and methanol for all other compounds.

Gramicidin S at *m/z* 1142, a strong MH<sup>+</sup> peak was observed. Soft ionization is obtained despite the high currents produced in the rf plasma. In the case of some of the samples, in particular the peptides, some fragmentation was obtained. This fragmentation appears to be due to decomposition during the nebulization–vaporization process and not due to collision-induced dissociation, as will be shown later in this work. In addition, He<sup>+</sup> or other buffer gas ions from the discharge are generally not observed because of charge exchange, and only minor background peaks from the H<sub>2</sub>O and/or MeOH cluster ions are observed. Interfering ion peaks from the solvent are rarely observed. Also, the fragmentation obtained from the rf plasma is comparable to the dc plasma, although in many cases the rf plasma source appears to provide slightly softer ionization.

**Detection Limits.** A second key property of the rf plasma source at atmospheric pressure is its superb sensitivity. This is demonstrated in Table II, which shows the results of quantitative work that was performed for samples of several different classes of compounds under single-ion-monitoring (SIM) conditions. These results were obtained with the rf plasma in He, but similar results were obtained for other buffer gases as well. In these experiments a known amount of sample was dissolved in the solvent, and lower concentrations were made by successive dilutions. The sample/solvent solution was then injected via syringe pump at a rate of 20 μL/min for ~0.5 min. The protonated molecule peak was monitored using ion counting electronics during this period. In the case of most of the small organic compounds of biological interest, a SIM detection limit in the low picogram

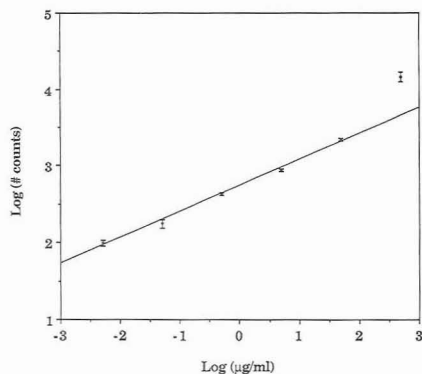


Figure 2. Quantitative measurement on tyramine using the API/rf plasma with liquid injection in methanol solvent and helium buffer gas.

region was generally observed. The detection limits shown in Table II are very comparable to those obtained using the dc plasma, although an improvement in detection limit of 1–2 times was usually obtained with the rf plasma. In addition, as shown in Figure 2, quantitation can be obtained for tyramine over at least 4 orders of magnitude, although above this regime the curve becomes nonlinear. The lower limit of detection was determined with a signal to noise ratio of 3 and was limited by background ions detected by the single-stage quadrupole. The excellent sensitivity is due to the high current density and the resulting efficient ionization of the sample under atmospheric pressure conditions. As in the case of the dc plasma, the limiting factor here appears to be the constant low background in the single quadrupole instrument. This might be eliminated with a tandem quadrupole device. Of course this excellent sensitivity has been obtained under SIM conditions, and the full-scan detection limit will be much higher. For tyramine, a full-scan sensitivity of 5.2 ng was obtained. Of course, the full-scan sensitivity could be improved markedly by a non-scanning device or a device with a much higher duty cycle in detection.

**Radiofrequency Power Level Effect on Sensitivity.** The sensitivity limits quoted in Table II are based upon optimized experimental conditions at a given rf power level. Several factors may influence the determined sensitivity limit and were thus investigated. In particular, the rf power can significantly affect the signal level. The sensitivity limits in Table II were obtained in 1 atm of He at a load power of <1 W. However, as shown in Figure 3, an increase in the rf power level from 2 to 5 W can increase the total ion yield by a factor of 3 and the yield of the  $MH^+$  by 1.5 times. Similar increases in ion current can also be observed in other buffer gases.

**Temperature Effects.** The temperature is another significant factor in the determined sensitivity limit. In Figure 4 is shown a plot of the effect of the nebulizer temperature on the signal intensity measured using the rf plasma source. In the case of tyramine, for example, there is a strong increase in the signal as the nebulizer temperature is increased over the range used in this experiment—nearly a factor of 10 times increase in signal over a range of 80 °C. This is almost certainly due to the enhanced efficiency for desolvation at higher temperature. In addition, an increase in the temperature also results in a decrease in the solvent background signal. The effect of the temperature on the rf plasma source ionization region was also investigated. An increase in the ionization chamber temperature once again significantly

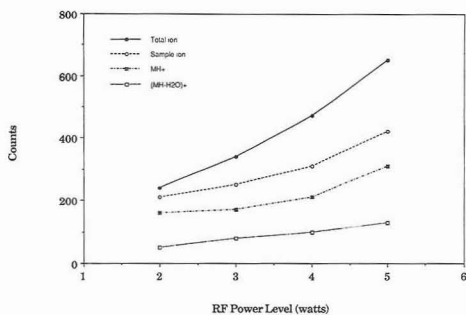


Figure 3. Effect of rf power level on signal intensity on tyramine in methanol solvent and helium buffer gas at given chamber/nebulizer temperatures (180/225 °C) and liquid flow rate (35  $\mu\text{L}/\text{min}$ ).

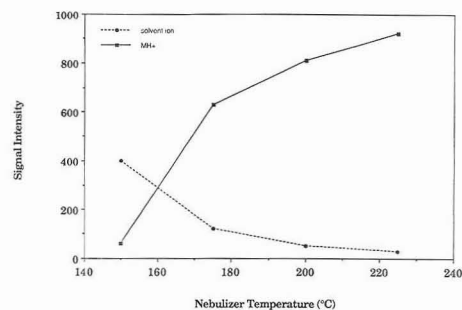


Figure 4. Effect of nebulizer temperature on signal intensity on tyramine in methanol solvent and helium buffer gas at given chamber temperature (180 °C) and liquid flow rate (20  $\mu\text{L}/\text{min}$ ).

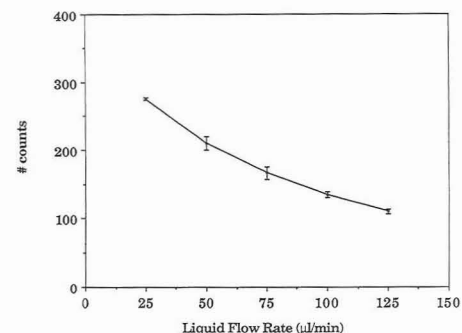


Figure 5. Effect of liquid flow rate of tyramine in methanol and helium buffer gas on the sensitivity at given chamber/nebulizer temperatures (180/225 °C).

enhances the signal at a given rf power level, sample introduction rate, and concentration. This is probably partially due to further enhanced desolvation in the discharge region at elevated temperature.

**Liquid Flow Rate and Solvent Composition Effects.** The effect of liquid injection flow rate on sensitivity was also investigated as shown in Figure 5. The results are very similar to those obtained with the dc discharge. As the flow rate is increased at a given temperature, the sensitivity decreases. This is probably due to the less efficient nebulization of the sample at the increased flow. The extra solvent also tends



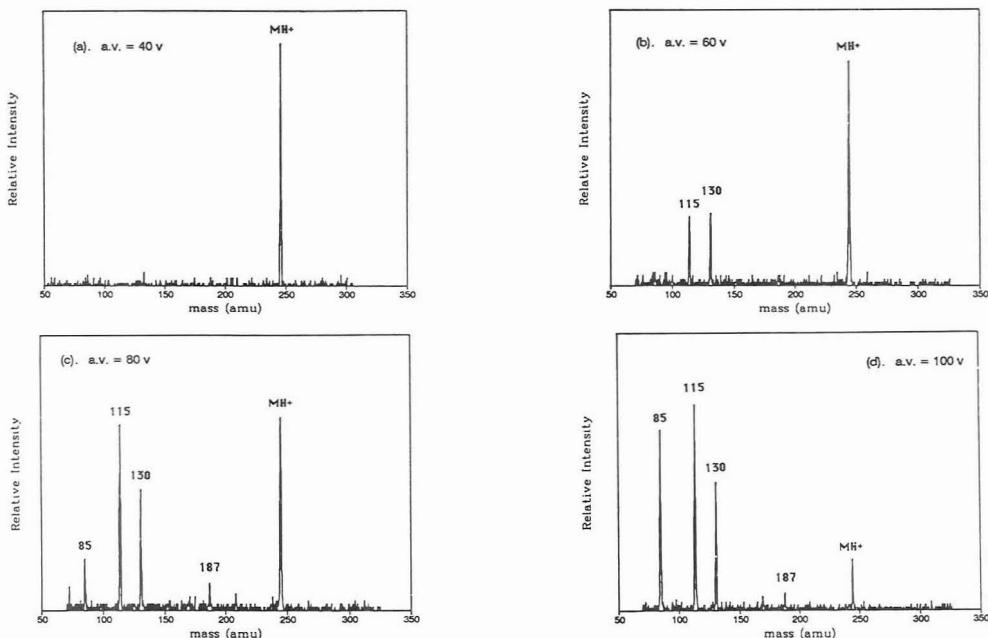


Figure 6. Collision-induced dissociation (CID) effect on Gly-Gly-Leu in 50:50 methanol:water solvent and helium buffer gas. The CID was induced by varying the voltage between the skimmers at (a) 40 V, (b) 60 V, (c) 80 V, and (d) 100 V.

to quench the plasma. The effect of solvent composition on sensitivity was also examined by varying it from 20:80 MeOH:H<sub>2</sub>O to 100% MeOH. At a temperature of 200 °C, which is sufficiently high to efficiently nebulize any of these solvent combinations, the solvent composition was not found to affect the sensitivity. In addition, neither the solvent flow rate nor the composition had any significant effect upon the mass spectrum observed for the different compounds studied in this work.

**Sources of Fragmentation.** (i) *Thermal Decomposition.* The conditions used in these experiments may affect the fragmentation patterns and, thus, the determination of the sensitivity. In most of the samples studied, relatively soft ionization with production of MH<sup>+</sup> was obtained. However, with many of the peptides listed in Table I, we found that some fragmentation always results. This fragmentation may be due to several phenomena, most likely thermal decomposition at the relatively high nebulization temperatures used. However, relatively high temperatures were required for vaporization and nebulization of these compounds by liquid injection. Over the temperature range studied, the fragmentation was not found to vary significantly.

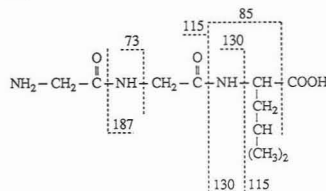
(ii) *Collision-Induced Dissociation (CID).* Other mechanisms for fragmentation may be either electron impact in the plasma at the high currents used in these experiments or relaxation of He\* metastables which may transfer a great deal of excess energy to the analyte. Another possibility for generating fragmentation is CID in the intermediate pressure region between the two skimmers. In order to check for CID, we varied the voltage difference across the two skimmers in order to see if the fragmentation changed as the difference increased. Over the normal range of voltages that would be used, no significant difference in fragmentation was observed as the voltage was varied. However, as the voltage was increased above this range, rather extensive fragmentation due to CID could be generated which varied as a function of

Table III. Comparison of MH<sup>+</sup> and Fragment Ion Intensities in Different Buffer Gases for Gly-Gly-Leu

buffer gas <sup>a</sup>	MH <sup>+</sup>	187	130	115	85	73
He	100	8	37	10	13	4
Ar	38	22	50	19	100	0
air	34	34	60	17	100	9
N <sub>2</sub>	12	18	77	22	100	1
CO <sub>2</sub> /He	25	36	80	14	100	24

<sup>a</sup> rf power levels in watts: He = 2, Ar = 3, air = 16, N<sub>2</sub> = 16, and CO<sub>2</sub>/He = 13.

Scheme I. Fragmentation Pattern of Gly-Gly-Leu (MW = 245)



voltage. This is illustrated in Figure 6a-d for the peptide Gly-Gly-Leu, where at low accelerating voltage, i.e., 40 V in Figure 6a, basically only the MH<sup>+</sup> is observed. However, as the voltage is successively raised up to 100 V in Figure 6b-d, extensive fragmentation is generated at the expense of the MH<sup>+</sup> which can be assigned as shown in the accompanying Scheme I.

**Buffer Gas Dependence of Spectra.** The mass spectrum obtained from the rf plasma source is very dependent upon the buffer gas used. This point is illustrated in Table III for the peptide Gly-Gly-Leu injected from MeOH/H<sub>2</sub>O (1:1) solvent at 230 °C into the rf plasma using various buffer gases.

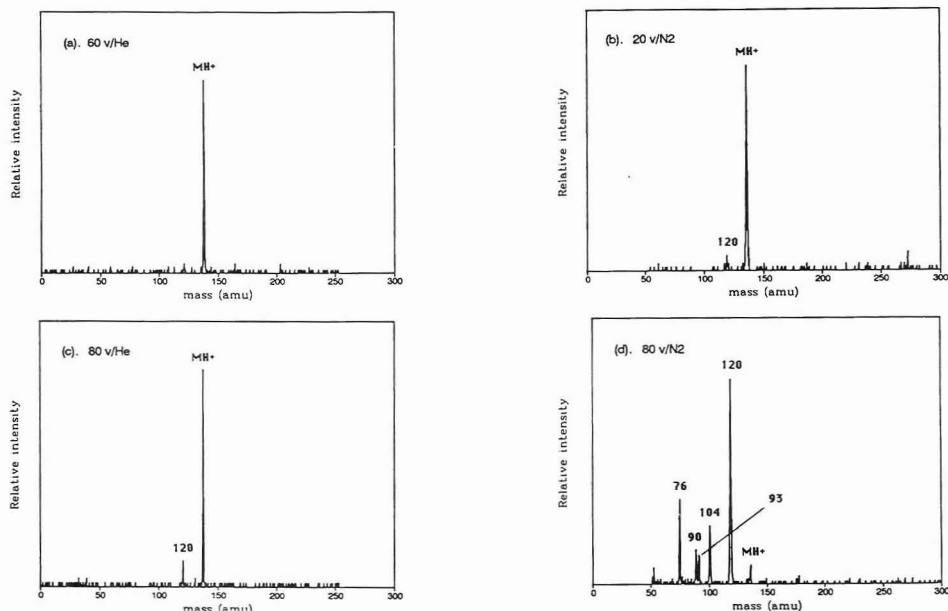
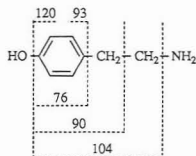


Figure 7. Comparison of CID between skimmers for tyramine in different buffer gases: Effect of buffer gas molecular weight on fragmentation for (a) 60 V in helium, (b) 20 V in nitrogen, (c) 80 V in helium, and (d) 80 V in nitrogen.

**Scheme II. Fragmentation Pattern of Tyramine (MW = 137)**



For the results shown in this table, an accelerating voltage of 60 V was used in all cases. The results show that under these conditions, when He is used as the buffer gas, then the  $MH^+$  is the base peak and little fragmentation is observed. However, when the heavier buffer gases are used, significant fragmentation results, and  $m/z$  85 becomes the base peak and  $MH^+$  becomes a relatively small peak in the spectrum. The increased fragmentation when the heavier buffer gases are employed is most likely due to the more effective collisional activation of the ions by these heavier gases in the expansion region between the two skimmers. This effect is also shown in Figure 7 for tyramine, where at an acceleration voltage of 60 V a strong  $MH^+$  peak with little fragmentation is observed for He buffer gas while for  $N_2$  the acceleration voltage has to be lowered to 20 V to achieve soft ionization. However, at an acceleration voltage of 80 V, the spectra change significantly where in the case of tyramine a strong  $MH^+$  with little fragmentation is still observed in He; whereas, if  $N_2$  is used as the buffer, then the  $MH^+$  peak becomes a minor peak and significant fragmentation results. This fragmentation is assigned as shown in Scheme II. Thus, although the rf plasma does operate in buffer gases other than He and can produce soft ionization, the results obtained will be very dependent upon the conditions used.

**Radiofrequency Power Level Effect on Fragmentation.** The observed fragmentation can also be affected by

the power level used in the rf plasma. This phenomenon is demonstrated in Figure 8 for tyramine ionized by the rf plasma in  $N_2$  at various power levels. The acceleration voltage between the skimmers has been raised sufficiently so that some fragmentation is observed at an rf plasma generated at 16 W. In this case the  $MH^+$  is observed, but the fragment at  $m/z$  120 is observed as the strongest peak in the spectrum. However, as the rf power is successively increased to 24 W, the  $MH^+$  almost disappears and other fragment ion peaks are observed beside the  $m/z$  120. This increased fragmentation may be due to several contributing effects. These might include the effects of the more energetic electrons in the plasma itself which induce fragmentation or, alternatively, the increased plasma potential may increase the ion kinetic energies and thus the extent of CID as the ions expand in the region between the skimmers. Nevertheless, we can conclude that the appearance and degree of fragmentation of the sample in the rf plasma source depends upon several factors that can be controlled in this experiment. Also, as demonstrated in Figure 8, an increase in the power level consequently results in a higher signal intensity.

In order to study further the utility of the rf plasma source for ionization and detection of organic samples from liquid injection, we have studied the use of this source for several different classes of molecules. The strengths and limitations of the rf plasma source are examined in the following sections:

**Catecholamines and Indoleamines.** An important group of molecules studied include the indoleamines, catecholamines, and their derivatives. The sensitive detection of these compounds from both blood and urine would be of great utility in the investigation of neuroblastomas and other neurogenic tumors, Parkinson's disease, and psychological stress.<sup>25</sup> These amines were examined in the positive mode since they generally have high proton affinities. In the case of each compound examined in Table I, the  $MH^+$  peak was detected with little or no fragmentation using the rf plasma source in

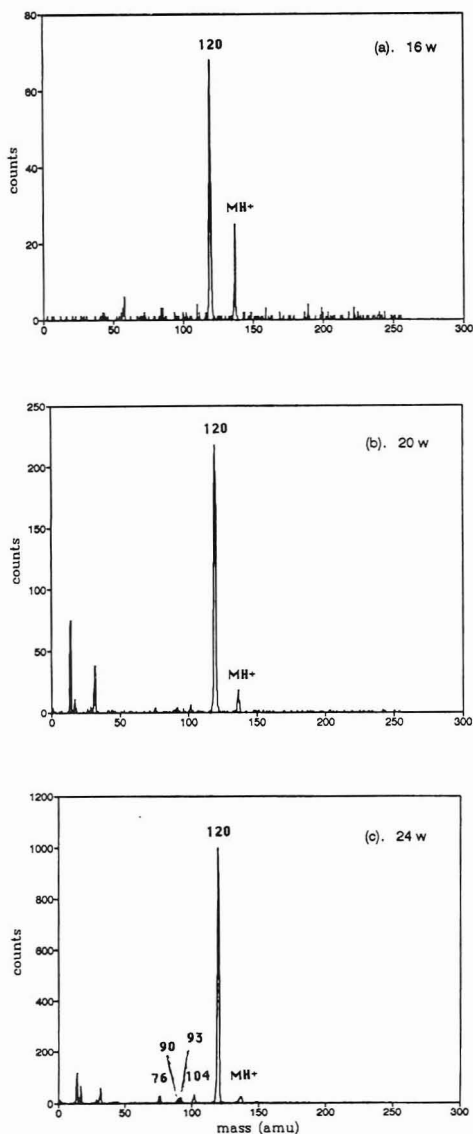


**Figure 8.** Effect of rf power level on signal intensity and fragmentation for tyramine in nitrogen buffer gas at (a) 16 W, (b) 20 W, and (c) 24 W.

He at 1 atm. Similar results were obtained for other buffer gases. A typical spectrum is shown in Figure 9 for serotonin, an important neurotransmitter and a very labile compound. This spectrum was taken at 205 °C with an rf load power of 1 W using injection from liquid methanol at a flow rate of 35  $\mu\text{L}/\text{min}$ . Even under these rather severe conditions, no fragmentation is observed. This remains basically true for all the compounds studied in this group. In the case of the dc plasma, some fragmentation was observed for melatonin under similar conditions; however, no fragmentation was observed using the rf plasma source. The results were also similar to those obtained by Kambara using a liquid injection-

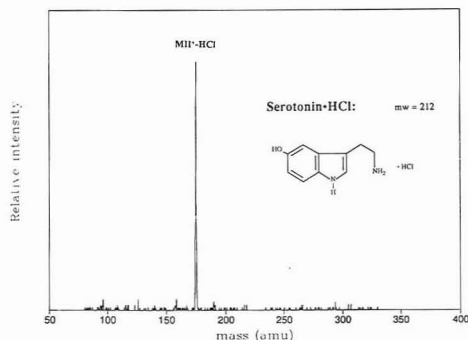


**Figure 9.** API/rf plasma mass spectrum of serotonin hydrochloride in helium from liquid injection in 50:50 methanol:water solvent.

nebulization method with a corona ionization source.<sup>9,10</sup> The ultimate sensitivity achieved for the detection of tyramine reached down to 1.5 pg, or 7 fmol. This general level of detection was achieved for most of this class of compounds.

**PTH-Amino Acids.** The detection of PTH-amino acids was studied using the rf plasma source in He and other buffer gases. The detection of PTH-amino acids is very important because these are the end products of Edman degradation, a procedure that is routinely used for protein sequencing. Extending the lower limit of protein sequencing, which is generally in the 50-pmol regime, would be especially useful for the sequencing of proteins that are available in very small quantities.<sup>26</sup> The results obtained for the detection of PTH-amino acids by the rf plasma using liquid injection-nebulization from methanol solvent are shown in Table I. In the examples studied the  $\text{MH}^+$  peak is observed without fragmentation. This lack of fragmentation would be particularly important for identification in Edman analysis. The soft ionization obtained is clearly improved, even compared to the dc plasma source where PTH-Asp and PTH-Glu are ionized with rather extensive fragmentation. The measured sensitivity as determined by successive dilutions for PTH-Ser was 4.0 pg. This limit is roughly comparable to that obtained by the dc plasma source but is nearly 3 orders of magnitude better than can be achieved routinely by Edman methods.

**Peptides.** Several underivatized oligopeptides have been studied using the rf plasma source in various atmospheric pressure buffers. As shown in Table I, the  $\text{MH}^+$  peak was observed in every case. In some of the peptides the  $\text{MH}^+$  was the base peak with little accompanying fragmentation. In other cases fragmentation was observed at the expense of the  $\text{MH}^+$ . Nevertheless, repeatable fragmentation is obtained which is easily interpretable in terms of the structure of the molecule. This was demonstrated for several examples in the previous work for the dc plasma. In comparison, the peptide Gly-Gly-Phe-Leu provided similar spectra for the dc and rf plasma sources as shown in Table I of this work and Figure 7 of ref 14. The spectra are similar, although there are differences in relative ion abundances. It should be noted that the conditions under which the two spectra were taken were not exactly the same. In both cases though, the base peak is the  $\text{MH}^+$  at  $m/z$  392. In addition, cleavages of the peptide bond produce the Y-type fragments  $Y_2$  and  $Y_3$  at  $m/z$  277 and 334, respectively. Although  $Y_1$  at  $m/z$  130 was not observed, the cleavage of the peptide bond occurred with the retention of the charge on the N-terminal end to produce the

(26) Robinson, R. *Tumors that Secrete Catecholamines*; John Wiley & Sons: Chichester, 1980.

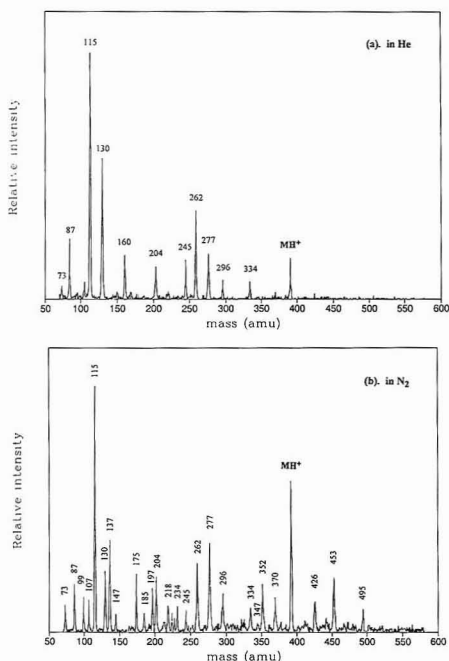
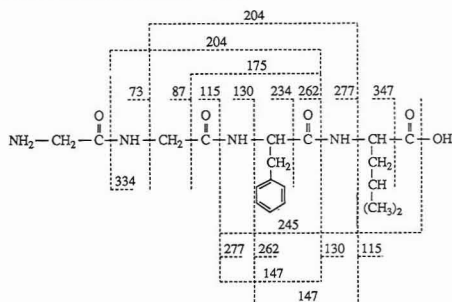


**Figure 10.** API/rf plasma spectra of Gly-Gly-Phe-Leu at an acceleration voltage of 80 V in (a) He and (b)  $N_2$ .

$B_3$  fragment at  $m/z$  262. These important fragments were produced by both the rf and dc plasma sources. The fragmentation that results in these experiments may be due to several effects, including thermal decomposition at the relatively high nebulization temperatures used for peptides (230–315 °C). Unfortunately, this high temperature was required for desolvation and detection of these species. Alternatively, some fragmentation may be due to either electron impact in the plasma or He metastables which may transfer charge and a great deal of excess energy to the analyte, thus causing fragmentation. These competing mechanisms can not be distinguished, but the method does provide reproducible spectra for identification and structural analysis.

Further fragmentation for structural analysis can be obtained via the use of CID. In comparison, the use of CID with a buffer gas between the two skimmers for Gly-Gly-Phe-Leu is shown in Figure 10 for both He and  $N_2$  buffer gases. In the case of CID induced by He, the high mass fragments (i.e.,  $m/z > 203$ ) are very similar to those obtained without CID. However, the use of CID in He results in a number of lower mass fragments, including  $Y_1$  at  $m/z$  130 so that the entire  $Y$  series, which represents cleavage at the peptide bond with charge retention on the carboxylic acid end, is observed. In addition, the  $B_2$  fragment at  $m/z$  115 is also now observed. This fragmentation contrasts with that obtained in  $N_2$ , where very extensive fragmentation is observed. In addition to the fragments observed with the use of He buffer, the  $N_2$ -induced CID results in a host of extra ion peaks, some of which can be assigned as internal fragments as shown in Scheme III, or others which result from rearrangements or clusters with  $N_2$ . Nevertheless, the results of Figure 10 demonstrate the ability to induce fragmentation of varying degrees with the use of different atmospheric pressure buffer gases in these experiments. The

### Scheme III. Fragmentation Pattern of Gly-Gly-Phe-Leu (MW = 392)



other peptides in this work can be similarly fragmented using either increasingly higher voltage as in Figure 6 or by varying the buffer gas as in Figure 10.

A quantitative study for the detection of Gly-Gly-Leu was performed using successive dilutions of the compound prepared in 50:50 water:methanol solvent. The tripeptide was introduced into the rf plasma source in He using liquid injection–nebulization at a nebulizer temperature of 235 °C. The lower limit of detection was 1 ng (~4 pmol) with a signal to noise ratio of 3. Although the molar sensitivity is not as good for some of the other species in Table II, it is nevertheless still excellent. However, as in the dc plasma,<sup>14</sup> as the size of the peptide increases the molar sensitivity becomes increasingly larger and, thus, will probably not be competitive with other techniques such as electrospray for larger peptides. The limitation here is probably the inability to efficiently desolvate larger peptides at the temperature range available in our setup. Nevertheless, even Gramicidin S, at  $m/z$  1142, could be detected in this work at an estimated concentration of 1 mg/mL.

**Steroids, Antibiotics, and Vitamins.** The detection of antibiotics and steroids is an important problem in the pharmaceutical industry and in drug testing and monitoring. This group of molecules of general biological interest is appropriately analyzed by LC/MS since they are relatively labile, but are sufficiently stable to provide strong intact molecular ion peaks in an API source, as shown in previous work.<sup>10</sup> Indeed, the steroids, antibiotics, and vitamins studied using the rf plasma source in He or other buffer gases invariably exhibit the  $MH^+$  peak with little or no fragmentation. In several cases a water molecule is lost during the nebulization–ionization process, but in most cases other significant fragmentation is not observed. The determined detection limit for valinomycin, for example, reaches down to 45 pg or ~40 fmol, whereas nicotinamide can be detected down to 100 fmol. The detection limit for antibiotics using the rf plasma source appeared to be significantly better than those achieved in previous work<sup>10</sup> by Kambara, where typically low nanogram sensitivity was obtained. However, it is difficult to make a valid comparison between these two experiments since different types of mass spectrometers were used under very different conditions. The detection limit for the steroid estrone was 170 pg, which appeared to be atypical of the steroids studied herein.

**Drugs.** Various drugs were examined which are of importance for clinical monitoring, forensic studies, and contraband detection and identification. This group of compounds is appropriately analyzed by LC/MS methods since they have high melting points (150 °C), but they are not particularly labile. In every case a strong  $MH^+$  peak is observed with no fragmentation. The results are very

comparable to those obtained in previous work using the dc plasma source. It should be noted that rather extensive fragmentation can be induced using heavy buffer gases in the CID region. A quantitative determination of the lower limit of detection for cocaine was performed using liquid injection from methanol solvent at 205 °C using the rf plasma. The lower limit of detection was 4 pg (13 fmol) with a signal to noise ratio of 3. The other drug compounds such as methadone and amitriptyline also were detected with sensitivities in the low picogram range. The detection limits for cocaine and these drug compounds generally appears to be several times improved with the use of the rf plasma source as compared to the dc plasma used in previous work.<sup>14</sup>

**Pesticides.** A number of phosphoroorganic pesticides which are relatively volatile but also labile were investigated by liquid injection into the rf plasma source. The use of various LC/MS methods has been important for the monitoring of these compounds in the environment. In studies with the rf plasma, the MH<sup>+</sup> was detected in almost every case with almost no fragmentation. These results can be compared to the dc plasma or Ni β API sources, where often significant fragmentation was observed in many of these same compounds.<sup>14</sup> The results obtained for these pesticides were obtained under similar conditions using both the dc and rf plasma. Two very illustrative examples include azinphos-ethyl and ronnel, in which the base peak is a relatively low mass fragment and the MH<sup>+</sup> may be of relatively low intensity using the dc plasma or the Ni β source. However, the rf plasma results in a strong MH<sup>+</sup> peak in both cases with only minor fragmentation. The cause of these differences between the results obtained with rf and dc plasmas is not clear; however, they may be due to differences in the degree of ionization by other mechanisms such as energetic metastable decay.

The pesticide dimethoate was quantitated using liquid methanol injection into the rf plasma at 150 °C. The lower limit of detection was 3.5 pg or 15 fmol. This is a factor of ~2.5 better than that obtained by the dc plasma. The detection here was performed in the positive mode, although these compounds could also be detected in the negative mode. However, the positive mode generally provides much better sensitivity for these phosphoroorganic compounds, with detection limits in the low picogram range. The actual concentration in the carrier can be calculated by knowing the flow rate of the buffer gas and the time of measurement. In the experiments reported in this work, He was used as the buffer and the calculated concentration of dimethoate was ~1 ppt. This measurement can be particularly important though in the case of the rf versus the dc plasma source since air can be used as the buffer gas in the rf source. Thus, the rf plasma could be used for real air sampling of related phosphoroorganic compounds that are used as chemical warfare agents.<sup>28</sup> The capability for real air sampling may be an important advantage of the rf plasma.

**Explosives.** Several key explosives were studied via liquid injection-nebulization into the atmospheric pressure rf plasma source. As shown in previous work, the negative ionization mode has proven to be optimal for detection.<sup>13,14</sup> The sensitive detection of explosives is important in several applications, including forensic studies following bomb explosions, monitoring of soil and water for explosives pollution due to improper disposal, and air monitoring for explosives detec-

tion.<sup>29,30</sup> In an attempt to determine the limitations for explosives detection for such applications, we studied the detection of TNT, RDX, and HMX. The latter two are particularly difficult to detect because of their high melting point and low volatility. These compounds were dissolved in methanol and injected into the rf plasma for ionization. In the case of TNT, a strong M<sup>-</sup> is detected as the base peak. Other peaks of much lower relative intensity are observed which are characteristic of the API mass spectrum of TNT. In the case of RDX, a relatively small M<sup>-</sup> is observed. The base peak is the (M + NO<sub>2</sub>)<sup>-</sup> as observed with the dc plasma and the Ni β source. In the case of HMX, a small M<sup>-</sup> peak is observed once again, and the base peak is observed at (M + NO)<sup>-</sup>. HMX has an extremely low vapor pressure and is very difficult to detect by heating alone;<sup>31</sup> however, a signal can be easily observed with the use of liquid injection nebulization and rf plasma ionization.

The lower limit of detection was quantitatively determined for TNT. Using liquid injection-nebulization into the rf plasma, a detection limit of 4.8 pg or ~21 fmol was determined with a signal to noise ratio of 3. The actual concentration in the He carrier was found to be 4.4 ppt. This experiment was performed with less than 1 W of load power from the rf power supply. This level of detection is certainly sufficient for forensic or soil-monitoring problems. In addition, the rf plasma can operate with air buffer and so at least in theory could be used for air monitoring, although the detection limits may not be quite sufficient for explosives monitoring in many applications.

## CONCLUSION

A radiofrequency plasma that can operate under atmospheric pressure conditions has been developed as an ionization source for organic species contained in the effluent of liquid injection. This rf plasma source can operate in an atmospheric pressure buffer of He, Ar, N<sub>2</sub>, air, or CO<sub>2</sub>. In the case of He, the rf plasma can operate at a load power of <1 W, while for the other buffer gases a higher power is needed to sustain the plasma that is usually less than 15 W. Even with the relatively high currents that result in the plasma, generally soft ionization results with the production of the protonated molecule, MH<sup>+</sup>. Often, some fragmentation may accompany the MH<sup>+</sup> which probably results from the heated nebulization of the samples, many of which are thermally labile, or from the presence of metastables in the plasma. In addition, CID can be induced by the buffer gas in between the two skimmers in the intermediate pressure region between the atmospheric pressure cell and the high vacuum region by increasing the acceleration voltage between the two skimmers. The use of a heavy buffer gas has been shown to be particularly useful for enhancing fragmentation for structural analysis. Furthermore, the ionization properties of the plasma have been characterized in regard to parameters such as the rf power level, buffer gas, temperature, and liquid flow rate and composition. The atmospheric pressure rf plasma source can provide very high sensitivity in detection, often in the low femtomole regime, for a variety of samples, including neurotransmitters, PTH-amino acids, drugs, pesticides, and explosives. This may correspond to as little as parts-per-trillion detection in the carrier gas. Quantitative measurements were performed, and linearity over 4 orders of magnitude was achieved.

The atmospheric pressure rf plasma source may find potential wide use as an ionization source for microbore liquid

(27) Crimmins, D. L.; Grant, G. A.; Mende-Mueller, L. M.; Niece, R.; Slaughter, C.; Speicher, D. W.; Yuxsel, K. V. In *Techniques in Protein Chemistry III*; Angeletti, R. H., Ed.; Academic Press: New York, 1992; pp 35-43.

(28) See *Proceedings of the 1989 U.S. Army Chemical Research, Development and Engineering Center Scientific Conference on Chemical Defense Research*; Williams, J. D., Ed.; Aberdeen Proving Ground, MD, Nov 1989.

(29) Yinon, J. *Mass Spectrom. Rev.* 1982, 1, 257.

(30) Yinon, J.; Zitrin, S. *The Analysis of Explosives*; Pergamon Press: Oxford, 1981.

(31) Huang, S. D.; Kolaitis, L.; Lubman, D. M. *Appl. Spectrosc.* 1987, 41, 1371-6.

chromatography detection of the relatively small organic molecules described in this work. It would, thus, most likely become a competitor to other API sources such as the Ni  $\beta$  and corona discharge sources with certain distinct advantages in several applications. In particular, the rf plasma source has the potential for enhanced sensitivity compared to the Ni  $\beta$  or corona discharge sources due to the high current densities produced in the plasma. In addition, Ni  $\beta$  and corona sources produce relatively small discharge currents, and the ion-molecule reactions can become easily saturated as the concentration of analyte increases. The rf plasma has shown linear detection over more than 4 orders of magnitude and still does not become easily saturated even as the concentration increases. Also, the corona source is located close to the orifice so that a limited sampling time may result in incomplete ionization, whereas the rf plasma source samples from a large volume of space sufficiently far from the orifice so that incomplete sampling is no longer a problem. The

atmospheric pressure dc plasma source also has some of these properties; however, the major advantage of the rf plasma is that it can operate in a variety of buffer gases other than He. The atmospheric rf plasma though cannot compete with electrospray in the nebulization and ionization of large molecules, but rather is most effective in the mass range under 500 amu.

#### ACKNOWLEDGMENT

We would like to thank Dr. J. Zhu for helpful suggestions during the early stages of this work. This work was supported in part under NSF Grant CHE 9022610 and by the National Center for Human Genome Research under Grant 1 P30 H 600209.

RECEIVED for review July 31, 1992. Accepted November 25, 1992.



# Collisional Fragmentation of Glycopeptides by Electrospray Ionization LC/MS and LC/MS/MS: Methods for Selective Detection of Glycopeptides in Protein Digests

Michael J. Huddleston, Mark F. Bean,\* and Steven A. Carr\*

SmithKline Beecham Pharmaceuticals, P.O. Box 1539, King of Prussia, Pennsylvania 19406

Mass spectrometric methods of glycopeptide-specific detection in liquid chromatography/electrospray mass spectrometry (LC/ESMS) of glycoprotein digests are explored using a variety of glycopeptide models and then applied to soluble complement receptor type 1, a 240-kDa glycoprotein containing 25 potential sites of N-glycosylation. The most specific method, requiring a triple quadrupole, involves monitoring of sugar oxonium fragment ions during precursor-ion scan ESMS/MS. Signals derived from nonglycosylated peptides are virtually eliminated, resulting in a total-ion current chromatographic trace of only the glycopeptides present in the digest. The corresponding mass spectra yield molecular weight and glycopeptide microheterogeneity information. An alternative and complementary approach that we term collisional-excitation scanning also involves fragmentation of glycopeptides to sugar oxonium ion fragments but does not involve any mass-selection process, permitting the experiment to be performed on a single quadrupole instrument. The resulting total ion chromatogram is similar to the UV chromatogram (215 nm), but a selected-ion chromatogram for carbohydrate-specific ions such as the N-acetylhexosamine oxonium ion ( $m/z$  204) produces a glycopeptide-specific trace. Although there can sometimes be peptide interferences in the spectra of the indicated glycopeptide-containing chromatographic peaks, this latter approach permits peptide mapping to be performed on the same data set that also indicates the location of glycopeptides in the chromatogram. Both methods are suitable for detection of glycopeptides with all common classes of oligosaccharides in either N- or O-linkage to the peptide.

## INTRODUCTION

Determining the locations, heterogeneity, and structures of oligosaccharides in recombinant glycoproteins is valuable to the biotechnology industry because such information can be used to correlate efficacy with structure and is often needed for regulatory purposes.<sup>1,2</sup> To date, most techniques for carbohydrate analysis have involved chemical or enzymatic release of carbohydrates prior to analysis.<sup>3,4</sup> However, characterizing glycopeptides, as opposed to analyzing the pool of released carbohydrates from a glycoprotein, has the advantage that the sequence context of each specific family of glycoforms is preserved. Several methods for locating glycopeptide-containing fractions in an HPLC map of a glycoprotein digest have been developed. The phenolsulfuric acid method, a classic colorimetric approach for oligosac-

charide detection, is still one of the more frequently used methods of glycopeptide detection and localization because it is simple and quantitative and can be performed on glycoproteins, glycopeptides, or oligosaccharides.<sup>5</sup> Nevertheless, localization of glycopeptides in a chromatographic run by this method does require testing of each of the isolated fractions separately. Glycopeptides can be selectively isolated from protein digests by appropriate use of lectin binding (concanavalin A or wheat germ agglutinin are often used); mass spectrometry can then be used for initial characterization of the molecular weight and microheterogeneity, although care must be taken to thoroughly desalt samples isolated from lectin columns.<sup>6</sup> Alternately, lectins can be made part of a glycopeptide-specific staining procedure.<sup>7</sup> Recently, there has been progress in adapting chemical methods to quick, high-throughput analyses using microtiter plates and microsample readers.<sup>8</sup> Glycopeptide structural information from the above methods is often scant or absent.

Several mass spectrometric (MS) techniques are used for locating glycopeptides. All of these have the advantage over chemical or lectin-based methods in that they yield molecular weight information. Together with prior knowledge of the recombinant protein sequence and of the range of carbohydrate structures previously characterized from the expression cell line used, molecular weight measurements can reveal a relatively detailed picture of the site of glycosylation, the oligosaccharide structural classes present, and their molecular heterogeneity. One of the earlier such methods involved analytical HPLC separation (with UV<sup>9</sup> or UV and mass spectrometric detection<sup>10</sup>) of the components of a protein digest before and after PNGase F enzymatic release of N-linked oligosaccharides followed by a search for differences between the two chromatograms. This method was limited to N-linked glycopeptides. Other MS methods depend on the frequently observed heterogeneity of the carbohydrate portion of the glycopeptide; a glycopeptide with more carbohydrate attached tends to elute slightly earlier in reversed-phase separations than the glycopeptide containing less carbohydrate. Although the chromatographic separation is insufficient for UV detection to resolve the peaks, the adjacent mass spectra appear quite different.<sup>11</sup> As a result, a diagonal line can be observed after plotting  $m/z$  versus time whereas peptides result in lines parallel to the  $m/z$  axis.<sup>12</sup> Alternately, a peak-pair searching algorithm can be used to

\* Authors to whom correspondence should be addressed.

(1) Cummings, D. A. *Glycobiology* 1991, 1, 115-130.  
(2) Goochee, C. F.; Gramer, M. J.; Andersen, D. C.; Bahr, J. B.; Rasmussen, J. R. *Bio/Technology* 1991, 9, 1347-1355.  
(3) Hardy, M. R.; Townsend, R. R. *Proc. Natl. Acad. Sci. U.S.A.* 1988, 85, 3289-3293.  
(4) Lee, Y. C. *Anal. Biochem.* 1990, 189, 151-162.

(5) Dubois, M.; Gilles, K. A.; Hamilton, J. K.; Rebers, P. A.; Smith, F. *Anal. Chem.* 1956, 28, 350-356.

(6) Bean, M. F.; Bangs, J. D.; Doering, T. L.; Englund, P. T.; Cotter, R. J. *Anal. Chem.* 1989, 61, 2686-2688.

(7) Hsi, K.-L.; Chen, L.; Hawke, D. H.; Zieske, L. R.; Yuan, P.-M. *Anal. Biochem.* 1991, 198, 238-245.

(8) Fox, J. D.; Robyt, J. F. *Anal. Biochem.* 1991, 195, 93-96.

(9) L'Italien, J. J. *J. Chromatogr.* 1986, 359, 213-220.

(10) Carr, S. A.; Roberts, G. D. *Anal. Biochem.* 1986, 157, 396-406.

(11) Hemling, M. E.; Roberts, G. D.; Johnson, W.; Carr, S. A.; Covey, T. E. *Biomed. Environ. Mass Spectrom.* 1990, 19, 677-691.

(12) Ling, V.; Guzzetta, A. W.; Canova-Davis, E.; Sultis, J. T.; Hancock, W. S.; Covey, T. R.; Shushan, B. I. *Anal. Chem.* 1991, 63, 2909-2915.

query LC/ESMS data by automatically searching the mass spectral data for characteristic  $m/z$  differences between spectral peaks such as those corresponding to hexose or *N*-acetylhexosamine.<sup>13</sup> Both of these methods fail in the absence of site microheterogeneity.

The need to find faster, more sensitive, more selective, and more universal techniques for locating glycopeptides during chromatography of glycoprotein digests becomes pressing when dealing with larger glycoproteins with many potential glycosylation sites. For example, the soluble complement receptor glycoprotein (sCR1) discussed in this paper is 240 kDa and has 25 potential sites of *N*-glycosylation. A tryptic digest of this glycoprotein is expected to produce 174 tryptic fragments, many of them glycopeptides. The HPLC separation of this digest is exceedingly complex, and most of the glycopeptides coelute with peptides in the digest. Thus, techniques for glycopeptide detection that rely solely on HPLC UV difference mapping before and after removal of carbohydrate<sup>9</sup> can only identify a small percentage of the glycopeptides present. Manually interrogating individual chromatographic fractions by chemical or mass spectrometric means quickly becomes unwieldy and time-consuming as the number of fractions increases. What we needed was an on-line HPLC method which not only detected the location of glycopeptide-containing fractions but also yielded structural information while retaining the peptide sequence context of the attachment site.

N-linked oligosaccharides expressed in mammalian cells have somewhat restricted heterogeneity with well-characterized structural types; the most common are represented by the following: deoxyhexose (fucose), hexose (mannose or galactose), *N*-acetylhexosamine (*N*-acetylglucosamine or *N*-acetylgalactosamine), and *N*-acetylneuraminic acid with the same Man<sub>5</sub>GlcNAc<sub>2</sub>-(Asn-X-Ser/Thr) core. O-linked oligosaccharides usually contain hexose (galactose) or *N*-acetylhexosamine (*N*-acetylglucosamine) with a common HexNAc-(Ser/Thr) core. Our objective was to develop methods for specific detection and molecular weight determination of all types of glycopeptides using liquid chromatography/electrospray mass spectrometry (LC/ESMS). In this paper we describe the collision-induced fragment ions of oligosaccharides and glycopeptides that may be exploited for selective detection of glycopeptides in complex digests. Neutral-loss scanning and parent- or precursor-ion scanning are compared. The analytical utility of collision-induced dissociation (CID) in Q2 of a triple quadrupole and CID in the ion source region of a single quadrupole, together with a novel method we refer to as *collisional-excitation scanning*, are discussed. Simultaneous with our initial presentation of this work on glycopeptide-specific detection,<sup>13,14</sup> Conboy and Henion presented preliminary data on the use of high-orifice voltage CID LC/ESMS for glycopeptide analysis.<sup>15,16</sup> An application of the methodology described in this paper to fetuin glycoprotein and its extension to the distinction of O- and N-linked glycopeptides has been published elsewhere.<sup>17</sup>

## EXPERIMENTAL SECTION

**Chemicals.** Man<sub>5</sub>GlcNAc, Gal-GalNAc-Ser, and the Asn-linked oligosaccharides illustrated in Figure 1 were obtained from

(13) Carr, S. A.; Armbruster, T.; Hemling, M. E.; Soneson, K. K.; Huddleston, M. J. Proceedings of the 39th ASMS Conference on Mass Spectrometry and Allied Topics, Nashville, TN, May 19-24, 1991; pp 483-484.

(14) Huddleston, M. J.; Bean, M. F.; Barr, J. R.; Carr, S. A. Proceedings of the 39th ASMS Conference on Mass Spectrometry and Allied Topics, Nashville, TN, May 19-24, 1991; pp 280-281.

(15) Conboy, J. J.; Henion, J. D. Proceedings of the 39th ASMS Conference on Mass Spectrometry and Allied Topics, Nashville, TN, May 19-24, 1991; pp 1415-1419.

(16) Conboy, J. J. Ph.D. Thesis, Cornell University, New York, 1992.

(17) Carr, S. A.; Huddleston, M. J.; Bean, M. F. *Protein Sci.*, in press.



**Figure 1.** Structures of model glycopeptides: (a) biantennary complex Asn-linked oligosaccharide,  $M(\text{monoisotopic or m.l.}) = 1754.6$ ; (b) same structure but with *N*-acetylneuraminic acid at the branch terminus,  $M(\text{m.l.}) = 2336.8$  (c) triantennary oligomannose Asn-linked oligosaccharide,  $M(\text{m.l.}) = 1996.7$ ; (d) O-linked disaccharide,  $M(\text{m.l.}) = 470.2$ .

BioCarb Chemicals (Accurate Chemical & Scientific Corp., Westbury, NY) and used without desalting or purification. A soluble, recombinant form of the CD4 surface glycoprotein (the lymphocytic receptor of the HIV virus) which lacks the transmembrane domain (known as soluble or sCD4) was expressed in Chinese hamster ovary cells and purified at SmithKline Beecham as published.<sup>18</sup> The secreted, truncated form of the HIV envelope protein gp120 (85 kDa) missing the first 31 amino acids from the mature form and containing the first four amino acids of tPA at the N-terminus was cloned, expressed in *Drosophila* cells, and purified at SmithKline Beecham as previously described.<sup>19</sup> The clone of soluble human complement receptor type I, a recombinant soluble form of type I complement receptor lacking the transmembrane and cytoplasmic domains<sup>20</sup> (sCR1, also known as TP-10 HD, 250 kDa) was received from T Cell Sciences, Inc. (Cambridge, MA), and the protein was expressed in Chinese hamster ovary cells.

**Enzymatic Digests.** The native glycoproteins gp120, sCD4, and sCR1 were each reduced and S-carboxymethylated prior to proteolytic digestion with trypsin by the same procedure. Reduction was performed in 0.5 M Tris-HCl buffer, pH, 8.3, containing 2 mM EDTA and 6 M guanidine hydrochloride with dithiothreitol in a 50-fold molar excess over cysteine. Denaturation and reduction were allowed to proceed under nitrogen for 3 h at 37 °C. An aliquot of aqueous iodoacetic acid (100-fold molar excess over DTT) that had been degassed and pH adjusted to 8.3 with NH<sub>4</sub>OH was added and the reaction allowed to continue for 1 h. The glycoprotein was dialyzed against 3.5 L of 50 mM NH<sub>4</sub>HCO<sub>3</sub> for 15 h at 4 °C and stored dried at -70 °C. Prior to proteolytic digestion, the samples were dissolved in 0.050 M NH<sub>4</sub>HCO<sub>3</sub> buffer at pH 8.5. TPCK-treated trypsin (Cooper Biomedical, Malvern, PA) dissolved in the same buffer was added in two equal portions 3 h apart to give a final enzyme-to-substrate ratio of 1:50. Digests were incubated at 37 °C for 6 h and halted by lowering the pH to ≤4 with dilute acetic acid.

**Flow Injection and Liquid Chromatography.** Oligosaccharide model compounds, Man<sub>5</sub>GlcNAc and Gal-GalNAc-Ser, were infused at 250 pmol/μL and the Asn-linked oligosaccharide models (Figure 1) flow injected at 100 pmol/μL in 50% methanol, 50% water, 0.2% formic acid (v/v/v) by means of a Model 22 syringe pump (Harvard Apparatus, S. Natick, MA). Chromatographic separations for microbore LC/MS/MS experiments were performed using a Brownlee Labs Micro Gradient System syringe pump and a 1.0 × 100-mm Aquapore column packed with 7-μm diameter particle, 30-nm pore size, C<sub>18</sub>-bonded silica (Applied Biosystems, Foster City, CA). The eluting solvent was run as a linear gradient from (A) 0.1% trifluoroacetic acid (TFA) in water

(18) Deen, K. C.; McDougal, J. S.; Inacker, R.; Folea-Wasserman, G.; Arthos, J.; Rosenberg, J.; Maddon, P. J.; Axel, R.; Sweet, R. W. *Nature* 1988, 331, 82-84.

(19) Culp, J. S.; Johansen, H.; Hellmig, B.; Beck, J.; Matthews, T. J.; Delers, A.; Rosenberg, M. *Bio/Technology* 1991, 9, 178-177.

(20) Weisman, H. P.; Barrow, T.; Leppo, M. K.; Marsh, H. C., Jr.; Carson, G. R.; Concino, M. F.; Boyle, M. P.; Roux, K. H.; Weisfeldt, M. L.; Fearon, D. T. *Science* 1990, 249, 146-151.

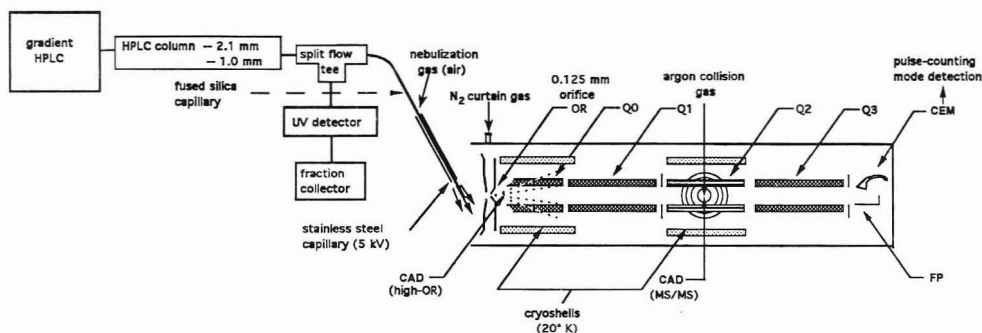


**Figure 2.** Diagram of the LC/ESMS system. OR = orifice. Q(0–3) = quadrupole rod sets 0–3 (Q1 and Q3 are mass analyzers). FP = faraday plate. CEM = channel-electron multiplier. High-OR refers to a relatively high voltage potential between OR and Q0, used to induce fragmentation of molecules prior to the first mass analyzer.

to (B) 90% acetonitrile, 10% H<sub>2</sub>O, 0.09% TFA using the following program: 0–60% B during 75 min and 60–100% B in 5 min at a flow rate of 40  $\mu$ L/min. For microbore LC/MS/MS analyses we injected ca. 800 pmol of protein digest. The microbore LC/MS setup is illustrated in Figure 2. The column effluent is split 10:1 by means of a (Valco, Houston, TX) low dead-volume "tee" union with fused-silica capillary tubing outlets (Polymicro Technologies, Phoenix, AZ) of different diameters and lengths to produce the desired split ratio. The major portion of the stream flowed through a 100- $\mu$ m-i.d. capillary to a Hewlett-Packard 1050 variable wavelength UV detector (Hewlett-Packard Co., San Fernando, CA) operated at 215 nm and then to a Gilson 203 fraction collector (Gilson Medical Electronics, Middleton, WI); the minor portion of the split stream passed to the electrospray nebulization needle tip through a 50- $\mu$ m-i.d. capillary.

**Mass Spectrometry.** Electrospray mass spectra were recorded on an API-III triple-quadrupole mass spectrometer (Perkin-Elmer Sciex Instruments, Thornhill, Canada) fitted with an articulated, pneumatically-assisted nebulization probe and an atmospheric pressure ionization source. The tuning and calibration solution consisted of an equimolar mixture of poly(propylene glycol) (PPG) 425, 1000, and 2000 ( $3 \times 10^{-6}$ ,  $1 \times 10^{-4}$ , and  $2 \times 10^{-4}$  M, respectively) in 50/50/0.1 H<sub>2</sub>O/methanol/formic acid (v/v/v), 1 mM NH<sub>4</sub>OAc. Calibration across the  $m/z$  range 10–2400 was effected by multiple-ion monitoring of eight NH<sub>4</sub>OAc/PPG solution ion signals. Mass-to-charge ratio assignments in the figures are the measured peak tops and will be more closely related either to the monoisotopic or to the average mass depending on the molecular weight. Although computed peak centroids traditionally yield better mass assignments than peak tops, the presence of various charge states and the resulting variation in peak widths in a single spectrum makes such centroiding error-prone.

The ion spray voltage was operated at 4.5 kV with 35–40 psi "zero" grade compressed air nebulization gas flowing at 0.8 L/min. A certain of nitrogen gas (99.999%) was used to keep atmospheric gases out of the analyzer at a flow rate of 1.2 L/min. Normal and precursor-ion mass spectra were acquired by scanning Q1. Product-ion spectra were taken by colliding the Q1-selected precursor ion of interest with argon gas in Q2 and scanning Q3 to analyze the fragment-ion products; precursor-ion scans were performed the same way except that Q1 was the scanning and Q3 the selecting quadrupole. Neutral-loss spectra required scanning Q1 and Q3 synchronously but offset one from the other by the  $m/z$  of interest. For all tandem MS experiments the 99.999% argon collision target gas thickness was  $(5\text{--}7 \times 10^{14})$  molecules/cm<sup>2</sup>, a figure computer-derived from a capacitance manometer reading of the gas inlet pressure and a formula for the downstream density of a free jet.<sup>21</sup> Precise collision energy measurements were not made, although these can be approximated as being somewhat greater than the ion charge state multiplied by the voltage potential (20–40 V) between the Q0 and Q2 quadrupoles.

Normal scan ESMS and LC/ESMS spectra were recorded at instrument conditions sufficient to resolve the isotopes of the PPG/NH<sub>4</sub><sup>+</sup> doubly-charged ion at  $m/z$  520 (85% valley definition). Although the observation of 0.5  $m/z$  isotope spacing is a reliable indication of a doubly-charged ion under normal conditions, such distinctions could not always be made with confidence for fast-scanning LC/ESMS where fast scan rates produce relatively small ion-current samples and nonideal spectral peak shape.

For precursor-ion tandem MS, the analyzing quadrupole (Q1) was operated at a resolution of about unit  $m/z$  (using a 35% peak valley definition at low  $m/z$  and a 60% peak valley definition at high  $m/z$ ), while the mass-selecting quadrupole Q3 was set to pass a 2–3-Da window around the ion of interest so as to enhance sensitivity. Orifice potential (OR), quadrupole rod offsets, and collision gas pressure were adjusted using the Man, GlcNAc model. Although the leeway for optimization is broad, we carefully adjust the instrument parameters for acquisition of LC/ESMS/MS spectra with low levels of analyte (<50 pmol). We have found that the optimal orifice potential is 55 V, although other values were used in earlier experiments (see figure legends). All tandem MS spectra have been smoothed once.

Collisional-excitation scanning (see Results and Discussion) can be implemented on the Sciex instrument in two ways: linear ramping of the orifice voltage with  $m/z$  is provided for in the software package; it is also possible to use multiple-ion monitoring with two very wide ion windows to maintain the sampling orifice potential high (140 V) during the low  $m/z$  scan window (150–500) and maintain it at a low (65 V) voltage in the second ion window which encompasses the scan from  $m/z$  500 to 2100 (see Figure 7). It is the latter approach that we now prefer, and we sometimes refer to this approach as a stepped orifice-voltage scan.

## RESULTS AND DISCUSSION

The carbohydrate nomenclature used in this paper employs the abbreviations Hex (hexose), HexNAc (*N*-acetylhexosamine), and NeuAc (*N*-acetylneuraminic acid) to refer to the carbohydrate residues without specifying which of the isobaric and mass spectrometrically equivalent isomers are actually present (e.g., mannose, glucose, etc. are a subset of hexose). In the mass spectra, loss of neutral carbohydrate moieties or pieces thereof from the charged parent ion are designated with a "–". For example, –Hex ( $\text{C}_6\text{H}_{10}\text{O}_6$ , 162 Da) indicates a loss of neutral dehydrohexose. Carbohydrate fragment ions with structures formally equivalent to oxonium ions are indicated with a "+" sign following the structure; for example Hex<sup>+</sup> ( $\text{C}_6\text{H}_{11}\text{O}_6^+$ ,  $m/z$  163) implies the oxonium ion of hexose. It is important to note that –Hex and Hex<sup>+</sup> (and the other corresponding carbohydrate fragment pairs) differ by one hydrogen (1 Da) from one another; this nomenclature simplifies annotation of the mass spectra. Designations such as (HexNAc-Asn + H)<sup>+</sup> and (Hex<sub>2</sub>HexNAc + H)<sup>+</sup> indicate

(21) French, J. B. *Can. Aeronaut. Space Inst. Trans.* 1977, 3, 77.

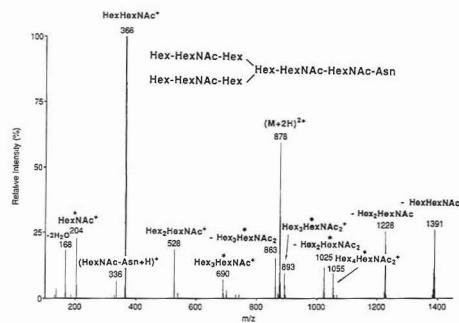


**Figure 3.** Product-ion MS/MS of  $m/z$  878.0 ( $M+2H$ ) $^{2+}$  for 500 pmol of Asn-linked oligosaccharide 1a. An asterisk (\*) indicates fragments formed by two-bond cleavages. Sum of 7 scans ( $m/z$  10–1800, step 1.0, 16.8 s/scan); orifice voltage = 55 V.

structures corresponding to smaller, intact molecules derived from the charged parent molecule by fragmentation and hydrogen rearrangement.

Because glycopeptides contain hexose or *N*-acetylhexosamine isomers which fragment in a predictable manner upon collisional excitation, it seemed reasonable that we would be able to recognize glycopeptides in a complex mixture by their characteristic collision-induced dissociation (CID) fragment ions. Moreover, such diagnostic fragment ions would allow selective identification of glycopeptide-containing chromatographic fractions during LC/MS analyses of enzymatic digests of glycoproteins. To test these hypotheses, we have employed pneumatically-assisted electrospray ionization on a triple-quadrupole mass analyzer in the configuration illustrated in Figure 2. Pneumatically-assisted electrospray has been shown previously to have advantages over continuous-flow fast atom bombardment for sensitive detection of glycopeptides.<sup>11</sup> Exploration of various normal and tandem MS scan modes (product-ion, precursor-ion, and neutral-loss) was initially performed on a small oligosaccharide model, Man<sub>1</sub>GlcNAc ( $M_r = 869.3$ ), and later on Asn-linked and Ser-linked oligosaccharides (Figure 1). The peptide-linked oligosaccharides were better glycopeptide models for our purposes in that formation of HexNAc $^+$  oxonium ion fragments required two-bond cleavages, as in true glycopeptides.

**Product-Ion Scanning for Model Glycopeptides.** The structurally-informative fragment ions shown in Figure 3 resulted from tandem MS selection of the ( $M+2H$ ) $^{2+}$  of the Asn-linked oligosaccharide (Figure 1a) for CID product-ion scanning. The results illustrate that low-energy (typically <150 eV) collisions of protonated glycopeptides yield an abundance of fragments that form by two-bond cleavages between saccharides (indicated by asterisks in the figure). Cleavages of the saccharide rings are not observed. Nearly all the observed fragmentation occurs along the branches (with charge localization either on GlcNAc-Asn or on the core GlcNAc adjacent to the mannose branch). Loss of one but not both of the branch arms is observed. The Hex-HexNAc $^+$  ion which is intense in this tandem mass spectrum might be expected to be relatively weaker in the case of high-mannose glycopeptides where formation of an equivalent ion requires loss not only of both branches but also of the GlcNAc-peptide core (a three-bond cleavage). We prefer  $m/z$  204 (HexNAc $^+$ ) as the most universal indicator of glycopeptides because its formation requires, in the worst case, only a two-bond cleavage, and because most O-linked carbohydrates are attached to Ser or Thr via *N*-acetylhexosamine.

**Neutral-Loss Scanning for a Model Oligosaccharide.** "Constant" or "fixed" neutral-loss scanning is a mode of

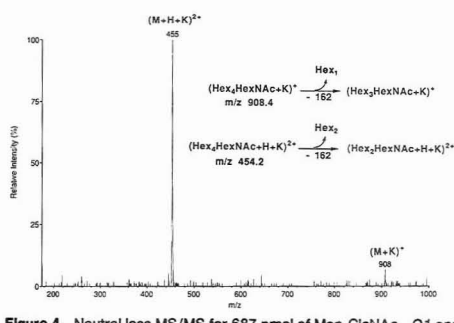


**Figure 4.** Neutral loss MS/MS for 687 pmol of Man<sub>1</sub>GlcNAc. Q1 and Q3 mass filters were offset one from the other by  $m/z$  161.8. Sum of 10 scans ( $m/z$  175–1000, step 0.2, 8.25 s/scan); orifice voltage = 80V.

analysis in which Q1 and Q3 are scanned synchronously but offset from one another by a constant, user selectable difference in the mass-to-charge ratio ( $m/z$ ). The only ions that arrive at the detector are those which dissociate in Q2, losing sufficient mass to be accepted by the offset second analyzer stage (Q3) of the triple quadrupole instrument. The spectrum displayed is that of the precursor ions (the Q1 scan).

So-called "constant neutral loss" scans require a little explanation for multiply-charged precursor ions. Although the two scanning quadrupoles, Q1 and Q3, are offset by a constant  $m/z$  difference in the ions they pass, the neutral loss in the collision gas region of Q2 cannot always be called "constant" because the mass will vary according to the charge state of the precursor ions. For example, in Figure 4 we observe neutral losses of Man<sub>1</sub> (162 Da) from the singly charged parent of Man<sub>1</sub>GlcNAc and loss of Man<sub>2</sub> (324 Da) from the double charged parent, in the same neutral-loss spectrum. In this case, the precursor and product  $m/z$  differ by 162 in both fragmentation pathways although the actual mass lost is different. Oddly, it would appear from the data that the neutral loss of dehydrohexose was derived not from the protonated molecule but from the potassium-cationized molecular species. The base peak in the normal-scan spectrum of this same compound corresponds to the ( $M+Na$ ) $^+$  while the ( $M+H$ ) $^+$  has a signal intensity equal to 25% of the base peak; neither are observed in the neutral loss data. Neutral-loss scans for an  $m/z$  difference of 203 (HexNAc) gave only weak data (not shown). Therefore, neutral-loss scanning for structure-specific detection in electrospray mass spectrometry, where observation of molecular ions with widely varying charge states is the rule rather than the exception, is not practical for our intended purposes. These difficulties also point to the need to modify the recommended terminology;<sup>22</sup> the words "constant" or "fixed" neutral loss are not appropriate in situations where there may be variation in the ion charge state. Here we have used the abbreviated term *neutral-loss scan*.

#### Precursor-Ion Scanning for Model Glycopeptides.

Precursor-ion scanning gives a spectrum of all precursor ions that dissociate to yield the selected product. This experiment provided useful information upon selection of the oxonium ions  $m/z$  204 (HexNAc $^+$ ) and  $m/z$  366 (Hex-HexNAc $^+$ , not shown) for the three model N-linked glycopeptides (Figure 1a–c) and the small O-linked glycopeptide Gal-GalNAc-Ser (Figure 1d). The spectra (Figure 5a–d) reveal predominantly unfragmented glycopeptide ion signals. Weak peaks which may arise from sample heterogeneity (loss of *N*-acetyl-

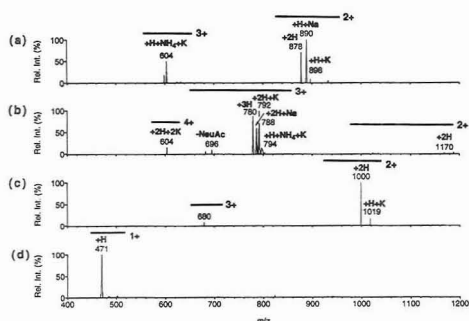


**Figure 5.** Comparison of precursor-ion MS/MS of  $m/z$  204.0 (HexNAc<sup>+</sup>) for 500 pmol of Asn-linked oligosaccharides 1a–d, respectively. Sum of 17 scans ( $m/z$  500–2100, step 0.5, 6.4 s/scan); orifice voltage = 55 V.

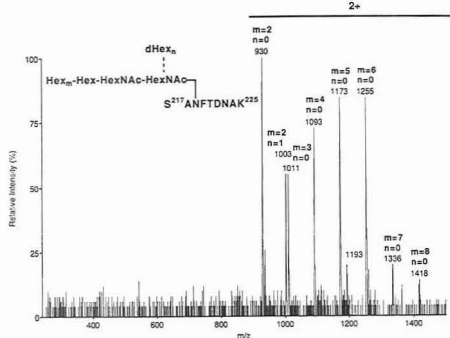


**Figure 6.** Precursor-ion MS/MS of  $m/z$  204.0 (HexNAc<sup>+</sup>) for ca. 120 pmol of an isolated oligomannose glycopeptide from the tryptic digest of gp120 glycoprotein.  $M_r(\text{av})$  for Hex<sub>9</sub>, dHex<sub>3</sub> = 2832.9. Sum of 24 scans ( $m/z$  250–1500, step 0.2, 12.5 s/scan); infusion rate 0.75  $\mu\text{L}/\text{min}$  in 1:1 MeOH–H<sub>2</sub>O with 10% acetic acid; orifice voltage = 90 V.

neuraminic acid) are observed in Figure 5b and can also be observed in pulsed amperometric detection HPLC for this same sample. However, it is not possible to reliably distinguish sample heterogeneity from fragmentation-derived sugar losses which result in ions of the same mass. The spectrum of the O-linked glycopeptide (Figure 5d) is similar to those obtained for the N-linked glycopeptides in that the only peaks observed were derived from protonated or cationized, intact glycopeptide. The information obtained is independent of the precursor-ion charge state, the type of glycopeptide (complex, as in Figure 5a,b, or oligomannose, as in Figure 5c) or whether it is N-linked or O-linked.

The precursor-ion scan experiment was repeated using glycopeptide-containing fractions isolated from glycoprotein digests by HPLC: an isolated oligomannose glycopeptide from gp120 and an isolated glycopeptide with a complex-type oligosaccharide from sCD4. For gp120, the mass spectra obtained by Q3 selection of either of the oxonium ion fragments  $m/z$  163 (Hex<sup>+</sup>) or 204 (HexNAc<sup>+</sup>) exhibited glycopeptide molecular weight related peaks clearly indicating the heterogeneity of the glycoforms at the given attachment sites; no interferences from peptide components in the isolated fractions were observed. For example, the precursor-ion scan of  $m/z$  204 for the gp120-derived glycopeptide (Figure 6) indicates that the carbohydrates attached are of the oligomannose class, varying in composition from Hex<sub>2</sub>HexNAc<sub>2</sub> to Hex<sub>9</sub>HexNAc<sub>3</sub>, in some cases with deoxyhexose (fucose) attached. For the glycopeptide with complex-type carbo-

hydrates from sCD4, selection of either the  $m/z$  204 (HexNAc<sup>+</sup>) or 366 (Hex-HexNAc<sup>+</sup>) product ions revealed the molecular weights of the various glycoforms (data not shown). In the case of sCD4, selection of  $m/z$  163 failed to yield precursor-ion spectra, presumably due to the absence of oligomannose glycopeptides for which this ion appears to be relatively selective. Although precursor-ion scans of the oxonium ions  $m/z$  147 (fucose) or  $m/z$  292 (*N*-acetylneuraminic acid) could be used to reveal the presence of these sugars, such information is in practice usually available from molecular weight considerations alone if the peptide sequence is also known. Collision-induced dissociation of glycopeptides to the HexNAc<sup>+</sup> oxonium ion ( $m/z$  204) has proven in these experiments to be general for oligosaccharides and glycopeptides containing *N*-acetylhexosamine either in the inner core or along the branches of the chains. Like peptide immonium ions, oxonium ion fragments can derive from two-bond cleavages. It seems likely that such multiple-bond cleavages are favored by low-energy, multiple collisions in carbohydrates as they are in peptides.<sup>23</sup> At present, we have not determined from which of the inner core *N*-acetylhexosamines the oxonium ion originates, although the data for the Gal-GalNAc-Ser glycopeptide clearly indicates that it can derive from the *N*-acetylhexosamine linking the carbohydrate to the peptide.

**Precursor-Ion Scanning LC/ESMS/MS and Normal LC/ESMS of a Tryptic Digest of sCR1 Glycoprotein.** Because  $m/z$  204 represents a fragment ion generic to all glycopeptide structural types, it was chosen for precursor-ion scanning LC/ESMS/MS experiments in which we used the mass spectrometer as a glycopeptide-specific HPLC detector, simultaneously acquiring mass spectral information on the molecular weight and heterogeneity of each glycopeptide during chromatography of a glycoprotein enzyme digest. We have performed this experiment on three reduced and carboxymethylated glycoprotein tryptic digests: sCD4 (two sites of glycosylation) (data not shown), GP120 (24 potential sites of *N*-glycosylation) (data shown for an isolated glycopeptide only, Figure 6), and sCR1 (25 potential sites of *N*-glycosylation) (Figures 7a, 8a, and 9). In addition we have compared these results with normal scanning LC/ESMS of the same digests. Representative data are discussed below.

The total ion current traces from precursor-ion scanning of  $m/z$  204 and normal  $m/z$  scanning during LC/ESMS of a tryptic digest of sCR1 are displayed in Figure 7a and 7b, respectively. The precursor-ion scan trace (Figure 7a) indicates 20 or more possible glycopeptides. The normal LC/ESMS total ion current trace (Figure 7b) is deceptively simple for there are more than 200 components that are poorly resolved even under the long gradient elution conditions used. In Figure 8 we compare the mass spectra for peak A (Figure 7) obtained by  $m/z$  204 precursor-ion scanning LC/ESMS/MS with the mass spectra obtained by normal scan LC/ESMS. Numerous peptide ion signals are observed in the normal  $m/z$  scan data (Figure 8b) (e.g.  $m/z$  617–665 and  $m/z$  860) together with the signals for the glycopeptide. In Figure 8a, the selectivity of the precursor-ion scanning method for glycopeptide detection is evident; we find a series of glycopeptide molecular weight-related signals separated by increments of *N*-acetylneuraminic acid and deoxyhexose, and there is no interference from nonglycosylated peptides. The mass spectrum of peak B from the precursor-ion LC/ESMS/MS experiment (Figure 9) represents a rather large biantennary glycopeptide ( $M_r(\text{av}) = 6221$  for the highest  $M_r$  component). Heterogeneity in the content of *N*-acetylneuraminic acid and deoxyhexose is again evident from the

(23) Bean, M. F.; Carr, S. A.; Thorne, G. C.; Reilly, M. H.; Gaskell, S. *J. Anal. Chem.* 1991, 63, 1473–1481.



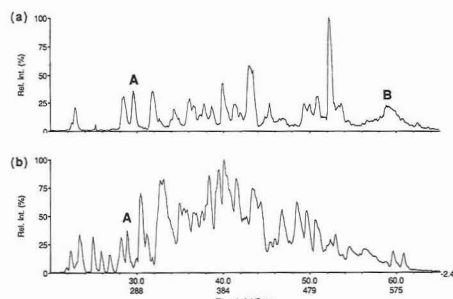


**Figure 7.** Comparison of total ion chromatograms for 800 pmol of a tryptic digest of reduced and carboxymethylated soluble complement receptor, type 1 (sCR1) scanned from  $m/z$  450 to 2400, step 0.3, 6.23 s/scan, orifice voltage = 80 V (not optimal): (a) precursor ions of  $m/z$  204 (HexNAC<sup>+</sup>), LC/ESMS/MS and (b) normal scan LC/ESMS.

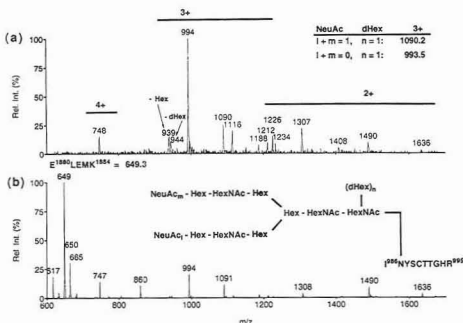


**Figure 8.** Comparison of the mass spectra for peak A (Figure 7a,b) obtained by (a) precursor-ion LC/ESMS/MS of  $m/z$  204 (HexNAC<sup>+</sup>) and (b) normal scan LC/ESMS.  $M_{(av)}$  of glycopeptide (NeuAc<sub>1</sub>, dHex<sub>1</sub>) = 3267.6. C = S-(carboxymethyl)cysteine.

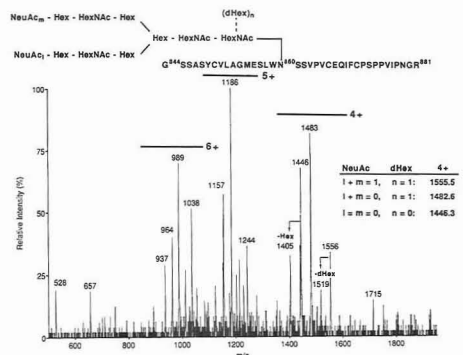


**Figure 9.** Precursor-ion (parents of  $m/z$  204.0) mass spectrum of region highlighted as peak B in Figure 7.  $M_{(av)}$  of glycopeptide (NeuAc<sub>1</sub>, dHex<sub>1</sub>) = 6221.2 (measured = 6219.7). C = S-(carboxymethyl)-cysteine.

$m/z$  spacings between peaks in the various parent-ion clusters. The spectra shown here are summed over the width of the chromatographic peak and therefore yield an approximate image of the glycoform heterogeneity at each of the given attachment sites.

The detected glycopeptides were assigned to their peptide context by subtracting the probable oligosaccharide mass from that of the glycopeptide, and then searching the protein sequence for candidate peptides with this mass that also contained the necessary consensus sequence for N-linked glycosylation (Asn-X-Ser/Thr). In the absence of any structural information on the carbohydrate, a list of possible peptide molecular weights is obtained by subtracting the masses of specific carbohydrate structures (guided by the known range of structures found on glycoproteins expressed in the given cell system) from the determined molecular weights of the glycopeptides. Of course this indirect method is only a starting point in the structural characterization. After the MS techniques described in this paper are used to locate glycopeptides in the chromatogram, the carbohydrate moieties of the isolated glycopeptides would be released by enzymatic or chemical means and the carbohydrates analyzed by other methods such as MS of the permethylated derivatives, or high-performance anion-exchange chromatography.<sup>24,25</sup>

**Collisional-Excitation Scanning.** In electrospray mass spectrometer systems the extent of fragmentation induced in the intermediate pressure region before the first mass filter (Q1) can be varied. Such collision-induced dissociations prior to mass analysis were an integral part of the design of early atmospheric pressure ionization sources, being used primarily to desolvate sample ions, although breaking of covalent bonds was also noted.<sup>26,27</sup> More recently, this technique of controlled fragmentation has been applied to partial sequencing of peptides.<sup>28,29</sup> On the Sciex instrument, CID before mass analysis is controlled by varying the voltage on the orifice itself (Figure 2). With an orifice voltage of 65 V, desolvation is achieved with minimal fragmentation, while 120 V results in marked fragmentation of covalent bonds. The effects of the two orifice voltages on the Asn-linked oligomannose glycopeptide 1c are shown in Figure 10a,b. In panel A, the orifice voltage was 140 V between  $m/z$  150 and 500, and then it was stepped down to 65 V from  $m/z$  501 to 2100; in panel B the orifice voltage was held constant at 120 V throughout the  $m/z$  scan. Although sequential loss of hexoses can be observed from the doubly-charged parent in both spectra, only the data from the constant high orifice potential experiment (Figure 10b) exhibits significant losses of from one to five hexoses from the singly charged molecule.

The orifice potential effects ion translational energy and the resultant conversion to excitation energy upon collisions with gas molecules in the analyzer region immediately after the orifice. This simple mode of CID has the advantage, when compared to tandem MS CID, of improved production resolution and ion intensity, but it has the disadvantage of not having any precursor-ion selectivity. Operating with higher orifice voltages has other implications: lower molecular charge states are favored, metal-cationized molecules often predominate over protonated molecules (presumably because they require higher excitation energies to dissociate), and overall sensitivity can be diminished for some samples. These effects are clearly illustrated in Figure 10, although we do not observe a sensitivity loss at higher orifice voltages for this

(24) Barr, J. R.; Anumula, K. R.; Vettesse, M. B.; Taylor, P. B.; Carr, S. A. *Anal. Biochem.* 1991, 192, 181-192.

(25) Carr, S. A.; Barr, J. R.; Roberts, G. D.; Anumula, K. R.; Taylor, P. B. *Methods Enzymol.* 1990, 193, 501-518.

(26) Buckley, J. A. Ph.D. Thesis, University of Toronto, Toronto, Canada, 1974.

(27) Buckley, J. A.; French, J. B.; Reid, N. M. *Can. Aeronaut. Space J.* 1974, 20, 231-233.

(28) Smith, R. D.; Loo, J. A.; Barinaga, C. J.; Edmonds, C. G.; Udseth, H. R. *J. Am. Soc. Mass Spectrom.* 1990, 1, 58-65.

(29) Katta, V.; Chowdhury, S. K.; Chait, B. T. *Anal. Chem.* 1991, 63, 174-178.



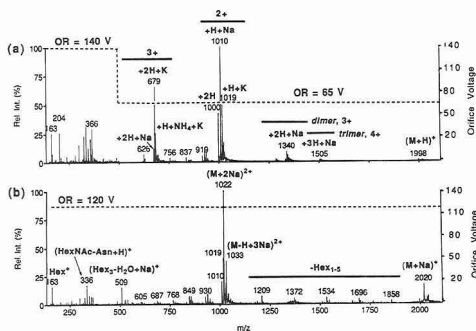


**Figure 10.** Comparison of the collisional-excitation scan mass spectrum (a) with the high orifice potential (120 V) scan spectrum (b) for 500 pmol of the triantennary oligomannose Asn-linked oligosaccharide illustrated in Figure 1c. Sum of 14 scans ( $m/z$  150–2100, step 0.33, 6 s/scan). The dotted line indicates that the orifice voltage was stepped from 140 to 65 V at  $m/z$  500 in (a) while it was maintained at a constant 120 V in (b).

molecule. The gas-phase molecular dimers and trimers seen at 65 V in Figure 10a are seen to dissociate at 120 V in Figure 10b.

Conboy and Henion<sup>15,16</sup> have shown that the use of high-orifice potentials throughout an LC/ESMS run resulted in abundant, diagnostic, low-mass fragments for glycopeptides. However, use of high-orifice potentials during the entire  $m/z$  scan can distort the apparent glycoform heterogeneity through fragmentation of the carbohydrate or peptide component of the glycopeptides; this is in contrast to spectra acquired with low orifice voltages where the molecular heterogeneity information provided by the data is relatively reliable. Some fragmentation of labile saccharide moieties occurs even at low orifice potentials (see Figure 10).

One means of maintaining the glycoform heterogeneity information and the sensitivity while inducing diagnostic fragmentation is to scan or step the orifice voltage (excitation energy) with mass (see the Experimental Section), as illustrated in Figure 10. During the low  $m/z$  portion of the scan (up to ca.  $m/z$  500), the high orifice voltage results in CID prior to the first mass analyzer and yields characteristic fragment-ion signals for the carbohydrate portion of the glycopeptide. These low-mass fragments include the oxonium ions and their related water-loss peaks, Hex<sup>+</sup> ( $m/z$  163), HexNAc<sup>+</sup> ( $m/z$  204), NeuAc<sup>+</sup> ( $m/z$  292), and Hex-HexNAc<sup>+</sup> ( $m/z$  366), as illustrated in Figures 10 and 11. The higher potential setting of the orifice was found to optimize at ca. 140 V for production of HexNAc<sup>+</sup> fragments using the oligomannose glycopeptide. The relatively low (65 V) orifice voltage used for the higher  $m/z$  region of the scan ( $m/z$  >500) declusters any attached solvent adducts but is insufficient to produce appreciable fragmentation so that intact glycopeptide ions predominate. The combination of the two orifice voltages in a single scan results in production of diagnostic, sugar-related fragments at the low  $m/z$  end and parent ions of intact glycopeptides at the high  $m/z$  end of the mass spectrum. We refer to this novel scanning procedure as *collisional-excitation scanning*. Such experiments can readily be performed on single quadrupoles outfitted with an electrospray ionization source. The Sciex data system permits linear scanning or stepped changes in the orifice potential; for simplicity we prefer the single step approach.

Collisional-excitation scan MS of the oligomannose Asn-linked glycopeptide model (Figure 1c) produces a variety of ion signals for the intact molecule (Figure 10) involving combinations of H<sup>+</sup>, NH<sub>4</sub><sup>+</sup>, Na<sup>+</sup>, and K<sup>+</sup> cations with one to

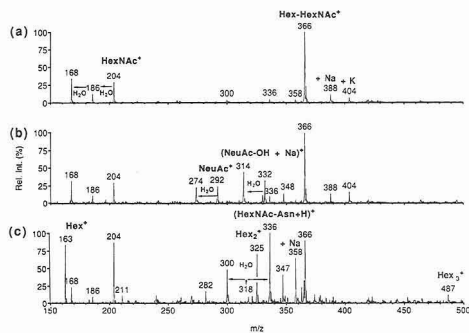


**Figure 11.** Comparison of the low  $m/z$  regions of the collisional-excitation scan mass spectra for 500 pmol of the Asn-linked oligosaccharides illustrated in Figure 1a–c, respectively. Orifice voltage was at 140 V from  $m/z$  150 to 500. See legend to Figure 10 for other details.

three charges per molecule as well as gas-phase dimers and trimers. We have found that commercially available oligosaccharide standards are often laden with salts, probably due to methods of isolation and purification which are not tailored to mass spectral analyses. No attempt was made to drive the cationization to one species other than to acidify the solvents with formic or acetic acid (see the Experimental Section). The spectral complexity observed in the flow injection ESMS analysis of commercially available glycopeptide models is largely due to the presence of excess salts that produce a variety of cationized forms. These complexities are not observed in LC/ESMS or LC/ESMS/MS analyses of glycoprotein digests employing salt-free, acidified mobile phases. In these cases proton transfer is the dominant cationization process observed (see Figures 8 and 9).

The low  $m/z$  region of the collisional-excitation scan mass spectra (Figure 11) for the three glycopeptide models of Figure 1 illustrate that there are two intense fragment ion signals common to both complex and high-mannose branched glycopeptides:  $m/z$  204 (HexNAc<sup>+</sup>) and 366 (Hex-HexNAc<sup>+</sup>). Signals at  $m/z$  163 (Hex<sup>+</sup>) are predictably more intense in the high-mannose spectra while 292 (NeuAc<sup>+</sup>) is distinctive for *N*-acetylneuraminic acid-containing glycopeptides. Because there are not terminal *N*-acetylhexosamines in any of these molecules, it is clear that the HexNAc<sup>+</sup> fragment ions must arise from two-bond cleavages.

## CONCLUSIONS

The data presented in this paper illustrate the utility of precursor-ion scanning LC/ESMS/MS for glycopeptide detection at a sensitivity level nearly equivalent to that of normal scan LC/ESMS but with greater specificity. The loss of resolution in the MS/MS method does not adversely affect interpretation of the data, although it is possible that poorer mass accuracy in LC/ESMS/MS might make distinction of hexosamines and hexoses (1-Da difference) problematic, if hexosamines were part of the structure. We should note that precursor-ion scanning for  $m/z$  204 occasionally detected peptides that fragmented to yield  $m/z$  204; for instance, in the sCD4 data (now shown) an intense  $y + 2H$  fragment ion corresponding to Gly-Lys from the tryptic peptide Val-Val-Leu-Gly-Lys was observed. The collisional-excitation LC/ESMS method, although a rather less selective method of glycopeptide detection, does allow simultaneous peptide mapping and improved sensitivity and mass accuracy and in

favorable cases has sufficient resolution to identify doubly-charged ions by their 0.5  $m/z$  isotope-cluster signals. We envision the two techniques to be complementary and use both in our analyses of glycoproteins.

There has been no effort in this paper to probe the *limits of analysis*, defined as the least quantities of analyte for which tandem mass spectra of essentially uncompromised quality could be obtained,<sup>23</sup> for the glycopeptide-specific LC/ESMS/MS. While the present studies have been carried out at the high picomole level of protein digest, we have successfully carried out identical studies on glycoproteins using as little as 25 pmol of material.<sup>17</sup> Improvements in sensitivity are due largely to the use of smaller internal diameter HPLC columns (packed fused-silica capillaries with i.d.  $\leq 0.32$  mm). By virtue of the very small peak elution volumes of these columns, the absolute concentration of peptide and glycopeptide entering the mass spectrometer is increased relative to the same amount of sample applied to a larger bore column.

A drawback to the use of these columns is that fraction collection is more difficult. Columns with diameters of 0.5 mm and larger therefore have an advantage since they permit collecting of fractions for further characterization of the oligosaccharide and peptide components where necessary.

#### ACKNOWLEDGMENT

The excellent technical assistance of Todd Armbruster in preparation of the sCR1 digest and of John Barr for digestion and isolation of the gp120 glycopeptide is gratefully acknowledged. We also thank James Conboy for useful discussions. This work was supported in part by a grant from the National Institutes of Health (GM-39526) to S. A. Carr.

RECEIVED for review September 28, 1992. Accepted December 22, 1992.

# Chiral Separation of Basic Drugs Using Cyclodextrin-Modified Capillary Zone Electrophoresis

Michel W. F. Nielen

Akzo Research Laboratories Arnhem, Corporate Research, Analytical and Environmental Chemistry Department, P.O. Box 9300, 6800 SB Arnhem, The Netherlands

Capillary zone electrophoresis (CZE) was successfully applied to the chiral separation of basic drugs after addition of a suitable cyclodextrin chiral selector to the electrophoresis buffer. Commercially available cyclodextrins ( $\alpha$ -,  $\beta$ -, and  $\gamma$ -cyclodextrin and heptakis(2,6-di-O-methyl)- $\beta$ -cyclodextrin) were evaluated for their enantioselectivity toward 10 compounds having rather complex molecular structures. In contrast to liquid chromatographic attempts, the enantiomers of all racemates investigated could be resolved with a resolution of more than 1.4, except for one ( $R_S$  1.1), and showed theoretical plate numbers up to 265,000 with good peak shapes. Apart from well-known parameters such as the concentration of the chiral selector added, the resolution was found to depend strongly on the applied field strength. It is shown and explained that the impact of the field strength on the electrophoretic mobilities and the coefficient of electroosmotic flow, and thus on the resolution, cannot be ignored, particularly at enantio-separations of cationic compounds. Quantitative aspects of chiral separations were studied, showing that less than 0.5% of an isomeric impurity, relative to the main optical isomer, can be determined while maintaining good accuracy, acceptable resolution, and good precision. The feasibility of increased sample throughput by injection of next samples while previous separation(s) are still in progress is demonstrated. The results obtained clearly show the potential of cyclodextrin-modified CZE toward quality control of enantioselective syntheses, enantio-purification schemes, and pharmaceutical formulations.

## INTRODUCTION

The separation of enantiomers is of primary importance in pharmaceutical analysis. Liquid chromatography (LC),<sup>1-3</sup> capillary gas chromatography (GC),<sup>4,5</sup> and supercritical fluid chromatography (SFC)<sup>6</sup> can be used for enantioselective separations. Since many drugs are rather involatile, polar, or even ionic, it is obvious that separation in the liquid phase will be favored. The main disadvantages of LC approaches using chiral stationary phases are (i) the columns are relatively expensive; (ii) the performance is often much lower than with regular LC columns; and (iii) many different types of these LC columns are required in order to cover a relatively narrow

range of racemic compounds. Capillary zone electrophoresis (CZE) offers rapid and efficient separations of ionic and ionizable compounds.<sup>7</sup> Initially, CZE was applied mainly to the field of biochemical analyses, but in recent years, its applicability has been demonstrated in all fields of chemical analysis.<sup>8,9</sup> CZE might be an attractive alternative for enantio-separations; one single CZE capillary can be subsequently filled with electrophoresis buffers containing different chiral selectors. Contrary to LC approaches with a chiral selector dissolved in the mobile phase, interactions of the enantiomers with the chiral selector will not be hindered by a packed stationary phase. Moreover, thanks to the small volume of a CZE system, rather expensive or commercially unavailable chiral selectors can be applied. Examples of chiral selectors used in CZE are maltodextrins,<sup>10</sup> bile salts,<sup>11,12</sup> chiral functionalized micelles,<sup>13</sup> cyclodextrins,<sup>14-25</sup> crown ethers,<sup>22</sup> cyclodextrins combined with SDS micelles,<sup>26</sup> cyclodextrins incorporated into a gel matrix,<sup>27</sup> and cyclodextrins coated on the capillary wall.<sup>28</sup> The cyclodextrins represent a range of cyclic glucopyranoses having a characteristic conical shape with a hydrophobic cavity and a polar exterior. Cyclodextrins (CD's) and their alkylated derivatives are able to form inclusion complexes with many substances, including racemic drugs. The complex constants are primarily determined by the size, geometry, hydrophobicity, and hydrogen-bonding

(7) Jorgenson, J. W.; Lukacs, K. D. *Anal. Chem.* 1981, 53, 1298-1302.

(8) Kuhn, W. G.; Monnig, C. A. *Anal. Chem.* 1992, 64, 389R-407R.

(9) Kuhn, W. G. *Anal. Chem.* 1990, 62, 403R-414R.

(10) Hulst, A. D.; Verbeke, N. Presented at the 4th International Symposium on High Performance Capillary Electrophoresis, Amsterdam, 1992.

(11) Cole, R. O.; Sepaniak, M. J.; Hinze, W. L. *J. High Res. Chromatogr.* 1990, 13, 579-582.

(12) Nishi, H.; Fukuyama, T.; Matsuo, M.; Terabe, S. *J. Chromatogr.* 1990, 515, 233-243.

(13) Dobashi, A.; Ono, T.; Hara, S.; Yamaguchi, J. *J. Chromatogr.* 1989, 480, 413-420.

(14) Snopek, J.; Jelinek, I.; Smolkova-Keulemansova, E. *J. Chromatogr.* 1988, 452, 571-590.

(15) Snopek, J.; Soini, H.; Novotny, M.; Smolkova-Keulemansova, E.; Jelinek, I. *J. Chromatogr.* 1991, 559, 215-222.

(16) Fanali, S. *J. Chromatogr.* 1989, 474, 441-446.

(17) Fanali, S.; Bocsk, P. *Electrophoresis* 1990, 11, 757-760.

(18) Fanali, S. *J. Chromatogr.* 1991, 545, 437-444.

(19) Sepaniak, M. J.; Cole, R. O.; Clark, B. K. *J. Liq. Chromatogr.* 1992, 15, 1023-1040.

(20) Wren, S. A. C.; Rowe, R. C. *J. Chromatogr.* 1992, 603, 235-241.

(21) Peterson, T. E.; Trowbridge, D. *J. Chromatogr.* 1992, 603, 298-301.

(22) Kuhn, R.; Stoeckel, F.; Erni, F. *Chromatographia* 1992, 33, 32-36.

(23) Ueda, T.; Kitamura, F.; Mitchell, R.; Metcalf, T.; Kuwana, Th.; Nakamoto, A. *Anal. Chem.* 1991, 63, 2979-2981.

(24) Cruzado, I.; Rawjee, Y.; Vigh, G. Presented at the 4th International Symposium on High Performance Capillary Electrophoresis, Amsterdam, 1992.

(25) Pluym, A.; van Ael, W.; de Smet, M. *Trends Anal. Chem.* 1992, 11, 27-32.

(26) Nishi, H.; Fukuyama, T.; Terabe, S. *J. Chromatogr.* 1991, 553, 503-516.

(27) Guttman, A.; Paulus, A.; Cohen, A. S.; Grinberg, N.; Karger, B. L. *J. Chromatogr.* 1988, 448, 41-53.

(28) Mayer, S.; Schurig, V. *J. High Res. Chromatogr.* 1992, 15, 129-131.

(1) Allenmark, S. G. *Chromatographic enantioseparation: Methods and applications*; Ellis Horwood: Chichester, 1988.

(2) Stouter, R. W. *Chromatographic separation of stereoisomers*; CRC Press: Boca Raton, FL, 1985.

(3) Maris, F. A.; Vervoort, R. J. M.; Hindriks, H. *J. Chromatogr.* 1991, 547, 45-58.

(4) Venema, A.; Henderiks, H.; van Geest, R. *J. High Res. Chromatogr.* 1991, 14, 676-680.

(5) Schurig, V.; Schleimer, M.; Jung, M.; Grosenick, H. Presented at the 14th International Symposium on Capillary Chromatography, Baltimore 1992.

(6) Juvancz, Z.; Markides, K. E. *LC-GC Int.* 1992, 5, 44-56.

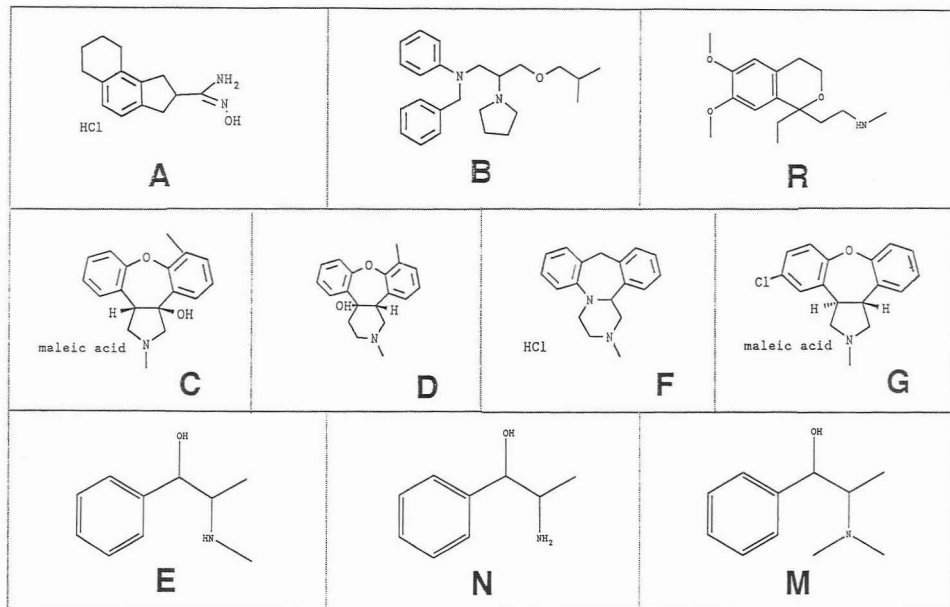


Figure 1. Molecular structures of the racemic drugs investigated.

ability of the analytes. Generally, the electrophoretic mobility of a CD-analyte complex will be much lower than the mobility of the free (uncomplexed) molecule. Consequently, separation of enantiomers will occur, provided that the complexation constants of the optical isomers are different. Chiral separations performed by cyclodextrin-modified CZE so far show baseline resolution and high plate numbers ( $N > 100\,000$ ) for derivatized amino acids, ephedrines, and epinephrines.<sup>16-19</sup> The feasibility toward structurally more complex drugs, such as thioridazines, ketotifen drugs, and quinagolide, has been demonstrated recently by Snopek et al.<sup>15</sup> and Kuhn et al.<sup>22</sup> In this study, cyclodextrin-modified CZE has been applied to the chiral separation of structurally complex basic drugs (Figure 1), most of them belonging to the cardiovascular or CNS-active compounds. Some ephedrines were included for comparison purposes. The impact of the applied field strength on the resolution, thus far ignored as an optimization parameter in cyclodextrin-modified CZE, has been studied in more detail. In addition, quantitative aspects of chiral separations using CZE have been studied, showing both the dependence of the resolution on the enantiomer ratio, the accuracy associated with, as well as calibration and precision data. The feasibility of increased sample throughput while maintaining adequate resolution has been studied preliminary. Data obtained have been compared critically with other LC<sup>3</sup> and CZE studies.

## EXPERIMENTAL SECTION

**Apparatus.** An Applied Biosystems (San Jose, CA) Model 270A capillary electrophoresis system<sup>23</sup> was used, equipped with a variable-wavelength UV absorbance detector and operated at 200 nm and a 0.5-s rise time. CZE was performed in a 70-cm  $\times$  50- $\mu$ m-i.d. fused silica capillary (Applied Biosystems); the length

to the detection window was 50 cm. A 70-cm  $\times$  50- $\mu$ m-i.d. C18-coated fused silica capillary (CElect-H250, Supelco, Bellefonte, PA) was used for some of the experiments. Separations were carried out in the constant voltage mode. The oven temperature was set at 30 °C, unless stated otherwise. Samples were introduced into the capillary via a controlled vacuum system; the injection time was 0.5 s which corresponds to a volume of approximately 1.5 nL (precision better than 1-2% according to the specs from the manufacturer). Sample injections were followed by a 0.5-s injection of water in order to wash the electrode and the outside of the fused silica capillary. Data were recorded using a Fisons Model VG-Multichrom integration system.

**Reagents.** Tris(hydroxymethyl)aminomethane (TRIS),  $\alpha$ -cyclodextrin,  $\beta$ -cyclodextrin,  $\gamma$ -cyclodextrin, (+)- and (-)-*N*-methyl-ephedrine, *D*-(+)-norephedrine hydrochloride, *L*-(-)-norephedrine, (+)-ephedrine hydrochloride, and (-)-ephedrine were obtained from Fluka (Buchs, Switzerland). Ephedrine, norephedrine, and *N*-methyl-ephedrine have been abbreviated in Figure 1 as E, N, and M, respectively. Heptakis(2,6-di-*O*-methyl)- $\beta$ -cyclodextrins were obtained from Sigma (St. Louis, MO) and Cyclolab (Budapest, Hungary). The other drugs under investigation (A, B, R, C, D, F, and G in Figure 1) were kindly provided by Organon Research (Akzo Pharma, Oss, The Netherlands); some of them have been used before in LC studies using chiral stationary phases.<sup>3</sup> All other chemicals were analytical-grade and obtained from J. T. Baker (Deventer, The Netherlands). Water was purified in an Alpha-Q (Millipore, Bedford, MA) apparatus.

**Procedures.** Electrophoresis buffers were prepared by dissolving 30 or 60 mM TRIS-base in water and adjusting the pH with concentrated phosphoric acid to the value desired (pH 2.4-3.3). CD's were dissolved in TRIS-phosphate buffer. Buffers were filtered through 0.45- $\mu$ m Spartan 30/B membrane filters (Schleicher & Schuell, Dassel, Germany) prior to use. Stock solutions of the drugs (1 mg/mL) were prepared in water, acidified with phosphoric acid to pH 2.5. Sample solutions were prepared by 10-30-fold dilution of the stock solutions with the electrophoresis buffer. The resolution between the optical isomers was

(29) Moring, S. E.; Colburn, J. C.; Grossman, P. D.; Lauer, H. H. *LC-GC Int.* 1990, 3, 46-54.

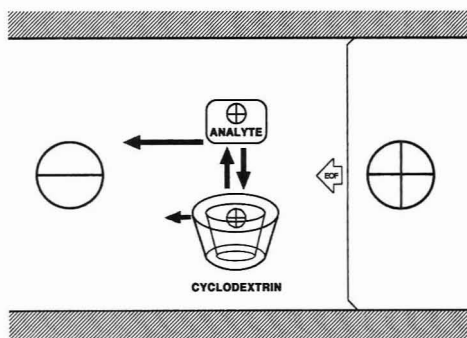


Figure 2. Separation mechanism in cyclodextrin-modified CZE.

calculated by using the triangle method<sup>30</sup> and the equation

$$R_S = 2[(t_2 - t_1)/(w_2 + w_1)] \quad (1)$$

in which  $t$  is the migration time and  $w$  the peak width. Plate numbers, apparent and electrophoretic mobilities, and the coefficient of electroosmotic flow were calculated using the equations in ref 31.

## RESULTS AND DISCUSSION

**Separation Principles.** The separations of the basic racemic drugs were carried out at acidic pH (2.4–3.3) throughout this study. Consequently the drugs and their CD complexes migrate toward the cathode as shown in Figure 2. The free CD's are uncharged and will move with the velocity of the electroosmotic flow, which is very low in this pH range. The CD's can be considered as a pseudostationary phase. One might argue that "electrokinetic capillary chromatography" (EKC)<sup>28</sup> should be the name for this separation mode. However, most of the EKC papers deal with uncharged analytes; in this work, the analytes do have a charge and are subjected to electric force. Therefore, "cyclodextrin-modified CZE" is to be preferred and used throughout this paper. Contrary to LC methods, an uncharged sample matrix (e.g. an excess of a chiral selector originating from an industrial enantiopurification process) does not interfere with the separation since the cationic analytes migrate much more rapidly than the neutral matrix components, the latter being simply washed out prior to the separation of the next sample. The separation in CD-modified CZE can be optimized by selection of a suitable CD type<sup>15</sup> (including mixtures of CD's<sup>19</sup>), the concentration of the CD,<sup>20,22</sup> the temperature<sup>22</sup>, the addition of other solvents such as alcohols or acetonitrile,<sup>18,20,22</sup> the choice of the counteranion,<sup>17</sup> and the pH<sup>19</sup> of the electrophoresis buffer. Recently, a theoretical model has been developed which predicts that the difference in apparent mobility of the optical isomers versus the concentration of CD will show a maximum. Unfortunately, band broadening due to diffusion, mass transfer and the electroosmotic flow were not included in the model for convenience. It should be noted that even small values of the electroosmotic flow might be significant for the resolution of basic compounds. The resolution equation in CZE,<sup>7</sup> assuming dispersion to be diffusion controlled only,

$$R_S = (0.25 \times N^{0.5}) [(\mu_{ep1} - \mu_{ep2})/(\mu_{epm} + \mu_{eof})] \quad (2)$$

in which  $\mu_{ep}$  is the electrophoretic mobility of the analyte,  $\mu_{epm}$  the mean of the two electrophoretic mobilities,  $\mu_{eof}$  the coefficient of electroosmotic flow, and  $N$  the number of theoretical plates, predicts that the maximum resolution will be obtained when the electroosmotic flow is in the opposite direction of the electrophoretic migration. In the present situation, the direction will be the same and the impact of changes in the (absolutely small) coefficient of electroosmotic flow and changes in the electrophoretic mobilities cannot be ignored, as will be shown below. Because of this, emphasis on resolution optimization rather than apparent mobility differences was preferred.

**Selection of Cyclodextrins.**  $\alpha$ -CD,  $\beta$ -CD, and  $\gamma$ -CD have increasing inner diameters of the hydrophobic cavity. The optimum fit of the compounds investigated (Figure 1) will be most likely a combination of inclusion of the aromatic part(s) and hydrogen bonding with a secondary hydroxyl group at the rim of the CD. The commercially available alkylated CD's are suspected for being mixtures.<sup>24</sup> Two brands of heptakis(2,6-di-*O*-methyl)- $\beta$ -CD's were compared for the separation of compounds B, F, N, and E. The results are shown in Figure 3A,B. The resolution for norephedrine (N) is the same and for ephedrine (E) only slightly different ( $R_S$  1.36 versus 1.27), but for compounds F ( $R_S$  1.61 versus 1.07) and B ( $R_S$  0.59 versus 0.66), different brands show significantly different enantioselectivities. The chiral separation of *N*-methylephedrine (M), not included in earlier ephedrine-type studies,<sup>16–18,21</sup> could be easily performed in the same CZE system, with high efficiency (144,000 plates) and baseline resolution ( $R_S$  1.56). Also mixtures of norephedrine and *N*-methylephedrine enantiomers could be resolved; however, mixtures of ephedrine and *N*-methylephedrine enantiomers showed partial overlap between (–)-*N*-methylephedrine and (+)-ephedrine. Baseline resolution of ephedrine racemates can be obtained after pH optimization (pH 10.0);<sup>32</sup> addition of heptakis(2,6-di-*O*-methyl)- $\beta$ -CD should be adequate for obtaining chiral separation of an *N*-methylephedrine and ephedrine mixture. No chiral separation could be obtained for norephedrine (N) and *N*-methylephedrine (M) using nonalkylated  $\alpha$ -,  $\beta$ -, or  $\gamma$ -CD. Only ephedrine (E) could be partially resolved using a system with 20 mM  $\beta$ -CD (saturated solution at room temperature) as a chiral selector. Increasing the saturation level of  $\beta$ -CD by specific additives such as urea might be an option<sup>33</sup> but was not considered in this work since the presence of an excess of urea might counteract the resolution improvement obtained at higher  $\beta$ -CD concentrations.<sup>34</sup> From the tetracyclic compounds C, D, F, and G, the F enantiomers could be resolved in any CD system except for the  $\alpha$ -CD. The  $\gamma$ -CD system, however, required rather high CD concentrations (100 mM) while showing less resolution than the  $\beta$ -CD or the heptakis(2,6-di-*O*-methyl)- $\beta$ -CD system.  $\beta$ -CD systems showed enantioselectivity toward all of the tetracyclic racemates. Minor differences in the molecular structure (cf. C, D, F, and G) had a strong impact on the resolution obtained. A typical electropherogram is shown in Figure 4. The double-charged F enantiomers migrate with the highest mobility (see also Figure 3). The structurally similar C and D enantiomers are almost baseline resolved. The G enantiomers, being the most hydrophobic, show the highest affinity for the  $\beta$ -CD selector; without  $\beta$ -CD, compound G is the second peak, but with  $\beta$ -CD added, the electrophoretic mobility decreased by a factor of 1.8. The C and G enantiomers could not be resolved with other CD's as chiral selector. The D enantiomers, on the other hand, showed

(32) Liu, Y.-M.; Sheu, S. J. *J. Chromatogr.* 1992, 600, 370–372.

(30) Snyder, L. R.; Kirkland, J. J. *Introduction to Modern Liquid Chromatography*, 2nd ed.; John Wiley & Sons, Inc.: New York, 1979; Chapter 2.

(31) Nielsen, M. W. F. *J. Chromatogr.* 1991, 542, 173–183.

(33) Pharr, D. Y.; Fu, Z. S.; Smith, T. K.; Hinze, W. L. *Anal. Chem.* 1989, 61, 275–279.

(34) Altria, K. D.; Goodall, D. M.; Rogan, M. M. *Chromatographia* 1992, 34, 19–24.

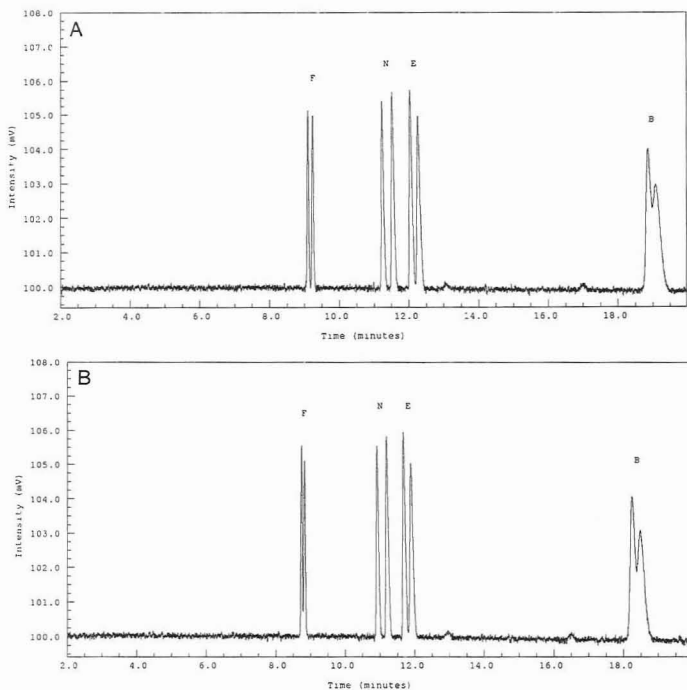


**Figure 3.** Separation of F, N, E, and B enantiomers using heptakis(2,6-di-O-methyl)- $\beta$ -CD obtained from two different manufacturers: (A) Sigma and (B) Cyclolab. Conditions: buffer, 30 mM TRIS-phosphate (pH 2.5) with 40 g/L of the alkylated  $\beta$ -CD; CZE at +30 kV and 30 °C, sample, F and B, 0.1 mg/mL; N and E,  $2 \times 10^{-4}$  M in buffer; other conditions, see the Experimental Section.

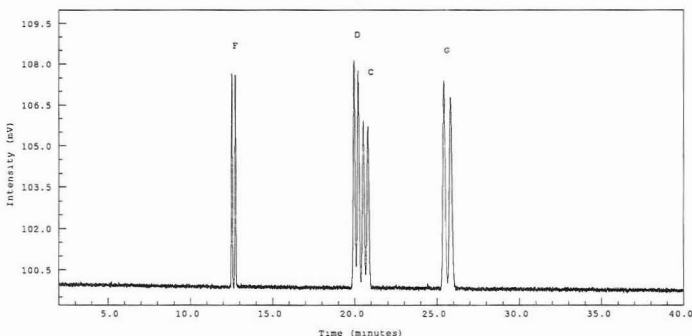


**Figure 4.** Separation of F, D, C, and G enantiomers in a  $\beta$ -CD system. Conditions: buffer, 30 mM TRIS-phosphate (pH 3) with 20 mM  $\beta$ -CD; CZE at +15 kV and 30 °C; samples, 0.1 mg/mL in buffer; other conditions, see the Experimental Section.

better resolution in an  $\alpha$ -CD system. Actually, the cavity of an  $\alpha$ -CD is too small for inclusion of the tetracycline compounds. In the case of the D enantiomers, however, the unsubstituted aromatic ring will enter the cavity while the hydroxyl group is in a favorable position for hydrogen bonding with the secondary hydroxyl groups at the rim of the CD. The electropherogram thus obtained is shown in Figure 5. It can be seen that the same system provided baseline resolution for the R enantiomers. Initially, the chiral separation of the A isomers turned out to be difficult; only the  $\beta$ -CD system provided some enantioselectivity ( $R_S$  0.63). It has been suggested that an increase in buffer concentration will

intensify the hydrophobic interactions with  $\beta$ -CD and increase the enantioselectivity.<sup>22</sup> Following that approach, the resolution of the A enantiomers was found to increase beyond unity at 60 mM TRIS-phosphate (Figure 6A) and even further at 100 mM.

The best separation performances obtained after screening of the  $\alpha$ -,  $\beta$ -, and  $\gamma$ -CD's and heptakis(2,6-di-O-methyl)- $\beta$ -CD's for their enantioselectivity toward the compounds shown in Figure 1 have been summarized in Table I. From this table it can be seen that all basic drugs studied show resolutions of more than 1.4, except for racemate A ( $R_S$  1.1). It should be noted that LC methods did not provide any



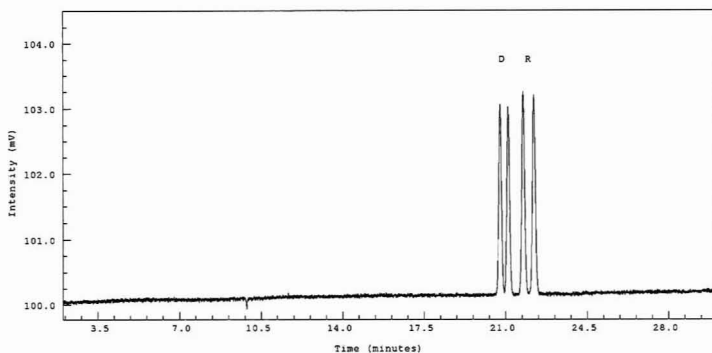


**Figure 5.** Separation of D and R enantiomers in an  $\alpha$ -CD system. Conditions: buffer, 30 mM TRIS-phosphate (pH 2.5) with 60 mM  $\alpha$ -CD; other conditions, see Figure 4.

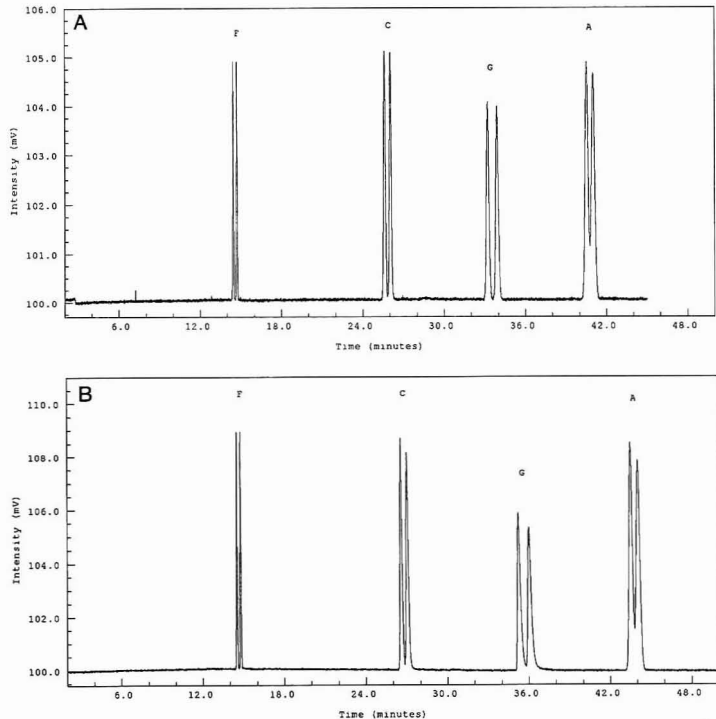


**Figure 6.** Separation of F, C, G, and A enantiomers in a  $\beta$ -CD system. Conditions: buffer, 60 mM TRIS-phosphate (pH 2.5) with 20 mM  $\beta$ -CD; CZE at +15 kV and 26 °C; samples, 0.1 mg/mL in buffer. CZE was performed in (A) an uncoated fused silica and (B) a C18-coated fused silica capillary. Other conditions, see the Experimental Section.

resolution for the enantiomers of compounds B and C, and the enantioseparation of A, D, F, and G by LC required the use of three different columns.<sup>3</sup> Contrary to LC results, peak symmetries in cyclodextrin-modified CZE are very good, and the plate numbers are up to 100-fold higher.

**Coated Capillaries.** Basic analytes are suspected for unintended interactions with uncoated fused silica capillaries. One way of suppression of these interactions is the use of coated CZE capillaries. In fact, early studies showing chiral separations of ephedrines and epinephrines by cyclodextrin-modified CZE were performed in polyacrylamide-coated capillaries.<sup>16-18</sup> We compared a C18-coated capillary with a

fused silica capillary, using the separation of Figure 6A as a model system. The result is shown in Figure 6B. From these figures, hardly any differences and certainly no improvements with the coated capillary can be seen. Migration times, resolutions, and plate numbers were similar, except for compound G; the plate number showed a decrease of ca. 20% and the peak showed considerable tailing in the coated capillary. Probably a relatively stronger hydrophobic interaction of compound G with the C18 phase is responsible for this observation. It was concluded that the excess of protonated amine (TRIS-phosphate buffer) and the acidic pH were sufficient means to suppress ionic interactions with

Table I. Optimum Separation Performance after Screening of Electrophoresis Buffers, Containing Different CD's, for Their Enantioselectivity toward the Racemic Drugs Shown in Figure 1

	compound									
	A	B	R	C	D	F	G	E	N	M
resolution	1.12	1.41	1.91	1.58	1.51	2.32	1.86	2.02	3.04	1.97
plate number	145 000	120 000	140 000	147 000	136 000	265 000	141 000	138 000	166 000	127 000
analysis time (min)	41	53	23	26	22	15	34	30	28	29
temperature (°C)	26	26	30	26	30	26	26	26	26	30
voltage (kV)	+15	+15	+15	+15	+15	+15	+15	+15	+15	+15
CD type	$\beta$	DM $\beta$	$\alpha$	$\beta$	$\alpha$	$\beta$	$\beta$	DM $\beta$	DM $\beta$	DM $\beta$
CD concn (mM)	20	40 <sup>a</sup>	60	20	60	20	20	40 <sup>a</sup>	40 <sup>a</sup>	40 <sup>a</sup>
TRIS concn (mM)	60	30	30	60	30	60	60	30	30	30
pH	2.5	2.5	2.5	2.5	2.5	2.5	2.5	2.5	2.5	2.5

<sup>a</sup> DM $\beta$  concentrations in grams per liter.

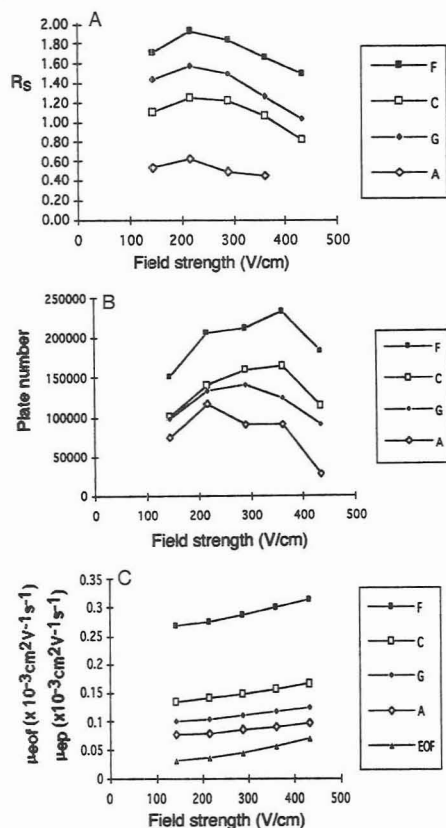


Figure 7. Impact of the applied field strength on (A) the resolutions, (B) the mean plate numbers, and (C) the mean electrophoretic mobilities of the enantiomers of F, C, G, and A. Conditions: see Figure 4, except for the pH, which was adjusted to 2.5.

the uncoated fused silica capillary, which was used further in all other experiments.

**Impact of the Applied Field Strength.** The impact of the applied field strength on the resolution was studied using the chiral separation of the F, C, G, and A racemates in the  $\beta$ -CD system. Conditions were the same as in Figure 4, except for the pH which was adjusted to pH 2.5. CZE was performed at 10, 15, 20, 25, and 30 kV, corresponding to field strengths

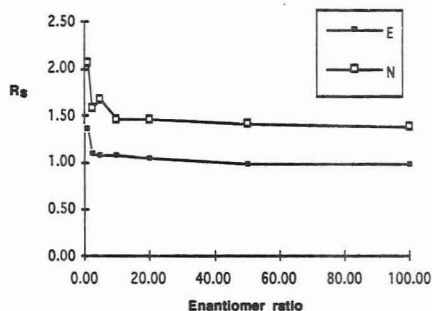


Figure 8. Resolution of N and E enantiomers versus the ratio of the (+) and (-) isomers. Conditions, see text.

of 144, 216, 289, 361, and 433 V/cm, respectively. The resolutions obtained showed optimum values at 15 kV (Figure 7A) and a rapid decrease at higher field strengths. The interaction of the analytes with the CD's (and thus the enantioselectivity) is diffusion-controlled and requires sufficient separation time; too high migration velocities will decrease the resolution. Interestingly, plots of the differences in apparent (or electrophoretic) mobilities of the enantiomers did not show any significant dependence on the applied field strength. Consequently optimization considering mobility differences only yields misleading results. Plots of the number of theoretical plates versus the field strength should show a linear dependence in CZE provided that dispersion is diffusion controlled only.<sup>7</sup> The situation is more complex in cyclodextrin-modified CZE, as can be seen in Figure 7B. It should be noted that the nonlinearity is unlikely caused by Joule heating. According to Nelson et al.,<sup>35</sup> the contribution of the radial temperature gradient—caused by Joule heating—to the total dispersion, must be negligible in this work, since the capillary dimensions were 50- $\mu\text{m}$  i.d./375- $\mu\text{m}$  o.d., forced air cooling was used, and the power generated never exceeded 1.1 W/m (the currents ranged from 8 up to 25  $\mu\text{A}$  only). Probably the increased dispersion due to mass transfer in and out of the CD's will be the main reason for the nonideal behavior of the plate number. The data in Figure 7B as such, however, do not explain the resolution optimum in Figure 7A. As mentioned above the difference in mobilities of the optical isomers did not change with the applied field strength; but the absolute values of the apparent mobilities did increase, even up to 50%. These increases originated from both an increase in  $\mu_{eof}$  (from 0.033 to 0.071  $\times 10^{-3} \text{ cm}^2 \text{ V}^{-1} \text{ s}^{-1}$ ), and increases in  $\mu_{ep}$  values as can be seen in Figure 7C. The more than 2-fold increase in  $\mu_{eof}$  at higher field strengths was neither

(35) Nelson, R. J.; Paulus, A.; Cohen, A. S.; Guttman, A.; Karger, B. L. *J. Chromatogr.* 1989, 490, 111-127.

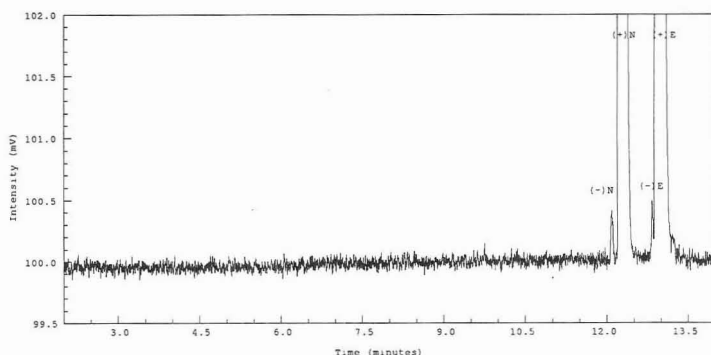


Figure 9. Separation of N and E enantiomers, having a 100-fold excess of the (+)-isomers relative to their (-)-isomers. Conditions, see text.

an exclusive phenomenon for TRIS-phosphate buffer—sodium phosphate showed a similar behavior—nor due to a big decrease in viscosity (Joule heating was relatively low, cf. above). The origin of this increase was not investigated in more detail. The increase in  $\mu_{ep}$  values was explained as follows: As stated above, the radial temperature gradient in our capillary could be ignored. The absolute rise in temperature at higher field strengths, however, will be significant and can be estimated to be ca. 5 °C,<sup>35</sup> thus accounting for a 10% increase in mobilities due to the lower bulk viscosity. In addition, the CD complex constants are known to be sensitive toward temperature changes:<sup>22</sup> even a minor temperature increase by Joule heating might be significant and decrease the CD complex constant. Remember that the  $\mu_{ep}$  of the free drugs is higher than the  $\mu_{ep}$  of the analyte-CD complex, so due to a decreased interaction of the analytes with the CD pseudostationary phase at higher field strengths, the mobilities observed will show an increase at higher fields. To summarize, the increased mobilities at higher field strengths are caused by a decrease in bulk viscosity and a decrease in interaction of the analytes with the CD's; the latter decrease most likely being caused by a thermal contribution, an increase in the velocity of the CD pseudostationary phase (due to the increase in electroosmotic flow) and a diffusion limitation due to the increase in analyte velocity as such.

Now the optimum in the resolution plots can be explained using eq 2 and the data from Figure 7B,C. At low field strengths, the increases in the plate numbers are more than sufficient for compensation of the increases in ( $\mu_{eof} + \mu_{epm}$ ), cf eq 2. At field strengths above 215 V/cm, the plate numbers do not increase sufficiently in order to compensate the increases in ( $\mu_{eof} + \mu_{epm}$ ). Consequently the resolutions tend to decrease after the initial increase, thus yielding the maxima in the resolution plots in Figure 7A. Such a resolution optimum will show up particularly at chiral separations of cationic analytes. Anionic compounds on the other hand are usually separated at an electroosmotic flow in a direction opposite to the electrophoretic migration. Then changes in  $\mu_{eof}$  and  $\mu_{ep}$  values, having opposite signs in that case, will have a much smaller impact, if any, on the resolution at higher field strengths. The latter statement is supported by recent data from Sepaniak et al.<sup>19</sup> who succeeded in the chiral separation of dansylated phenylalanine at pH 9 within 90 s, using a field strength of 700 V/cm.

**Quantitative Aspects of Cyclodextrin-Modified CZE.** Many papers about the use of cyclodextrins in capillary electrophoresis show chiral separations, but quantitative data are often not included. In practice one is not only interested in good resolution but moreover in the accurate determination of minor optical impurities relative to the main isomer. These

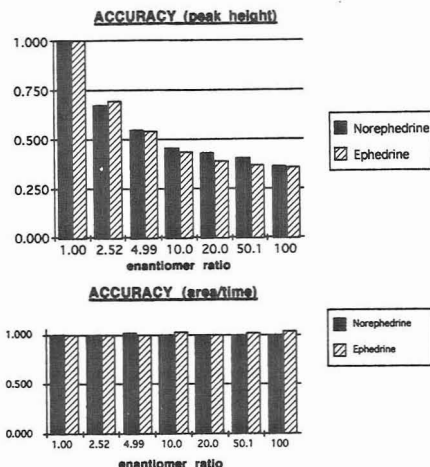
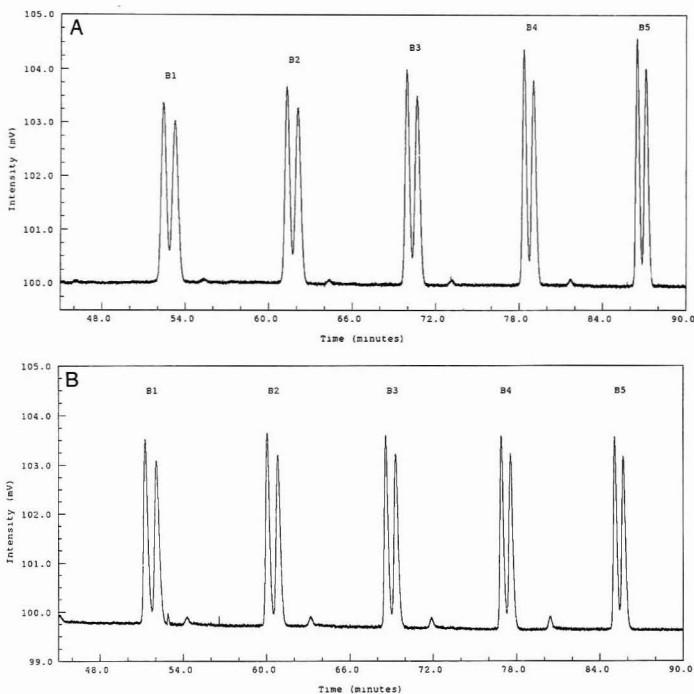


Figure 10. Enantiomer ratios found divided by the ratios prepared versus the enantiomer ratio of the (+)- and (-)-isomers. Conditions, see text.

aspects were studied using norephedrine (N) and ephedrine (E), whose individual optical isomers are readily available. The chiral separations were carried out at +25 kV and using an electrolyte of 30 mM TRIS-phosphate (pH 3) with 40 g/L heptakis(2,6-di-O-methyl)- $\beta$ -CD added. Synthetic mixtures were prepared having a 2.5-, 5-, 10-, 20-, 50-, and 100-fold excess ( $2.5 \times 10^{-3}$  versus  $2.5 \times 10^{-5}$  M) of the (+)-isomers relative to the (-)-isomers. Each sample was analyzed in duplicate. The response factors of the enantiomers in a CD environment are different,<sup>17</sup> so peak heights and peak areas/time were normalized using the responses obtained at an enantiomer ratio of 1:1. The resolutions as a function of the enantiomer ratio are shown in Figure 8. From this figure, it can be seen that the resolutions decrease rapidly when the enantiomer ratio increases. Nevertheless, even at 100-fold excess of the main optical isomers, resolutions of 1.4 (N) and 1.0 (E) remain of the initial 2.1 (N) and 1.4 (E), see also Figure 9. According to Table I, only the A enantiomers show an initial resolution of less than 1.4 at a 1:1 enantiomer ratio; consequently, only in the case of the A enantiomers, the detectable enantiomer ratio at a desired resolution of 1.0 will be definitely lower than 100:1. The accuracies of the enantiomer ratios found versus the ratios prepared are shown in Figure 10. It can be seen that quantitation by peak heights fails already below an enantiomer ratio of 2.5:1. It is obvious



**Figure 11.** Increased sample throughput in the separation of the B enantiomers using (A) five hydrodynamic (0.5 s vacuum) injections and (B) five electrokinetic (20 s at +5 kV) injections at 10-min intervals, while the separations of the previous samples are still in progress. Conditions, see text.

that peak areas (corrected for migration time) have to be used; even at a 100-fold excess of the main optical isomers, the enantiomer ratios can be determined with good accuracy (0.998 for N and 1.04 for E). The area/time data of the (-)-isomers were used to calculate the linearities of the calibration curves, covering a range of  $(2.5\text{--}83) \times 10^{-6}$  M. The calibration plots were linear, having correlation coefficients ( $n = 7$ ) of 0.9997 and 0.9998 for (-)-norephedrine and (-)-ephedrine, respectively. These values can compete with the data in ref 21, in which a narrow range (12.5–37.5 ppm epinephrine) was covered and the use of an internal standard was stated to be essential. Actually, we have been running our apparatus for almost 3 years in rather different application fields, and we never found a need for an internal standard to improve our precision and/or linearity data. The detection limits of (-)-norephedrine and (-)-ephedrine were calculated to be  $1 \times 10^{-5}$  M. The highest enantiomer ratios which could be detected reliably were 200:1. The precisions at enantiomer ratios of 1:1 were determined at 20 kV using a mixture of the F, N, E, and B racemates. The relative standard deviations of the peak areas/time of the individual optical isomers ranged from 1.2 to 2.5% RSD ( $n = 6$ ). The precisions of the enantiomer ratios were even better of course (the optical isomers are each others internal standard): 0.2–1.5% RSD ( $n = 6$ ). At higher enantiomer ratios, the precision might decrease because of an increase in integration errors for the minor optical isomer. However, using the N and E data of the accuracy test (which was carried out in duplicate), the precisions determined were still better than 1.6%, except for the experiments at a 100-fold excess, which showed precisions of 6.9 and 2.9% for the N and the E enantiomers, respectively.

**Analysis Time.** It was demonstrated above that an initial resolution of 1.4 at an enantiomer ratio of 1:1 is still adequate for quantitative chiral separation. The optimum resolutions presented in Table I are more than sufficient for most of the compounds investigated. Consequently, the analysis times of those compounds can be shortened by performing the chiral separations at higher field strengths, thereby compromising the resolution (cf. above). Following this approach, the analysis times can be reduced by 50% for the chiral separations of the R, F, G, E, N, and M racemates, while maintaining sufficient resolution for quantitative analysis. The chiral separations of the A and B racemates took more than 40 min (cf. Table I), which is very long for a CZE method. The resolutions of the A, B, and to a lesser extent the C and D enantiomers do not allow the use of much higher field strengths, and the sample throughput has to be increased in an alternative way. The separation of the B enantiomers, normally taking about 50 min, was used as a model system. The conditions were the same as in Table I, except for the temperature which was set to 30 °C. The samples were injected either hydrodynamically (0.5 s vacuum) or electrokinetically (20 s at +5 kV). Five samples were injected at 10-min intervals while the CZE separation(s) of previous sample(s) were still in progress. The results are shown in Figure 11A,B. At least five samples can be analyzed within 90 min (throughput 18 min/sample) without intermediate washing of the CZE capillary, provided that the sample matrix is known and reproducible (which is true in enantiosyntheses or enantiopurification plants, and in pharmaceutical formulations). Figure 11A represents hydrodynamic injections; that is, the separation is not only interrupted (voltage off), but the

next injection also induces a hydrodynamic flow (parabolic profile) in the capillary. The additional dispersion associated with, can be clearly seen by comparing samples B1 and B5, whose separations were interrupted four times and not at all, respectively. The resolution increased from 1.05 up to 1.20 and the plate number from 90.000 up to 135.000, in the order of B1 to B5. Figure 11B, representing electrokinetic injections, shows that the interruptions as such are irrelevant as compared with the dispersion originating from the hydrodynamically induced parabolic flow profile in Figure 11A; the electrokinetic injections caused only a minor decrease (instead of an increase) of the resolution (from 1.3 to 1.2) and the plate number (from 145.000 to 140.000) in the order of B1 to B5. Thus despite the long analysis time required for sufficient chiral resolution, the sample throughput can be increased to a similar level as for the other drugs.

### CONCLUSION

Chiral separations of structurally complex basic drugs were successfully performed by cyclodextrin-modified capillary zone electrophoresis using uncoated fused silica capillaries. Contrary to LC methods, 9 out of the 10 drugs investigated

showed resolutions higher than 1.4. The resolution was found to be strongly dependent on the applied field strength, around 215 V/cm being the optimum. This behavior was explained by the impact on the resolution of the increase in the coefficient of electroosmotic flow and in electrophoretic mobilities at higher field strengths. The separation systems described showed good precision, linearity, and accuracy; 0.5% of an optical impurity relative to the main isomer could be determined. The sample throughput was improved by repeated injections while the separations of previous samples were still in progress.

It can be concluded that cyclodextrin-modified CZE offers an attractive, reliable, and (in its use) inexpensive alternative to chromatographic separation methods and should be the method of choice wherever possible. Nevertheless, LC methods using chiral stationary phases still have the benefit of the possibility of upscaling toward the semipreparative level, and therefore they will continue to have a position in this field.

RECEIVED for review September 4, 1992. Accepted December 17, 1992.

# Kinetic Detection Method for the Quantification of Isoenzymes on Electrophoretic Media

Robin S. Hampton and Sarah C. Rutan\*

Department of Chemistry, Virginia Commonwealth University, Richmond, Virginia 23284-2006

A method has been developed for the quantitative determination of isozymes that combines electrophoresis, charge-coupled device imaging, denaturation, and kinetic analysis. Detection of the isozymes after electrophoresis is achieved by introducing a substrate that upon reaction with the isozymes forms a colored or fluorescent product. A tetrazolium dye and 4-methylumbelliferyl phosphate (MUP) are used to visualize lactose dehydrogenase (LDH) and alkaline phosphatase (ALP), respectively. The rate of product formation can be related to the activity of the isozymes. Poorly resolved bands can be distinguished by the addition of a denaturant, guanidine hydrochloride that differentially deactivates the isozymes. The data are then analyzed using zero- and first-order kinetic models. Studies with LDH show that this method is as accurate and precise as traditional fixed time methods of analysis for the quantification of well-separated isozyme bands on planar separation media, with an average precision of 6.4% as compared to 7.4% with a fixed time analysis. The ALP studies provided information on the capability of the method for quantification of poorly resolved bands after electrophoresis. Linear calibration curves were obtained for the bovine intestinal and liver ALP in the range of 0-200 and 0-700 units/L, respectively. The deactivation constant is consistent for liver isozyme samples containing 180-640 units/L.

## INTRODUCTION

Several methods have been developed over the past decade for the quantification of enzymes separated by electrophoresis methods. Because enzymatic activity is detected on a planar surface, the identification of the various isozymes for well-separated species can be determined by comparison with known samples run under identical conditions in the lane adjacent to the unknown sample.<sup>1</sup> More recent advances in this area have addressed the quantification of those isozymes that are not well resolved by the initial separation process. The main thrust of new ideas in this area has been the introduction of charge-coupled device (CCD)<sup>2</sup> imaging systems as an improvement over video cameras and densitometers<sup>3,4</sup> that have been used as detection systems for these analyses.<sup>2,4-9</sup>

In the proposed method, the detection of the isozymes after cellulose acetate electrophoresis is achieved by introducing

a substrate, which forms a colored or fluorescent product when catalyzed by the isozymes. Consecutive images are then taken of the electrophoresis membrane with a CCD camera during the time period of the reaction. The rate of product formation can be related to the activity of the isozymes present in the samples. This general approach has been proposed previously for thin-layer chromatographic separation and analysis of amino acids.<sup>10</sup>

In order to characterize our method we have looked at two enzyme systems. The first, lactose dehydrogenase (LDH), provides well-resolved bands after electrophoresis and is used to compare this method with other typical methods of analysis. LDH (L-lactate:NAD-oxidoreductase (EC 1.1.1.27)) is a clinically important enzyme which gives rise to five isozymes. The release of the isozymes due to injury or hepatobiliary, hematologic, renal, or neoplastic diseases causes alterations in the isozyme distribution pattern. The resulting patterns have been shown to be characteristic for those particular diseases. We felt that it was important to characterize a well-resolved isozyme system before we attempted a more difficult unresolved system.

The second enzyme, alkaline phosphatase (ALP), does not give resolved bands for all of its isozymes and is used to assess the ability of the kinetic analysis method to resolve overlapped bands. Alkaline phosphatase, orthophosphoric monoester phosphohydrolase (EC 3.1.3.1), is an enzyme found in human serum with isozymes derived from liver, bone, intestinal, and placental tissues. Other methods of analysis that have been used to study ALP include zone electrophoresis, isoelectric focusing, affinity chromatography, and high-performance liquid chromatography,<sup>11-19</sup> but none of these methods are completely satisfactory for the quantification of ALP isozymes. Improvements in the ability to reliably quantify the isozymes present in serum should provide improved diagnostic criteria for a variety of disease states.<sup>20,21</sup>

\* Address correspondence to this author.

- (1) Gabriel, O.; Gersten, D. M. *Anal. Biochem.* 1992, 203, 1-21.
- (2) Sutherland, J. C.; Lin, B.; Monteleone, D. C.; Mugavero, J. A.; Sutherland, B. M.; Trunk, J. *Anal. Biochem.* 1987, 163, 446-457.
- (3) Regnault, C.; Delvordre, P.; Bonnier, H.; Postaire, E. *J. Chromatogr.* 1992, 607, 159-162.
- (4) Oldham, P. B. *Anal. Instrum.* 1990, 19, 49-77.
- (5) Hasselgrove, J. C.; Lyons, G.; Rubenstein, N.; Kelly, A. *Anal. Biochem.* 1985, 150, 449-456.
- (6) Drury, H. A.; Clark, K. W.; Hermes, R. E.; Fesser, J. M.; Thomas, L. J., Jr.; Donis-Keller, H. *Biotechniques* 1992, 12 (6), 892-901.
- (7) Lanan, M.; Grossman, D. W.; Morris, M. D. *Anal. Chem.* 1992, 64, 1967-1972.

- (8) Pickett, S. C.; Johnston, R. F.; Miller, M. F.; Barker, D. L. *Am. Lab.* 1990, 22, 34-40.
- (9) Ribeiro, E. A.; Sutherland, J. C. *Anal. Biochem.* 1991, 194, 174-184.
- (10) Corcoran, C. A.; Rutan, S. C. *Anal. Chim. Acta* 1989, 224, 315-328.
- (11) Van Hoof, V. O.; Lepoutre, L. G.; Hoylaerts, M. F.; Chevigne, R.; De Broe, M. E. *Clin. Chem.* 1988, 34 (9), 1857-1862.
- (12) Moss, D. W.; Campbell, D. M.; Anagnostov-Kakaras, E.; King, E. *J. Biochem. J.* 1961, 81, 441-447.
- (13) Ramasamy, I. *Clin. Chim. Acta* 1991, 199, 243-252.
- (14) Schriber, W. E.; Whitta, L. *Clin. Chem.* 1986, 32 (8), 1570-1573.
- (15) Onica, D.; Sundblad, L.; Waldenlind, L. *Clin. Chim. Acta* 1986, 155, 285-294.
- (16) Anderson, D. J.; Branum, E. L.; O'Brien, J. F. *Clin. Chem.* 1990, 36 (2), 240-246.
- (17) Rhone, D. P.; Mizuno, F. M. *Am. J. Clin. Pathol.* 1973, 59, 531-541.
- (18) Rosalki, S. B.; Foo, A. Y. *Clin. Chem.* 1984, 30, 1182-1186.
- (19) Vessell, E. S.; Bearn, A. G. *Proc. Soc. Exp. Biol. Med.* 1957, 94, 96.
- (20) McComb, R. B.; Bowers, G. N., Jr.; Posen, S. *Alkaline Phosphatase*; Plenum Press: New York, 1979; Chapter 6.
- (21) McComb, R. B.; Bowers, G. N., Jr.; Posen, S. *Alkaline Phosphatase*; Plenum Press: New York, 1979, p 550.



The use of various chemicals to cause differential inhibition of the ALP isozymes has been used by several investigators as a means of resolving and quantifying these isozymes. The list of possible chemical inhibitors includes urea, *l*-tryptophan, *l*-phenylalanine, and guanidine hydrochloride (GuHCl).<sup>22</sup> Miggiano and co-workers have studied the time dependence of urea deactivation of ALP isozymes<sup>23</sup> using a pseudo-first-order kinetic model which revealed unique inactivation profiles for each isozyme. Alternatively, Shephard and Peake used GuHCl to selectively deactivate the four major ALP isozymes found in serum.<sup>24</sup> They concluded that GuHCl had several advantages over urea as an inhibitor, including faster inhibition, improved reproducibility, and the ability to use a lower reagent concentration. However, Tillyer has shown that the errors associated with this type of approach may be larger than acceptable in clinical laboratories.<sup>25</sup> Fitzpatrick and Pardue used simulated data to establish an understanding of the factors which affect the simultaneous determination of catalysts (enzymes) when inhibited by a common inhibitor.<sup>26</sup> Their analysis is based on the use of a first-order inhibition model. Recently, these authors followed up this study by evaluating various reaction conditions for absorbance and fluorescence-based methods to quantify two component mixtures of ALP.<sup>27,28</sup> The data for both methods were analyzed using curve fitting of the inhibition kinetic data. The upper activity limit for these methods was 322 units/L, which is less than the average activity found in sera with elevated levels of ALP. Although their method is fairly precise for two isozyme systems, it becomes increasingly more difficult to use when additional isozymes are present. Solution-phase studies using two isozymes of ALP in the presence of GuHCl showed that the deactivation rates for the two isozymes differ and that this difference can be exploited to quantify the isozymes when present in the same sample.<sup>27-29</sup>

Electrophoresis has been used for many years as a means of separating ALP isozymes. Although agarose gels are popular as a separation media in clinical labs, for the purpose of these experiments cellulose acetate has several advantages over agarose gels. One of our main concerns is that the thickness of the agarose gels would result in slower diffusion and thus affect either the reaction between the enzyme and the denaturant or the reaction between the enzyme and the substrate. Cellulose acetate has the added advantages of being cheaper, more reproducible, and readily available. This separation method takes approximately 40 min, and there are several commercially available procedures, including those from Helena<sup>30</sup> and Gelman Sciences.<sup>31</sup>

Enzymes kinetics in the presence of a denaturant can be described quantitatively by the following equation:<sup>32,33</sup>

$$[P] = \frac{k_2[E]_0(1 - e^{-k_3t})}{k_3} \quad (1)$$

Equation 1 is the kinetic model used for data analysis, where

(22) McComb, R. B.; Bowers, G. N., Jr.; Posen, S. *Alkaline Phosphatase*; Plenum Press: New York, 1979; pp 268-275.

(23) Miggiano, G. A. D.; Mordente, A.; Pileri, M.; Martovana, G. E.; Meucci, E.; Castelli, A. *Enzyme* 1984, 32, 162-169.

(24) Shephard, M. D. S.; Peake, M. J. *J. Clin. Pathol.* 1986, 39, 1025-1030.

(25) Tillyer, C. R. *Clin. Chem.* 1988, 34, 2490-2493.

(26) Fitzpatrick, C. P.; Pardue, H. L. *Anal. Chem.* 1989, 61, 2551-2556.

(27) Fitzpatrick, C. P.; Pardue, H. L. *Clin. Chem.* 1992, 38, 238-246.

(28) Fitzpatrick, C. P.; Pardue, H. L. *Clin. Chem.* 1992, 38, 247-255.

(29) Lewis, W. H., Jr.; Rutan, S. C. *Anal. Chem.* 1991, 63, 627-629.

(30) Warren, B. M. *The Isozymes of Alkaline Phosphatase*; Helena Laboratories: Beaumont, TX, 1981.

(31) *Alk-Phos Isozyme Reagent Set*; Gelman Sciences: Ann Arbor, MI, 1985.

(32) Lehninger, A. L. *Principles of Biochemistry*; Worth Publishers: New York, 1982; pp 211-219.

(33) Weiser, W. E.; Pardue, H. L. *Anal. Chem.* 1986, 58, 2523-2527.

the  $\Delta P$ ,  $P_0$  (the background contribution), and the deactivation constant,  $k_3$ , are determined from a nonlinear least-squares fit of the data.  $\Delta P$  is defined as the preexponential factor, as shown in eq 2, where  $k_2[E]_0$  is the enzyme activity. The

$$\Delta P = \frac{k_2[E]_0}{k_3} \quad (2)$$

data analysis method used is a nonlinear regression based on the extended Kalman filter, a recursive, digital parameter estimation method which has been used previously for kinetic data analysis.<sup>29,34</sup>

## EXPERIMENTAL SECTION

**Chemicals and Solutions.** LDH marker (Gelman Sciences, Ann Arbor MI), a solution containing all of the five isozymes of LDH, was used as the LDH sample. The reagents and procedures for LDH analysis were provided by Gelman Sciences. The procedure for visualization of LDH isozymes is a colorimetric technique based on the reduction of a tetrazolium dye, 2,5-diphenyl-3-(4,5-dimethylthiazol-2-yl)-2H-tetrazolium bromide, that was prepared as directed by Gelman.<sup>35</sup> The procedure was followed directly except for the changes described below.<sup>36</sup>

Stock solutions of alkaline phosphatase (ALP), Type XXXIII from bovine liver and Type I from bovine intestine (Sigma, St. Louis, MO), were made to contain approximately 100 and 50 units/L, respectively. These activities are based on the reported values of 9.7 and 2.0 units/mg solid as determined by Sigma. A unit is defined as the amount of enzyme required to hydrolyze 1.0  $\mu$ mol of *p*-nitrophenyl phosphate per minute at pH 10.4 and 37 °C.<sup>37</sup> Dilutions of these stock solutions were prepared in the range of 0-100 units/L for the liver isozyme and 0-50 units/L for the intestinal isozyme. All ALP sample solutions were prepared in 2-amino-2-methyl-1-propanol (2A2M1P) (Eastman Kodak Co., Rochester, NY) buffer which contained  $2.5 \times 10^{-5}$  M  $MgCl_2$  (Mallinckrodt, Paris, KY). The pH was adjusted to 10.0 by the addition of concentrated HCl.  $Mg^{2+}$  was added to the buffer solution because its presence is responsible for maintaining the ALP structure required for catalytic activity.<sup>38</sup>

The ALP substrate was 4-methylumbelliferyl phosphate (MUP, Sigma, St. Louis, MO). ALP hydrolyzes MUP to form a highly fluorescent product, 4-methylumbelliferone (MU). MU fluoresces at 460 nm when excited at 366 nm. MUP was chosen because it is one of the most sensitive substrates for ALP and it allows for detection of product early in the reaction.<sup>28</sup> MUP was made in two different buffers. The substrate concentration in each buffer solution was the same (2.23 mM), and both buffer concentrations were 0.9 M. The first buffer, 2A2M1P, was chosen because 2-amino alcohols can act as phosphoryl group acceptors, in place of  $H_2O$ . This causes the reaction product to be a 2-aminoalkyl phosphate rather than inorganic phosphate, resulting in an increased rate of dissociation of the product from the enzyme. Ethylaminoethanol (EAE) buffer (Eastman Kodak, Rochester, NY) was the second buffer used. The EAE buffer solutions also contained  $5.65 \times 10^{-5}$  M  $ZnCl_2$  and 3.74 M NaCl (both from J. T. Baker Chemical Co., Phillipsburg, NJ) and  $2.5 \times 10^{-5}$  M  $MgCl_2$ . The EAE solution was brought to pH 10.0 by the addition of concentrated NaOH. GuHCl (4 M), the denaturant, was prepared in deionized water. All the above solutions were refrigerated when not in use and are stable for 3 days under these conditions. Because the concentration of 4MUP must be greater than the Michaelis-Menten constant,  $K_m$ , a concentration of approximately 2.2 mM was used. For solution studies, Lewis found that this was approximately 100 times the  $K_m$  for bovine intestinal isozyme, which had the highest  $K_m$  of the isozymes

(34) Rutan, S. C. *Chemom. Intell. Lab. Syst.* 1989, 6, 191-201.

(35) Vesell, E. S.; Bearn, A. G. *Proc. Soc. Exp. Biol. Med.* 1957, 45, 753.

(36) *LDH Isozyme Substrate Set*; Gelman Sciences, Ann Arbor, MI, 1985.

(37) McComb, R. B.; Bowers, G. N., Jr.; Posen, S. *Alkaline Phosphatase*; Plenum Press: New York, 1979; Chapter 7.

(38) Bosron, W. F.; Anderson, R. A.; Falk, M. C.; Kennedy, F. S.; Vallee, B. L. *Biochemistry* 1977, 16, 610-614.

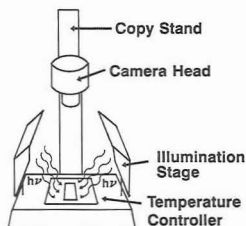


Figure 1. Schematic diagram of CCD imaging instrumentation.

studied.<sup>29</sup> We have since determined that the apparent  $K_m$  of the isozymes on the cellulose acetate is approximately 10 times that observed in solution and have increased the substrate concentration for subsequent experiments to 22 mM.

**Apparatus.** Electrophoresis was done in a Speratek electrophoresis chamber (Gelman Sciences, Ann Arbor, MD). The electrophoresis was carried out in high-resolution buffer (tris-barbital-sodium barbital (TRIS), pH 8.8) on cellulose acetate electrophoresis strips (Sephraphore III). Each electrophoresis strip can accommodate eight samples in parallel lanes. A Speratek-8 applicator was used to apply uniform quantities (8  $\mu$ L) of sample to the electrophoretic membrane. The substrate transfer strips were nitrocellulose membranes. All electrophoresis materials were purchased from Gelman Sciences, and the Gelman procedures for electrophoresis were followed.<sup>31,36</sup>

A CCD camera system (Star I, Photometrics, Tucson, AZ) equipped with a Thompson CCD (TH7883, PM Grade) was mounted on a Bogen TC-1 copy stand. An illumination stage (Reprostar II, Camag, Wrightsville Beach, NC) was used to illuminate the gels with either white light or UV light at 366 nm. A microscope stage warmer (MP 100 DM), (Kitazato, New York, NY) was placed on the illumination stage and could be used to thermostat the membrane during data collection. The camera head temperature is controlled by a thermoelectric cooler (LC 200, Photometrics, Tucson, AZ). The camera had a Nikon 50-mm lens with the  $f$  stop set at 22. The images were transferred to a Data World 386-33-MHz computer through a National Instruments IEEE-488 board. The computer is used for storage and analysis of the images and is equipped with a dual-mode caching disk controller and extended memory to improve disk access time and storage capabilities. An entire image can be stored on the hard disk in approximately 10 s. The imaging system was contained within a light-proof closet (Camag, Wrightsville Beach, NC). A schematic diagram of this instrument is shown in Figure 1.

**Procedure.** Electrophoresis was based on the procedures published by Gelman for LDH and ALP separations. For electrophoresis, sample solutions are applied to alternate lanes of the membrane. Two ice packs are used to cool the chamber during electrophoresis. After electrophoresis, the membrane is placed on a glass slide within the imaging chamber. The transfer strip, soaked in substrate, is placed on the electrophoresis membrane for 15 s. The transfer strip is carefully lifted from the membrane to prevent band broadening or mixing of the isozyme bands. After substrate application, a repetitive image program, CCD, is used to collect and store sequential images. CCD was written using Microsoft C, version 6.0 (Microsoft Corp., Redmond, WA) and allows the analyst to control the camera settings and data acquisition and storage. Typically, 30 2-s exposures are taken at 30-s intervals, using the high gain setting. The delay time between substrate application and the first image is noted for use in the kinetic analysis program. In all experiments, the elapsed time between substrate application and the acquisition of the first image was less than 1 min. If GuHCl is to be added to the membrane, it is added to the membrane after the substrate via a transfer strip for 10 s.

Storage of a complete image (576  $\times$  384 pixels) requires approximately 440K bytes of disk storage space. Deleting unnecessary data reduces the image size to 349  $\times$  116 pixels which requires only 79K bytes of disk space. To correct the images for the unique light sensitivity of each pixel a dark image ( $I_D$ ) and

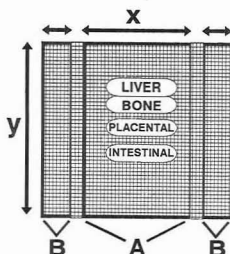


Figure 2. Diagram of electrophoretic membrane after electrophoresis, illustrating data summation and background subtraction process. Box A contains isozyme intensity data; the boxes B contain background signal data.

a flat field frame ( $I_F$ ) are needed. The dark image, taken while the shutter is closed, corrects for the background dark current. The flat field frame is the response of each of the pixels to a uniformly illuminated image. In the case of ALP, this is a transfer strip that has been soaked in a solution of the fluorescent product, MU. For the LDH analysis, a blank membrane is used. This flat fielding correction is calculated as<sup>39</sup>

$$I_C = \frac{(I_R - I_D)M}{(I_F - I_D)} \quad (3)$$

where  $I_C$  is the corrected image,  $I_R$  is the original image, and  $M$  is the mean pixel intensity for  $I_F - I_D$ . This calculation is done by a PASCAL (Turbo Pascal v.6.0, Borland International, Scotts Valley, CA) computer program, FLATF. The next stage of data analysis is accomplished by a program ZERO, for zero-order data, and a program FIRST for first-order data. Both programs were also written in PASCAL. The coordinates of a box containing all the information for a single lane are determined. This box is shown in Figure 2, box A, and the same size box is used for each lane on the membrane. The pixel intensities within this box are summed across the X direction so that each lane is represented by a vector of intensity values in the Y direction. The columns (Figure 2, boxes labeled B) to either side of box A are summed in the X direction and put in a second vector which represents the background intensity. The background vector is subtracted from the data vector for each lane to give an electropherogram. This procedure is done for every image collected in a single timed experiment.

For each position along the Y-axis, the intensity values vs time give rise to a kinetic profile for the reaction. These profiles are fit using an appropriate kinetic model, and the enzyme activity for each position along the Y-axis is determined. A plot of the activity vs position is made, where the area under the curve is directly proportional to the total activity of the enzyme present on the membrane.

## RESULTS AND DISCUSSION

In order for the proposed technique to be useful, the kinetic data must be reproducible. There are several variables which can affect the results from these experiments including temperature, ionic strength, transfer method for both substrate and denaturant, and moisture content of the membrane during imaging. Originally we thought that cooling of the membrane as the solutions evaporated might affect the rate of reaction of the isozymes. This was investigated by placing a thermistor on top of the membrane and monitoring the surface temperature during the reaction. The only change in the temperature occurred within the first minute, and this was less than a half a degree increase; this change did not have an appreciable effect on the reaction kinetics. Throughout

(39) STAR I Camera System: Image Processing Software; Photometrics: Tucson, AZ, 1989.

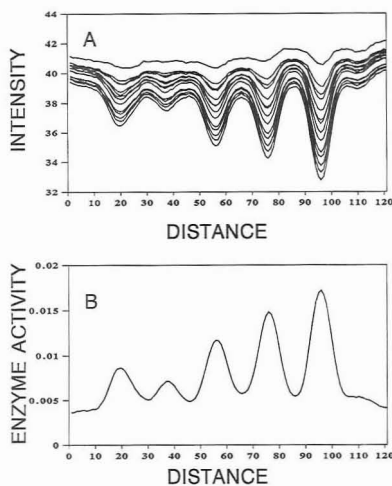


**Figure 3.** (a) Multiple electropherograms of LDH isozymes. Images were taken every 15 s. Distance is expressed as pixel number. (b) Activity profile of LDH isozymes obtained by zero order kinetic analysis of electropherograms in A. Activity is expressed as the slopes of the kinetic profiles, counts/second.

the remainder of the experiment the temperature remained constant ( $\pm 0.1$  °C).

The process of transferring solution to the surface of the membrane is another potential source of variability. Requirements for successful substrate introduction are as follows: excess substrate ( $[S] \gg K_m$ ) is introduced, substrate introduction is rapid, lateral diffusion of the isozyme bands is minimized, and a minimum amount of isozyme is removed from the membrane by the transfer strip. We have taken images of the transfer strips after contact with the electrophoresis membrane and found that only a small amount of product appears over time. There appeared to be a uniform transfer for all lanes on the membrane, and therefore we believe this is not an important source of variability. During some of the experiments we noticed a shifting of the peak maxima as the reaction proceeds which we ascribed to directional diffusion of the isozymes within the membrane. The diffusion was always toward to point of enzyme application. Although we do not yet understand this phenomenon, this can be corrected using the data analysis programs ZERO and FIRST by aligning the peak maxima before kinetic analysis. This correction only works well for data with a large signal to noise ratio. In a second effort to correct for the shifting peak maxima, we used a 10-min electrophoresis of the membrane prior to application of sample. Peak maxima in subsequent experiments did not shift. This also provided another advantage of reducing the effect of contaminants such as fingerprints and dust particles or other irregularities in the membrane and provided a more consistent background signal.

A comparison was made between this kinetic method and a fixed-time method of analysis. The conventional method of LDH analysis records the intensity of the bands after a fixed period of time, usually with a densitometer. The kinetic method is based on the series of consecutive electropherograms shown in Figure 3A. Because LDH is observed using a colorimetric reaction, the bands increase in the negative direction, as an increasing amount of light is absorbed. The profile obtained from the calculated activity values for these data are shown in Figure 3B. A zero-order model was used

**Table I. Results of Kinetic and Fixed Time Analysis for LDH Isozymes**

isozyme	kinetic <sup>a</sup> % area	fixed time <sup>b</sup> % area	kinetic <sup>a</sup> RSD (%) <sup>c</sup>	fixed time <sup>b</sup> RSD (%) <sup>c</sup>
LDH 1	13.1 $\pm$ 2.1	13.0 $\pm$ 1.3	16	10
LDH 2	5.6 $\pm$ 0.4	5.0 $\pm$ 0.9	6.2	17
LDH 3	19.3 $\pm$ 0.7	19.9 $\pm$ 0.9	3.8	4.3
LDH 4	27.1 $\pm$ 0.9	26.1 $\pm$ 0.9	3.4	3.3
LDH 5	34.9 $\pm$ 0.9	36.1 $\pm$ 0.9	2.6	2.4

<sup>a</sup> Based on a zero-order kinetic fit. Images were taken every 30 s for 10.5 min. <sup>b</sup> Based on analysis of one image taken after 10.5 min. <sup>c</sup> Relative standard deviation.

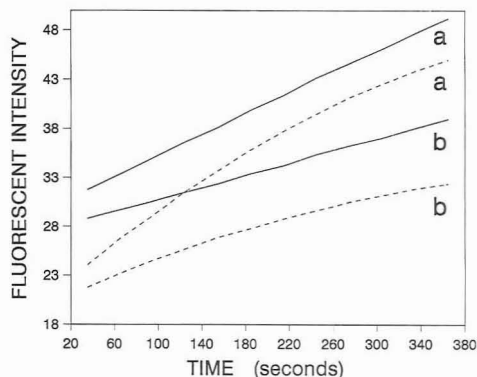


**Figure 4.** Kinetic profiles at the peak maximum for several activities of liver ALP isozyme: (—) in the absence of the denaturant GuHCl, (---) in the presence of GuHCl. The activities (units/L) are (a) 644 and (b) 362.

since no denaturant was present. The area under each of the peaks in Figure 3B is directly related to the activity of the isozyme present in the initial sample. A comparison of these areas and the areas obtained from a single image taken after 10.5 min was made, and the resulting data are shown in Table I. Because the kinetic method of analysis is based on data obtained over a longer period of time with more data points, it is expected to be a more precise method; however, the two methods gave results with similar relative standard deviations. Some of the larger errors (i.e., LDH 1) for both methods are due to uncertainties in determining the baseline for integration.

The next series of experiments was designed to ascertain the sensitivity of the method and to determine if the method could be used to detect the low levels of ALP isozymes found in serum. ALP bovine isozymes were used in this evaluation. Kinetic profiles for two activities of liver ALP are shown in Figure 4 (solid lines). The linearity of these profiles is indicative of a zero-order kinetic process. The results for the regression analyses of calibration curves derived from these data are shown in Table II. Although these values encompass the normal range of isozyme activities in serum we have also extended these ranges to 1000 and 250 units/L for liver and intestinal isozymes, respectively. Some additional calibration data for these activity ranges are also shown in Table II. This extended range of activities is useful for characterizing samples with elevated isozyme levels. The difference in the slopes for the liver and intestinal isozymes has been confirmed by solution phase experiments and is probably due to differences in the specific activity of the isozymes toward MUP as compared to the specific activity toward *p*-nitrophenyl phosphate, the substrate used by Sigma in determining the enzyme activities.

**Table II. Regression Analysis**

isozyme	activity range <sup>c</sup>	GuHCl	N <sup>d</sup>	slope	intercept	std <sup>e</sup> error
liver <sup>c</sup>	0-90	no	8	0.00269 ± 0.00019	0.018 ± 0.010	0.016
int	0-40	no	8	0.0181 ± 0.0013	0.055 ± 0.030	0.047
liver <sup>b</sup>	180-640	no	6	0.0193 ± 0.0010	-0.14 ± 0.41	0.38
liver <sup>b</sup>	180-640	yes (4M)	6	0.0316 ± 0.0014	-1.15 ± 0.55	0.51
int <sup>b</sup>	40-150	no	6	0.00777 ± 0.00038	-0.048 ± 0.037	0.035
int <sup>b</sup>	40-150	yes (4M)	6	0.00255 ± 0.00037	0.040 ± 0.036	0.034

<sup>a</sup> Selected kinetic profiles shown in Figure 4 (solid lines). <sup>b</sup> Data shown in Figure 5. <sup>c</sup> Activity expressed in units per liter. <sup>d</sup> Number of data points. <sup>e</sup> Standard error of linear regression results.

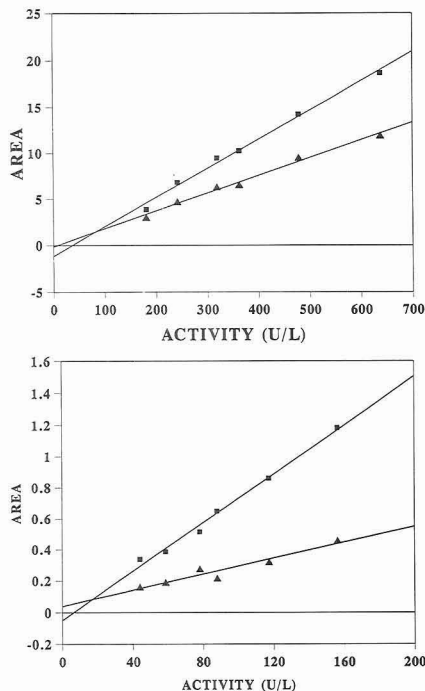


**Figure 5.** Calibration curves and least-squares fit for (A) liver ALP and (B) intestinal ALP: (■) without GuHCl; (▲) with GuHCl (4 M).

The differences in the rate of enzyme deactivation in the presence of the denaturant, GuHCl, has been exploited to distinguish overlapped bands for mixtures containing two isozymes. The rate constants,  $k_3$ , for the GuHCl deactivation of liver and intestinal isozymes are different. For the intestinal isozyme, significant deactivation by GuHCl is not observed. However, kinetic profiles for the liver isozyme reacting with GuHCl are no longer linear but are curved, demonstrating a first-order deactivation of the isozyme. Figure 4 (dotted curves) shows examples of kinetic profiles observed for two samples of the liver isozyme in the presence of GuHCl. Calibration curves for liver and intestinal isozymes with and without GuHCl are shown in Figure 5A,B. The calculation of the calibration curve in the presence of GuHCl assumes that the sole effect of the GuHCl is the first-order deactivation of the enzyme over the time period measured. The values shown are the resulting estimates for the activity before the addition of GuHCl. Initially, the reason for the lower slope in the presence of GuHCl was not known. However, recent

**Table III. Deactivation Constant for Liver ALP<sup>a</sup>**

activity (units/L)	deactivation constant ( $10^{-3} \text{ s}^{-1}$ ) <sup>b</sup>	activity (units/L)	deactivation constant ( $10^{-3} \text{ s}^{-1}$ ) <sup>b</sup>
638	2.5 ± 0.4	319	2.8 ± 0.2
479	3.4 ± 0.3	243	2.4 ± 0.2
363	2.8 ± 0.2	181	2.1 ± 0.2

overall:  $(2.7 \pm 0.4) \times 10^{-3} \text{ s}^{-1}$

<sup>a</sup> Results for a first-order fit in the presence of 3 M GuHCl. <sup>b</sup> The average of 15 pixels at the top of the peak.

experiments in our laboratory have shown that the difference in ionic strength of the substrate solution and the GuHCl solution can account for this change in slope.<sup>40</sup> The ionic strength of the MUP buffer was 0.9 M and the ionic strength of the GuHCl solution was 4 M.

In order to confirm this hypothesis, an experiment was done where the ionic strength of the substrate solution was adjusted to match that of the GuHCl solution. In this case, EAE was used as the buffer, since 2A2MIP was insoluble in high ionic strength solutions.<sup>41</sup> GuHCl was introduced between the fifth and sixth images, and the GuHCl transfer strip was kept on the membrane for 10 s. The initial portion of the data (images 1-5) was linear, and after the fifth image, the profile began to exhibit curvature. We fit the first five points to a zero-order kinetic model, and the remaining points to a first-order kinetic model. The apparent decrease in activity seen for the data shown in Figure 5A,B was not observed here, confirming our assumption that the ionic strength plays a role in producing the lower slopes observed for GuHCl calibration curves.

If a differential kinetic method is to be reliable, the deactivation constant for each isozyme should depend only on the GuHCl concentration and the type of isozyme. The  $k_3$  values across one band on the electrophoresis membrane are reasonably consistent near the peak maximum. Table III lists the deactivation constant,  $k_3$ , for several different samples of the liver isozyme and demonstrates that the deactivation constant is also consistent for samples with varying activities. This will be especially significant for distinguishing the bone and liver isozymes of ALP which cannot be completely resolved using electrophoresis.

## CONCLUSIONS

The long-term goal of the work presented here is to develop a new procedure which will permit the separation and quantitation of all the ALP isozymes present in serum. We have shown that the combination of electrophoresis and imaging with kinetic analysis can be used to separate and quantify individual isozymes of LDH and ALP. The use of a denaturing agent, such as GuHCl, allows us to differentiate

(40) Wong, J. T.; Hampton, R. S.; Rutan, S. C.; Chlebowski, J. F. *Clin. Chem.* 1992, 38, 2560-2561.

(41) McComb, R. B.; Bowers, G. N., Jr. *Clin. Chem.* 1972, 18, 97.

between two isozyme forms that are not fully resolved by electrophoresis. The deactivation constants for the isozymes are independent of activity. This method should be useful for the separation and quantification of other isozyme systems as well. Any system which can produce either an absorbance or a fluorescent signal can be monitored with this method. The relatively short analysis time required should be beneficial for clinical diagnosis. Investigations of human serum containing ALP isozymes with this method are currently underway.

#### ACKNOWLEDGMENT

We are thankful to Jan Chlebowski, Greg Miller, and Will Lewis, Jr., for their helpful comments and suggestions during the course of this research. Financial support from the Department of Energy and the Jeffress Trust is gratefully acknowledged.

RECEIVED for review July 13, 1992. Accepted January 4, 1993.

# Capillary Electrophoresis/Electrospray Ionization Mass Spectrometry: Improvement of Protein Detection Limits Using On-Column Transient Isotachophoretic Sample Preconcentration

Toni J. Thompson, Frantisek Foret,<sup>†</sup> Paul Vouros, and Barry L. Karger\*

Barnett Institute, Department of Chemistry, Northeastern University, Boston, Massachusetts 02115

On-column transient isotachophoretic sample preconcentration has been utilized for decreasing concentration detection limits in capillary electrophoresis (CE)/electrospray ionization mass spectrometry analysis (ESI/MS) of protein samples. Mixtures of model proteins have been separated in the cationic mode using a coated capillary and have been analyzed by mass spectrometry coupled on-line to an electrospray interface with a coaxial sheath flow arrangement. Complex formation, between  $\beta$ -lactoglobulins A and B and the BGE, was found to occur under certain conditions. The detection level was evaluated using capillary zone electrophoresis (CZE)/MS, capillary isotachopheresis (CITP)/MS and the on-column combination of transient CITP/CZE/MS. In CZE/MS, the sample concentration necessary to obtain a reliable full scan spectrum was in the range of  $10^{-5}$  M ( $\sim 500$  fmol injected in a 75- $\mu$ m-i.d. capillary). In the CITP/MS mode, a sample could in principle be preconcentrated by several orders of magnitude. The isotachopheretically stacked zones overlapped one another, and the minor components, focused to very narrow zones of less than 1 s, could not be reliably identified. However, isotachopheresis represents an ideal preconcentration technique for CZE whereby the benefits of both CITP and CZE are maintained. By proper selection of running buffers, the on-column combination of both CITP and CZE (transient CITP/CZE) was used to decrease the concentration detection limits for a full scan CZE/MS analysis by a factor of 100 to  $\sim 10^7$  M. Such an approach can be employed with currently available commercial CE equipment.

## INTRODUCTION

There is currently a great deal of interest in the development of capillary electrophoresis/mass spectrometry (CE/MS) for the separation and identification of charged species ranging from small ions to proteins.<sup>1-5</sup> The importance of this combination stems from the advantageous features of both CE and MS. Capillary electrophoresis provides significant separation efficiency and analytical speed for a broad range of substances in solution, while mass spectrometry provides peak identification. Furthermore, the flow rates from the capillary column are compatible with on-line coupling to MS.

In an early report on coupling capillary electrophoresis to a mass spectrometer,<sup>6</sup> an on-line valve was used to transfer CITP-separated zones into a mass spectrometer equipped with an electron ionization source. Although this technique should properly be referred to as an off-line technique, the potential of mass spectrometry for identification of analytes separated by capillary electrophoresis was clearly demonstrated. The first reports of the on-line coupling of CZE to MS used an electrospray source for the ionization and transfer of analyte ions into a quadrupole mass spectrometer.<sup>1,2</sup> Later, fast atom bombardment (FAB) was also employed for the ionization and sample transfer into the mass spectrometer.<sup>4,7-9</sup> Recently, other types of mass spectrometers such as time of flight<sup>10</sup> and ion trap<sup>11</sup> have been tested for coupling to CE.

For the determination of high molecular weight ions, electrospray ionization has an advantage in the formation of multiply-charged ions that can be conveniently analyzed by a mass spectrometer in the  $m/z$  range up to 4000. Exact molar masses can then be easily calculated from the observed distribution of charge states of the molecule.<sup>12</sup> With respect to coupling of CE to MS, electrospray has the further advantage of operating at atmospheric pressure so that hydrodynamic flow in the separation capillary (with its attendant parabolic flow profile) does not result or can be simply overcome.

Mass detection levels for proteins determined by CZE/MS are typically in the high femtomole range,<sup>3</sup> but when the concentration of the sample injected is considered, the detection level is frequently insufficient ( $\sim 10^{-5}$  M). One solution to this detection level problem is the use of selected ion recording,<sup>13</sup> which is known to significantly decrease the detection limits as compared to full scan analyses; however, this method requires prior knowledge of ions that will be present in the sample. In cases where detection limits of a CE/MS analysis are an issue, sample preconcentration, preferably in an on-line arrangement, should be considered as a possible method to improve detection without the loss of accuracy. Several approaches for decreasing the concentration detection limits for CE analyses by on-column preconcentration have been described. Principally, they can

(6) Kennler, E.; Kaniansky, D. *J. Chromatogr.* 1981, 209, 306-309.

(7) Moseley, M. A.; Deterding, L. J.; Tomer, K. B.; Jorgenson, J. W. *J. Chromatogr.* 1989, 480, 233-245.

(8) Moseley, M. A.; Deterding, L. J.; Tomer, K. B.; Jorgenson, J. W. *Rapid Commun. Mass Spectrom.* 1989, 3, 87-96.

(9) Wolf, S.; Norwood, C.; Jackim, E.; Vouros, P. *J. Am. Soc. Mass Spectrom.* 1992, 3, 757-761.

(10) Hallen, R. W.; Shumate, C. B.; Siems, W. F.; Tsuda, T.; Hill, H. H., Jr.; *J. Chromatogr.* 1989, 480, 233-245.

(11) Schwartz, J. C.; Jardine, I. Poster presented at The 40th ASMS Conference on Mass Spectrometry and Allied Topics, Washington, DC, (TP57) May 31-June 5, 1992.

(12) Fenn, J. B.; Mann, M.; Meng, C. K.; Wong, S. F.; Whitehouse, C. M. *Science* 1989, 246, 64-71.

(13) Moseley, M. A.; Jorgenson, J. W.; Shabanowitz, J.; Hunt, D. F.; Tomer, K. B. *J. Am. Soc. Mass Spectrom.* 1992, 3, 289-300.

\* Author to whom correspondence should be addressed.

<sup>†</sup> On leave from Institute of Analytical Chemistry, Veveri 97, 611 42 Brno, Czechoslovakia.

(1) Olivares, J. A.; Nguyen, N. T.; Yonker, C. R.; Smith, R. D. *Anal. Chem.* 1987, 59, 1232-1236.

(2) Lee, E. D.; Muck, W.; Henion, J. D.; Covey, T. R. *J. Chromatogr.* 1988, 455, 313-321.

(3) Thibault, P.; Paris, C.; Pleasance, S. *Rapid Commun. Mass Spectrom.* 1991, 5, 484-490.

(4) Moseley, M. A.; Deterding, L. J.; Tomer, K. B.; Jorgenson, J. W. *Anal. Chem.* 1991, 63, 109-114.

(5) Garcia, F.; Henion, J. D. *Anal. Chem.* 1992, 64, 985-990.



be divided into two classes—sorption<sup>14,15</sup> and electrophoretic techniques.<sup>16–20</sup> While the sorption techniques require a precolumn and somewhat complex instrumentation, the use of electrophoretic techniques is simpler and more general.

This study has as its goal the development of a simple preconcentration technique for CZE/MS where higher sample volumes could be injected. The use of sample stacking via low conductivity sample matrices as a means of increasing injection volume<sup>16</sup> was first tested. Next, CITP was investigated, followed by a combination of CITP and CZE. The on-line coupling of CITP to ESI/MS has been previously demonstrated.<sup>21</sup> While the concentrating capability of CITP is excellent, the optimization of separation conditions, particularly in the case of protein analysis, is not straightforward. On the other hand, when ITP is used solely as a preconcentration technique, the selection of leading and terminating electrolytes can be easily accomplished. The coupling of CITP as a preconcentration step to CZE was already explored with UV<sup>18–20,22</sup> and fluorescence<sup>23</sup> detectors and recently with a mass spectrometer.<sup>24</sup> So far, coupled column systems were solely explored where preconcentration was carried out in a CITP wide bore pre-separation tube connected to a CZE capillary of smaller internal diameter. This technique permits sample preconcentration by at least 3 orders of magnitude; however, it requires somewhat complicated instrumentation. Recently we have demonstrated the possibility of on-column transient CITP preconcentration of protein samples where both CITP preconcentration and CZE separation proceed in one capillary on a commercial instrument equipped with a UV detector.<sup>22</sup>

The present work reports results on the use of on-column transient CITP sample preconcentration for decreasing the detection limits of protein determination by CE/ESI/MS. This method is compared to sample stacking via low conductivity sample matrices and CITP alone. It will be shown that transient CITP provides a simple means of decreasing detection limits by 2 orders of magnitude over normal CZE.

## EXPERIMENTAL SECTION

**Mass Spectrometer and Interface.** The mass spectrometer was a Finnigan MAT TSG700 (Finnigan, San Jose, CA) triple quadrupole equipped with an electrospray ionization source. Several modifications to the electrospray interface (Figure 1) were necessary to couple CE with ESI/MS. The stainless steel needle supplied with the instrument was replaced with a polyimide coated fused silica capillary used in CE. This change was made to eliminate any junctions that could be detrimental to the separation and to enable the end of the capillary to be located at the electrospray needle tip. The interface utilized a coaxial liquid sheath, as shown previously,<sup>25</sup> as well as a coaxial gas sheath.<sup>2</sup> The liquid sheath tube supplied by the manufacturer was replaced by stainless steel tubing (Small Parts, Inc., Miami Lakes, FL) of ~0.4-mm i.d. and ~0.7-mm-o.d., and the gas sheath

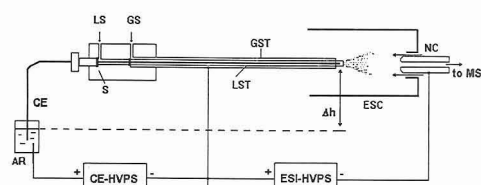


**Figure 1.** Diagram of the capillary electrophoresis/electrospray interface. S is septum, LST is liquid sheath tube, LS is liquid sheath entry port, GST is gas sheath tube, GS is gas sheath entry port, AR is anode reservoir, CE is CE capillary, NC is nitrogen curtain drying gas, ESC is cylindrical electrospray electrode, ESI-HVPS is the electrospray high voltage power supply,  $\Delta h$  is the height difference between the anode and cathode ends of the column, and CE-HVPS is the capillary electrophoresis high-voltage power supply. See the Experimental Section for further details.

tip was also replaced with a tip having an orifice of 1.0-mm i.d. The liquid sheath tip was narrowed to ~0.5 mm to improve the electrospray stability.<sup>26</sup> The fused silica separation capillary terminated 0.5 mm inside the liquid sheath tip. A silicone septum was also added to prevent back flow of sheath liquid along the capillary.

Figure 1 further shows that the difference in height ( $\Delta h$ ) between the anode reservoir and the tip of the electrospray needle (the cathode end of CZE column) was ~10 cm. A partial vacuum was created due to the flow of the gas sheath at the capillary tip, and with the ends of the capillary at equal height, a significant bulk liquid flow toward the cathode took place. In order to compensate for this pressure drop, the level of the anode reservoir was lowered. Capillary isotachopheresis was employed to determine the level at which no bulk flow occurred. The capillary was first filled with the leading electrolyte (0.01 M ammonium acetate, pH 5), and then ~150 nL of  $10^{-5}$  M methyl green dye was siphon injected. The injection end of the capillary was then placed in the terminating electrolyte reservoir (0.001 M acetic acid), and the current was applied. The current was turned off when the dye had focused into a narrow 2-mm-long band. Movement of the zone could easily be observed through the polyimide coating of the capillary, due to the high concentration of this focused dye. The height of the reservoir was adjusted until no movement of the dye was observed in either the forward or the reverse direction.

The electrospray needle, as shown in Figure 1, was maintained at ground potential while the sampling orifice was at about -4000 V when operating in the positive ion mode. The drying gas (nitrogen curtain) for the electrospray was maintained at about 100 °C at a flow rate of 6 L/min, while the sheath gas flow was set at approximately 2 L/min. The liquid sheath consisted of 1% acetic acid in 50% 2-propanol/water, flowing at a rate of 4.0  $\mu\text{L}/\text{min}$ . Tuning and calibration of the mass spectrometer were performed using a 5 pmol/ $\mu\text{L}$  myoglobin solution. The third quadrupole of the mass spectrometer was scanned from  $m/z$  600 to 2000 at 1 scan/s for all analyses while the first and second quadrupoles were operated in the rf only mode. The quadrupole manifold was heated to 70 °C, and the electron multiplier was set at 1.5 kV with the conversion dynode at -15 kV.

**Capillary Electrophoresis.** The electrophoresis apparatus was made in-house using a CZE1000R (Spellman, Plainville, NY) high-voltage power supply. The CE columns were fused silica capillaries (Polymicro Technologies, Phoenix, AZ) 75- $\mu\text{m}$  i.d., 360- $\mu\text{m}$  o.d., and 50-cm length, coated in-house with linear polyacrylamide.<sup>27</sup> The polyacrylamide coating minimized adsorption by proteins to the capillary walls and eliminated electroosmotic flow within the capillary. The voltage for the CZE and transient CITP analyses was 18 kV with a resultant current of 6  $\mu\text{A}$ . The constant current applied during the CITP analyses was 6  $\mu\text{A}$  with voltage increasing from 7 to 17 kV.

**Solutions.** The standard proteins were purchased from Sigma Chemical Co. (St. Louis, MO) and were used without further

(14) Guzman, N. A.; Trebilcock, M. A.; Advis, J. P. *J. Liquid Chromatogr.* 1991, 14 (5) 997–1015.

(15) Cai, J.; El Rassi, Z. *J. Liquid Chromatogr.* 1992, 15 (6&7), 1179–1192.

(16) Aebersold, R.; Morrison, H. D. *J. Chromatogr.* 1990, 516, 79–88.

(17) Chien, R. L.; Burgi, D. S. *J. Chromatogr.* 1991, 559, 141–152.

(18) Kaniansky, D.; Marak, J. *J. Chromatogr.* 1990, 498, 191–204.

(19) Foret, F.; Sustacek, V.; Boeck, P. *J. Microcol. Sep.* 1990, 2, 299–303.

(20) Stegehuis, D. S.; Irth, H.; Tjaden, U. R.; van der Greef, J. *J. Chromatogr.* 1991, 538, 393–402.

(21) Smith, R. D.; Fields, S. M.; Loo, J. A.; Barinaga, C. J.; Udseth, H. R.; Edmonds, C. G. *Electrophoresis* 1990, 11, 709–717.

(22) Foret, F.; Szoko, E.; Karger, B. L. *J. Chromatogr.* 1992, 608, 3–12.

(23) Stegehuis, D. S.; Tjaden, U. R.; van der Greef, J. *J. Chromatogr.* 1992, 591, 341–349.

(24) Tinke, A. P.; Reinhoud, N. J.; Niessen, W. M. A.; Tjaden, U. R.; van der Greef, J. *Rapid Commun. Mass Spectrom.* 1992, 6, 560–563.

(25) Smith, R. D.; Barinaga, C. J.; Udseth, H. R. *Anal. Chem.* 1988, 60, 1948–1952.

(26) Chowdhury, S. K.; Chait, B. T. *Anal. Chem.* 1991, 63, 1660–1664.

(27) Hjerten, S. *J. Chromatogr.* 1985, 347, 191–197.

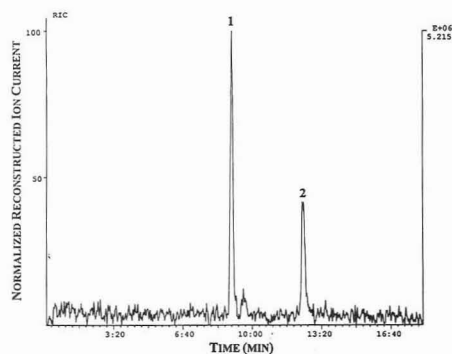


**Figure 2.** CZE/MS full scan ( $m/z$  600–2000) reconstructed ion electropherogram of 9.0  $\mu\text{M}$  cytochrome *c* (1) and 5.4  $\mu\text{M}$  myoglobin (2) in the BGE. Injection volume: 50 nL (injected quantity of 450 and 270 fmol, respectively). BGE: 0.02 M 6-aminohexanoic acid + acetic acid, pH 4.4. CE conditions: constant voltage 18 kV, current 6  $\mu\text{A}$ .

purification. The samples were dissolved in either the background electrolyte or distilled/deionized water for CZE separations. The CZE background electrolyte (BGE) was 0.02 M 6-aminohexanoic acid in water, adjusted to pH 4.4 with glacial acetic acid. The CITP leading electrolyte was 0.01 M ammonium acetate adjusted to pH 4.4 with glacial acetic acid, and the terminating electrolyte was 0.001 M acetic acid. For the transient CITP experiments, the samples were diluted in the CITP leading electrolyte buffer and the background electrolyte was the same as that used in the CZE experiments. All buffer chemicals were purchased from Sigma.

**Sample Injection.** The CE column was first washed with the background electrolyte or, in the case of CITP, with the leading electrolyte. The sample was then siphon injected by inserting the column into the sample vial and elevating the vial by 20 cm for 10–150 s, producing an injection volume of 50–750 nL.

## RESULTS AND DISCUSSION

In order to provide a baseline from which to judge the preconcentration methods, initial studies were performed with CZE/MS, with the sample dissolved in the background electrolyte. Figure 2 shows the full scan reconstructed ion electropherogram (RIE) of 50 nL of a sample containing cytochrome *c* and myoglobin in which the proteins were diluted in the background electrolyte (6-aminohexanoic acid) to a concentration of  $\sim 10^{-5}$  M. This injection volume of 50 nL is larger than typically used in CZE and was chosen so that reliable mass spectra could be obtained. In this figure, the signal to noise ratio (S/N) for cytochrome *c* is 12:1. An improved S/N may be obtained by dissolving the sample in water or low concentration buffer<sup>17</sup> with subsequent focusing of the larger volume injected. Figure 3a shows the full scan RIE of 150 nL of a sample containing lysozyme (1), cytochrome *c* (2), ribonuclease A (3), myoglobin (4),  $\beta$ -lactoglobulin A (5),  $\beta$ -lactoglobulin B (6), and carbonic anhydrase (7) dissolved in water. An example of the spectra obtained by averaging the scans under the peaks is shown in Figure 3b, and the deconvolution of that spectrum is shown in Figure 3c. Initial preconcentration across the sample/BGE boundary was responsible for improved detection signal of 3.5 times that of the sample dissolved in the BGE.

Few of the proteins in Figure 3a were still detectable in the RIE of a 1:10 dilution ( $10^{-6}$  M) of this sample with water as shown in Figure 4a. While mass spectra of separated proteins could still be obtained, clearly the zone identification of an unknown component at these concentrations would be difficult. The analysis time was significantly longer with, for

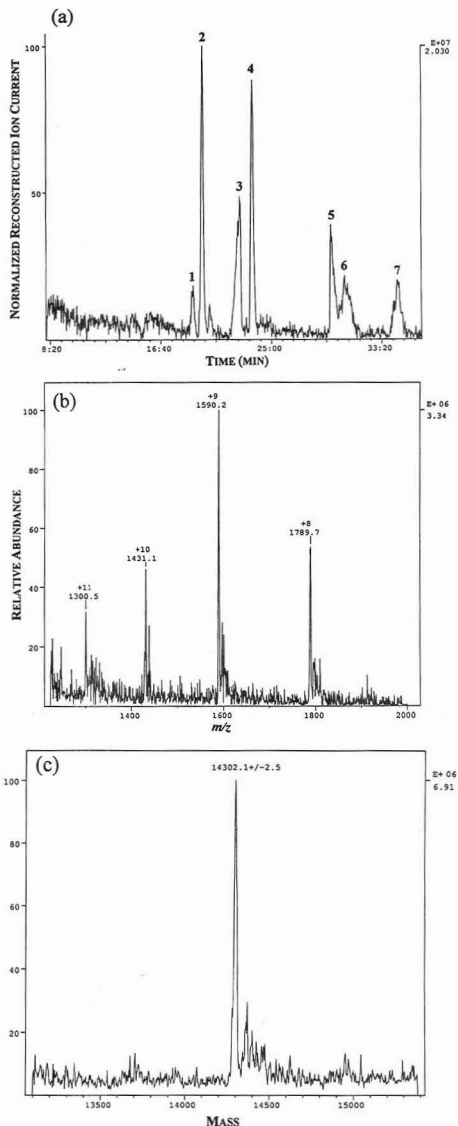


**Figure 3.** (a) CZE/MS full scan ( $m/z$  600–2000) reconstructed ion electropherogram of a 150-nL injection of 12  $\mu\text{M}$  each of lysozyme (1), cytochrome *c* (2), ribonuclease A (3), myoglobin (4),  $\beta$ -lactoglobulin A (5),  $\beta$ -lactoglobulin B (6), and carbonic anhydrase (7) dissolved in water. BGE: 0.02 M 6-aminohexanoic acid + acetic acid, to pH 4.4; (b) spectrum of lysozyme taken from averaging the scans under the peak; (c) deconvoluted spectrum of lysozyme.  $M_r$  for lysozyme is 14 306.<sup>34</sup> CE conditions as in Figure 2.

example, cytochrome *c* eluting 12 min later in Figure 3a and 23 min later in Figure 4a than in Figure 2 where the sample was dissolved in the BGE. The increased migration time is due to the voltage drop across the initial sample zone caused by the low electrical conductivity of the zone compared with the BGE. The electric field strength is not uniform through-

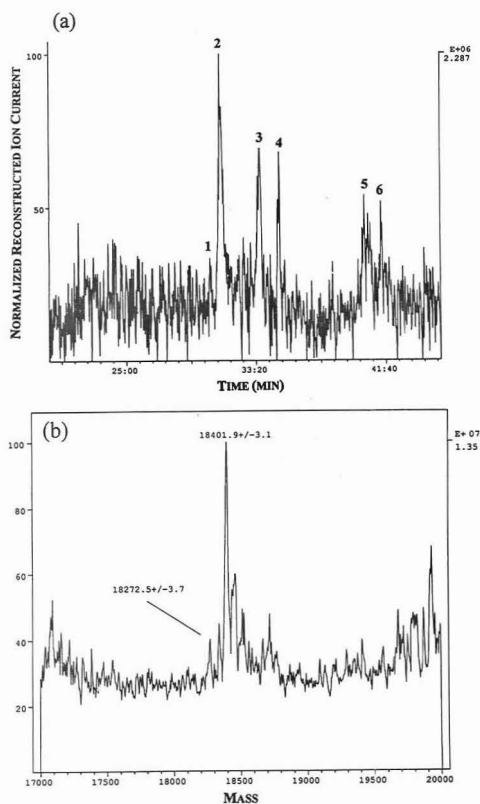


**Figure 4.** (a) CZE/MS full scan ( $m/z$  600–2000) reconstructed ion electropherogram of a 150-nL injection of 1.2  $\mu$ M each of lysozyme (1), cytochrome *c* (2), ribonuclease A (3), myoglobin (4),  $\beta$ -lactoglobulin A (5),  $\beta$ -lactoglobulin B (6), and carbonic anhydrase (not detected) dissolved in water. BGE: 0.02 M 6-aminohexanoic acid + acetic acid, pH 4.4; (b) deconvoluted spectrum of  $\beta$ -lactoglobulin B.  $M_r$  for  $\beta$ -lactoglobulin B is 18 277.<sup>34</sup> Note the complex formation at  $M_r = 18 401.9$ . The molecular weight of 6-aminohexanoic acid is 130. CE conditions as in Figure 2.

out the capillary but is lower in the BGE than in the original sample zone, resulting in slower migration of the sample ions. This could be overcome by working with constant current; however, excessive sample Joule heating would result. Thus, when a sample is dissolved in water or dilute electrolyte, sample deterioration may occur due to low ionic strength and increased Joule heat generation across the sample zone.<sup>28</sup>

The deconvolution of the spectra of both the  $\beta$ -lactoglobulin A and  $\beta$ -lactoglobulin B in Figures 3a and 4a led to the interesting observation of two values of mass, one at the correct mass for the protein and one at 130 mass units greater. The charge states corresponding to these peaks are identical, indicating that some form of complexation with the protein was occurring. Since 6-aminohexanoic acid (BGE constituent) has a molecular weight of 130, and the standard deviation of mass for both the complexed and uncomplexed protein was  $<3.0$ , the resulting increase of 130 in mass suggests the protein is complexing with the BGE. Figure 4b shows the deconvoluted spectrum of  $\beta$ -lactoglobulin B. At low concentrations

the  $\beta$ -lactoglobulin/BGE complex was significantly more abundant than the uncomplexed species. This result indicates that one needs to be cautious in interpreting data obtained in CZE with buffered electrolytes. As has been reported,<sup>29</sup> it may be possible to eliminate complex formation by increasing the nozzle to skimmer voltage to break up a complex in the source; however, this was not pursued here since the intent of this study was not to explore complexation; moreover, in this process, the sample may be fragmented leading potentially to interpretation errors.

As noted, one drawback of CZE is the limited volume of the sample that can be injected into the column without deterioration of the separation. In this study, the maximum volume that could be injected when the sample was dissolved in the BGE was 50 nL, and when the sample was dissolved in water the maximum injection volume was 150 nL. Although the injection volume could in principle be further increased with water as the sample matrix, the injection volume was still limited by the fact that the analysis time would increase significantly with the water matrix. The analysis time could be decreased by using uncoated capillaries with attendant electroosmotic flow, but in this case some proteins could adsorb to the capillary wall. This would be especially true for the basic proteins in this study.

Capillary isotachopheresis was next tested in an attempt to increase further the volume injected. Figure 5a shows the CITP/MS reconstructed ion electropherogram of a sample containing lysozyme (1), ribonuclease A (2), and  $\beta$ -lactoglobulin A (3) with 6-aminohexanoic acid added as a low molecular weight spacer to separate ribonuclease A from  $\beta$ -lactoglobulin A. In this case, large amounts of sample (250 nL, 50 pmol) were injected. A region of increased signal is visible prior to the elution of the  $\beta$ -lactoglobulin A zone. The increased signal is likely due to detection of a mixed zone of 6-aminohexanoic acid and  $\beta$ -lactoglobulin A. The deconvoluted spectrum of this region is shown in Figure 5b. As in the CZE/MS electropherogram, the analysis of this region suggested that a complex was formed between the spacer and  $\beta$ -lactoglobulin A.

The analytes in CITP elute in a stack of narrow bands. In the analysis of samples of trace concentration, these bands could become extremely narrow such that the mass spectrometer could not scan over the necessarily wide  $m/z$  range at the speed required to prevent overlap of the eluting peaks. A typical example of the narrow zones possible in CITP with UV detection is in Figure 6, which shows the separation of the same proteins as in Figure 5a, but the amount injected was 5 times less. Narrow ITP zones could easily be detected since the time constant of the UV detector was 0.1 s. This sample amount injected (5 pmol of each) could not be reliably detected by the mass spectrometer under the conditions specified because the time-based length of all three protein zones was only 12 s and the shortest zone was only 2 s wide. With the requirement of at least 1 s/scan for full scan analysis, reliable mass spectra of individual trace components could not be obtained. In principle, the rate of elution of ITP zones could be slowed by decreasing the electric field so that wider bands in terms of time could allow MS scanning. However, lower fields would lead to poorer resolution and longer migration times in CITP. Furthermore, separation at high fields, with a subsequent reduction in the field strength after UV detection, would be difficult to precisely control. Finally, optimization of protein separations by CITP is not straightforward.

An advantage of CITP, however, is the possibility of injecting and focusing relatively large sample volumes. On

(28) Vinther, A.; Soeberg, L.; Nielsen, J.; Pedersen, J.; Biederman, K. *Anal. Chem.* 1992, 64, 1878–191.

(29) Loo, J. A.; Udseth, H. R.; Smith, R. D. *Rapid Commun. Mass Spectrom.* 1988, 2, 207–210.

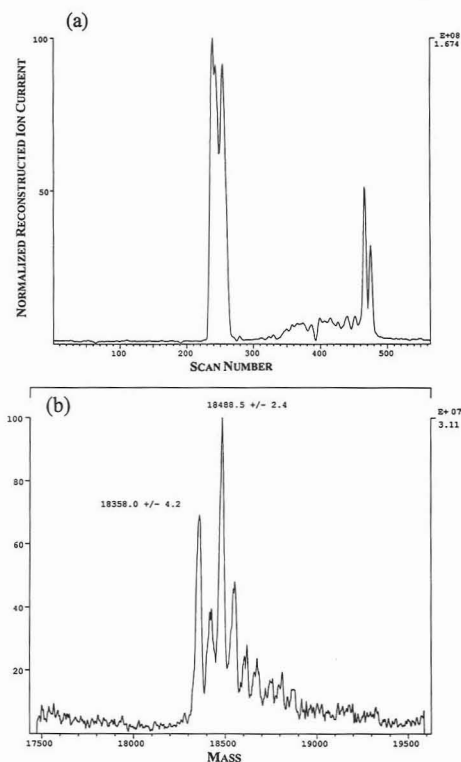


**Figure 5.** (a) CITP/MS full scan ( $m/z$  600–2000) reconstructed ion electropherogram of a 250-nL injection of 200  $\mu$ M of lysozyme, ribonuclease A,  $\beta$ -lactoglobulin A with 6-aminohexanoic acid added as a spacer. Leading electrolyte: 0.01 M ammonium acetate + acetic acid to pH 4.4. Terminating electrolyte: 0.001 M acetic acid. The  $\beta$ -lactoglobulin A peak is split in two due to instability in the electrospray process. (b) Deconvoluted spectrum of  $\beta$ -lactoglobulin A complexed with 6-aminohexanoic acid. CE conditions: constant current 6  $\mu$ A, voltage increased from 7 to 17 kV.  $M_r$  = 18 362 for  $\beta$ -lactoglobulin A.

the other hand, CZE offers the advantage of better peak separation, generally with peak widths of sufficient time for full scan MS of proteins. We, therefore, combined the advantages of CITP and CZE by employing transient CITP prior to CZE analysis.<sup>22</sup> Using a simple mixture of two standard proteins, the utility of transient CITP was tested. The sample was diluted in  $5 \times 10^{-3}$  M ammonium acetate with ammonium serving as the leading ion with the 6-aminohexanoate cation of the BGE acting as the terminating ion during the transient CITP migration.

Initially, the column was filled with the BGE, followed by siphon injection of 750 nL of the sample dissolved in ammonium acetate buffer. The end of the column was then returned to the BGE reservoir. The ammonium ions (which have high mobility) moved ahead of the sample ions when the field was applied. At this point the sample ions stacked behind the ammonium zone in a narrow band and began moving at constant velocity (as in CITP). The ammonium ions, however, continued to move through the slower BGE. Consequently, the concentration of ammonium ions in the ammonium zone rapidly decreased below the concentration

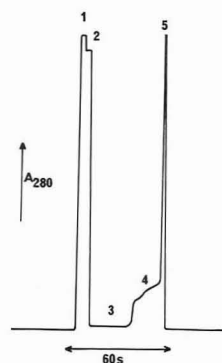


**Figure 6.** CITP analysis with UV detection of 25 nL of 200  $\mu$ M lysozyme (1), ribonuclease A (2), 6-aminohexanoic acid (3), mixed zone of (3) and (5), and  $\beta$ -lactoglobulin A (5).  $A_{280}$  = UV absorbance at 280 nm. Leading electrolyte: 0.01 M ammonium acetate + acetic acid, pH 4.4. Terminating electrolyte: 0.001 M acetic acid, pH 4.4. CE conditions: constant current 6  $\mu$ A, voltage increased from 7 to 17 kV.

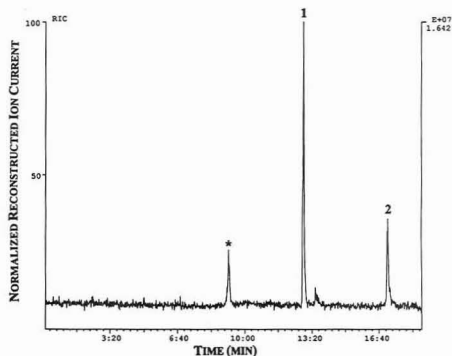


**Figure 7.** Transient CITP/MS full scan ( $m/z$  600–2000) reconstructed ion electropherogram of 450 nm cytochrome *c* (1) and 270 nM myoglobin (2) in 0.005 M ammonium acetate buffer. The peak marked (\*) is from the rear boundary of the ammonium zone. Injection volume = 750 nL (injected quantity of 337 and 202 fmol, respectively). BGE: 0.02 M 6-aminohexanoic acid + acetic acid, pH 4.4. CE conditions as in Figure 2.

necessary for ITP migration.<sup>30</sup> At this point, the zones separated as in CZE.

Using transient CITP, we were able to inject and detect sample concentrations that were significantly lower in magnitude than in CZE without preconcentration. Figure 7 shows the full scan reconstructed ion electropherogram of the protein sample containing cytochrome *c* (1) and myoglobin (2) diluted in  $5 \times 10^{-3}$  M ammonium acetate to a concentration of  $10^{-7}$  M, which is roughly 100 times lower than in Figure 2 (sample dissolved in BGE) and is 30 times lower than Figure 3a (sample dissolved in water). Furthermore, under this condition, the peaks in Figure 7 are narrower and more intense than those in Figures 2 and 3a, resulting in higher signals; however, the comparison of separation efficiency is not possible since due to the focusing step, a shorter migration length is available for the consecutive CZE separation.

Next, transient CITP/MS of the protein mixture containing lysozyme (1), cytochrome *c* (2), ribonuclease A (3), myoglobin

(30) Gebauer, P.; Boeck, P.; Thormann, W. *J. Chromatogr.* 1992, 608, 47–57.

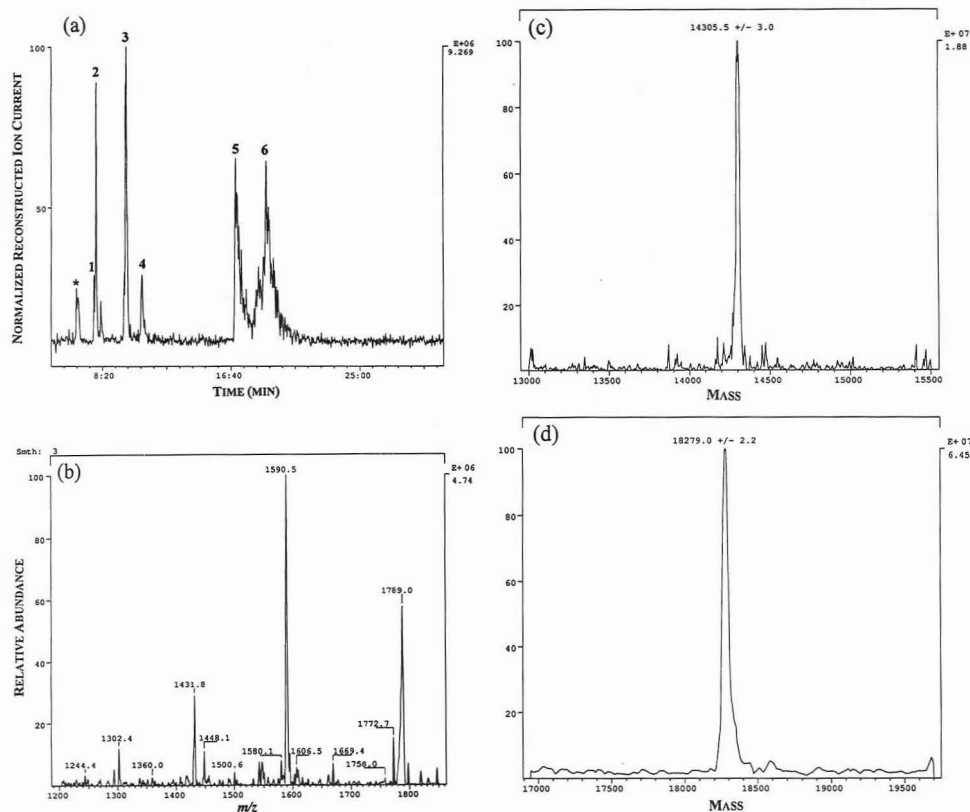


**Figure 8.** (a) Transient CITP/MS full scan ( $m/z$  600–1850) reconstructed ion electropherogram of  $\sim 500$  nM each of lysozyme (1), cytochrome *c* (2), ribonuclease A (3), myoglobin (4),  $\beta$ -lactoglobulin A (5),  $\beta$ -lactoglobulin B (6), and carbonic anhydrase (not detected) in 0.005 M ammonium acetate buffer. The peak marked (\*) is from the rear boundary of the ammonium zone. Injection volume = 750 nL. BGE: 0.02 M 6-aminohexanoic acid + acetic acid, pH 4.5. CE conditions as in Figure 2. (b) The spectrum of lysozyme obtained by averaging the scans under the peak in the electropherogram. (c) The deconvoluted spectrum of lysozyme. (d) The deconvoluted spectrum of  $\beta$ -lactoglobulin B.

(4),  $\beta$ -lactoglobulin A (5),  $\beta$ -lactoglobulin B (6), and carbonic anhydrase (not labeled) was performed. The sample concentration was  $\sim 5 \times 10^{-7}$  M for each protein. Figure 8a shows the full scan reconstructed ion electropherogram of the analysis of this mixture. When compared to Figure 3a, the increased sensitivity is apparent from the fact that the total ion currents for the peaks of greatest intensity are equivalent while the sample concentration is 24 times less in Figure 8a. In addition, the spectra, obtained from averaging the scans under the peaks shown in Figure 8b–d, indicate increased signal to noise ratios over what was obtained in Figures 3 and 4, and the biomasses calculated for these spectra are more accurate as a result of this greater signal to noise ratio.

Further examination of Figure 8a shows that there is an additional peak (\*) eluting ahead of lysozyme (also in Figure 7). This peak is caused by the rear boundary of the ammonium zone, resulting in transient increase in the ion current of the electrospray at that point. In addition, in Figure 8d, the intensity of the complex of 6-aminohexanoic acid with  $\beta$ -lactoglobulin A is much lower when compared to Figure 4b since the protein concentration is significantly higher, due to sample focusing, in Figure 8d. At the same time, the concentration of 6-aminohexanoic acid in the protein zone is significantly lower due to the electroneutrality principle.  $\beta$ -lactoglobulins A and B in Figure 8 as in Figures 3a and 4a

reveal broad bands probably due to the known multimer formation of these proteins in the pH range of 4–5.<sup>31</sup> Finally, carbonic anhydrase is missing in Figure 8 as a result of the fact that this protein does not preconcentrate under the specific conditions, because its effective mobility at this pH ( $7 \times 10^{-5}$  cm<sup>2</sup>/V-s as calculated from Figure 3a) is less than that of the BGE ( $15 \times 10^{-5}$  cm<sup>2</sup>/V-s). For preconcentrating proteins of low mobilities, the BGE would need to contain a co-ion with an effective electrophoretic mobility less than 6-aminohexanoic acid such as  $\beta$ -alanine ( $5 \times 10^{-5}$  cm<sup>2</sup>/V-s at pH 4.4). The selection of BGE co-ion can be made by comparing the electrophoretic mobilities of the sample components obtained by preliminary CZE experiments with those found in published tables.<sup>32</sup>

## CONCLUSIONS

As found with UV detection,<sup>22,33</sup> on-column transient isotachopheric sample preconcentration can be successfully used for improvement of the concentration detection limits

(31) Grinberg, N.; Blanco, R.; Yarmush, D. M.; Karger, B. L. *Anal. Chem.* 1989, 61, 514–520.

(32) Pospichal, J.; Gebauer, P.; Bocek, P. *Chem. Rev.* 1989, 89, 419–430.

(33) Foret, F.; Szoko, E.; Karger, B. L. *Electrophoresis*, submitted.

(34) Smith, R. D.; Loo, J. A.; Edmonds, C. G.; Barinaga, C. J.; Udseth, H. R. *Anal. Chem.* 1990, 62, 882–899.

in CZE/ESI/MS. This enhancement is a result of the preconcentration of a large sample volume injected into the capillary. In the most simple case described here, two conditions must be fulfilled. First, the injected sample must be supplemented by co-ions with high electrophoretic mobility that can act as leading ions for the ITP migration in the early stages of the separation. In the case of cationic separation demonstrated here, ammonium can be selected as a universal leading ion since its electrophoretic mobility is among the highest of all cations. Furthermore, ammonium ion, unlike other highly mobile inorganic ions such as sodium or potassium, does not interfere with the electrospray process. Depending on the original salt concentration of the sample, the addition of an ammonium salt in a 0.001–0.01 M concentration will be generally satisfactory in practice. If necessary, a desalting pretreatment step can be performed prior to CE analysis. The second condition requires that the background electrolyte used for CZE separation contain a co-ion with low electrophoretic mobility that can serve as a terminating ion during the transient ITP migration. Suitable

substances can be found among organic amines, amino acids, and Good's buffers, and the respective electrophoretic mobilities are listed in tables.<sup>32</sup> When the proper BGE is selected and a well-coated capillary is used to prevent adsorption, transient on-column ITP preconcentration provides reproducible and quantitative results. In a separate study,<sup>33</sup> quantitation of protein samples with concentrations less than  $10^{-8}$  M was achieved using UV detection.

#### ACKNOWLEDGMENT

The authors thank Beckman Instruments for support of this work. The authors also acknowledge Finnigan MAT Corporation for their instrument support and helpful discussions. Contribution no. 542 from the Barnett Institute, Northeastern University, Boston, MA 02115.

RECEIVED for review August 11, 1992. Accepted December 30, 1992.



# Graphitized Carbon Black Extraction Cartridges for Monitoring Polar Pesticides in Water

Antonio Di Corcia\* and Roberto Samperi

Dipartimento di Chimica, Università "La Sapienza", Piazza Aldo Moro 5, 00185 Roma, Italy

Antonio Marcomini and Susanna Stelluto

Dipartimento di Scienze Ambientali, Università di Venezia, Calle Larga S. Marta 2137, 30123 Venezia, Italy

Our previously reported procedure for analyzing pesticides in aqueous samples involving liquid-solid extraction by graphitized carbon black (GCB) followed by liquid chromatography was appropriately modified for extending the analysis to very polar pesticides and pesticide metabolites. For this purpose, a 1-g GCB reversible extraction cartridge was adopted. Pesticide reextraction was performed by back-flushing the cartridge with a suitable eluant phase. The advantages of back-flush over forward flush desorption are illustrated. On extracting 2 L of drinking water spiked with the pesticides considered, the performance of the GCB cartridge was compared to that of a 1-g C<sub>18</sub> bonded silica cartridge as well as to those of discontinuous and continuous liquid-liquid extraction (LLE) techniques. The influence of the presence of humic substances in water on the quality of the analysis of the pesticides considered was assessed. The limits of quantification (5 times the limit of detection) of this method for the pesticides considered by analyzing municipal waters were below 0.1 µg/L, except for vamidothion and cymoxanil. Quantitative recoveries of even the most polar pesticides were obtained by submitting to the analysis volumes of ground and surface water samples no greater than 1 and 0.5 L, respectively.

## INTRODUCTION

In the last 20 years, the technique of extracting organic compounds from aqueous samples by means of suitable solid sorbents has drawn a growing interest as it eliminates several well-known problems associated with the use of liquid-liquid extraction (LLE). Following the introduction of bonded-phase porous silica in small, low-cost cartridges from various suppliers, the use of liquid-solid extraction (LSE) has expanded substantially and it has been included in many analytical procedures elaborated for determining a large variety of pesticides.<sup>1-7</sup> In spite of this growing popularity, the U.S. EPA, revising overall pesticide analytical methods, has very recently elaborated methods still involving the use of the LLE technique.<sup>8</sup> Probably, the reasons for this choice are that only few studies<sup>9-12</sup> have investigated the extent to

which naturally occurring materials, such as suspended particulate matter and humic substances, may affect the LSE of pesticides. Moreover only little information<sup>13-15</sup> is found in the literature on the capability of sorbent cartridges of retaining highly polar pesticides, when extracting large volumes of water. This matter deserves more attention since a recent trend in agriculture involves the use of pesticides that are more water soluble than their predecessors and pesticide residues often occur at concentrations lower than 1 µg/L.

Very recently at our laboratory we developed a multiresidue HPLC method<sup>15</sup> for monitoring 89 pesticides in environmental waters at part per trillion levels. To extract pesticides, we use small extraction cartridges filled with graphitized carbon black (GCB). This well-known adsorbent has already proved to be effective in extracting polar compounds, such as phenols<sup>16</sup> and chloroanilines<sup>17</sup> from water samples. Direct comparison between GCB cartridges and octadecyl-bonded silica (C<sub>18</sub>) showed that the former adsorbent has a much higher ability to extract some polar pesticides from water.<sup>14</sup> With respect to C<sub>18</sub>, an additional advantage of using GCB is that base-neutral/acid fractionation of the extracted pesticides can be achieved by differential elution, by suitably exploiting the presence on the GCB surface of sites able to exchange anions.<sup>18,19</sup>

The object of this work has been that of evaluating the feasibility of a general scheme of multicomponent trace analysis, based on LSE extraction and HPLC-UV quantitation, for monitoring in natural waters a large number of pesticides, having a very broad range of polarities. In view of this, we paid particular attention to the extractability from large water volumes of those pesticides and pesticide metabolites that, being highly soluble in water, are supposed to be difficult to extract by both the LLE and LSE techniques. For this purpose, we adopted a 1-g GCB cartridge, whose design allows the reextraction of the analytes to be performed by back-flush elution.

## EXPERIMENTAL SECTION

**Reagents and Chemicals.** Excepting aldicarb and butocarbim sulfoxides and cymoxanil, all authentic pesticides were

\* To whom correspondence should be addressed.

- (1) Junk, G. A.; Richard, J. *J. Anal. Chem.* 1988, 60, 451-454.
- (2) Sauer, W. A.; Gilbert, J. *J. Liq. Chromatogr.* 1980, 3 (11), 1735-1742.
- (3) Wells, M. J. M.; Michael, J. L. *Anal. Chem.* 1987, 59, 1739-1742.
- (4) Marvin, C. H.; Brindle, I. D.; Hall, C. D.; Chiba, M. *Anal. Chem.* 1990, 62, 1495-1498.
- (5) Hinkley, D. A.; Bidleman, T. F. *Environ. Sci. Technol.* 1989, 23, 995-1000.
- (6) Tatar, V.; Popl, M. *Fresenius' Z. Anal. Chem.* 1985, 322, 419-422.
- (7) West, S. D.; Dorulla, G. K.; Poole, G. M. *J. Assoc. Off. Anal. Chem.* 1983, 66, 111-114.
- (8) Munch, D. J.; Graves, R. L.; Maxey, R. A.; Engel, T. M. *Environ. Sci. Technol.* 1990, 24, 1446-1451.
- (9) Junk, G. A. In *Organic Pollutants in Water*; Suffet, H. I., Malayandi, M., Eds.; ACS Symposium Series 214; American Chemical Society: Washington, DC, 1987; p 201.

- (10) Leoni, V.; Puccetti, G.; Colombo, R. J.; D'Ovidio, A. M. *J. Chromatogr.* 1976, 125, 399.
- (11) Johnson, W. E.; Fendinger, N. J.; Plimmer, J. R. *Anal. Chem.* 1991, 63, 1510-1513.
- (12) Di Corcia, A.; Carfagnini, G.; Marchetti, M. *Ann. Chim.* 1987, 77, 825-835.
- (13) Bellar, T. A.; Budde, W. L. *Anal. Chem.* 1988, 60, 2076-2083.
- (14) Di Corcia, A.; Marchetti, M. *Anal. Chem.* 1991, 63, 580-585.
- (15) Di Corcia, A.; Marchetti, M. *Environ. Sci. Technol.* 1992, 26, 66-74.
- (16) Di Corcia, A.; Marchetti, M.; Samperi, R. *Anal. Chem.* 1986, 58, 2048-2052.
- (17) Di Corcia, A.; Samperi, R. *Anal. Chem.* 1990, 62, 1490-1494.
- (18) Andreolini, F.; Borra, C.; Caccamo, F.; Di Corcia, A.; Samperi, R. *Anal. Chem.* 1987, 59, 1720-1725.
- (19) Campanella, L.; Di Corcia, A.; Samperi, R.; Gambacorta, A. *Mater. Chem.* 1982, 7, 429-438.

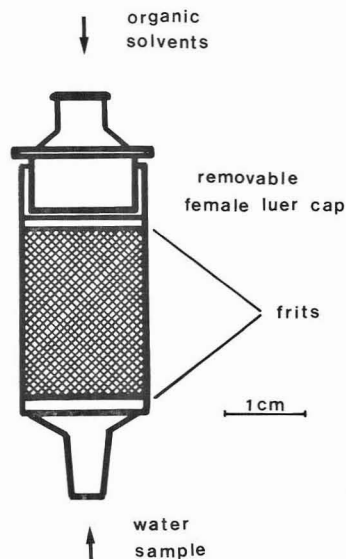


Figure 1. Schematic view of the 1-g GCB extraction cartridge.

purchased from Riedel-de-Haen, Selze, Germany.

Cymoxanil was from Eurobase, Milan, Italy. Aldicarb and butocarboxim sulfonides were individually prepared according to a procedure reported more extensively elsewhere.<sup>20</sup> Aldicarb and butocarboxim were separately dissolved in methanol-water (1:1) and oxidized at 4 °C by addition of a slightly excess amount of sodium metaperiodate. After 3 days, the reaction was blocked by adding sodium thiosulfate. As determined by HPLC analysis, the yield of the reaction was about 95%. Individual standard solutions were prepared by dissolving 50 mg of each analyte in 50 mL of methanol. By the chromatographic system adopted, it was not possible to separate all the analytes considered by a single chromatographic run. For recovery studies, we prepared two distinct composite working standard solutions by mixing 50–400  $\mu$ L of each pesticides standard solution and diluting to 10 mL with methanol.

In particular, the composition of solution 1 was as follows (in parentheses the concentrations of the analytes expressed as mg/L are reported): omethoate (20), butocarboxim sulfonide (20), aldicarb sulfonide (20), butoxycarboxim (20), aldicarb sulfone (10), methomyl (10), deisopropylatrazine (5), dicrotophos (10), fenuron (5), metatiron (10), vamidothion (40), isocarbamid (10), chloridazon (5), dimethoate (20), mevinphos (10), butocarboxim (20), aldicarb (20), metoxuron (5), bromacil (20), metribuzin (10), dichlorvos (40). The composition of solution 2 was oxamyl (10), monocrotophos (10), desethylatrazine (5), cymoxanil (40), hexazinone (10), and phosphamidon (10).

Humic acid sodium salts were supplied by Aldrich Chemical Co. (Milwaukee, WI). A humic acid solution having a concentration equivalent to an organic carbon content (DOC) of about 200 mg/L was prepared according to a previously reported procedure<sup>11</sup> but by avoiding the further dilution with water of the concentrated humic acid solution after centrifugation. Ascorbic acid was from Carlo Erba (Milan, Italy). For HPLC, distilled water was further purified by the Elgastat UHQPS apparatus (Elga, Buchs, England). Methanol and acetonitrile of gradient grade was from Riedel-de-Haen. All other solvents were of reagent grade and were used as supplied.

GCB (74–130  $\mu$ m), commercially referred to as Carbo-graph, was supplied from Carbochimica, Roma, Italy.

Void, reversible plastic tubes (see Figure 1) and plastic frits

for preparing extraction cartridges were kindly supplied from Supelco Inc. (Bellefonte, PA). The extraction cartridge was prepared by packing 1 g of GCB and locating polyethylene frits above and below the sorbent bed. To avoid crushing the Carbo-graph particles, which results in a decrease of the permeability of the cartridge, the upper frit was placed gently on the sorbent bed. Before processing water samples, the cartridge was washed with 8 mL of methylene chloride–methanol and 4 mL of methanol followed by 20 mL of 10 g/L ascorbic acid in HCl-acidified water (pH 2). The trap was fitted into a side arm filtering flask and connected to the water sample-containing bottle through a Teflon tube. Liquids were forced to pass through the cartridge by vacuum (20–30 mmHg) from a water pump.

**Procedure.** Aqueous samples were fortified with known volumes of either working standard solution 1 or 2. When tap water was analyzed, 0.5 g of  $\text{Na}_2\text{S}_2\text{O}_3 \cdot 5\text{H}_2\text{O}$ /L of water was added to avoid oxidation of some pesticides and other unwanted effects that have been previously discussed.<sup>14</sup> Sodium thiosulfate was preferred to the sodium sulfite used previously,<sup>14</sup> as the latter salt was observed to provoke some degradation of aldicarb and butocarboxim, probably due to a Bertagnini addition reaction-like mechanism occurring between sodium bisulfite and the two carbamates.

Environmental water samples were collected in empty solvent bottles and stored at 4 °C until used. Ground water samples having a dissolved organic carbon (DOC) concentration between 0.8 and 1.5 mg/L were collected from various sources near Rome and Venice. Surface water samples (4.3–8.9 mg/L DOC) were sampled from rivers and lakes situated between Florence and Rome. Unless they contained large amounts of suspended sediments, water samples were extracted unfiltered. When necessary, Whatman GF/C glass-fiber pads (pore size 10  $\mu$ m) were used. Pesticide-amended aqueous samples were agitated for 30 s and, after 10 min, connected to the sorbent cartridge by the Teflon tube. Water was forced to pass through the cartridge at a flow rate of about 100 mL/min by reducing the pressure in the vacuum apparatus to the minimum. After the sample had passed through the cartridge, the water pump was disconnected, and the cartridge was turned upside down and washed with 5 mL of distilled water, at a moderate flow rate. Most of the water was expelled by vacuum for 1 min. The residual water content was further decreased by slowly passing 0.9 mL of methanol through the cartridge. Again, the trap was air-dried for 1 min. By doing so, it was roughly estimated that 250–300  $\mu$ L of water was still present in the cartridge and carried through the rest of the procedure. Then, the water pump was disconnected, a round-bottom glass vial with an inside diameter of about 1.4 cm was set beneath the cartridge, and the analytes were eluted by passing through the trap, at flow rates of about 5–6 mL/min, 1 mL of methanol followed by 6 mL of methylene chloride–methanol (80:20, v/v). The last drops of the eluant system were forced out by a further decrease of the pressure into the flask. When glass vials narrower than those described above were used, a persistent double layer, the higher one consisting of water–methanol and the lower one consisting of methylene chloride–methanol, was formed during the solvent blow down step. In these conditions, the final extract may still contain some methylene chloride, that interferes with the subsequent separation and quantification by HPLC.

Concentration of the extract down to about 0.25 mL was performed by a water bath at 27 °C under a nitrogen stream for solvent removal. In these conditions, no trace of methylene chloride was present in the final extract.<sup>15</sup> After the final extract volume was measured by a 500- $\mu$ L syringe, 25  $\mu$ L of it was injected into the HPLC apparatus. If higher volumes of the extract were injected, a consistent broadening of the early eluting peaks was noted.

**HPLC Analysis.** Liquid chromatography was carried out with a Varian (Walnut Creek, CA) Model 5000 chromatograph equipped with a Rheodyne Model 7125 injector having a 50- $\mu$ L loop and with a Model 2550 UV detector (Varian). Columns (25 cm  $\times$  4.6-mm i.d.) filled with 5- $\mu$ m siliceous materials (Supelco) were used. The primary column contained a LC-18 DB packing and the confirmation column contained a LC-CN (cyano) packing. For separating pesticides by the primary column the initial mobile-phase composition was as follows: solvent A, water containing 2% methanol; solvent B, acetonitrile. With the

**Table I. Liquid Chromatography Retention Times and Recovery of Pesticides Added to 2-L Aliquots of a Drinking Water Sample by Extracting Them with Both 0.3- and 1-g GCB Cartridges (Spike Level: 0.3–1.2 µg/L)**

pesticide	class	water solubility, <sup>a</sup> g/L	retn time, min		recovery, <sup>b</sup> %	
			C <sub>18</sub>	CN	0.3-g GCB	1.0-g GCB
1. omethoate	phosphorothioate	miscible	5.9	3.7	31	78
2. butocarbomim sulfoxide	metabolite		6.6	3.4	60	102
3. aldicarb sulfoxide	metabolite		7.6	3.4	30	91
4. butoxyacarbomim	carbamate	208	9.7	6.2	42	98
5. aldicarb sulfone	carbamate	10	10.2	6.2	8	72
6. oxamyl	carbamate	280	10.4	7.4	84	101
7. methomyl	carbamate	58	11.3	7.8	88	100
8. monocrotophos	phosphate	1000	12.5	7.7	90	98
9. atrazine, deisopropyl-	metabolite		12.6	8.4	98	102
10. dicrotophos	phosphate	miscible	14.8	9.4	90	97
11. fenuron	phenylurea	4	17.0	10.0	98	99
12. metatritron	triazinone	2	17.6	10.9	86	95
13. vamidothion	phosphorothioate	4000	18.2	11.4	93	97
14. isocarbamid	carbamate	13	18.8	10.4	92	99
15. atrazine, desethyl-	metabolite		19.0	11.5	100	97
16. chloridazon	pyridazinone	0.4	19.4	13.4	102	100
17. dimethoate	phosphorodithioate	25	20.2	12.7	83	96
18. mevinphos	phosphate	miscible	23.2	12.7	90	92
19. cymoxanil	urea	1	23.4	10.8	92	92
20. butocarbomim	carbamate	0.35	24.4	12.6	89	93
21. aldicarb	carbamate	6	26.2	12.8	92	95
22. metoxuron	phenylurea	0.7	27.4	22.2	98	97
23. hexazinone	triazinedione	33	28.4	18.2	101	96
24. bromacil	uracil	1	28.8	17.4	100	97
25. phosphamidon	phosphate	miscible	29.6	20.4	101	98
26. metribuzin	triazinone	1	30.2	15.4	99	100
27. dichlorvos	phosphate	10	31.6	14.3	85	88

<sup>a</sup> Values taken from various sources. <sup>b</sup> Mean values calculated from three determinations.

primary column, acetonitrile was programmed linearly from 5% to 30% after 35 min. The addition of methanol to water served to improve both the symmetry and sharpness of the peak for cymoxanil. With the confirmational column, solvent A was water and solvent B was a water-methanol-acetonitrile (50:25:25) mixture. The initial mobile-phase composition was 0% B, that was programmed linearly to 32% after 24 min. The temperature of the columns was held at 30 °C. The flow rate of the mobile phase was 1.5 mL/min. The analytes were monitored with the detector set at 210 nm. Moreover, although very pure, acetonitrile was not as pure as the water used by us for the gradient elution. When operating at low AUFS ranges with the UV detector set at 210 nm, this resulted in a certain base-line drift that disturbed correct quantification of the analytes. A less pronounced drift was obtained by contaminating water with a little amount of methanol.

The concentrations of the pesticides in water were calculated by measuring manually the peak height of each pesticide and comparing them with those obtained from standard solutions. These were prepared by taking known and appropriate volumes of the working standard solutions, evaporating the methanol, and reconstituting the residue with 250 µL of water-methanol (50:50 v/v). For each pesticide considered, we observed that the response of the UV detector was linearly related to injected amounts within the range 0.025–2 µg.

## RESULTS AND DISCUSSION

For this study, we selected 23 pesticides and 4 pesticide metabolites by adopting the criteria of considering those pesticides of common use that have a water solubility equal to about or higher than 0.5 g/L and that are UV-absorbing species. For analyzing the selected compounds, we adopted the HPLC technique, as many of them are not easily amenable to analysis by standard GC methods. According to these criteria, Table I lists the selected pesticides together with some of their properties and retention times on both the primary column (C<sub>18</sub>-DB) and the confirmational column (cyano). In our experience, the use of a confirmational column is effective for decreasing the probability of false positives. However, the goal of obtaining a high-confidence identification of target compounds in complex mixtures can be reached

only by the use of a mass spectrometer as a structurally-specific HPLC detector.

In the same table recovery data obtained by extracting 2-L aliquots of a pesticide-amended drinking water sample with the cartridge under evaluation and with a previously adopted 300-mg GCB cartridge<sup>15</sup> are reported for comparison. It appears that the 1-g extraction cartridge is of more effective use for extending the multicomponent analysis of organic pollutants to very polar analytes.

Figure 2 shows typical chromatograms relative to a procedural blank from the extraction cartridge under evaluation and from analyzing 2 L of chlorine-free, municipal water samples spiked with selected pesticides at the individual level of 0.25 µg/L.

Extracting water samples spiked with the pesticides considered at concentrations lower than 1 ppb by the 1-g GCB cartridge and reextracting the analytes in the conventional mode, that is by allowing the organic solvent mixture to flow through the sorbent bed in the same way as that followed by the water sample, led to about 30 and 50% losses of metribuzin and metatritron, respectively, as shown in Table II. Doubling the volume of the eluant system did not improve the recovery of these two compounds. On the other hand, no significant loss of the two pesticides was observed if, before reextracting the analytes, the cartridge was turned upside down and it was back-flushed with the eluant system. In a previous paper,<sup>14</sup> we showed that a few quinone groups contaminating the GCB surface<sup>19</sup> were responsible for partial irreversible adsorption of particular compounds able to react with them. This unwelcome effect was eliminated by pretreating the 300-mg GCB cartridge with an aqueous solution of ascorbic acid, that reduces quinones to less reactive hydroquinones. Partial loss of the two analytes observed during desorption from the 1-g GCB extraction cartridge in the conventional mode may be explained by assuming that (i) when the aqueous sample is passed through the GCB bed, hydroquinones are in part reconverted to quinones by oxygen dissolved in water; (ii) chemisorption effects by quinones occur only in an anhydrous environment, and (iii) metribuzin and

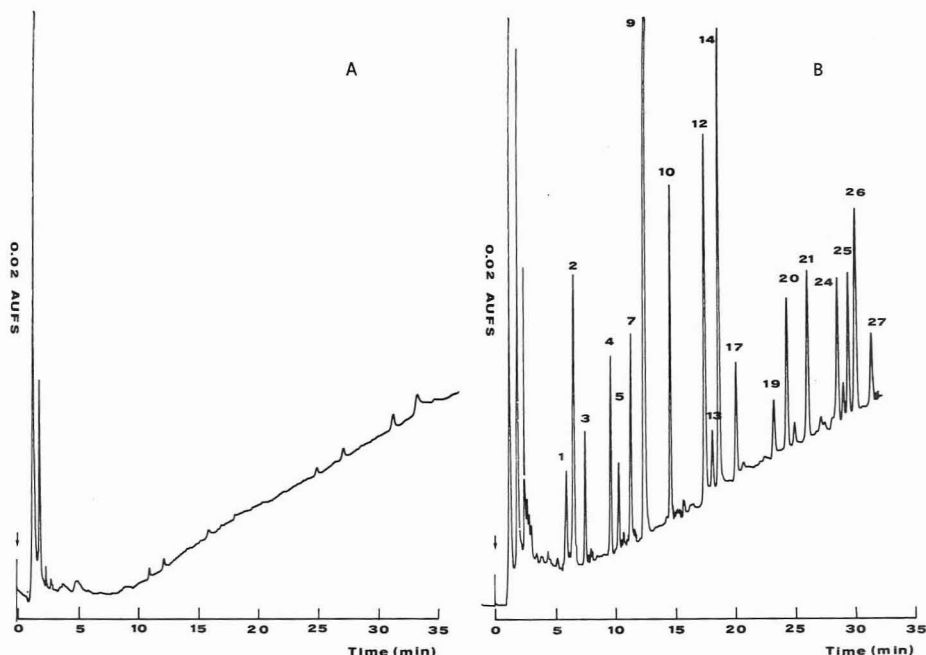


Figure 2. Chromatograms obtained on injecting the concentrated eluate from (A) a procedural blank and (B) analysis of 2 L of chloroform-free municipal water spiked with selected pesticides and pesticide metabolites at the individual level of  $0.25 \mu\text{g/L}$ . Chromatograms were recorded with the UV detector set at 210 nm and at 20 mAU full-scale sensitivity. Peak numbering corresponds to that reported in Table I.

Table II. Recovery of Metribuzin and Metamitron Extracted from 2-L Aliquots of Drinking Water by Both Back-Flushing and Forward Flushing Desorption

compd	recovery, <sup>a</sup> %			
	1-g GCB		0.3-g GCB	
	forward flushing	back-flushing	forward flushing	back-flushing
metamitron	51	93	85	92
metribuzin	72	98	98	100

<sup>a</sup> Mean values obtained from three determinations.

metamitron contained in the water sample are adsorbed on the initial part of the sorbent bed.

When these assumptions are accepted, partial irreversible adsorption of the two pesticides can take place during their elution along the sorbent column with the organic solvent mixture. The advantage of using back-flush elution over forward flush elution is that of avoiding an excessive time of contact between the two eluates and the quinone groups spread along the sorbent column. This hypothesis was substantiated by observing that, when a smaller extraction cartridge was used, such as that containing 300 mg of GCB, only a moderate loss of metamitron was obtained by forward flush desorption.

When a large-size extraction cartridge is used, an inherent advantage of desorbing the analytes by reversing the cartridge is that small volumes of the eluant phase can suffice to reextract even those adsorbates that, having a large affinity for the sorbent surface, are slowly eluted by any eluant system. With low eluate volumes, time for the solvent removal is saved and the risk of evaporative loss of the most volatile analytes is reduced. The extent of the advantage of back-flushing

Table III. Eluant Phase Volumes Needed for Reextracting Some Selected Pesticides by Both Forward Flushing and Back-Flushing the 1-g GCB Extraction Cartridge

compd	volume, <sup>a</sup> mL			
	forward elution		back-flush elution	
	neutral phase	acid phase	neutral phase	acidic phase
	Neutral			
diuron	9 <sup>b</sup>		3	
linuron	6		3	
azinphos ethyl	9		3	
coumaphos	18		6	
DDT	6		3	
	Acids			
bromoxynil		6		3
dinitro- <i>o</i> -cresol		24		6
dinoseb		6		3
pentachlorophenol		24		6

<sup>a</sup> Volume of the mobile phase sufficient for eluting 90% of the adsorbed analyte. <sup>b</sup> Mean values obtained from triplicate experiments.

over forward flushing desorption was evaluated by extracting with the 1-g GCB cartridge 2 L of a water sample spiked with some selected pesticides considered in our previous study.<sup>15</sup> Neutral pesticides were desorbed by the same solvent mixture as that reported in the Experimental Section, while acidic compounds were eluted by using a suitably acidified methylene chloride-methanol mixture.<sup>15</sup> Fractions (3 mL) of each eluant system were separately collected and, after solvent removal, analyzed by HPLC. Results reported in Table III show that, by reversing the cartridge, the analyte reextraction was achieved by making use of much lower volumes of both mobile phases. It is also noteworthy that by back-flushing the cartridge with the neutral solvent mixture, the possibility

**Table IV. Recovery Data Obtained on Extracting, with Various Techniques, Pesticides Added to 2 L of a Municipal Water Sample (Spike Level: 1–4 µg/L)**

compd	% recovery ± RSD <sup>a</sup>			
	DLLE	CLLE	C <sub>18</sub>	GCB
omethoate	58 ± 7.9	68 ± 8.2	3 ± 45	83 ± 6.2
butocarboxim sulfoxide	13 ± 14	17 ± 11	3 ± 42	102 ± 4.8
aldicarb sulfonide	16 ± 17	23 ± 12	4 ± 29	93 ± 5.2
butoxycarboxim	74 ± 6.9	83 ± 4.8	4 ± 32	98 ± 2.8
aldicarb sulfone	58 ± 11	61 ± 14	6 ± 21	75 ± 8.3
oxamyl	51 ± 10	67 ± 9.6	24 ± 12	101 ± 2.1
methomyl	64 ± 11	70 ± 7.3	10 ± 20	100 ± 2.0
monocrotophos	68 ± 5.3	86 ± 7.6	42 ± 16	98 ± 2.7
deisopropylatrazine	87 ± 4.3	94 ± 4.9	15 ± 14	102 ± 3.8
dicrotophos	78 ± 8.3	89 ± 4.3	83 ± 10	98 ± 3.0
fenuron	60 ± 7.8	85 ± 6.8	19 ± 12	99 ± 2.8
metamitron	79 ± 4.2	87 ± 2.1	28 ± 12	95 ± 4.5
vimidithion	57 ± 8.4	70 ± 7.4	87 ± 5.4	98 ± 3.8
isocarbamid	74 ± 10.4	95 ± 8.4	78 ± 6.2	97 ± 3.4
desethylatrazine	85 ± 4.1	95 ± 2.4	30 ± 13	97 ± 3.7
chloridazon	75 ± 4.2	90 ± 4.1	31 ± 11	100 ± 3.0
dimethoate	78 ± 5.9	90 ± 6.2	22 ± 14	98 ± 4.3
mevinphos	79 ± 6.7	84 ± 5.7	92 ± 6.0	94 ± 4.6
cymoxanil	89 ± 9.1	93 ± 7.2	28 ± 11	94 ± 3.4
butocarboxim	82 ± 4.9	90 ± 2.3	63 ± 9.2	95 ± 4.0
aldicarb	68 ± 12	78 ± 12	55 ± 9.4	99 ± 4.0
metoxuron	83 ± 5.1	89 ± 4.2	101 ± 3.3	97 ± 2.6
hexazinone	75 ± 11	91 ± 8.9	88 ± 4.0	98 ± 3.4
bromacil	74 ± 7.3	89 ± 5.3	87 ± 5.0	97 ± 1.9
phosphamidon	84 ± 9.5	90 ± 11	94 ± 3.7	98 ± 2.5
metribuzin	79 ± 7.4	92 ± 7.9	70 ± 7.2	96 ± 3.3
dichlorvos	64 ± 8.4	80 ± 5.9	64 ± 9.3	85 ± 10
grand mean	69	79	46	96

<sup>a</sup> Mean values obtained from four determinations.

of isolating acidic analytes from the base-neutral cartridge is not precluded. Definitively, when using a 1-g GCB extraction cartridge, the analyte desorption is much more conveniently performed by back-flushing elution, also considering that, in this way, chemisorption effects occurring for particular analytes, discussed above, are circumvented.

For the polar pesticides considered in this study, the extraction efficiency of the 1-g GCB cartridge was compared with those obtained by using discontinuous LLE (DLLE) and continuous LLE (CLLE) as well as by a 1-g C<sub>18</sub> extraction cartridge. Experiments were performed by adding pesticides to 2-L aliquots of chlorine-free municipal water sample and analyzing. DLLE of the water sample was performed by using three separate 120-mL portions of methylene chloride and following a previously reported procedure.<sup>13</sup> CLLE was carried out by bubbling 120 mL of methylene chloride through the aqueous sample for 3 h.<sup>21</sup> Water samples were passed through the two cartridges filled respectively with the C<sub>18</sub> and GCB materials, by the maximum flow rates possible with the apparatus used. The measured flow rates were about 15 and 100 mL/min, respectively, for the C<sub>18</sub> and GCB cartridges. The reextraction of the analytes from the GCB cartridge was carried out as reported in the Experimental Section, while 10 mL of methanol was used for the analyte desorption from the C<sub>18</sub> sorbent cartridges. Recovery data obtained by using the various extraction techniques are reported in Table IV. As can be seen, the 1-g C<sub>18</sub> extraction cartridge is inadequate to the multicomponent analysis of pesticides in the ppb region. Better results were obtained by the LLE technique. In particular, the CLLE technique appears to be more effective than the popular DLLE technique for extracting polar compounds from water. Compared to the DLLE technique, additional advantages of CLLE are that it is less laborious and more amenable to automation and requires a substantially

lower solvent volume. Even this technique, however, failed to extract two very polar pesticide metabolites, butocarboxim and aldicarb sulfoxides.

Among the various extraction techniques compared, that employing a 1-g GCB cartridge had the highest ability to retain hydrophilic pesticides from large water volumes. Recoveries better than 90% were obtained for the pesticides considered, except for omethoate, aldicarb sulfone, and dichlorvos. Reanalysis by another GCB cartridge of the water sample extracted by the first cartridge showed that omethoate and aldicarb sulfone were partly lost in the water effluent. Some loss of dichlorvos was found to occur during the solvent reduction step.

Johnson et al.<sup>11</sup> have recently shown that the extraction efficiency of a C<sub>18</sub> cartridge for certain selected pesticides was seriously affected when pesticides were dissolved in a distilled water sample containing Aldrich humic acids (10 mg/L DOC) to simulate a natural water sample with a high DOC. Additional experiments and considerations led the authors to the conclusion that loss of pesticides was not caused by saturation effects but by a mechanism of association of pesticides with humic acids. These latter substances, passing unadsorbed through the chemically bonded silica bed, are able to drag with them smaller, associated organic molecules. In order to verify whether a similar, negative effect could take place when the extraction procedure proposed by us was used, experiments similar to those performed by the authors cited above were repeated. Water samples (1 L) with a 5 and 10 mg/L DOC were prepared by adding suitable volumes of the Aldrich humic acid solution to distilled water. These samples were then amended with the pesticides considered in this study and also with those considered by Johnson et al. Spike levels ranged from 2 to 8 µg/L. After about 1.5 h, each spiked water sample was extracted by two in-line 1-g GCB cartridges. Experiments were done in duplicate. After the water sample was passed through the two cartridges in tandem, they were disconnected and pesticides were reextracted from both cartridges. Analysis by HPLC of the final extracts showed that when water samples with 5 mg/L DOC were analyzed, all the pesticides were completely retained by the first cartridge. On the contrary, when 1 L of the water sample with 10 mg/L DOC was analyzed, relative amounts equal to 35, 18, 20, and 39%, respectively, of omethoate, butocarboxim sulfoxide, aldicarb sulfonide, and aldicarb sulfone, that were not found in the first cartridge, were extracted from the second one. In particular, for the pesticides considered by Johnson et al., no anomalous effect due to the presence in water of humic acids was evident. Therefore, the only effect caused by the presence of a relatively high amount of humic substances in water was that of partially saturating the GCB cartridge. The results obtained by us do not exclude the occurrence of some kind of association between the pesticides considered in these experiments and humic acids. It is possible that the pesticide-humic acid complex passing through the GCB bed is captured by the anion-exchange sites existing on the GCB surface. Pesticides are then released by humic acids specifically adsorbed to the sorbent surface, when the organic system is passed through the cartridge.

With respect to the LLE technique, a serious disadvantage of the LSE technique is that, when environmental water samples are extracted, competitive adsorption processes between the components of the aqueous matrix and the analytes can overload the column to the point that the accuracy of the analysis is seriously affected. The only effective way of estimating the influence of the matrix effect on the accuracy of an analytical procedure making use of LSE is that of analyzing a reasonably large number of environmental aqueous samples from various sources after spiking them with the analytes of interest. The accuracy of the method under consideration was assessed by spiking with

(21) Stelluto, S.; Marcomini, A.; Di Corcia, A.; Marchetti, M.; Capri, S.; Liberatori, A. *Ann. Chim.* 1990, 80, 369, 377.



Table V. Accuracy of This Method for the Determination of Selected Pesticides in Various Aqueous Environmental Matrices (Spike Level: 1-4 µg/L)

	ground water (14 samples)				river water (8 samples)			
	1.0 L		2.0 L		0.5 L		1.0 L	
	av recovery, %	range	av recovery, %	range	av recovery, %	range	av recovery, %	range
omethoate	92	84-101	72	49-84	94	92-102	84	74-94
butocarbonyl sulfoxide	98	92-103	94	87-97	98	95-102	93	83-100
aldicarb sulfoxide	95	90-101	90	82-94	98	94-100	91	80-96
butoxycarbonyl	97	96-103	92	86-94	98	95-100	98	94-101
aldicarb sulfone	91	82-96	48	43-62	93	86-96	71	57-86
oxamyl	99	93-103	100	94-102	100	97-103	99	95-101
methomyl	100	94-101	101	95-100	99	95-102	100	95-102
monocrotophos	98	93-102	98	94-101	100	96-104	104	97-109
deisopropylatrazine	99	96-101	99	94-100	99	93-101	98	94-99
dicrotophos	98	93-100	96	93-99	98	94-100	97	93-101
fenuron	101	96-104	100	97-101	101	96-103	102	96-106
metamitron	96	88-100	95	90-100	95	91-101	96	89-100
vamidothion	96	95-101	99	94-101	97	94-100	98	94-102
isocarbamid	98	94-99	98	95-99	98	93-101	98	96-102
desethylatrazine	100	95-102	98	94-100	103	96-108	107	98-111
chloridazon	96	94-99	97	93-98	98	97-100	96	96-101
dimethoate	97	93-99	99	94-100	100	95-102	98	95-102
mevinphos	95	94-100	96	94-100	97	94-99	97	94-100
cymoxanil	93	84-97	94	88-101	95	88-100	95	90-102
butocarbonyl	96	95-99	97	93-99	96	94-98	95	94-97
aldicarb	97	93-99	98	94-100	98	97-100	96	95-99
metoxuron	98	94-100	96	95-99	97	94-103	100	98-106
hexazinone	97	95-99	101	97-104	99	96-101	102	95-104
bromacil	98	94-100	98	93-102	98	95-100	97	94-99
phosphamidon	97	96-99	96	95-99	97	94-100	96	94-99
metribuzin	94	94-98	95	93-99	93	92-96	97	94-100
dichlorvos	84	81-93	86	83-94	85	80-91	88	80-90

Table VI. Percent Recovery<sup>a</sup> of Some Selected Pesticides after Partial Solvent Removal

compound	final volume, µL				
	180	230	250	280	180 <sup>b</sup>
dichlorvos	81	85	95	91	85
molinate	78	86	94	97	74
butylate	56	67	83	90	60
trifluralin	66	85	91	96	85
DDT	69	80	96	99	98

<sup>a</sup> Mean values obtained from triplicate experiments. <sup>b</sup> Recoveries after addition of 50 µL of methanol to 180 µL of the final extract.

the pesticides considered several ground and surface water specimens from different sources located around Rome, Florence, and Venice. The DOC contents of the ground water samples ranged between 0.8 and 1.5 mg/L, while the DOC contents of the surface water samples were in the range between 4.3 and 8.9 mg/L. Mean recoveries calculated from these measurements (Table V) show that aldicarb sulfone was largely lost when analyzing 2 and 1 L, respectively, of ground and surface water samples. Moreover, under these conditions, omethoate and aldicarb sulfone recoveries were distributed in an unacceptably wide range. These results indicate that, when the analysis of these two pesticides has to be performed in the aquatic environment, the volumes of ground and surface waters to be submitted to the extraction procedure should not exceed 1 and 0.5 L, respectively.

In trace analysis, the volume of the eluate from the sorbent cartridge is generally reduced under a gentle nitrogen stream. The final volume of the extract is the result of a compromise aimed to maximize the enrichment factor without significant evaporative losses. When using LSE coupled to RP-HPLC, an additional positive effect of minimizing the extract volume by solvent evaporation is that the relative amount of water in the eluate increases. This makes the final extract more compatible with the mobile phase of the RP-HPLC system with the result that larger volumes of the extract can be injected into the HPLC column without peak broadening. For the pesticides considered, suitable experiments showed

that the final volume of the eluate from the GCB cartridge could be made as low as 180 µL with only a moderate loss of the most volatile pesticide, namely dichlorvos (Table VI). In these conditions, 35 µL of the final extract could be injected into the HPLC column with only a moderate peak broadening of the first three eluted analytes. However, when the eluate blow-down experiments were extended to two volatile pesticides, such as butylate and molinate, and two nonvolatile, hydrophobic pesticides, namely DDT and fenvalerate, significant losses of these compounds were noted if the extract volume was made lower than 250 µL. Adsorption effects on the glass walls of the vial could be responsible for the apparent loss of the two hydrophobic analytes, considering that a progressive decrease of the eluate volume increases the water content of the moiety in which the analytes are dissolved. In conclusion, when a general multicomponent analysis has to be performed, the final extract volume should not be made lower than about 250 µL. In this case, to avoid peak broadening of the early eluting compounds, the maximum volume of the final extract injectable into the HPLC column should not be higher than 25 µL.

For the polar pesticides under evaluation, considering the analysis of 2 L of drinking water, concentrating the relative extract to 180 µL, and injecting 35 µL of this, the estimated limits of quantitation (5 times the limits of detection) ranged between 13 and 85 ng/L, except for dichlorvos, vamidothion, and cymoxanil, whose limits of quantitation were respectively 110, 130, and 195 ng/L.

#### ACKNOWLEDGMENT

We are grateful to Silvio Capri (IRSA, CNR, Italy) for DOC measurements of real water samples.

RECEIVED for review March 10, 1992. Accepted December 21, 1992.



# Determination by Heteronuclear NMR Spectroscopy of the Complete Structure of the Cell Wall Polysaccharide of *Streptococcus sanguis* Strain K103<sup>†</sup>

G. Prabhakar Reddy, Chi-Chou Chang, and C. Allen Bush\*

Department of Chemistry & Biochemistry, University of Maryland Baltimore County, Baltimore, Maryland 21228

Although complete structures of complex polysaccharides have traditionally been determined by chemical degradative methods, a number of recent developments in instrumentation have greatly facilitated this task. We illustrate the application of several of these methods in a determination of the complete covalent structure of the polysaccharide from *Streptococcus sanguis* K103, which is composed of an octasaccharide repeating subunit linked by phosphodiester bonds. Carbohydrate analysis by HPAE-PAD and by reverse-phase chromatography of benzoylated derivatives of the hydrolysis products of the polysaccharide gave glucose (3 mol), galactose (1 mol), rhamnose (2 mol), *N*-acetylglucosamine (1 mol), and galactose 6-phosphate (1 mol). Circular dichroism of the *O*-benzoylated monosaccharides showed the absolute configurations to be *D* for all residues except for rhamnose, which is *L*. The <sup>1</sup>H NMR spectrum was completely assigned by two-dimensional homonuclear methods (DQF-COSY, NOESY, HOHAHA). The stereochemistry of pyranosides was assigned from <sup>3</sup>J<sub>HH</sub> coupling constant values determined from these experiments. The <sup>13</sup>C spectrum was assigned by <sup>1</sup>H-detected heteronuclear multiple-quantum correlation (<sup>1</sup>H/<sup>13</sup>C HMQC) and by the hybrid method of HMQC-COSY. The glycosidic linkage positions of the polymer were determined by <sup>1</sup>H-detected multiple-bond correlation (<sup>1</sup>H/<sup>13</sup>C HMBC) and by 2D-NOESY spectra. The position of the phosphodiester linkage was determined by splitting observed in the <sup>13</sup>C resonances due to <sup>31</sup>P couplings leading to the overall structure given in Chart I.

## INTRODUCTION

Determination of the complete covalent structure of the complex carbohydrate of a glycoprotein, glycolipid, or bacterial polysaccharide is a rather more subtle and difficult task than sequencing a protein or polynucleotide. Not only must the sequence of monosaccharides be determined, but the linkage position, anomeric configuration, and the absolute configuration are also required. It is notoriously difficult to predict the outcome of chemical reactions involving sugars of highly varied functionality, and this fact has complicated the development of routine chemical procedures for degradation and sequence analysis. Although some enzymatic methods have been shown to be extremely valuable, the number of known endo- and exoglycosidases is too limited to provide a general method for structure determination. Therefore there is considerable interest in development of new methods based on analytical instrumentation. We describe the integration of three recently introduced methods in the determination of the structure of the cell wall polysaccharide of *Streptococcus sanguis* strain K103.

<sup>†</sup> Research supported by NIH Grant DE-09445. This study was presented at the 31st Annual Meeting of the Eastern Analytical Symposium, Somerset, NJ, Nov 16-20, 1992.

The antigenic and lectin receptor activities of the cell wall polysaccharides of the viridans streptococci depend on distinct structural domains at the reducing as well as at the non-reducing terminal. Lectin-mediated interactions between different bacteria have been demonstrated among members of the human flora and are thought to contribute to the formation of mixed microbial communities on teeth.<sup>1-3</sup> Previous studies in our laboratory on the structures of the cell wall polysaccharides of *Streptococcus oralis* 34,<sup>4</sup> *Streptococcus mitis* J22,<sup>5</sup> *S. oralis* ATCC 10557,<sup>6</sup> *S. oralis* C104,<sup>7</sup> and *Streptococcus gordonii* 338<sup>8</sup> have shown that each functions as a receptor molecule for the galactose- and *N*-acetylgalactosamine-reactive fimbrial lectins of *Actinomyces viscosus* and *Actinomyces naeslundii* in the early stages of dental plaque formation. The polysaccharide structures are made up of different hexa- or heptasaccharide repeating units linked by phosphodiester bonds. Recognition of these structures by the lectins of *Actinomyces* sps. was postulated to depend on the exposure of internal Gal β-(1→3)GalNAc or GalNAc β-(1→3)Gal by the flexible Gal; β-(1→6) linkage.

As part of our continuing investigations of the structural basis for the lectin-carbohydrate binding, the polysaccharide from *Streptococcus sanguis* K103 was isolated and studied. This polysaccharide is a receptor for the castor bean lectin (RCA 120) but not for *Actinomyces*, and it does not appear to be antigenically related to those of the strains SS34, SS38, J22, C104, and 10557, (J. O. Cisar, unpublished results). To further explore the lectin and antigenic properties of streptococcal polysaccharides, the structure of the polysaccharide from *S. sanguis* K103 was determined by high-resolution NMR. In the course of these studies we have attempted to evaluate the steps which are essential to the structure determination of complex polysaccharides by NMR spectroscopy.

## MATERIALS AND METHODS

**Isolation of the Polysaccharide.** The cell wall polysaccharide of *S. sanguis* K103 was isolated by similar methods

(1) McIntire, F. C.; Crosby, L. K.; Vatter, A. E.; Cisar, J. O.; McNeil, M. R.; Allen Bush, C. A.; Tjoa, S. S.; Fennessey, P. V. *J. Bacteriol.* 1988, 170, 2229-2235.

(2) Cisar, J. O.; Brennan, M. J.; Sandburg, A. L. In *Molecular Basis of Oral Microbial Adhesion*; Mergenhagen, S. E., Rosan, B., Eds.; American Society for Microbiology: Washington, DC, 1985; pp 159-163.

(3) Cisar, J. O. In *Microbial Lectins and Agglutinins: Properties and Biological Activity*; Mirelman, D., Ed.; John Wiley and Sons: New York, 1986; pp 183-196.

(4) Abeysunwardana, C.; Allen Bush, C. A.; Susan, S. T.; Fennessey, P. V.; McNeil, M. R. *Carbohydr. Res.* 1989, 191, 279-283.

(5) Abeysunwardana, C.; Allen Bush, C. A.; Cisar, J. O. *Biochemistry* 1990, 29, 234-243.

(6) Abeysunwardana, C.; Allen Bush, C. A.; Cisar, J. O. *Biochemistry* 1991, 30, 6528-6539.

(7) Abeysunwardana, C.; Allen Bush, C. A.; Cisar, J. O. *Biochemistry* 1991, 30, 8568-8577.

(8) Reddy, G. P.; Abeysunwardana, C.; Allen Bush, C. A.; Cisar, J. O. Proceedings of the 11th International Symposium on Glycoconjugates, Toronto, ON, Canada, June 30-July 5, 1991; *Glycoconjugate J.* 1991, 8 (3), 235 (abstract).

described previously for the other strains.<sup>5-7</sup> Briefly, crude cell walls were prepared from bacteria cultured in 20 L of complex media and digested with mutanolysin (M-3765, Sigma Chemical Co., St. Louis, MO) to solubilize the polysaccharide. The soluble fraction, obtained after precipitation of protein in the presence of cold 5% trichloroacetic acid, was applied to a column of DE52 anion exchanger (Whatman BioSystem Ltd., Maidstone, Kent, England) equilibrated with 10 mM sodium phosphate, pH 8.0, and eluted with this buffer followed by a gradient (0–100 mM) of NaCl in starting buffer. The K103 polysaccharide emerged as the anionic component in the extract and was recovered from fractions and further purified by gel filtration.

**Sugar Composition.** The carbohydrate composition of the polysaccharide was determined by high-performance anion-exchange chromatography with pulsed amperometric detection (HPAEC-PAD) with the Dionex Bio-Lc system.<sup>9</sup> A sample of polysaccharide (200 µg) was hydrolyzed with 4 N trifluoroacetic acid (TFA; 200 µL, 100 °C, 2 h). After TFA was evaporated under a stream of nitrogen, the sample was taken up in 200 µL of deionized water and analyzed by the HPAEC-PAD system using the CarboPac PA1 column (4 × 250 mm). Neutral monosaccharides and amino sugars resulting from the acid hydrolysis were eluted with 15 mM NaOH at 1 mL/min. Phosphorylated monosaccharides were eluted by the following gradient:<sup>10</sup> solvent A was 100 mM NaOH; solvent B was 100 mM NaOH containing 1 M sodium acetate; the flow rate was 1 mL/min. The column was equilibrated in 90% A and 10% B, and the sample was injected. The samples were eluted with a two-stage linear gradient from 10% to 20% solvent B in 20 min and from 20% to 50% solvent B in 30 min. Peaks were identified by comparing the retention times with that of standard monosaccharides and monosaccharide phosphates (Sigma).

The carbohydrate composition of the polysaccharide was also determined by HPLC as perbenzoylated methyl glycosides (monosaccharides) according to the method of Jentoft.<sup>11</sup> The polysaccharide sample (1 mg) was methanolized with 1 N HCl in MeOH at 80 °C for 4 h. Following re-N-acetylation of any hexosamine present, constituent methyl glycosides were perbenzoylated as described earlier.<sup>5</sup> The peaks (UV absorbance at 230 nm) in the reverse-phase chromatography (Spherisorb C-18 ODS-II, 3 µm, 15 cm; Alltech Associates) were assigned from the retention times of perbenzoylated methyl glycosides prepared from standard monosaccharides. The O-benzoylated sugars all partition to the toluene phase in the toluene-water partition which precedes the HPLC analysis in this protocol. The phosphorylated monosaccharide, which is not cleaved in the methanolysis step, was recovered from the aqueous layer. The water layer was dried and treated with 0.5 mL of cold HF at 4 °C for 24 h to cleave the phosphate. It was dried and perbenzoylated by the above methods in order to identify the phosphorylated sugar and to determine its absolute configuration.

**CD Spectroscopy.** The absolute stereochemistry of the sugar components was determined by circular dichroism spectroscopy (Jasco J-710) in the region 200–270 nm on perbenzoylated monosaccharides collected from HPLC as described.<sup>12</sup> All the samples were dissolved in acetonitrile with a sample cell of 1 cm thickness holding a 3-mL volume. Spectra were multiply scanned, smoothed, and treated with baseline correction with the help of the J-710 software. Before CD spectra were recorded, the concentration of each sample was determined from UV absorbance using the extinction coefficient of the benzoylated chromophore at 229.5 nm ( $\epsilon$  15 300) and that of the acetamido chromophore ( $\epsilon$  1175).

**NMR.** Spectra were recorded on a General Electric GN-500 spectrometer. The observed <sup>1</sup>H chemical shifts are reported relative to internal standard sodium 4,4-dimethyl-4-silapentane-1-sulfonate (DSS) with acetone as an internal standard at 2.225 ppm. The carbon chemical shifts are reported to internal acetone (31.07 ppm). The polysaccharide sample (25 mg) was exchanged

in D<sub>2</sub>O (99.8 atom % D) and lyophilized three times. The final sample was prepared by dissolving the dried sample in 500 µL of high-purity D<sub>2</sub>O (99.96 atom % D).

Two-dimensional spectra were recorded at 25 °C without sample spinning. Data were acquired in phase-sensitive mode using the method of States et al.<sup>13</sup> in the GN-500. DQF-COSY,<sup>14</sup> TQF-COSY,<sup>15</sup> and NOESY<sup>13</sup> were recorded at 500 MHz with standard pulse sequences. A phase-sensitive homonuclear Hartman-Hann spectrum (HOHAHA) was recorded<sup>16,17</sup> with isotropic mixing by the MLEV-17 method using the pulse sequence of Bax and Davis.<sup>18</sup> Typically, 2 × 256 × 1024 or 2 × 384 × 1024 data sets were collected and zero filled in  $t_1$  to give a final data matrix of 1K × 1K real points. The spectral width was 2403 Hz in the <sup>1</sup>H dimension and 12 500 Hz in the <sup>13</sup>C dimension for all the heteronuclear two-dimensional experiments for a digital resolution in <sup>13</sup>C and <sup>1</sup>H dimensions of ±0.1 and ±0.005 ppm/point, respectively. Broad-band <sup>1</sup>H-decoupled <sup>13</sup>C spectra were obtained at 125 MHz with a 12.5-kHz spectral width and 32K complex data points. The 90° <sup>13</sup>C pulse length was 12 µs, and MLEV-16 decoupling was used.<sup>19</sup> <sup>1</sup>H-<sup>13</sup>C correlation spectra were recorded in the proton-detected mode using standard X-nucleus decoupling hardware in the GN-500 with a 5-mm RPT probe. The pulse sequence for single-bond correlation spectra (HMQC) was that of Bax et al.<sup>20</sup> WALTZ-16<sup>21</sup> decoupling at the carbon frequency was used during acquisition. Multiple-bond-correlation spectra (HMBC) were recorded in phase-sensitive mode using the pulse sequence of Bax and Summers.<sup>22</sup> Delays of 3.4 ( $1/\rho_{CH}^2$ ) and 50 ms ( $1/nJ_{CH}$ ) were used with a 1.5-s relaxation delay between acquisitions. The HMQC-COSY experiment,<sup>23</sup> combining <sup>1</sup>H-detected heteronuclear multiple-quantum coherence (HMQC) with homonuclear correlation (COSY), was recorded without <sup>13</sup>C decoupling during the acquisition.

NMR data processing was carried out on VAX station 3200 using the FTNMR program of Dennis Hare, (Hare Research Inc, Woodinville, WA). GN data were transferred via ethernet to the Vax station and converted to readable files by an in-house program (GENET). Experimental details and processing parameters of the spectra are given in the figure captions.

## RESULTS

The <sup>1</sup>H NMR spectrum (Figure 1) of the *S. sanguis* K103 polysaccharide in D<sub>2</sub>O at 500 MHz shows eight resonances in the anomeric region, with three of them (4.615, 4.501, and 4.443 ppm) having a doublet line shape of approximately 8 Hz. The resonance having a semiquartet at 5.629 ppm suggests an anomeric proton of an  $\alpha$ -glycosyl phosphate residue. The high-field region of the spectrum shown in Figure 2 contains two methyl resonances at 1.330 and 1.249 ppm ( $d$ ,  $J$  = 6.0 Hz) and a sharp peak at 2.126 ppm consistent with the presence of two 6-deoxy sugars and an acetamido sugar.

The <sup>13</sup>C spectrum (Figure 1) of the polysaccharide shows eight carbon signals in the region expected for anomeric resonances and the HMQC spectrum (Figure 1) shows that they correlate with the anomeric <sup>1</sup>H resonances, confirming the presence of eight sugar residues in the repeating subunit.

(13) States, D. J.; Hakerborn, R. A.; Ruben, D. J. *J. Magn. Reson.* 1982, 48, 286–292.

(14) Rance, M.; Sorensen, O. W.; Bodenhausen, G.; Wagner, G.; Ernst, R. R.; Wuthrich, K. *Biochem. Biophys. Res. Commun.* 1983, 117, 479–485.

(15) Piantini, U.; Sorensen, O. W.; Ernst, R. R. *J. Am. Chem. Soc.* 1982, 104, 6800–6801.

(16) Braunschweiler, L.; Ernst, R. R. *J. Magn. Reson.* 1983, 53, 521–528.

(17) Davis, D. J.; Bax, A. *J. Am. Chem. Soc.* 1985, 107, 2820–2821.

(18) Bax, A.; Davis, D. G. *J. Magn. Reson.* 1985, 65, 355–360.

(19) Levitt, M. H.; Freeman, R.; Frenkiel, T. *J. Magn. Reson.* 1982, 47, 328–330.

(20) Bax, A.; Griffey, R. H.; Howkins, B. L. *J. Magn. Reson.* 1983, 55, 301–315.

(21) Shaka, A. J.; Keeler, J.; Frenkiel, T.; Freeman, T. *J. Magn. Reson.* 1983, 52, 335–338.

(22) Bax, A.; Summers, M. F. *J. Am. Chem. Soc.* 1986, 108, 2093–2094.

(23) Gronenborn, A. M.; Bax, A.; Wingfield, P. T.; Clore, G. M. *FEBS Lett.* 1989, 243, 93–98.

(9) Hardy, M. R.; Townsend, R. R.; Lee, Y. C. *Anal. Biochem.* 1988, 170, 54–62.

(10) *Dionex Technical Note; TN 20; Dionex Corp. Sunnyvale, CA, March 1989.*

(11) Jentoft, N. *Anal. Biochem.* 1985, 148, 424–433.

(12) Kalurachchi, K.; Bush, C. A. *Anal. Biochem.* 1989, 179, 209–215.

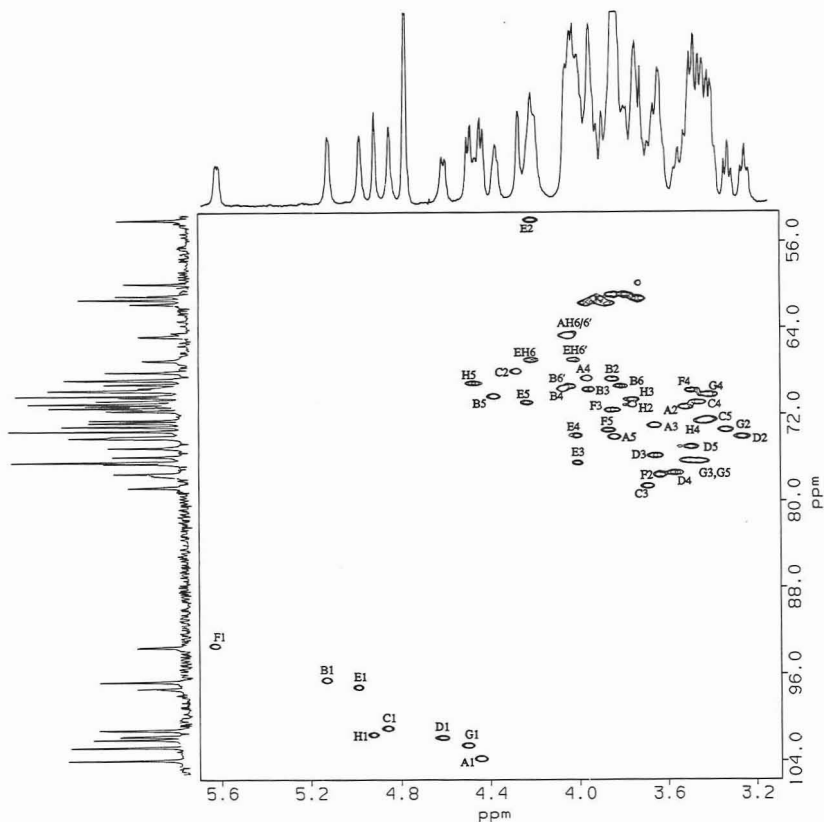


**Figure 1.** Phase-sensitive,  $^{13}\text{C}$ -decoupled,  $^1\text{H}$ -detected multiple-quantum-correlation spectrum ( $^1\text{H}[^{13}\text{C}]$  HMQC) of the polysaccharide from *S. sanguis* K103 at 500 MHz. The data matrix was  $2 \times 384 \times 1\text{K}$  complex points with 48 scans per  $t_1$  value. The spectral window was  $\pm 6250$  Hz in the  $F_1$  dimension ( $^{13}\text{C}$ ) and  $\pm 1201$  Hz in the  $F_2$  dimension ( $^1\text{H}$ ). Relaxation delays of 1.5-s, 3.40-ms ( $1/2 J_{\text{CH}}$ ), and 426-ms acquisition time were used in the experiment. Data were apodized in  $t_2$  by Gaussian line broadening of 3 Hz and  $90^\circ$  sine-bell apodization with zero filling in the  $t_1$  dimension to obtain a  $1\text{K} \times 1\text{K}$  real matrix. Peaks are labeled with a capital letter identifying the residue followed by the number assigning the carbon (proton) atom. The 1D proton spectrum and 1D carbon spectrum are shown on top and left, respectively.

The  $^{13}\text{C}$  resonances at 17.50 and 17.68 ppm (not shown) are consistent with the assignment to the methyl carbon of two 6-deoxy sugars. The resonance at 54.17 ppm is characteristic for a carbon atom attached to a nitrogen, as in an *N*-acetamido sugar. Further evidence for an acetamido sugar is provided by the resonance at 175.21 ppm characteristic of a carbonyl carbon and one at 23.04 ppm for methyl carbon (data not shown).

Carbohydrate analysis by the HPAEC-PAD method gave 3 mol of glucose (Glc), 2 mol of rhamnose (Rha), 1 mol of *N*-acetylglucosamine (GlcNAc), and 1 mol of galactose (Gal) when the column was eluted with 15 mM NaOH, thus accounting for only seven residues. It was observed previously with the polysaccharides of similar strains<sup>5-7</sup> that cleavage of the phosphate attached to C-6 of the nonreducing terminal was incomplete under the hydrolysis conditions employed for the carbohydrate analysis, thus leaving it as a 6-phosphorylated monosaccharide. Expecting similar results for this polysaccharide, we eluted the column with the acetate gradient described under Materials and Methods, which is used to identify phosphorylated sugars.<sup>10</sup> A peak at  $24.4 \pm 0.5$  min corresponds to the retention time of standard gal-6- $\text{PO}_4$ . Reverse-phase HPLC of the *O*-benzoyl derivatives

identified the same seven sugar residues as found by HPAEC-PAD chromatography, suggesting that acidic methanolysis does not cleave the phosphorylated sugar. But after HF treatment of the aqueous layer in the toluene-water partition, followed by perbenzoylation, a peak corresponding to galactose was detected in HPLC.

CD bands were detected in the 230-nm region for the *O*-benzoylated monosaccharides. The absolute configuration of each sugar was deduced by the exciton chirality method.<sup>12</sup> The data (Table I) clearly show the assignment of both rhamnose residues to the L configuration and the three glucose residues to the D configuration. If the two rhamnose residues had opposite configuration, the CD signals would be expected to cancel, and if the three glucose residues were not all D, cancellation would reduce the observed  $\Delta\epsilon$  and  $A$  values to  $1/3$  the value in standards. It is also evident from the data that the other two sugars, GlcNAc and two galactoses, are in the D configuration. The chromatographic and CD data indicate that the polysaccharide is composed of 3 mol of D-Glc, 2 mol of L-Rha, 2 mol of D-Gal, and 1 mol each of *N*-acetyl-D-glucosamine and phosphate. These data are consistent with an octasaccharide repeating unit polymerized through a phosphodiester linkage.

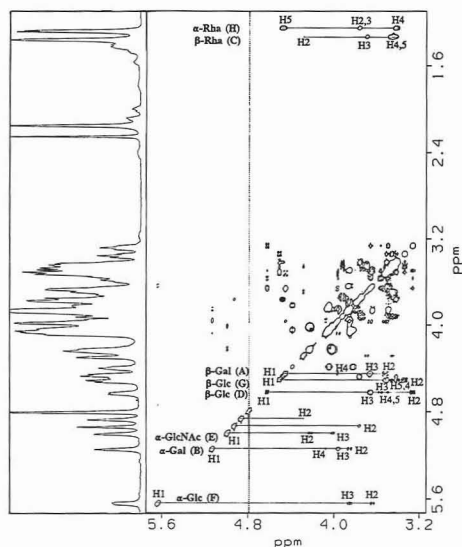


**Figure 2.** Homonuclear Hartman-Hann spectrum (HOHAHA) of the polysaccharide from *S. sanguis* K103 at 500 MHz. The spin-locking time was 70 ms. The data matrices were  $2 \times 256 \times 1\text{K}$  complex points with 32 scans per  $t_1$  value. Gaussian line broadening with 6 and 3 Hz was used in the  $t_2$  and  $t_1$  dimensions respectively. Spectra were zero filled in  $t_1$  to obtain  $1\text{K} \times 1\text{K}$  real matrices.

**Table I.** Circular Dichroism Data for Perbenzoylated Methyl Glycosides

perbenzoylated methyl glycoside	$A^\circ$	long wavelength		short wavelength	
		$\Delta\epsilon$	$\lambda$	$\Delta\epsilon$	$\lambda$
<b>standards</b>					
$\alpha$ -D-Gal	70	46.55	237.6	-23.48	221.8
$\beta$ -D-Gal	68	46.70	237.5	-20.82	221.9
$\alpha$ -D-Glc	11	10.03	233.8	-1.19	219.4
$\beta$ -D-Glc	19	15.16	235.6	-3.74	219.5
$\alpha$ -L-Rha	80	60.77	236.6	-19.05	221.2
$\alpha$ -L-Fuc	-87	-69.25	236.6	18.07	221.4
$\alpha$ -D-Man	-59	-43.89	238.4	14.92	222.6
$\alpha$ -D-GalNAc	15	9.95	238.3	-4.56	222.5
$\alpha$ -D-GlcNAc	-23	-17.37	239.1	5.82	223.4
<b>K103</b>					
$\alpha$ -D-Gal	70	46.76	237.7	-22.82	221.9
$\beta$ -D-Gal	66	47.54	237.6	-18.44	221.1
$\alpha$ -D-Glc	11	9.93	235.4	-1.55	219.4
$\beta$ -D-Glc	19	15.25	235.1	-3.75	219.6
$\alpha$ -L-Rha	80	63.18	236.8	-17.09	221.5
$\alpha$ -D-GlcNAc	-22	-16.52	238.7	5.85	223.1
$\alpha$ -D-Gal-6-PO <sub>4</sub>	69	48.18	237.5	-20.93	222.2
$\beta$ -D-Gal-6-PO <sub>4</sub>	66	48.77	237.6	-16.86	222.1

$^\circ A = \Delta\epsilon(\text{long } \lambda) - \Delta\epsilon(\text{short } \lambda)$ . See ref 12.

Identification of the stereochemistry of the individual sugar components was straightforward and similar to the methods reported earlier.<sup>5-7</sup> The well-separated downfield  $^1\text{H}$  anomeric signals provided a good starting point in tracing out the individual spin systems, based on their characteristic multiplicity patterns and vicinal coupling constant values,<sup>24</sup> observed in the DQF-COSY spectrum.<sup>25,26</sup>

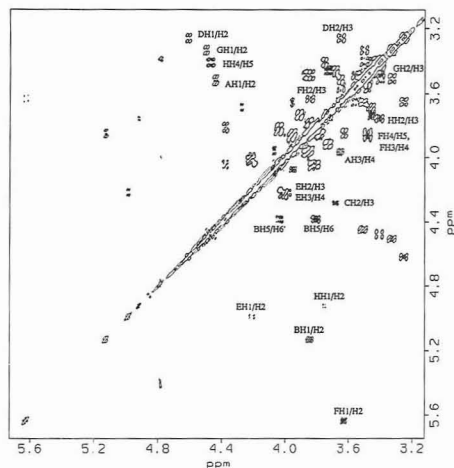


**Figure 3.**  $^1\text{H}$  phase-sensitive homonuclear DQF-COSY spectrum of the polysaccharide from *S. sanguis* K103 at 500 MHz. The data matrix was  $2 \times 256 \times 1\text{K}$  complex points, 32 scans per  $t_1$  value. Sine-bell apodization with  $30^\circ$  and  $65^\circ$  phase shifts were used in the  $t_2$  and  $t_1$  dimensions, respectively. Data were zero filled in the  $t_1$  dimension to obtain a final data matrix with  $1\text{K} \times 1\text{K}$  real points. Both positive and negative contours are shown in the plot.

The H-1/H-2 cross peak for the most downfield resonance, residue F, at 5.629/3.633 ppm shows displacement of resonances in  $\omega_1$  and  $\omega_2$  cross sections, apparently due to long-range coupling of  $^{31}\text{P}$  in the DQF-COSY spectrum (Figure 3). The H-2/H-3 cross peak is well separated and shows partial cancellation of the central components, indicating equal  $J_{23}$  and  $J_{34}$  coupling constants. The assignment of H-4 and H-5 was not possible from the DQF-COSY spectrum due to overlapping of H-3/H-4 and H-4/H-5 cross peaks giving a distorted multiplet structure. The cross section taken through the anomeric (H-1) proton in the HOHAHA spectrum (Figure 2) for this residue clearly shows connectivity up to H-3, and the line shape of the H-3 resonance (pseudotriplet) identifies it as the gluco configuration having equal  $J_{23}$  and  $J_{34}$  coupling constants ( $\approx 9$  Hz). Due to the close proton chemical shift values of H-3 and H-5 for this residue, we have relied on heteronuclear experiments, HMQC and HMBC, for the exact assignments of the chemical shift and the coupling constants. For strongly coupled proton resonances, the intrasite long-range  $^1\text{H}$ - $^{13}\text{C}$  connectivities observed in the HMBC spectrum (Figure 4) provide chemical shift information. The long-range intrasite correlations observed in the HMBC spectrum depend on the relative stereochemistry of the sugar unit. Correlation peaks are generally observed between resonances for residues with relatively large two- and three-bond  $^{13}\text{C}$ - $^1\text{H}$  coupling constants, which have been reported for peracetylated methyl glycosides by Morat et al.<sup>27</sup> Thus the anomeric proton (residue F) gave long-range correlation peaks to C-3 and C-5 as shown in the HMBC spectrum (Figure 4). Once the carbon chemical shift is known, the proton chemical shift value can easily be obtained from the HMQC spectrum. In this way, resonance assignments up to H-5 were obtained and cross sections taken through C-3 (Figure 5a) and C-4 (Figure 5b) of the HMQC spectrum for residue F show a pseudotriplet line shape for both the resonances,

(24) Altona, A.; Hasnoot, C. A. G. *Org. Magn. Reson.* 1980, 13, 417-429.

(25) Dabrowski, J.; Eijchart, A.; Kordowicz, M.; Hainfland, P. *Magn. Reson. Chem.* 1987, 25, 338-331.

(26) Berman, E. *Eur. J. Biochem.* 1987, 165, 385-391.

(27) Morat, C.; Taravel, F. R.; Vignon, M. R. *Magn. Reson. Chem.* 1988, 26, 264-270.

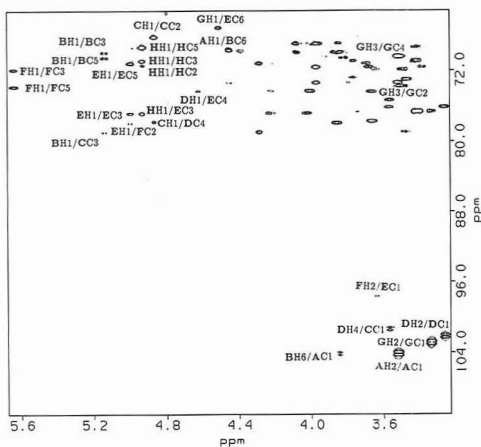


**Figure 4.**  $^1\text{H}$ -detected,  $^1\text{H}$ - $^{13}\text{C}$  multiple-bond-correlation spectrum ( $^1\text{H}$ - $^{13}\text{C}$ HMBC) of the polysaccharide at 500 MHz. The data matrix was  $2 \times 384 \times 1\text{K}$  complex points with 32 scans per  $t_1$  value. The spectral window was  $\pm 6250$  Hz in the  $F_1$  dimension and  $\pm 1201$  Hz in  $F_2$ . Relaxation delays of 3.4 ( $1/2 J_{\text{CH}}$ ) and 50 ms ( $1/2 J_{\text{CH}}$ ) were used in the experiment. Data were apodized in  $t_2$  by Gaussian line broadening of 3 Hz and  $90^\circ$  sine-bell apodization in  $t_1$  together with zero filling to obtain a  $1\text{K} \times 1\text{K}$  real matrix. The data are presented in mixed mode, absorption in  $F_1$ , and absolute value in  $F_2$ .

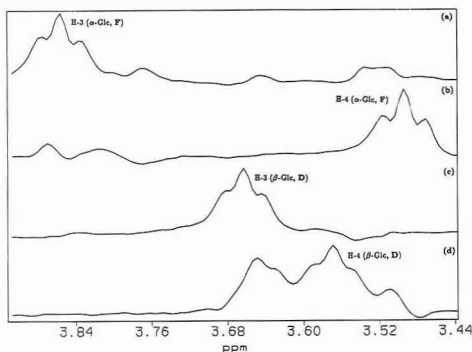


**Figure 5.** Cross section taken through C-3 (a) and C-4 (b) for residue F,  $\alpha$ -Glc, and cross section taken through C-3 (c) and C-4 (d) for residue D,  $\beta$ -Glc, from the HMBC spectrum.

confirming the gluco configuration. The assignments of H-6 and H-6' were obtained by the HMQC-COSY method, which is described below. The anomeric configuration was found to be  $\alpha$  for this residue on the basis of the observed  $J_{12}$  coupling constant ( $\approx 3.1$  Hz) and an H-1/H-2 cross peak observed in the NOESY spectrum (Figure 6). Thus residue F is identified as  $\alpha$ -glucose.

Cross-peak connectivity from the downfield anomeric resonance at 5.129 ppm yielded proton assignments up to H-4 for residue B, from both DQF-COSY (Figure 3) and HOHAHA spectra (Figure 2). Cross-peak fine structure of the H-1/H-2 and H-3/H-4 cross peaks in the DQF-COSY spectrum shows small active couplings for  $J_{12}$  and  $J_{34}$  ( $\approx 3.4$  Hz), indicating a sugar residue having the  $\alpha$ -galactopyranose configuration.<sup>5,6</sup> As expected for sugars with the galactopyranose configuration, the H-4/H-5 cross peak was not observed in the DQF-COSY spectrum due to the small coupling ( $J_{45} < 1$  Hz). The H-1 proton for this residue gave an intrasite cross peak to C-3 and C-5 in the HMBC spectrum (Figure 4),

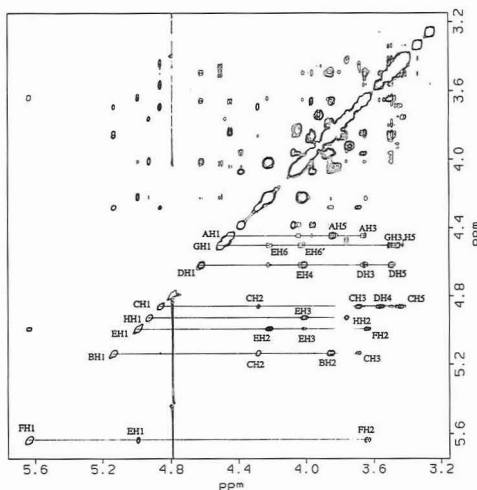


**Figure 6.** Phase-sensitive NOESY spectrum of the *S. sanguis* K103 polysaccharide at 500 MHz. The data matrix was  $2 \times 256 \times 1\text{K}$  complex points with 32 scans per  $t_1$  value. The spectral width was 2403.84 Hz, with 300-ms mixing time. Processing parameters are shifted sine bell with  $65^\circ$  in  $t_1$  and Gaussian line broadening with 3.0 Hz in the  $t_2$  dimension, respectively, with zero filling in the  $t_1$  dimension to obtain  $1\text{K} \times 1\text{K}$  real points.

and the corresponding H-5 resonance was assigned from the HMQC spectrum. The H-6 and H-6' resonance assignments were obtained from either DQF-COSY (Figure 3), TQF-COSY (data not shown), or HMQC-COSY spectra.

The anomeric resonance at 4.998 ppm, residue E, gave a cross peak to the H-2 resonance at 4.212 ppm in the DQF-COSY spectrum (Figure 3). Further, in the HMQC spectrum (Figure 1), the H-2 resonance correlated with a carbon resonance appearing at 54.17 ppm identifying this residue as the *N*-acetamido sugar detected in the chromatographic carbohydrate analysis. The large distorted cross peak for the H-2/H-3 resonance (Figures 2 and 3) indicates close chemical shift values for the H-3 and H-4 resonances and prevents observation of connectivity beyond H-3 in the DQF-COSY spectrum. Heteronuclear experiments (described below) were used to obtain accurate assignments and multiplet shapes of the individual resonances for this acetamido sugar, labeled as residue E. However the residue must be  $\alpha$ -*N*-acetylglucosamine since the carbohydrate analysis by both the HPAEC-PAD and reverse-phase HPLC methods showed the presence of only one acetamido sugar in the polysaccharide.

The proton resonances at 4.922 and 4.858 ppm appeared as an unresolved singlets ( $J_{12} < 2$  Hz). The anomeric resonance at 4.922 ppm, assigned as residue H, gave a cross peak to the H-2 proton at 3.758 ppm, and correlation starting from the methyl signal (H-6) at 1.249 ppm was traced out in the DQF-COSY spectrum (Figure 3) to H-3 (3.758 ppm), which had the same chemical shift as H-2 (3.758 ppm). The HOHAHA spectrum (Figure 2) also supported the assignment of this residue as rhamnose. For a situation such as this in which the H-2 and H-3 resonances have identical chemical shift values, the HMQC-COSY spectrum can be utilized in assigning accurate chemical shift and multiplet shapes as will be described below. The anomeric configuration of this residue was determined to be  $\alpha$  from the 2D NOESY spectrum (Figure 6), which shows NOE connectivity from H-1 to H-2 as the only intrasite NOE cross peak.<sup>5</sup>



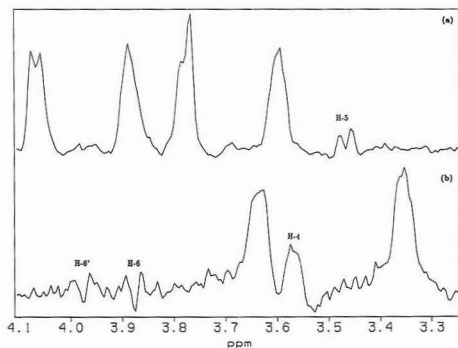


**Figure 7.** Cross sections of the phase-sensitive HMQC-COSY spectrum of the polysaccharide at 500 MHz recorded without  $^{13}\text{C}$  decoupling during the acquisition. The data matrix was  $2 \times 256 \times 1\text{K}$  complex points with 64 scans per  $t_1$  value. The spectral window was  $\pm 6250$  Hz in the  $F_1$  dimension and  $\pm 1201$  Hz in the  $F_2$  dimension. Relaxation delay of 1.5 s was used. Gaussian line broadening (3 Hz) in  $t_2$  and sine-bell apodization in  $t_1$  were used prior to Fourier transformation. Data were zero filled in the  $t_1$  dimension to obtain a  $1\text{K} \times 1\text{K}$  real matrix with digital resolution of  $\pm 0.005$  (H) and  $\pm 0.1$  ppm/point ( $^{13}\text{C}$ ). Cross section taken through C-6 (a) for residue G,  $\beta$ -Glc, and cross section taken through C-5 (b) for residue D,  $\beta$ -Glc, from the HMQC-COSY spectrum.

The other narrow resonance at 4.858 ppm, assigned as residue C, showed an H-1/H-2 cross peak in the HOHAHA spectrum (Figure 2) and in the DQF-COSY spectrum at lower contour level. The remaining assignments were straightforward starting from the upfield methyl proton at 1.330 ppm in the HOHAHA and DQF-COSY spectra, confirming that residue C is the second rhamnose. The anomeric configuration is  $\beta$  since the NOESY spectrum (Figure 6) gave intraresidue NOE cross peaks to H-2, H-3, and H-5.<sup>5</sup>

The anomeric resonance at 4.615 ppm ( $J_{12} = 8$  Hz), residue D, shows an H-1/H-2 cross peak with partial cancellation of the central components in the DQF-COSY spectrum, indicating equal  $J_{12}$  and  $J_{23}$  coupling constants. Exact values of the  $J_{12}$  and  $J_{23}$  coupling constants were obtained from the well-resolved H-2 resonance in the resolution-enhanced 1D spectrum (Figure 1). The connectivity was traced out from the DQF-COSY spectrum starting from the anomeric resonance up to H-5 and was further confirmed with the HOHAHA spectrum (Figure 2). Due to the cancellation of the central components in the DQF-COSY spectrum, the exact line shapes were obtained from the HMQC spectrum, which clearly shows the resonances for H-3 (Figure 5c) and H-4 (Figure 5d) as pseudotriplets, indicating equal  $J_{23}$ ,  $J_{34}$ , and  $J_{45}$ . The large coupling constants identify residue D as glucose in the  $\beta$ -configuration. Further, the NOE cross peaks (Figure 6) observed between H-1 to H-3 and H-5 confirm this residue as  $\beta$ -glucose. The H-6 and H-6' for this residue were assigned from the HMQC-COSY spectrum. In this spectrum, a cross section taken through C-5 (Figure 7b) showed relay peaks to H-6 and H-6'.

The proton resonance at 4.501 ppm, residue G, gave a cross peak to the H-2 resonance at 3.332 ppm in the DQF-COSY spectrum, and the exact coupling constants  $J_{12}$  and  $J_{23}$  were obtained from the well-resolved H-2 (triplet) resonance from the 1D spectrum (Figure 1). Due to the close chemical shift values for the H-3, H-4, and H-5 protons for this residue, the DQF-COSY spectrum and HOHAHA spectrum failed to provide accurate assignments for these resonances. As a result of identical carbon chemical shift values for C-3 and C-5, the HMQC spectrum also gave unresolved cross peaks for H-3/

C-3 and H-5/C-5 resonances. The problem was resolved in the long-range heteronuclear correlation spectrum HMBC, Figure 4. The assignment up to H-3 was easily obtained from the DQF-COSY spectrum (Figure 3) and the H-3 resonance in the HMBC spectrum gave cross peaks to C-2 and C-4, thus providing the assignment of H-4 from the HMQC spectrum (Figure 1). Further, a cross peak from H-4 to C-6 for this residue in the HMBC spectrum enabled assignment of the corresponding H-6 and H-6' from the HMQC spectrum. The assignments for this residue were completed by observation of a HMBC cross peak from H-6 to C-5. The pseudotriplet line shape obtained from the isolated H-4/C-4 cross peak in the HMQC or in the HMQC-COSY spectrum clearly identifies this residue as the gluco configuration. The anomeric configuration for this residue was identified as  $\beta$  on the basis of NOESY cross peaks observed from H-1 to H-3 and H-5 as well as from the  $J_{12}$  coupling constant (8.2 Hz).

The remaining proton resonance at 4.443 ppm, residue A, showed a large active coupling ( $J_{12} = 8$  Hz) in the H-1/H-2 cross peak in the DQF-COSY spectrum and a small active coupling ( $J_{34} = 3.6$  Hz) in the H-3/H-4 cross peak, indicating a  $\beta$ -galactopyranose configuration.<sup>5,6</sup> As expected, no cross peak was observed between H-4 and H-5 due to the small  $J_{45}$  coupling ( $< 1$  Hz). The H-5 resonance for this residue was obtained from the NOESY spectrum (Figure 6) as the anomeric proton gave a cross peak to the H-3 and H-5 resonances. The resonances of H-6 and H-6', which appeared at the same chemical shift values, were obtained from the HMQC-COSY spectrum.

Although most of the assignments were derived from the homonuclear (HOHAHA, NOESY, DQF-COSY) and simple heteronuclear methods (HMQC, HMBC), some problems resulting from chemical shift overlap were encountered in these experiments. They were overcome by the hybrid experiment, HMQC-COSY, which utilizes the advantage of greater spectral dispersion in the  $^{13}\text{C}$  dimension combined with homonuclear correlation. A cross section taken through a particular carbon frequency shows direct correlation peaks that are analogous to the diagonal peak in the COSY spectrum in addition to relay peaks to vicinal protons. Large vicinal proton couplings give stronger relay peaks while smaller couplings tend to give weaker relay peaks. When this experiment is recorded without  $^{13}\text{C}$  decoupling during acquisition, direct peaks are split by  $^1\text{J}_{\text{CH}}$  coupling displacing them from peaks of vicinal protons which are strongly coupled. Thus the relay peaks which are not split by  $^{13}\text{C}$  coupling appear between the components of the direct peak, thereby allowing accurate assignments of both chemical shift and proton multiplet shape.

The utility of the HMQC-COSY method can be demonstrated in assigning proton and carbon resonances for residue E,  $\alpha$ -GlcNAc, which posed problems in both the DQF-COSY and HOHAHA spectra. As we already identified the H-2/C-2 cross peak for this residue from the DQF-COSY and HMQC spectrum, the cross section taken through the C-2 carbon in the HMQC-COSY spectrum showed relay peaks to the vicinal protons, H-1 and H-3 (Figure 8a), thus providing assignment of H-3 and C-3. The cross section taken through C-3 identifies the vicinal protons, H-2 and H-4 (Figure 8b), providing the exact chemical shift of the H-4 proton. The cross section taken through C-4 showed a relay peak to the H-5 proton (Figure 8c), enabling the assignment of the corresponding C-5 from the HMQC spectrum. Finally, the cross section taken through the C-5 resonance (Figure 8d) identified the relay peaks to the H-6 and H-6' protons. The same approach was used to verify the assignments obtained by the other experiments for residue F,  $\alpha$ -Glc. The cross section taken through C-3 for this residue in the HMQC-



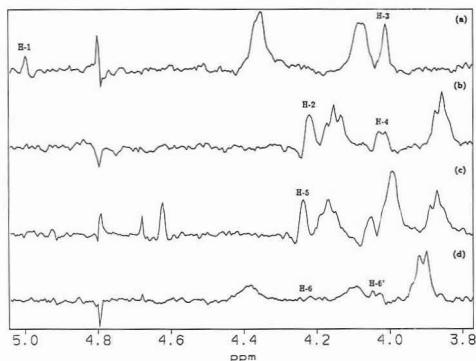


Figure 8. Cross section taken through C-2 (a), C-3 (b), C-4 (c), and C-5 (d) for residue E,  $\alpha$ -GlcNAc, from the HMQC-COSY spectrum.

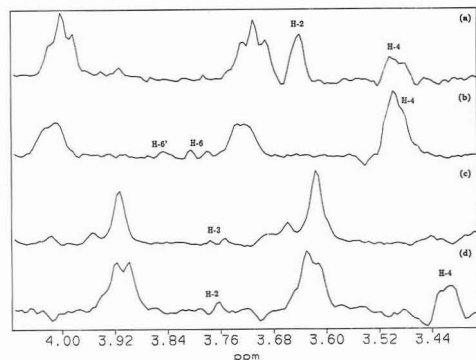


Figure 9. Cross section taken through C-3 (a) and C-5 (b) for residue F,  $\alpha$ -Glc, and cross section taken through C-2 (c) and C-3 (d) for residue H,  $\alpha$ -Rha, from the HMQC-COSY spectrum.

COSY spectrum shows relay peaks to H-2 and H-4 (Figure 9a), and the cross section from C-5 not only identifies H-4, but also H-6 and H-6' (Figure 9b).

The assignment for  $\alpha$ -Rha (residue H) is complicated by strong coupling of the H-2 and H-3 proton resonances at 3.758 ppm. But the dispersion in the carbon dimension (C-2 at 71.40 ppm and C-3 at 70.88 ppm) allows interpretation of the cross sections through C-2 and C-3 of the HMQC-COSY spectrum, providing accurate  $^1\text{H}$  chemical shifts. In the cross section from C-2 at 71.40 ppm (Figure 9c), the H-2 signal was split by  $^1J_{\text{CH}}$ , revealing a relay peak at 3.758 ppm from the H-3 proton. The cross section taken through C-3 (70.88 ppm) gave a relay peak at 3.758 ppm (Figure 9d) due to the vicinal proton H-2, which had the same chemical shift value as H-3 (3.758 ppm) in addition to a relay peak at 3.409 ppm from the H-4 resonance. Thus, one can effectively assign both chemical shift and multiplet shape from the HMQC-COSY spectrum even in case of  $^1\text{H}$  chemical shift degeneracy.

We have found the HMQC-COSY spectrum to be especially useful in connecting the H-6 and H-6' resonances with H-5 of their respective sugars in the polysaccharide. Although the triple-quantum-filtered COSY (TQF-COSY) has been found useful for assignment of H-5 and H-6 of galactose residues, it is less useful for glucose residues.<sup>5,6</sup> We have not observed cross peaks arising from H-5 to H-6 and H-6' in the TQF-COSY spectrum for the glucose residues in the polysaccharide (data not shown), perhaps as a result of a small coupling between H-5 and one of the H-6 resonances. The

HOHAHA spectrum also failed to provide the connectivity to the H-6 and H-6', but the connectivities were observed in the HMQC-COSY spectrum, either in cross sections taken through C-5 giving relay peaks to H-6 and H-6' or in cross sections taken through C-6 giving relay peaks to H-5. As an example, Figure 7b shows the cross section taken through C-5, for residue D, giving relay peaks to H-6,6' and Figure 7a shows the cross section taken through C-6, for residue G, showing the relay peak to its H-5 proton. Similar approaches were used in identifying the rest of the H-6,6' connectivities for the other sugars in the polysaccharide. (All these connectivities observed for this polysaccharide are summarized in Table III.)

Given the complete proton and carbon assignments in Table II, the glycosidic linkage positions are readily assigned from the data of the HMBC spectrum (Figure 4). All the anomeric protons except H-1 of  $\alpha$ -glucose (residue F) gave correlation to the aglycon carbon atom through  $^3J_{\text{CH}}$  coupling across the glycosidic linkage, defining the linkage position of the respective monosaccharides forming the repeating unit of the polysaccharide. The anomeric proton of  $\beta$ -Gal, residue A, showed long-range correlation to B C-6, defining the linkage as  $\beta$ -Gal(1 $\rightarrow$ 6)- $\alpha$ -Gal. The anomeric proton of residue B ( $\alpha$ -Gal), in addition to intraresidue cross peaks to its C-3 and C-5 gave an interresidue cross peak to C C-3 ( $\beta$ -Rha), defining the linkage  $\alpha$ -Gal(1 $\rightarrow$ 3)- $\beta$ -Rha. The anomeric proton of  $\beta$ -Rha (residue C) showed an interresidue correlation to D C-4, indicating the linkage  $\beta$ -Rha(1 $\rightarrow$ 4)- $\beta$ -Glc in the polysaccharide. Further, the H-1 proton of residue D ( $\beta$ -Glc) shows an interresidue long-range correlation to E C-4, and the anomeric proton of residue E ( $\alpha$ -GlcNAc) gave a long-range correlation to F C-2, in addition to intraresidue cross peaks to C-3 and C-5, thus defining the linkage  $\beta$ -Glc(1 $\rightarrow$ 4)- $\alpha$ -GlcNAc(1 $\rightarrow$ 2)- $\alpha$ -Glc in the polysaccharide. The two remaining residues,  $\alpha$ -Rha (residue H) and  $\beta$ -Glc (residue G), were found to be linked to the same residue, i.e.,  $\alpha$ -GlcNAc (residue E), as shown by their long-range interresidue cross peaks observed in the HMBC spectrum. The anomeric proton of  $\alpha$ -Rha (residue H) in addition to the intraresidue cross peaks to C-2, C-3, and C-5, showed a clear interresidue cross peak to E C-3, indicating the linkage as 1 $\rightarrow$ 3 to the  $\alpha$ -GlcNAc (residue E). The remaining anomeric proton for residue G ( $\beta$ -Glc) gave a long-range interresidue cross peak to E C-6, defining its linkage position as 1 $\rightarrow$ 6 to the same  $\alpha$ -GlcNAc (residue E), thus providing complete linkage assignments in the polysaccharide. As summarized in Table III, the 2D-NOESY spectrum (Figure 6) also showed correlation cross peaks defining the glycosidic linkages described above.

No interresidue long-range correlation cross peak was observed for the anomeric proton of the  $\alpha$ -Glc (residue F) in either the HMBC or the NOESY spectrum, indicating involvement in the phosphodiester linkage forming the repeating unit. The position of the phosphodiester linkage is suggested by the  $^{31}\text{P}$  scalar couplings observed in the resolution-enhanced  $^{13}\text{C}$  spectrum (data not shown). Both C-1 ( $^2J_{\text{PC}} \approx 6.0$  Hz) and C-2 ( $^3J_{\text{PC}} \approx 7.0$  Hz) of residue F ( $\alpha$ -Glc) show  $^{13}\text{C}$ - $^{31}\text{P}$  coupling, and the anomeric  $^1\text{H}$  resonance is also split by  $^{31}\text{P}$  coupling.  $^{13}\text{C}$ - $^{31}\text{P}$  coupling is also observed at C-6 ( $J_{\text{PC}} \approx 3.5$  Hz) for residue A ( $\beta$ -Gal), suggesting a phosphodiester linkage between C-1 of  $\alpha$ -Glc (residue F) and C-6 of  $\beta$ -Gal (residue A).

All the observed long-range inter- and intraresidue cross peaks observed in the HMBC spectrum, as well as the data from the other experiments, are summarized in Table III. These linkage assignments, together the phosphodiester linkage between  $\alpha$ -Glc (residue F) and  $\beta$ -Gal (residue A), yielded the structure shown in Chart I for the repeating unit of the polysaccharide from *S. sanguis* K103.

Table II. Chemical Shifts of *Streptococcus sanguis* K103 Polysaccharide in D<sub>2</sub>O at 25 °C

assgnmt	residue							
	α-Glc F	α-Gal B	α-GlcNAc E	α-Rha H	β-Rha C	β-Glc D	β-Glc G	β-Gal A
	<sup>1</sup> H Chemical Shifts <sup>a</sup>							
H-1	5.629	5.129	4.988	4.922	4.858	4.615	4.501	4.443
H-2	3.633	3.849	4.212	3.758	4.278	3.259	3.333	3.513
H-3	3.849	3.956	4.000	3.758	3.686	3.654	3.509	3.658
H-4	3.484	4.071	4.014	3.410	3.463	3.564	3.405	3.964
H-5	3.869	4.379	4.235	4.476	3.424	3.490	3.458	3.838
H-6	3.787	3.816	4.216	1.249	1.330	3.871	3.738	4.05
H-6'	3.854	4.039	4.028			3.968	3.918	4.05
	<sup>13</sup> C Chemical Shifts <sup>b</sup>							
C-1	93.63	96.81	97.47	101.86	101.30	102.13	102.86	104.05
C-2	77.78	68.99	54.17	71.40	68.25	74.33	73.70	71.62
C-3	71.85	69.95	76.70	70.88	78.89	76.11	76.54	73.34
C-4	70.04	69.90	74.25	72.71	71.16	77.67	70.42	68.93
C-5	73.70	70.58	71.16	69.38	72.91	75.25	76.52	74.38
C-6	61.15	69.70	67.19	17.50	17.68	61.94	61.50	64.95

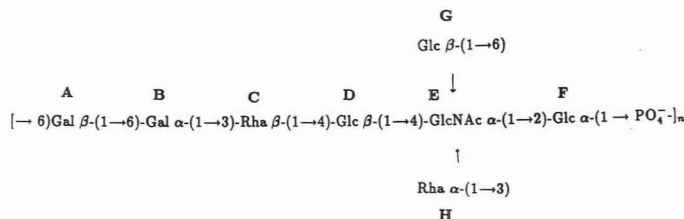
<sup>a</sup> <sup>1</sup>H NMR chemical shifts are with reference to internal DSS with acetone as the internal standard (2.225 ppm downfield from DSS). <sup>b</sup> <sup>13</sup>C NMR chemical shifts are with reference to internal DSS with acetone as the internal standard (31.07 ppm downfield from DSS).

Table III. Summary of Observed Connectivities in NMR Spectra of the Polysaccharide from *Streptococcus sanguis* K103 in D<sub>2</sub>O at 25 °C<sup>a</sup>

expt	α-Glc F	α-Gal B	α-GlcNAc E	α-Rha H	β-Rha C	β-Glc D	β-Glc G	β-Gal A
HOHAHA								
H-1	H-2,3	H-2,3,4	H-2,3	H-2	H-2	H-2,3,4,5	H-2,3,4,5	H-2,3,4
H-6				H-2,3,4,5	H-2,3,4,5			
NOESY								
H-1	H-2, EH-1 <sup>b</sup>	H-2, CH-2, CH-3 <sup>b</sup>	H-2, FH-2 <sup>b</sup>	H-2, EH-3 <sup>b</sup>	H-2,3,5, DH-4 <sup>b</sup>	H-3,5, EH-4 <sup>b</sup>	H-3,5, EH-6,6' <sup>b</sup>	H-3,5, BH-6 <sup>b</sup>
HMQC-COSY								
C-1		H-2	H-2			H-2	H-2	H-2
C-2	H-3	H-1,3	H-1,3	H-3	H-3	H-1,3	H-1	H-1
C-3	H-2,4	H-4	H-2,4	H-2,4	H-2,4	H-2,4	H-4	H-4
C-4	H-3,5	H-3	H-5	H-3,5	H-3,5	H-3,5	H-3,5	H-3
C-5	H-4,6,6'	H-6,6'	H-6,6'	H-4,6	H-4,6	H-4,6,6'	H-4,6,6'	H-6,6'
C-6	H-5	H-5	H-5	H-5	H-5	H-5	H-5	H-5
HMBC								
H-1	F3, F5	B3, B5, C3 <sup>b</sup>	E3, E5, F2 <sup>b</sup>	H2, H3, H5, E3 <sup>b</sup>	C2, D4 <sup>b</sup>	E4 <sup>b</sup>	E6 <sup>b</sup>	B6 <sup>b</sup>
H-2	E1, F3	B4	E3, E4	H3	C3, C4	D1, D3	G1, G3	A1, A3
H-3	F2	B2	E4	H4	C4	D4, D2	G2, G4	A2
H-4	F3, F5, F6	B2, B3	E3	H3, H5	C3, C5	D3, D5	G3, G6	A3, A2
H-5		B6						A4, A6
H-6			E5	H4, H5	C4, C5		G5	

<sup>a</sup> The individual residues are identified by capital letters, and the <sup>13</sup>C resonance is identified by a capital letter followed by a number for the carbon atom assigned. All protons show signals arising from one-bond correlations with their attached carbon atoms in HMQC. <sup>b</sup> Interresidue connectivities.

## Chart I



## CONCLUSIONS

A number of problems may be encountered in the use of the heteronuclear <sup>1</sup>H-<sup>13</sup>C NMR method for determination of a polysaccharide structure given a sample of sufficient size to make a 5–15 mM solution, which is required for these <sup>1</sup>H-detected experiments with natural-abundance <sup>13</sup>C. Approximately 10–20 mg of polysaccharide was used in the experiments reported here. First, strongly coupled <sup>1</sup>H signals

prevent tracing of the spin system and determination of multiplet pattern which is required for identification of the stereochemistry of the pyranoside sugars. We have described how this problem can be generally solved by HMQC-COSY. If the <sup>13</sup>C chemical shifts are also close, HMBC spectra are often useful. Second, gauche protons may have small <sup>3</sup>J<sub>HH</sub> preventing tracing of the spin system of the sugar ring. Examples in this polysaccharide are the small *J*<sub>4,5</sub> in pyranosides with the galacto configuration and small *J*<sub>1,2</sub> in sugars

with the manno configuration such as rhamnose. We have described how HMBC can overcome this difficulty since it follows  $J_{CH}$  rather than  $J_{HH}$ . NOESY spectra may also be useful in this case since the gauche protons with small coupling are close in space and have large NOE. A problem related to the small coupling constants is short  $T_2$  and wide NMR lines resulting from long rotational correlation times of the polysaccharide. Internal motion in the polymer alleviates this problem and is related to polysaccharide structure and dynamics. The line widths for the polysaccharide from *S. sanguis* K103 and related polymers having the teichoic acid type linkage are relatively narrow.<sup>28</sup> Application of this method to polymers with less internal flexibility, such as the capsular polysaccharide of *Vibrio vulnificus*, was possible at a higher NMR probe temperature.<sup>29</sup>

(28) Abeygunawardana, C.; Bush, C. A. Determination of the Chemical Structure of Complex Polysaccharides by Heteronuclear NMR Spectroscopy. In *Advances in Biophysical Chemistry*; Bush, C. A. Ed.; JAI Press: Greenwich, CT, in press.

(29) Reddy, G. P.; Hayat, U.; Abeygunawardana, C.; Fox, C.; Wright, A. C.; Maneval, D. R.; Bush, C. A.; Morris, G. M., Jr. *J. Bacteriol.* 1992, 174, 2620-2630.

(30) Gerwig, G. J.; Kamerling, J. P.; Vliegthart, J. F. G. *Carbohydr. Res.* 1978, 62, 349-357.

Although the absolute configurations of the monosaccharides in this polysaccharide are those most commonly found, the great variability of the structures of bacterial polysaccharides requires an unambiguous determination. The CD method used in this work, which is a natural adjunct of the HPLC method for carbohydrate analysis, gives the absolute configurations of all the sugars including amino sugars and sugar phosphates. The method is distinct from the more commonly used method involving high-resolution chromatography of glycosides with chiral alcohols.<sup>30</sup> It has the added advantage that a sound theoretical basis for distinguishing optical isomers is provided by the chiral exciton theory.

#### ACKNOWLEDGMENT

We thank Dr. J. O. Cisar, National Institute of Dental Research (NIDR, Bethesda, MD) for providing the purified sample of *S. sanguis* K103 polysaccharide and for his continuing interest in this research project. We acknowledge Dr. C. Abeygunawardana for his helpful advice on the NMR experimental techniques.

RECEIVED for review October 20, 1992. Accepted December 23, 1992.

# Effect of Model Organic Compounds on Potentiometric Stripping Analysis Using a Cellulose Acetate Membrane-Covered Electrode

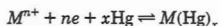
Joseph H. Aldstadt and Howard D. Dewald\*

Department of Chemistry, Clippinger Laboratories, Ohio University, Athens, Ohio 45701-2979

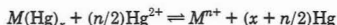
The effects of model surfactants (sodium dodecyl sulfate, Triton X-100), proteins (ovalbumin, gelatin), and carbohydrates (agar, starch) as well as D-camphor and humic acid on a cellulose acetate dialysis membrane-modified mercury film electrode (CM-MFE) in potentiometric stripping analysis (PSA) are described. The CM-MFE (1000 amu molecular weight cutoff) minimized interference by these compounds to the PSA measurement. The constant current stripping analysis (CCSA) mode was found to provide a more stable response than the use of Hg(II) as chemical oxidant with the CM-MFE. Results presented for urine and natural water samples demonstrate the analytical utility of the CM-MFE in PSA.

## INTRODUCTION

Potentiometric stripping analysis (PSA) is a powerful technique for rapidly measuring trace levels of heavy metals.<sup>1,2</sup> As with the more commonly used technique of anodic stripping voltammetry (ASV), a metal analyte (*M*) is first preconcentrated as a mercury amalgam during the "deposition step":



ASV and PSA differ, however, during the second step, known as the "stripping step". In ASV, a potential waveform is applied, and the current arising from oxidation of the metal analyte out of the amalgam is measured. In PSA, the metal analyte is stripped from the amalgam using oxidants in solution. The potentiostat is disconnected following the deposition step, and the time required to pass through the metal's redox potential is measured. Using mercuric ion as the stripping agent, the stripping step in PSA is described by:



In a variation of PSA, called constant current stripping analysis (CCSA), the metal analyte is stripped by a constant oxidizing current passed through the working electrode rather than by a chemical oxidant. In either PSA or CCSA, the time required to oxidize the analyte is directly proportional to the concentration of the metal ion.

The adsorption of proteins and surfactants or the accumulation of reaction products on the electrode surface can result in a gradual loss of electrode activity when a mercury electrode is used in the determination of heavy metals in complex mixtures.<sup>3-6</sup> An obvious way to improve selectivity in PSA

is by using modified electrodes to protect the surface from adsorptive interferences.

In stripping analysis, two general categories of polymer-modified electrodes (PMEs) have been used to improve method selectivity: specific and nonspecific. Specific PMEs are ion-exchanging polymers ("ionomers") that selectively preconcentrate analyte within the polymer, while nonspecific PMEs serve to control access to the electrode surface by acting as diffusion barriers. The perfluorosulfonate cation-exchange resin Nafion has been used as a specific PME material in anodic stripping voltammetry (ASV)<sup>7,8</sup> and PSA<sup>9</sup> for the determination of heavy metals in various environmental and clinical samples. For nonspecific PMEs, cellulose acetate films<sup>10,11</sup> and cellulose acetate dialysis membrane-covered electrodes<sup>12-14</sup> have been reported in ASV. The cellulose acetate films used by Wang and Hutchins-Kumar could be prepared with molecular weight cutoffs as low as ~200 amu, while commercially available dialysis membranes with lower limits of 1000 amu were employed by Smart and Stewart.

We have found that the nonspecific cellulose acetate PME material is more advantageous in routine analytical applications than the specific Nafion PME material, primarily as a result of significant preconcentration by the Nafion. Six or more replicates per sample are required to obtain a steady signal using a Nafion-modified MFE in ASV, and consecutive samples show a carry-over effect.<sup>15</sup> The nonspecific cellulose acetate dialysis membrane-modified MFE (CM-MFE) does not preconcentrate analyte as severely, thereby requiring fewer replicates per sample and minimizing carryover. The primary disadvantage of using a CM-MFE arises from the presence of the relatively thick membrane at the redox surface in decreasing the sensitivity. However, we have observed that relative to an unmodified MFE, the sensitivity of a CM-MFE (1000 amu cutoff) is reduced by a factor of ~18 in ASV but only by a factor of ~6 in PSA.

For a nonspecific polymer such as cellulose acetate, a process of dialysis occurs across the solution-membrane-electrode interphases. The driving force in dialysis is the concentration gradient across the membrane where the permeability of the membrane governs partitioning between the membrane and adjacent phases. The flux (*J*) across the membrane is defined

(7) Hoyer, B.; Florence, T. M.; Batley, G. E. *Anal. Chem.* 1987, 59, 1608-1614.

(8) Hoyer, B.; Florence, T. M. *Anal. Chem.* 1987, 59, 2839-2842.

(9) Huiliang, H.; Jagner, D.; Renman, L. *Anal. Chim. Acta* 1988, 207, 17-26.

(10) Wang, J.; Hutchins, L. D. *Anal. Chem.* 1985, 57, 1536-1541.

(11) Wang, J.; Hutchins-Kumar, L. D. *Anal. Chem.* 1988, 58, 402-407.

(12) Schimpff, W. K. Dissertation, University of Michigan, 1971.

(13) Stewart, E. E.; Smart, R. B. *Anal. Chem.* 1984, 56, 1131-1135.

(14) Smart, R. B.; Stewart, E. E. *Environ. Sci. Technol.* 1985, 19, 137-140.

(15) Aldstadt, J. H.; Dewald, H. D. *Anal. Chem.* 1992, 64, 3176-3179.

(1) Jagner, D. *Analyst (London)* 1982, 107, 593-599.

(2) Hussam, A.; Coetzee, J. *Anal. Chem.* 1985, 57, 581-585.

(3) Brezonik, P. L.; Brauner, P. A.; Stumm, W. *Water Res.* 1976, 10, 605-612.

(4) Cominoli, A.; Buffle, J.; Haerd, W. *J. Electroanal. Chem.* 1980, 110, 259-275.

(5) Sagberg, P.; Lund, W. *Talanta* 1982, 29, 457-460.

(6) Nelson, A.; Mantoura, R. F. C. *J. Electroanal. Chem.* 1984, 164, 265-272.

as

$$J = \frac{dx}{dt} C_s = P(C_s - C_d)$$

where  $x$  is the direction perpendicular to the membrane surface,  $t$  is the time,  $P$  is the permeability of the membrane, and  $C_s$  and  $C_d$  are the concentrations of analyte on the sample and detector sides of the membrane surface, respectively ( $C_s$  and  $C_d$  will differ from the bulk concentrations except at equilibrium).<sup>16</sup> The electrochemical driving force across the membrane gives rise to a steeper concentration gradient from the change of oxidation state upon amalgamation (in a 1:1 stoichiometry). The use of CCSA with a dialysis membrane-modified electrode for the method described herein eliminates an opposing gradient of divalent cations within the membrane [i.e., analyte vs the Hg(II) oxidant], thereby increasing the dialysis efficiency.

Electroanalytical techniques for studying the effect of complex organic compounds that differ in the excitation, response, measurement duration, and type of electrode have different specific sensitivities to these substances.<sup>17</sup> Although many applications of PSA with a MFE in complex matrices (e.g., urine, milk, and blood) have been reported,<sup>18-20</sup> a thorough characterization of the MFE in PSA by the major classes of interfering substances (proteins, carbohydrates, and surfactants) does not exist. We report here our results using the MFE and the CM-MFE in PSA for several model compounds of these classes.

## EXPERIMENTAL SECTION

**Apparatus.** A Radiometer TraceLab Model PSU20 potentiometric stripping analyzer with Model SAM20 sample station was used for all measurements. A 3-mm i.d. glassy carbon disc working electrode, saturated calomel reference electrode (SCE), and platinum wire auxiliary electrode were also obtained from Radiometer.

**Reagents and Supplies.** All reagents were prepared in water that was de-ionized and then doubly distilled. Heavy metal standards (nitrate salts) were prepared volumetrically from atomic absorption standards (Fisher Scientific, Pittsburgh, PA). A pH of 3 (the isoelectric point of cellulose acetate<sup>21</sup>) was maintained in solutions for analysis in order to minimize ion exchange within the membrane as well as to prevent the formation of metal hydroxides. OPTIMA-grade nitric acid (Fisher Scientific) was used for the adjustment of pH; reagent-grade nitric acid (Fisher Scientific) was used elsewhere. Pb(II) and Cd(II) samples (50 ppb each) were prepared in 10 mM KNO<sub>3</sub> (pH 3.0).

Model organic compounds were prepared at 250 mg/L from technical grade stock and stored at 4 °C. Sodium dodecyl sulfate (SDS) (Pierce), Triton X-100 (Z. D. Gilman, Inc.), humic acid (Janssen Chimica), ovalbumin (Merck), and gelatin (Fisher Scientific) were prepared by dissolution in reagent water. D-Camphor (Eastman) was dissolved in 1 mL of 95% (v/v) ethanol before aqueous dilution. The agar (Sargent-Welch) and starch (Fisher Scientific) solutions were prepared (without preservative) using standard procedures.<sup>22</sup>

Spectrum Spectra/por 7 cellulose acetate dialysis membranes (20 μm thickness and ~10 Å pore diameter) with a nominal molecular weight cutoff of 1000 amu were obtained from Fisher Scientific. As permeability decreases exponentially with in-

creasing solute size,<sup>23</sup> a sharp molecular weight cutoff point does not exist with these membranes.

Urine samples were obtained from laboratory personnel while natural water samples were gathered from the Hocking River near Athens, OH, downstream of a sewage treatment facility. All samples were acidified to 0.5 M using nitric acid and were stored in polyethylene containers. Each sample was spiked with Pb(II) and Cd(II) standards immediately prior to analysis.

**Procedures. Container Cleaning.** Heavy metal reagent solutions were stored in polyethylene containers that had been soaked in 0.1 M HNO<sub>3</sub> for at least 1 week.

**Electrode Polishing.** The working electrode was polished on a felt pad with 0.05 μm γ-Al<sub>2</sub>O<sub>3</sub> (Buehler Ltd., Lake Bluff, IL), followed by rinsing with 6 M nitric acid and reagent water before drying in the air.

**MFE Preparation.** MFEs were prepared in solution ex situ using 0.40 mM Hg(NO<sub>3</sub>)<sub>2</sub> in 0.13 M HNO<sub>3</sub> for 20 min at -900 mV (all potentials are vs SCE). Mercury films were obtained by holding the potential at -900 mV for 30 s and then stepping the potential to -100 mV for 5 s. Forty of these 35-s periods were run consecutively. Following this cycling period, the potential was held at -100 mV for 120 s. Stripping was performed using 40 μM Hg(NO<sub>3</sub>)<sub>2</sub> and dissolved oxygen as oxidants or with the constant current stripping analysis (CCSA) mode (1-5 μA).

**CM-MFE Preparation.** The membranes were prepared and stored as described by Stewart and Smart.<sup>13</sup> Spectra/por 7 cellulose acetate dialysis membranes were heated for 20 min at 70 °C in reagent water, followed by 48 h at 4 °C in reagent water to remove traces of the sodium azide preservative. To prevent degradation by cellulytic microbes, the tubing was stored at 4 °C and transferred to freshly boiled reagent water daily. Stock dialysis membranes (i.e., unwashed) were refrigerated per the manufacturer's instructions. Care was exercised so that the membrane was neither stretched nor allowed to dry out.<sup>24</sup> Membranes (11-mm diameter) were cut with a cork borer on a glass plate before placement on the polished glassy carbon surface. A preformed cap (9 × 12 mm) made of heat-shrink PTFE tubing was used to hold the membrane in place on the end of the working electrode. The CM-MFE was prepared as described above for the MFE except that 4.0 mM Hg(NO<sub>3</sub>)<sub>2</sub> in 0.13 M HNO<sub>3</sub> was used. The CM-MFE was stored overnight by polarizing it at -100 mV in 10 mM KNO<sub>3</sub> under a blanket of nitrogen. Stripping with the CM-MFE was performed using CCSA (5-15 μA).

**PSA.** A relative standard deviation of <5% ( $n = 4$ ) was required for the Pb(II) peak area response before proceeding with the addition of an organic interferent. The sample solution was equilibrated for 5 min with gentle stirring upon addition of each organic interferent. Between sample replicates, approximately 2 min elapsed in order to save and plot the data. The following electrochemical protocol was typically used for PSA measurements: initial (deposition) potential of -900 mV; final potential of -300 mV; deposition time of 60-120 s for the model organic compounds, 120-300 s for the river water and urine samples. The solution was stirred during the deposition step and was quiescent for 15 s prior to and during the stripping step. Prior to each deposition period, the electrode was held at -100 mV for 15 s to remove impurities (e.g., contaminating copper ion). Solutions were not deaerated.

The power of the background subtraction procedure determines the success of trace-level PSA<sup>25</sup> and ASV<sup>26</sup> techniques. The standard PSA background correction method<sup>27</sup> subtracts the usually faint capacitance-dominated signal from the sample signal by repeating a brief (~1 s) deposition immediately after the stripping of the sample has completed. In typical PSA methods this is effective, but with a PME—especially a specific PME such as Nafion under typical experimental conditions used

(16) Martins, E.; Bengtsson, M.; Johansson, G. *Anal. Chim. Acta* 1985, 169, 31-42.

(17) Cosovic, B.; Vojvodic, V. *Limnol. Oceanogr.* 1982, 27, 361-369.

(18) Almestrand, L.; Jagner, D.; Renman, L. *Talanta* 1986, 33, 991-995.

(19) Almestrand, L.; Jagner, D.; Renman, L. *Anal. Chim. Acta* 1987, 193, 71-79.

(20) Almestrand, L.; Betti, M.; Chi, H.; Jagner, D.; Renman, L. *Anal. Chim. Acta* 1988, 209, 339-343.

(21) Heyde, M. E.; Peters, C. R.; Anderson, J. E. *J. Colloid Interface Sci.* 1985, 167, 111-115.

(22) *Standard Methods for the Examination of Water and Wastewater*; APHA: Washington, DC, 1981; p 401.

(23) Colton, C. K.; Smith, K. A.; Merrill, E. W.; Farrell, P. C. *J. Biomed. Mater. Res.* 1971, 5, 459-488.

(24) Kesting, R. E. *Synthetic Polymer Membranes*, 2nd ed.; Wiley-Interscience: New York, 1985; Chapter 4.

(25) Turner, D. R.; Robinson, S. G.; Whitfield, M. *Anal. Chem.* 1984, 56, 2387-2392.

(26) Whang, C.-W.; Page, J. A.; vanLoon, G. *Anal. Chem.* 1984, 56, 539-542.

(27) Graneli, A.; Jagner, D.; Josefson, M. *Anal. Chem.* 1980, 52, 2220-2223.

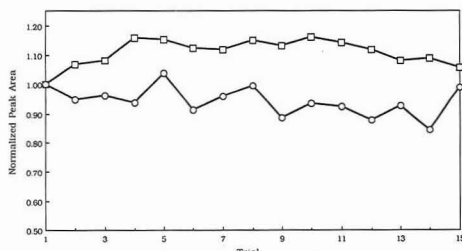


**Figure 1.** Effect of oxidant on Pb(II) determination (50 ppb) with the CM-MFE. With 40  $\mu$ M Hg(II) and dissolved oxygen as oxidant (O) and with a constant current (5  $\mu$ A) applied during the stripping step (□).

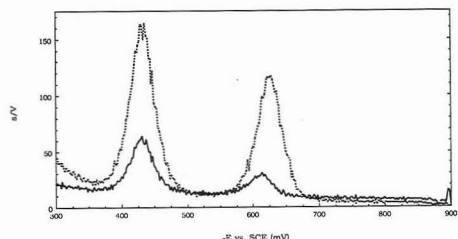


**Figure 2.** Comparison of the response using a MFE (---) and a CM-MFE (—) to Pb(II) and Cd(II) using CCSA (50 ppb each). Raw data (without background correction, smoothing, or filtering) is shown.

in this study—the background signal is large because analyte preconcentration maintains a higher concentration of analyte within the membrane near the MFE surface. We found that, even for nonspecific PME's such as cellulose acetate dialysis membranes, the background can approach ~25–50% of the sample signal. Therefore, the Radiometer digital curve-fitting "BASE" routine<sup>29</sup> was used for background correction with the CM-MFE, as it was found that subtraction of a short deposition period potentiogram yielded a distorted peak shape as a result of changes in peak potential between the sample and background. Each sample response was measured in quadruplicate, with averaging of the last three replicates. Peak area data were corrected for dilution, and both peak area and peak potential data were normalized to the average initial background (i.e., no added interferent) value.

## RESULTS AND DISCUSSION

**Choice of Oxidant.** A typical comparison of the response using Hg(II) as oxidant and the electrode as oxidant (i.e., CCSA) for the CM-MFE is shown in Figure 1. The normalized peak area signal for 15 repetitive measurements on the same 50 ppb Pb(II) sample solution had a relative standard deviation (RSD) of 9.7% with Hg(II) as oxidant and 4.1% with CCSA for the Pb(II) signal. It was also noted that the use of a digital filter (eight-point average and nine-point Savitzky-Golay algorithm) yielded consistently higher RSD values for this type of data, perhaps because the smoothing of the very sharp peaks observed resulted in large differences in peak heights prior to integration.

**MFE vs CM-MFE.** Figure 2 depicts typical results for CCSA with a MFE and CM-MFE. The Pb(II) and Cd(II) peak potentials were  $-458 \pm 1$  and  $-655 \pm 1$  mV, respectively, for the MFE and  $-446 \pm 2$  and  $-621 \pm 1$  mV, respectively, for the CM-MFE ( $n = 32$ ). The stripping potential in CCSA is governed by the Nernst equation. Uncompensated resistance

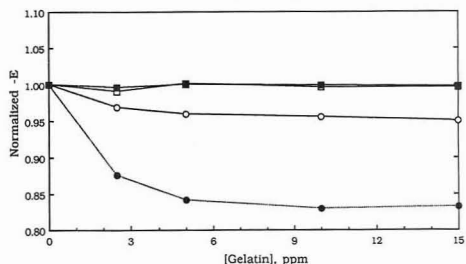
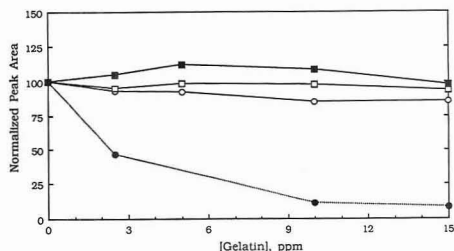


**Figure 3.** Response to gelatin addition for the MFE (O) and CM-MFE (□) for Cd(II) (closed symbols) and Pb(II) (open symbols) determinations (50 ppb each); peak area response (a, top) and peak potential response (b, bottom).

between the reference and working electrode (MFE versus CM-MFE) will cause the potential to shift.

**Model Organic Compounds.** The effect of each of the eight model organic compounds on the Cd(II) and Pb(II) normalized peak area and normalized peak potential responses with a bare MFE and with a CM-MFE is discussed below (Table I).

**Proteins.** Gelatin and ovalbumin were chosen to model proteinaceous material found in clinical samples and in natural waters as a result of microbial activities. Low concentrations of the globular protein gelatin (MW 75 000), a maxima suppressor in polarography, have been reported in ASV to cause 57–65% decreases in the Cd(II) peak current at pH 3–5 and severe shifts in peak potential.<sup>14,29–31</sup> As shown in Figure 3a, for a bare MFE we observed a 50% decrease in the Cd(II) peak area signal at a gelatin concentration of 3 ppm and over 90% decrease at 15 ppm gelatin. With a bare MFE we observed a 15% decrease in the Pb(II) peak area. Use of the CM-MFE resulted in stable Pb(II) and Cd(II) peak area signals over the range of interferent concentrations tested. As shown in Figure 3b, the Pb(II) and Cd(II) peak potentials were relatively unchanged with a CM-MFE while the Pb(II) and Cd(II) peak potentials for a bare MFE shifted positive by over 5% and 17% at 15 ppm of gelatin, respectively.

Ovalbumin (MW 45 000), a protein with high hydrophobic amino acid content, exhibited effects similar to those observed for gelatin. As shown in Figure 4a, a severe decrease in the Cd(II) peak area signal is observed at an ovalbumin concentration of 15 ppm for the bare MFE while the Pb(II) signal changed 15%. A >15% positive shift of the Cd(II) peak potential was found for the bare MFE (Figure 4b). Peak potential drift was not observed with the CM-MFE.

**Carbohydrates.** Starch and agar were chosen to model the complex polysaccharides found in clinical samples and in natural waters as a result of phytoplankton activity. A 6%

(28) TraceLab Trace Element Laboratory Programmer's Manual (Version 2.1), Radiometer A/S, 1991.

(29) Wang, J.; Luo, D. B. *Talanta* 1984, 31, 703–707.

(30) Wang, J.; Taha, Z. *Electroanalysis* 1990, 2, 383–387.

(31) Kubiak, W. W.; Wang, J. *Talanta* 1989, 36, 821–824.



**Table I. Comparison of Normalized Peak Area and Peak Potential Data for Model Organic Compounds (15 ppm) at 50 ppb Pb(II) and Cd(II)**

	normalized peak area (100%)				normalized peak potential (1.000) <sup>a</sup>			
	Cd MFE	Cd CM-MFE	Pb MFE	Pb CM-MFE	Cd MFE	Cd CM-MFE	Pb MFE	Pb CM-MFE
gelatin	8.7	97.9	85.0	93.5	0.833 (-114)	0.997 (-2)	0.950 (-23)	0.996 (-2)
ovalbumin	7.9	99.0	85.6	97.1	0.816 (-121)	0.995 (-3)	0.921 (-37)	0.995 (-2)
SDS <sup>b</sup>	119.0	109.0	125.0	135.0	1.006 (+4)	1.017 (+11)	1.020 (+8)	1.019 (+8)
Triton X-100	86.9	115.0	156.0	107.0	0.889 (-73)	0.911 (-56)	0.848 (-70)	0.973 (-12)
humic acid	101.0	102.0	75.9	51.9	0.990 (-4)	1.004 (+1)	1.001 (+2)	1.005 (+1)
camphor	108.0	105.0	81.6	109.0	0.992 (-5)	1.002 (+3)	0.985 (-7)	1.001 (+2)
starch	111.0	102.0	90.5	107.0	1.000 (0)	1.060 (+35)	0.985 (-7)	1.015 (+6)
agar <sup>b</sup>	108.0	125.0	91.3	135.0	1.000 (0)	1.001 (+1)	0.991 (-4)	1.000 (0)

<sup>a</sup> The shift in units of mV relative to the analyte metal ion without added interferent is shown in parentheses next to the normalized value.

<sup>b</sup> A gradual increase in signal suggested contamination of the interferent stock.

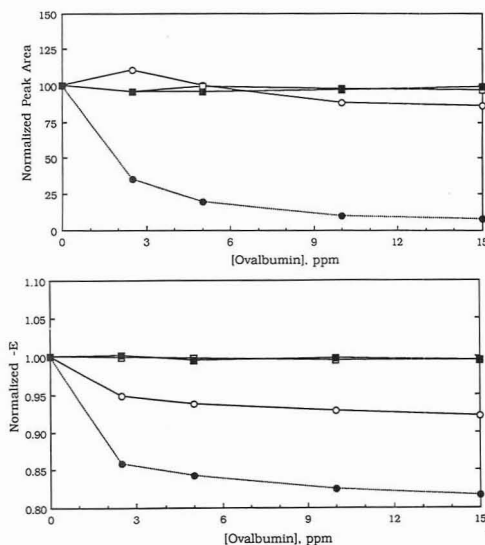


**Figure 4.** Response to ovalbumin addition for the MFE (O) and CM-MFE (□) for Cd(II) (closed symbols) and Pb(II) (open symbols) determinations (50 ppb each); peak area response (a, top) and peak potential response (b, bottom).

negative shift in the Pb(II) peak potential when using the CM-MFE was observed, while a gradual increase in the agar peak area response suggested interfering trace metals in the technical grade preparation (Table I). A lack of significant changes in the peak area and peak potential responses was noted, in contrast to previous ASV work where decreases in the peak current with a bare MFE were observed at low pH.<sup>14,29</sup>

**Surfactants.** The anionic surfactant SDS (MW 288) and the nonionic surfactant Triton X-100 (MW 647) were studied. Like Wang and Luo,<sup>29</sup> we observed erratic responses in the presence of SDS and a gradual increase in the peak area signals for both Pb(II) and Cd(II), suggestive of trace concentrations of contaminating heavy metals in the stock solutions. Minor changes in peak potential were observed in the presence of SDS with either electrode (Table I).

The Triton behavior was the most complex of the eight model compounds studied. For PSA with a bare MFE as shown in Figure 5a, the Pb(II) peak area signal at concentrations of >5 ppm increased dramatically while the Cd(II) peak area signal decreased by approximately 15%. Using the CM-MFE, both peak area signals stabilized significantly. The peak potential signals shifted positive by 10–15% at 15 ppm with the bare MFE and 5–10% with the CM-MFE

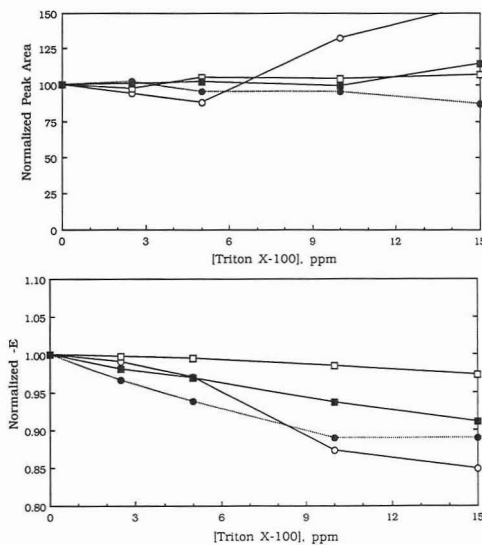


**Figure 5.** Response to Triton addition for the MFE (O) and CM-MFE (□) for Cd(II) (closed symbols) and Pb(II) (open symbols) (50 ppb each); peak area response (a, top) and peak potential response (b, bottom).

(Figure 5b). It is important to note that in ASV with a CM-MFE, Triton was shown to be the most problematic interferent on the normalized Cd(II) peak current signal.<sup>14</sup>

**Humic Acid.** Humic acids are model compounds for the organic matter found in natural waters.<sup>32</sup> They are known to interfere in electroanalytical measurements by complexation with heavy metals as well as by a poorly understood adsorptive mechanism.<sup>3,33</sup> Wang and Luo observed severe decreases in the Cd(II) and Pb(II) peak currents in ASV with a bare MFE in the presence of humic acids.<sup>29</sup> Our observations (Figure 6) reveal little change in the Cd(II) peak area signal with either electrode, while the Pb(II) peak area signal decreases regardless of the electrode used. This suggests that complexation in the bulk solution is the major mechanism for interference with the Pb(II) measurement. The more severe decrease in the Pb(II) peak area signal is caused by the use of a longer deposition time for the CM-MFE. The peak potentials remain unchanged with either electrode (Figure 6b).

(32) Schnitzer, M.; Khan, S. U. *Humic Substances in the Environment*; Marcel Dekker: Chur, 1972.

(33) Zur, C.; Ariel, M. *Anal. Chim. Acta* 1977, 88, 245–251.

(34) Laitinen, H. A.; Chambers, L. M. *Anal. Chem.* 1964, 36, 5–11.

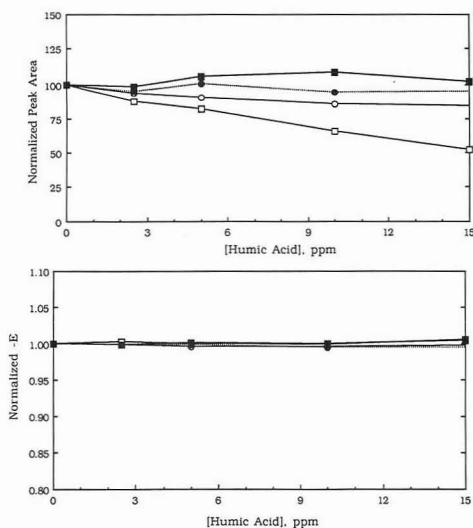


**Figure 6.** Response to humic acid addition for the MFE (O) and CM-MFE (□) for Cd(II) (closed symbols) and Pb(II) (open symbols) (50 ppb each); peak area response (a, top) and peak potential response (b, bottom).

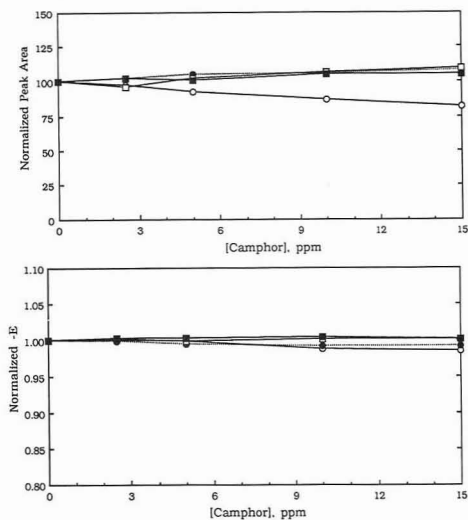


**Figure 7.** Response to camphor addition for the MFE (O) and CM-MFE (□) for Cd(II) (closed symbols) and Pb(II) (open symbols) (50 ppb each); peak area response (a, top) and peak potential response (b, bottom).

**Camphor.** D-Camphor, a plasticizer of cellulose esters and ethers (MW 152), exhibited qualitatively similar effects to those observed by Stewart and Smart for Cd(II).<sup>14</sup> Namely, a decrease of nearly 20% was seen for the Pb(II) peak area signal with a bare MFE; the use of the CM-MFE eliminated this trend as shown in Figure 7a. The peak potentials for both metal ions and electrodes changed little (Figure 7b).

**Environmental and Clinical Application.** The determination of Cd(II) in river water and urine samples was

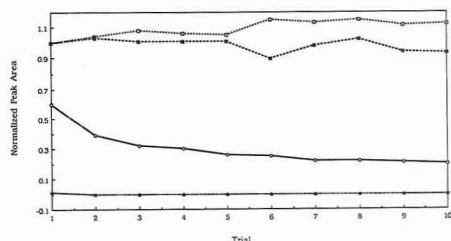


**Figure 8.** Stability of Cd(II) peak area signal in acidified natural water (open symbols) and urine (closed symbols) samples with a bare MFE (O) and with a CM-MFE (□). The clinical sample required a brief equilibration period before analysis. The deposition time was 300 s with a constant current during the stripping stage of 5  $\mu$ A.

attempted with the bare MFE and the CM-MFE using CCSA. As shown in Figure 8, the peak area response in river water decreased to  $\sim$ 20% of the initial value by the tenth replicate and became uninterpretable by the second replicate for the urine sample. Using the CM-MFE, the peak area response remained relatively steady throughout the 10 trials in both matrices, with a RSD of 3.6% and 4.7% for the river water and urine samples, respectively.

## CONCLUSIONS

In general, the Pb(II) response to the model organic compounds was much less affected than the Cd(II) response. For the model proteins, the diversity of amino acid functional groups provides proteins with both complexation and adsorption capacities. Because protein adsorption is a major source of electrode fouling in clinical samples, the ability of the CM-MFE in PSA to prevent protein fouling is significant. The use of cellulose acetate films with low molecular weight cutoffs would minimize further interference by peptides. With the model carbohydrate compounds, even the bare MFE in PSA is an improvement over a bare MFE in ASV. With humic acid, one can use PSA with the CM-MFE to discriminate adsorption from complexation. Since PSA in the constant current mode is essentially a chronopotentiometric measurement, it can be used to its advantage as a sensitive indicator of adsorption processes.<sup>34</sup> Most significantly, determinations in the presence of Triton X-100 have been shown to be a problem in ASV with the CM-MFE,<sup>14</sup> whereas with PSA the CM-MFE performed well in Triton's presence.

Finally, although these results using the CM-MFE in PSA show promise, Florence points out<sup>7</sup> that a membrane coating ultimately cannot eliminate all interferences in a sample from reaching the electrode surface. Even interfering components that are excluded from the electrode surface may still complicate the signal by their accumulation at the outer membrane surface. We are currently investigating the use of the CM-MFE in a flow injection analysis system to address this issue.

## ACKNOWLEDGMENT

We gratefully acknowledge Radiometer America A/S for providing the TraceLab system. We have benefitted greatly from discussions with Nick Georgopoulos of Radiometer. This work was supported in part by the Research Challenge Program at Ohio University.

RECEIVED for review November 9, 1992. Accepted January 8, 1993.

# Voltammetric Study on a Condensed Monolayer of a Long Alkyl Cyclodextrin Derivative as a Channel Mimetic Sensing Membrane

Kazunori Odashima, Minoru Kotato, Masao Sugawara,<sup>1</sup> and Yoshio Umezawa<sup>2\*</sup>

Department of Chemistry, Faculty of Science, Hokkaido University, Kita 10-Jo Nishi 8-Chome, Sapporo, Hokkaido 060, Japan

For a fundamental study on the development of signal-amplifying chemical sensors that mimic biological ion channels, a control of membrane permeability based on the blocking of an intramolecular channel by host-guest complexation has been investigated for a condensed monolayer of a long alkyl derivative of  $\beta$ -cyclodextrin having a channel-like structure (6<sup>A</sup>, 6<sup>B</sup>, 6<sup>C</sup>, 6<sup>D</sup>, 6<sup>E</sup>, 6<sup>F</sup>, 6<sup>G</sup>, 6<sup>H</sup>-heptadeoxy-6<sup>A</sup>, 6<sup>B</sup>, 6<sup>C</sup>, 6<sup>D</sup>, 6<sup>E</sup>, 6<sup>F</sup>, 6<sup>G</sup>, 6<sup>H</sup>-heptakis(dodecylthio)- $\beta$ -cyclodextrin tetradecaacetate). To obtain experimental evidence for such a mode of permeability control, an approach based on horizontal touch cyclic voltammetry was carried out for this condensed monolayer, which was formed at the air/water interface by applying a controlled high surface pressure to minimize the permeability through the intermolecular voids between the membranous cyclodextrin molecules. By comparing the permeabilities for three kinds of electroactive markers that differ in the steric bulkiness and/or hydrophobicity, rigid evidence was obtained for the ability of this cyclodextrin derivative to function as an intramolecular channel. The permeability of this channel for a sterically permeable marker (*p*-quinone) was shown to be able to be controlled by blocking the channel with a guest molecule. By using this condensed monolayer, the selectivity of permeability inhibition was examined for several organic guests. The molecular response ratio as a measure of signal transduction efficiency was up to 10.4.

## INTRODUCTION

The analyte-triggered open/close switching of membrane permeability would be one of the most promising approaches toward highly sensitive and selective sensing membranes because it could lead to a chemical amplification of analyte concentration. Such a mode of control of the membrane permeability is effected in a most sophisticated and efficient manner in ligand-gated ion channels that function in biomembranes.<sup>1,2</sup> As a simplest starting point for the development of a novel class of sensors that would be designated as "ion channel sensors",<sup>3-12</sup> we have reported a series of voltammetric

sensors that exploit charged and ordered membranes of Langmuir-Blodgett (LB) type deposited directly on glassy carbon electrodes. These LB membranes contained valinomycin (1)<sup>3,4</sup> or long alkyl derivatives of polyamine hosts (2, 3)<sup>5</sup> as the receptors that are capable of forming host-guest complexes with cations and anions, respectively (see Figure 1 for the structures). Host-guest complexation by these membranous receptors induced changes in the cyclic voltammograms of electroactive marker compounds added in the sample solutions. These voltammetric changes could be ascribed to a guest-induced modulation of the permeability for these markers as a result of a change in the net charge and/or assembly of the ordered membrane. The magnitude of permeability change induced by adding a guest to a given concentration depended on the guest structure, resulting in a voltammetric discrimination of guests.<sup>4,5</sup> Of the LB membrane sensors examined, the one containing a long alkyl derivative of  $\beta$ -cyclodextrin (3) exhibited an interesting selectivity which was different from that of the corresponding sensor containing a simple macrocyclic polyamine (2).<sup>5</sup> The voltammetric selectivity of the former sensor possibly reflects a shape-discriminating effect due to the inclusion of guest molecules within the  $\beta$ -cyclodextrin cavity.

All of these LB membrane sensors are based on the control of permeation of the marker ions through the intermolecular voids between the membranous host molecules. Of the host molecules examined, the long alkyl derivative of  $\beta$ -cyclodextrin (3)<sup>13,14</sup> is characteristic in that it has a channel-like structure in which the cyclodextrin cavity is expected to function as a receptor site and channel entrance. However, since the marker ions used ( $[\text{Fe}(\text{CN})_6]^{4-}$ ,  $[\text{Ru}(\text{bpy})_3]^{2+}$ , L-ascorbic acid) are sterically not permeable through the  $\beta$ -cyclodextrin cavity, the controlling mode that can be expected for the sensor composed of host 3 as well as for the other LB membrane sensors is the control of permeability through the intermolecular voids between the membranous host molecules (Figure

(6) Sugawara, M.; Sazawa, H.; Umezawa, Y. *Langmuir* 1992, 8, 609-612.

(7) Uto, M.; Michaelis, E. K.; Hu, I. F.; Umezawa, Y.; Kuwana, T. *Anal. Sci.* 1990, 6, 221-225.

(8) Minami, H.; Sugawara, M.; Odashima, K.; Umezawa, Y.; Uto, M.; Michaelis, E. K.; Kuwana, T. *Anal. Chem.* 1991, 63, 2787-2795.

(9) Minami, H.; Uto, M.; Sugawara, M.; Odashima, K.; Umezawa, Y.; Michaelis, E. K.; Kuwana, T. *Anal. Sci.* 1991, 7 (Supplement), 1675-1676.

(10) Umezawa, Y.; Sugawara, M.; Kataoka, M.; Odashima, K. In *Ion-Selective Electrodes*, 5; Pungor, E., Ed.; Akadémiai Kiadó (Pergamon Press): Budapest (Oxford), 1989; pp 211-234.

(11) Odashima, K.; Umezawa, Y. In *Biosensor Technology. Fundamentals and Applications*; Buck, R. P., Hatfield, W. E., Umaña, M., Bowden, E. F., Eds.; Marcel Dekker: New York, 1990; pp 71-93.

(12) Odashima, K.; Sugawara, M.; Umezawa, Y. *Trends Anal. Chem.* 1991, 10, 207-215.

(13) Takahashi, H.; Irinatsu, Y.; Kozuka, S.; Tagaki, W. *Mem. Fac. Eng., Osaka City Univ.* 1985, 26, 93-99.

(14) Takahashi, H.; Tagaki, W. *Yukagaku* 1988, 37, 1027-1031.

<sup>1</sup> Present address: Department of Chemistry, Faculty of Science, The University of Tokyo, Hongo 7-3-1, Bunkyo-Ku, Tokyo 113, Japan.

<sup>2</sup> Permanent address: Department of Chemistry, Faculty of Science, The University of Tokyo, Hongo 7-3-1, Bunkyo-Ku, Tokyo 113, Japan.

(1) Miller, C., Ed. *Ion Channel Reconstitution*; Plenum Press: New York, NY, 1986.

(2) Stein, W. D. *Channels, Carriers, and Pumps: An Introduction to Membrane Transport*; Academic Press: San Diego, CA, 1990.

(3) Sugawara, M.; Kojima, K.; Sazawa, H.; Umezawa, Y. *Anal. Chem.* 1987, 59, 2842-2846.

(4) Sugawara, M.; Kataoka, M.; Odashima, K.; Umezawa, Y. *Thin Solid Films* 1989, 180, 129-133.

(5) Nagase, S.; Kataoka, M.; Naganawa, R.; Komatsu, R.; Odashima, K.; Umezawa, Y. *Anal. Chem.* 1990, 62, 1252-1259.



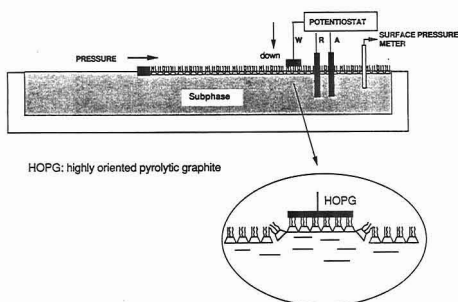


**Figure 3.** Experimental system for the measurement of surface pressure-molecular area ( $\pi$ -A) isotherms and the horizontal touch cyclic voltammetry. W, working electrode; R, reference electrode; A, auxiliary electrode.

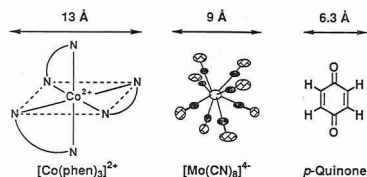


**Figure 4.** Appropriate dimensions of the three electroactive compounds used in the present study as the markers for membrane permeability.

Tokyo, Japan) equipped with a glass Wilhelmy plate and a Teflon-coated trough ( $14 \times 70 \text{ cm}^2$ ) was used for both  $\pi$ -A isotherm measurements and horizontal touch cyclic voltammetry. The temperature of subphase solutions was kept at  $17.0 \pm 0.1^\circ \text{C}$  for all experiments. Monolayers were obtained by spreading  $100 \mu\text{L}$  of a  $0.25$ – $0.30 \text{ mM}$  chloroform solution of cyclodextrin derivative 4 at the air/water interface on the subphase solutions. After the monolayer was allowed to stand for 15 min for complete evaporation of chloroform,  $\pi$ -A isotherms were recorded with a compression velocity of  $17.9 \text{ mm min}^{-1}$  ( $25.1 \text{ cm}^2 \text{ min}^{-1}$ ). The molecular area of 4 extrapolated at zero surface pressure ( $A_0$ ) and the collapse pressure of the monolayer were determined from the  $\pi$ -A isotherms.

**Horizontal Touch Cyclic Voltammetry.** The horizontal touch cyclic voltammetry was carried out as described by Zhang and Bard<sup>22</sup> using a three-electrode configuration: a highly oriented pyrolytic graphite (HOPG) electrode as a working electrode, an Ag/AgCl electrode (Type HS-205C, Toa Electronics Ltd., Tokyo, Japan) as a reference electrode, and a platinum wire as an auxiliary electrode. The HOPG block (area,  $12 \times 12 \text{ mm}^2$ ; initial width, 2 mm; Union Carbide Corp., Cleveland, OH; kindly provided by Professor Stephen G. Weber, Department of Chemistry, University of Pittsburgh) was first connected to a silver wire with silver paste (Nilaco Corp., Tokyo, Japan), and then its surface was cleaved by peeling off with an adhesive tape to obtain a fresh basal plane of the graphite surface.

The experimental system for the horizontal touch cyclic voltammetry is shown in Figure 3. A computer-controlled electroanalysis system (Model CYSY-1, Cypress Systems, Inc., Lawrence, KS) equipped with an X-Y recorder (Model 7440A, Hewlett-Packard Co., Palo Alto, CA) was used with the three-electrode configuration. The monolayer prepared as above was compressed to a preset surface pressure ( $50 \text{ mN m}^{-1}$ ) at the same barrier movement velocity as described above for the  $\pi$ -A isotherm measurements. The HOPG electrode was initially held above the air/water interface with its surface parallel to the interface. After the compressed monolayer was allowed to stand for 30 min, the HOPG electrode was first lifted down with a motor-driven lifter at a displacement speed of  $2 \text{ mm min}^{-1}$  and brought into contact with the monolayer, and then was lifted up by  $1 \text{ mm}$  at the same speed. This operation was carried out for eliminating a possibility of vertical compression that could disorder the oriented monolayer.<sup>22</sup> In the present experiments,

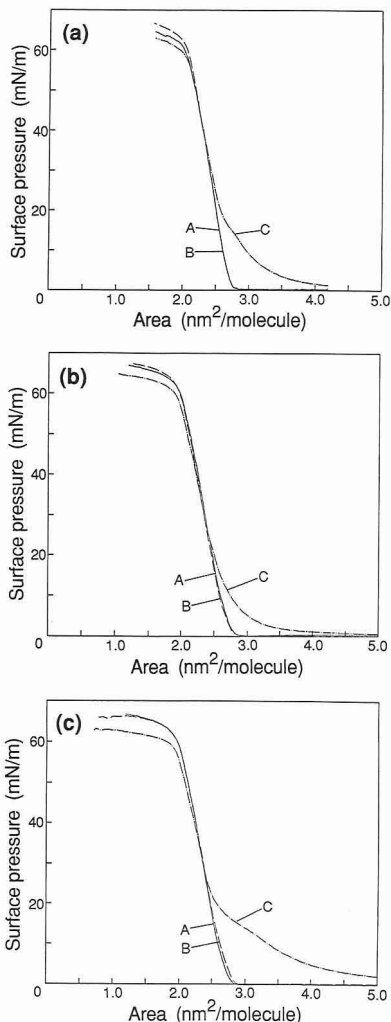


**Figure 5.**  $\pi$ -A isotherms measured at  $17.0 \pm 0.1^\circ \text{C}$  for the long alkyl derivative of  $\beta$ -cyclodextrin (4) in the presence or absence of cyclohexanol (10 mM) as a guest and (a)  $[\text{Co}(\text{phen})_3]^{2+}$  (0.10 mM), (b)  $[\text{Mo}(\text{CN})_6]^{4-}$  (1.0 mM), or (c) *p*-quinone (1.0 mM) as a marker. The composition of the subphase solution for each curve was as follows. Curve A: 0.1 M acetate buffer (pH 6.0) containing no guest or marker. Curve B: the acetate buffer containing a marker. Curve C: the acetate buffer containing a marker and guest.

no difference in cyclic voltammograms was observed by changing the lifting distance from 0 to 3 mm.

The most convenient method for adding a guest into the subphase solution would be a simple injection of the corresponding guest solution. However, this method is not suitable in this case because it practically requires a stirring of the subphase solution, which will cause a distortion of the cyclodextrin monolayer at the air/water interface. Accordingly, the guest had to be introduced by the exchange method composed of the first and second cycles as follows. In the first cycle, a cyclic voltammogram was recorded first in the absence of the cyclodextrin monolayer on a buffer solution containing no guest. Then, the cyclodextrin monolayer was prepared as described above and allowed to stand for 30 min for stabilization at the preset surface pressure ( $50 \text{ mN}$

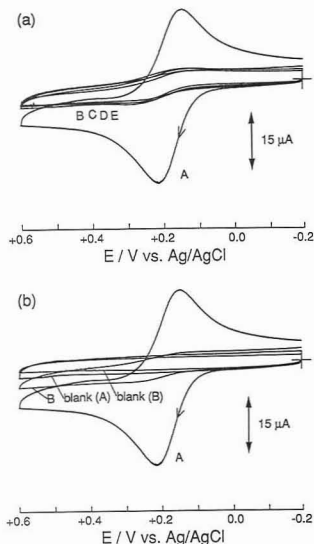


**Figure 6.** Cyclic voltammograms of  $[\text{Co}(\text{phen})_3]^{2+}$  (0.10 mM) as a permeability marker, measured on 0.1 M acetate buffer solution (pH 6.0) at  $17.0 \pm 0.1$  °C. (a) The effects of the condensed cyclodextrin monolayer and the cyclohexanol guest. Curve A: measured in the absence of the cyclodextrin monolayer on the buffer solution containing no guest. Curve B: measured in the presence of a condensed monolayer of cyclodextrin derivative 4 on the buffer solution containing no guest. Curves C–E: measured in the presence of the condensed cyclodextrin monolayer on the buffer solution containing cyclohexanol as a guest. The concentrations of cyclohexanol were 5, 10, and 20 mM for curves C, D, and E, respectively. The marker was added as  $[\text{Co}(\text{phen})_3](\text{ClO}_4)_2$ . The surface pressure for compressing the cyclodextrin monolayer was controlled at  $50 \text{ mN m}^{-1}$ . The starting point of the potential scan ( $-0.2 \text{ V}$ ) is shown with a cross. The direction of the potential scan is indicated with an arrow. (b) The background currents recorded in the presence and absence of the cyclodextrin monolayer on the buffer solution containing no marker or guest are shown as "blank (A)" and "blank (B)", respectively. Curves A and B are those shown in Figure 6a.

$\text{min}^{-1}$ ). The HOPG electrode was brought into contact with the monolayer (vide supra) and kept at an initial potential for 30 s, and then a cyclic voltammogram was recorded. After the measurement, the monolayer and the subphase solution were discarded and the trough was thoroughly washed. The HOPG surface was cleaved by peeling off with an adhesive tape to obtain a fresh surface. In the second cycle, a cyclic voltammogram was recorded again in the absence of the cyclodextrin monolayer on the buffer solution containing no guest in order to ensure that the surface area of the HOPG electrode did not change by peeling off its surface. Then, the buffer solution was discarded, the trough thoroughly washed, and the same buffer solution containing a guest was introduced into the trough as a subphase solution. The condensed cyclodextrin monolayer was prepared, and a cyclic voltammogram was recorded in the same manner as described above. For each combination of marker and guest, these cycles were repeated two or three times.

The potential scan for cyclic voltammograms was conducted at a sweep rate of  $100 \text{ mV s}^{-1}$  for all markers. In the case of  $[\text{Co}(\text{phen})_3]^{2+}$ , the scan was made from an initial potential of  $-0.2 \text{ V}$  toward anodic and then back to cathodic directions over a potential window of 0.8 V ranging from  $+0.6$  to  $-0.2 \text{ V}$  (see Figure 6). In the case of  $[\text{Mo}(\text{CN})_6]^{4-}$ , the scan was made from an initial potential of  $+0.3 \text{ V}$  toward anodic and then back to cathodic directions over a potential window of 0.7 V ranging from  $+0.9$  to  $+0.2 \text{ V}$  (see Figure 7). In the case of *p*-quinone, the scan was made from an initial potential of  $+0.2 \text{ V}$  toward cathodic

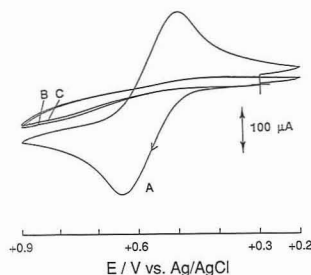


**Figure 7.** Cyclic voltammograms of  $[\text{Mo}(\text{CN})_6]^{4-}$  (1.0 mM) as a permeability marker, measured on 0.1 M acetate buffer solution (pH 6.0) at  $17.0 \pm 0.1$  °C. Curve A: measured in the absence of the cyclodextrin monolayer on the buffer solution containing no guest. Curve B: measured in the presence of a condensed monolayer of cyclodextrin derivative 4 on the buffer solution containing no guest. Curve C: measured in the presence of the condensed cyclodextrin monolayer on the buffer solution containing 10 mM cyclohexanol as a guest. The marker was added as  $\text{K}_4[\text{Mo}(\text{CN})_6]$ . The surface pressure for compressing the cyclodextrin monolayer was controlled at  $50 \text{ mN m}^{-1}$ . The starting point of the potential scan ( $+0.3 \text{ V}$ ) is shown with a cross. The direction of the potential scan is indicated with an arrow.

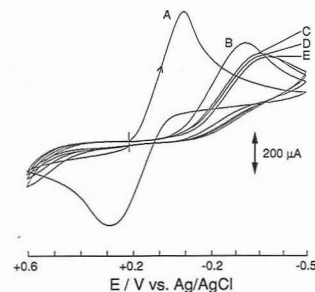


**Figure 8.** Cyclic voltammograms of *p*-quinone (1.0 mM) as a permeability marker, measured on 0.1 M acetate buffer solution (pH 6.0) at  $17.0 \pm 0.1$  °C. Curve A: measured in the absence of the cyclodextrin monolayer on the buffer solution containing no guest. Curve B: measured in the presence of a condensed monolayer of cyclodextrin derivative 4 on the buffer solution containing no guest. Curves C–E: measured in the presence of the condensed cyclodextrin monolayer on the buffer solution containing cyclohexanol as a guest. The concentrations of cyclohexanol were 5, 10, and 20 mM for curves C, D, and E, respectively. The surface pressure for compressing the cyclodextrin monolayer was controlled at  $50 \text{ mN m}^{-1}$ . The starting point of the potential scan ( $+0.2 \text{ V}$ ) is shown with a cross. The direction of the potential scan is indicated with an arrow.

and then back to anodic directions over a potential window of 1.1 V ranging from  $+0.6$  to  $-0.5 \text{ V}$  (see Figure 8). The potential ranges for the integration of these peaks were  $-0.1$  to  $+0.6 \text{ V}$ ,  $+0.3$  to  $+0.9 \text{ V}$ , and  $+0.2$  to  $-0.5 \text{ V}$  for  $[\text{Co}(\text{phen})_3]^{2+}$ ,  $[\text{Mo}(\text{CN})_6]^{4-}$ , and *p*-quinone, respectively.

Since integrated currents calculated from the cyclic voltammogram area varied with the HOPG block used, each series of experiments was carried out with a single block of HOPG. Within the series of experiments for each marker, typical repeatability (mean deviation) of the integrated current in the absence of the cyclodextrin monolayer was as follows:  $[\text{Co}(\text{phen})_3]^{2+}$  (0.10 mM),  $58.9 \pm 1.6 \mu\text{C}$  (2.7%) for 10 runs;  $[\text{Mo}(\text{CN})_6]^{4-}$  (1.0 mM),  $649 \pm 7.1 \mu\text{C}$  (1.1%) for 10 runs; *p*-quinone (1.0 mM),  $2322 \pm 34 \mu\text{C}$  (1.5%) for 14 runs. In the case that the integrated current in the absence of the cyclodextrin monolayer greatly deviated from these values, the electrode surface was peeled off again until the expected integrated current was obtained.



## RESULTS AND DISCUSSION

**Long Alkyl Derivative of Cyclodextrin as a Sensory Element.** Host 4<sup>19,20</sup> as well as host 3<sup>13,14</sup> is one of the new type of cyclodextrin derivatives developed by Tagaki et al.,<sup>27</sup> which have a characteristic structure that all of the primary hydroxyl groups are substituted with long alkyl chains. This structural feature allows the secondary hydroxyl side to face the aqueous solution to accommodate a guest molecule into the cavity. It has been shown mainly by  $\pi$ -A isotherm studies that these cyclodextrin derivatives form oriented mono- and multilayers either with or without a guest.<sup>19,28-30</sup> Since this type of cyclodextrin derivative has a channel-like structure with an interfacial receptor site, the development of a novel type of sensing membrane is expected, provided that an open/close switching of the permeability of the membrane is effected by the blocking of the channel with a guest molecule (Figure 2b).

**Advantage of Horizontal Touch Cyclic Voltammetry for Studying Intramolecular Channel Function.** The first step for developing such a channel mimetic sensing membrane is to obtain rigid experimental evidence for the intramolecular channel function of the channel mimetic sensory element. There have been a number of studies aimed at the development of artificial ion channels based on derivatives of cyclodextrin and crown ethers.<sup>31-38</sup> Some of these studies have given experimental results showing a marked increase in the membrane permeability by incorporation of these molecules into liposomes.<sup>31,33,34,36,37</sup> However, it has always been difficult to unambiguously attribute the permeability increase to their intramolecular channel function because a possibility of leak outside the channel must also be taken into account; the incorporation of these channel compounds could result in an increase of leak outside the channel by a microscopic distortion of the surrounding lipids.

In the present study, an approach based on horizontal touch cyclic voltammetry was carried out to overcome this fundamental problem. This technique, first used by Fujihira<sup>21</sup> and recently sophisticated by Bard,<sup>22-24</sup> enables investigation on the electrochemical properties of oriented monolayers at varying packing densities under an appropriately controlled surface pressure. By applying a surface pressure that is sufficiently high for the formation of a closest packed monolayer, the intermolecular voids between the membranous molecules will be minimized so that the leak of the markers outside the intramolecular channels is expected to be suppressed to a minimum.

As the guests to block the channel and control the membrane permeability, uncharged organic molecules have been chosen because it is essential for examining the

intramolecular channel function that the permeability for the electroactive marker is controlled only by the steric factor and not complicated by the electrostatic factor. When an uncharged guest is used, the permeability for the marker will be controlled by the proportion of the channels that are sterically blocked by the guest molecule. On the other hand, if a charged guest is used, the permeability for the marker will be greatly affected by a change in the membranous charge due to the host-guest complexation with this guest. As observed in our previous studies,<sup>3-6</sup> such a change in the membranous charge would cause a change in the charge-charge interaction between the membrane and marker or in the packing density of the membrane. These effects are unsuitable for the purpose of the present study because they could cause a permeability change regardless of the steric capability of marker compounds to pass through the intramolecular channel.

In the present study, cyclohexanol, benzyl alcohol, 1-adamantanol, adenosine, and cytidine have been chosen as uncharged guests that can be accommodated into the  $\beta$ -cyclodextrin cavity and block the channel to sterically inhibit the permeation of marker compounds. The permeability change induced as a result of host-guest complexation by the cyclodextrin derivative (4) in a condensed monolayer has been compared for the electroactive markers that are sterically permeable (*p*-quinone) and not permeable ([Co(phen)<sub>3</sub>]<sup>2+</sup>, [Mo(CN)<sub>6</sub>]<sup>4-</sup>) through the  $\beta$ -cyclodextrin cavity (channel entrance). Appropriate dimensions of these marker compounds are shown in Figure 4.

**$\pi$ -A Isotherms of Cyclodextrin Derivative 4.** To determine the surface pressure to be applied in the horizontal touch cyclic voltammetric measurements, a  $\pi$ -A isotherm study was carried out with the same conditions as those for the horizontal touch cyclic voltammetry. Figure 5a-c shows the  $\pi$ -A isotherms of the long alkyl cyclodextrin derivative (4) in the presence or absence of cyclohexanol as a guest and [Co(phen)<sub>3</sub>]<sup>2+</sup>, [Mo(CN)<sub>6</sub>]<sup>4-</sup>, or *p*-quinone as a marker in the subphase solution (Figure 5a, 5b, and 5c, respectively). These  $\pi$ -A isotherms indicate the formation of a monolayer of cyclodextrin derivative 4. For the purpose of examining the intramolecular channel function, a condensed monolayer must be formed in which the intermolecular voids between the membranous cyclodextrin molecules that would cause a leak of the marker are minimized. Accordingly, the surface pressure to be applied must be sufficiently high, but should not be so high as to cause a collapse of the monolayer when in contact with the HOPG electrode.

From the  $\pi$ -A isotherm measured on a buffer solution containing no guest or marker, the molecular area extrapolated at zero surface pressure ( $A_0$ ) was estimated to be  $271 \pm 2 \text{ \AA}^2$  molecule<sup>-1</sup>. This value is close to that observed on pure water at the same temperature ( $261 \pm 4 \text{ \AA}^2$  molecule<sup>-1</sup>, figure not shown) and also to the reported value at the same conditions ( $259 \text{ \AA}^2$  molecule<sup>-1</sup>).<sup>19,28</sup> These  $A_0$  values indicate that the membranous cyclodextrin molecules are oriented with their cavity entrance (the acetylated secondary hydroxyl side) facing the subphase solution. However, since these  $A_0$  values are greater than that calculated from the base area of the cylindrical structure of  $\beta$ -cyclodextrin ( $200\text{--}210 \text{ \AA}^2$  molecule<sup>-1</sup> for the secondary hydroxyl side), the above monolayer at zero surface pressure with a molecular area of  $260\text{--}270 \text{ \AA}^2$  molecule<sup>-1</sup> is still in an expanded state. This is possibly due to the free rotation of the *O*-acetyl groups attached to the secondary hydroxyl groups of the  $\beta$ -cyclodextrin. By further compressing the monolayer, the molecular area decreased and reached just before the membrane collapse to a minimum value of ca.  $200 \text{ \AA}^2$  molecule<sup>-1</sup>, corresponding to the base area of  $\beta$ -cyclodextrin.

(27) Tagaki, W. *Yukagaku* 1988, 37, 394-401 and the references cited therein.

(28) Kawabata, Y.; Matsumoto, M.; Nakamura, T.; Tanaka, M.; Manda, E.; Takahashi, H.; Tamura, S.; Tagaki, W.; Nakahara, H.; Fukuda, K. *Thin Solid Films* 1988, 159, 353-358.

(29) Taneva, S.; Ariga, K.; Okahata, Y.; Tagaki, W. *Langmuir* 1989, 5, 111-113.

(30) Taneva, S.; Ariga, K.; Tagaki, W.; Okahata, Y. *J. Colloid Interface Sci.* 1989, 131, 561-566.

(31) Tabushi, I.; Kuroda, Y.; Yokota, K. *Tetrahedron Lett.* 1982, 23, 4601-4604.

(32) van Beijnen, A. J. M.; Nolte, R. J. M.; Zwikker, J. W.; Drenth, W. *Recl. Trav. Chim. Pays-Bas* 1982, 101, 409-410.

(33) Nevel, J. G.; Nolte, R. J. M. *Tetrahedron Lett.* 1984, 25, 2263-2266.

(34) Kragten, U. F.; Roks, M. F. M.; Nolte, R. J. M. *J. Chem. Soc., Chem. Commun.* 1985, 1275-1276.

(35) Jullien, L.; Lehn, J. M. *Tetrahedron Lett.* 1988, 29, 3803-3806.

(36) Carmichael, V. E.; Dutton, P. J.; Fyles, T. M.; James, T. D.; Swan, J. A.; Zojaji, M. *J. Am. Chem. Soc.* 1989, 111, 767-769.

(37) Nakano, A.; Xie, Q.; Mallen, J. V.; Echegoyen, L.; Gokel, G. W. *J. Am. Chem. Soc.* 1990, 112, 1287-1289.

(38) Voyer, N. *J. Am. Chem. Soc.* 1991, 113, 1818-1821.

As shown in Figure 5a-c, an addition of either marker compound (0.10 mM of  $[\text{Co}(\text{phen})_3]^{2+}$ , or 1.0 mM of  $[\text{Mo}(\text{CN})_6]^{4-}$  or *p*-quinone) did not affect the  $\pi$ -A isotherm. However, an addition of the guest (10 mM cyclohexanol) induced some expansion at the beginning of the monolayer formation (surface pressure below ca. 25 mN m<sup>-1</sup>). Since the formation of a host-guest inclusion complex with an uncharged guest should not affect the  $\pi$ -A isotherm, the expansion at low surface pressures can be ascribed to the insertion of the hydrophobic guest molecules between the membranous cyclodextrin molecules. In the later stage of the monolayer formation at higher surface pressures, almost no expansion was induced by the guest, indicating the formation of a condensed monolayer in which the guest molecules that initially existed between the membranous cyclodextrin molecules were squeezed out. The complex formation caused some decrease in the stability of the cyclodextrin monolayer as indicated by decreased collapse pressures in the presence of the guest in the subphase solution (Figure 5a-c). With regard to the other guests used for the selectivity study, i.e., benzyl alcohol (10 mM), 1-adamantanol (0.3 mM), adenosine (10 mM), and cytidine (10 mM), almost no expansion of the monolayer was induced even at low surface pressures (figures not shown).

Based on these  $\pi$ -A isotherm results, the surface pressure for the horizontal touch cyclic voltammetric measurements has been set to 50 mN m<sup>-1</sup>, which is close to but somewhat lower than the collapse pressure of this cyclodextrin monolayer. A higher surface pressure just below the collapse pressure caused a collapse of the monolayer when the HOPG electrode was brought into contact with it. By controlling at 50 mN m<sup>-1</sup>, the molecular area of the membranous cyclodextrin would be limited to ca. 210 Å<sup>2</sup> molecule<sup>-1</sup> and the intermolecular voids between the cyclodextrin molecules that could cause a leak of the marker are expected to be minimized.

**Permeability of Marker Compounds through the Cyclodextrin Monolayer.** Permeability through the monolayer of cyclodextrin derivative 4 has been estimated from the accessibility of electroactive markers to the electrode surface, which in turn can be estimated from the peak potential and area of cyclic voltammograms (Figures 6-8). The calculation of the voltammogram area has been made by integration of either oxidation or reduction peak that corresponds to the initial process of the redox cycle, i.e., the oxidation peak in the case of  $[\text{Co}(\text{phen})_3]^{2+}$  and  $[\text{Mo}(\text{CN})_6]^{4-}$ , and the reduction peak in the case of *p*-quinone. Permeability through the condensed cyclodextrin monolayer as well as the effect of cyclohexanol as a guest was found to be quite different, depending on whether the electroactive marker used is sterically permeable (*p*-quinone) or not permeable ( $[\text{Co}(\text{phen})_3]^{2+}$ ,  $[\text{Mo}(\text{CN})_6]^{4-}$ ) through the  $\beta$ -cyclodextrin cavity (channel entrance).

(a)  **$[\text{Co}(\text{phen})_3]^{2+}$  as a Permeability Marker.** Figure 6a shows the cyclic voltammograms of  $[\text{Co}(\text{phen})_3]^{2+}$  as a permeability marker. The heterogeneous electron transfer rate constant (electrochemical standard rate constant;  $k^0$ ) of the  $[\text{Co}(\text{phen})_3]^{3+/2+}$  redox couple is reported to be  $6 \times 10^{-2}$  cm s<sup>-1</sup> in water (1 M KCl) at 25 °C.<sup>39</sup> Such a fast electron transfer kinetics of  $[\text{Co}(\text{phen})_3]^{2+}$  is a favorable property for using this compound as a marker for the membrane permeability. Since this marker is initially in the reduced form, a change in the area of the oxidation peak ( $[\text{Co}^{\text{II}}(\text{phen})_3]^{2+} \rightarrow [\text{Co}^{\text{III}}(\text{phen})_3]^{3+} + e^-$ ; the lower half of the cyclic voltammograms in Figure 6) would be a proper measure of the change in the accessibility of this marker to the electrode surface. Accordingly, the permeability change was estimated from the change in the area of the oxidation peak.

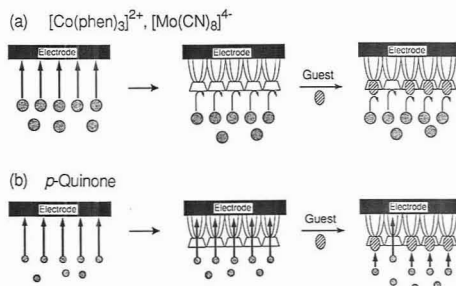


**Figure 9.** Schematic representation of the permeability for the marker compounds through the condensed cyclodextrin monolayer. Figures 9a and 9b represent the behaviors of the markers that are sterically (a) not permeable ( $[\text{Co}(\text{phen})_3]^{2+}$ ,  $[\text{Mo}(\text{CN})_6]^{4-}$ ) and (b) permeable (*p*-quinone) through the  $\beta$ -cyclodextrin cavity (channel entrance).

For the calculation of the voltammogram area, the background current must be taken into account because the voltammogram peak was much smaller than those for  $[\text{Mo}(\text{CN})_6]^{4-}$  and *p*-quinone (both 1.0 mM concentration) due to a lower solubility of  $[\text{Co}(\text{phen})_3]^{2+}$ ; the measurements had to be carried out at 0.10 mM concentration. However, the background currents in both the presence and absence of the cyclodextrin monolayer gave essentially horizontal lines from -0.1 V (Figure 6b). As a result, a background-corrected integration could be made simply by integrating the oxidation peaks of  $[\text{Co}(\text{phen})_3]^{2+}$  (curves A and B in Figure 6) from -0.1 V (see the Experimental Section).

It is evident from Figure 6a that the presence of the cyclodextrin monolayer causes a dramatic decrease in the area of the oxidation peak with no apparent peak potential within the potential window (curve A vs B). By correcting for the background currents in the presence and absence of the cyclodextrin monolayer (Figure 6b), the decrease in the area of the oxidation peak was estimated to be 85%. Furthermore, the change in the cyclic voltammogram upon an addition of cyclohexanol as a guest (up to 20 mM) was very small (curve B vs C-E in Figure 6a) as compared to the corresponding changes when *p*-quinone was used as a marker (vide infra; Figure 8). These observations can be explained by considering the steric incapability of the marker  $[\text{Co}(\text{phen})_3]^{2+}$  (ca. 13-Å minimum diameter; Figure 4) to pass through the  $\beta$ -cyclodextrin cavity (ca. 7.5-Å diameter). Consequently, the access of this marker to the electrode surface would be efficiently inhibited by the cyclodextrin monolayer, and in addition, the host-guest complexation with cyclohexanol that blocks the channel would not affect the marker permeability (Figure 9a).

(b)  **$[\text{Mo}(\text{CN})_6]^{4-}$  as a Permeability Marker.** Figure 7 shows the cyclic voltammograms of  $[\text{Mo}(\text{CN})_6]^{4-}$  as a permeability marker. This marker also has a favorable property because the electron transfer is even more feasible as compared to  $[\text{Co}(\text{phen})_3]^{2+}$ ; the heterogeneous electron transfer rate constant ( $k^0$ ) of the  $[\text{Mo}(\text{CN})_6]^{3-/4-}$  redox couple is reported to be  $5 \times 10^{-1}$  cm s<sup>-1</sup> in water (0.2 M KCl) at room temperature.<sup>40</sup> Since this marker is initially in the reduced form, a change in the area of the oxidation peak ( $[\text{Mo}^{\text{IV}}(\text{CN})_6]^{4-} \rightarrow [\text{Mo}^{\text{V}}(\text{CN})_6]^{3-} + e^-$ ; the lower half of the cyclic voltammograms in Figure 7) would be a proper measure of the change in the accessibility of this marker to the electrode surface. Accordingly, the permeability change was estimated from the change in the area of the oxidation peak. The background

(39) Bartelt, H. *Electrochim. Acta* 1971, 16, 629-635.

(40) Saji, T.; Maruyama, Y.; Aoyagi, S. *J. Electroanal. Chem. Interfacial Electrochem.* 1978, 86, 219-222.

correction was not made because the measurements at a marker concentration of 1.0 mM (10-fold as compared to the case of  $[\text{Co}(\text{phen})_3]^{2+}$ ) gave much larger voltammetric peaks, and as a result the background current was negligible either in the presence or absence of the cyclodextrin monolayer.

Similarly as in the case of using  $[\text{Co}(\text{phen})_3]^{2+}$  as a marker, a marked inhibition of electron transfer was observed in the presence of the cyclodextrin monolayer (curve A vs B; 70% decrease in the area of the oxidation peak). The change in the cyclic voltammogram upon an addition of cyclohexanol (10 mM) was very small (curve B vs C). These observations, again, can be explained by the steric incapability of the marker  $[\text{Mo}(\text{CN})_6]^{4-}$  (ca. 9-Å minimum diameter; Figure 4) to pass through the  $\beta$ -cyclodextrin cavity (Figure 9a).

**(c) Degree of Integrity of the Condensed Cyclodextrin Monolayer in Contact with the HOPG Electrode.** Despite the fact that  $[\text{Mo}(\text{CN})_6]^{4-}$  as well as  $[\text{Co}(\text{phen})_3]^{2+}$  is much too large to pass through the  $\beta$ -cyclodextrin cavity (channel entrance), and that the intermolecular voids between the membranous cyclodextrin molecules should be minimized under a controlled high surface pressure, a complete inhibition of electron transfer was not attained for either of these markers. This could be ascribed, in principle, to the following two reasons: (i) A leak of the markers through the defects (bare spots or large pinholes) that exist in the monolayer. (ii) A long-range electron transfer between the electrode and markers that are separated from each other at some distance by the existence of the cyclodextrin monolayer. Of these two possible reasons, (i) is considered to be the main reason on the basis of the following discussions.

The theoretical study by Savéant et al.<sup>41</sup> demonstrates that partial blocking of an electrode surface by membranous molecules or polymers, which generates a large number of microscopic electroactive sites still free from the membranous material, causes a change in the shape of cyclic voltammograms. As the fractional coverage of the electrode surface increases, the current decreases according to a net decrease in the surface area, and in addition, the anodic to cathodic peak distance becomes larger according to an apparent decrease of the heterogeneous electron transfer rate constant. As the fractional coverage further increases, the current further decreases and the voltammogram bears a sigmoidal shape. At this stage, the electrode has a number of microscopic active sites, which are sufficiently separated with each other to act as an array of microelectrodes. Such voltammetric changes have been clearly observed by Bilewicz and Majda<sup>42,43</sup> for a series of evaporated gold electrodes modified with Langmuir-Blodgett type composite monolayers of 1-octadecanethiol and 1-octadecanol under different surface pressures. Finally, under a complete coverage of the electrode, the current is further reduced and the voltammogram loses its sigmoidal character. Under such a condition, the current contains a significant component due to electron tunneling across the membrane or film.<sup>42-46</sup>

In view of the above discussion, the shapes of curve B in Figures 6 and 7 can be regarded as in the stage of a large anodic to cathodic peak separation because no apparent voltammetric peak was observed within the potential window in either of these curves. Although the peak separation seems to be greater in the case of  $[\text{Mo}(\text{CN})_6]^{4-}$  (curve B in Figure 7), the voltammogram is not yet in the stage of bearing a

typical sigmoidal shape. Accordingly, the electrode reaction takes place at a large number of sites that are not covered or only loosely covered with an organized monolayer of the cyclodextrin molecules, in other words, the defects (bare spots or large pinholes) that exist in the cyclodextrin monolayer. The total area of these pinholes should amount to 15 or 30% of the electrode surface area when calculated on the basis of the 85 and 70% net decrease in the area of the oxidation peaks for  $[\text{Co}(\text{phen})_3]^{2+}$  and  $[\text{Mo}(\text{CN})_6]^{4-}$ , respectively.

The recent study by Chang and Bard<sup>47</sup> demonstrates up to 1–10% defect in the HOPG surface on the basis of direct observation by scanning tunneling microscopy; the surface of freshly cleaved HOPG surface contains not only atomically smooth planes but also various morphologies of graphite. Although the existence of these defects may favor the formation of large pinholes, this factor alone cannot explain such a large total area of pinholes as described above (15 or 30% of the area of the electrode surface). In fact, almost complete inhibition of electron transfer has been observed by Uchida et al.<sup>48</sup> in the case of a condensed monolayer of stearic acid deposited on an HOPG electrode by the Langmuir-Blodgett method.

A factor that might partly explain this discrepancy is the generation of defects in the monolayer that could occur by a contact with the HOPG electrode. This would be favored by the presence of edges in the HOPG electrode and/or by the unbalanced cross-sectional areas within the molecule of cyclodextrin derivative 4 as compared to simple alkane derivatives. In the long alkyl derivative of cyclodextrin (4), the cross-sectional areas of the cyclodextrin moiety and the long alkyl chains (in total) are ca. 200 and 140 Å<sup>2</sup>, respectively.

Another factor that should be considered is the possibility of a decrease in the electron-transfer rate. When an electrode surface is covered with membranous molecules or polymers, an anodic to cathodic peak separation could be induced in cyclic voltammograms not only by a simple decrease in the electrode area (ref 41) but also by a decrease in the electron-transfer rate. In other words, the peak separation could also result from a factor that does not reflect the total area of "bare spots" at which the electron transfer proceeds without a decrease of the rate. Since the anodic to cathodic peak separation, regardless of the reason, would cause a part of the voltammogram peak to be pushed out of the potential window, an estimation of the total area of "bare spots" from voltammogram areas (vide supra) might lead to an overestimation if the peak separation was at least partly due to the kinetic effect described above.

In the present case, the decrease in the electron-transfer rate, if occurred, would be ascribed to the existence of defects that are not actually "bare spots" but rather the spots covered with a loosely packed cyclodextrin monolayer. In these spots, a disordered arrangement of the cyclodextrin molecules would lead to a situation in which the markers are not able to sufficiently access the electrode surface but a long-range electron transfer between the markers and the electrode surface is still possible.

**(d) *p*-Quinone as a Permeability Marker.** Figure 8 shows the cyclic voltammograms of *p*-quinone as a permeability marker. Since this marker is initially in the oxidized form, a change in the area of the reduction peak (quinone + 2H<sup>+</sup> + 2e<sup>-</sup> → hydroquinone; the upper half of the cyclic voltammograms in Figure 8) would be a proper measure of the change in the accessibility of this marker to the electrode surface. Accordingly, the permeability change was estimated from the change in the area of the reduction peak. As in the

(41) Amatore, C.; Savéant, J. M.; Tessier, D. *J. Electroanal. Chem. Interfacial Electrochem.* 1983, 147, 39–51.

(42) Bilewicz, R.; Majda, M. *Langmuir* 1991, 7, 2794–2802.

(43) Bilewicz, R.; Majda, M. *J. Am. Chem. Soc.* 1991, 113, 5464–5466.

(44) Porter, M. D.; Bright, T. B.; Allara, D. L.; Chidsey, C. E. D. *J. Am. Chem. Soc.* 1987, 109, 3559–3568.

(45) Chidsey, C. E. D.; Loiacono, D. N. *Langmuir* 1990, 6, 682–691.

(46) Miller, C.; Cuendet, P.; Grätzel, M. *J. Phys. Chem.* 1991, 95, 877–886.

(47) Chang, H.; Bard, A. J. *Langmuir* 1991, 7, 1143–1153.

(48) Uchida, I.; Ishino, A.; Matsue, T.; Itaya, K. *J. Electroanal. Chem. Interfacial Electrochem.* 1989, 266, 455–460.

case of  $[\text{Mo}(\text{CN})_6]^{4-}$  (vide supra), the background correction was not made because the background current was negligible both in the presence and absence of the cyclodextrin monolayer.

As shown in Figure 8, the presence of the cyclodextrin monolayer caused some decrease in the area of the cyclic voltammogram of *p*-quinone (curve A vs B). But in this case, the magnitude of change was much smaller (31% decrease in the reduction peak) than in the case of  $[\text{Co}(\text{phen})_3]^{2+}$  or  $[\text{Mo}(\text{CN})_6]^{4-}$ . In addition, the voltammetric reduction peak was retained within the potential window though the peak potential shifted to the negative direction (+0.03 V  $\rightarrow$  -0.24 V).

Compared to  $[\text{Co}(\text{phen})_3]^{2+}$  and  $[\text{Mo}(\text{CN})_6]^{4-}$ , the electron transfer is much less feasible in *p*-quinone; the heterogeneous electron-transfer rate constant ( $k^0$ ) of the *p*-quinone/hydroquinone redox couple is reported to be  $1.4 \times 10^{-4} \text{ cm s}^{-1}$  in water (1 M HClO<sub>4</sub>) at 25 °C.<sup>49</sup> For such a marker, a greater shift as well as broadening of the cyclic voltammogram peak is expected to be induced by the presence of the cyclodextrin monolayer. As a result, a part of the voltammogram peak might be pushed out of the potential window, which is set for the measurement of the cyclic voltammogram of *p*-quinone in the absence of the cyclodextrin monolayer, in other words, for the measurement with the bare HOPG electrode. Since the permeability is estimated from the voltammogram area in the presence of the cyclodextrin monolayer relative to that for the bare electrode, the permeability for *p*-quinone with a slower electron-transfer kinetics might be underestimated.

Despite such an unfavorable factor for *p*-quinone, a well-defined voltammetric peak was still observed within the potential window and the decrease in the voltammogram area was much smaller as compared to  $[\text{Co}(\text{phen})_3]^{2+}$  and  $[\text{Mo}(\text{CN})_6]^{4-}$ . These voltammetric behaviors clearly indicate a much more feasible access of *p*-quinone to the electrode surface. To interpret these results, it must be taken into account that *p*-quinone (ca. 6.3 Å shorter width; Figure 4) is sterically permeable through the  $\beta$ -cyclodextrin cavity (channel entrance) and that the cyclodextrin monolayer is sufficiently condensed so that the intermolecular voids are minimized. These points, taken together, support the permeation of *p*-quinone through the intramolecular channel formed within the cyclodextrin derivative 4 (Figure 9b). Since the difference between the voltammograms for *p*-quinone and the other two bulky markers is quite remarkable, an incomplete integrity of the cyclodextrin monolayer in contact with the HOPG electrode (vide supra) does not invalidate the above discussion.

As mentioned above, the cyclodextrin monolayer caused a shift of the reduction peak potential of *p*-quinone to the negative direction. Such a shift of the voltammetric peak is consistent with the discussions in section c because the noncavity part of the cyclodextrin molecules causes "partial blocking" of the electrode surface (Figure 10). In this case, the "fractional coverage" could be as high as 79% if a complete integrity of the oriented and condensed monolayer was assumed.

An addition of the guest in the subphase solution caused further decrease in the voltammogram area (curve B vs C in Figure 8). Furthermore, the extent of decrease became greater by increasing the concentration of the guest in the subphase (curve C  $\rightarrow$  D  $\rightarrow$  E). These observations can be most reasonably explained by a channel blocking effect of the cyclohexanol guest, leading to an inhibition of the permeation of *p*-quinone that can sterically pass through the  $\beta$ -cyclodextrin cavity (Figure 9b). The shift of voltammetric peak

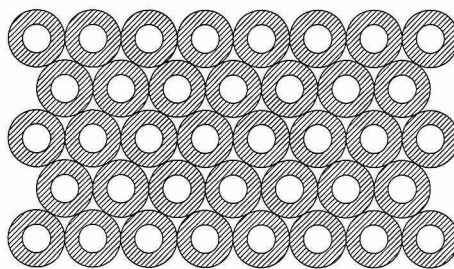


**Figure 10.** Schematic representation of the closest-packed monolayer of the cyclodextrin molecules facing its base to the aqueous subphase solution. The shaded area indicates the noncavity part of the cyclodextrin molecules.

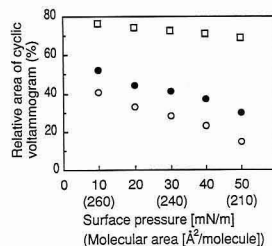


**Figure 11.** Dependence of the cyclic voltammogram area on the surface pressure applied to the cyclodextrin monolayer. The expected molecular areas were indicated in the parentheses in the abscissa. *p*-Quinone (□; 1.0 mM),  $[\text{Mo}(\text{CN})_6]^{4-}$  (●; 1.0 mM), and  $[\text{Co}(\text{phen})_3]^{2+}$  (○; 0.1 mM) were examined as the markers for permeability. Measured on 0.1 M acetate buffer solution (pH 6.0) at  $17.0 \pm 0.1$  °C. The ordinate indicates the voltammogram area relative to that measured for the same marker in the absence of the cyclodextrin monolayer. The voltammogram areas were calculated by the integration of the following peaks in the potential ranges indicated. *p*-Quinone: the reduction peak in a potential range from +0.2 to -0.5 V.  $[\text{Mo}(\text{CN})_6]^{4-}$ : the oxidation peak in a potential range from +0.3 to +0.9 V.  $[\text{Co}(\text{phen})_3]^{2+}$ : the oxidation peak in a potential range from -0.1 to +0.6 V.

to the negative direction by increasing the concentration of the guest (curve B  $\rightarrow$  C  $\rightarrow$  D  $\rightarrow$  E) is consistent with an increase in the fractional coverage of the electrode surface as a result of the channel blocking by host-guest complexation with cyclohexanol.

**Dependence of Marker Permeability on Surface Pressure.** Figure 11 shows the dependence of the cyclic voltammogram area on the surface pressure applied to the cyclodextrin monolayer. All of the cyclic voltammetric measurements described so far were carried out at the highest surface pressure (50 mN m<sup>-1</sup>) on the abscissa. By increasing the surface pressure from 10 to 50 mN m<sup>-1</sup>, in other words, by decreasing the molecular area from ca. 260 to 210 Å<sup>2</sup> molecule<sup>-1</sup>, the voltammogram areas for all three markers decreased almost linearly. However, an important point to be emphasized here is that the magnitude of the decrease was different between the markers; the decrease for *p*-quinone was much smaller than that for the other two bulky markers, i.e.,  $[\text{Co}(\text{phen})_3]^{2+}$  and  $[\text{Mo}(\text{CN})_6]^{4-}$ .

This observation can also be explained by considering the steric capability of *p*-quinone to pass through the  $\beta$ -cyclodextrin cavity (vide supra). By increasing the surface pressure, the total area of the intermolecular voids in the monolayer would be smaller, but the number of the cyclodextrin molecules (the number of channels) that are in contact with the electrode surface would increase. The dependence

(49) Laczse, P.-C.; Pham, M. C.; Delamar, M.; Dubois, J.-E. *J. Electroanal. Chem. Interfacial Electrochem.* 1980, 108, 9-16.



**Table I. Guest-Induced Decrease in the Area of the Cyclic Voltammogram of *p*-Quinone in the Presence of a Condensed Monolayer of the Long Alkyl Derivative of  $\beta$ -Cyclodextrin (4)<sup>a</sup>**

guest	concentration of guest (M)	relative area of cyclic voltammogram (%) <sup>b</sup>	guest-induced decrease (%)
without guest		69.2	
cyclohexanol	$1.0 \times 10^{-2}$	$62.5 \pm 1.5$	6.7
adenosine	$1.0 \times 10^{-2}$	$63.7 \pm 1.2$	5.5
cytidine	$1.0 \times 10^{-2}$	$64.6 \pm 0.3$	4.6
benzyl alcohol	$1.0 \times 10^{-2}$	$65.3 \pm 0.7$	3.9
1-adamantanol	$3.0 \times 10^{-4}$	$64.5 \pm 1.3$	4.7

<sup>a</sup> Measured at  $17.0 \pm 0.1$  °C in the presence of a condensed monolayer of  $\beta$ -cyclodextrin derivative 4 on 0.1 M acetate buffer (pH 6.0) as a subphase solution. Surface pressure was controlled at 50 mN m<sup>-1</sup>. The concentration of *p*-quinone as a marker was 1.0 mM. <sup>b</sup> Calculated as a percentage of the voltammogram peak area relative to that measured in the absence of the cyclodextrin monolayer (bare electrode). Scan rate: 100 mV s<sup>-1</sup>. The integration was made for the reduction peak in a potential range from +0.2 to -0.5 V (see the Experimental Section for the details). The average values of two or three runs are shown.

of the voltammogram area on the surface pressure for the markers that are sterically too large to pass through the  $\beta$ -cyclodextrin cavity ([Co(phen)<sub>3</sub>]<sup>2+</sup>, [Mo(CN)<sub>6</sub>]<sup>4-</sup>) would be controlled only by their permeability through the intermolecular voids. The surface pressure dependence shown in Figure 11 for these two bulky markers is consistent with this expectation. On the other hand, the surface pressure dependence for *p*-quinone that can sterically pass through the  $\beta$ -cyclodextrin cavity would be controlled by the permeability through both intermolecular voids and intramolecular channels. The fact that the decrease in the voltammogram area upon an increase in the surface pressure is much smaller for *p*-quinone (Figure 11) indicates a characteristic aspect of this cyclodextrin monolayer to retain a considerable part of the permeability despite the decrease in the total area of the intermolecular voids between the membranous molecules. These observations further support the intramolecular channel function of the cyclodextrin derivative 4 (Figure 9b).

Another point that should be considered is the fact that a dramatic increase in the voltammogram area upon a decrease in the surface pressure was observed for both of the two bulky markers, regardless of whether the marker is hydrophilic ([Mo(CN)<sub>6</sub>]<sup>4-</sup>) or hydrophobic ([Co(phen)<sub>3</sub>]<sup>2+</sup>). Such a behavior is quite different from a much smaller surface pressure dependence for *p*-quinone, which is sterically smaller than [Mo(CN)<sub>6</sub>]<sup>4-</sup> or [Co(phen)<sub>3</sub>]<sup>2+</sup> and can pass through the  $\beta$ -cyclodextrin cavity. These results indicate that the main factor controlling the permeability through the intramolecular

channel of the cyclodextrin derivative is the steric bulkiness rather than the hydrophobicity of the marker. Such an aspect is characteristic of the cyclodextrin monolayer, as compared to monolayers of simple alkane derivatives. Bilewicz and Majda<sup>42</sup> have recently examined the permeability of electroactive marker compounds through a series of Langmuir-Blodgett type composite monolayers of 1-octadecanethiol/1-octadecanol mixture and found that the permeability for [Os(2,2'-bipyridyl)<sub>2</sub>]<sup>2+</sup> (hydrophobic) was greater than that for [Ru(NH<sub>3</sub>)<sub>6</sub>]<sup>3+</sup> (hydrophilic). These results have been ascribed to a more feasible access of the hydrophobic marker to the electrode surface despite its larger size, indicating that the permeability through the intermolecular voids is controlled mainly by the hydrophobicity and not by the steric bulkiness of the marker.

**Selectivity of Permeability Control.** In the present study, the voltammetric responses to several uncharged guests, i.e., benzyl alcohol, 1-adamantanol, adenosine, and cytidine, in addition to cyclohexanol, were examined using *p*-quinone as a marker for the permeability change. The results are shown in Table I. It has been shown by the  $\pi$ -A isotherm study that none of these guests causes expansion of the cyclodextrin monolayer at high surface pressures (vide supra), confirming the incapability of these guests to be inserted between the membranous cyclodextrin molecules in a condensed monolayer. Accordingly, for this condensed monolayer membrane, a new type of selectivity is expected that is based on the ability of these guests to decrease the membrane permeability by blocking the intramolecular channel of the membranous cyclodextrin molecule. Between the guests examined, some differences were observed for the change in the voltammogram area. Although the repeatability of the experiments was close to these small differences, a trend of selectivity was observed when the averaged values were compared. Since an incomplete integrity of the present cyclodextrin monolayer is suggested by the earlier discussions, the voltammogram area might not be zero even if all of the cyclodextrin channels are blocked by the guest. Accordingly, the differences of the change in the voltammogram area between the guests in Table I might be underestimated.

Only in the case of 1-adamantanol, the measurement was carried out at a concentration of 0.3 mM because of its low solubility in water. Since the guest-induced decrease in the voltammogram area was negligible for 0.3 mM cyclohexanol, the selectivity of such a voltammetric response could be regarded as 1-adamantanol >> cyclohexanol > adenosine > cytidine > benzyl alcohol. The greatest decrease in the voltammogram area by 1-adamantanol, reflecting the greatest inhibition of marker permeability by this guest, is consistent with the stronger binding ability of the parent  $\beta$ -cyclodextrin

**Table II. Molecular Response Ratio of the Long Alkyl Derivative of  $\beta$ -Cyclodextrin (4) for Cyclohexanol Guest<sup>a</sup>**

	concentration of guest (mM)	amount of electron transfer <sup>b</sup>	decrease in the amount of electron transfer <sup>c</sup>	molecular response ratio <sup>d</sup>
without the cyclodextrin monolayer	0	$(7.18 \pm 0.01) \times 10^{15}$		
with the cyclodextrin monolayer	0	$(5.10 \pm 0.12) \times 10^{15}$		
	5	$(4.60 \pm 0.04) \times 10^{15}$	$5.0 \times 10^{14}$	7.3
	10	$(4.49 \pm 0.09) \times 10^{15}$	$6.1 \times 10^{14}$	8.9
	20	$(4.39 \pm 0.13) \times 10^{15}$	$7.1 \times 10^{14}$	10.4

<sup>a</sup> Measured at  $17.0 \pm 0.1$  °C for a condensed monolayer of  $\beta$ -cyclodextrin derivative 4 on 0.1 M acetate buffer (pH 6.0) as a subphase. Surface pressure was controlled at 50 mN m<sup>-1</sup>. The concentration of *p*-quinone as a marker was 1.0 mM. <sup>b</sup> Calculated from the area of the reduction peak of cyclic voltammograms. Scan rate: 100 mV s<sup>-1</sup>. Potential range for the integration: +0.2 to -0.5 V. The average of two to four runs is shown with the mean deviation. <sup>c</sup> Calculated as the guest-induced decrease in the amount of electron transfer for each concentration of the guest. The average value is shown. <sup>d</sup> Defined as the guest-induced change in the amount of electron transfer relative to the estimated number of the cyclodextrin molecules in the monolayer that are in contact with the electrode. The average value is shown. See text for the details.

for 1-adamantanol ( $K_s = 1.6 \times 10^3 \text{ M}^{-1}$  at 23 °C)<sup>50</sup> as compared with cyclohexanol ( $K_s = 5.0 \times 10^2 \text{ M}^{-1}$  at 25 °C)<sup>51</sup> in aqueous solution.

**Molecular Response Ratio.** The molecular response ratio was calculated (see ref 5), which was defined in this case as the guest-induced change in the amount of the electron transfer between the electrode and marker (*p*-quinone) relative to the estimated number of the cyclodextrin molecules in the monolayer that are in contact with the electrode. This value would be a direct and convenient measure for the efficiency of signal transduction. A channel mimetic mode of signal transduction could, in principle, lead to an amplification of the signal.

The amount of the electron transfer from the electrode to the marker *p*-quinone in the presence or absence of the cyclohexanol guest was estimated from the area of the reduction peak of cyclic voltammograms. From these values, the decrease in the amount of the electron transfer upon the addition of each concentration of guest in the subphase solution was calculated. On the other hand, if a complete integrity of the cyclodextrin monolayer was assumed, the number of the membranous cyclodextrin molecules that would be in contact with the electrode surface could be estimated as  $6.86 \times 10^{13}$  on the basis of the molecular area of  $210 \text{ \AA}^2$  molecule<sup>-1</sup> at an applied surface pressure of  $50 \text{ mN m}^{-1}$ . Based on these values, the molecular response ratios of cyclodextrin derivative 4 under the present experimental conditions were calculated (Table II). As expected, the molecular response ratio increased by increasing the concentration of the guest so that the permeation of more markers would be inhibited by the channel blocking as a result of host-guest complexation. A molecular response ratio up to 10.4 (1.7/s) was obtained under the present conditions.

## CONCLUSIONS

A long alkyl derivative of  $\beta$ -cyclodextrin (4) was exploited as a channel mimetic sensory element. The permeability of a condensed monolayer of 4 was controlled by blocking the intramolecular channel with organic guests. To obtain rigid experimental evidence for the ability of this cyclodextrin derivative to function as an intramolecular channel, an

approach based on horizontal touch cyclic voltammetry was carried out for a condensed monolayer of 4, in which intermolecular voids between the membranous cyclodextrin molecules that would cause a leak of electroactive marker compounds were minimized. The permeability for a marker that can sterically pass through the  $\beta$ -cyclodextrin cavity (channel entrance) as in the case of *p*-quinone was shown to be able to be controlled by blocking the channel with organic guests. Consequently, it has been shown that this type of cyclodextrin derivative affords a new type of channel mimetic sensory element that displays a selectivity based on the ability of each guest to decrease the membrane permeability by blocking the intramolecular channel of the membranous host molecule. Further design of host molecules to improve the complexation ability and selectivity as well as to introduce more suitable channel components would lead to artificial "ion channel sensors" with an efficient chemical amplification of analyte concentration to attain a higher sensitivity.

## ACKNOWLEDGMENT

We gratefully acknowledge Professor Stephen G. Weber, Department of Chemistry, University of Pittsburgh, Pittsburgh, PA, for providing highly oriented pyrolytic graphite (HOPG) used as the working electrode and the Research Laboratory of Nihon Shokuhin Kako Co. (Shizuoka, Japan) for supplying  $\beta$ -cyclodextrin. We also acknowledge Hiroki Hashimoto and Hiroyuki Sazawa, Department of Chemistry, Faculty of Science, Hokkaido University, for helpful assistance in the synthesis of the long alkyl cyclodextrin derivative and in the horizontal touch voltammetric measurements, respectively. This work was supported from the Grant-in-Aids for Scientific Research (Y.U., K.O.) by the Ministry of Education, Science and Culture, Japan, and from the Japan-U.S. Cooperative Science Program (Y.U.) cosponsored by the Japan Society for the Promotion of Science and the U.S. National Science Foundation. The supports from the Iketani Science and Technology Foundation (Tokyo, Japan) to Y.U. and from the Tokuyama Science Foundation (Tokyo, Japan) and the Tokyo Biochemical Research Foundation (Tokyo, Japan) to K.O. are also acknowledged. Finally, we express our appreciation to the reviewers of this paper for valuable comments.

(50) Syamala, M. S.; Ramamurthy, V. *Tetrahedron* 1988, 44, 7223-7233.

(51) Matsui, Y.; Mochida, K. *Bull. Chem. Soc. Jpn.* 1979, 52, 2808-2814.

RECEIVED for review May 27, 1992. Accepted December 1, 1992.



# Scanning Tunneling Microscopy of Carbon Surfaces: Relationships between Electrode Kinetics, Capacitance, and Morphology for Glassy Carbon Electrodes

Mark T. McDermott, Christie Allred McDermott, and Richard L. McCreery\*

Department of Chemistry, The Ohio State University, 120 West 18th Avenue, Columbus, Ohio 43210

Polished, fractured, heat-treated, and laser-activated glassy carbon (GC) surfaces were examined by scanning tunneling microscopy (STM) in ambient air. Polished electrodes, as well as those which were vacuum heat treated (VHT) or laser activated (25 mW/cm<sup>2</sup>) after being polished, were comparably smooth in 2.5- $\mu$ m STM scans, exhibiting root-mean-square roughness (RMSR) of  $\sim$ 4 nm. Fractured, unpolished surfaces were significantly rougher (RMSR  $\sim$ 20 nm) and exhibited numerous nodules with diameters in the range of 50-300 nm. Polished surfaces laser activated at high-power density (70 MW/cm<sup>2</sup>) showed unexpected features along polishing scratches, apparently caused by local melting. The heterogeneous electron-transfer rate constant ( $k^0$ , cm/s) and capacitance ( $C^0$ ,  $\mu$ F/cm<sup>2</sup>) were also determined for the STM-characterized surfaces. Although rougher surfaces generally exhibited higher  $C^0$ , major differences in  $k^0$  were observed for surfaces with similar roughness and appearance. The results are consistent with the dominance of surface cleanliness in the mechanism of laser activation. Combined with past results based on adsorption, the morphological data indicate that differences in surface roughness are unimportant for laser activation of Fe(CN)<sub>6</sub><sup>4-/3-</sup> kinetics. Furthermore, the STM images reveal morphological effects of laser activation and polishing which were not apparent from previous electrochemical results.

## INTRODUCTION

Effective applications of solid electrodes in analysis, synthesis, and energy conversion result in part from an understanding of electrode surface properties and their effects on electron transfer. Glassy carbon (GC) is widely used as an electrode for analysis and as a substrate for modified electrodes largely because of its hardness, wide potential range, durability, and cost. However, the surface properties of a typical GC electrode are not thoroughly understood due to the variety of procedures used to prepare these electrodes and the large number of variables at the surface. The many procedures and associated effects on electrode kinetics and capacitance have been reviewed recently.<sup>1</sup> Because these surfaces are not well-defined, the major factors which determine electrochemical behavior have not been completely determined. The relationship between surface structural variables of GC and electrochemical phenomena such as heterogeneous electron-transfer kinetics and differential capacitance is the subject of this report.

Surface properties of carbon electrodes which affect electrochemical reactivity may be classified into four

categories: carbon microstructure, surface roughness, physisorbed impurities, and chemisorbed species, particularly oxides. The microstructural properties of various carbon materials are determined by their microcrystallite size, which will in turn determine the relative distribution of basal plane and edge plane regions at the surface. Graphite edge plane has been shown to differ greatly in electrochemical behavior from basal regions on ordered graphite surfaces.<sup>1-10</sup> However, the electrode activity will also be affected by the remaining three variables: roughness may determine the number of active sites, physisorbed impurities may cover or block active sites, and oxides may alter the mechanism of electron transfer altogether. Whether or not these variables are important to the behavior of a given electrode is determined by the electrode material and preparation history.

Our group and others have reported a number of surface preparations for GC electrodes. Pertinent examples of pretreatment methods are polishing,<sup>11-13</sup> laser activation,<sup>14-19</sup> vacuum heat treatment,<sup>13,20-22</sup> and exposure of the fresh bulk carbon by fracturing a GC rod in situ.<sup>17,18,23,24</sup> The purpose of these and other preparation schemes is to modify one or more of the GC surface variables mentioned above in order to affect electron-transfer rates of target redox systems. However, the effect of any particular electrode preparation procedure on the many GC surface factors remains unclear. For example, fracturing a GC electrode in solution should yield a surface relatively free of chemisorbed and physisorbed impurities with a microcrystallite size representative of the bulk carbon material. A polished surface, on the other hand,

(5) Bowling, R.; Packard, R.; McCreery, R. L. *J. Am. Chem. Soc.* 1989, 111, 1217-1223.

(6) Bowling, R.; Packard, R. T.; McCreery, R. L. *Langmuir* 1989, 5, 683-688.

(7) Rice, R. J.; McCreery, R. L. *Anal. Chem.* 1989, 61, 1637-1641.

(8) Robinson, R. S.; Sternitzke, K.; McDermott, M. T.; McCreery, R. L. *J. Electrochem. Soc.* 1991, 138, 2412-2418.

(9) McDermott, M. T.; Kneten, K.; McCreery, R. L. *J. Phys. Chem.* 1992, 96, 3124-3130.

(10) Kneten, K. R.; McCreery, R. L. *Anal. Chem.* 1992, 64, 2518-2524.

(11) Kamau, G. N.; Willis, W. S.; Rusling, J. F. *Anal. Chem.* 1985, 57, 545-551.

(12) Hu, I.; Karweik, D. H.; Kuwana, T. *J. Electroanal. Chem.* 1985, 188, 59-72.

(13) Wightman, R. M.; Deakin, M. R.; Kovach, P. M.; Kuhr, P. M.; Stutts, K. J. *J. Electrochem. Soc.* 1984, 131, 1578-1583.

(14) Poon, M.; McCreery, R. L. *Anal. Chem.* 1986, 58, 2745-2750.

(15) Poon, M.; McCreery, R. L. *Anal. Chem.* 1987, 59, 1615-1620.

(16) Poon, M.; McCreery, R. L.; Engstrom, R. *Anal. Chem.* 1988, 60, 1725-1730.

(17) Rice, R. J.; Pontikos, N.; McCreery, R. L. *J. Am. Chem. Soc.* 1990, 112, 4617-4622.

(18) Pontikos, N. M.; McCreery, R. L. *J. Electroanal. Chem.* 1992, 324, 229-242.

(19) Strein, T. G.; Ewing, A. G. *Anal. Chem.* 1991, 63, 194-198.

(20) Fagan, D. T.; Hu, I.; Kuwana, T. *Anal. Chem.* 1985, 57, 2759-2763.

(21) Stutts, K. J.; Kovach, P. M.; Kuhr, W. G.; Wightman, R. M. *Anal. Chem.* 1983, 55, 1632-1634.

(22) Hance, G. W.; Kuwana, T. *Anal. Chem.* 1987, 59, 131-134.

(23) Rice, R.; Allred, C.; McCreery, R. J. *Electroanal. Chem.* 1989, 263, 163-169.

(24) Allred, C. D.; McCreery, R. L. *Anal. Chem.* 1992, 64, 444-448.

\* Author to whom correspondence should be addressed.

(1) McCreery, R. L. In *Electroanal. Chemistry*; Bard, A. J., Ed.; Dekker: New York, 1991; Vol. 17, pp 221-374.

(2) Randin, J. P.; Yeager, E. J. *Electrochem. Soc.* 1971, 118, 711-714.

(3) Randin, J. P.; Yeager, E. J. *Electroanal. Chem.* 1972, 36, 257-276.

(4) Randin, J. P.; Yeager, E. J. *Electroanal. Chem.* 1975, 58, 313-322.

possesses a number of impurities and a microcrystalline structure quite different from that of the bulk carbon.<sup>18,23,24</sup> The fractured surface exhibits large heterogeneous electron-transfer rate constants ( $k^0$ ) for the ferro-/ferricyanide redox system compared to polished GC surfaces, but it is not clear whether this increase in rate is due to differences in microcrystallite size, microscopic roughness, surface cleanliness, or a combination of these variables.

There have been a number of surface techniques employed to study the surface structure of GC electrodes. Techniques commonly employed are X-ray photoelectron spectroscopy (XPS) and Auger electron spectroscopy (AES),<sup>11,12,20,21,25</sup> Raman spectroscopy,<sup>17,18,23</sup> surface-enhanced Raman spectroscopy (SERS),<sup>26,27</sup> and scanning electron microscopy (SEM).<sup>14,18,25,28</sup> Scanning tunneling microscopy (STM) has been used extensively to characterize highly ordered pyrolytic graphite (HOPG) electrodes at atomic resolution, including examination of the effects of electrochemical and chemical oxidation.<sup>30-32</sup> In several cases, defects on HOPG surfaces have been associated with increased chemical and electrochemical reactivity.<sup>3,31-35</sup> In an SEM study of GC by Bodalbhaj and Brajter-Toth,<sup>29</sup> the electrodeposition of copper at active sites was correlated with roughness and electron-transfer kinetics for  $\text{Fe}(\text{CN})_6^{4-/3-}$ . It was concluded that treatments which increase the density of copper nucleation sites also increase the electron-transfer rate. These techniques have been useful for understanding carbon electrode structure/reactivity relationships, but the structural models for GC surfaces remain incomplete at the scale below the SEM resolution limit of  $\sim 100 \text{ \AA}$ . A few reports of atomic scale STM of GC have appeared,<sup>36-38</sup> but in no case was the observed morphology related to electrochemical behavior. Furthermore, the variety of GC preparation procedures and test redox systems has made it difficult to compare the performance of different surfaces under otherwise identical conditions. Accordingly, the current effort involves the use of STM to provide surface morphological information about GC surfaces resulting from several pretreatment procedures and comparison of the electrode kinetics and capacitance of these surfaces. STM is particularly attractive because of high spatial resolution, especially in the vertical direction. In addition, SEM images of polished GC have been shown to be modified by the presence of a carbon microparticle layer.<sup>28</sup>

Electrochemically activated GC surfaces which had previously been polished have been imaged by two groups. Wang et al. compared surface roughness and topography imaged by STM for two different methods of electrochemical pretreatment (ECP)<sup>39</sup> and also used STM to investigate GC surface passivation due to phenol oxidation.<sup>40</sup> Freund et al. compared STM images and atomic force microscopy (AFM) images of

polished as well as electrochemically pretreated GC.<sup>41</sup> Both STM studies of electrochemically activated GC concluded that ECP resulted in a rougher surface relative to the initial polished surface. We report here an STM study of a number of other standard pretreatment procedures for GC electrodes. The surface morphology and relative roughness of conventionally polished, laser-irradiated, fractured, and vacuum heat treated GC surfaces are correlated with the electrochemical behavior as determined by the heterogeneous electron-transfer rate constant,  $k^0$ , for ferro-/ferricyanide and differential capacitance,  $C^0$ , for these surfaces. An essential component of our approach is observation of both STM images and electrochemical behavior on the same GC surface in order to reduce common problems with surface reproducibility. By comparing STM morphology and electrochemical activity for polished, laser-activated, fractured, and heat-treated GC, insights into electrode structure/reactivity relationships were obtained.

## EXPERIMENTAL SECTION

**Reagents.** All solutions were prepared with water obtained from a Nanopure II system (Barnstead, Dubuque, IA). Potassium ferrocyanide was used as received from Baker (Phillipsburg, NJ). Potassium chloride was used as received from Jenne Chemical (Cincinnati, OH). Solutions of 1 mM  $\text{K}_3\text{Fe}(\text{CN})_6$  in 1 M KCl were made fresh daily and purged with purified argon prior to use.

**Electrode Preparation.** Glassy carbon (GC-20) working electrodes were obtained from Tokai and employed in one of three different mechanical shapes: a 3-mm-diameter GC rod, a GC disk cut from a 2-mm-thick plate and sanded to shape, and GC microelectrodes fabricated as described previously.<sup>18,24</sup> All electrodes (GC disks and microelectrodes) used in the correlation of roughness and morphology with electrochemical behavior (Figures 1-3 and Tables I-III) were manufactured from a single 2-mm-thick plate of Tokai GC-20. The high-resolution STM images of fractured GC in Figure 4 were taken on a 3-mm-diameter Tokai GC-20 rod because of the ease of mounting and lack of sample tilt compared to fractured GC microelectrodes. No differences were observed in the STM images between fractured 3-mm GC rods and fractured GC microelectrodes. The electrochemical cell was made of Teflon and was equipped with a quartz window through which the electrode could be laser irradiated. Disk electrode areas were defined by a viton o-ring, and microelectrode areas (ca.  $0.5 \times 0.5 \text{ mm}$ ) were defined by the exposed electrode face surrounded by a sheath of epoxy. The three-electrode cell was completed with a Bioanalytical Systems (West Lafayette, IN) Ag/AgCl (3 M NaCl) reference electrode and a platinum wire auxiliary electrode.

Polished electrodes were prepared by polishing with 600-grit silicon carbide paper followed by 1-, 0.3-, and 0.05- $\mu\text{m}$  alumina (Buehler, Lake Bluff, IL) slurries on Microcloth polishing cloth (Buehler). Slurries were prepared from dry alumina and Nanopure water. Polished electrodes were sonicated in Nanopure water for  $\sim 5 \text{ min}$  before placement in the electrochemical cell. Care was taken to ensure that a drop of water remained on the polished electrode during insertion into the Teflon cell until anolyte solution was added. In-situ laser activation of polished electrodes in Nanopure water was performed with a Nd:YAG laser (Model 580-10, Quantel) operating at 1064 nm with 9-ns pulses. In order to partially average spatial and temporal variations of the laser intensity, three successive pulses were applied to the electrode. For this study, power densities of 25 and 70 MW/cm<sup>2</sup> were utilized. Fracturing procedures were as described previously.<sup>16,17,22,23</sup> Fractured surfaces were created in situ by breaking a GC microelectrode flush with the surface of the embedding epoxy (Eccobond 55, Emerson and Cuming, Inc., Woburn, MA). Electrochemical measurements were taken immediately after fracturing. Heat treatment procedures were similar to those of Fagen et al.<sup>22</sup> Rate constant and capacitance data were obtained

(25) Engstrom, R. C.; Strasser, V. A. *Anal. Chem.* 1984, 56, 136-141.

(26) Almsmeyer, Y. W.; McCreery, R. L. *Anal. Chem.* 1991, 63, 1289-1295.

(27) Almsmeyer, Y. W.; McCreery, R. L. *Langmuir* 1991, 7, 2370-2375.

(28) Kazee, B.; Weisshaar, D. E.; Kuwana, T. *Anal. Chem.* 1985, 57, 2739-2740.

(29) Bodalbhaj, L.; Brajter-Toth, A. *Anal. Chim. Acta* 1990, 231, 191.

(30) Gewirth, A.; Bard, A. J. *J. Phys. Chem.* 1988, 92, 5563.

(31) Chang, H.; Bard, A. J. *J. Am. Chem. Soc.* 1990, 112, 4598.

(32) Chang, H.; Bard, A. J. *J. Am. Chem. Soc.* 1991, 113, 5588.

(33) Bowling, R.; Packard, P.; McCreery, R. L. *J. Am. Chem. Soc.* 1988, 111, 1217.

(34) Bowling, R.; McCreery, R. L.; Pharr, C. M.; Engstrom, R. C. *Anal. Chem.* 1989, 61, 2763.

(35) Snyder, S. R.; White, H. S.; Lopez, S.; Abruna, H. D. *J. Am. Chem. Soc.* 1990, 112, 1333.

(36) Hu, C. Z.; Feng, L.; Andrade, J. D. *Carbon* 1988, 26, 543-555.

(37) Ellings, V.; Wudl, F. *J. Vac. Sci. Technol. A* 1988, 6 (2), 412-414.

(38) Brown, N. M. D.; You, H. X. *J. Mater. Chem.* 1991, 310, 127-138.

(39) Wang, J.; Martinez, T.; Yaniv, D. R.; McCormick, L. D. *J. Electroanal. Chem.* 1990, 278, 379-386.

(40) Wang, J.; Martinez, T.; Yaniv, D. R.; McCormick, L. D. *J. Electroanal. Chem.* 1991, 313, 120-140.

(41) Freund, M. S.; Brajter-Toth, A.; Cotton, T. M.; Henderson, E. R. *Anal. Chem.* 1991, 63, 1047-1049.

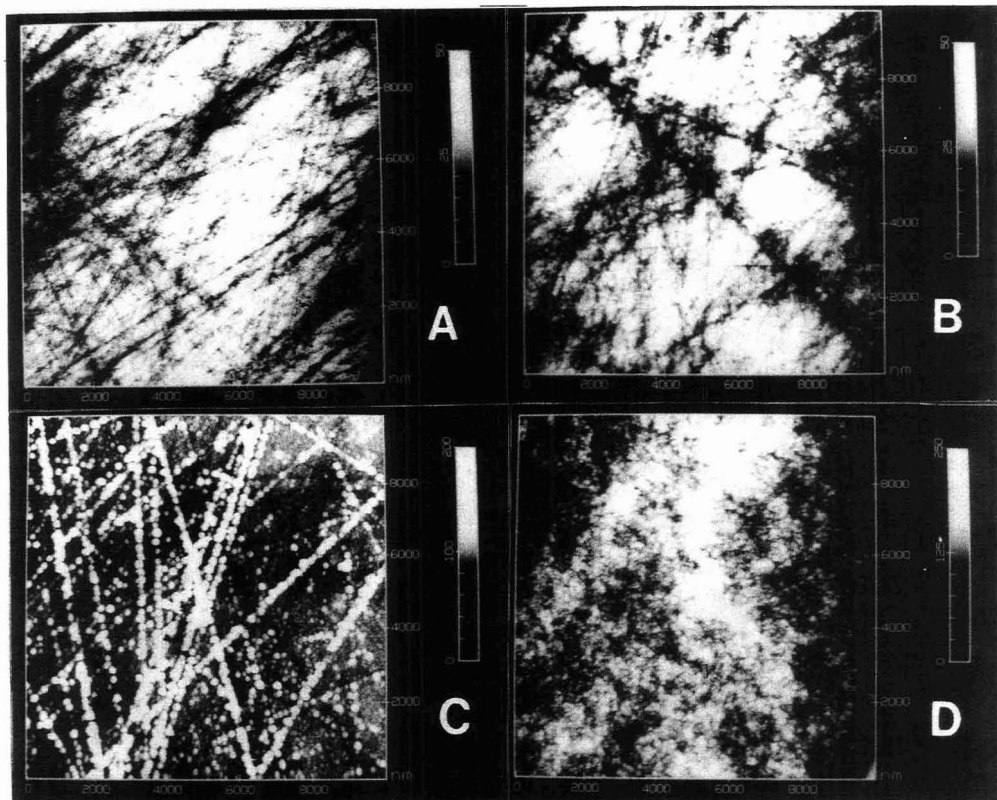


**Figure 1.** Images, 10 000 nm (full-scale  $x$  and  $y$ ), of GC electrodes after different pretreatment conditions: (A) polished GC,  $z$  scale 0–50 nm; (B) polished/laser-activated (25 MW/cm<sup>2</sup>) GC,  $z$  scale 0–50 nm; (C) polished/laser-activated (70 MW/cm<sup>2</sup>) GC,  $z$  scale 0–200 nm; (D) fractured GC,  $z$  scale 0–250 nm.

on a polished surface first and then this surface was removed from solution and deactivated by exposure to ambient air for ~12 h. After electrochemical kinetics and capacitance were again observed, the same surface was then heat treated and the last set of electrochemical data was obtained. Vacuum heat treatment (VHT) was carried out in an UHV chamber at  $10^{-8}$ – $10^{-9}$  Torr. GC disks were mounted on a sample probe tip, and the temperature was raised by ohmic heating. Heating and temperature sensing occurred on the back side of a GC disk electrode (1.5 mm thick), such that a 700 °C temperature was achieved 1–2 h. Heat-treated electrodes were exposed to ambient air for ~30 s while being inserted into the Teflon cell and bathed in analyte solution.

Highly oriented pyrolytic graphite (HOPG) was obtained from Arthur Moore (Union Carbide, Parma, OH). HOPG electrodes were cleaved with adhesive tape or with a razor blade as described previously.<sup>9,10</sup>

**Electrochemical Measurements.** Electrode areas were determined by chronoamperometry on a 5-s time scale in 1 mM Fe(CN)<sub>6</sub><sup>4-/3-</sup> in 1 M KCl. Linear sweep cyclic voltammetry experiments and  $k^0$  determination were performed as described previously<sup>9,10,15,24</sup> utilizing a function generator (Tektronix Inc., Beaverton, OR) and an Advanced Idea Mechanics (Columbus, OH) potentiostat. Differential capacitance measurements were performed by the method of Gileadi<sup>42,43</sup> and described by us previously<sup>9,17,18,23</sup> using a 100-Hz, 20-mV peak-to-peak triangle

wave centered at 0.0 V. All reported  $C^0$  values are normalized to the projected electrode area, as determined from chronoamperometry. All potentials stated are relative to the Ag/AgCl (3 M NaCl) electrode. Simulated voltammograms were calculated with the finite difference approach, and the computer program was provided by Dennis Evans,<sup>44</sup> with a constant value of the transfer coefficient.

**STM Conditions.** STM images were obtained with a Nanoscope II (Digital Instruments Inc., Santa Barbara, CA). Most images were obtained with electrochemically etched 0.01-in.-diameter tungsten wire tips, as recommended by the manufacturer. Mechanically cut Pt/Ir (80/20) tips (Digital Instruments) were also used for comparison, but no significant differences between the two types of tips were observable in the STM images at the relatively low resolution utilized for most of this work. All images were taken in ambient air, and no changes were noted in the images for many hours after initial scans.

Low-resolution images (150-nm full scale and greater) were obtained with the 12 × 12 μm scan head in the "height" image mode (constant current) with a bias voltage of 500 mV and a set-point current of 0.5 nA. High-resolution images (25-nm full scale and lower) were taken with a 0.7 × 0.7 μm scan head in the "current" image mode (constant height) with bias voltages of 20–100 mV and set-point current of 2–5 nA.

GC samples were mounted with silver paste to a thin metal plate through which the bias voltage was applied. All polished

(42) Gileadi, E.; Tshernikovski, N. *Electrochim. Acta* 1971, 16, 579–584.

(43) Babai, M.; Tshernikovski, N.; Gileadi, E. *J. Electrochem. Soc.* 1972, 119, 1018–1021.

(44) Corrigan, D. A.; Evans, D. H. *J. Electroanal. Chem.* 1980, 106, 287.

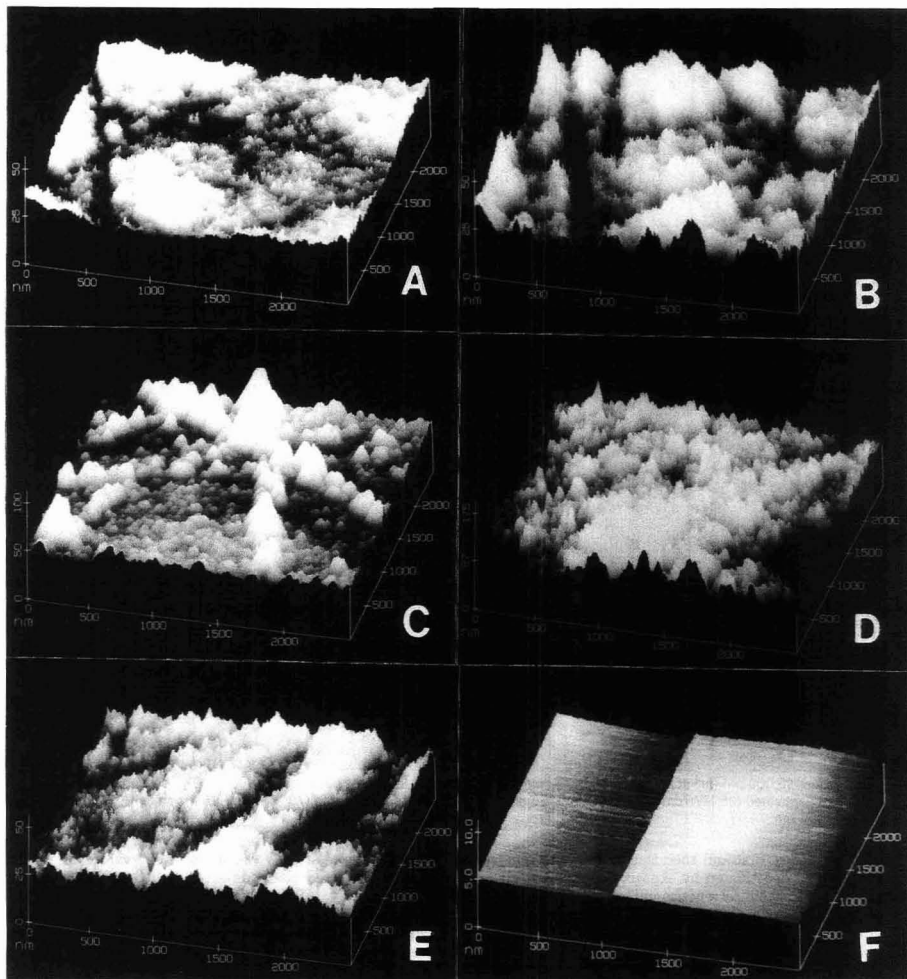


**Figure 2.** Images, 2500 nm, of electrodes under different pretreatment conditions: (A) polished GC, z scale 0–50 nm; (B) polished/laser-activated ( $25 \text{ MW/cm}^2$ ) GC, z scale 0–50 nm; (C) polished/laser-activated ( $70 \text{ MW/cm}^2$ ) GC, z scale 0–100 nm; (D) fractured GC, z scale 0–175 nm; (E) polished/vacuum heat treated GC, z scale 0–50 nm; (F) highly ordered pyrolytic graphite, z scale 0–10 nm.

surfaces yielded similar STM images, at the resolution employed, regardless of the electrode configuration (large disk or micro-electrode). Images of fractured surfaces were obtained on the piece fractured from the electrode rather than the electrode itself, since the electrode would not fit in the STM sample region. Different surfaces as well as several different areas of each surface were examined to obtain representative images.

## RESULTS

Figure 1 shows  $10 \times 10 \mu\text{m}$  survey scans of typical GC surfaces that were evaluated electrochemically. Due to image curvature which occurs with large scan areas, the images were software flattened but not smoothed or filtered. STM height scales are shown on the right sides of the plots along with the topographic grey scale; higher points appear as lighter shades. The images shown in Figure 1 are polished, polished/laser-irradiated at  $25 \text{ MW/cm}^2$  (denoted P/L 25), polished/laser-

irradiated at  $70 \text{ MW/cm}^2$  (denoted P/L 70), and fractured surfaces. The polished (Figure 1A) and P/L 25 (Figure 1B) surfaces appear similar in morphology, with polishing scratches visible in both images, and in height, with features not exceeding 50 nm in height. The P/L 70 (Figure 1C) and the fractured (Figure 1D) surfaces cover a greater height range and exhibit distinct morphological features. The P/L 70 surface exhibits isolated protrusions (shown as bright lines) that appear to originate from the polishing scratches that were present on the surface before laser irradiation. The fractured surface displays protrusions or nodules with diameters ranging from 50 to 300 nm. We have previously reported nodules on fractured GC electrodes based on SEM images.<sup>18</sup>

Parts A–D of Figure 2 show the same types of surfaces plotted in a 3-D perspective and on a smaller x, y scale. In

**Table I. STM Results for Seven Carbon Electrode Surfaces**

surface	samples	images	RMSR (nm)	$Z_{\max}$ (nm)
polished	6	13	$4.1 \pm 1^a$	$36 \pm 8^a$
P/L 25	4	10	$4.4 \pm 1$	$37 \pm 10$
P/L 70	6	17	$11 \pm 4$	$96 \pm 33$
fractured	5	10	$20 \pm 5$	$140 \pm 30$
P/DEAC	2	4	$4.7 \pm 1$	$38 \pm 7$
P/VHT	3	6	$4.5 \pm 0.6$	$37 \pm 4$
HOPG	1	1	0.24	2.0

<sup>a</sup> Standard deviation of RMSR and  $Z_{\max}$  for the number of images examined.

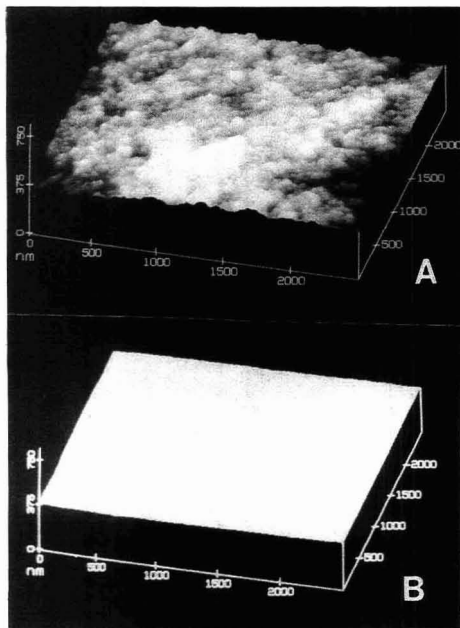


**Figure 3.** Image, 2500 nm, of (A) fractured GC plotted in a 1:1 aspect ratio compared to a similar image of (B) polished GC.  $z$  scale is 0–750 nm.

addition, images of polished/VHT (denoted P/VHT) and highly oriented pyrolytic graphite surfaces are shown in Figure 2E and F. Note the difference in  $z$ -axis scale from image to image. With this mode of image display, the differences in the surface morphologies are particularly noticeable. Polished, P/L 25, and P/VHT surfaces (Figure 2A, B, and E) appear similar, with all images employing identical height scales and exhibiting polishing scratches. The distinctive morphologies of the fractured and P/L 70 surfaces (Figure 2C and D) are apparent and will be discussed in detail below. Again, these surfaces exhibit greater height variation than the other surfaces. Figure 2F is a typical HOPG basal plane surface containing a step defect for comparison with the other images.

To provide a quantitative comparison of surface roughness, the root-mean-square roughness (RMSR) function of the Nanoscope II software was employed. RMSR is defined as the standard deviation of the height of the surface calculated from all points obtained during a given scan. For example, the image of HOPG in Figure 2F yields an RMSR of 0.24 nm, while that of fractured GC (Figure 2D) yields 20.4 nm.

Although RMSR has not been established as a rigorous quantitative measure of surface roughness, it does provide a comparison for different surfaces. An additional but less statistically useful parameter is  $Z_{\max}$ , which is the difference between the minimum and maximum surface heights.  $Z_{\max}$  and RMSR results are listed in Table I. Note that both values also include standard deviations of  $Z_{\max}$  and RMSR for the number of images indicated.

Figure 3 illustrates how the fractured surface, which exhibits the highest  $Z_{\max}$  and RMSR, would appear if plotted with a 1:1 aspect ratio between the  $x$ ,  $y$  scale and the  $z$  scale. In Figure 2, and in typical STM images, the  $z$  scales are expanded in order to enhance surface features. In Figure 3, the distance on the  $z$  axis was adjusted to equal those of the  $x$  and  $y$  axes. A polished surface (from Figure 2A) is plotted similarly for comparison. Without expansion of the  $z$ -axis scale, both surfaces appear much smoother.

The unusual morphology of the fractured GC surface is shown at successively higher magnification in Figure 4. Image 4A shows the variation in nodule diameter, while 4B shows an intersection of three nodules with ca. 200-nm diameters. Images C and D show the top of the upper left nodule of Figure 4B, with a full-scale scan range of 25 nm. Note that the apparent roughness persists even on a scale of ca. 1 nm.

**Electrochemical Results.** Table II shows electron-transfer rate constants and capacitance for the six types of surfaces examined by STM. The relatively large area of several electrode types limited the scan rate to 10 V/s or less, so rate constants above 0.1 cm/s are lower limits of the true values. As noted by several authors,<sup>12,13,17</sup> the variability of  $k^\circ$  for  $\text{Fe}(\text{CN})_6^{4-/3-}$  on polished GC is quite large due to variations in cleanliness but is often in the range of  $10^{-3}$ – $10^{-2}$  cm/s. The  $k^\circ$  values obtained here are somewhat higher than typical, but do show a large standard deviation (50%) typical of polished surfaces.

Laser activation at either 25 or 70 MW/cm<sup>2</sup> or fracturing led to reliably large  $k^\circ$  values. Since the  $\Delta E_p$ 's for these surfaces were near the reversible limit of 57 mV,  $k^\circ$  determinations based solely on  $\Delta E_p$  are of limited accuracy. Figure 5 shows a comparison of the experimental voltammogram for  $\text{Fe}(\text{CN})_6^{4-/3-}$  at a fractured GC surface and a simulated response for  $k^\circ = 0.40$  and  $\nu = 10$  V/s. A  $k^\circ$  of 0.40 was the lowest which yielded a good fit to the experiment, so a  $k^\circ$  estimate of  $>0.4$  cm/s is reliable in this case. The aberrant background on the experimental voltammogram is due to the differences in the background current between the  $\text{Fe}(\text{CN})_6^{4-/3-}$  voltammogram and that obtained in supporting electrolyte, leading to inaccurate background subtraction. The background current on activated GC varies with time, making background subtraction incomplete. A more rigorous investigation of  $\text{Fe}(\text{CN})_6^{4-/3-}$  kinetics has been performed on these surfaces at scan rates which yielded a more reliable rate constant of 0.5 cm/s.<sup>17</sup> The fractured GC and the P/L 70 surfaces exhibited rate constants at least 6 times greater than that of the initial polished electrode ( $>0.4$  vs 0.060 cm/s). The rate constant value for the P/L 25 electrode is larger than that of the original polished surface by more than a factor of 5 ( $>0.3$  vs 0.060 cm/s). Recall that although the STM data show that the fractured and P/L 70 surfaces possess distinct morphologies with high  $Z_{\max}$  and RMSR values, the morphology and the  $Z_{\max}$  and RMSR values of the P/L 25 surface are very similar to those acquired for the polished surface.

Finally, the P/VHT surfaces yielded rate constant values similar to the polished surface. These results are consistent with those of Kuwana et al.<sup>20</sup> The  $\Delta E_p$  for  $\text{Fe}(\text{CN})_6^{4-/3-}$  at 10 V/s increased from 98 to 230 mV upon deactivation in ambient air, but after heat treatment, reactivation of the



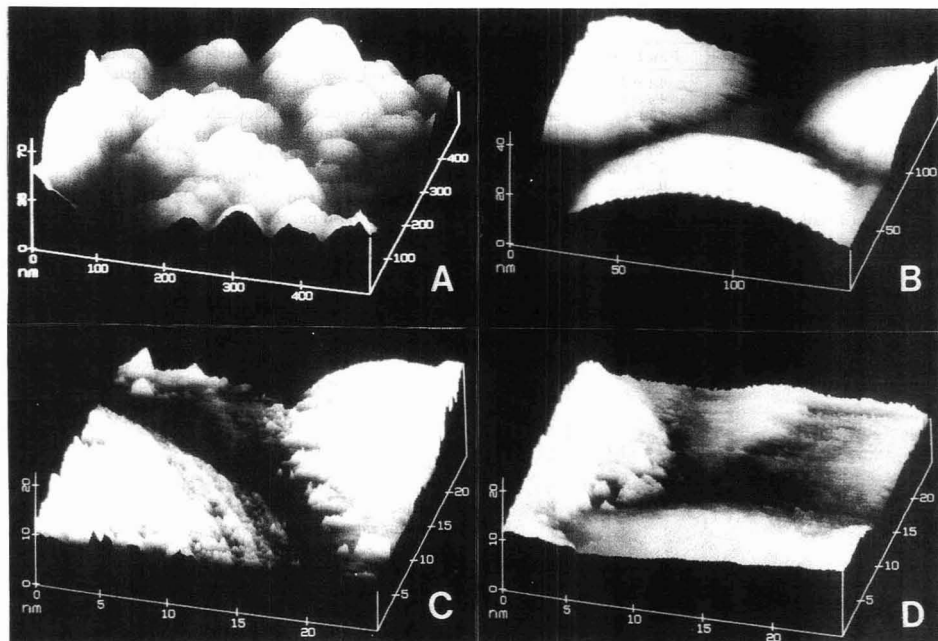


**Figure 4.** Fractured GC under higher resolution conditions: (A) 500-nm scan with z scale 0–70 nm; (B) 200-nm scan with z scale 0–40 nm; (C) 25-nm scan with z scale 0–20 nm; (D) 25-nm scan with z scale 0–20 nm. Images C and D were acquired at the upper left corner of sample in image B.

**Table II. Electrochemical Results**

surface	RMSR (nm) <sup>a</sup>	$\Delta E_p$ (mV) <sup>b</sup>	$k^0$ of $\text{Fe}(\text{CN})_6^{4-/3-}$ (cm/s)	$C^0$ <sup>c</sup> ( $\mu\text{F}/\text{cm}^2$ )	$N^d$
polished	4.1	$98 \pm 29$	$0.06 \pm 0.03$	$33 \pm 6$	14
P/L 25	4.4	$71 \pm 12$	$>0.3$	$34 \pm 7$	4
P/L 70	11.0	$62 \pm 6$	$>0.4$	$120 \pm 31$	3
fractured	20.0	$58 \pm 4$	$>0.4$	$75 \pm 16$	4
P/DEAC	4.7	$232 \pm 42$	$(8.4 \pm 4) \times 10^{-3}$	$15 \pm 2$	3
P/VHT	4.5	$96 \pm 13$	$0.065 \pm 0.020$	$40 \pm 5$	3
HOPG <sup>e</sup>	0.24	$>1200$	$<1 \times 10^{-6}$	$<1.0$	

<sup>a</sup> Values repeated from Table I. <sup>b</sup>  $\nu = 10$  V/s. <sup>c</sup> Based on chronoamperometric area. <sup>d</sup> For electrochemical results, not RMSR. <sup>e</sup> Values from ref. 8.

electrode occurred to a level equal to or greater than that of the initial polished surface.

Differential capacitance ( $C^0$ ) values are also shown in Table II. The fractured and P/L 70 surfaces exhibit higher  $C^0$  values than the other surfaces as well as the largest variation in capacitances.  $C^0$  values for polished, P/L 25, and VHT surfaces are similar. Note that deactivation decreased  $C^0$  by a factor of 2 while decreasing  $k^0$  of  $\text{Fe}(\text{CN})_6^{4-/3-}$  by a factor of 7 from the original polished surface. The significant influence of adsorbed airborne impurities on the activity of GC is illustrated in these decreases in  $k^0$  of  $\text{Fe}(\text{CN})_6^{4-/3-}$  and  $C^0$  from the polished to the P/DEAC surface. We have observed that exposure of a polished GC surface to air for even a few seconds leads to lower rate constants for  $\text{Fe}(\text{CN})_6^{4-/3-}$ . As noted in the Experimental Section, great care was taken to ensure that a drop of water remained on the electrode surface during handling after polishing and sonication. Also note that the marked decrease in electro-

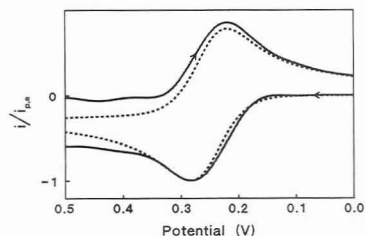


**Figure 5.** Experimental (solid line) and simulated (dashed line) cyclic voltammograms of 1 mM  $\text{Fe}(\text{CN})_6^{4-/3-}$  on fractured GC in 1 M KCl at  $\nu = 10$  V/s. Simulation assumed  $\alpha = 0.5$ ,  $k^0 = 0.4$  cm/s, and  $D_{\text{red}} = 6.32 \times 10^{-6}$  cm<sup>2</sup>/s.

chemical activity through exposure to ambient conditions followed by reaction via VHT was not accompanied by significant morphological changes.

## DISCUSSION

The STM results discussed above are relevant to two issues regarding GC surface structure: morphological characteristics of GC electrodes under different pretreatment conditions and the quantitation of microscopic roughness and electrochemical activity. Previous insight on the morphology of GC electrodes prepared according to the methods reported here has originated from scanning electron microscopy.<sup>18,28,29</sup> Although SEM provides the necessary magnification for elementary image analysis, the resolution (particularly in the vertical direction) is poor compared to STM. Electrode roughness has been investigated previously by indirect means such as



**Table III. Effect of Laser Power on Surface Protrusions for P/L Surfaces**

power density (MW/cm <sup>2</sup> )	no./ image <sup>a</sup>	% coverage <sup>b</sup>	av ht (nm) <sup>c</sup>
25	0		
30	0.5	1.3	20
40	2	4.5	20
50	5.6	10	26
70	12	42	57

<sup>a</sup> Average number of protrusions per 10 × 10 μm scan image based on four images. <sup>b</sup> Percentage of the total area in a 10 × 10 μm scan covered by protrusions. <sup>c</sup> Average height of protrusions for a given power density.

adsorption and differential capacitance measurements.<sup>17,18,20,29,45</sup> One would expect that  $k^\circ$  and capacitance should scale with microscopic area of the electrode, all else being equal, and that activation may be caused in part by increases in surface roughness.

At first glance, there does appear to be a correlation between the STM determined RMSR,  $k^\circ$ , and  $C^\circ$ . The surfaces with the largest  $k^\circ$  and  $C^\circ$  (fractured and P/L 70) also exhibit the highest RMSR. Further consideration, however, reveals that the correlation is inconsistent. Polished, P/L 25, P/VHT, and P/DEAC surfaces have RMSR values which vary by less than 15%, while their  $k^\circ$ 's vary by at least a factor of 50. Laser activation at 25 MW/cm<sup>2</sup> leads to an increase in  $k^\circ$  of more than a factor of 5, yet the RMSR increase is only ~7%. These results are consistent with those presented previously based on SEM and phenanthrenequinone (PQ) adsorption.<sup>17,18</sup> They also confirm the conclusions from other laboratories that changes in microscopic roughness are not sufficient to explain the effects of activation procedures on kinetics and adsorption.<sup>29,45</sup> Large increases in  $k^\circ$  occurred upon laser activation with only minor changes in morphology and microscopic area as determined from phenanthrenequinone adsorption.<sup>17</sup> In the case of the fractured surface, the higher RMSR is due to nodules and obviously implies higher roughness. On the basis of PQ adsorption, the fractured surface has about twice the microscopic area of the polished or P/L 25 surfaces.<sup>18</sup> Thus variations in roughness could reasonably account for a factor of ~2 in  $k^\circ$ , but the major source(s) for  $k^\circ$  variation must lie elsewhere.

We have previously attributed  $k^\circ$  increases caused by laser activation to the removal of adsorbed impurities.<sup>17</sup> This conclusion is reinforced by the VHT experiments of Fagan et al.<sup>20</sup> and Stutts et al.,<sup>21</sup> repeated here with the addition of STM characterization. Deactivation and subsequent VHT led to minimal changes in RMSR from the polished surface yet yielded large variation in  $k^\circ$ . As expected for impurity adsorption, the capacitance decreases for the P/DEAC surface. The low  $C^\circ$  values reported by Fagan et al. were not observed here, probably due to the very different frequency domains used in the capacitance measurements. Taken together with results from other laboratories, the STM and electrochemical results strongly support the conclusion that the major factor controlling  $k^\circ$  for Fe(CN)<sub>6</sub><sup>4-/3-</sup> on GC is surface cleanliness, with surface roughness playing a minor role. Stated semiquantitatively, roughness accounts for a factor of ~2 in observed  $k^\circ$  on GC, while surface cleanliness can affect  $k^\circ$  for Fe(CN)<sub>6</sub><sup>4-/3-</sup> by factors as large as several hundred.

The second major issue addressed by the STM examination deals with the morphological effects of various pretreatments, particularly laser activation. The unique features of the fractured surface are obvious from SEM or STM. The increased roughness leads to increases in capacitance and  $k^\circ$

for fractured surfaces compared to P/L 25 surfaces, but these effects are not large (a factor of ~2). The major consequence of in-situ fracturing with regard to  $k^\circ$  enhancement is the avoidance of impurity adsorption. At least at the resolution employed here, the morphological differences between fractured and polished surfaces do not appear to have major consequences for observed kinetics. The effect of polishing is to flatten the tops of nodules, yielding the surfaces of Figures 1A and 2A, accompanied by the undesired consequence of impurity adsorption.

While laser activation at 25 MW/cm<sup>2</sup> had no observable morphological effects at the resolution employed, higher power densities led to qualitatively distinct features. The protrusions apparent in Figure 2C formed along polishing scratches (apparent in Figure 1C). Atomic force microscope images of these features were very similar in appearance, indicating that they are not an artifact due to multiple tunneling points as the STM tip negotiates the scratches. The density and height of the protrusions increase with power density (Table III). At 30 MW/cm<sup>2</sup> and lower, they are very infrequent or not present, while at 70 MW/cm<sup>2</sup>, they cover more than 40% of the surface. We have reported previously that significant excursions in  $C^\circ$  and PQ adsorption occur at powers above 30 MW/cm<sup>2</sup><sup>18</sup> and that a surface temperature simulation predicts that local melting should occur with a threshold between 30 and 40 MW/cm<sup>2</sup> for GC.<sup>46</sup> It is likely that the protrusions are caused by local melting, perhaps followed by expansion of heated, entrapped gases. The localization of protrusions on polishing scratches may result from the lower reflectivity inside the scratches, resulting in more efficient coupling of the laser light into the GC. In addition, the thermal conductivity near scratches could be different, leading to localized temperature variations.

The high-resolution images of the top of a nodule on the fractured surface (Figure 4C and D) are not of sufficient resolution to image individual atoms. The apparent roughness, which is on a much smaller scale than that shown in Figures 1 and 2, could be due to genuine morphological features or to variations in electronic interactions between the tip and the surface during scanning. Although these features are reproducible, it is not yet clear what they represent. A few reports here appeared on high-resolution STM of disordered carbon materials.<sup>36-38</sup> Atomic resolution was achieved, although the polishing procedures employed leaves some doubt about the condition of the surface. Unusual arrangements of carbon atoms were observed, perhaps because of deviations of the electronic structure of disordered carbons from that of HOPG. The high-resolution images on the fractured surface obtained here are of value because the fractured surface is unmodified by polishing and should be more representative of bulk structure. Attempts to obtain atomic scale images of the fractured surface are currently being made.

## SUMMARY

The foremost conclusion drawn from the correlation of electrochemical properties with STM images is that some phenomenon other than surface roughening is responsible for increases in electrode activity toward Fe(CN)<sub>6</sub><sup>4-/3-</sup> upon laser or VHT activation. This statement is especially apparent with comparison of the polished and P/L 25 surfaces. Results show that laser activation at 25 MW/cm<sup>2</sup> causes no changes in capacitance and roughness, but causes a drastic increase in activity as evidenced by the heterogeneous rate constant for Fe(CN)<sub>6</sub><sup>4-/3-</sup>. These results are consistent with a mech-

anism in which electrode activity is determined by exposure of active sites and activation occurs through a cleaning process. STM images of polished, P/L 25, P/VHT, and P/DEAC electrodes show them to be similar in morphology, indicating that any changes induced by laser activation at low power densities and vacuum heat treatment at temperatures of  $\sim 700$  °C are minimal. Fractured and P/L 70 surfaces exhibit distinct morphologies with a large amount of roughness and some variability in electrochemical behavior. Morphological characteristics of the P/L 70 surface are attributed to possible melting of the GC substrate at high laser power densities, beginning at 30–40 MW/cm<sup>2</sup>. Investigation of these surfaces with AFM and with STM at higher resolution is currently underway.

#### ACKNOWLEDGMENT

The authors thank Robert S. Robinson for assistance with STM techniques and initial STM examinations of GC surfaces and Roy Tucker for assistance with UHV heat treatment. The work was supported by the Air Force Office of Scientific Research, an ACS Analytical Division Fellowship sponsored by Eli Lilly and Co. to C.A.M., and an Amoco Foundation Doctoral Fellowship to M.T.M.

RECEIVED for review July 27, 1992. Accepted December 30, 1992.

## TECHNICAL NOTES

### Fluorocarbon-Based Immobilization of a Fluoroionophore for Preparation of Fiber Optic Sensors

Timothy L. Blair, Tadeusz Cynkowski, and Leonidas G. Bachas\*

Department of Chemistry and Center of Membrane Sciences, University of Kentucky, Lexington, Kentucky 40506

#### INTRODUCTION

Fiber optic chemical sensors (FOCS) are based on interactions of an immobilized reagent phase with an analyte in a sample solution. Typically, optical fibers are used as optical waveguides that carry light to and from a species-selective reagent phase. Interactions with the analyte induce changes in the optical properties of the reagent phase. Monitoring of this change in the optical signal allows for the determination of the analyte.

Immobilization of reagents for optical sensors can be achieved in a number of ways. Reagents have been entrapped within polymer matrices<sup>1,2</sup> or behind semipermeable membranes.<sup>3,4</sup> Solid supports (e.g., glass beads or polymer films) with covalently-attached reagents can be affixed at the sensing tip<sup>5,6</sup> or the reagents can be covalently attached to the fiber itself.<sup>7</sup> Recently, Ogasawara et al. reported a FOCS based on a dynamic immobilization scheme.<sup>8</sup> In this approach, C<sub>18</sub>-alkyl chains were covalently attached to an optical fiber, resulting in a hydrophobic region at the fiber surface. Hydrophobic reagents were then associated with this surface. The technique was used to develop a sensor for riboflavin binding protein based on its ability to quench the fluorescence of 3-octylriboflavin which was associated with the fiber optic surface. Immobilization has also been accomplished by adsorption of reagents on polymeric supports,<sup>9-11</sup> such as poly(tetrafluoroethylene) (PTFE).<sup>12</sup>

PTFE provides an excellent surface for immobilization of reagents. The reagent phase adsorbed on the PTFE is more accessible to the analyte than when immobilized on resin beads.<sup>12</sup> The inert surface may also eliminate problems associated with nonspecific adsorption on the surface of the FOCS. Indeed, Bright et al. have reported that the stability of immunosurfaces prepared using functionalized PTFE membranes is improved over conventional quartz surfaces,<sup>6</sup> a fact that can be attributed to reduced denaturation due to

nonspecifically adsorbed portions of the antibody.<sup>13</sup> However, the inertness of PTFE also makes immobilization difficult. In 1988, Kobos et al. reported an enzyme electrode in which the enzyme was immobilized on a PTFE membrane.<sup>14</sup> This was achieved by modifying the enzyme with perfluoroalkyl groups that could be embedded in the membrane.

We have synthesized the fluorogenic crown ether 5 (Figure 1) for the development of an optical sensor for alkaline earth metal ions. This fluoroionophore is immobilized at the tip of the FOCS through the covalently-attached perfluorinated alkyl chain, which can be embedded in a PTFE membrane.

#### EXPERIMENTAL SECTION

**Reagents.** The following reagents were used as received from Aldrich (Milwaukee, WI): diaza-18-crown-6 (1,4,10,13-tetraoxa-7,16-diazacyclooctadecane), formalin (37% formaldehyde solution in water with 10-15% methanol), benzyl chloroformate, Sure/Seal dimethylformamide (DMF), and triethylamine. Perfluorooctanoyl chloride and 4-methylumbelliferone were obtained from Strem Chemicals (Newburyport, MA) and Eastman Kodak (Rochester, NY), respectively. Tris(hydroxymethyl)aminomethane (Tris) was from Research Organics (Cleveland, OH) and (ethylenedinitrilo)tetraacetic acid (EDTA) from Mallinkrodt (Paris, KY). All salt solutions were prepared using analytical reagent-grade chemicals and deionized (Milli-Q water purification system, Millipore, Bedford, MA), distilled water.

**Synthesis.** The starting material for the synthesis of ionophore 5 (Figure 1) was commercially available diaza-18-crown-6, 1. Attempted monoacylation of 1 with perfluorooctanoyl chloride failed to yield the desired monosubstituted derivative 4. However, the diazacrown ether 1 could be readily converted to monocabamate 2 by treatment with benzyl chloroformate.<sup>15</sup>

*N*-Carbobenzoxy-*N'*-(perfluorooctanoyl)-1,4,10,13-tetraoxa-7,16-diazacyclooctadecane (3). Triethylamine (0.17 mL) was added to a solution of 2 (115 mg, 0.29 mmol) in 4 mL of anhydrous benzene, followed by perfluorooctanoyl chloride (130 mg, 0.30 mmol) in 1 mL of benzene. The resulting mixture was then stirred at room temperature under argon for 18 h. A 10% aqueous NaOH solution (1 mL) was added, and the layers were separated after 10 min. After adding 15 mL of benzene, the benzene solution was washed successively with 10% NaOH, 10% HCl, water, and brine and was dried over sodium sulfate. Chromatography on silica gel yielded 181 mg (0.23 mmol, 79% yield) of 3 [<sup>1</sup>H NMR (CDCl<sub>3</sub>) δ 3.5-3.9 (24 H, m), 5.15 (2 H, s), 7.35 (5 H, s)].

*N*-(Perfluorooctanoyl)-1,4,10,13-tetraoxa-7,16-diazacyclooctadecane (4). Product 3 (700 mg, 0.88 mmol) was hydrogenated in 10 mL of methanol in the presence of 10% Pd/C (30 mg). The catalyst was filtered off and the filtrate evaporated. After recrystallization from benzene-heptane, 394 mg (0.60 mmol, 68% yield) of product 4 was obtained [<sup>1</sup>H NMR (CDCl<sub>3</sub>) δ 3.25 (4 H, t), 3.6-4.0 (20 H, m)].

(13) Betts, T. A.; Catena, G. C.; Haug, J.; Litwiler, K. S.; Zhang, J.; Zagrobelny, J.; Bright, F. V. *Anal. Chim. Acta* 1991, 246, 55-63.

(14) Kobos, R. K.; Eveleigh, J. W.; Stepler, M. L.; Haley, B. J.; Papa, S. L. *Anal. Chem.* 1988, 60, 1996-1998.

(15) Lehn, J. M.; Simon, J.; Wagner, J. *Now. J. Chem.* 1977, 1, 77-84.

(1) Seiler, K.; Wang, K.; Kuratli, M.; Simon, W. *Anal. Chim. Acta* 1991, 224, 151-160.

(2) Kawabata, Y.; Kamichika, T.; Imasaka, T.; Ishibashi, N. *Anal. Chim. Acta* 1990, 62, 2054-2055.

(3) Freeman, M. K.; Bachas, L. G. *Anal. Chim. Acta* 1990, 241, 191-125.

(4) Arnold, M. A.; Ostler, T. J. *Anal. Chem.* 1986, 58, 1137-1140.

(5) Posch, H. E.; Leiner, M. J. P.; Wolfbeis, O. S. *Fresenius' Z. Anal. Chem.* 1989, 334, 162-165.

(6) Bright, F. V.; Litwiler, K. S.; Vargo, T. G.; Gardella, J. A. *Anal. Chim. Acta* 1992, 262, 323-330.

(7) Tromberg, B. J.; Sepaniak, M. J.; Vo-Dinh, T.; Griffin, G. D. *Anal. Chem.* 1987, 59, 1226-1230.

(8) Ogasawara, F. K.; Wang, Y.; Bobbitt, D. R. *Anal. Chem.* 1992, 64, 1637-1642.

(9) ZhuJun, Z.; Seitz, W. R. *Anal. Chem.* 1986, 58, 220-222.

(10) Narayanaswamy, R.; Russell, D. A.; Sevilla, F. *Talanta* 1988, 35, 83-88.

(11) Chau, L. K.; Porter, M. D. *Anal. Chem.* 1990, 62, 1964-1971.

(12) Wyatt, W. A.; Bright, F. V.; Hietje, G. M. *Anal. Chem.* 1987, 59, 2272-2276.

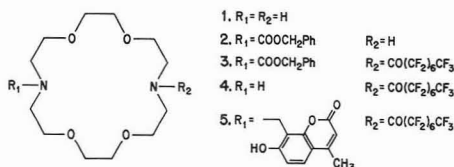


Figure 1. Structures of ionophore 5 and precursors 1-4.

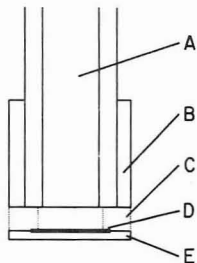


Figure 2. Construction of FOCS: (A) bifurcated fiber optic bundle, (B) PTFE sleeve, (C) 2-mm-long spacer, (D) PTFE membrane with immobilized ionophore, and (E) PTFE support for membrane.

**Condensation of 4 with 4-Methylumbelliferone.** Product 4 (131.7 mg, 0.20 mmol), 4-methylumbelliferone (37 mg, 0.21 mmol), triethylamine (0.2 mL), and formalin (0.15 mL) were dissolved in 6 mL of anhydrous DMF. The resulting solution was stirred at 55 °C under argon for 22 h. The solvent was evaporated, and the residue was dissolved in 20 mL of chloroform. The solution was washed with 10% tartaric acid and brine and was then dried over sodium sulfate. Chromatography on silica gel yielded 90 mg (0.11 mmol, 53% yield) of 5 as a colorless oil [ $^1H$  NMR ( $CDCl_3$ )  $\delta$  2.4 (3 H, s), 2.9 (4 H, s), 3.5-4.0 (20 H, m), 4.15 (2 H, s), 6.1 (1 H, s), 6.8 (1 H, d), 7.4 (1 H, d), 8.0 (1 H, s)]; FAB-MS 846 ( $M^+$ ), 601, 440, 231, 173].

**Apparatus.** All spectroscopic measurements were made using an Oriol (Stratford, CT) modular spectrophotometer, configured as described earlier.<sup>3</sup> The major components of the instrument include a tungsten-filament lamp, a grating monochromator (set at 358 nm), a glass bifurcated fiber optic bundle, a high-pass filter with a 420-nm cut off, a photomultiplier tube (PMT), and a photomultiplier readout device interfaced with a strip-chart recorder. The high-pass filter was placed in front of the PMT to discriminate against the exciting radiation.

**Probe Construction and Procedure.** The probe construction is shown in Figure 2. A previously-swollen piece of PTFE membrane (FHUP 047 00, Millipore) was placed in the PTFE housing and was immersed in a 0.50 mM solution of 5 (in HPLC-grade methanol from Fisher, Fair Lawn, NJ) for several hours. The probe was washed with deionized water and placed in 0.010 M Tris-HCl (pH 7.5)/0.50 mM EDTA for approximately 1 h. The probe was then immersed in fresh 0.010 M Tris-HCl (pH 7.5) and allowed to equilibrate. The change in signal was monitored as the concentration of analyte was varied by additions of standard solutions to the buffer. The probe was placed in the EDTA buffer before each experiment.

## RESULTS AND DISCUSSION

Recently, interest has grown in the development of optical sensors for metal ions. One class of compounds which may provide an appropriate chromogenic metal-selective reagent for development of such a sensor is crown ethers. The ability of crown ethers to complex alkali and alkaline earth ions has led to their use in a variety of applications,<sup>16,17</sup> including ion chromatography, phase-transfer systems, and ion-selective

electrodes. Covalent attachment of a chromophore to the crown ether skeleton has allowed the spectrophotometric determination of metal ions.<sup>18,19</sup> FOCS can be developed by immobilization of such a modified crown ether at the tip of an optical fiber.

In 1987, Alder et al. reported a fiber optic sensor based on an immobilized chromogenic crown ether, a "crowned" nitrophenylazophenol.<sup>20</sup> The reagent was adsorbed on ground Amberlite XAD-2 resin (a styrene/divinylbenzene copolymer), which was trapped at the end of an optical fiber by a porous PTFE membrane. The probe responded reversibly to aqueous potassium ions in the concentration range  $10^{-3}$ - $10^{-1}$  M and gave a  $K^+/Na^+$  selectivity ratio of 6.4. The response times ranged from 2 to 7 min, depending on the change in concentration. The same group later reported that the probe was actually more selective for the more highly-charged calcium ion, with a  $Ca^{2+}/K^+$  selectivity ratio of 8.3.<sup>21</sup> This probe construction was used with a number of different chromogenic crown ethers to produce optical sensors for potassium ions.<sup>22</sup>

The fluorogenic crown ether 5 was synthesized in order to evaluate the feasibility of using fluorocarbon-based immobilization of fluoroionophores in fiber optic sensors. A perfluorinated alkyl chain was substituted on one of the nitrogens of the diazacrown ether, and 4-methylumbelliferone (a fluorogenic tag) was attached to the other. Monoacylation of the diazacrown ether skeleton with perfluorooctanoyl chloride proved to be impractical, producing only the di-substituted species. However, a monosubstituted carbamate could easily be prepared.<sup>15</sup> After acylation of the remaining nitrogen, the carbamate group could be cleaved to allow attachment of the fluorophore. The fluoroionophore was immobilized by the covalently-bound perfluoroalkyl group, which embedded itself in a PTFE membrane positioned at the tip of a bifurcated fiber optic bundle.

Diazacrown ethers with two pendant chromogenic side arms have been shown to exhibit selectivity for divalent alkaline earth metal ions over monovalent alkali metals.<sup>23</sup> Similar monoazacrowns with a single chromogenic side arm are also selective for divalent cations.<sup>24,25</sup> This suggests that the diazacrown 5 with a single chromogenic side arm would also be selective for alkaline earth metal ions. Association of the diaza-crown 5 with a metal ion results in the loss of a proton from the methylumbelliferone moiety. Deprotonation of umbelliferone induces a change in the fluorescence intensity which is proportional to the concentration of metal in solution.<sup>26,27</sup>

Calibration curves for  $Ca^{2+}$  and  $Mg^{2+}$  in the 0-5 mM range are shown in Figure 3. The probe exhibits similar responses to the two divalent cations. The detection limit for  $Ca^{2+}$  is 0.1 mM as determined by the  $Ca^{2+}$  concentration that gives a signal that is 3-fold higher than the peak-to-peak noise level of the blank. This detection limit is 2.5-fold better than that reported by Ashworth et al. using chromogenic crown

(18) Lohr, H. G.; Vogtle, F. *Acc. Chem. Res.* 1985, 18, 65-72.

(19) Takagi, M.; Ueno, K. *Top. Curr. Chem.* 1984, 21, 39-65.

(20) Alder, J. F.; Ashworth, D. C.; Narayanaswamy, R. *Analyst* 1987, 112, 1191-1192.

(21) Ashworth, D. C.; Huang, H. P.; Narayanaswamy, R. *Anal. Chim. Acta* 1988, 213, 251-257.

(22) Al-Amir, S. M. S.; Ashworth, D. C.; Narayanaswamy, R.; Moss, R. E. *Talanta* 1989, 36, 645-650.

(23) Katayama, Y.; Fukuda, R.; Iwasaki, T.; Nita, K.; Takagi, M. *Anal. Chim. Acta* 1988, 204, 113-125.

(24) Fery-Forgues, S.; Le Bris, M.-T.; Guette, J.-P.; Valeur, B. *J. Chem. Soc., Chem. Commun.* 1988, 384-385.

(25) Wickstrom, T.; Dale, J.; Lund, W.; Buoen, S. *Anal. Chim. Acta* 1988, 211, 223-229.

(26) Blair, T. L.; Desai, J.; Bachas, L. G. *Anal. Lett.* 1992, 25, 1823-1834.

(27) Fink, D. W.; Koehler, W. R. *Anal. Chem.* 1970, 42, 990-993.

(16) Takagi, M.; Nakamura, H. *J. Coord. Chem.* 1986, 15, 53-82.

(17) Forrest, H.; Pacey, G. E. *Talanta* 1989, 36, 335-340.

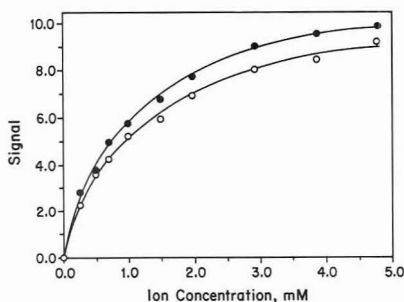


Figure 3. Calibration curves for  $\text{Ca}^{2+}$  (●) and  $\text{Mg}^{2+}$  (○). "Signal" refers to percent change in fluorescence intensity.

ethers immobilized on XAD-2 resin,<sup>21</sup> and it is 100-fold better than reported by Kawabata et al. using a chlortetracycline fluoroionophore immobilized on an ion exchange membrane.<sup>28</sup> This may be attributed to a stronger association of the  $\text{Ca}^{2+}$  with the fluoroionophore 5. The response can be reversed by immersing the probe in an EDTA solution.

The probe gives a response time of less than 1 min in all our studies. This is a significant improvement over the response times obtained with immobilization techniques that involve adsorption of the reagent on particles that are entrapped behind a membrane at the tip of the sensor.<sup>21</sup> The response time of the latter type of probe is limited by the time required for diffusion of the analyte across the microporous membrane and to the region of the probe where the transduction occurs. With immobilization on the surface of the PTFE membrane, the need for such diffusion is eliminated and the response time is limited only by mass

transport to the FOCS surface and the kinetics of the immobilized reagent-analyte interaction.

The introduction of multiple or branched perfluorinated carbon chains may help to prevent leaching of the reagent off the membrane and improve the lifetime of the probe. Indeed, de Miguel et al. report that multiple-stranded or branched-chain perfluoroalkyl groups are more retained on a perfluorinated stationary phase than singly-stranded analogues.<sup>29</sup> The signal of our probe decreased by about 35% in a 24-h period. This may be due to a combination of leaching of the reagent off the membrane and/or decomposition of the fluoroionophore. However, the same membrane could be regenerated by immersion in the original reagent solution. The reproducibility of the calibration curve, as determined by relative standard deviations of triplicate data points, is typically about 25%. This relatively low reproducibility can be attributed to the factors mentioned above. Incorporation of multiple-stranded perfluoroalkyl groups in the fluoroionophore used should also improve the reproducibility of the sensor response.

In conclusion, we have demonstrated the feasibility of using a fluorocarbon-based immobilization method for the development of fiber optic sensors. A fiber optic probe using an immobilized fluorogenic crown ether ionophore was constructed which responds to  $\text{Ca}^{2+}$  and  $\text{Mg}^{2+}$  with response times of less than 1 min.

#### ACKNOWLEDGMENT

This work was supported in part by grants from the U.S. Department of the Interior (through the Kentucky Water Resources Research Institute) and the National Science Foundation (EHR-9108764).

(28) Kawabata, Y.; Tahara, R.; Imasaki, T.; Ishibashi, N. *Anal. Chim. Acta* 1988, 212, 267-271.

(29) de Miguel, I.; Exbrayat, S.; Samain, D. *Chromatographia* 1987, 24, 849-853.

RECEIVED for review August 12, 1992. Accepted December 7, 1992.

## Detection of Carbohydrates by Capillary Electrophoresis with Pulsed Amperometric Detection

Thomas J. O'Shea and Susan M. Lunte\*

Center for Bioanalytical Research, University of Kansas, 2095 Constant Avenue, Lawrence, Kansas 66047

William R. LaCourse

Department of Chemistry, University of Maryland, Baltimore County, 5401 Wilkens Avenue, Baltimore, Maryland 21228

### INTRODUCTION

Carbohydrates are important in a number of biological processes. They are a significant energy source for both plants and animals and play a substantial role in biological recognition of proteins. The analysis of carbohydrates in protein samples is becoming increasingly important with the emergence of a number of biotechnology-derived pharmaceuticals into the marketplace.

Capillary electrophoresis (CE) is a powerful tool for the separation of a wide variety of biological compounds. The distinguishing characteristics of CE are its ability to analyze extremely small volumes and the high separation efficiencies that can be obtained. The analysis of carbohydrates is a particularly challenging analytical problem since these compounds possess no unique chromophore or fluorophore necessary for direct detection. Carbohydrates have been detected using CE with indirect fluorescence detection.<sup>1</sup> However, this method suffers from high concentration detection limits, lacks specificity, and requires isolation of the sugars from other charged species prior to analysis of any biological samples.

Two groups have employed precolumn derivatization with UV or fluorescence detection for carbohydrate analysis. Honda and co-workers separated 12 monosaccharides by CE-UV following precolumn derivatization with 2-aminopyridine.<sup>2</sup> Although the separation of the monosaccharides was quite impressive, detection was limited to millimolar concentrations of the carbohydrates. A more sensitive method was reported by Liu et al., who were able to successfully detect carbohydrates at the nanomolar level using a two-step reaction including reductive amination and precolumn derivatization by 3-(4-carboxybenzoyl)-2-quinolinecarboxaldehyde.<sup>3</sup> The disadvantage of this process is that it takes several hours to accomplish, including 1-2 h for the reduction step and an additional hour for the derivatization reaction. In addition, other amines present in the sample can interfere with the analysis.

Electrochemical detection is an ideal method of detection for microcolumn-based separation systems because detection is based on a reaction at an electrode surface.<sup>4-6</sup> Therefore, in contrast to optical methods where the response of the detector is dependent on path length, cell volumes can be made very small with no decrease in sensitivity. This is a particular advantage in CE, where the path length is typically less than 100  $\mu\text{m}$ . Capillary electrophoresis-electrochemistry has been used extensively for the analysis of catecholamines

in single cells and for the detection of analytes obtained during microdialysate perfusion.<sup>7-10</sup> Detection limits for electroactive compounds usually are in the nanomolar range.

Pulsed amperometric detection (PAD) at Au electrodes following high-performance anion-exchange chromatography (HPAEC) has become the method of choice for the determination of carbohydrates in a variety of samples, including foods and beverages, biotechnologically derived products, and physiological fluids.<sup>11-13</sup> PAD at noble metal electrodes exploits surface-catalyzed oxidations of various functional groups (e.g., aldehyde, alcohol, amine, and sulfur-containing moieties). The high electrocatalytic activity at Au or Pt electrodes for a constant applied potential is often accompanied by fouling of the electrode surface.<sup>14</sup> LaCourse and Johnson have used pulsed voltammetry (PV) to evaluate and optimize carbohydrate response at a gold electrode.<sup>15</sup> PAD overcomes fouling of electrodes by combining amperometric detection with alternated anodic and cathodic polarizations to clean and reactivate the electrode surface. Hence, PAD utilizes multistep potential-time wave forms ( $E_t$ ) to maintain uniform and reproducibly high electrode activity.

Although there are numerous studies employing PAD at macroelectrodes, little has been done with PAD at microelectrodes. Recently, Ewing et al. employed PV to obtain voltammetric information in static biological microenvironments at Pt microelectrodes.<sup>16</sup> In this paper, the feasibility of PAD as a detection method for capillary electrophoresis is explored. This is the first report involving PAD at a microelectrode in a flowing stream. A system has been developed using off-column detection and a gold wire microelectrode. The separation and detection by CE-PAD of several charged carbohydrates of biological interest will be presented. In addition, the use of this detector for the determination of glucose in blood will be demonstrated.

### EXPERIMENTAL SECTION

**Reagents.** All carbohydrates were obtained from Sigma Chemical Co. (St. Louis, MO) and used as received. Semiconductor-grade sodium hydroxide pellets, used in the preparation

- (1) Garner, T. W.; Yeung, E. S. *J. Chromatogr.* 1990, 515, 639-644.
- (2) Honda, S.; Iwase, S.; Makino, A.; Fujiwara, S. *Anal. Biochem.* 1989, 176, 72-77.
- (3) Liu, J.; Shirato, O.; Wiesler, D.; Novotny, M. *Proc. Natl. Acad. Sci. U.S.A.* 1991, 88, 2302-2306.
- (4) Wallingford, R. A.; Ewing, A. G. *Anal. Chem.* 1987, 59, 1762-1766.
- (5) Curry, P. D.; Engstrom-Silverman, C. E.; Ewing, A. G. *Electroanalysis* 1991, 3, 587-596.
- (6) O'Shea, T. J.; Greenhagen, R. D.; Lunte, S. M.; Lunte, C. E.; Smyth, M. R.; Radzik, D. M.; Watanabe, N. *J. Chromatogr.* 1992, 593, 305-312.

- (7) Olefirowicz, T. M.; Ewing, A. G. *Anal. Chem.* 1990, 62, 1872-1876.
- (8) O'Shea, T. J.; Telting-Diaz, M.; Lunte, S. M.; Lunte, C. E.; Smyth, M. R. *Electroanalysis* 1992, 4, 463-468.
- (9) O'Shea, T. J.; Weber, P. L.; Bammell, B. P.; Lunte, C. E.; Lunte, S. M. *J. Chromatogr.* 1992, 608, 189-195.
- (10) Chien, T. B.; Wallingford, R. A.; Ewing, A. G. *J. Neurochem.* 1990, 54, 633-638.
- (11) Johnson, D. C.; LaCourse, W. R. *Anal. Chem.* 1990, 62, 589A-597A.
- (12) LaCourse, W. R.; Johnson, D. C. *Carbohydr. Res.* 1991, 215, 159-178.
- (13) Johnson, D. C.; LaCourse, W. R. *Electroanalysis* 1992, 4, 367-380.
- (14) Gilman, S. In *Electroanalytical Chemistry*; Bard, A. J., Ed.; Marcel Dekker: New York, 1967; Vol. 2, pp 111-192.
- (15) LaCourse, W. R.; Johnson, D. C. *Anal. Chem.* 1993, 65, 50-55.
- (16) Chen, T. K.; Lau, Y. Y.; Wong, D. K. Y.; Ewing, A. G. *Anal. Chem.* 1992, 64, 1264-1268.



of the operating buffer, were also obtained from Sigma. All other chemicals were analytical reagent grade. All solutions were prepared in NANOpure water (Sybron-Barnstead, Boston, MA) and passed through a membrane filter (0.2- $\mu\text{m}$  pore size) before use. Stock solutions of carbohydrates were prepared daily.

**Apparatus.** Electrophoresis in the capillary was driven by a high-voltage power supply (Spellman Electronics Corp., Plainview, NY). Polyimide-coated fused-silica capillary columns of 360- $\mu\text{m}$  o.d. and 75- $\mu\text{m}$  i.d. were obtained from Polymicro Technologies (Phoenix, AZ). Sample introduction was accomplished using a pressure injection system, and the volume injected was calculated in the continuous-fill mode by recording the time required for the sample to reach the detector.

The microelectrode was constructed using a 50- $\mu\text{m}$ -diameter gold wire (Johnson Matthey Electronics, Hertfordshire, UK) which was bonded to a length of copper wire using silver epoxy (Ted Pella Inc., Redding, CA). Capillary tubes were pulled with a List-Model (Greenvale, NY) Model 3A vertical pipet puller to a narrow tip. The gold wire was inserted through the capillary until it protruded approximately 0.5 cm from the tip. Silicon adhesive was then applied to the tip at the junction of the capillary and the gold wire. Once cured, the gold wire was cut to the desired length, 300–350  $\mu\text{m}$ , using surgical scissors. The gold electrode was then washed with ethanol followed by copious amounts of deionized water.

The construction of the complete CE system with electrochemical detection has been described in detail elsewhere.<sup>6</sup> The exception is the preparation of the Nafion joint, which is used to isolate the detection end of the column from the effects of the applied electrical field. Due to the large currents (ca. 40  $\mu\text{A}$ ) generated using the hydroxide electrolyte in this study, a modification of the design was used to further lower the resistance across the Nafion joint. Thus, the final section of capillary was epoxied to a glass slide and a fracture was made at a previously prepared score mark. The fracture was then covered with Nafion solution (5 wt % solution in a mixture of lower molecular weight alcohols and 10% water) which was purchased from Sigma. This was allowed to dry fully. This joint was then submerged in the cathodic buffer reservoir and the system completed as described previously.<sup>6</sup> A three-electrode configuration was used, and the electrode connections were made to an EG&G Princeton Applied Research (Princeton, NJ) Model 400 electrochemical detector, which provided the potential wave form and current output. A Ag/AgCl reference and a platinum auxiliary electrode were employed in the CE-EC experiments. A Faraday cage was used to shield the electrochemical cell from external noise sources.

**Pulsed Voltammetry (PV) Experiments.** Pulsed voltammetric data were obtained at a 50- $\mu\text{M}$  Au electrode with a computer-controlled potentiostat (Model RDE-4; Pine Instrument Co., Grove City, PA) using a DAS-20 high-speed A/D-D/A expansion board (MetraByte Corp., Taunton, MA) in an IBM-AT-compatible computer (Gateway Co., Sioux Falls, SD). The reference electrode employed was a SCE. Pulse voltammetry wave forms were generated with ASYST Scientific software (Asyst Software Technologies, Inc., Rochester, NY).

**Separation Conditions.** For the CE separations, a capillary length of 95 cm with an applied voltage of 25 kV was employed. The run buffer was 10 mM NaOH containing 8 mM sodium carbonate, pH 12. For detection of carbohydrates, the following PAD wave form was employed:  $E_1$  (detection) +325 mV,  $t_1$  199 ms;  $E_2$  (oxidative cleaning) +800 mV,  $t_2$  166 ms;  $E_3$  (reactivation) -600 mV,  $t_3$  249 ms applied. All potentials are vs Ag/AgCl.

**Sample Preparation.** For the determination of glucose levels in blood, 20  $\mu\text{L}$  of human blood was diluted in 1 mL of operating buffer, filtered, and centrifuged in a Gelman Sciences (Ann Arbor, MI) two-spin filtration unit. The filtered sample was injected directly.

## RESULTS AND DISCUSSION

**Pulsed Voltammetry of Glucose.** Figure 1 shows the current-potential ( $i$ - $E$ ) response during the positive scans for glucose at a Au microelectrode in 10 mM NaOH-8 mM  $\text{Na}_2\text{CO}_3$ . Only the data for the positive scans are shown

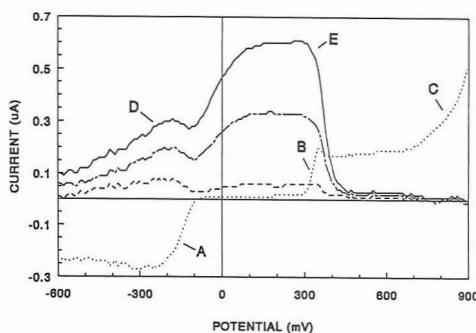


**Figure 1.** Pulse voltammetric response of glucose at a Au microelectrode in 10 mM NaOH-8 mM  $\text{Na}_2\text{CO}_3$ . Conditions: partially deaerated with  $\text{N}_2$ . Wave form:  $E_{\text{det}} = -600$  to  $+900$  mV,  $t_{\text{det}} = 500$  ms,  $t_{\text{cat}} = 240$  ms,  $t_{\text{int}} = 200$  ms;  $E_{\text{oxid}} = 800$  mV,  $t_{\text{oxid}} = 166$  ms;  $E_{\text{red}} = -600$  mV,  $t_{\text{red}} = 249$  ms. Summation of nine PAD cycles per point. Solutions: (---) residual; (- - -) 10  $\mu\text{M}$  glucose; (- · - ·) 50  $\mu\text{M}$  glucose; (—) 100  $\mu\text{M}$  glucose.

because this response is relevant to the PAD wave forms (in which the anodic response is measured following a positive step from the cathodic potential  $(E_{\text{red}})$  to the detection potential  $(E_{\text{det}})$ , which is much greater than  $E_{\text{red}}$ ). The cathodic and anodic signals for the residual correspond to reduction of dissolved  $\text{O}_2$  (wave A; ca. -600 to -100 mV), the formation of surface oxide (wave B; greater than ca. +300 mV), and  $\text{O}_2$  evolution from water anodization (wave C, greater than ca. +700 mV). The "background-corrected" PV responses for glucose at 10, 50, and 100  $\mu\text{M}$  are also shown in Figure 1. Glucose produces a two-step anodic response during the positive scan. The first anodic step corresponds to the oxidation of the aldehyde group to the carboxylate anion in this alkaline media (wave D; ca. -600 to ca. -100 mV). The second step has the form of the peak (wave E; ca. -100 to +450 mV) and corresponds to the combined oxidations of the aldehyde and alcohol groups of glucose. The anodic signal during the positive scan is inhibited (greater than ca. +300 mV) corresponding to the onset of oxide formation (wave B). This is as expected for detections which are catalyzed at oxide-free surfaces.<sup>11,13</sup> Any  $E_{\text{det}}$  value in the range of 0 to +300 mV vs SCE will be acceptable for detection of glucose by PAD under these conditions. Application of this potential in PAD will enable the universal and direct detection of virtually all carbohydrates. By judicious selection of the detection potential, the applicability of this system can be extended to simple alcohols<sup>11</sup> and aliphatic amines and amino acids,<sup>17,18</sup> as well as numerous sulfur compounds.<sup>19,20</sup>

**Determination of Glucose.** Glucose was the analyte of choice for the initial investigation of the performance of the detector with CE because of its general importance in a number of biological systems and its proven record with PAD detection. The column appeared to be quite stable at the high pH with migration times not exceeding 3% RSD within 1 day. A column used continuously over a 3-week period showed variations in migration times of not more than 10% RSD. Eight successive injections of  $1 \times 10^{-4}$  M glucose exhibited RSDs for migration time and peak height of 1.1% and 3.3%, respectively.

(17) Polta, J. A.; Johnson, D. C. *J. Liq. Chromatogr.* 1983, 6, 1727-1743.

(18) Welch, L. E.; LaCourse, W. R.; Mead, D. A.; Johnson, D. C. *Anal. Chem.* 1989, 61, 555-559.

(19) Polta, T. Z.; Johnson, D. C. *J. Electroanal. Chem.* 1986, 209, 159-169.

(20) Ngovitchai, A.; Johnson, D. C. *Anal. Chim. Acta* 1988, 215, 1-12.

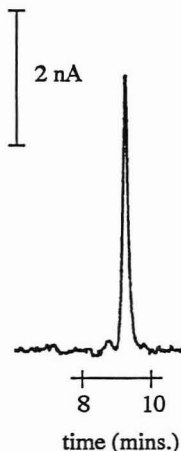


Figure 2. Electropherogram of  $1 \times 10^{-5}$  M glucose using a  $75\text{-}\mu\text{m}$  capillary column; operating buffer,  $10\text{ mM NaOH-}8\text{ mM Na}_2\text{CO}_3$ ; separation voltage,  $25\text{ kV}$ ; PAD wave form as described in the Experimental Section.

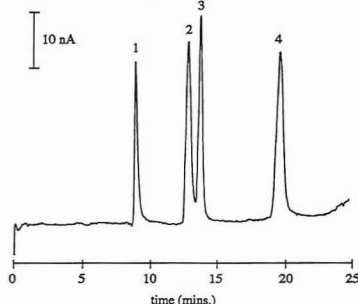


Figure 3. Separation of  $1 \times 10^{-4}$  M (1) glucosaminic acid, (2) glucosamine 6-sulfate, and (4) glucosamine 6-phosphate. Separation conditions as outlined in Figure 2.

The PAD response for glucose was linear over the range  $1 \times 10^{-5}$  to  $1 \times 10^{-3}$  M with a correlation coefficient of 0.9997 ( $n = 7$ ). Calibration curves prepared over this range yielded slopes of  $299\text{ nA/mM}$ . A detection limit of  $9 \times 10^{-7}$  M based on a  $S/N = 3$  was estimated from the electropherogram obtained from an injection of  $1 \times 10^{-5}$  M glucose shown in Figure 2. Based on an injection volume of  $25\text{ nL}$ , this corresponds to a mass detection limit of  $22.5\text{ fmol}$ . The mass detection limits are 5-fold higher than those reported using indirect detection;<sup>1</sup> however, in the latter method  $5\text{-}\mu\text{m}$  capillaries were employed, which leads to increased mass sensitivity. Therefore, although mass detection limits are comparable, because the injection volume is smaller in  $5\text{-}\mu\text{m}$  columns, the concentration detection limit is poorer with indirect detection. In this study,  $75\text{-}\mu\text{m}$ -i.d. capillaries were used. The mass detection limit could be substantially improved by the use of columns of smaller inner diameter.

**Separation of Charged Carbohydrates.** CE-PAD was employed for the separation and detection of several biologically important charged carbohydrates, including glucosamine, glucosaminic acid, glucosamine 6-sulfate, and glucosamine 6-phosphate. Figure 3 shows the separation achieved for these four compounds, with glucosaminic acid

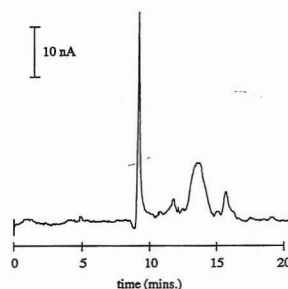


Figure 4. Electropherogram of human blood. Peak corresponds to  $85\text{ }\mu\text{M}$  glucose. Separation conditions as outlined in Figure 2.

and glucosamine 6-sulfate nearly baseline-resolved.

Garner and Yeung achieved a separation of the "neutral" sugars sucrose, glucose, and fructose in less than 10 min at a similar pH using  $20\text{-}\mu\text{m}$  capillaries.<sup>1</sup> However, many other sugars exhibited the same migration time as these three. Under the conditions reported here, we were not able to achieve the high efficiencies necessary for this separation of these three neutral sugars. This could be due to the fact that a larger amount of current is generated by the hydroxide electrolyte in a  $75\text{-}\mu\text{m}$  capillary than in a  $20\text{-}\mu\text{m}$  capillary, leading to Joule heating. An additional factor is the time constant of the detector, which is designed for LC applications. Future research will involve the evaluation of new buffer systems, complexing agents, and other additives to better facilitate the separation of uncharged carbohydrates.

**Determination of Glucose in Blood.** To investigate the selectivity of the detector for the analysis of carbohydrates in real samples, the determination of glucose in blood was examined. Illustrated in Figure 4 is the electropherogram of a 1:50 dilution of human blood; the only sample pretreatments were centrifugation and filtration. The glucose peak represents an injection of  $85\text{ }\mu\text{M}$  glucose, which corresponds to a concentration in the blood of  $4.25 \pm 0.13\text{ mM}$  ( $n = 3$ ). This agrees well with that reported in the literature.<sup>21</sup> Only a few other small peaks are present in the electropherogram, demonstrating the high degree of selectivity this technique has toward carbohydrates.

There are several potential advantages of this method over other methods for carbohydrate analysis. In CE-PAD, unlike LC-PAD, buffers of high pH can be employed for the separation without column degradation. Capillaries are also much less expensive than the ion-exchange columns presently used for LC separations. The small volumes required for analysis by CE make it possible to apply this method in those cases where one is limited by sample size. In addition, this method permits direct detection, eliminating problems inherent in derivatization procedures currently employed for CE analysis (dilution of sample, incomplete reaction, side products, long reaction times). The high degree of selectivity has been demonstrated by the electropherogram of glucose in blood.

One drawback of this technique is the high pH necessary for electrochemical detection of carbohydrates, which limits the pH range that can be employed for the separation. However, this problem can be overcome either by using Pt electrodes, which may allow one to work at lower pH values, or through postcolumn addition of base using one of the previously described methods for postcolumn derivatiza-

(21) *The Merck Manual*, 15th ed.; Berkow, R., Ed.; Merck Sharp & Dohme Research Laboratories: Rahway, NJ, 1987; p 2413.

tion.<sup>22,23</sup> Oxygen can be a problem when Pt electrodes are employed; however, deoxygenation has been shown to be relatively simple to accomplish with CE because of the small volume of buffer involved.<sup>24</sup>

The emphasis of future studies will be on the separation and detection of carbohydrates present on glycoproteins. The use of this method for the detection of other PAD-active

functional groups, such as amines and alcohols, will also be investigated.

#### ACKNOWLEDGMENT

The authors thank Nancy Harmony for help in the preparation of the manuscript. This work was supported by the Center for Bioanalytical Research and the Kansas Technology Enterprise Corp.

(22) Rose, D. J.; Jorgenson, J. W. *J. Chromatogr.* 1988, 447, 117-131.

(23) Pentoney, S., Jr.; Huang, X.; Burgi, D.; Zare, R. N. *Anal. Chem.* 1988, 60, 2625-2629.

(24) O'Shea, T. J.; Lunte, S. M. *Anal. Chem.*, 1993, 65, 247-250.

RECEIVED for review October 5, 1992. Accepted December 30, 1992.

## Ion Chromatography of Sulfur Dioxide, Sulfate Ion, and Dithionate Ion in Aqueous Mineral Leachates

Lloyd M. Petrie,\* M. Emmelyn Jakel, Richard L. Brandvig, and Joseph G. Kroening

Bureau of Mines, U.S. Department of Interior, 5629 Minnehaha Avenue South, Minneapolis, Minnesota 55417

### INTRODUCTION

The U.S. Bureau of Mines is conducting research on in situ leach mining of  $Mn^{4+}$  and  $Mn^{3+}$  oxide ores, a process reliant on mineral-fluid geochemistry.<sup>1</sup> Acidic aqueous  $SO_2$  is being evaluated because of its low cost and prior evidence that  $SO_2$  selectively dissolves manganese oxides before iron oxides and other host minerals.<sup>2,3</sup> Process development requires monitoring several parallel reductive leaching reactions:



The above formulas represent the number of oxygen atoms required to balance the overall equations shown. The actual coordination of most manganese oxides is six O atoms octahedrally arranged about  $Mn^{4+}$  or  $Mn^{3+}$  centers.

The objective of this work was to develop a sampling/analysis procedure for low-level determination of S speciation for the above reductive dissolution reactions. Accurate leachate concentrations of  $SO_2$ ,  $SO_4^{2-}$ , and  $S_2O_6^{2-}$  are needed to determine fundamental kinetics and process engineering parameters (e.g. product/reactant ratios).

The aqueous samples requiring S speciation determination are from laboratory batch, column, and core leaching experiments. These samples contained total concentration levels for S = 1-35 g/kg, Mn = 0.1-40 g/kg, and Fe = 0-2 g/kg. Dissolved oxygen was not periodically measured and oxygen was not excluded during solution handling because field operations use oxygenated solutions.

First, sample handling procedures were needed. Determining S speciation in aqueous media is challenging due to  $SO_2$  volatility and  $Mn^{2+}$ -catalyzed oxidation of S(IV) equilibria products,  $HSO_3^-$  and  $SO_3^{2-}$ .<sup>4,5</sup> Below pH 1.5,  $SO_2$  is the abundant form, whose high vapor pressure<sup>6</sup> (e.g. 359 kPa at 22 °C; 426 kPa at 27 °C) requires sealed vessels and gas-tight syringes. Eckert and co-workers<sup>7-9</sup> reported (1) significant  $Mn^{2+}$ -catalyzed oxidation for pH 3 to 5, (2) a proposed metal coordination-free radical mechanism for  $HSO_3^-$  oxidation, and (3) S(IV) oxidation inhibition below pH 5 with phenolic antioxidants (e.g. pyrogallol and hydroquinone). Schroeter

reviewed earlier work on inhibition of S(IV) oxidation.<sup>10</sup> In the absence of trace metals, dilute solutions of ethanol and formaldehyde prevent S(IV) oxidation.

Second, sample-specific chemical analysis methods for S(IV),  $SO_4^{2-}$ , and  $S_2O_6^{2-}$  were needed. Iodate titration for S(IV) was not sensitive enough for some samples.<sup>11</sup> A number of methods have been developed for airborne  $SO_2$ , but they generally rely on oxidation of  $SO_2$  to  $SO_4^{2-}$  before instrumental analysis.<sup>12,13</sup> Kim and co-workers compared AOAC-approved methods for  $SO_2$  in grapes,<sup>14</sup> including two ion exclusion LC methods. Bartroli and co-workers recently reported a p-aminazobenzene calorimetric method for  $SO_2$  in wine.<sup>15</sup> Of the five  $SO_4^{2-}$  standard methods for water and wastewaters,<sup>16</sup> two have the necessary sensitivity and range—ion chromatography with chemical suppress/conductivity detection and methylthymol blue autoanalysis.

Fewer analytical methods have been developed for  $S_2O_6^{2-}$ . The most frequent approach is sequential oxidation of S species to  $SO_4^{2-}$ ,  $SO_4^{2-}$  analysis at each step and calculation of  $S_2O_6^{2-}$  or other S oxyanions.<sup>17-19</sup> We sought a direct determination method of  $S_2O_6^{2-}$ . Rabin and Stanbury reported a reversed-phase ion-pair chromatography method for polythionates, including  $S_2O_6^{2-}$ .<sup>20</sup> Unfortunately,  $SO_4^{2-}$  and  $S_2O_6^{2-}$  co-eluted in their system. Subsequently, they developed a simple anion method using Wescan equipment and 4.0 mM potassium phthalate eluent to resolve  $SO_4^{2-}$  and  $S_2O_6^{2-}$  peaks.<sup>21</sup> Dionex recommended their anion mobile phase ion chromatography system.<sup>22</sup> Lastly, FTIR spectrometry can detect high levels of  $SO_2$ ,  $SO_3^{2-}$ ,  $SO_4^{2-}$ , and  $S_2O_6^{2-}$  in aqueous media, a capability examined in a forthcoming report.

Due to its analytical range, speed, accuracy, specificity, and potential for field applications, ion chromatography was selected as the most promising analytical methodology for measurement of S(IV),  $SO_4^{2-}$ , and  $S_2O_6^{2-}$  in our mineral leaching studies.

### EXPERIMENTAL SECTION

References to specific products does not imply endorsement by the Bureau of Mines. A Dionex 4000i ion chromatography with conductivity detection and Spectra-Physics 4270 integrator was used. Peak area quantitation was performed for all samples

(10) Schroeter, L. C. Reference 4, pp 55-62.

(11) *Standard Methods for the Examination of Water and Wastewater*, 17th ed.; Franson, M., Ed.; Am. Public Health Assoc.: Washington, D.C., 1989; pp 4-200-4-201.

(12) Bhatt, A.; Gupta, V. *Analyst* 1983, 108, 374-9.

(13) Hallberg, B.; Rulling, J.; Hultman, A.; Hultgren, M. *Scand. J. Work Environ. Health* 1984, 10, 305-9.

(14) Kim, H.; Conca, K.; Richardson, M. *J. Assoc. Off. Anal. Chem.* 1990, 73, 983-9.

(15) Bartroli, J.; Escalada, M.; Jorquera, C.; Alonso, J. *Anal. Chem.* 1991, 63, 2532-5.

(16) Reference 12, pp 4-204-4-210.

(17) Williams, W. J. *Handbook of Anion Determination*; Butterworths: New York, 1979; pp 501-3.

(18) Siskos, P.; Diamandis, E.; Gillieron, E.; Colbert, J. *Talanta* 1983, 30, 980-2.

(19) Babiker, B. *Analyst* 1988, 113, 351-3.

(20) Rabin, S.; Stanbury, D. *Anal. Chem.* 1985, 57, 1130-2.

(21) Sarala, R.; Islam, M. A.; Rabin, S. B.; Stanbury, D. M. *Inorg. Chem.* 1990, 29, 1133-42.

(22) *Methods Development Using Anion Mobile Phase Ion Chromatography*; Tech. Note 12R; Dionex Corp.: Sunnyvale, 1984.

(1) Marozas, D. C.; Paulson, S. E.; Petrie, L. M. SME National Meeting, Denver, CO, Feb 25-28, 1991, Preprint No. 91-177.

(2) Petrie, L. M. Department of Interior, Bureau of Mines Open File Report, 1991, No. 6-91.

(3) Pahlman, J. E.; Khalafalla, S. E. Department of Interior, Bureau of Mines Report of Investigation, 1988, No. 9150.

(4) Schroeter, L. C. *Sulfur Dioxide - Applications in Foods, Beverages, and Pharmaceuticals*; Pergamon Press: New York, 1966; pp 7-18.

(5) Cotton, F. A.; Wilkinson, G. *Advanced Inorganic Chemistry*, 5th ed.; Wiley-Interscience: New York, 1988; pp 519-21.

(6) *CRC Handbook of Chemistry and Physics*, 71st ed.; Lide, D. R., Ed.; CRC Press: Boca Raton, 1990; pp 6-78.

(7) Huss, A.; Lim, P. K.; Eckert, C. A. *J. Phys. Chem.* 1982, 86, 4224-8.

(8) Huss, A.; Lim, P. K.; Eckert, C. A. *J. Phys. Chem.* 1982, 86, 4229-33.

(9) Lim, P. K.; Huss, A.; Eckert, C. A. *J. Phys. Chem.* 1982, 86, 4233-37.

with the peak width = 30 and peak threshold = 12 for the 4270.  $\text{SO}_3^{2-}$  and  $\text{SO}_4^{2-}$  were determined with a Dionex AS4A column and 1.8 mM  $\text{Na}_2\text{CO}_3$  + 1.7 mM  $\text{NaHCO}_3$  eluent at 2 mL/min.  $\text{S}_2\text{O}_8^{2-}$  was determined with Dionex MPIC-NG1 column and 1 mM  $\text{Na}_2\text{CO}_3$  + 2 mM tetrabutylammonium hydroxide + 20 wt % acetonitrile at 1.5 mL/min. Total S was determined, without dilution, using a Philips 1410 XRF spectrometer. A Copenhagen Radiometer ABU80 autotitrator was used for iodometric titrations.

ACS reagent-grade chemicals were used. The only source found for  $\text{Na}_2\text{S}_2\text{O}_8$  was Pfaltz and Bauer. Type I water was used for sample dilutions and final rinses of acid-washed glass and plasticware.

Leaching solutions were prepared by bubbling gaseous  $\text{SO}_2$  from compressed gas cylinders into tightly-capped HDPE bottles equipped with a recirculating water line to mix the gas and water. A 5 psi  $\text{N}_2$  overpressure was applied to contain the volatile  $\text{SO}_2$  in the solutions. CAUTION:  $\text{SO}_2$  gas and acidic  $\text{SO}_2$  solutions pose significant inhalation hazards. Additional important information is contained in the MSDS. They should be handled in a hood, and personal protection equipment should be used.

Each sample batch for ion chromatography or manganese analysis included a prep blank, spiked sample, and blind check standard. The analyst provided a calibration verification standard (CVS) and calibration blank. Total S sample batches included all QC samples but the spiked sample and CVS.

Stock standards for  $\text{SO}_3^{2-}$  ion chromatography were prepared in 1 w/w % formaldehyde and were stable for a minimum of 4 weeks. The stock standards were diluted 100-fold with type I water to prepare calibration standards. These standards were stable for 2 weeks.

Two diluents were used to dilute samples for ion chromatography. The initial dilution was made with IC diluent no. 1 (1 wt % formaldehyde + 0.25 m NaCl + 0.02 m HCl). Final dilutions were made with IC diluent no. 2 (0.1 wt % formaldehyde + 0.025 m NaCl + 0.002 m HCl, pH 2.44).

Samples for ion chromatography were not exposed to air during collection. First, a gas-tight syringe was partially filled with a known mass of IC diluent no. 1. A small stirring bar was placed in the syringe to facilitate mixing. Second, Tygon tubing was attached to the solution sampling port, and sufficient leachate was drained to fill the tubing. Third, the needle from the gastight syringe was immediately injected into the filled Tygon tubing, and several milliliters of fresh leachate were drawn into the syringe. Fourth, the sample port valve closed and the syringe was removed. Fifth, the contents of the syringe were gently handshaken to achieve complete mixing. If additional dilutions were needed, diluent no. 2 was used.

## RESULTS AND DISCUSSION

**(a) Sample Handling.** Regardless of analytical method, a sample handling procedure was needed to preserve S speciation by preventing  $\text{SO}_2$  volatilization and S(IV) oxidation to  $\text{SO}_4^{2-}$ . Volatilization losses were minimized through staff awareness and use of gas-tight syringes.

Since ion chromatography required large dilutions (1–3000-fold) of collected leachates, the diluted concentrations of  $\text{SO}_2$ ,  $\text{SO}_3^{2-}$ , and  $\text{S}_2\text{O}_8^{2-}$  were equal to that for dissolved  $\text{O}_2$  and  $\text{Mn}^{2+}$ , making Mn-catalyzed oxidation of S(IV) to  $\text{SO}_4^{2-}$  significant. To devise a S(IV) preservation procedure, Eckert's work<sup>7-9</sup> provided a starting point. First, EDTA complexation of  $\text{Mn}^{2+}$  was attempted. When leachates were diluted with pH 3–4 EDTA solutions, the high  $\text{Mn}^{2+}$  concentrations resulted in Mn hydroxide precipitation and variable degrees of S(IV) preservation. Next, attention was focused on organic antioxidants. Diluents containing 0.5–5 wt % mannitol and ethanol prevented S(IV) oxidation in the absence of  $\text{Mn}^{2+}$ . Diluents containing  $10^{-3}$  m hydroquinone at pH 1 and 5 failed to prevent complete oxidation of S(IV) when  $1.67 \times 10^{-4}$  M  $\text{Mn}^{2+}$  was present. This was a surprising result since Eckert reported effective prevention of S(IV) oxidation for  $[\text{Mn}^{2+}] = 1.49 \times 10^{-4}$  M,  $[\text{O}_2] = 0.0018$  M,  $[\text{S(IV)}] = 0.015$  M,  $[\text{hydroquinone}] \leq 1.5 \times 10^{-6}$  M, and pH  $\leq 5.9$

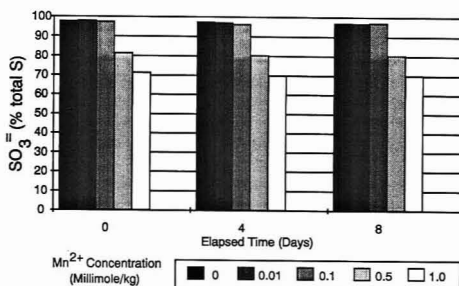


**Figure 1.** Prevention of Mn-catalyzed oxidation of S(IV) through 8 days in the presence of 0–1.0 mmol/kg  $\text{Mn}^{2+}$ . Preservation was at pH 2.44 with a 0.1 wt % formaldehyde + 0.025 m NaCl + 0.002 m HCl buffer.

This can be explained by the fact that they added the phenolic antioxidants to the S(IV) solutions before introducing  $\text{Mn}^{2+}$ . To simulate our leachates, we added  $\text{Mn}^{2+}$  before diluting with hydroquinone.

Satisfactory S(IV) preservation was achieved with formaldehyde by recalling that  $\text{HSO}_3^-$  undergoes nucleophilic addition to the carbonyl C atom of formaldehyde according to eq 4:<sup>23</sup>



With S(IV) part of an organic bisulfite ion, it cannot readily complex  $\text{Mn}^{2+}$  atoms as proposed in the mechanism for  $\text{Mn}^{2+}$ -catalyzed  $\text{O}_2$  oxidation.<sup>8</sup>  $\text{HSO}_3^-$  is the primary S(IV) oxyanion between pH 2 (63 mol %) and pH 4 (96 mol %). To test formaldehyde preservation, 0.0397 m  $\text{Na}_2\text{SO}_3$  in 0.2 m HCl samples with varying amounts of  $\text{MnCl}_2$  were diluted with IC no. 2 (0.1 wt % formaldehyde + 0.025 m NaCl + 0.002 m HCl), giving diluted samples at pH 2.44. Figures 1 summarizes the results of these tests. S(IV) oxidation was prevented for solutions where  $[\text{Mn}^{2+}]$  was  $\leq 0.1$  mmol/kg through 8 days, the maximum holding time anticipated for IC analysis of leaching test samples.

**(b)  $\text{SO}_3^{2-}$  and  $\text{SO}_4^{2-}$  Ion Chromatography.** Determination of  $\text{SO}_3^{2-}$  in natural waters using conventional ion chromatography with suppressed conductivity detection is well-known. With a S(IV) preservation procedure, conventional anion chromatography can be used to determine S(IV) as  $\text{SO}_3^{2-}$  since the eluent is at pH 10.2. Five stock  $\text{SO}_3^{2-}$  standards were diluted to 5–100 ppm  $\text{SO}_3^{2-}$  with IC no. 2 (0.1 wt % formaldehyde + 0.025 m NaCl + 0.002 m HCl) and analyzed in triplicate.  $\text{SO}_3^{2-}$  peaks were well-shaped with a flat baseline. Linear regression of the data produced a correlation coefficient = 0.9993. Retention times for  $\text{SO}_3^{2-}$  were 5.41–5.55 min.

A condition common to diluted manganese leachates is high  $\text{SO}_3^{2-}$  concentrations relative to  $\text{SO}_4^{2-}$ . This effect was investigated for 50 ppm  $\text{SO}_3^{2-}$  with increasing  $\text{SO}_4^{2-}$ : $\text{SO}_3^{2-}$  ratios (i.e. 1:1, 3:1, 10:1). For ratios 1:1 and 3:1, the  $\text{SO}_3^{2-}$  measured concentrations were 50.2 and 50.0 ppm, respectively. Since the  $\text{SO}_3^{2-}$  peak was not fully resolved at ratio 10:1, 3:1 can be considered the practical maximum  $\text{SO}_4^{2-}$ : $\text{SO}_3^{2-}$  ratio.

Figure 2 is a typical chromatogram for a column leachate diluted to a final sample matrix of 0.1 wt % formaldehyde + 0.025 m NaCl + 0.002 m HCl. The  $\text{SO}_3^{2-}$  peak (22 ppm) has the same peak shape as the 25 ppm  $\text{SO}_3^{2-}$  standard solution. The  $\text{SO}_3^{2-}$  retention time is 5.39 min vs an average 5.46 min for the 25 ppm  $\text{SO}_3^{2-}$  standard. This indicates that

(23) Morrison, R. T.; Boyd, R. N. *Organic Chemistry*, 2nd ed.; Allyn and Bacon: Boston, 1966; p 639.

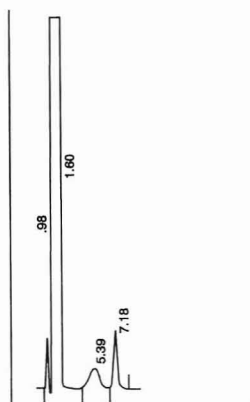


Figure 2. Typical leachate chromatogram diluted with 0.1 wt % formaldehyde + 0.025 m NaCl + 0.002 m HCl showing  $\text{SO}_3^{2-}$  (5.39 min, 22 ppm) and  $\text{SO}_4^{2-}$  (7.18 min, 11.0 ppm).

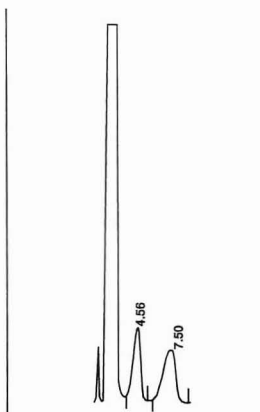


Figure 3. Typical leachate chromatogram diluted with 0.1 wt % formaldehyde + 0.025 m NaCl + 0.002 m HCl showing  $\text{SO}_4^{2-}$  (4.56 min) and  $\text{S}_2\text{O}_6^{2-}$  (7.50 min, 48.3 ppm).

as the preserved sample is introduced onto the column bisulfite ion dissociates, producing  $\text{SO}_3^{2-}$  as the only S(IV) form at eluent pH of 10.2. Since the  $\text{SO}_4^{2-}$  concentration (11.0 ppm) is similar to that of  $\text{SO}_3^{2-}$ , there is good resolution for both two peaks.

(c)  **$\text{S}_2\text{O}_6^{2-}$  Ion Chromatography.** Conventional suppressed anion chromatography will not detect  $\text{S}_2\text{O}_6^{2-}$ . However, Dionex has a mobile-phase ion-pair column (MPIC-NG1) column that can detect  $\text{S}_2\text{O}_6^{2-}$  and  $\text{SO}_4^{2-}$  with the same suppression and conductivity detection system. On the MPIC-NG1, retention times for  $\text{S}_2\text{O}_6^{2-}$  and  $\text{SO}_4^{2-}$  were approximately 7.5 and 4.6 min, respectively.

Stock  $\text{S}_2\text{O}_6^{2-}$  standards were again diluted with IC no. 2 (0.1 wt % formaldehyde + 0.025 m NaCl + 0.002 m HCl). Calibration for  $\text{S}_2\text{O}_6^{2-}$  was split into a low and high range, covering 5–50 and 50–200 ppm, respectively. Five standard calibration curves were run for each range. The high calibration curve was linear (correlation coefficient = 0.999). The low calibration curve was also relatively linear (correlation coefficient = 0.991).

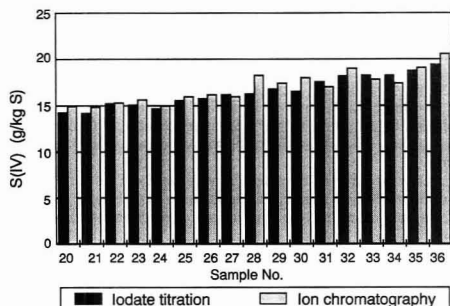


Figure 4. Comparison of S(IV) determination for column leachates by (a) iodate titration and (b) ion chromatography for  $\text{SO}_3^{2-}$  in g/kg S.

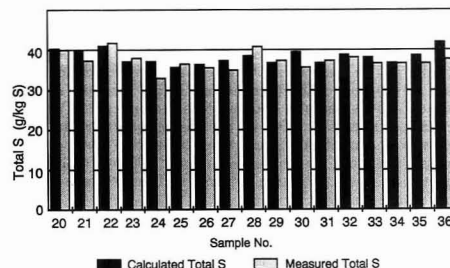


Figure 5. Comparison of total S determination for column leachates by (a) calculated sum of ion chromatography results for  $\text{SO}_3^{2-}$  +  $\text{SO}_4^{2-}$  +  $\text{S}_2\text{O}_6^{2-}$  and (b) X-ray fluorescence spectrometry in g/kg S.

Since retention times for  $\text{S}_2\text{O}_6^{2-}$  and  $\text{SO}_4^{2-}$  were close on the NG1,  $\text{SO}_4^{2-}$  interference with  $\text{S}_2\text{O}_6^{2-}$  peaks was a concern. Mixed  $\text{SO}_4^{2-}$ - $\text{S}_2\text{O}_6^{2-}$  standards with varying  $\text{SO}_4^{2-}$ : $\text{S}_2\text{O}_6^{2-}$  ratios were prepared in IC no. 2. Acceptable resolution was achieved up to a 10:1 ratio. For that sample, the calculated  $\text{S}_2\text{O}_6^{2-}$  value (27.8 ppm) compared well with the measured value (27.7 ppm). For manganese leachates, the  $\text{SO}_4^{2-}$ : $\text{S}_2\text{O}_6^{2-}$  ratio rarely exceeded the 10:1 ratio.

Figure 3 is a typical chromatogram for an IC no. 2 diluted column leachate, displaying first  $\text{SO}_4^{2-}$  at 4.56 min and then  $\text{S}_2\text{O}_6^{2-}$  at 7.50 min. The large peaks before  $\text{SO}_4^{2-}$  and  $\text{S}_2\text{O}_6^{2-}$  are due to the diluent matrix. The measured  $\text{S}_2\text{O}_6^{2-}$  concentration was 48.3 ppm. However, the NG1 column was not used for  $\text{SO}_4^{2-}$  determinations for two reasons. First, as seen in Figure 3, the matrix peaks and the  $\text{SO}_4^{2-}$  peak were not completely resolved. Second,  $\text{SO}_3^{2-}$  and  $\text{SO}_4^{2-}$  co-eluted in the samples, making quantitative measurement of  $\text{SO}_4^{2-}$  impossible with this column. Coelution was confirmed by running a standard with known  $\text{SO}_3^{2-}$  and  $\text{SO}_4^{2-}$  concentrations through the NG1 and AS4A columns in series. The NG1  $\text{SO}_4^{2-}$  peak was larger than expected and yet correct determination was achieved for both  $\text{SO}_3^{2-}$  and  $\text{SO}_4^{2-}$  on the AS4A column.

(d) **Comparison of IC Results to Other Analytical Results.** In addition to ion chromatography for  $\text{SO}_3^{2-}$ ,  $\text{SO}_4^{2-}$ , and  $\text{S}_2\text{O}_6^{2-}$ , S(IV) was determined by iodate titration, and total S was determined by X-ray fluorescence spectrometry, providing external accuracy checks of the IC methods.

First, the standard iodate titrations for S(IV) were performed on undiluted subsamples of the same leachates analyzed by ion chromatography. Figure 4 shows the comparison between iodate titration and ion chromatography for some of the samples from port 2 of a large column leaching experiment. Except for sample 28 (11.6%) and sample 30



(8.2%) results, the relative percent differences between ion chromatography and iodate titration were between 0.6% and 5.7%.

Second, X-ray fluorescence (XRF) spectrometry was used to determine total S in the same large column leaching samples. In Figure 5, these "measured" total S results are compared to "calculated" total S summed from the ion chromatography data for  $\text{SO}_3^{2-}$ ,  $\text{SO}_4^{2-}$ , and  $\text{S}_2\text{O}_6^{2-}$ . Given the possibilities for accumulated sampling and analysis errors in this comparison, the results were good. For the 17 comparisons, relative percent differences were between 0.1% and 2.9%.

### CONCLUSIONS

We have described sample preparation and ion chromatography procedures that permit rapid, low-level, accurate measurement of S(IV) as  $\text{SO}_3^{2-}$ ,  $\text{SO}_4^{2-}$ , and  $\text{S}_2\text{O}_6^{2-}$  in aqueous mineral leachates. By using a pH 2.44 buffered diluent containing formaldehyde,  $\text{Mn}^{2+}$ -catalyzed oxidation of S(IV) to  $\text{SO}_4^{2-}$  was prevented. These methods are applicable to a

wide range of aqueous samples from the food, manufacturing, and environmental sectors, particularly when  $\text{Mn}^{2+}$ ,  $\text{Fe}^{3+}$ , and other metal catalysts are present in the samples. The IC method for  $\text{S}_2\text{O}_6^{2-}$  may be useful for environmental studies of  $\text{SO}_2$  reactivity since partial oxidation of  $\text{SO}_2$  can form  $\text{SO}_3^-$  radical which dimerizes to form  $\text{S}_2\text{O}_6^{2-}$ . It is important to remember these methods use standard commercial instrumentation, columns, and eluents.

### ACKNOWLEDGMENT

We thank Stan Peterson and Dale Breed, Twin Cities Research Center, Bureau of Mines, for their efforts in collecting and preparing samples for the work reported here. We wish to also thank the Dionex Corporation for their technical assistance in  $\text{S}_2\text{O}_6^{2-}$  IC methods development.

RECEIVED for review October 1, 1992. Accepted December 21, 1992.

## Multiplexed Fluorescence Detector for Capillary Electrophoresis Using Axial Optical Fiber Illumination

John A. Taylor and Edward A. Yeung\*

Ames Laboratory-USDOE and Department of Chemistry, Iowa State University, Ames, Iowa 50011

It is obvious that irrespective of which basic technology is eventually selected to sequence the entire human genome,<sup>1,2</sup> there are substantial gains to be made if a high degree of multiplexing of parallel runs can be implemented. Such multiplexing should not involve expensive instrumentation and should not require additional personnel, or else the main objective of cost reduction will not be satisfied even though the total time for sequencing is reduced. A corollary is that if a certain basic technology can be readily and efficiently highly multiplexed, then it may ultimately become the method of choice to sequence the entire human genome. In fact, present-day sequencing runs are already being performed in slab gels with multiple lanes to achieve multiplexing. Unfortunately, slab gels are not readily amenable to a high degree of multiplexing and automation. Difficulties include uniform gel preparation over a large area, reproducibility over different gels, loading of sample wells, large physical size of the medium, uniform cooling, large amounts of media, buffer, and samples needed, and long run times for extended reading of bases. The introduction of ultrathin slab gels<sup>3,4</sup> does address some of these difficulties. Still, it is hard to imagine how 1000 lanes can be run simultaneously in one instrument.

In the last 2 years, several research groups have shown that capillary gel electrophoresis (CGE) is an attractive alternative to slab gel electrophoresis (SGE) for DNA sequencing.<sup>5-9</sup> The medium used, buffer composition, separation mechanism, sequencing chemistry, and tagging chemistry for CGE are all derived from proven SGE schemes. A 25-fold increase in the sequencing rate per capillary (per lane) has already been demonstrated. This is a direct consequence of the small internal diameter of the capillary tubes, typically around 50-75  $\mu\text{m}$ , greatly reducing Joule heating associated with the electrical current. Gel distortions and temperature gradients that can affect resolution of the bands are thus virtually absent. More importantly, much higher electric fields can be applied to speed up the separation. For comparison, conventional SGE are limited to field strengths below 50 V/cm while CGE have been successfully used for sequencing up to 500 V/cm.<sup>7</sup> The unique aspect ratio of capillary gels (25-50 cm long) provides uniform field strengths, and the large surface-to-volume ratio favors efficient heat removal. These combine to produce much sharper bands than are possible in slab gels.

Part of the improvement in sequencing speed in CGE is counteracted by the inherent ability of slab gels for accommodating multiple lanes in a single run. So, unless capillary

gels can be highly multiplexed and run in parallel, the above-mentioned advantages cannot lead to real improvements in sequencing the human genome. Fortunately, the capillary format is in fact well suited for multiplexing. Already mentioned is the substantial reduction of Joule heating per lane, even given the high applied fields, so that the overall cooling requirement and electrical requirement remain manageable. The cost of materials per lane is much reduced because everything, including sample sizes, is smaller. The reduced band dimensions are ideal for excitation by laser beams and for imaging onto solid-state array detectors. The use of electromigration injection provides reproducible sample introduction with little band spreading and with little effort. Commercial capillary electrophoresis instruments have already incorporated the necessary robotics for such an operation. The small band sizes, however, put stringent requirements on detection. It is not possible to use large amounts of DNA fragments because of overloading and plugging of the gel pores.<sup>6</sup> So, recently proposed multiplexing schemes such as multiple hybridization<sup>8</sup> and multiple tagging<sup>9</sup> cannot be readily implemented in CGE.

Parallel sequencing runs in a set of up to 24 capillaries have been demonstrated recently.<sup>10</sup> To provide sensitive laser-excited fluorometric detection, a confocal illumination geometry couples a single laser beam to a single photomultiplier tube. Observation is one capillary at a time, and the capillary bundle is translated across the excitation/detection region at 20 mm/s by a mechanical stage. This provides adequate observation time for each capillary (to achieve a reasonable signal-to-noise ratio for base calling), but fast enough to repeat the scan every second (to achieve reasonable temporal resolution). That study<sup>10</sup> clearly demonstrates that capillaries can be run in parallel for DNA sequencing.

There are some subtle features inherent to the confocal excitation scheme<sup>10</sup> that may limit its use for very large numbers (thousands) of capillaries. Since data acquisition is sequential and not truly parallel, the ultimate sequencing speed will be determined by the observation time needed per DNA band for an adequate signal-to-noise ratio. Having more capillaries in the array or being able to translate the array across the detection region faster will not increase the overall sequencing speed. That is, to achieve the same signal-to-noise ratio, if the state-of-the-art sequencing speed of 1000 bases/h per lane<sup>7</sup> is used, the number of parallel capillaries<sup>10</sup> will have to be reduced proportionately regardless of the scan speed. The use of a translational stage may become problematic for a large capillary array. It has been shown<sup>11</sup> that bending of the capillaries can result in degradation in the separation efficiency. This is attributed to distortions in the gel and multipath effects. The amount of bending and cycling naturally increases with the number in the array. Sensitive laser-excited fluorescence detection also requires careful alignment both in excitation and in light collection so that

(1) Joint U.S. Department of Energy and U.S. Department of Health and Human Services Report DOE/ER-0452P, Understanding Our Genetic Inheritance—The U.S. Human Genome Project: The First Five Years; Washington, DC, April 1990.

(2) National Research Council Report of the Committee on Mapping and Sequencing the Human Genome, Board of Basic Biology, Commission on Life Sciences; National Academy Press: Washington, DC, 1988.

(3) Stegemann, J.; Schwager, C.; Erfle, H.; Hewitt, N.; Voss, H.; Zimmermann, J.; Ansoorge, W. *Nucleic Acids Res.* 1991, 19, 675-6.

(4) Brumley, R. L.; Smith, L. M. *Nucleic Acid Res.* 1991, 19, 412-6.

(5) Cohen, A. S.; Najarian, D. R.; Paulus, A.; Guttman, A.; Smith, J. A.; Karger, B. L. *Proc. Natl. Acad. Sci. U.S.A.* 1988, 85, 9680-3.

(6) Drossman, H.; Luckey, J. A.; Kostichka, A. J.; D'Cunha, J.; Smith, L. M. *Anal. Chem.* 1990, 62, 900-903.

(7) Sverdlow, H.; Zhang, J. Z.; Chen, D. Y.; Harke, H. R.; Grey, R.; Wu, S.; Dovichi, N. J.; Fuller, C. *Anal. Chem.* 1991, 63, 2835-2841.

(8) Church, G. M.; Kieffer-Higgins, S. *Science* 1988, 240, 185-188.

(9) Arlinghaus, H. F.; Thonnard, N.; Spaar, M. T.; Sachleben, R. A.; Larimer, F. W.; Foote, R. S.; Woychik, R. P.; Brown, G. M.; Sloop, F. V.; Jacobson, K. B. *Anal. Chem.* 1991, 63, 402-407.

(10) Huang, X. C.; Quesada, M. A.; Mathies, R. A. *Anal. Chem.* 1992, 64, 967-972.

(11) Hjerten, S., Paper M-3, EuChem Conference on Capillary Electro-separations, Storlien, Sweden, 1991.

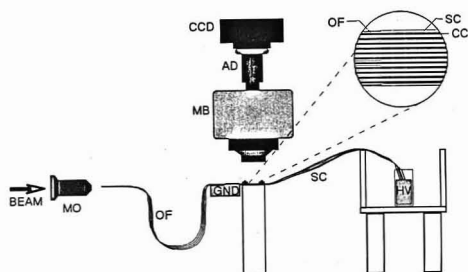


**Figure 1.** Multiplexed detection in capillary electrophoresis. CCD, charge-coupled device camera; AD, adapter column; MB, microscope body (eyepiece not shown); OF, optical fibers; SC, separation capillary; CC, capillary with black coating; MO, 10 $\times$  microscope objective; GND, buffer reservoir at ground potential; HV, buffer reservoir at positive high potential.

efficient coupling with the small i.d. tubing and discrimination of stray light are possible.<sup>12</sup> The translational movement thus has to maintain flatness to the order of the confocal parameter<sup>10,13,14</sup> (around 25  $\mu$ m) or else the cylindrical capillary walls will distort the spatially selected image. Multiple lenses and beamsplitters, beam scanning optics, or translational stages are therefore all unattractive. The latter two also have inherently a low duty cycle which works against multiplexing.

Recently, we have developed an axial beam excitation scheme for capillary electrophoresis.<sup>15</sup> The excitation laser is coupled via an optical fiber which in turn is inserted into the capillary tube. Observation is outside the capillary walls perpendicular to the axis. In one mode of operation, total internal reflection of the excitation beam is achieved, so that no stray light from the quartz walls or the polyimide coating reaches the phototube. Axial-beam excitation also provides longer absorption/fluorescence pathlengths, increasing the signal. Detection at the picomolar level was demonstrated. We report here the use of this excitation geometry to simultaneously monitor 10 capillary tubes undergoing electrophoresis. This represents a truly parallel multiplexing scheme for monitoring large arrays of capillaries. The system has no moving parts. Data rates are compatible with state-of-the-art run times in CGE and are fast enough even if there is another order of magnitude increase in DNA sequencing rates per lane in the future.

## EXPERIMENTAL SECTION

**Excitation.** A schematic diagram of the multiplexing apparatus is shown in Figure 1. Approximately 500 glass optical fibers (0.002-in. o.d., P31735, Edmond Scientific, Barrington, NJ) were grouped together and inserted into a 1/8-in.-i.d. heat shrinking tube. After heating, a razor blade was used to cleave the heat shrink casing and the enclosed fibers. This fiber bundle was inserted into the laser beam path by a microscope objective (Bausch and Lomb, Rochester, NY 16 mm, 10 $\times$ , BM2888). The 488-nm laser beam (2011-30SL, Cyonics, San Jose, CA) was partially focused by the objective to provide a beam spot size that overlaps the desired number of fibers in the illumination zone. A total laser power of 5 mW was thus divided among 10–12 optical fibers. The free end of each illuminated fiber was inserted 1.5 cm into a different fused silica capillary as discussed previously.<sup>15</sup>

**Detection.** The capillary array in the detection region was imaged onto a charge-coupled device (CCD) camera (Photomet-

rics, Tuscon, AZ, Series 200) through the camera extension of a binocular microscope (Bausch and Lomb, Stereo Zoom 7). The CCD camera was operated in a 25 to 1 column binning mode.<sup>16,17</sup> This allowed compression of 200 columns and 375 rows of image data into a 8  $\times$  375 array. Data extraction from the CC200 memory and analysis was carried out on a PC-compatible 80386-based computer equipped with an IEEE interface. Each frame of data, corresponding to a 0.1-s CCD exposure taken every 0.9 s, was stored in an individual file. The choice of exposure time (0.1 s) guarantees that even the sharpest and fastest moving bands in typical CE runs are not broadened due to blurring. Naturally, it is possible to eventually synchronize the reading of the CCD with the movement of the bands and gain 1 order of magnitude in sensitivity.<sup>18</sup> The time between exposures (0.8 s) is dictated by the camera-to-disk transfer rate of our particular computer hardware and software (0.5 s) and our attempt to limit the total amount of data collected. The total storage space for the 400 data files collected during a run was under 4 megabytes. With proper binning and using state-of-the-art CCD hardware and software, a data rate of 10 Hz can be achieved. Using a simple BASIC algorithm, the intensities of selected 3  $\times$  5 element regions representing each separation capillary were summed. These time-dependent sums are then plotted as electropherograms.

**Separation.** Silica capillaries (Polymicro Technologies, Phoenix, AZ, 75- $\mu$ m i.d., 150- $\mu$ m o.d., No. TSP075150, length = 27 cm) were prepared by removing 1 cm of polyimide coating with boiling sulfuric acid 25 cm from the injection end. Equilibration consisted of flushing with 0.1 M NaOH followed by filling with running buffer (10 mM bicarbonate adjusted to pH = 9) and applying a 5-kV potential for at least 10 h prior to fiber insertion. Solutions of riboflavin (BioRad) and fluorescein (Eastman Kodak) were prepared in running buffer. The electrophoretic separation was driven at +7.5 kV using a high-voltage power supply (Glassman, Whitehouse Station, NJ, Model PS/MJ30P0400-11) with a platinum electrode at the high-voltage end and a chrommel electrode at ground.

## RESULTS

**General Considerations.** Perhaps the most serious limitation of axial detection schemes concerns photochemical bleaching. This can result from the relatively long exposure of the analyte band to the intense excitation beam. Proper attention to this problem in instrument design is essential. Our earlier experiments,<sup>15</sup> where light was propagated along the entire capillary using total internal reflectance, utilized an organic absorber, Orange G, to block photochemical damage until the analyte reached the detection region. In the present case, with partial internal reflection,<sup>19</sup> only a small fraction of the incident laser intensity remains in the capillary after 1 cm of travel. A small bend (2-cm radius) in the capillary after the detection region prohibits any further light travel, thus rendering the use of an organic absorber unnecessary. An additional electronic shutter in the beam path, which opens synchronously with the CCD shutter, blocks the incident beam during the 80% of time when no signal is being collected and should greatly reduce photochemical damage in the detection region. The lack of photochemical bleaching is confirmed by comparing peak heights in single capillaries with different amounts of cumulative exposure to laser excitation.

The relative ease of capillary mounting and optical alignment shown previously has been preserved in this apparatus. To replace a single capillary in the array, two brackets are loosened, the malfunctioning or broken capillary is removed, and a new capillary slid into its place. Assuming that the fiber bundle has already been positioned properly relative to the microscope objective, alignment of the excitation beam

(12) Yeung, E. S.; Sepaniak, M. J. *Anal. Chem.* 1980, 52, 1465A–1481A.

(13) Hernandez, L.; Marquina, R.; Escalona, J.; Guzman, N. J. *Chromatogr.* 1990, 502, 247–255.

(14) Hernandez, L.; Escalona, J.; Joshi, N.; Guzman, N. J. *Chromatogr.* 1991, 559, 193–196.

(15) Taylor, J. A.; Yeung, E. S. *Anal. Chem.* 1992, 64, 1741–1744.

(16) Sweedler, J. V.; Bilhorn, R. B.; Epperson, P. M.; Sims, G. R.; Denton, M. B. *Anal. Chem.* 1988, 60, 282A–291A.

(17) Epperson, P. M.; Sweedler, J. V.; Bilhorn, R. B.; Sims, G. R.; Denton, M. B. *Anal. Chem.* 1988, 60, 327A–335A.

(18) Sweedler, J. V.; Shear, J. B.; Fishman, H. A.; Zare, R. N.; Scheller, R. H. *Anal. Chem.* 1991, 63, 496–502.

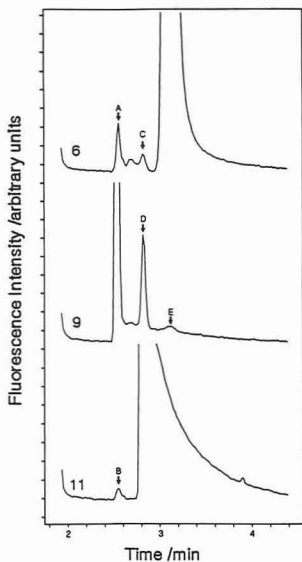


**Figure 2.** Crosstalk between separation channels in the absence of spacers. Thirteen capillaries were placed side by side and numbered consecutively. Peaks A and B are reflections of the fluorescence signal in capillary 9, C and D arise from the signal in capillary 11, and E represents interference from capillary 6. The eluted fluorophore is 3,3'-diethylthiadicarbocyanine iodide (DTDCI), appearing at different times due to variations among the capillaries. The scale is deliberately magnified to show the artifacts.

involves nothing more than the insertion of the optical fiber into the new capillary. Although this can be accomplished by hand even with unaided vision, use of the microscope, which is already in place, speeds up the process. The distance between the tip of the optical fiber and the observation zone does affect the net excitation intensity. This is not critical, however, since variations can be corrected for by calibration standards.

Crosstalk between the separation channels is another important design consideration in multiplexed detectors. This must be eliminated or reduced to a predetermined level before applications such as DNA sequencing can be addressed. Crosstalk has two causes: signal light reflections from the walls of adjacent capillaries and scatter from optics inside the microscope. When capillaries are placed next to each other, false peaks are observed in nearby capillaries, as shown in Figure 2. Our approach is simply to place spacers, which are the same 150- $\mu\text{m}$ -o.d. capillaries coated with black ink, between each of the separation capillaries. Using this method we reduced crosstalk to well below 1% of the observed signal. Naturally, more sophisticated masks can be built to eliminate crosstalk completely.

**Mobility and Quantitation.** Electropherograms for 10 parallel separations of riboflavin and fluorescein are shown in Figure 3. The retention times for the two components are similar to those reported previously.<sup>19</sup> This indicates that the electroosmotic flow normally present in an open capillary is not significantly disturbed by fiber insertion. The individual retention times in the 10 capillaries vary noticeably. The relative standard deviations (RSD) for the migration times of riboflavin ( $t_1$ ) and for the migration times of

fluorescein ( $t_2$ ) are around 3% and 5.5%, respectively. Since the 10 capillaries are unrelated, even the relative migration times of fluorescein ( $t_2/t_1$ ) show a 4% RSD. Also, the calculated mobilities ( $\mu$ ) of fluorescein (related to  $1/t_2 - 1/t_1$ ) give a RSD of 5%. Repeat experiments show similar results. This is to be expected given the uncontrolled nature of the surfaces inside each capillary, variations in temperature, variations in capillary i.d., variations in fiber-optic o.d., and differences in the length of insertion of the fiber. However, for a given capillary, run-to-run reproducibility was much better. The ranges of RSD for  $t_1$ ,  $t_2$ ,  $t_2/t_1$ , and  $\mu$  are 0.4–1.1%, 0.4–3.4%, 0.4–2.4%, and 0.4–2.4%, respectively. These are not too different from typical run-to-run variations in capillary electrophoresis in the absence of temperature control and for constant voltage operation.

Figure 3 also shows large variations in the peak areas among the 10 parallel capillaries. The RSD ranges from 70% for riboflavin ( $A_1$ ), 95% for fluorescein ( $A_2$ ), and 29% for the relative areas ( $A_2/A_1$ ). Large differences are expected due to nonuniform coupling of excitation energy into each capillary and variations in pixel sensitivities across the CCD. These dominate over the variations of individual capillary surfaces and geometries. For a given capillary, run-to-run reproducibility (RSD ranges) for  $A_1$ ,  $A_2$ , and  $A_2/A_1$  are 6–28%, 6–29%, and 3.6–17%, respectively. Injection bias is responsible for these variations. These are more pronounced than variations in migration times because factors like unequal time constants for electromigration injection, ubiquitous injection,<sup>20</sup> and the particular characteristics of the capillary entrance affect the injected amount but not the migration times. It is interesting to note that the peak areas are not correlated with the migration times. This indicates that photochemical bleaching<sup>15</sup> is not important in these experiments.

## DISCUSSION

Several important observations can be made. First, truly simultaneous multiplexing of capillary electrophoresis was achieved because the CCD camera looks at all capillaries at all times, with data rates fast enough for sequencing at >1 base/s per lane. Second, there are no moving parts and the injection (HV) end of the capillary bundle can be freely manipulated without affecting alignment. Third, the 5-mW excitation laser simply irradiates the entrance of the optical fiber bundle without critical alignment of the optics to achieve distribution of energy into each capillary. Fourth, there are variations in the excitation energies reaching each capillary, but that can be calibrated for in the same way the individual CCD pixels are normalized. Fifth, there are variations in absolute and relative migration times for the two compounds in the set of electropherograms. This is expected due to the uncontrolled nature of the capillary walls (electroosmotic flow), different temperatures, and different geometries in each capillary. However, recently we developed a migration index and an adjusted migration index to specifically correct for these variations.<sup>21</sup> These corrections can be implemented in the next generation of the instrument. Sixth, there are variations in the relative peak heights and areas among the capillaries for the same injected sample concentration. This is again expected due to bias at injection due to differences in electroosmotic flow rates, geometries, and injection time constants of the capillaries. Recently,<sup>20</sup> we developed a correction scheme to address this exact problem and have been able to reduce injection bias to <5%, which is adequate for DNA sequencing. Alternatively, an approach based on

(19) Whang, C. W.; Yeung, E. S. *Anal. Chem.* 1992, 64, 502–506.

(20) Lee, T. T.; Yeung, E. S. *Anal. Chem.* 1992, 64, 1226–1231.

(21) Lee, T. T.; Yeung, E. S. *Anal. Chem.* 1991, 63, 2842–2848.

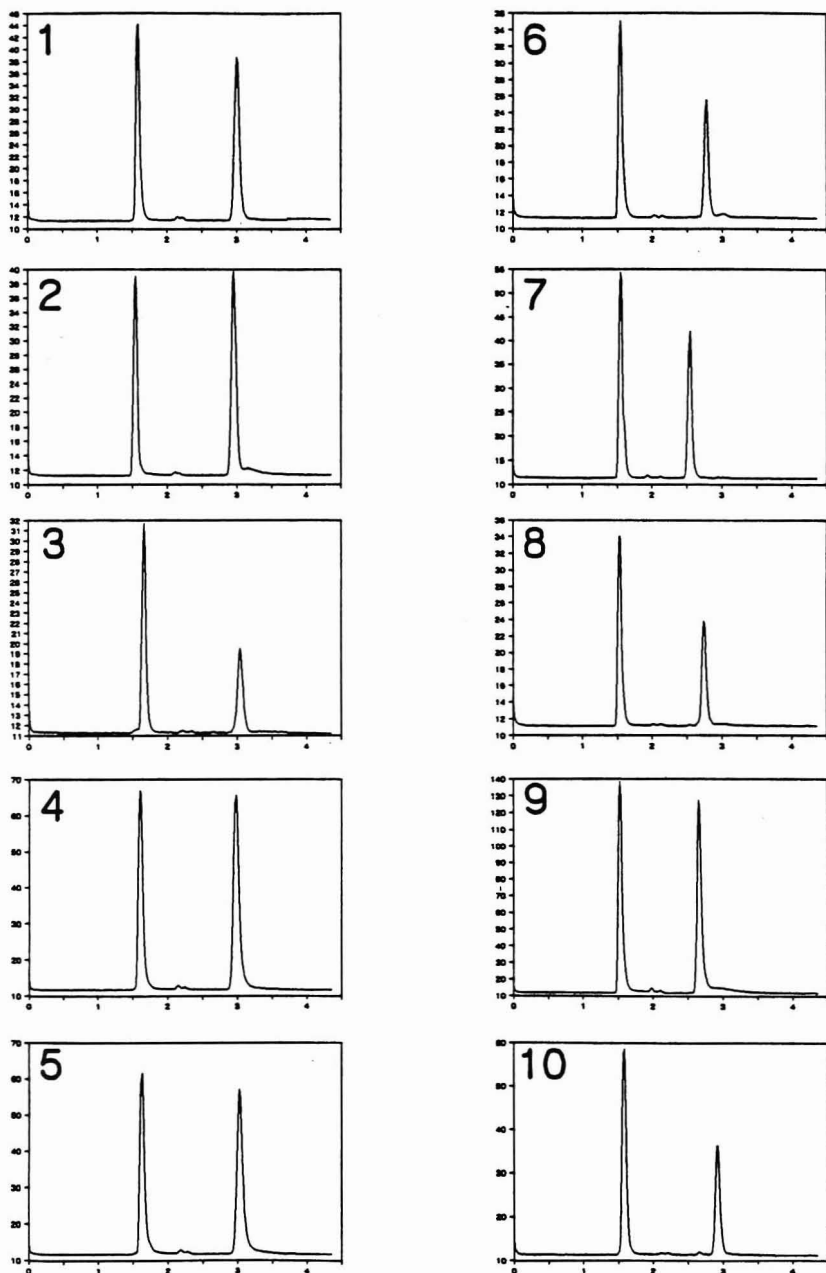


Figure 3. Simultaneous electrophoretic separations of riboflavin and fluorescein. Riboflavin concentration,  $5 \times 10^{-5}$  M; fluorescein concentration,  $6 \times 10^{-7}$  M; injection time at 7500 V, 5 s; time axis is in minutes.

two internal standards can be used.<sup>22</sup> These corrections can be incorporated in future experiments.

We expect this scheme to be capable of true multiplexing of 1024 capillaries in DNA sequencing runs. This number is

based on the number of column elements already available in modern solid-state imagers. An optical system can be devised based on our results for 10 capillaries. Fiber bundles to 1000 are readily available at a low cost. A 1-5-W argon ion laser can be used to illuminate one end of the fiber bundle,

(22) Dose, E. V.; Guichon, G. A. *Anal. Chem.* 1991, 63, 1154-1158.

conveniently distributing 0.4–2 mW of light to each fiber. The other end of the fiber bundle can be fanned out into a flat sheet on a guide, which is simply a set of parallel grooves to fix the location of each fiber to maintain a constant spacing; 1024 separation capillaries can also form a flat sheet on another guide. Insertion of the fibers (<50 mm) into the capillaries (~75 mm) should then be straightforward. The imaging optics can be a standard distortion-free camera lens, matching each of the optical windows on the capillaries to each pixel column on the detector. Several rows of pixels can be binned<sup>16–18</sup> to provide increased dynamic range without degrading resolution. The data rate of CCD cameras, even in the high-sensitivity, slow-scan mode, can be around 10 Hz. Since all channels are monitored at all times, true multiplexing is achieved. At a later stage, one can convert this to a charge-injection device (CID) camera. The advantage is that random access of data logging and even nondestructive reads are possible. One should be able to further increase the data rate by 1 order of magnitude, making the system compatible with any future increases in the speed of CGE. Data storage is also substantially reduced because the information can be evaluated before binning or reading multiple frames.<sup>23</sup> Also, once a base is identified, the other three lanes in the set of four need not be read or be subjected to data processing. A

(23) Koutny, L. B.; Yeung, E. S. An Expert System for Data Acquisition to Achieve Constant Signal-to-Noise: Application to Imaging of DNA Sequencing Gels. *Anal. Chem.* 1993, 65, 148–152.

(24) Smith, L. M.; Sanders, J. Z.; Kaiser, R. J.; Hughes, P.; Dodd, C.; Connell, C. R.; Heiner, C.; Kent, S. B.; Hood, L. E. *Nature* 1986, 321, 674–679.

second-generation imaging design can also include color filters to accommodate the four-color sequencing process<sup>7,24</sup> utilizing different parts of the CID detector.

To compensate for slight variations in migration times from one capillary to the next<sup>19</sup> one can use the migration index we developed.<sup>21</sup> All that is needed is separate current measurements in each capillary. If series resistors are connected to each of the capillaries, the resulting voltage can be monitored sequentially by an A/D converter and a desktop computer. Our work here shows that measurements every 0.1 s are sufficient. So, this is a simple task for 1000 capillaries using commercially available serial interface boards. The injection bias can also be corrected in an analogous manner<sup>20</sup> to maintain faithful intensity determinations. Our migration index has not yet been applied to sequencing gels. However, we have obtained preliminary results on a small number of sequencing runs. The results are promising in that variations in length, voltage, and diameter are properly accounted for. Naturally, more work to validate this correction scheme is needed and will be pursued in the future.

#### ACKNOWLEDGMENT

Ames Laboratory is operated for the U.S. Department of Energy by Iowa State University under Contract No. W-7405-Eng-82. This work was supported by the Director of Energy Research, Office of Health and Environmental Research.

RECEIVED for review August 20, 1992. Accepted November 23, 1992.



Differential Visualization of Transparent Testa Mutants in *Arabidopsis thaliana*

John J. Sheahan and Garry A. Reznitz\*

Hawaii Biosensor Laboratory, Department of Chemistry, University of Hawaii, Honolulu, Hawaii 96822

## INTRODUCTION

Destruction of the ozone layer is resulting in increased levels of UV-B (280-320 nm) radiation.<sup>1-4</sup> This presents a potential threat to living organisms.<sup>5</sup> If UV-B radiation continues to increase at current rates, the impact on vegetation could become significant.

UV-B stress in crops may affect photosynthesis, soluble proteins, lipids, carbohydrates, nonphotosynthetic pigments, nucleic acids, plant hormones, and ion transport. This may result in a wide range of morphological or anatomical effects, such as changes in leaf area, weight, bronzing, glazing, or chlorosis, as well as altered seedling growth, dry matter production, dry matter allocation, or yield.<sup>6</sup>

Fortunately, plants can protect themselves from UV-B injury. For instance, growth reduction, wall thickening, increased cell layers, nocturnal fluxes through UV-B susceptible metabolic pathways, orientation of cellular organelles distal to the UV-B light source, epicuticular waxes, trichomes, enhanced DNA repair, antioxidative capacities, and phenolic production are all possible forms of protection, most of which have been reviewed previously.<sup>6</sup>

Of these, phenolic production has been the most thoroughly characterized. The absorbance of hydroxycinnamic acid derivatives in the range of 320-390 nm, and of flavonoids in the range of 270 to 340 nm, suggests that both offer UV-B protection.<sup>7</sup> Flavonoid accumulation has a linear fluence-effect relationship and a fast response after UV-B induction and occurs in the outer cell layers of plants.<sup>8</sup> All of this suggests that flavonoids are a major class of UV-B protectants, but some of them have other roles. This is not surprising considering that there are approximately 2000 flavonoid structures<sup>9</sup> in the 12 flavonoid classes of Figure 1. Of the 12 classes, the three most abundant and widespread are the anthocyanins, flavones, and flavonols. Each is produced in relatives of *Arabidopsis*.<sup>10</sup>

Of these three classes, flavonols serve as the major UV-B protectants. They are more abundant than the flavones.<sup>11</sup> Several lines of evidence also suggest that they are more efficient UV-B protectants than the anthocyanins: their colorless nature indicates that they do not attenuate photosynthetically active radiation (PAR), their accumulation in mustard (a relative of *Arabidopsis*) cotyledons is not blocked by UV-B stress,<sup>12</sup> and they accumulate in the upper epidermis, rather than the lower epidermis as is the case for

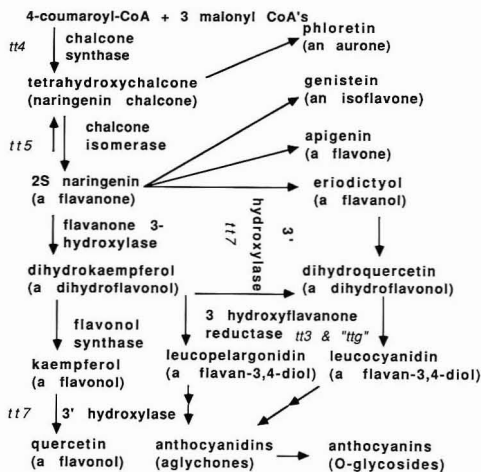


Figure 1. Flavonoid biosynthesis in *A. thaliana*. Several transparent testa mutants are shown in italics, and their stained fluorescence is shown in Figure 2.

anthocyanins,<sup>13</sup> all of which suggests that flavonols are the major class of flavonoid UV-B protectants in *Arabidopsis*.

The two major groups of flavonols are the kaempferol and quercetin glycosides. The fact that they are almost universal in the leaves of higher plants<sup>9</sup> indicates that they are the primary flavonoid UV-B protectants in crop species. With this in mind, we developed a staining procedure that detects quercetin glycosides in plant tissue.<sup>14</sup>

## EXPERIMENTAL SECTION

Wild-type (wt) seeds of the *Wassilewskija* ecotype were obtained from Ken Feldman, Du Pont, P.O. Box 80402 Wilmington, DE 19880-0402. They were the same ecotype as Dupont's T-DNA insertional mutant library, and they had an orange fluorescence that was indistinguishable from 20 other wild-type ecotypes (data not shown). This result suggests that the staining procedure will have limited use in breeding programs, but does not preclude its use for mutant isolation.

The chalcone-synthase mutant (*tt4* locus, F142 line, AIS accession number 1361) was obtained from the *Arabidopsis* Information Service, A. R. Kranz, Botanisches Institut, J. W. Goethe-Universität Seismayerstr. 70, Postfach 111 932, D-6000 Frankfurt am Main 11, Federal Republic of Germany. It has a null allele for the *tt4* locus which maps to chromosome 5 at position 14.9.<sup>15</sup> Since a chalcone synthase clone maps to chromosome 5 position 14.8,<sup>16</sup> it seems likely that the *tt4* locus is responsible for chalcone production. Because chalcone is the precursor for all flavonoids, and chalcone synthase is present as a single copy per haploid genome in *Arabidopsis*,<sup>17</sup> all tissues of the mutant are likely to lack flavonoids. This is further supported by the lack of pigmentation in the seed coat and stem of the mutant.

(13) Wellmann, E. *Ber. Dtsch. Bot. Ges.* 1974, 87, 275-279.

(14) Sheahan, J. J.; Reznitz, G. A. *Biotechniques* 1992, 13, 890-883.

(15) Koorneef, M. *Arabidopsis Information Service* 1990, 27, 1-4.

(16) Chang, C.; Bowman, J. L.; DeJong, J. L.; Lander, E. S.; Meyerowitz, E. M. *Proc. Natl. Acad. Sci. U.S.A.* 1988, 85, 6856-6860.

(17) Feinbaum, R. L.; Ausubel, F. M. *Mol. Cell. Biol.* 1988, 8 (5), 1985-1992.

- (1) Blumthaler, M.; Ambach, W. *Science* 1990, 248, 206-208.
- (2) Blumthaler, M.; Ambach, W. *Photochem. Photobiol.* 1991, 54 (3), 492-492.
- (3) Green, A. E. S. *Physiol. Plant.* 1983, 58, 351-359.
- (4) Webb, A. R. *Photochem. Photobiol.* 1991, 54 (5), 789-794.
- (5) Bormann, J. F. *Photochem. Photobiol. B: Biol.* 1989, 4, 145-158.
- (6) Teramura, A. H. *Physiol. Plant.* 1983, 58, 415-427.
- (7) Schnabl, H.; Weissenböck, G.; Sachs, G.; Scharf, H. J. *Plant Physiol.* 1989, 135, 249-252.
- (8) Wellmann, E. In *The Encyclopedia of Plant Physiology, New Series, 16B, Photomorphogenesis*; Shropshire, W., Jr., Mohr, H., Eds.; Springer-Verlag: New York, 1983; p 749.
- (9) Harborne, J. B. In *Secondary Plant Products*; Bell, E. A., Charlwood, B. V., Eds.; Springer-Verlag: New York, 1980; pp 329-402.
- (10) Giannasi, D. E. In *The Flavonoids*; Harborne, J. B., Ed.; Chapman and Hall: London, 1988; p 489.
- (11) Wollenweber, E.; Jay, M. In *The Flavonoids*; Harborne, J. B., Ed.; Chapman and Hall: London, 1988; pp 233-302.
- (12) Wellmann, E.; Schneider-Zeibert, U.; Beggs, C. J. *Plant Physiol.* 1984, 75, 997-1000.

The remaining transparent testa mutants were obtained from Mary Anderson, Nottingham *Arabidopsis* Stock Centre, School of Biological Sciences, University of Nottingham, University Park, Nottingham NG7 2RD U.K. The chalcone flavanone isomerase mutant (*tt5*, NW 86) and the dihydroflavonol 4-reductase mutant (*tt3*, NW 84) have also been identified, and their corresponding genes have been cloned by genomic subtraction.<sup>18</sup> The flavonoid 3'-hydroxylase mutant (*tt7*, NW 88) has been identified by thin-layer chromatography and maps to the late flowering gene *fy* at the end of chromosome 5.<sup>19</sup> The *ttg* locus has not been identified in *Arabidopsis thaliana*. However, its lack of leaf hairs and the presence of flavonols suggests that it is equivalent to the *e* and *g* mutants of *Matthiola* which lack dihydroflavonol 4-reductase (3-hydroxyflavanone reductase) activity.<sup>20</sup>

Seedlings were germinated in 3 ppm Norflurazon (Trade names Solcomax and Zorial which is made by Sandoz Crop Protection, Chicago IL). Its signal word is caution, and it is in toxicity class IV, suggesting low toxicity. It interfered with carotenoid biosynthesis at the level of phytoene desaturation.<sup>21</sup> Because carotenoids were unable to protect the photosynthetic apparatus, seedlings were bleached white in the presence of light. On the second day after their germination, they were harvested and soaked in staining solution for 1 h. The solution consisted of 3.75 × 10<sup>-3</sup>% (v/v) Triton X-100 and 0.25% (w/v) diphenylboric acid 2-aminoethyl ester (see refs 22-24; Sigma, Chemical Abstracts Registry No. 524-95-8; also called Naturstoff Agent, NA). Its toxicological properties have not been thoroughly investigated, but it has an oral rat LD50 of 78 000 mg/kg, which suggests low toxicity.

The seedlings were removed and placed on a Petri plate containing 1% agar and 0.5% graphite to provide a dark photographic background. The stained seedlings were then excited with a long-wave UV light source (Model UVGL-25 UVP, Inc., San Gabriel, CA 91778). Photographs were taken through a visible microscope with a 2× fluorescence objective onto Kodacolor Gold 1600 ASA film. The final magnification was 30× for 4-in. × 6-in. prints. A 0.5-h exposure had specific fluorescent coloration, but the images and background were underdeveloped. Longer exposures improved their resolution but decreased the specificity of color development and are not shown.

## RESULTS AND DISCUSSION

Flavonol research has been hampered by the lack of flavonol coloration. Flavonol synthase (FS) mutants have not been identified, and FS has not been cloned apparently for that reason. Flavonoid 3'-hydroxylase (F3'H) is shared by anthocyanin biosynthesis, so mutants have been isolated, and a F3'H gene (the "blue" gene) has apparently been cloned by Calgene Pacific (personal communication), but is not yet available to the research community.

All of the upstream enzymes shown in Figure 1 have been cloned. The occurrence of colored pigments downstream of their biosynthetic pathway is responsible for the rapid progress in this area, and the same progress could be achieved with flavonol biosynthesis if the flavonols were visible. Thus we developed a staining procedure for this purpose.

It provides phenolic precursors with a faint blue fluorescence as is shown for *tt4* (a chalcone synthase mutant) in

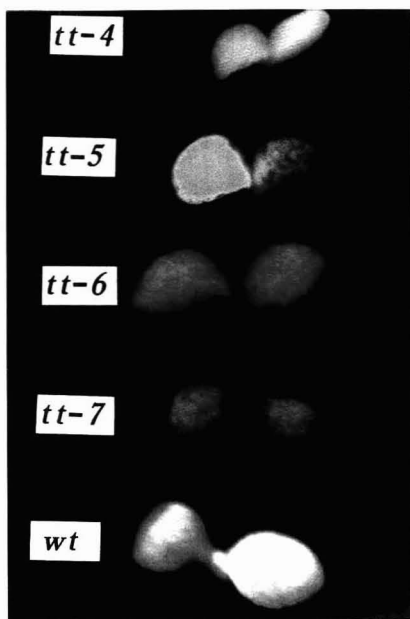


**Figure 2.** Fluorescence of *A. thaliana* transparent testa mutants whose lesions are shown in Figure 1. The blue *tt4* is a chalcone-synthase mutant, the off-white *tt5* is a chalcone isomerase mutant, the red *tt6* is unidentified, and the green *tt7* is a flavonoid 3'-hydroxylase mutant. Both *ttg* and *tt3* lack dihydroflavonol 4-reductase (3-hydroxyflavanone reductase) activity and have an orange fluorescence which is characteristic of wild-type.

Figure 2. The blue fluorescence is less pronounced in *tt5* (a chalcone isomerase mutant). Since the *tt5* accumulates fewer sinapate esters than *tt4*,<sup>25</sup> these results suggest that phenolic precursors are responsible for the blue fluorescence. The stain also provides 4',4'-dihydroxyflavones and -flavonols with a green fluorescence<sup>14,20-22,26</sup> as is shown for *tt7* (a flavonoid 3'-hydroxylase mutant), and 3',4'-equivalents<sup>14,20-22,26</sup> with an orange fluorescence as is shown for wild-type. This orange fluorescence was also observed in *ttg*, *tt1*, *tt2*, *tt3*, *tt8*, *tt9*, and *tt10*. The reddish fluorescence of *tt6* suggests that it also has 3',4'-equivalents, but it has not yet been identified.

The staining procedure is an improvement over previous methods utilizing ammonia<sup>27</sup> in that it does not require etiolated tissue and its fluorescence is more stable and is specific for flavonoids. This specificity was demonstrated by the transparent testa mutants with altered anthocyanin content. These include *tt4*, *tt5*, *tt6*, and *tt7*, all of which lack wild-type fluorescence. Of the remaining transparent testa mutants, only *ttg* and *tt3* have altered anthocyanin content. They do not have altered fluorescence, however, because their lesions are specific to the anthocyanin biosynthesis as is shown in Figure 1.

The T-DNA insertional mutant library at Dupont was also screened for mutants with altered fluorescence. Two mutants

(18) Shirley, B. W.; Hanley, S.; Goodman, H. M. *Plant Cell* 1992, 4, 333-347.

(19) Koornneef, M.; Luiten, W.; Vlaming, P. de; Schram, A. W. *Arabidopsis Information Service* (Frankfurt am Main) 1982, 19, 113-115.

(20) Heller, W.; Forkmann, G.; Britsch, L.; Grisebach, H. *Planta* 1985, 165, 284-287.

(21) Sandman, G.; Boger, P. In *Encyclopedia of Plant Physiology: Photosynthesis III*. Vol. 19. Sites of herbicide inhibition of the photosynthetic apparatus; Staehelin, L. A., Arntzen, C. J., Eds.; Springer-Verlag: Berlin, 1986; p 595.

(22) Brasseur, T.; Angenot, L. *J. Chromatogr.* 1986, 351, 351-355.

(23) Brasseur, T.; Angenot, L. *Phytochemistry* 1987, 26 (12), 3331-3334.

(24) Budzianowski, J. *J. Chromatogr.* 1991, 540, 469-474.

(25) Jiayang, Li; Tsai-Mei, Ou-Lee; Raba, R.; Amundson, R. G.; Last, R. L., submitted to *Plant Cell*.

(26) Markham, K. R. *Techniques of Flavonoid Identification*; Academic Press: New York, 1982; p 24.

(27) Schmelzer, E.; Jahnen, W.; Hahlbrock, K. *Proc. Natl. Acad. Sci. U.S.A.* 1988, 85, 2989-2993.

with a green fluorescence were isolated. Complementation tests revealed that both were allelic to *tt7*. These results further demonstrate the specificity of the staining procedure for flavonoids in *A. thaliana*.

### CONCLUSIONS

The lack of flavonol coloration has hampered flavonol research, so we developed a staining procedure that overcame this problem. We have shown that the proposed staining procedure differentially stains flavonoids in chlorophyll-bleached tissue of *A. thaliana*.

A flavonol synthase (FS) mutant has not been identified, and FS is the only gene in flavonol biosynthesis which has not yet been cloned. The unique fluorescence and visible coloration of *tt6* will require further investigation as to whether it is a flavonol synthase mutant or a flavanone 3-hydroxylase mutant.

Flavonoid 3'-hydroxylase (F3'H) is also unavailable to the scientific community. A T-DNA insertional mutant library screen identified two F3-H mutants, and attempts to clone a tagged gene are in progress.

Besides identifying mutants with which to clone the last of the flavonol biosynthetic genes, this staining procedure provides visual markers which were not before available. Unlike other model organisms, *Arabidopsis* has few pigments with which to analyze rare forms of genetic recombination. This paper demonstrates several visual markers which will be used for that purpose.

### ACKNOWLEDGMENT

We gratefully acknowledge financial support from the National Science Foundation. We also thank Joseph De Franks for providing an aliquot of Norfluorazon, A. R. Kranz for supplying the chalcone-synthase mutant, Robert Reiter and Sandra Russel for assistance in screening the T-DNA insertional mutant library at Dupont, and Terry Lyttle for the use of his microscope.

RECEIVED for review September 29, 1992. Accepted December 3, 1992.

**AUTHOR INDEX**

- Aldstadt, J. H., 922
- Bachas, L. G., 945
- Bean, M. F., 877
- Blair, T. L., 945
- Brandvig, R. L., 952
- Bush, C. A., 913
- Carr, S. A., 877
- Castro, A., 849
- Chang, C.-C., 913
- Changsong, L., 863
- Cynkowski, T., 945
- Dewald, H. D., 922
- Di Corcia, A., 907
- Fairfield, F. R., 849
- Foret, F., 900
- Hampton, R. S., 894
- Huddleston, M. J., 877
- Jakel, M. E., 952
- Karger, B. L., 900
- Kasthurikrishnan, N., 857
- Koropchak, J. A., 857
- Kotato, M., 927
- Kroening, J. G., 952
- LaCourse, W. R., 948
- Lakowicz, J. R., 853
- Lubman, D. M., 866
- Lunte, S. M., 948
- Marcomini, A., 907
- McCreery, R. L., 937
- McDermott, C. A., 937
- McDermott, M. T., 937
- Nielen, M. W. F., 885
- Odashima, K., 927
- O'Shea, T. J., 948
- Petrie, L. M., 952
- Rechnitz, G. A., 961
- Reddy, G. P., 913
- Rutan, S. C., 894
- Samperi, R., 907
- Sheahan, J. J., 961
- Shera, E. B., 849
- Stelluto, S., 907
- Sugawara, M., 927
- Taylor, J. A., 956
- Thompson, R. B., 853
- Thompson, T. J., 900
- Umezawa, Y., 927
- Vouros, P., 900
- Weijun, J., 863
- Yeung, E. A., 956
- Zhao, J., 866

# ACS PUBLICATIONS

Essential Resources for the Chemical Sciences

## Enhance Your Work Ensure Your Future

### Accounts of Chemical Research

Editor: Fred W. McLafferty  
Cornell University  
12 issues a year. ISSN 0001-4842  
Member \$28 Nonmember \$177

### Analytical Chemistry

Editor: Royce W. Murray  
University of North Carolina, Chapel Hill  
24 issues a year. ISSN 0003-2700  
Member \$36 Nonmember (Personal) \$78  
Nonmember (Institutional) \$415

### Biochemistry

Editor: Gordon G. Hammes  
Duke University  
51 issues a year. ISSN 0006-2960  
Member \$107 Nonmember \$1,186

### Bioconjugate Chemistry

Editor: Claude F. Meares  
University of California, Davis  
6 issues a year. ISSN 1043-1802  
Member \$29 Nonmember \$273

### Biotechnology Progress

Editor: Jerome S. Schultz  
University of Pittsburgh  
6 issues a year. ISSN 8756-7938  
Member \$30 Nonmember \$325

### Chemical & Engineering News

Editor: Michael Heylin  
51 issues a year. ISSN 0009-2347  
Nonmember \$110

### Chemical Research in Toxicology

Editor: Lawrence J. Marnett  
Vanderbilt University  
6 issues a year. ISSN 0893-228X  
Member \$46 Nonmember \$311

### Chemical Reviews

Editor: Josef Michl  
University of Colorado, Boulder  
8 issues a year. ISSN 0009-2665  
Member \$33 Nonmember \$346

### Chemistry & Industry

Editor: Andrew Miller  
Society of Chemical Industry  
Available exclusively in North America  
through a marketing agreement between  
ACS and SCI.  
24 issues a year. ISSN 0009-3068  
Member \$59 Nonmember \$330

### Now Monthly!

### Chemistry of Materials

Editor: Leonard V. Interrante  
Rensselaer Polytechnic Institute  
12 issues a year. ISSN 0897-4756  
Member \$49 Nonmember \$375

### NEW EDITOR!

### CHEMTECH

Editor: Abraham P. Gelbein  
12 issues a year. ISSN 0009-2703  
Member \$39 Nonmember (Personal) \$79  
Nonmember (Institutional) \$370

### Energy & Fuels

Editor: John W. Larsen  
Lehigh University  
6 issues a year. ISSN 0887-0624  
Member \$48 Nonmember \$345

### Environmental Science & Technology

Editor: William H. Glaze  
University of North Carolina, Chapel Hill  
12 issues a year. ISSN 0013-936X  
Member \$43 Nonmember (Personal) \$89  
Nonmember (Institutional) \$444

### Industrial & Engineering Chemistry Research

Editor: Donald R. Paul  
University of Texas, Austin  
12 issues a year. ISSN 0888-5885  
Member \$64 Nonmember \$567

### Inorganic Chemistry

Editor: M. Frederick Hawthorne  
University of California, Los Angeles  
26 issues a year. ISSN 0020-1669  
Member \$90 Nonmember \$949

### Journal of Agricultural and Food Chemistry

Editor: Irvin E. Liener  
University of Minnesota  
12 issues a year. ISSN 0021-8561  
Member \$32 Nonmember \$335

### Journal of the American Chemical Society

Editor: Allen J. Bard  
University of Texas, Austin  
26 issues a year. ISSN 0002-7863  
Member \$96 Nonmember \$1,055

### Journal of Chemical & Engineering Data

Editor: Kenneth N. Marsh  
Texas A&M University  
4 issues a year. ISSN 0021-9568  
Member \$36 Nonmember \$309

### Journal of Chemical Information and Computer Sciences

Editor: George W.A. Milne  
National Institutes of Health  
6 issues a year. ISSN 0095-2338  
Member \$20 Nonmember \$180

### Journal of Medicinal Chemistry

Editor-in-Chief: Philip S. Portoghese  
University of Minnesota  
26 issues a year. ISSN 0022-2623  
Member \$54 Nonmember \$586

### The Journal of Organic Chemistry

Editor: Clayton H. Heathcock  
University of California, Berkeley  
26 issues a year. ISSN 0022-3263  
Member \$75 Nonmember \$785

### NEW EDITOR!

### Journal of Physical and Chemical Reference Data

Editor: Jean W. Gallagher  
National Institute of Standards and  
Technology  
6 issues a year. ISSN 0047-2689  
Member \$85 Nonmember \$420

### Now Weekly!

### The Journal of Physical Chemistry

Editor: Mostafa A. El-Sayed  
University of California, Los Angeles  
51 issues a year. ISSN 0022-3654  
Member \$97 Nonmember \$1,140

### Langmuir

Editor: William A. Steele  
The Pennsylvania State University  
12 issues a year. ISSN 1074-7463  
Member \$68 Nonmember \$715

### Macromolecules

Editor: Field H. Winslow  
AT&T Bell Laboratories  
26 issues a year. ISSN 0024-9297  
Member \$83 Nonmember \$920

### Organometallics

Editor: Dietmar Seyferth  
Massachusetts Institute of Technology  
12 issues a year. ISSN 0276-7333  
Member \$79 Nonmember \$850

Rates listed are for one-year, U.S. prices only.  
For rates outside the U.S., contact ACS.  
Rates are valid through December 31, 1993.

#### For subscription information write:

American Chemical Society • Member and Subscriber Services • P.O. Box 3337 • Columbus, Ohio 43210

Or call TOLL FREE (U.S. only) 1-800-333-9511

Outside the U.S. call 614-447-3776 • FAX: 614-447-3671

#### For nonmember rates in Japan, contact:

Maruzen Company, Ltd. • 3-10 Nihonbashi 2-chome, Chuo-ku • Tokyo 103, Japan

# *When Precision is Important*



## **Choose the NEW AC-350 Calorimeter from LECO!**

- Integral water measuring and bomb filling station
- Accurate over a wide ambient temperature range
- 16-bit DSP controller ensures high precision
- Extended calibration stability
- Isoperial Methodology

*For more information, contact:*



LECO Corporation; 3000 Lakeview Avenue  
St. Joseph, Michigan 49085-2396, U.S.A.  
Phone: 616-983-5531; Fax: 616-983-3850

LECO is a registered trademark of LECO Corporation